THERMODYNAMIC AND KINETIC STUDIES OF GALENA IN THE PRESENCE AND ABSENCE OF POTASSIUM ETHYL XANTHATE

by

Mark David Pritzker

Dissertation submitted to the Faculty of the

Virginia Polytechnic Institute and State University

in partial fulfillment of the requirements for the degree of

DOCTOR OF PHILOSOPHY

in

Materials Engineering Science

APPROVED:

R. H. Yoon, Chairman

G. V. Gibbs

K. Reifsnider

P. E. Richardson

G. Sanzone

T. C. Ward

J. P. Wightman

April, 1985

Blacksburg, Virginia

THERMODYNAMIC AND KINETIC STUDIES OF GALENA IN THE PRESENCE AND ABSENCE OF POTASSIUM ETHYL XANTHATE

by

Mark David Pritzker

Committee Chairman: Roe-Hoan Yoon
Mining and Minerals Engineering

(ABSTRACT)

A study of the electrochemistry of the PbS-H_2O and PbS-KEX-H_2O systems has been made by carrying out thermodynamic calculations, electrochemical experiments and microflotation tests. Particular attention has been paid to how well this system can be described by equilibrium thermodynamics.

The thermodynamic calculations are more comprehensive than previous ones of this type since they are based on a mass balance which includes both insoluble and soluble species. The data they provide include equilibrium concentrations of all dissolved species at any E_h and pH and an E_h-pH stability diagram for each collector addition. Also, two- and three-dimensional plots showing the effect of E_h and pH on xanthate uptake by the galena surface have been presented for the first time. These are particularly useful because they can be directly compared to observed flotation data.

The results of voltammetry, IGP and potential-step experiments suggest that the oxidation of galena at pH 6.8 and 9.2 begins at a

potential below the value predicted by bulk thermodynamics with the electrosorption of OH^- and the formation of a metal-deficient sulfide and a surface lead oxide. When oxidation becomes extensive enough, bulk products, S^o and PbO, begin to nucleate. Thiosulfate is detected at pH 9.2, but only becomes significant at high potentials.

The electrochemical experiments indicate that xanthate adsorbs onto galena via a one-electron transfer chemisorption reaction in the first monolayer and via the formation of PbX_2 in subsequent layers. It also appears that galena oxidation and xanthate adsorption are competitive processes that tend to inhibit each other.

Ground galena exhibits natural floatability at pH 9.2 as long as oxidation extends to the formation of a metal-deficient sulfide, but not to bulk PbO. When 10^{-5} M xanthate is added, the upper potential limit for flotation agrees well with the value predicted from thermodynamics for the decomposition of PbX_2. The lower limit, on the other hand, is at least 200 mv lower than any of the predicted values.

PbS dissolves anodically at pH 1.1 and 4.6 to form Pb^{2+} and S^o first by a random surface process and then by a nucleation and growth mechanism once oxidation becomes extensive enough. At pH 0, the relation between the open-circuit potential and mineral solubility, as predicted by the thermodynamic calculations, agrees quantitatively with that determined experimentally. However, as the pH is increased to 1.1 and 4.6, the system becomes increasingly less reversible.

ACKNOWLEDGMENT

The author has worked with Dr. R. H. Yoon for a major part of the last nine years - as an undergraduate at McGill University, as a Physical Scientist at the Canada Centre for Mineral and Energy Technology, and as a graduate student at Virginia Polytechnic Institute and State University. The guidance, inspiration and enthusiasm that this friend and advisor has shown throughout this collaboration are sincerely appreciated.

The author is also grateful to Dr. Ron Woods, who made many invaluable suggestions for possible experiments and spent many hours discussing the results of this work. Special thanks are also given to , who provided much assistance in designing some of the experimental equipment and who participated in many discussions concerning this research.

The author expresses his gratitude to for the Presidential Fellowship and the Mining and Minerals Resources Research Institute Fellowship that he received during his stay at Virginia Tech.

Sincere gratitude is also expressed to and for their technical support, and to , and for their work in conducting some of the experiments and analysis.

The friendship of the many graduate students the author came to know at Virginia Tech, particularly that of and , is also appreciated.

Finally, the author wishes to extend particular thanks to

for her continuing support and enthusiasm, for typing and reading the dissertation, and without whom this manuscript could not have been completed.

TABLE OF CONTENTS

page

ABSTRACT ii

ACKNOWLEDGMENT iv

TABLE OF CONTENTS vi

LIST OF FIGURES xiii

LIST OF TABLES xxviii

I. INTRODUCTION 1

1.1 **General** 1

1.2 **Scope of the Work** 3

1.3 **Current Trends in Electrochemical Research on the Solution and Flotation Chemistry of Sulfides** . . . 4

1.4 **Objectives of This Study** 20

II. THERMODYNAMIC CALCULATIONS OF THE GALENA-ETHYL XANTHATE SYSTEM 24

2.1 **Introduction** 24

2.1.1 General 24

2.1.2 Literature Review 25

2.2 **Approach Used for the Calculations** 26

2.2.1 Outline of Procedure 26

2.2.2 Example of Derivation of a Mass Balance Equation 35

2.3 **Results** 40

2.3.1 E_h-pH Diagrams 41

a. Case I 43

0 and 10^{-7} M KEX 43
10^{-6} M KEX 45
10^{-5} M KEX 47
10^{-4} M KEX 47

b. Case II 50

0 M KEX 50
10^{-7} M KEX 52
10^{-6} M KEX 54
10^{-5} M KEX 54
10^{-4} M KEX 54

c. Case III 58

0 M KEX 58
10^{-7} M KEX 60
10^{-6} M KEX 60
10^{-5} M KEX 60
10^{-4} M KEX 60

2.4 **Discussion** 64

2.4.1 Oxidation and Collectorless Flotation of Galena . 64

2.4.2 Reduction of Galena 76

2.4.3 Relation Between Solution Chemistry and Electro-Kinetics of the Galena-Water System 76

2.4.4 Effect of E_h, pH, and Xanthate Addition on the Formation of PbX_2 and X_2 80

a. Effect of E_h 81

b. Effect of pH 99

2.4.5 Contour Diagram and Three-Dimensional Plots . . 111

a. Lead solubility 111

b. Xanthate uptake 119

2.4.6 Stability of Xanthate-Bearing Species 119

2.5 **Summary** 128

III. EXPERIMENTAL STUDIES REGARDING THE SOLUTION AND FLOTATION CHEMISTRY OF GALENA AT pH 6.8 AND 9.2 131

3.1 **Introduction** 131

3.1.1 General 131

3.1.2 Literature Review 132

3.1.3 Linear Sweep Voltammetry 139

3.1.4 Intermittent Galvanostatic Polarization 143

3.2 **Experimental** 146

3.2.1 Materials 146

3.2.2 Preparation of Galena Electrode 148

3.2.3 Electrochemical Measurements 148

3.2.4 Microflotation Tests 151

3.3 **Results and Discussion** 152

3.3.1 In the Absence of Xanthate 152

a. Single sweep voltammetry at pH 9.2 152

Effect of anodic limit 152
Effect of stirring 156
Charge analysis of voltammetry peaks 156
Identification of A_2 peak 170

b. Cyclic voltammetry at pH 9.2 172

Identification of C_1 peak 172
Effect of cycling on oxidation 174

c. IGP experiments at pH 9.2 183

d. Chronoamperometry experiments at pH 9.2 . . . 194

e. Single sweep voltammetry at pH 6.8 196

Identification of A_1, C_1 and C_2 peaks 196

f. Cyclic voltammetry at pH 6.8 203

g. IGP experiments at pH 6.8 210

h. Chronoamperometry experiments at pH 6.8 . . . 217

3.3.2 In the Presence of Xanthate 220

a. Single sweep voltammetry at pH 9.2 220

Effect of xanthate concentration 220
Effect of anodic limit at 10^{-3} M KEX 229
Anodic limits up to 445 mv at 10^{-3} M KEX . . . 232
Anodic limit of 495 mv at 10^{-3} M KEX 234
Anodic limit of 545 mv at 10^{-3} M KEX 239
Effect of anodic limit at 10^{-4} M KEX 240
Anodic limits below 495 mv at 10^{-4} M KEX . . . 243
Anodic limits of 495 and 545 mv at 10^{-4} M KEX . 247

b. Cyclic voltammetry at 10^{-3} M KEX and pH 9.2 . . 248

c. IGP experiments at pH 9.2 250

d. Single sweep voltammetry at pH 6.8 253

Effect of xanthate concentration 253
Initial xanthate adsorption 253
Anodic limits up to 345 mv at 10^{-3} M KEX . . . 260
Anodic limit of 345 mv at 10^{-3} M KEX 260
Anodic limits up to 245 mv at 10^{-4} M KEX . . . 263

e. IGP experiments at pH 6.8 266

f. Chronoamperometry experiments at 10^{-3} M KEX and at pH 6.8 and 9.2 270

g. Microflotation tests at pH 9.2 273

3.4 **Summary** 277

IV. ELECTROCHEMICAL STUDIES OF GALENA AT pH 1.1 AND 4.6 280

4.1 **Introduction** 280

4.1.1 General 280

4.1.2 Literature Review 282

4.2 **Experimental** 286

4.3 **Results and Discussion** 287

4.3.1 Electrochemical Experiments at pH 1.1 287

a. Chronoamperometry 287

b. Single sweep voltammetry 293

Identification of A_1, C_1 and C_2 peaks 293
Identification of A_2 and A_3 peaks 305

c. Intermittent galvanostatic polarization . . . 310

4.3.2 Voltammetry Experiments at pH 4.6 319

Identification of peaks 319
Effect of anodic limit 325
Effect of scan rate 327
Effect of Pb^{2+} concentration 330

4.3.3 Effect of Open-Circuit Potentials on the Dissolution of Galena 341

a. In 1 M $HClO_4$ solution (pH 0) 341

b. In 0.1 M $HClO_4$ solution (pH 1.1) 346

c. In 0.5 M CH_3COOH/0.5 M CH_3COONa solution (pH 4.6) 349

4.4 **Summary** 352

V. POSSIBLE MECHANISMS FOR GALENA OXIDATION AND XANTHATE ADSORPTION 354

5.1 **Introduction** 354

5.1.1 General 354

5.1.2 Electronic Properties of Galena 354

5.2 **Galena Oxidation and Xanthate Adsorption at pH 9.2 and 6.8** 356

5.2.1 Galena Oxidation at pH 9.2 356

a. Mechanism for initial stages of galena oxidation 357

b. Formation of bulk oxidation products 365

c. Thiosulfate formation 366

5.2.2 Galena Oxidation at pH 6.8 369

5.2.3 Chemisorption of Xanthate at pH 9.2 and 6.8 . . 374

5.2.4 Xanthate Adsorption and Sulfide Oxidation as Competitive Processes 379

5.3 **Galena Oxidation at pH 1.1 and 4.6** 386

5.3.1 Mechanism Change with Extent of Reaction . . . 386

5.3.2 Dissolution by a Random Surface Process 388

5.3.3 Dissolution by a Nucleation and Growth Mechanism . 391

VI. SUMMARY AND CONCLUSIONS 402

6.1 **Introduction** 402

6.2 **Role of Thermodynamics in Describing Galena Aqueous Chemistry** 402

6.2.1 In the Absence of Xanthate 402

6.2.2 In the Presence of Xanthate 407

6.3 **Contributions from the Present Study** 410

6.3.1 Thermodynamic Calculations 410

6.3.2 Electrochemical Experiments at pH 9.2 and 6.8 . . 413

6.3.3 Electrochemical Experiments at pH 1.1 and 4.6 . . 416

6.4 **Recommendations for Future Research** 419

REFERENCES 425

APPENDIX I. Sample Computer Program 443

APPENDIX II. Sample Derivation of the Relationship Between Charges Associated With a Reaction Sequence . . . 483

APPENDIX III. Expressions for the Amount of PbO Generated and Consumed During Each Cyclic Scan at pH 9.2 . . 487

APPENDIX IV. Equilibrium Ratio for the Occupation of the Surface Sites by X^- and OH^- 490

VITA 493

LIST OF FIGURES

		page
Figure 1.1	The establishment of a mixed potential between separate anodic and cathodic reactions.	6
Figure 1.2	Schematic diagram showing the effect of oxygen partial pressure on the mixed potential for the aqueous oxidation of a sulfide.	9
Figure 1.3	Typical electrode used for the electrochemical studies of conducting minerals.	13
Figure 1.4	(a) Electrochemical cell set-up for a three-electrode system. (b) Schematic diagram showing the electric connections used for three-electrode potentiostatic experiments.	15
Figure 1.5	Schematic diagram of the particle-bed electrode set-up used by Richardson and co-workers (Walker et al., 1984a,b; Richardson et al., 1984).	17
Figure 2.1	Effect of pH on the equilibrium concentration of the dissolved species in the PbS-H_2O system for Case I at E_h = 200 mv, T = 298°K and P = 1 atm.	42
Figure 2.2	E_h-pH diagram of the PbS-H_2O system for Case I at T = 298°K and P = 1 atm.	44
Figure 2.3	E_h-pH diagram of the PbS-KEX-H_2O system for Case I at a collector addition of 10^{-6} M KEX, T = 298°K and P = 1 atm.	46
Figure 2.4	E_h-pH diagram of the PbS-KEX-H_2O system for Case I at a collector addition of 10^{-5} M KEX, T = 298°K and P = 1 atm.	48
Figure 2.5	E_h-pH diagram of the PbS-KEX-H_2O system for Case I at a collector addition of 10^{-4} M KEX, T = 298°K and P = 1 atm.	49
Figure 2.6	E_h-pH diagram of the PbS-H_2O system for Case II at T = 298°K and P = 1 atm.	51

Figure 2.7 E_h-pH diagram of the PbS-KEX-H_2O system for Case II at a collector addition of 10^{-7} M KEX, T = 298°K and P = 1 atm. 53

Figure 2.8 E_h-pH diagram of the PbS-KEX-H_2O system for Case II at a collector addition of 10^{-6} M KEX, T = 298°K and P = 1 atm. 55

Figure 2.9 E_h-pH diagram of the PbS-KEX-H_2O system for Case II at a collector addition of 10^{-5} M KEX, T = 298°K and P = 1 atm. 56

Figure 2.10 E_h-pH diagram of the PbS-KEX-H_2O system for Case II at a collector addition of 10^{-4} M KEX, T = 298°K and P = 1 atm. 57

Figure 2.11 E_h-pH diagram of the PbS-H_2O system for Case III at T = 298°K and P = 1 atm. 59

Figure 2.12 E_h-pH diagram of the PbS-KEX-H_2O system for Case III at a collector addition of 10^{-6} M KEX, T = 298°K and P = 1 atm. 61

Figure 2.13 E_h-pH diagram of the PbS-KEX-H_2O system for Case III at a collector addition of 10^{-5} M KEX, T = 298°K and P = 1 atm. 62

Figure 2.14 E_h-pH diagram of the PbS-KEX-H_2O system for Case III at a collector addition of 10^{-4} M KEX, T = 298°K and P = 1 atm. 63

Figure 2.15 Comparison of the effect of E_h at pH 8.0 on the natural floatability of galena (-o-) and the percent distribution (---) of various sulfur-bearing species from the calculations of Case III. The flotation data are reproduced from Guy and Trahar (1984). The solid vertical lines show the upper and lower potential limits of the stability for the indicated phases. 70

Figure 2.16 Comparison of the effect of E_h at pH 8.0 and a 10^{-2} M Na_2S addition on the floatability of galena (-o-) and the calculated percent distribution (---) of various sulfur-bearing species. The flotation data are reproduced from Guy and Trahar (1984). The calculations are based on the assumption that oxidation can proceed as far as the formation of S^o. 73

Figure 2.17 Comparison of the effect of E_h at pH 8.0 and a 10^{-2} M Na_2S addition on the floatability of galena (-o-) and the calculated percent distribution (---) of various sulfur-bearing species. The flotation data are reproduced from Guy and Trahar (1984). The calculations are based on the assumption that oxidation can proceed only as far as the formation of polysulfide. 74

Figure 2.18 E_h-pH diagram showing the regions of minimum lead solubility (---) calculated for Case III in the absence of collecter. The solubility remains constant at a minimum over a range of E_h and pH values in the two shaded regions. 79

Figure 2.19 Effect of E_h on % PbX_2 for Case I and a collector addition of 10^{-6} M KEX. The number next to each curve denotes the pH. 82

Figure 2.20 Effect of E_h on % PbX_2 for Case I and a collector addition of 10^{-5} M KEX. The number next to each curve denotes the pH. 83

Figure 2.21 Effect of E_h on % PbX_2 for Case I and a collector addition of 10^{-4} M KEX. The number next to each curve denotes the pH. 84

Figure 2.22 Effect of E_h on % PbX_2 for Case II and a collector addition of 10^{-7} M KEX. The number next to each curve denotes the pH. 85

Figure 2.23 Effect of E_h on % PbX_2 for Case II and a collector addition of 10^{-6} M KEX. The number next to each curve denotes the pH. 86

Figure 2.24 Effect of E_h on % PbX_2 for Case II and a collector addition of 10^{-5} M KEX. The number next to each curve denotes the pH. 87

Figure 2.25 Effect of E_h on % PbX_2 for Case II and a collector addition of 10^{-4} M KEX. The number next to each curve denotes the pH. 88

Figure 2.26 Effect of E_h on % PbX_2 for Case III and a collector addition of 10^{-6} M KEX. The number next to each curve denotes the pH. 89

Figure 2.27 Effect of E_h on % PbX_2 for Case III and a collector addition of 10^{-5} M KEX. The number next to each curve denotes the pH. 90

Figure 2.28 Effect of E_h on % PbX_2 for Case III and a collector addition of 10^{-4} M KEX. The number next to each curve denotes the pH. 91

Figure 2.29 Comparison of the effect of E_h on the flotation recovery of galena (-o-) and on % PbX_2 (---) calculated for a collector addition of 10^{-5} M KEX and pH 8.0. The flotation data are the results reported by Guy and Trahar (1984) for a collector level of $2x10^{-5}$ M KEX and pH 8.0. The Roman numeral next to each solid curve denotes the case number. 93

Figure 2.30 Effect of E_h on the flotation recovery of galena at a collector addition of $2x10^{-5}$ M KEX and pH 11.0 (from Guy and Trahar, 1984). 98

Figure 2.31 Effect of pH on % PbX_2 for Case I and a collector addition of 10^{-6} M KEX. The number next to each curve denotes the E_h (mv). 100

Figure 2.32 Effect of pH on % PbX_2 for Case I and a collector addition of 10^{-5} M KEX. The number next to each curve denotes the E_h (mv). 101

Figure 2.33 Effect of pH on % PbX_2 for Case I and a collector addition of 10^{-4} M KEX. The number next to each curve denotes the E_h (mv). 102

Figure 2.34 Effect of pH on % PbX_2 for Case II and a collector addition of 10^{-7} M KEX. The number next to each curve denotes the E_h (mv). 103

Figure 2.35 Effect of pH on % PbX_2 for Case II and a collector addition of 10^{-6} M KEX. The number next to each curve denotes the E_h (mv). 104

Figure 2.36 Effect of pH on % PbX_2 for Case II and a collector addition of 10^{-5} M KEX. The number next to each curve denotes the E_h (mv). 105

Figure 2.37 Effect of pH on % PbX_2 for Case II and a collector addition of 10^{-4} M KEX. The number next to each curve denotes the E_h (mv). 106

Figure 2.38 Effect of pH on % PbX_2 for Case III and a collector addition of 10^{-6} M KEX. The number next to each curve denotes the E_h (mv). 107

Figure 2.39 Effect of pH on % PbX_2 for Case III and a collector addition of 10^{-5} M KEX. The number next to each curve denotes the E_h (mv). 108

Figure 2.40 Effect of pH on % PbX_2 for Case III and a collector addition of 10^{-4} M KEX. The number next to each curve denotes the E_h (mv). 109

Figure 2.41 Contour plot showing the effect of E_h and pH on log $[Pb^{+2}]$ for Case I of the PbS-H_2O system. 112

Figure 2.42 Three-dimensional block diagram showing the effect of E_h and pH on log $[Pb^{2+}]$ for Case I of the PbS-H_2O system. 113

Figure 2.43 Contour plot showing the effect of E_h and pH on log $[Pb^{+2}]$ for Case II of the PbS-H_2O system. 114

Figure 2.44 Three-dimensional block diagram showing the effect of E_h and pH on log $[Pb^{2+}]$ for Case II of the PbS-H_2O system. 115

Figure 2.45 Contour plot showing the effect of E_h and pH on log $[Pb^{2+}]$ for Case III of the PbS-H_2O system. 116

Figure 2.46 Three-dimensional block diagram showing the effect of E_h and pH on log $[Pb^{2+}]$ for Case III of the PbS-H_2O system. 117

Figure 2.47 Contour plot showing the effect of E_h and pH on % PbX_2 for Case II and a collector addition of 10^{-5} M KEX. 120

Figure 2.48 Three-dimensional block diagram showing the effect of E_h and pH on % PbX_2 for Case II and a collector addition of 10^{-5} M KEX. 121

Figure 2.49 Contour plot showing the effect of E_h and pH on % PbX_2 for Case III and a collector addition of 10^{-5} M KEX. 122

Figure 2.50 Three-dimensional block diagram showing the effect of E_h and pH on % PbX_2 for Case III and a collector addition of 10^{-5} M KEX. 123

Figure 3.1 Linear sweep voltammograms of a galena electrode immersed in a 0.1 M $Na_2B_4O_7$ solution (pH 9.2) containing 0 M KEX (---) and 9.5×10^{-3} M KEX (—) (from Woods, 1971). 135

Figure 3.2 Electrochemical cell used by Lamache et al. (1984) in their studies on galena particle beds. 137

Figure 3.3 Schematic diagram of the instrumentation used for linear sweep voltammetry. 141

Figure 3.4 (a) Change in the concentration profile of species A which is being oxidized during an anodic scan.
(b) The shape of the voltammogram resulting from the depletion of A from the electrode surface during the anodic scan and of B during the reverse scan. 142

Figure 3.5 Typical response of the electrode potential to the application of short (1 second) on/off current pulses. 145

Figure 3.6 Typical IGP trace obtained after repeatedly applying short on/off current pulses and recording on a slow chart speed. 147

Figure 3.7 Schematic diagram of the instrumentation used for IGP experiments. 150

Figure 3.8 The effect of the anodic limit on the single sweep voltammograms for a galena electrode immersed in a 0.05 M $Na_2B_4O_7$ solution (pH 9.2). No stirring. Scan rate = 20 mv/sec. 153

Figure 3.9 The effect of stirring on the single sweep voltammograms for a galena electrode immersed in a 0.05 M $Na_2B_4O_7$ solution (pH 9.2). Scan rate = 20 mv/sec. 157

Figure 3.10 Cyclic voltammograms of a galena electrode in a 0.05 M $Na_2B_4O_7$ solution (pH 9.2) for potential sweeps between -455 and 345 mv. No stirring. Scan rate = 20 mv/sec. The number next to each curve denotes the cycle number. 173

Figure 3.11 Cyclic voltammograms of a galena electrode in a 0.05 M $Na_2B_4O_7$ solution (pH 9.2) for potential sweeps between -555 and 445 mv. No stirring. Scan rate = 20 mv/sec. The next to the curve denotes the cycle number. 177

Figure 3.12 Effect of lowering the cathodic limit during the cyclic scan of a galena electrode in a 0.05 M $Na_2B_4O_7$ solution (pH 9.2). Anodic limit held at 245 mv. No stirring. Scan rate = 20 mv/sec. 182

Figure 3.13 IGP diagrams obtained after applying current pulses of 0.05 mA/cm^2 to a galena electrode immersed in an unstirred 0.05 M $Na_2B_4O_7$ solution (pH 9.2). Anodic pulses applied initially for 0 (a), 2 (b), 3 (c) and 6 (d) minutes before reversal of current. 185

Figure 3.14 Effect of stirring on IGP diagram obtained by applying a current pulse of 0.05 mA/cm^2 to a galena electrode immersed in a 0.05 M $Na_2B_4O_7$ solution (pH 9.2). 188

Figure 3.15 Effect of stirring on IGP diagram obtained by applying a current pulse of 0.10 mA/cm^2 to a galena electrode immersed in a 0.05 M $Na_2B_4O_7$ solution (pH 9.2). 191

Figure 3.16 IGP diagram obtained after applying a current pulse of 0.5 mA/cm^2 to a galena electrode immersed in a stirred 0.05 M $Na_2B_4O_7$ solution (pH 9.2). 192

Figure 3.17 Current-time curves obtained after applying potential of 45, 145, 245, 345 and 495 mv to a galena electrode immersed in an unstirred 0.05 M $Na_2B_4O_7$ solution (pH 9.2). 195

Figure 3.18 The effect of the anodic limit on the single sweep voltammograms for a galena electrode immersed in a stirred 0.05 M KH_2PO_4/0.05 M Na_2HPO_4 solution (pH 6.8). Scan rate = 20 mv/sec. 197

Figure 3.19 The effect of the anodic limit on the single sweep voltammograms for a galena electrode immersed in an unstirred 0.05 M KH_2PO_4/0.05 M Na_2HPO_4 solution (pH 6.8). Scan rate = 20 mv/sec. 198

Figure 3.20 The effect of stirring on the single sweep voltammograms for a galena electrode immersed in a 0.05 M KH_2PO_4/0.05 M Na_2HPO_4 solution (pH 6.8). Scan rate = 20 mv/sec. 201

Figure 3.21 Cyclic voltammograms of a galena electrode in an unstirred 0.05 M KH_2PO_4/0.05 M Na_2HPO_4 solution (pH 6.8) for potential sweeps between -600 and 345 mv. Scan rate = 20 mv/sec. The number next to each curve denotes the cycle number. 204

Figure 3.22 Cyclic voltammograms of a galena electrode in a stirred 0.05 M KH_2PO_4/0.05 M Na_2HPO_4 solution (pH 6.8) for potential sweeps between -600 and 345 mv. Scan rate = 20 mv/sec. The number next to each curve denotes the cycle number. 205

Figure 3.23 Cyclic voltammograms of a galena electrode in an unstirred 0.05 M KH_2PO_4/0.05 M Na_2HPO_4 solution (pH 6.8) for potential sweeps between -400 and 295 mv. Scan rate = 20 mv/sec. The number next to each curve denotes the cycle number. 208

Figure 3.24 The effect of decreasing the cathodic limit during the cyclic scan of a galena electrode in a stirred 0.05 M KH_2PO_4/0.05 Na_2HPO_4 solution (pH 6.8). Anodic limit held at 345 mv. Scan rate = 20 mv/sec. 209

Figure 3.25 IGP diagrams obtained after applying current pulses of 0.1 mA/cm^2 to a galena electrode immersed in a stirred 0.05 M KH_2PO_4/0.05 M Na_2HPO_4 solution (pH 6.8). Anodic pulses applied initially for 0 (a), 3 (b) and 6 (c) minutes before reversal of current. 211

Figure 3.26 IGP diagrams obtained after applying current pulses of 0.2 mA/cm^2 to a galena electrode immersed in a stirred 0.05 M KH_2PO_4/0.05 M Na_2HPO_4 solution (pH 6.8). Anodic pulses applied initially for 3 (a) and 6 (b) minutes before reversal of current. 214

Figure 3.27 IGP diagrams obtained after applying current pulses of 0.2 mA/cm^2 to a galena electrode immersed in a stirred 0.05 M KH_2PO_4/0.05 M Na_2HPO_4 solution (pH 6.8). Anodic pulses applied initially for 9.5 (a) and 14 (b) minutes before reversal of current. 215

Figure 3.28 Current-time curves obtained after applying potentials of 45, 145, 245 and 295 mv to a galena electrode immersed in an unstirred 0.05 M KH_2PO_4/0.05 M Na_2HPO_4 solution (pH 6.8). 218

Figure 3.29 Current-time curves obtained after applying potentials of 345 and 495 mv to a galena electrode immersed in an unstirred 0.05 M KH_2PO_4/0.05 M Na_2HPO_4 solution (pH 6.8). 219

Figure 3.30 Single sweep voltammograms for a galena electrode immersed in a 0.05 M $Na_2B_4O_7$ solution (pH 9.2) containing 0 (---), 10^{-4} (——) and 10^{-3} (• • •) M KEX. No stirring. Scan rate = 20 mv/sec. 221

Figure 3.31 Effect of scan rate on the single sweep voltammograms for a galena electrode immersed in a 0.05 M $Na_2B_4O_7$ (pH 9.2) + 10^{-3} M KEX solution. No stirring. 223

Figure 3.32 Effect of scan rate on the single sweep voltammograms for a galena electrode immersed in a 0.05 M $Na_2B_4O_7$ (pH 9.2) + 10^{-4} M KEX solution. No stirring. 227

Figure 3.33 Effect of anodic limits between 45 and 295 mv on the single sweep voltammograms for a galena electrode immersed in a 0.05 M $Na_2B_4O_7$ (pH 9.2) + 10^{-3} M KEX solution. No stirring. Scan rate = 20 mv/sec. 230

Figure 3.34 Effect of anodic limits between 345 and 545 mv on the single sweep voltammograms for a galena electrode immersed in a 0.05 M $Na_2B_4O_7$ (pH 9.2) + 10^{-3} M KEX solution. No stirring. Scan rate = 20 mv/sec. 231

Figure 3.35 Effect of anodic limits between 245 and 395 mv on the single sweep voltammograms for a galena electrode immersed in a 0.05 M $Na_2B_4O_7$ (pH 9.2) + 10^{-4} M KEX solution. No stirring. Scan rate = 20 mv/sec. 241

Figure 3.36 Effect of anodic limits between 445 and 545 mv on the single sweep voltammograms for a galena electrode immersed in a 0.05 M $Na_2B_4O_7$ + 10^{-4} M KEX solution. No stirring. Scan rate = 20 mv/sec. 242

Figure 3.37 Cyclic voltammograms of a galena electrode in an unstirred 0.05 M $Na_2B_4O_7$ (pH 9.2) + 10^{-3} M KEX for potential sweeps between -655 and 245 mv. Scan rate = 20 mv/sec. 249

Figure 3.38 IGP diagrams obtained after applying current pulses of 0.02 mA/cm^2 to a galena electrode immersed in an unstirred solution containing 0.05 M $Na_2B_4O_7$ (pH 9.2) + 0 (a), 10^{-4} (b) and 10^{-3} (c) M KEX. 251

Figure 3.39 Single sweep voltammograms for a galena electrode immersed in a 0.05 M KH_2PO_4/0.05 M Na_2HPO_4 (pH 6.8) + 0 (a), 10^{-4} (b) and 10^{-3} (c) M KEX solution. No stirring. Scan rate = 20 mv/sec. 254

Figure 3.40 Effect of scan rate on the single sweep voltammograms for a galena electrode immersed in a 0.05 M KH_2PO_4/0.05 M Na_2HPO_4 (pH 6.8) + 10^{-3} M KEX solution. Scan rate varied from 5 to 25 mv/sec. No stirring. 255

Figure 3.41 Effect of scan rate on the single sweep voltammograms for a galena electrode immersed in a 0.05 M KH_2PO_4/0.05 M Na_2HPO_4 (pH 6.8) + 10^{-3} M KEX solution. Scan rate varied from 30 to 50 mv/sec. No stirring. 256

Figure 3.42 Effect of scan rate on the single sweep voltammograms for a galena electrode immersed in a 0.05 M KH_2PO_4/0.05 M Na_2HPO_4 (pH 6.8) + 10^{-4} M KEX solution. No stirring. 257

Figure 3.43 Effect of anodic limit on the single sweep voltammograms for a galena electrode immersed in a 0.05 M KH_2PO_4/0.05 M Na_2HPO_4 (pH 6.8) + 10^{-3} M KEX solution. No stirring. Scan rate = 20 mv/sec. 261

Figure 3.44 Effect of anodic limit on the single sweep voltammograms for a galena electrode immersed in a 0.05 M KH_2PO_4/0.05 M Na_2HPO_4 (pH 6.8) + 10^{-4} M KEX solution. No stirring. 264

Figure 3.45 IGP diagrams obtained after applying current pulses of 0.1 mA/cm^2 to a galena electrode immersed in an unstirred solution containing 0.05 M KH_2PO_4/0.05 M Na_2HPO_4 (pH 6.8) + 0 (a) and 10^{-3} (b) M KEX. 267

Figure 3.46 IGP diagrams obtained after applying current pulses of 0.2 mA/cm^2 to a galena electrode immersed in a solution containing 0.05 M KH_2PO_4/0.05 M Na_2HPO_4 (pH 6.8) + 10^{-3} M KEX. Anodic pulses applied initially for: (a) 3 minutes while stirred; (b) 6 minutes while stirred; and (c) 6 minutes while unstirred before current reversal. 268

Figure 3.47 Current-time curves obtained after applying potentials of 45, 145, 245, 295, and 345 mv to a galena electrode immersed in a 0.05 M KH_2PO_4/0.05 M Na_2HPO_4 (pH 6.8) + 10^{-3} M KEX solution. No stirring. 271

Figure 3.48 Current-time curves obtained after applying potentials of 45, 145, 245, and 345 mv to a galena electrode immersed in a 0.05 M $Na_2B_4O_7$ (pH 9.2) + 10^{-3} M KEX solution. No stirring. 272

Figure 3.49 Effect of E_h on the galena recovery obtained after 1 minute of microflotation in a 0.05 M $Na_2B_4O_7$ solution (pH 9.2). 274

Figure 3.50 Comparison of the effect of E_h on the microflotation recovery of galena (-o-) and on the calculated % PbX_2 (——) at a collector addition of 10^{-5} M KEX and pH 9.2. The Roman numeral next to each curve for % PbX_2 denotes the case number. 276

Figure 4.1 Current-time curves for the initial stages of oxidation after applying potentials of 545, 645, 945, 1045, and 1245 mv to a galena electrode immersed in a 0.1 M $HClO_4$ solution (pH 1.1). Solution stirred. 289

Figure 4.2 Current-time curves obtained over a longer duration applying potentials of 545, 645, 945, 1045 and 1245 mv to a galena electrode immersed in a 0.1 M $HClO_4$ solution (pH 1.1). 290

Figure 4.3 The effect of stirring and of extending the anodic limit from 545 to 645 mv on the single sweep voltammograms for a galena electrode in a 0.1 M $HClO_4$ solution (pH 1.1). Scan rate = 20 mv/sec. 294

Figure 4.4 Voltammogram obtained for a rotating galena disc electrode in a solution of pH 1 (reproduced from Nicol et al., 1978). 298

Figure 4.5 Effect of extending the anodic limit from 345 to 745 mv on the voltammograms for a galena electrode immersed in a 0.1 M $HClO_4$ solution (pH 1.1). No stirring. Scan rate = 20 mv/ sec. 300

Figure 4.6 Single sweep voltammogram for a galena electrode in an unstirred 0.1 M $HClO_4$ solution (pH 1.1) after scanning between -800 and 1245 mv. Scan rate = 20 mv/sec. 302

Figure 4.7 Single sweep voltammogram for a galena electrode in a stirred 0.1 M $HClO_4$ solution (pH 1.1) after scanning between -800 and 1245 mv. Scan rate = 20 mv/sec. 303

Figure 4.8 Effect of stirring on the voltammogram for a galena electrode in a 0.1 M $HClO_4$ solution (pH 1.1) after holding its potential at -755 mv for 5 minutes. 306

Figure 4.9 Effect of anodic limit on the voltammogram for a galena electrode in a 0.1 M $HClO_4$ solution (pH 1.1) after holding its potential at -755 mv for 5 minutes. No stirring. Scan rate = 20 mv/sec. 309

Figure 4.10 IGP diagrams obtained after applying current pulses of 3.9 mA/cm^2 to a galena electrode immersed in an unstirred (a) and stirred (b) 0.1 M $HClO_4$ solution (pH 1.1). 311

Figure 4.11 IGP diagrams obtained after applying current pulses of 3.9 mA/cm^2 to a galena electrode immersed in an unstirred 0.1 M $HClO_4$ solution (pH 1.1). The difference in the two cases is that after initial anodic pulses (7 minutes), (a) cathodic polarization maintained long enough to remove all oxidation products and (b) cathodic polarization terminated before all oxidation products removed. 314

Figure 4.12 IGP diagrams obtained after applying current pulses of 3.9 mA/cm^2 to a galena electrode immersed in a stirred 0.1 M $HClO_4$ solution (pH 1.1). The difference in the two cases is that after initial anodic pulses (7 minutes), (a) cathodic polarization maintained long enough to remove all oxidation products and (b) cathodic polarization terminated before all oxidation products removed. 315

Figure 4.13 Effect of stirring on the single sweep voltammograms for a galena electrode immersed in a 0.5 M CH_3COOH/0.5 M CH_3COONa solution (pH 4.6). Potential scan between -755 and 645 mv. Scan rate = 20 mv/sec. 320

Figure 4.14 Effect of stirring on the cathodic portion of the single sweep voltammograms for a galena electrode immersed in a 0.5 M CH_3COOH/0.5 M CH_3COONa solution (pH 4.6). Potential scan between -625 and 545 mv. Scan rate = 20 mv/sec. 324

Figure 4.15 Effect of the anodic limit on the single sweep voltammograms for a galena electrode immersed in a stirred 0.5 M CH_3COOH/0.5 M CH_3COONa solution (pH 4.6). Scan rate = 20 mv/sec. 326

Figure 4.16 Effect of scan rate on the single sweep voltammograms for a galena electrode immersed in a stirred 0.5 M CH_3COOH/0.5 M CH_3COONa solution (pH 4.6). 328

Figure 4.17 Effect of anodic limit on the single sweep voltammograms for a galena electrode immersed in an unstirred 0.5 M CH_3COOH/0.5 M CH_3COONa solution (pH 4.6) + 10^{-3} M Pb^{2+} solution. Scan rate = 20 mv/sec. 332

Figure 4.18 Effect of anodic limit on the single sweep voltammograms for a galena electrode immersed in a stirred 0.5 M CH_3COOH/0.5 M CH_3COONa solution (pH 4.6) + 10^{-3} M Pb^{2+} solution. Scan rate = 20 mv/sec. 333

Figure 4.19 Effect of Pb^{2+} ion addition on the cathodic portion of the single sweep voltammograms for a galena electrode immersed in a stirred 0.5 M CH_3COOH/0.5 M CH_3COONa solution (pH 4.6) solution. Scan rate = 20 mv/sec. 338

Figure 4.20 Effect of anodic limit and stirring on the single sweep voltammograms for a galena electrode immersed in a 0.5 M CH_3COOH/0.5 M CH_3COONa (pH 4.6) + 10^{-3} M Pb^{2+} solution. Scan rate = 20 mv/sec. 339

Figure 4.21 Relation between the open-circuit potential and dissolved lead concentration obtained for a galena electrode immersed in a stirred 1 M $HClO_4$ solution (pH 0.0). Experimental data (o) reproduced from Brodie (1969). Calculated curve (——) determined from the computations of this study. 342

Figure 4.22 Relation between the open-circuit potential and dissolved lead concentration obtained for a galena electrode immersed in a stirred 0.1 M $HClO_4$ solution (pH 1.1). Cell contents either closed (▲) or open (o) to atmosphere during experiments. Roman numeral next to each solid curve denotes the case number of the corresponding calculations. 347

Figure 4.23 Experimental relation between the open-circuit potential and dissolved lead concentration obtained for a galena electrode immersed in a stirred 0.5 M CH_3COOH/0.5 M CH_3COONa solution (pH 4.6). Cell contents either closed (▲) or open (o) to atmosphere during experiments. 350

Figure 5.1 Plot of 1/i versus time for the chronoamperometry data obtained for the galena electrode in an unstirred 0.05 M $Na_2B_4O_7$ solution (pH 9.2). 362

Figure 5.2 Possible arrangement of oxygen on the lead surface after oxidation: (a) Regular array in which oxygens are on the same side of the interface; (b) Alternating array after some oxygens have exchanged places with lead cations. 367

Figure 5.3 Plot of 1/i versus time for the chronoamperometry data obtained for the galena electrode in an unstirred 0.05 M KH_2PO_4/0.05 M Na_2HPO_4 solution (pH 6.8). 372

Figure 5.4 Plot of 1/i versus time for the chronoamperometry data obtained for the galena electrode immersed in unstirred 0.05 M $Na_2B_4O_7$ (pH 9.2) + 10^{-3} M KEX and unstirred 0.05 M KH_2PO_4/0.05 M Na_2HPO_4 (pH 6.8) + 10^{-3} M KEX solutions. 376

Figure 5.5 Competition of X^- and OH^- anions for the galena surface during oxidation: (a) Total oxide layer when little or no xanthate is added. (b) Mixed oxide-xanthate surface when intermediate concentrations of xanthate are added. (c) Total xanthate surface when high concentrations of xanthate are added. 381

Figure 5.6 Schematic diagrams showing two types of nucleation and growth: (a) Side and plan view of two-dimensional pits growing in a plane parallel to the electrode surface; (b) Side view of a three-dimensional pit with the geometry of a right circular cone growing across and into the electrode surface. 393

Figure 5.7 Theoretical current-time transients for two-dimensional instantaneous nucleation and growth according to Eq. [5.26] (a); two-dimensional progressive nucleation and growth according to Eq. [5.27] (b); and successive layer-by-layer growth of two-dimensional centers for progressive nucleation (Armstrong and Harrison, 1969) (c). 395

Figure 5.8 Theoretical current-time curve for three-dimensional nucleation and growth of right circular cones according to Eq. [5.29] (Armstrong et al., 1966). 397

LIST OF TABLES

		page
Table 2.1	Standard Free Energy Data Used in this Study ($T = 298.15^{o}K$; $P = 1$ atm)	30
Table 2.2	Reactions Considered in this Study and the Corresponding Equilibrium Data ($T = 298.15^{o}K$; $P = 1$ atm)	31
Table 3.1	Possible Reaction Sequences in the Galena-Water System at pH 9.2	160
Table 3.2	Charge Ratios Q_{C1}/Q_{A1} and Q_{C2}/Q_{A1} from the Single Sweep Scans as a Function of Anodic Limit	165
Table 3.3	Molar Ratios $S_2O_3^{2-}/S^o$ Resulting from the Oxidation of Galena During Single Sweep Scans to Different Anodic Limits	169
Table 3.4	Charge Ratios Q_{C1}/Q_{A1} and Q_{CT}/Q_{A1} Obtained During Cyclic Scans Between -455 and 345 mv	175
Table 3.5	Molar Ratios $n_{S_2O_3^{2-}}/n_{S^o}$ and $(n_{PbO})_A/(n_{PbO})_C$ Obtained During Cyclic Scans Between -555 and 445 mv	180
Table 3.6	Effect of Scan Rate on the Charge Density of the Anodic Pre-Wave at pH 9.2 and 10^{-3} M KEX	224
Table 3.7	Effect of Scan Rate on the Charge Density of the Anodic Pre-Wave at pH 9.2 and 10^{-4} M KEX	228
Table 3.8	Charge Ratios Q_{CT}/Q_{A1} Obtained from the Voltammograms for 10^{-3} M KEX at pH 9.2	233
Table 3.9	Charge Ratios Q_{C1}/Q_{A1} Obtained as a Function of Anodic Limit for 10^{-4} M KEX and pH 9.2	244
Table 3.10	Molar Ratios $n_{S_2O_3^{2-}}/n_{S^o}$ Obtained During Oxidation at 10^{-4} M KEX and pH 9.2	246
Table 3.11	Effect of Scan Rate on the Charge Density of the Anodic Pre-Wave at pH 6.8 and 10^{-3} M KEX	259

Table 4.1 Measured Q/M Ratios for a Galena Electrode Held at Different Potentials at pH 1.1 291

Table 4.2 The Effect of Scan Rate on the Anodic and Cathodic Charges at pH 4.6 329

Table 4.3 Dissolved Lead Concentration as a Function of Rest Potential at pH 4.6 351

Table 5.1 Fit of Chronoamperometry Data for Galena Oxidation at pH 9.2 According to an Equation of the Form $1/i = mt + b$ 363

Table 5.2 Fit of Chronoamperometry Data for Galena Oxidation at pH 6.8 According to an Equation of the Form $1/i = mt + b$ 373

Table 5.3 Fit of Chronoamperometry Data for Xanthate Adsorption at pH 9.2 and 6.8 According to an Equation of the Form $1/i = mt + b$ 377

CHAPTER I.

INTRODUCTION

1.1 General

The processing of sulfide ores is, in general, extremely complicated and includes many stages between the time the ore is mined and the final metal is produced. Two of the steps that have been the focus of a great deal of attention over the years are flotation and leaching. Because of the great differences in the objectives and nature of these two processes, mineral scientists and engineers have, for the most part, studied them separately.

Sulfide ores typically contain only a few percent by weight of the desired metal(s) and, consequently, it is necessary to physically remove the undesired minerals prior to chemical processing. This involves finely grinding the ore in order to liberate the various minerals from each other and then separating them, almost always by flotation.

Flotation is a physicochemical process whereby certain mineral particles in a slurry attach themselves to rising air bubbles. Since sulfides are not strongly hydrophobic, chemical reagents called collectors are added to the pulp in order to selectively adsorb onto the desired minerals and enhance their affinity for the bubbles. The floated mineral concentrate is collected in the froth layer at the top of the slurry and then sent for chemical treatment.

Chemical extraction may follow several different routes depending upon technical and economic factors. One possibility is to pyrometallurgically reduce the sulfide to a metal, and then to purify it in a series of refining processes. A second alternative is to convert the sulfide to an oxide by roasting and then to leach out the metal, usually in an acidic aqueous solution. A third route involves use of the direct leach of the metal from the sulfide concentrate and subsequent purification. It is the type of leaching in this last approach which is most relevant to the present study.

There are obvious differences between flotation and leaching of sulfides. The aim of the first process is to produce a hydrophobic film on the mineral, which usually requires moderately alkaline and oxidizing conditions for optimum results. The purpose of the second is to dissolve out metal from throughout the mineral particle. In most cases, a low pH and a highly oxidizing environment achieve this most effectively.

Despite this, the two processes do have several things in common. Many of the controlling reactions in either case are electrochemical in nature and, consequently, can be studied using similar experimental techniques. Furthermore, both are oxidation processes and result in the formation of product layers on the mineral surface, which can have a significant effect on further reaction.

Because of these similarities, there should be a great deal in common between the descriptions of flotation and leaching of sulfides. From this point of view, the two should not necessarily be treated as

separate disciplines.

1.2 Scope of the Work

This dissertation will be divided into six chapters. The remainder of Chapter I will serve as a general introduction to the main body of the work and will contain a discussion of the current trends in sulfide research and of the objectives of this study.

The next three chapters will be devoted to a description and discussion of the research itself. The topics to be covered are:

Chapter II - thermodynamic calculations for the galena-water-ethyl xanthate system;

Chapter III - electrochemical experiments on the galena-water-ethyl xanthate system at pH 9.2 and 6.8;

Chapter IV - electrochemical experiments on the galena-water system at pH 1.1 and 4.6.

Since the topics are somewhat independent of each other, the chapters will be written with self-contained formats. Each will have its own Introduction, Experimental and Results and Discussion sections. Because comparing the results of the thermodynamic calculations to the observed behavior is one of the major themes of this research, there will be repeated references throughout Chapters III and IV to the results obtained in Chapter II.

Chapter V will include a discussion of the possible mechanisms of galena oxidation and xanthate adsorption. In Chapter VI, the relation

between the results of Chapters II, III and IV will be dealt with more comprehensively. Included will be some discussion of why galena chemistry follows thermodynamic behavior in some instances but not in others. This final chapter will also contain a summary of the major findings of this research and recommendations for future work.

1.3 Current Trends in Electrochemical Research on the Solution and Flotation Chemistry of Sulfides

The interactions between galena (PbS) and water and between galena and aqueous solutions of the flotation collector, potassium ethyl xanthate (KEX, which has the formula $CH_3CH_2OCS_2K$), have been of extreme importance to researchers from both a practical and a fundamental viewpoint. Although galena has probably been the most extensively studied sulfide mineral, many questions still exist concerning various aspects of its solution and flotation chemistry.

Much of the early work done involved subjecting galena to various aqueous environments and analyzing the reaction products using wet chemical and spectroscopic techniques. Because most base-metal sulfides, including galena, are semiconductors and can support and/or participate in reactions that involve the transfer of electrons, the direction of research in recent years has swung overwhelmingly toward viewing sulfide oxidation and xanthate adsorption reactions as electrochemical in nature. In fact, the biggest disagreements between researchers currently center not around whether electron transfer reactions are involved, but what the products of these reactions are.

Two theories that have been very successful in explaining adsorption of xanthate onto sulfides are the mixed potential model and the semiconductor-adsorption model. The former focuses on the solution side of the solid/liquid interface and assumes that the surface potential is determined by anodic and cathodic reactions occurring there. The latter takes the view that the potential drop across the space charge layer in the solid controls the adsorption of xanthate. The scope of this study is restricted to a study of the chemistry pertaining to the solution side of the solid/liquid interface. What follows is a brief description of the mixed potential model, as it is viewed today.

When a semiconducting sulfide, such as galena, is immersed in water, both anodic and cathodic reactions occur on its surface. Since the mineral is not connected to any external circuit to act as a source or sink for excess electrons, its potential will adjust itself to a value where the anodic and cathodic rates are equal. This is termed the open-circuit or rest potential, which is shown schematically is Figure 1.1. If the cathodic reaction is just the reverse of the anodic one, then the system is in thermodynamic equilibrium and the open-circuit potential will be the same as the Nernst potential of the redox couple. If, however, the reactions are not simply the reverse of each other, then the system is not at thermodynamic equilibrium. It will come to rest at the mixed potential, which is not a thermodynamic quantity and which lies somewhere between the reversible potentials of the separate anodic and cathodic reactions.

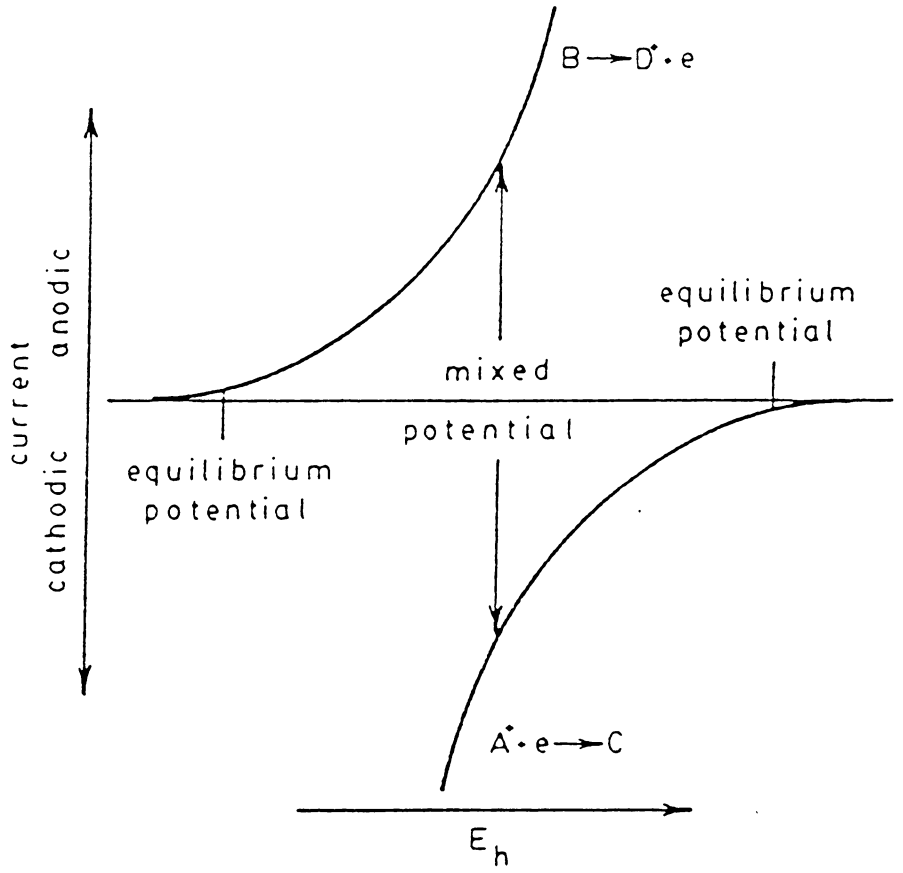


Figure 1.1 The establishment of a mixed potential between separate anodic and cathodic reactions.

The presence of oxygen determines the mechanism of both the oxidation of sulfides and the adsorption of xanthate. When there is a sufficient quantity of dissolved oxygen, the reduction of oxygen readily occurs on most sulfide surfaces whether xanthate is present or not. The mixed potential theory will then apply to this situation.

At the conditions typical of sulfide flotation (i.e., moderately alkaline pH), the cathodic reaction is:

$$1/2\ O_2 + H_2O + 2e \longrightarrow 2OH^-. \qquad [1.1]$$

Whereas there is unanimity among most researchers concerning this reduction reaction, agreement over the identity of the anodic reaction on galena has been quite a different matter. In the absence of xanthate, alternatives include:

$$PbS + H_2O \longrightarrow PbO + S^o + 2H^+ + 2e, \qquad [1.2]$$

$$2PbS + 5H_2O \longrightarrow 2PbO + S_2O_3^{2-} + 10H^+ + 8e, \qquad [1.3]$$

$$PbS + 5H_2O \longrightarrow PbO + SO_4^{2-} + 10H^+ + 8e. \qquad [1.4]$$

Although reaction [1.4] is thermodynamically favored, sulfide oxidation can be sluggish and evidence to support the occurrence of the other two has been reported (Gardner and Woods, 1979b).

Several possibilities have been envisaged for the oxidation of xanthate. Firstly, it can involve the chemisorption of xanthate via the process:

$$X^- \longrightarrow X_{ads} + e, \qquad [1.5]$$

where X^- represents a xanthate ion. Secondly, xanthate can be oxidized to dixanthogen, X_2, according to:

$$2X^- \longrightarrow X_2 + 2e. \qquad [1.6]$$

In both cases, the mineral acts as an electrocatalyst for the anodic and cathodic reactions. However, galena can also be directly involved in the oxidation via a reaction in which lead ethyl xanthate is formed. As in the case of oxidation in the absence of xanthate, three possibilities have been considered:

$$PbS + 2X^- \longrightarrow 2PbX_2 + S^o + 2e, \qquad [1.7]$$

$$2PbS + 4X^- + 3H_2O \longrightarrow 2PbX_2 + S_2O_3^{2-} + 6H^+ + 8e, \qquad [1.8]$$

$$PbS + 2X^- + 4H_2O \longrightarrow PbX_2 + SO_4^{2-} + 8H^+ + 8e. \qquad [1.9]$$

These are somewhat analogous to reactions [1.2], [1.3] and [1.4]. Galena is rendered floatable by any of these routes because X_{ads}, X_2 and PbX_2 can each make the surface hydrophobic.

As the solution is deoxygenated, the rate of the oxygen reduction will slow down and the rest potential will approach the Nernst potential of the anodic reaction. This is shown schematically in Figure 1.2. When the solution is sufficiently deoxygenated, the reverse of the anodic reaction will become the predominant cathodic reaction and equilibrium will be reached when the circuit is opened.

The first idea that a mixed potential mechanism could apply to sulfide flotation originated with Salamy and Nixon (1953). It has proven to be very successful since it can explain the numerous

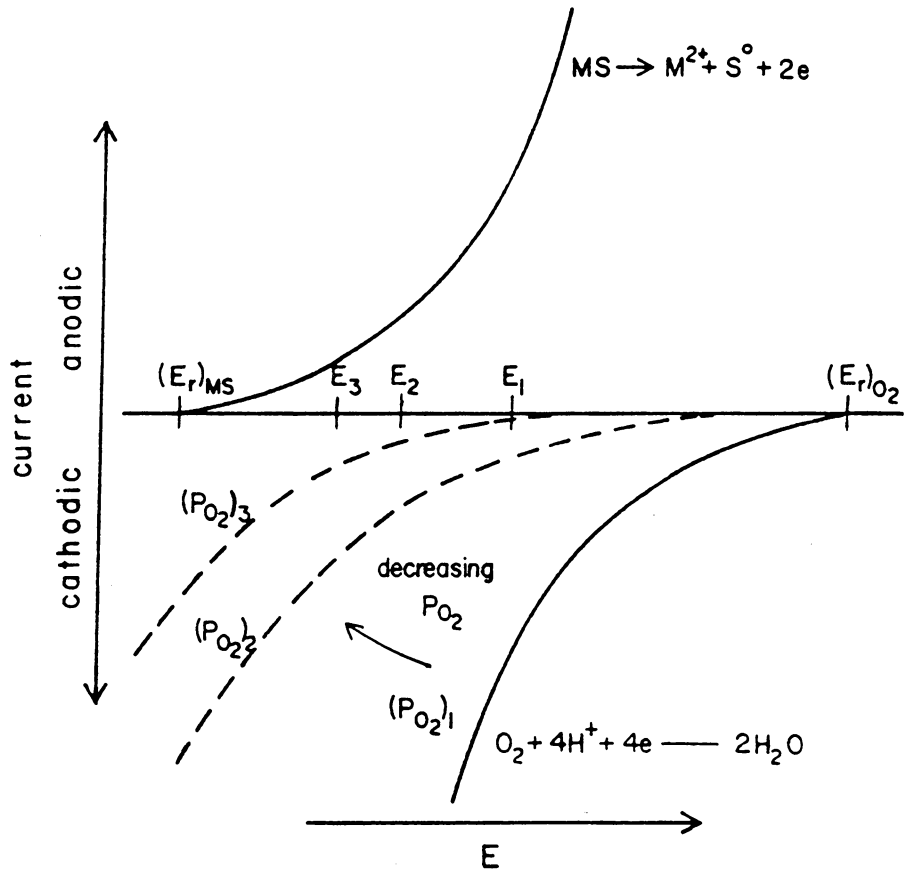


Figure 1.2 Schematic diagram showing the effect of oxygen partial pressure on the mixed potential for the aqueous oxidation of a sulfide.

observations that the presence of oxygen not only enhances xanthate adsorption but also that it is required for it to occur to any appreciable extent (Plaksin and Bessonov, 1957; Poling and Leja, 1963; Tolun and Kitchener, 1964; Gaudin and Finkelstein, 1965; Finkelstein, 1970, to name a few). An increase in the oxygen content will increase the rate of oxygen reduction (reaction [1.1]). This forces the anodic reactions to speed up in order to supply the additional electrons for oxygen reduction.

Another strength of the mixed potential theory is that it embodies many of the earlier flotation theories (Taggart et al., 1934; Cook and Nixon, 1950; Sutherland and Wark, 1955; Gaudin, 1957). For example, Taggart et al. (1934) observed a near-stoichiometric balance between the amount of xanthate adsorbed onto galena and the amount of sulfate, thionate, thiosulfate and carbonate ions released into the solution, and proposed an ion-exchange type of mechanism, e.g.,

$$PbSO_4 + 2X^- \longrightarrow PbX_2 + SO_4^{2-}. \qquad [1.10]$$

Although this reaction itself is not an electrochemical reaction, the oxidation of the galena to produce $PbSO_4$ on the surface that occurred prior to the contact with xanthate can be viewed as an electrochemical reaction, i.e.;

$$PbS + 4H_2O \longrightarrow PbSO_4 + 8H^+ + 8e. \qquad [1.11]$$

Thus, the combination of reactions [1.10] and [1.11] would yield the anodic adsorption reaction [1.9].

The most common approach that has been taken among researchers studying sulfides is to compare an observed rest potential, or the potential on a voltammogram at which a faradaic process begins, with equilibrium potentials for different possible reactions that have been calculated from thermodynamic data (e.g., Allison et al., 1972). Whether the system is at equilibrium or not, the rest potential must be greater than or equal to the reversible potential for the anodic process taking place. Likewise, it must be less than or equal to that for the cathodic reaction. These criteria can be used to eliminate certain reactions from consideration.

However, when dealing with surface reactions, caution should be exercised in using thermodynamics for two reasons. Firstly, many of the reactions involving sulfides proceed very slowly and do not reach equilibrium in a time frame relevant to flotation and most laboratory experiments. In addition, reactions that do reach equilibrium may not be the thermodynamically most favored ones. Secondly, the reversible potentials are calculated from thermodynamic data for bulk phases, which may be significantly different from that for the formation of submonolayers of a surface species on a pre-existing surface (Woods, 1984). Therefore, thermodynamics alone cannot be relied upon to describe the solution and flotation chemistry of sulfides.

With all the emphasis on the electrochemistry of sulfides, it is not surprising that the electrode potential (E_h) has become one of the most often studied variables in flotation. Although some time has elapsed since the first reports of potential measurements in industrial

flotation circuits were made (Woodcock and Jones, 1970a, 1970b; Leonov and Badenikov, 1973; Natarajan and Iwasaki, 1973), there has recently been an upsurge in interest in using E_h measurements to monitor or control flotation (Heyes and Trahar, 1979; Castro and Larrondo, 1981; Agar et al., 1982; Woods, 1984; Trahar, 1983a; Rand and Woods, 1984). Woods (1984) has pointed out, however, that a considerable amount of further research is needed in order to determine the effect of potential on flotation in the various recycle streams in a circuit before it can be used for control purposes.

Numerous investigations have been conducted that are more concerned with the fundamental aspects of the effect of potential; in fact, it is becoming increasingly rare to find an article on sulfide flotation that does not deal with the electrode potential. Some of these include the work of Heyes and Trahar (1984), Guy and Trahar (1984) and Walker et al. (1984a) on the flotation of chalcopyrite ($CuFeS_2$), galena, chalcocite (Cu_2S), pyrite (FeS_2) and pyrrhotite (FeS) in the absence of collectors. Similar studies on systems containing xanthate have been reported by Gardner and Woods (1973), Heyes and Trahar (1977), Trahar (1983a), Guy and Trahar (1984), Richardson et al. (1984), and Adam and Iwasaki (1984).

In virtually all of the early work and in most of the work being done presently, mineral electrodes have been made by cutting a pure specimen, which is then attached to a wire lead and mounted in epoxy resin, as shown in Figure 1.3. The electric circuit used in most experiments consists of the mineral electrode (working electrode), a

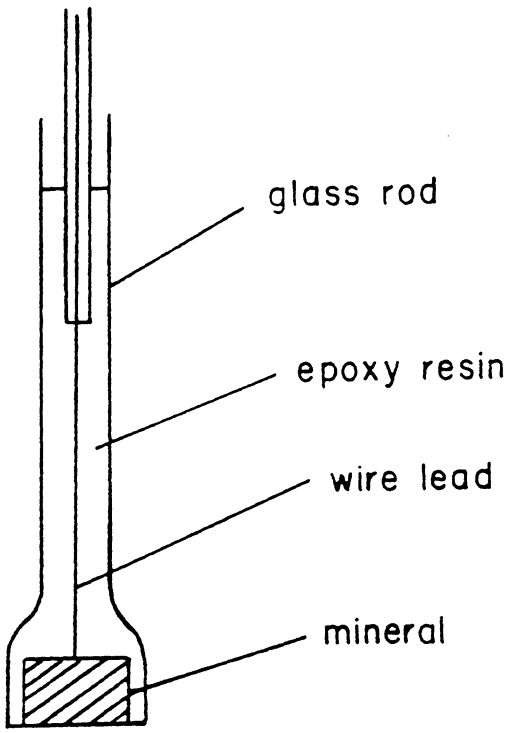
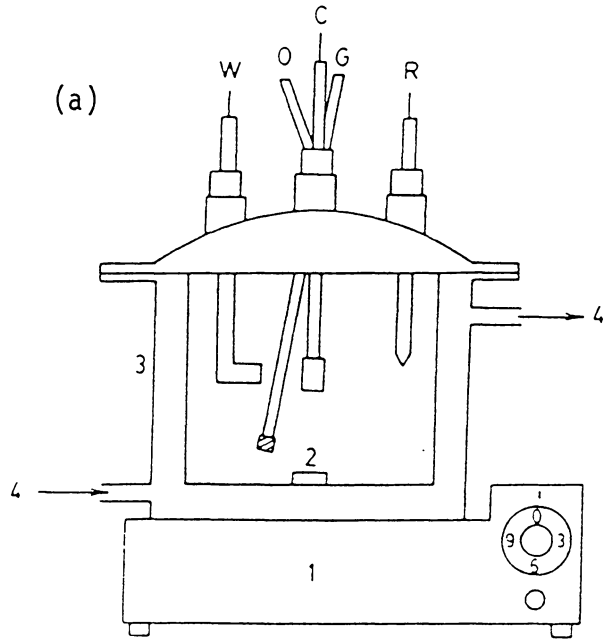


Figure 1.3 Typical electrode used for the electrochemical studies of conducting minerals.

reference electrode (typically a saturated calomel electrode) and a counter electrode (a large surface area conductor such as a platinum foil) immersed in an electrolytic solution and connected to a potentiostat or galvanostat (Figure 1.4). When operating the system potentiostatically, a voltage is applied across the working and reference electrodes. At an appropriate potential, a faradaic reaction at the mineral surface will begin and a current will flow. It is desirable that none of this current passes between the working and the reference electrode since this will alter the applied voltage. Consequently, the measured current is made to flow to the counter electrode by placing a high impedance between the working and the reference electrode.

Employing such a working electrode has several advantages. Proper electrical contact between the mineral and the potentiostat is assured by directly attaching a wire between them. Also, consecutive experiments with the same working electrode can be very conveniently done by polishing the mineral surface after a test run and immersing it again in the solution. However, there are certain disadvantages with this set-up. The surface area of the exposed mineral surface (typically 0.5-1.0 cm^2) is very small compared to the volume of the solution. Then, not only will there be a relatively low current signal, but it will not be possible to detect changes in the concentration of any soluble species. This makes it impossible to directly study the effect of potential on flotation recovery or collector adsorption when the mineral is in this form. Furthermore, because only single mineral



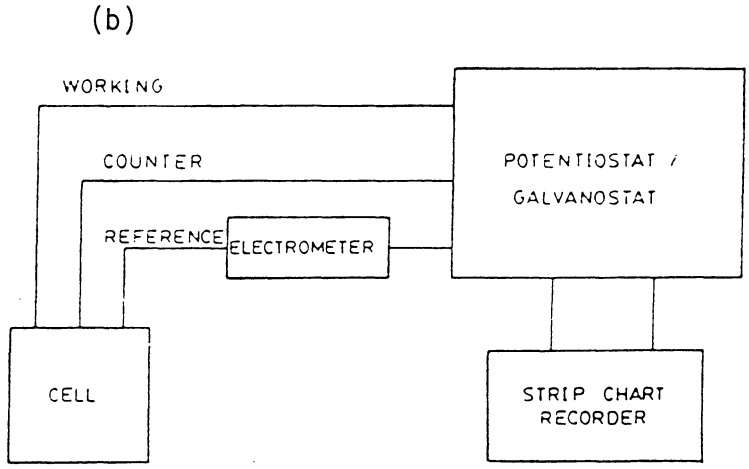


Figure 1.4 (a) Electrochemical cell set-up for a three-electrode system.
(b) Schematic diagram showing the electric connections used for three-electrode potentiostatic experiments.

systems can be studied at one time, galvanic interactions between different minerals and competition between different minerals for the collector cannot be directly investigated. These phenomena can have tremendous effects on the behavior of industrial flotation circuits.

A serious criticism that has been leveled against the electrochemical research on sulfides is that the collector concentrations used (often in the range of 10^{-3} to 10^{-2} M xanthate) are usually much higher than those in a typical flotation circuit (10^{-5} to 10^{-4} M). Researchers have had to resort to such high collector levels in order to detect evidence for electrosorption because of the low mineral surface area and because xanthate adsorption and mineral oxidation often occur at similar potentials.

In order to overcome some of these difficulties, researchers have begun to use ground minerals in their electrochemical experiments. Two approaches have been used. In one, an indicator electrode (usually platinum) and a reference electrode, immersed in a suspension containing the minerals, measure the open-circuit potential. The potential is varied by adding various amounts of oxidizing or reducing agents. Once the mineral is conditioned, flotation or adsorption tests can easily be done. In the second method, the mineral particles are packed in a bed and the electrolyte is pumped through it. A three-electrode system is used, which involves placing a platinum wire working electrode and a Luggin capillary connected to the reference electrode in the particle bed and immersing the counter electrode somewhere in the solution (Figure 1.5). As long as there is good wire-to-particle and particle-

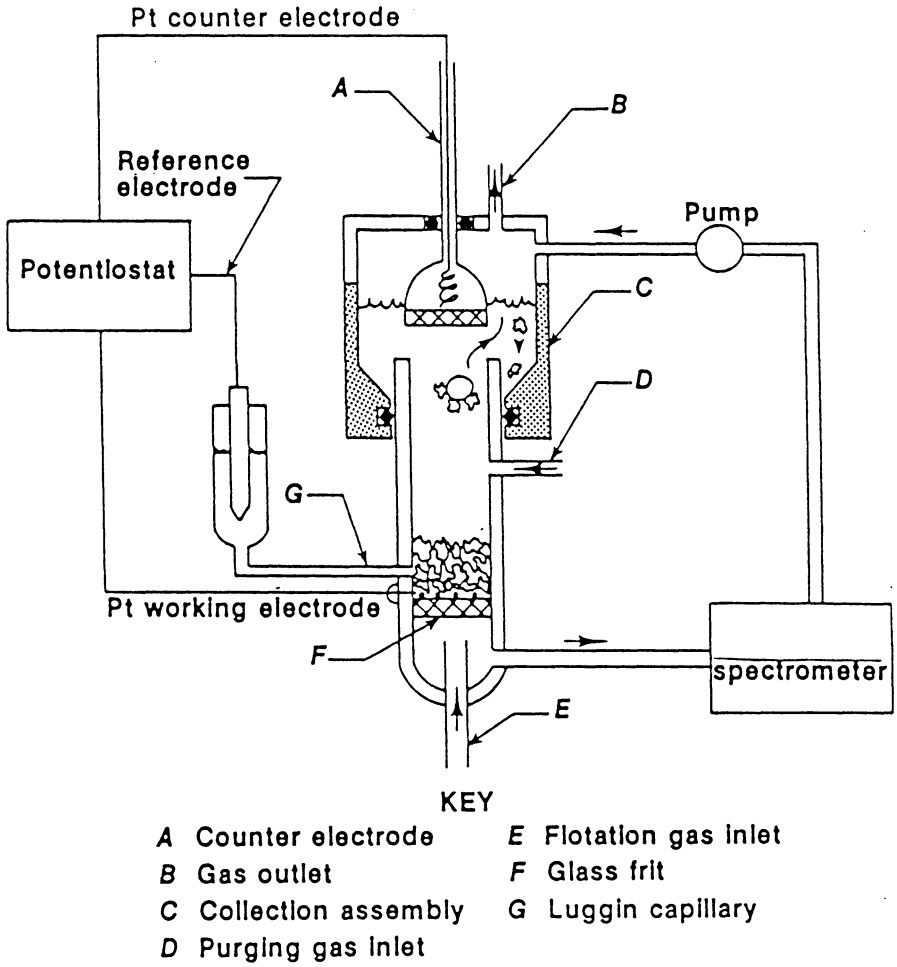


Figure 1.5 Schematic diagram of the particle-bed electrode set-up used by Richardson and co-workers (Walker et al., 1984a,b; Richardson et al., 1984).

to-particle contact, different potentials can be applied to the bed from a potentiostat.

The first method is very convenient to use and has been used in flotation plants (Woodcock and Jones, 1970a,b; Natarajan and Iwasaki, 1973; Rand and Woods, 1984), in laboratory-scale batch flotation tests on actual ores (Heyes and Trahar, 1979, 1984; Luttrell and Yoon, 1984; Guy and Trahar, 1984), and in microflotation tests on pure single-mineral systems (Luttrell and Yoon, 1982). Extreme caution should be taken, however, in interpreting the meaning of the potential measurements. The recorded values are determined by the dominant anodic and cathodic reactions at the indicator electrode. If the nature of the reactions or the kinetics of the reactions occurring on the mineral are different from that on the indicator, then the actual potential on the mineral surface may not be the same as that measured. Furthermore, Rand and Woods (1984) have found that the measured potential can vary depending on the material used as the indicator electrode, the roughness of the electrode surface, the amount of stirring and the pulp density.

In many cases, the reaction involving the oxidizing or reducing agent that is present dominates what occurs on the particle surfaces and on the indicator electrode. Therefore, changes at the mineral/solution interface will likely be reflected by changes in the monitored potentials. Although the ideal choice is to use the same mineral for the indicator electrode as is being floated, the surface of such an electrode may be altered during the course of a measurement (e.g., it may be oxidized) so that it can no longer respond to changes in the

solution.

The use of a packed-bed offers several advantages:

i) the potential can be controlled in either a closed- or open-circuit manner,

ii) better control of the mineral potential is usually possible,

iii) chemical reagents are not needed to vary the potential, and

iv) electrochemical experiments, e.g., voltammetry and chronoamperometry, can be conducted simultaneously with flotation and adsorption tests.

At the same time, however, there are some drawbacks associated with the packed-bed:

i) experimentation tends to be more cumbersome and time-consuming than with the other method,

ii) even if the particles are tightly packed, a considerable electrical resistance can still exist across the bed,

iii) control of the bed potential is usually lost when flotation is begun, and

iv) if reagent is introduced into the cell after the solution has already been flowing, it circulates and comes into contact with the bed by plug-flow.

If there is high enough resistance across the bed, not only can the potential of the particles be appreciably different from what is applied, but potential gradients in the bed will also occur. The

difficulty in achieving potential control depends on the type of mineral (e.g., experience in this laboratory has shown that galena seems to cause more problems than other sulfides), the size of the particles in the bed and how tightly the bed is packed.

The most notable proponents of the packed-bed electrode have been Richardson and his co-workers (Walker et al., 1984a,b; Richardson et al., 1984; O'Dell et al., 1984). Using their flow-through cell in conjunction with a rapid-scan UV spectrophotometer, they have been able to look at the effect of potential on mineral dissolution, xanthate adsorption and flotation for several sulfide systems. Navarro and Gutierrez (1980a,b) also used a three-electrode system, although somewhat different from that of Richardson, to study the electrochemistry and flotation of a bed of galena particles.

1.4 **Objectives of This Study**

As mentioned previously, researchers have investigated the solution and flotation chemistry of galena both from thermodynamic and kinetic viewpoints. Although thermodynamics has been very useful in numerous cases, it has not been in many other instances. Consequently, some debate has arisen over how much it should be used in describing the aqueous chemistry of galena (and other sulfides) in general.

One of the main objectives of this study will be to examine this question more closely. The approach will be from several different angles, all of which will concentrate on the electrochemical aspects of the galena system. The first phase of the work will center around an

extensive set of thermodynamic calculations over the entire E_h and pH region. In the second phase, electrochemical experiments will be conducted on a galena electrode at four different pH values between 1.1 and 9.2. Some of the predictions based on these calculations will be compared to data from these experiments and from the literature in order to determine what aspects of the behavior of this system are controlled by thermodynamics.

Another aim of these calculations is to more fully extend the application of thermodynamics to the study of mineral-water systems. In the previous work of this kind, mass balance considerations were incorporated with the thermodynamics, but these were restricted only to the solution part of the system. Solid phases were not included in the mass balances and only the concentrations of the soluble species were assumed to have finite values. The approach taken in the present study is, however, to include the entire system, both solid and aqueous phases, in the mass balance calculations. Consequently, only the initial quantity of mineral and any reagents added to the solution must be known.

Although the resulting calculations are somewhat more complicated than the previous ones, they yield detailed information concerning, for example, the concentration of dissolved species and the amount of xanthate taken up by the mineral that could not be obtained beforehand. These data can be presented as functions of E_h or pH on two-dimensional diagrams or as combined functions of E_h and pH on three-dimensional diagrams. Another objective of this work will be to demonstrate the

usefulness of these plots for comparing predicted behavior with observed behavior.

It was mentioned in the previous section that many aspects of galena aqueous chemistry are not properly understood despite the fact that a considerable amount of research has already been expended in this direction. Many details have been learned concerning galena oxidation and the adsorption of xanthate onto galena, for example, and it is now generally accepted that there are many similarities between the two and that they are often closely connected with each other. However, few attempts have been made to put all of this information together in the form of a comprehensive mechanism. The electrochemical experiments conducted at pH 9.2 and 6.8 in this study will be designed and interpreted from the viewpoint that galena oxidation and xanthate adsorption are competitive dynamic processes. It is hoped that the results can be useful in developing a kinetic model that simultaneously takes into account such important variables as pH, collector concentration, electrode potential and time. Such a model might tidy up some loose ends and resolve some apparent discrepancies in the literature.

Other factors besides thermodynamics and kinetics, such as mass and charge transfer, can become extremely important when dealing with heterogeneous reactions that may or may not involve the transfer of electrons. For example, the accumulation of an insoluble product layer on a conducting mineral may dramatically affect the rate at which reactants and products (including electrons) can be transported to and from the reaction sites. Many of the non-thermodynamic effects that are

often observed can be attributed to such changes. This will also be considered when the results of the electrochemical experiments in this study are analyzed.

CHAPTER II.

THERMODYNAMIC CALCULATIONS OF THE GALENA-ETHYL XANTHATE SYSTEM

2.1 Introduction

2.1.1 General

Although kinetics and mass transfer must be considered in order to understand the dynamics of a process, only thermodynamics can determine whether the process will begin in the first place. Experience has shown that the adsorption of xanthate onto sulfide minerals occurs quite rapidly and that only a small surface coverage is required for flotation to be possible (Gaudin, 1957). For these reasons, it is often more important for a mineral engineer to know the conditions at which adsorption is possible rather than how quickly or to what extent this reaction proceeds. Knowledge of the thermodynamics is the necessary starting point for the proper design and operation of a sulfide-xanthate flotation process.

It has become common practice among researchers doing electrochemical work on sulfides to invoke thermodynamics by comparing the potentials at which a reaction begins with the Nernst equation for that proposed reaction. However, few attempts have been made to do a comprehensive series of calculations in which many different soluble and insoluble species are considered simultaneously. The most ambitious study has been that done by Hepel and Pomianowski (1977) on the Cu-H_2O-KEX system. Although the authors conceded that this was not the most

relevant system to flotation, they stated that they had tackled this case because a sulfide system was too complicated.

A more logical step is, of course, to study a sulfide system. Galena (and synthetic lead sulfide) has probably been the sulfide most widely studied by mineral processors, hydrometallurgists, geochemists, chemists and physicists alike. Yet, there is a great deal that is still uncertain concerning its interactions with water and xanthate. With the vast amount of data available in the literature concerning it, the galena-ethyl xanthate system is perhaps the ideal choice for which a comprehensive set of thermodynamic calculations can be carried out.

The calculations to be described are more rigorous than those done previously because they are based on a mass balance that includes insoluble species as well as soluble ones. As mentioned previously in Section 1.4, one of the main objectives of this work is to extend the use of thermodynamic calculations for mineral systems and to present a few novel ways in which the data can be presented and applied. Consequently, a considerable emphasis in this chapter will be placed on discussing the approach taken in setting up and executing the calculations. This chapter will contain portions that have previously been published (Pritzker and Yoon, 1984a,b; Pritzker et al., 1984).

2.1.2 Literature Review

Many investigators have attempted to relate the behavior of sulfide flotation systems to the reaction products predicted by thermodynamic calculations. DuRietz (1957, 1976) compared the solubilities of

minerals and metal-reagent salts (e.g., metal xanthates) in order to explain the selectivity of flotation and depression in different systems. With the recognition of the electrochemical nature of these systems, many researchers (Elgillani and Fuerstenau, 1968; Fuerstenau et al., 1968; Chander and Fuerstenau, 1975; Janetski et al., 1977; Hepel and Pomianowski, 1977; Brion et al., 1980) began to use E_h-pH stability diagrams for the interpretation of their experimental results.

With regard to the galena and galena-xanthate systems, Burkin et al. (1964) showed that unless a suspension of galena in water is subjected to strongly reducing conditions, oxidized species, e.g., $PbSO_4$, PbO or $HPbO_2^-$, are stable, whereas PbS is not. From this, they concluded that, in most circumstances encountered in flotation practice, the interaction between the collector and these oxidation products is what determines the adsorption mechanism. No metastable species were considered in their calculations. Toperi and Tolun (1969), on the other hand, related the results of their electrochemical and bubble contact experiments to an E_h-pH diagram constructed assuming that the oxidation of sulfide ions does not proceed past thiosulfate.

2.2 **Approach Used for the Calculations**

2.2.1 Outline of Procedure

The calculations carried out in this study are similar to previous ones dealing with the construction of E_h-pH diagrams, but with two important distinctions:

1) The mass balance includes not only lead-, sulfur- and xanthate-bearing dissolved species, but any solid species, as well. Previous work of this kind (on other mineral systems) has failed to include solid species in the mass balance.

2) Solution of the mass balance equations yields the concentrations of all dissolved species and the weights of all precipitated phases under any E_h-pH conditions. Previous work has been limited to determining the phase boundaries on an E_h-pH diagram.

Despite the fact that the increased rigor of these calculations requires more extensive and costly computer computations, much more information concerning the flotation chemistry of the system in question can be obtained.

The most important assumptions that have been made in carrying out these calculations are that:

a) only one type of mineral is present,

b) all reactions are reversible so that the Nernst equation can be used to define half-cell potentials,

c) the potential on the mineral surface is uniform, and

d) the activity coefficients of all species are taken to be unity.

The validity of assumption (d) has been borne out by resulting calculations which showed that the concentrations are usually dilute. Probably the most crucial assumptions are (b) and (c). Although arguments can be raised against the galena-xanthate-water system being reversible and equipotential (Szeglowski, 1960; Granville et al.,

1972), these assumptions are necessary to allow it to be handled on a thermodynamic basis.

Mass balance equations for lead-bearing, sulfur-bearing and xanthate-bearing species (both soluble and insoluble) have been derived in terms of the appropriate equilibrium constants and solved to determine not only the concentrations of the various dissolved species, but also the amount of precipitates formed. In previous work of this kind, it was often necessary to arbitrarily fix the total solubility of an element over a range of E_h and pH. In a real flotation system, however, the solubility is a function of E_h and pH and, thus, cannot be independently controlled. In the present work, no such assumptions need to be made.

At ambient conditions, the thermodynamics dictates that the oxidation of sulfur should proceed as far as the formation of sulfate (+6 oxidation state of sulfur). However, under the conditions typically encountered in flotation practice, sulfide oxidation is sluggish and so species such as elemental sulfur and thiosulfate can exist although they are not thermodynamically favored (Eadington and Prosser, 1969; Gardner and Woods, 1979b; Guy and Trahar, 1984). Consequently, the calculations have been done for the following cases:

Case I. oxidation of sulfide proceeds to sulfate,

Case II. oxidation of sulfide proceeds only as far as the formation of thiosulfate, and

Case III. oxidation of sulfide proceeds only as far as the formation of elemental sulfur.

The derivation of the working equations begins by considering a given amount of galena and potassium ethyl xanthate to be present in a given volume of water. This places a constraint on the total amount of lead- (N_{Pb}), sulfur- (N_S) and xanthate- (N_X) bearing species, both soluble and insoluble, in the system. In Table 2.1, all the species that have been considered in these calculations are listed along with their free energies of formation. (Note that xanthate species have not been included since their free energies are not available from the literature. Thermodynamic data has, instead, been reported for reactions in which they participate and are presented in Table 2.2).

Separate mass balance equations are written for the lead-, sulfur- and xanthate-bearing species to account for the quantities N_{Pb}, N_S and N_X. Contained in these equations are terms for the concentrations of each of the aqueous and gaseous species listed in Table 2.1 and the amount of whatever condensed phase(s) is(are) present. The concentration of each soluble lead-bearing species can be expressed in terms of a common ion (Pb^{2+} in these calculations) through use of the reactions and equilibrium relationships given in Table 2.2. Sulfur-bearing species can likewise be written in terms of SO_4^{2-} (Case I), $S_2O_3^{2-}$ (Case II) or S^{2-} (Case III), and xanthate-bearing species in terms of X^-.

A different mass balance equation results by specifying the one, two or three condensed phases that may be stable together. In addition, the case when no condensed phases are present has also been considered. The identity of the insoluble species not only affects the coefficients

Table 2.1

Standard Free Energy Data Used in this Study (T = 298.15°K; P = 1 atm)

Dissolved Species	ΔG_f^o (kcal/mole)	References
Pb^{2+}	- 5.81	Latimer (1952)
$PbOH^+$	- 52.82	Sillen and Martell (1964)
$Pb(OH)_2$	- 95.74	" "
$Pb(OH)_3^-$	-136.75	" "
$Pb(OH)_4^{2-}$	-178.91	" "
Pb_2OH^{3+}	- 59.72	" "
$Pb_3(OH)_4^{2+}$	-212.40	" "
$Pb_4(OH)_4^{4+}$	-223.80	" "
$Pb_6(OH)_8^{4+}$	-430.30	" "
Pb^{4+}	72.30	Latimer (1952)
PbO_3^{2-}	- 66.34	Pourbaix (1966)
PbO_4^{4-}	- 67.42	Pourbaix (1966)
S^{2-}	21.80	Latimer (1952)
HS^-	3.01	" "
$H_2S(aq)$	- 6.54	" "
SO_4^{2-}	-177.34	" "
HSO_4^-	-179.94	" "
H_2SO_4	-177.34	" "
$S_2O_3^{2-}$	-127.2	Pourbaix (1966)
$HS_2O_3^-$	-129.5	" "
$H_2S_2O_3$	-129.9	" "
S_2^{2-}	19.8	" "
S_3^{2-}	18.0	" "
S_4^{2-}	16.6	" "
S_5^{2-}	15.7	" "
H_2O	- 56.69	Latimer (1952)
Gaseous Species		
H_2S	- 7.89	Latimer (1952)
Solid Species		
PbO_2	- 52.34	Latimer (1952)
Pb_2O_3	- 98.42	Pourbaix (1966)
Pb_3O_4	-147.60	Latimer (1952)
$Pb(OH)_2$	-100.60	Latimer (1952)
$PbSO_4$	-193.89	Latimer (1952)
PbS (galena)	- 23.10	Vaughan and Craig (1978)
PbS_2O_3	-134.0	Latimer (1952)

Table 2.2

Reactions Considered in This Study and the Corresponding Equilibrium Data (T = 298.15°K; P = 1 atm)

Reaction	Equilibrium Constant	E_h^o (mv)	Reference[a]
Dissolved substances only:			
$Pb^{2+} + H_2O = PbOH^+ + H^+$	$^*\beta_{11} = 10^{-7.10}$		
$Pb^{2+} + 2H_2O = Pb(OH)_2(aq) + 2H^+$	$^*\beta_{21} = 10^{-17.20}$		
$Pb^{2+} + 3H_2O = Pb(OH)_3^- + 3H^+$	$^*\beta_{31} = 10^{-28.70}$		
$Pb^{2+} + 4H_2O = Pb(OH)_4^{2-} + 4H^+$	$^*\beta_{41} = 10^{-39.36}$		
$2Pb^{2+} + H_2O = Pb_2OH^{3+} + H^+$	$^*\beta_{12} = 10^{-6.30}$		
$3Pb^{2+} + 4H_2O = Pb_3(OH)_4^{2+} + 4H^+$	$^*\beta_{43} = 10^{-23.32}$		
$4Pb^{2+} + 4H_2O = Pb_4(OH)_4^{4+} + 4H^+$	$^*\beta_{44} = 10^{-19.22}$		
$6Pb^{2+} + 8H_2O = Pb_6(OH)_8^{4+} + 8H^+$	$^*\beta_{86} = 10^{-42.60}$		
$Pb^{4+} + 2e = Pb^{2+}$		1694	
$PbO_3^{2-} + 6H^+ + 2e = Pb^{2+} + 3H_2O$		2375	
$PbO_4^{4-} + 8H^+ + 2e = Pb^{2+} + 4H_2O$		3581	
$SO_4^{2-} + 8H^+ + 8e = S^{2-} + 4H_2O$		149	
$SO_4^{2-} + 9H^+ + 8e = HS^- + 4H_2O$		252	
$SO_4^{2-} + 10H^+ + 8e = H_2S(aq) + 4H_2O$		303	
$SO_4^{2-} + H^+ = HSO_4^-$	$K_1 = 10^{1.91}$		
$SO_4^{2-} + 2H^+ = H_2SO_4$	$\beta_{21} = 1.00$		

$S_2O_3^{2-} + 6H^+ + 8e = 2S^{2-} + 3H_2O$ -4

$S_2O_3^{2-} + 8H^+ + 8e = 2HS^- + 3H_2O$ 200

$S_2O_3^{2-} + 10H^+ + 8e = 2H_2S(aq) + 3H_2O$ 303

$S_2O_3^{2-} + H^+ = HS_2O_3^-$ $K_1 = 10^{1.69}$

$S_2O_3^{2-} + 2H^+ = H_2S_2O_3$ $\beta_{21} = 10^{1.98}$

$X^- + H^+ = HX$ $K_1 = 10^{1.64}$

One gaseous substance:

$SO_4^{2-} + 10H^+ + 8e = H_2S(g) + 4H_2O$ 311

$S_2O_3^{2-} + 10H^+ + 8e = 2H_2S(g) + 3H_2O$ 318

$S^o + 2H^+ + 2e = H_2S(g)$ 171

One condensed substance:

$PbO_2(s) + 4H^+ + 2e = Pb^{2+} + 2H_2O$ 1450

$Pb_2O_3(s) + 6H^+ + 2e = 2Pb^{2+} + 3H_2O$ 1806

$Pb_3O_4(s) + 8H^+ + 2e = 3Pb^{2+} + 4H_2O$ 2094

$Pb^{2+} + 2e = Pb(s)$ -126

$Pb(OH)_2(s) + 2H^+ = Pb^{2+} + 2H_2O$ $K_{So} = 10^{13.63}$

$PbSO_4(s) = Pb^{2+} + SO_4^{2-}$ $K_{So} = 10^{-7.67}$

$PbS(s) = Pb^{2+} + S^{2-}$ $K_{So} = 10^{-28.79}$

$PbS_2O_3 = Pb^{2+} + S_2O_3^{2-}$ $K_{So} = 10^{-0.73}$

$S^o + 2e = S^{2-}$ -476

$S^o + H^+ + 2e = HS^-$ -65

$S^o + 2H^+ + 2e = H_2S(aq)$ 142

$2S^o + 2e = S_2^{2-}$ -429

$3S^o + 2e = S_3^{2-}$		-390	
$4S^o + 2e = S_4^{2-}$		-360	
$5S^o + 2e = S_5^{2-}$		-340	
$X_2(l) = X_2(aq)$	$K_{So} = 10^{-4.90}$		2
$X_2(l) + 2e = 2X^-$		-60	3
$PbX_2(s) = Pb^{2+} + 2X^-$	$K_{So} = 10^{-16.7}$		4

References

1. Iwasaki and Cooke (1958), Majima (1961), Tornell (1966), Hopstock (1968)
2. Tipman and Leja (1975)
3. Average value of Kakovskii and Arashkevich (1969), Majima and Takeda (1968), Goldstick (1959), DuRietz (1957), Tolun and Kitchener (1963)
4. DuRietz (1976)

[a]In the case where no reference number is given, the equilibrium constant or standard electrode potential has been calculated from the free energy data (Table 2.1).

of the mass balance equations due to its stoichiometry, but also introduces an additional thermodynamic relationship between the soluble species (e.g., if PbS is stable, then $[Pb^{2+}]$ and $[S^{2-}]$ are related to each other by the corresponding solubility product). The equilibrium constant, or standard electrode potential, pertaining to each condensed phase is also included in Table 2.2.

The equations are then combined in order to eliminate the term(s) for the insoluble species. In so doing, one is left with a single equation in one unknown (usually $[Pb^{2+}]$), which can then be solved for a given E_h and pH. The secant method has been used whenever a polynomial equation arises. Once $[Pb^{2+}]$ is known, the concentration of each of the other dissolved species is then determined from the equilibrium relationship between Pb^{2+} and that species.

One of the important aspects of this approach for the calculations is that one obtains as many equations as there are unknowns. Consequently, the concentration of none of the species has to be arbitrarily fixed.

In order to determine which condensed phase(s) is(are) most stable at a particular E_h and pH, the following iterative procedure has been used:

1. To begin with, a solid phase is arbitrarily assumed to be stable.
2. The appropriate equation(s) is(are) solved for particular values of E_h and pH.
3. The concentration of the particular dissolved species needed to determine whether any of the other possible precipitated phases

listed above are more stable is determined.

4. The solubility products and electrode potentials for the condensed species are then checked to see if any other precipitated phase can also be present under these conditions. When one such case is found, the mass balance equation for that particular species is immediately solved and a new set of concentrations of the significant soluble species is determined. If the solubility product of the original solid is still exceeded, then the two are considered to co-exist.
5. Step 4 is repeated with the remaining solids under consideration. This whole cycle is continued until the most stable species is(are) found.
6. Steps 1-5 are repeated as E_h and pH are systematically varied.
7. The equilibrium concentrations of all the other dissolved species are calculated over the entire ranges of E_h (-200 mv to +200 mv) and pH (0 to 14).

By keeping track of the values of E_h and pH at which particular phase transitions occur, an E_h-pH stability diagram can be generated.

2.2.2 Example of Derivation of a Mass Balance Equation

It will be instructive to go through a detailed derivation of one of the mass balance equations. Consider the case when $PbSO_4(s)$ and $PbX_2(s)$ are stable together. Under these conditions, the following two equilibrium conditions prevail:

$$PbSO_4(s) = Pb^{2+}(aq) + SO_4^{2-}(aq), \quad K_{So} = [Pb^{2+}][SO_4^{2-}] = 10^{-7.47} \quad [2.1]$$

$$PbX_2(s) = Pb^{2+}(aq) + 2X^{-}(aq), \quad K_{So} = [Pb^{2+}][X^{-}]^2 = 10^{-16.7}. \quad [2.2]$$

Mass balances for lead-, sulfur- and xanthate-bearing species yield:

$$\text{lead:} \quad n_{PbSO_4} + n_{PbX_2} + \Sigma(Pb) = N_{Pb} \quad [2.3]$$

$$\text{sulfur:} \quad n_{PbSO_4} + \Sigma(S) = N_S \quad [2.4]$$

$$\text{xanthate:} \quad 2n_{PbX_2} + \Sigma(X) = N_X \quad [2.5]$$

where n_{PbSO_4} = number of moles of $PbSO_4$ per liter of solution

n_{PbX_2} = number of moles of PbX_2 per liter of solution

$\Sigma(Pb)$, $\Sigma(S)$, $\Sigma(X)$ = total number of moles of dissolved lead-, sulfur- and xanthate-bearing species, respectively, per liter of solution

N_{Pb}, N_S, N_X = total number of moles of lead-, sulfur- and xanthate-bearing species, respectively, per liter of solution.

Since all the species are in equilibrium with each other, the concentration of each of the metal-bearing species can be expressed in terms of one of these species. For example, the equilibrium between Pb^{2+} and $PbOH^{+}$ can be written as:

$$Pb^{2+} + H_2O = PbOH^{+} + H^{+}.$$

The equilibrium constant for this equation, ${}^{*}\beta_{11}$, can be determined from

the free energy data in Table 2.1. In the present work, the notations for the equilibrium constants of the various reactions follow the rules used by Sillen and Martell (1964). $[PbOH^+]$ can then be expressed in terms of $[Pb^{2+}]$ by the relation:

$$[PbOH^+] = {}^*\beta_{11}\,[Pb^{2+}]/[H^+] \qquad [2.6]$$

This is also done for the other lead-bearing species, for the sulfur-bearing (in terms of $[SO_4^{2-}]$, pH, E_h) species and for the xanthate-bearing ($[X^-]$, pH, E_h) species. Consequently, the terms $\Sigma(Pb)$, $\Sigma(S)$ and $\Sigma(X)$ in equations [2.3], [2.4], and [2.5] become:

$$\Sigma(Pb) = 6\,\frac{{}^*\beta_{86}}{[H^+]^8}\,[Pb^{2+}]^6 + 4\,\frac{{}^*\beta_{44}}{[H^+]^4}\,[Pb^{2+}]^4 + 3\,\frac{{}^*\beta_{43}}{[H^+]^4}\,[Pb^{2+}]^3 + 2\,\frac{{}^*\beta_{12}}{[H^+]}\,[Pb^{2+}]^2 + B_1\,[Pb^{2+}] \qquad [2.7]$$

$$\Sigma(S) = B_2\,[SO_4^{2-}] \qquad [2.8]$$

$$\Sigma(X) = (1 + K_1^{HX}[H^+])\,[X^-] + (2)\cdot 10^{\frac{2F(E_h - E^{\circ}_{X_2(aq)/X^-})}{2.303RT}}\,[X^-]^2 \qquad [2.9]$$

where

$$B_1 = 1 + \frac{{}^*\beta_{11}}{[H^+]} + \frac{{}^*\beta_{21}}{[H^+]^2} + \frac{{}^*\beta_{31}}{[H^+]^3} + \frac{{}^*\beta_{41}}{[H^+]^4} + 10^{\frac{2F(E_h - E^{\circ}_{Pb^{2+}/Pb^{4+}})}{2.303RT}} + 10^{\frac{2F(E_h - E^{\circ}_{Pb^{2+}/PbO_3^{2-}})}{2.303RT} + 6pH} + 10^{\frac{2F(E_h - E^{\circ}_{Pb^{2+}/PbO_4^{4-}})}{2.303RT} + 8pH}$$

$$B_2 = 1 + K_1^S\,[H^+] + \beta_{12}[H^+]^2 + 10^{\frac{-8F(E_h - E^{\circ}_{S^{2-}/SO_4^{2-}})}{2.303RT} - 8pH}$$

$$+ 10^{\frac{-8F(E_h - E^{\circ}_{HS^-/SO_4^{2-}})}{2.303RT} - 9pH} + 10^{\frac{-8F(E_h - E^{\circ}_{H_2S(aq)/SO_4^{2-}})}{2.303RT} - 10pH}$$

$$+ 10^{\frac{-8F(E_h - E^{\circ}_{H_2S(g)/SO_4^{2-}})}{2.303RT} - 10pH}$$

It should be noted that the decomposition of ethyl xanthate into carbon disulfide and ethyl alcohol that has been observed by several workers (Iwasaki and Cooke, 1958; Majima, 1961; Tornell, 1966; Hopstock, 1968; Pomianowski and Leja, 1963; Tipman and Leja, 1975) has not been accounted for in these calculations since no free energy data for this reaction could be found in the literature.

The mass balance equations contain terms that are controllable and/or fixed (i.e., N_{Pb}, N_S, N_X) as well as those that vary and cannot be arbitrarily assigned (i.e., n_{PbSO_4}, n_{PbX_2}). Obviously, it is preferable to eliminate the latter from the working equations. From Eqs. [2.4] and [2.5]:

$$n_{PbSO_4} = N_S - \Sigma(S)$$

$$n_{PbX_2} = 1/2\ (N_X - \Sigma(X)).$$

Substituting these into Eq. [2.3] yields:

$$N_S - \Sigma(S) + 1/2\ (N_X - \Sigma(X)) + \Sigma(Pb) = N_{Pb},$$

which after rearranging becomes:

$$\Sigma(Pb) - \Sigma(S) - 1/2\,\Sigma(X) - N_{Pb} + N_S + 1/2\ N_X = 0. \qquad [2.10]$$

When Eq. [2.10] is expanded by substituting Eqs. [2.7], [2.8] and [2.9], Eq. [2.11] results:

$$6\frac{{}^{*}\beta_{86}}{[H^+]^8}[Pb^{2+}]^6 + 4\frac{{}^{*}\beta_{44}}{[H^+]^4}[Pb^{2+}]^4 + 3\frac{{}^{*}\beta_{43}}{[H^+]^4}[Pb^{2+}]^3 + 2\frac{{}^{*}\beta_{12}}{[H^+]}[Pb^{2+}]^2$$

$$+ B_1[Pb^{2+}] - B_2[SO_4{}^{2-}] - 1/2\ (1 + K_1{}^{HX}[H^+])\ [X^-]$$

$$- 10^{\frac{2F(E_h - E^o{}_{X_2(aq)/X^-})}{2.303RT}}[X^-]^2 - (N_{Pb} - N_S - 1/2\ N_X) = 0 \qquad [2.11]$$

This can be reduced to a polynomial equation in one unknown, $[Pb^{2+}]$, by using Eqs. [2.1] and [2.2]:

$$[SO_4{}^{2-}] = \frac{K_{So}{}^{PbSO}}{[Pb^{2+}]}$$

$$[X^-] = \left(\frac{K_{So}{}^{PbX}}{[Pb^{2+}]}\right)^{1/2}$$

After substituting these in and multiplying through by $[Pb^{2+}]$, the final equation is obtained:

$$6\frac{{}^{*}\beta_{86}}{[H^+]^8}[Pb^{2+}]^7 + 4\frac{{}^{*}\beta_{44}}{[H^+]^4}[Pb^{2+}]^5 + 3\frac{{}^{*}\beta_{43}}{[H^+]^4}[Pb^{2+}]^4 + 2\frac{{}^{*}\beta_{12}}{[H^+]}[Pb^{2+}]^3$$

$$+ B_1[Pb^{2+}]^2 - (N_{Pb} - N_S - 1/2\ N_X)\ [Pb^{2+}]$$

$$- 1/2\ (K_{So}{}^{PbX_2})^{1/2}\ (1 + K_1{}^{HX}[H^+])\ [Pb^{2+}]^{1/2}$$

$$- K_{So}{}^{PbSO_4}\ B_2 - K_{So}{}^{PbX_2} \cdot 10^{\frac{2F(E_h - E^0X_2(aq)/X^-)}{2.303RT}} = 0 \qquad [2.12]$$

This can be solved numerically for different E_h and pH values. The secant method has been used in this work. Once $[Pb^{2+}]$ is known, $[SO_4{}^{2-}]$ and $[X^-]$ can be calculated from Eq. [2.1] and [2.2], respectively, while the concentrations of the other species can be obtained from equations such as [2.6].

A listing of one of the Fortran computer programs that was written to do the calculations (the one shown is for Case III) can be found in Appendix I.

2.3 **Results**

The input data to the computer program were chosen to correspond to the case when 0.45 moles of galena are placed in 1 liter of solution. A series of computations over the entire E_h-pH range was carried out for each of the following additions of potassium ethyl xanthate: 0, 10^{-7}, 10^{-6}, 10^{-5}, 10^{-4} M.

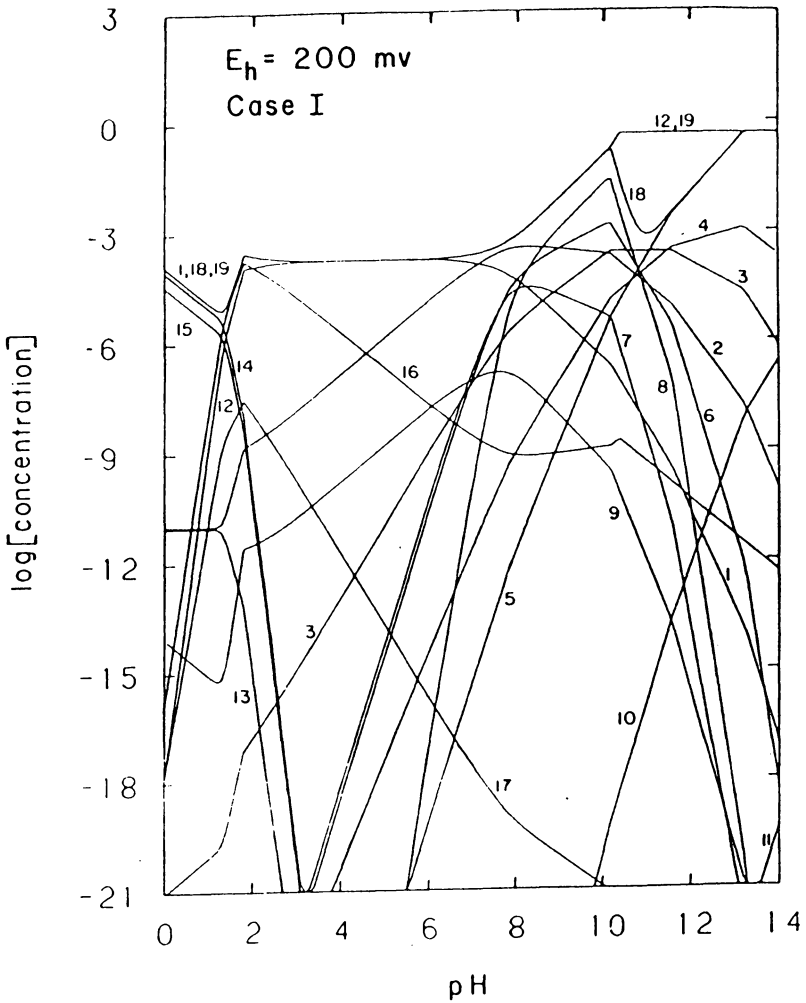
As mentioned earlier, in some of the previously reported thermodynamic calculations of this kind, it has usually been assumed

that the total solubility of an element is constant. Since a constraint has been placed only on the initial amount of mineral added to the system, the lead and sulfur solubility would be expected to vary with E_h and pH. Figure 2.1 shows a plot of the calculated concentrations of the dissolved species as a function of pH at E_h = 200 mv for Case I of the PbS-H_2O system. Examination of curves 18 and 19 in this figure shows that the total concentration of lead- and sulfur-bearing species in solution can vary significantly with pH.

2.3.1 E_h-pH Diagrams

Figures 2.2, 2.6 and 2.11 show the E_h-pH diagrams constructed from the results of the thermodynamic calculations carried out for Cases I, II and III, respectively, in the absence of xanthate. In each diagram, the domains of predominance of the soluble lead-bearing and sulfur-bearing species are shown by the dotted lines. The E_h-pH regions in which various insoluble phases are present are indicated by solid lines. The concentrations of the species on either side of a boundary are equal along the boundary.

Since the solubility of the mineral is not affected by the presence of xanthate unless exceedingly high concentrations are added, the positions of the boundary lines are independent of the collector addition. For the sake of clarity, only dissolved lead-bearing species occurring in E_h-pH regions where no solid lead-bearing species is stable have been included in the diagrams for the cases where xanthate is present.



Key:

1 = Pb^{2+}

2 = $PbOH^{+}$

3 = $Pb(OH)_2$

4 = $Pb(OH)_3^-$

5 = $Pb(OH)_4^{2-}$

6 = $Pb_3(OH)_4^{2+}$

7 = $Pb_4(OH)_4^{4+}$

8 = $Pb_6(OH)_8^{4+}$

9 = Pb_2OH^{3+}

10 = PbO_3^{2-}

11 = PbO_4^{4-}

12 = SO_4^{2-}

13 = HS^-

14 = $H_2S(aq)$

15 = $H_2S(g)$

16 = HSO_4^-

17 = H_2SO_4

18 = Pb_{tot}

19 = S_{tot}

Figure 2.1 Effect of pH on the equilibrium concentration of the dissolved species in the PbS-H_2O system for Case I at E_h = 200 mv, T = 298°K and P = 1 atm.

a. Case I:

0 and 10^{-7} M KEX: At 10^{-7} M KEX, no xanthate-bearing precipitate (i.e., PbX_2 or X_2) is found to form, and so its diagram is identical to that when no xanthate is added (Figure 2.2). PbX_2 does not form because there are not enough plumbous ions for its solubility product (pK_{So} = 16.7) to be exceeded. The predominant reactions involving the oxidation of galena that would be expected on the basis of these calculations are:

$$PbS \longrightarrow Pb^{2+} + S^{o} + 2e \qquad [2.13] \qquad pH < 1.0$$

$$PbS + 4H_2O \longrightarrow Pb^{2+} + HSO_4^{-} + 7H^{+} + 8e \qquad [2.14] \qquad 1.0 < pH < 1.9$$

$$PbS + 4H_2O \longrightarrow PbSO_4 + 8H^{+} + 8e \qquad [2.15] \qquad 1.9 < pH < 10.1$$

$$2PbS + 10H_2O \longrightarrow PbSO_4 + Pb(OH)_2 + SO_4^{2-} + 18H^{+} + 16e \qquad [2.16] \qquad 10.1 < pH < 10.4$$

$$PbS + 6H_2O \longrightarrow Pb(OH)_2 + SO_4^{2-} + 10H^{+} + 8e \qquad [2.17] \qquad 10.4 < pH < 12.7$$

$$PbS + 8H_2O \longrightarrow Pb(OH)_4^{2-} + SO_4^{2-} + 12H^{+} + 12e \qquad [2.18] \qquad pH > 12.7$$

The reduction of galena occurs via:

$$PbS + 2H^{+} + 2e \longrightarrow Pb^{o} + H_2S \qquad [2.19] \qquad pH < 7.0$$

$$PbS + H^{+} + 2e \longrightarrow Pb^{o} + HS^{-} \qquad [2.20] \qquad 7.0 < pH < 13.7$$

$$PbS + 2e \longrightarrow Pb^{o} + S^{2-} \qquad [2.21] \qquad pH > 13.7$$

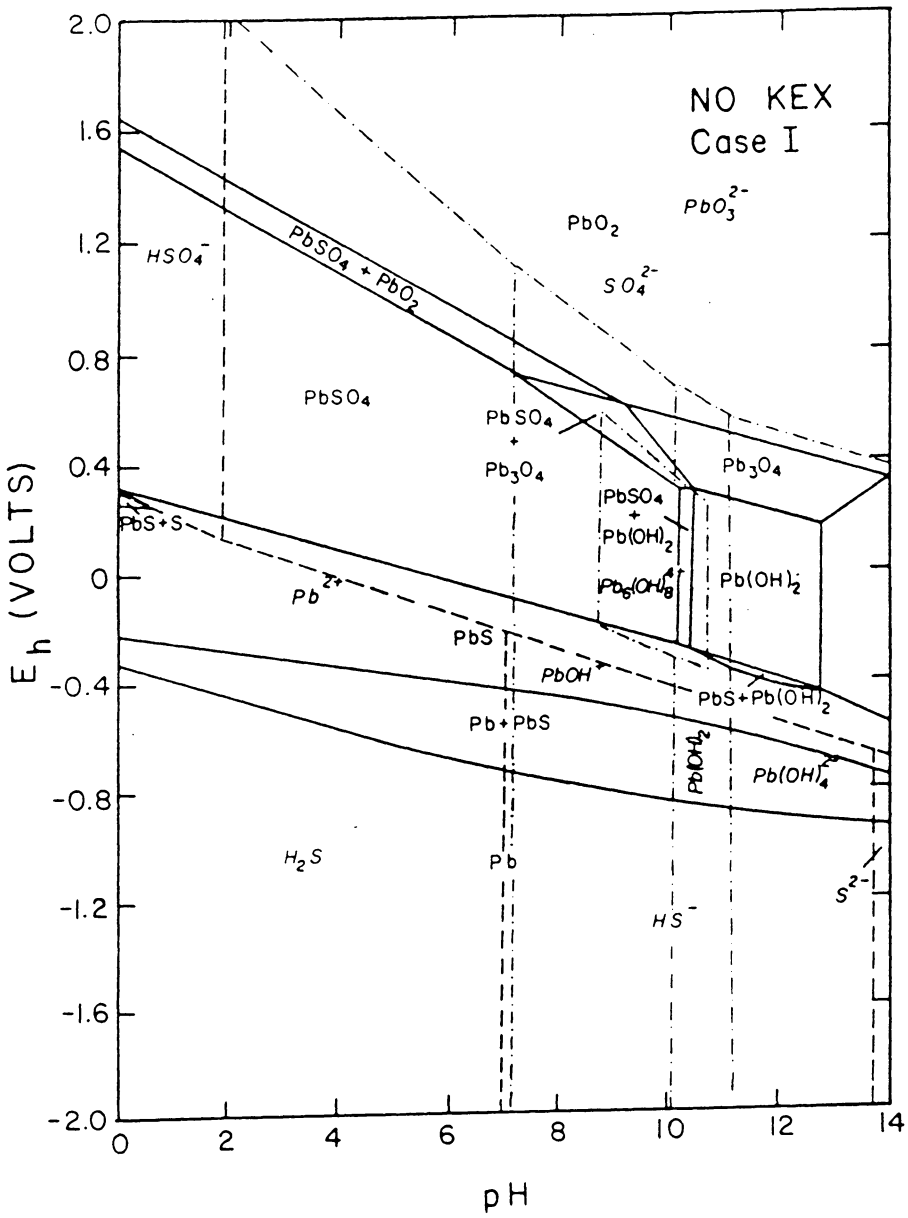


Figure 2.2 E_h-pH diagram of the PbS-H_2O system for Case I at T = 298°K and P = 1 atm.

It is interesting to note that the polynuclear species, $Pb_6(OH)_8^{4+}$, is the predominant lead-bearing species in the E_h-pH region between pH 8.6 and 10.7 and from E_h = -400 mv to E_h ~ 600 mv. The domain for $Pb_6(OH)_8^{4+}$ is the only one for a dissolved species in Case I that is affected by the total amount of mineral considered in the system. The larger the amount of mineral present, the larger it becomes. Since all the other lead species on the diagram are mononuclear, the equilibrium between any two of them is independent of their particular concentrations as long as they are equal to each other.

Another interesting result of these calculations is the existence of a region above pH 11 in which no solid is stable and $Pb(OH)_4^{2-}$ and SO_4^{2-} are the predominant species present. This region arises entirely due to the fact that a limit has been placed on the total amount of lead and sulfur in the system. Had a much larger amount of mineral been considered, the domains for Pb_3O_4 and $Pb(OH)_2$ would have grown sufficiently to cover this region.

10^{-6} M KEX: As can be seen in Figure 2.3, lead xanthate does become stable when 10^{-6} M KEX is added. It is found to co-exist primarily with $PbSO_4$ in a region bounded by E_h = 280 mv, pH = 8.4, and the $PbSO_4$/PbS line. PbX_2 also co-exists with PbS in a thin region between pH = 1.0 and pH 8.4 and just below the $PbSO_4$/PbS line. The formation of PbX_2 in both these regions can be attributed to the reaction:

$$PbS + 2X^- + 4H_2O \longrightarrow PbX_2 + SO_4^{2-} + 8H^+ + 8e. \qquad [2.22]$$

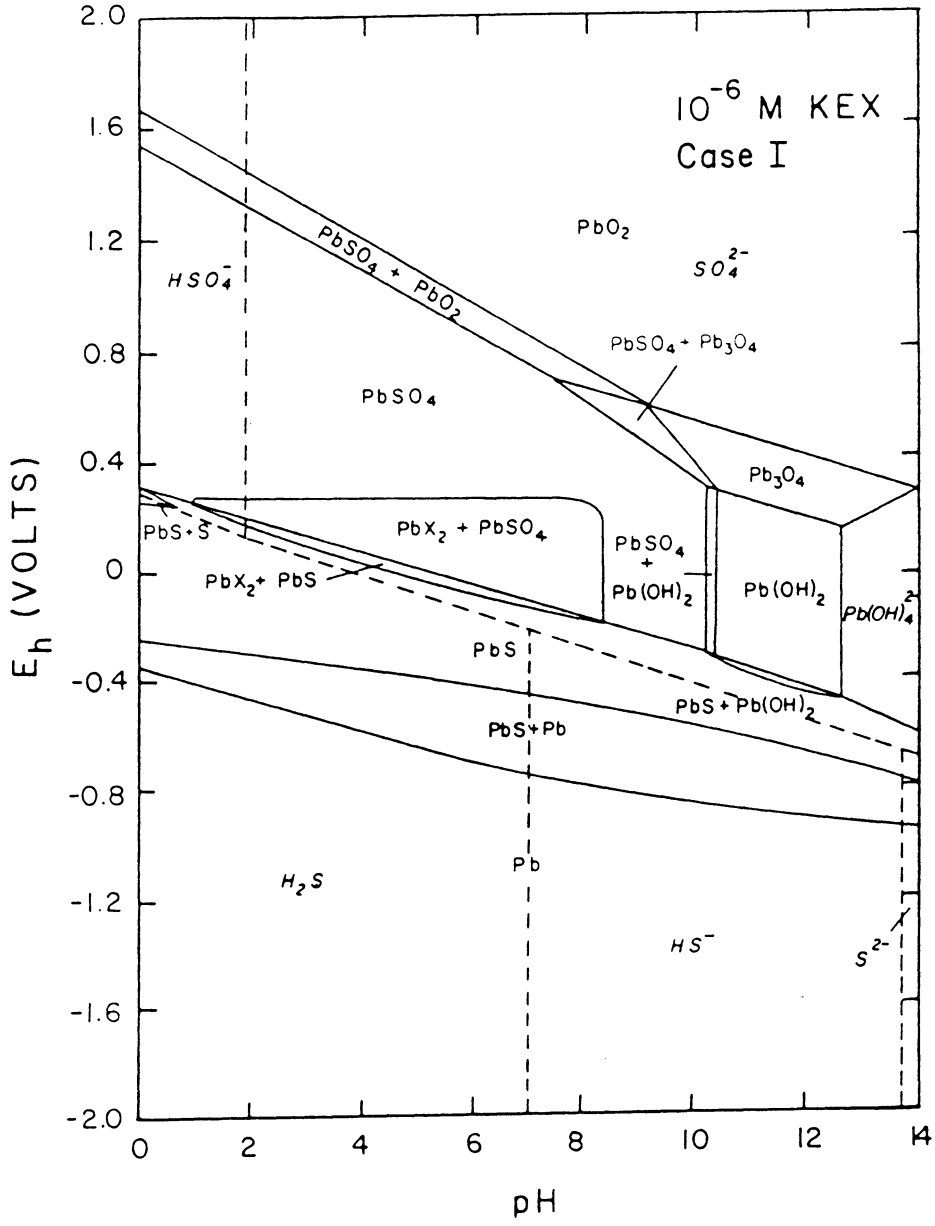


Figure 2.3 E_h-pH diagram of the PbS-KEX-H_2O system for Case I at a collector addition of 10-6 M KEX, T = 298°K and P = 1 atm.

The upper boundary for the PbX_2 + $PbSO_4$ domain at E_h = 280 mv arises because of the limit of the amount of KEX added to the system. As the pH rises, $[Pb^{2+}]$ decreases due to hydrolysis and, consequently, a higher $[X^-]$ is needed in order to precipitate PbX_2. The requirement reaches the limit of 10^{-6} M at pH 8.4. It should also be noted that the domain in which PbS and PbX_2 co-exist is much smaller in comparison because PbS is much more insoluble than $PbSO_4$.

10^{-5} M KEX: Upon increasing the KEX addition to 10^{-5} M (Figure 2.4), the regions in which PbX_2 co-exists with PbS and $PbSO_4$ have grown considerably. PbX_2 and $PbSO_4$ co-exist in the region bounded by E_h = 320 mv, pH = 0, pH = 10.2 and the $PbS/PbSO_4$ line. The positions of these boundaries are determined by the same mass balance constraints as in the case of 10^{-6} M KEX. Also, at this xanthate level, PbX_2 does co-exist with Pb^o and S^o, although in very small regions.

10^{-4} M KEX: At 10^{-4} M KEX, there is enough xanthate in the system for the formation of liquid ethyl dixanthogen, $X_2(l)$, according to the reaction:

$$2X^- \longrightarrow X_2(l) + 2e \qquad [2.23]$$

to be possible (Figure 2.5). The line marking the lower limit of the $X_2(l)$ domain is along E_h = 320 mv, up to pH 8.0, and then slopes downward to E_h = 180 mv at pH 11.1. Beyond this, it remains level.

Under more reducing conditions, PbX_2 is found to co-exist with $PbSO_4$, PbS, Pb^o, S^o, as is the case for 10^{-5} M, and with $Pb(OH)_2$ for the

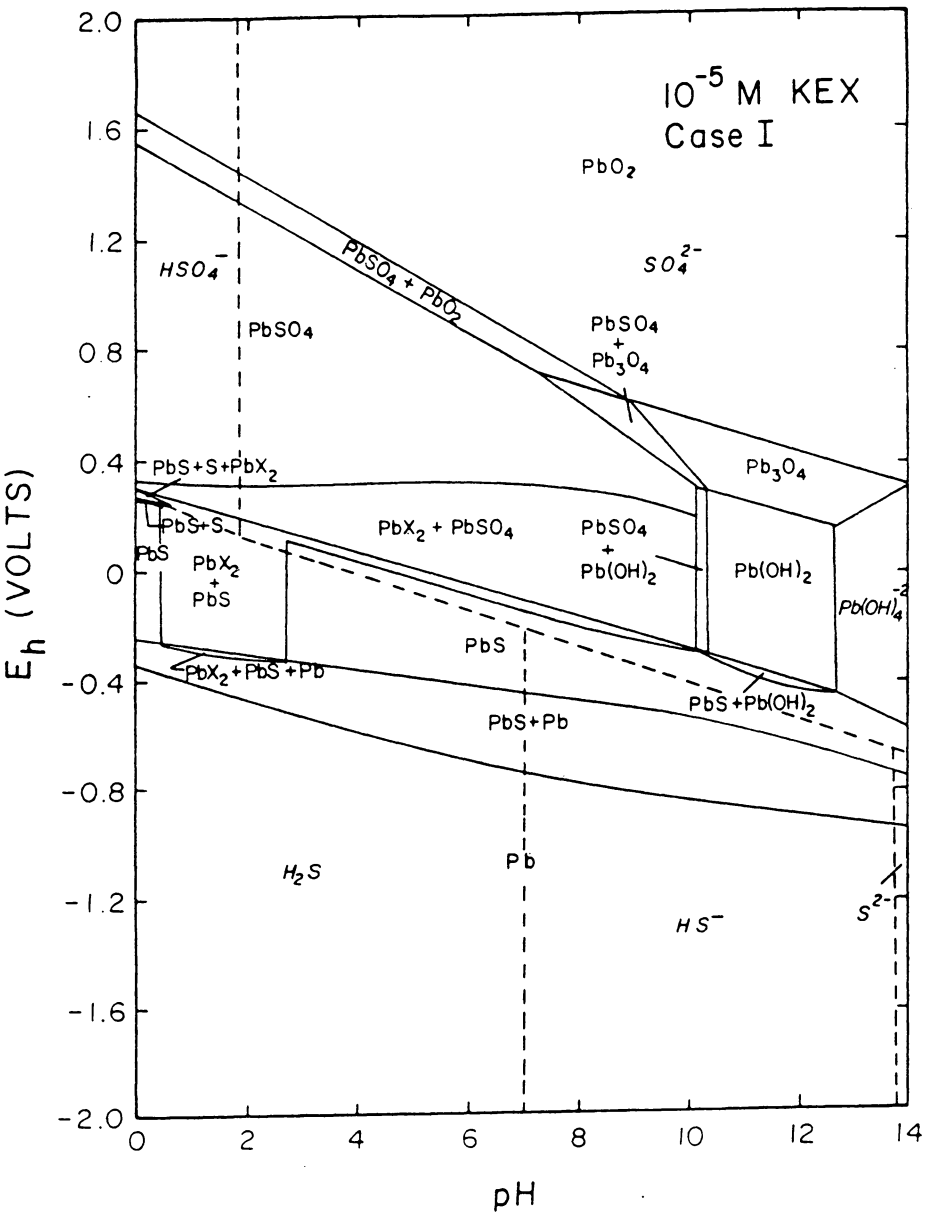


Figure 2.4 E_h-pH diagram of the PbS-KEX-H_2O system for Case I at a collector addition of 10^{-5} M KEX, T = 298°K and P = 1 atm.

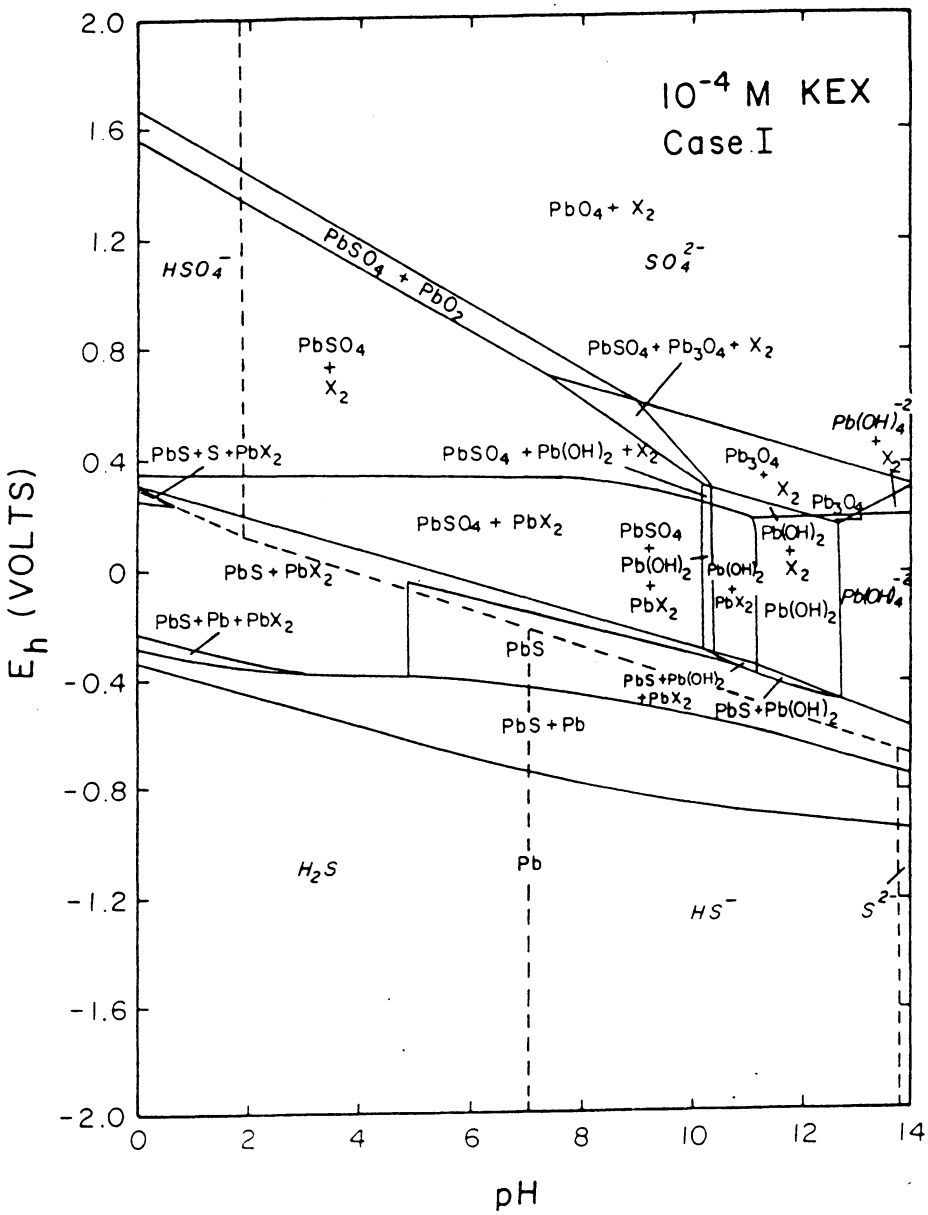


Figure 2.5 E_h-pH diagram of the PbS-KEX-H_2O system for Case I at a collector addition of 10-4 M KEX, T = 298°K and P = 1 atm.

first time, i.e.,

$$2PbS + 2X^- + 10H_2O \longrightarrow Pb(OH)_2 + PbX_2 + 2SO_4^{2-} + 18H^+ + 16e \quad [2.24]$$

The $PbSO_4 + PbX_2$ region has remained virtually the same size as at 10^{-5} M KEX, while that for $PbS + PbX_2$ has grown, extending from pH 0 to pH 4.8. Even at this high xanthate concentration, however, there is still a large E_h-pH range in which PbS exists alone. This supports the general understanding that xanthate adsorption is not favored under reducing conditions.

b. Case II:

0 M KEX: The results for the case in which the oxidation of sulfur proceeds only as far as thiosulfate differ primarily from the first case under acidic oxidizing conditions (Figure 2.6). Lead thiosulfate does not become stable, with the result that the mineral completely dissolves in this E_h-pH region.

Oxidation of galena proceeds principally by the reactions:

$$PbS \longrightarrow Pb^{2+} + S^o + 2e \quad [2.13] \quad pH < 2.8$$

$$2PbS + 3H_2O \longrightarrow 2Pb^{2+} + HS_2O_3^- + 5H^+ + 8e \quad [2.25] \quad 0.3 < pH < 1.8$$

$$2PbS + 3H_2O \longrightarrow 2Pb^{2+} + S_2O_3^{2-} + 6H^+ + 8e \quad [2.26] \quad 1.8 < pH < 5.7$$

$$4PbS + 10H_2O \longrightarrow Pb_4(OH)_4^{4+} + 2S_2O_3^{2-} + 16H^+ + 16e \quad [2.27]$$

$$5.7 < pH < 7.3$$

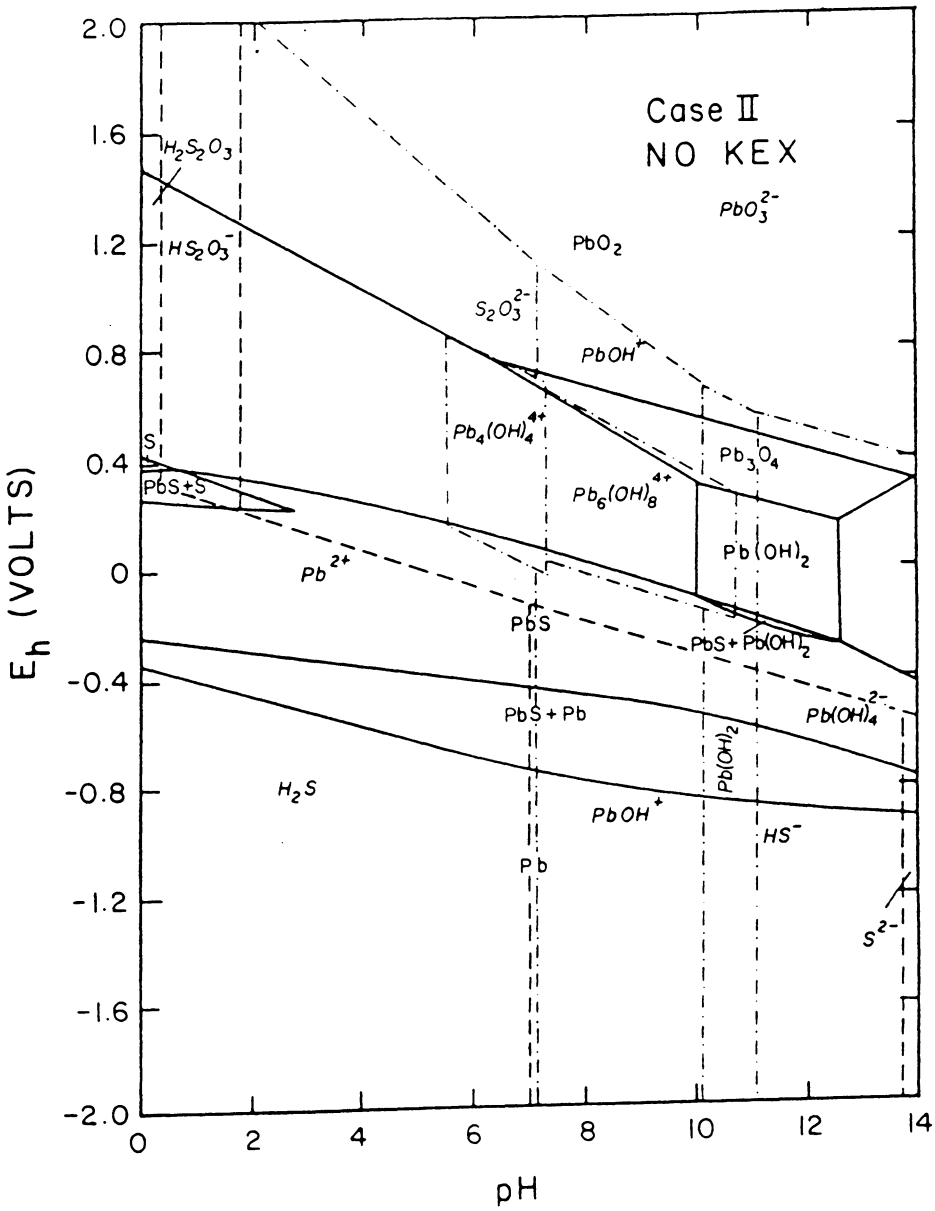


Figure 2.6 E_h-pH diagram of the PbS-H_2O system for Case II at T = 298°K and P = 1 atm.

$$6PbS + 17H_2O \longrightarrow Pb_6(OH)_8^{4+} + 3S_2O_3^{2-} + 26H^+ + 24e \qquad [2.28]$$

$7.3 < pH < 10.1$

$$2PbS + 7H_2O \longrightarrow 2Pb(OH)_2 + S_2O_3^{2-} + 10H^+ + 8e \qquad [2.29]$$

$10.1 < pH < 12.7$

$$2PbS + 11H_2O \longrightarrow 2Pb(OH)_4^{2-} + S_2O_3^{2-} + 14H^+ + 8e \qquad [2.30] \quad pH > 12.7$$

whereas reduction once again occurs by reactions [2.19], [2.20] and [2.21].

The region in which $Pb_6(OH)_8^{4+}$ is the most abundant soluble lead-bearing species is larger than it is in Case I and extends to a lower pH (7.2 as compared to 8.6). In addition, between pH 5.6 and 7.2, another polynuclear ion, $Pb_4(OH)_4^{4+}$, predominates, whereas it never did in the previous case. These differences reflect the fact that the solubility of galena under these E_h-pH conditions is higher in Case II than in Case I.

The boundaries separating the sulfoxy ions and the sulfide ions are also influenced by the amount of the sulfur considered. As the amount increases, these lines move toward lower potentials, thereby enlarging the stability domains of the sulfoxy species.

10^{-7} M KEX: Because of the high solubility of the system in Case II, PbX_2 exists, even as low as 10^{-7} M KEX (Figure 2.7). The reaction in which PbX_2 is formed may be represented as follows:

$$2PbS + 4X^- + 3H_2O \longrightarrow 2PbX_2 + S_2O_3^{2-} + 6H^+ + 8e. \qquad [2.31]$$

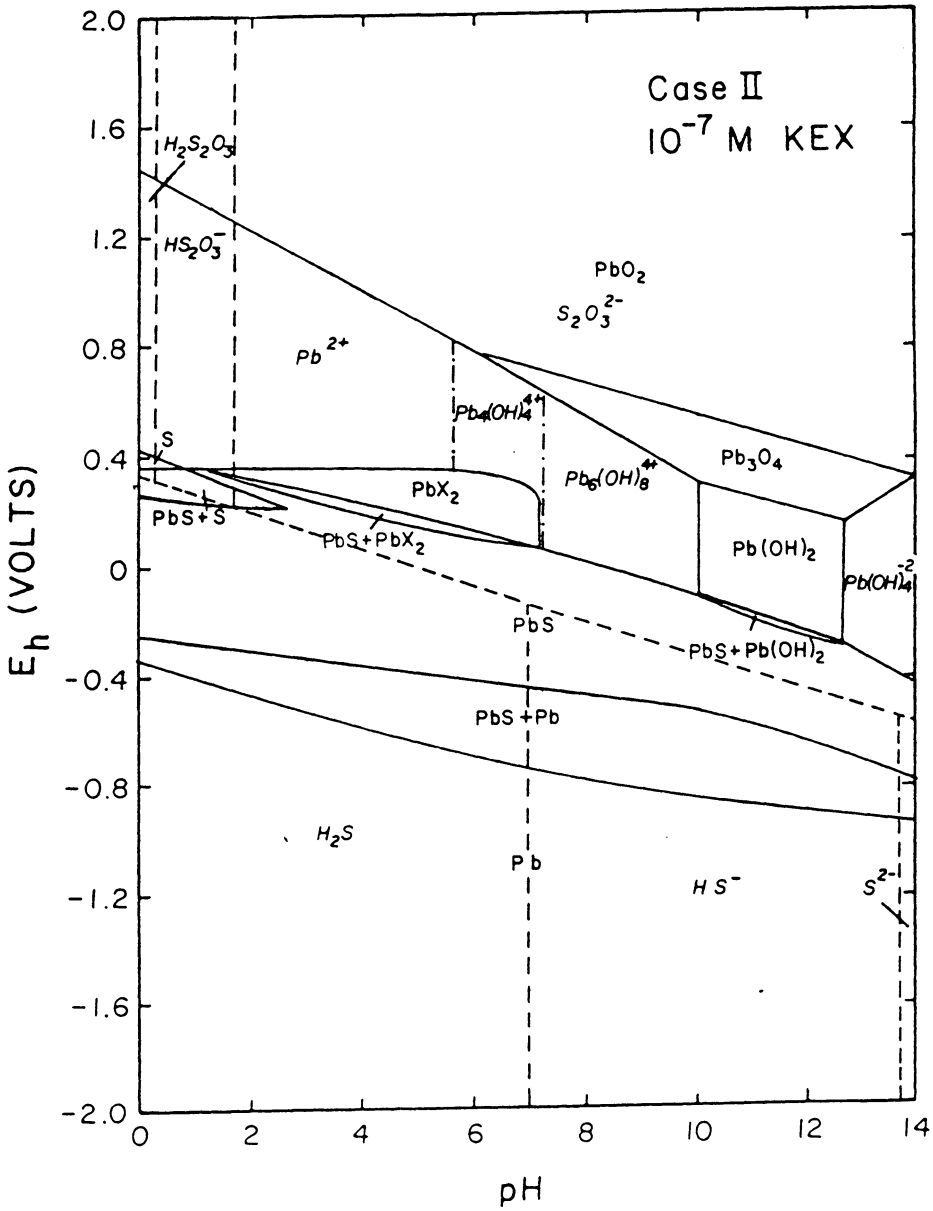


Figure 2.7 E_h-pH diagram of the PbS-KEX-H_2O system for Case II at a collector addition of 10^{-7} M KEX, T = 298°K and P = 1 atm.

The region in which PbX_2 is stable extends from pH 1.2 to pH 7.2 and from 60 mv to 350 mv. Beyond this upper potential limit, PbX_2 decomposes by the reaction,

$$PbX_2 \longrightarrow Pb^{2+} + X_2(aq) + 2e. \qquad [2.32]$$

Liquid dixanthogen, $X_2(l)$, which may also render galena floatable if it adsorbs, cannot form at this low collector concentration.

10^{-6} M KEX: When the KEX concentration is increased to 10^{-6} M, PbX_2 is found to be stable up to 400 mv and at a pH as high as 8.8 (Figure 2.8). At higher E_h values, PbX_2 is the only stable solid phase, but at lower E_h values, it can co-exist with PbS. It can co-exist with S^o only at very low pH.

10^{-5} M KEX: At 10^{-5} M KEX (Figure 2.9), PbX_2 is stable up to just above pH 10.0 and over a wider potential range than at the lower concentrations. Also, PbX_2 remains stable in a tiny pH region above pH 10.2 where $Pb(OH)_2$ exists. The appropriate reactions can be expressed as:

$$2PbS + 5H_2O + 2X^- \longrightarrow PbX_2 + Pb(OH)_2 + S_2O_3^{2-} + 8H^+ + 8e \qquad [2.33]$$

It should be recalled that for Case I no such corresponding reaction occurs at this collector addition.

10^{-4} M KEX: At this collector level, the upper pH limit for PbX_2 reaches 11.1 and the region in which PbX_2 and PbS co-exist has grown (Figure 2.10). In addition, the lower potential limit has dropped

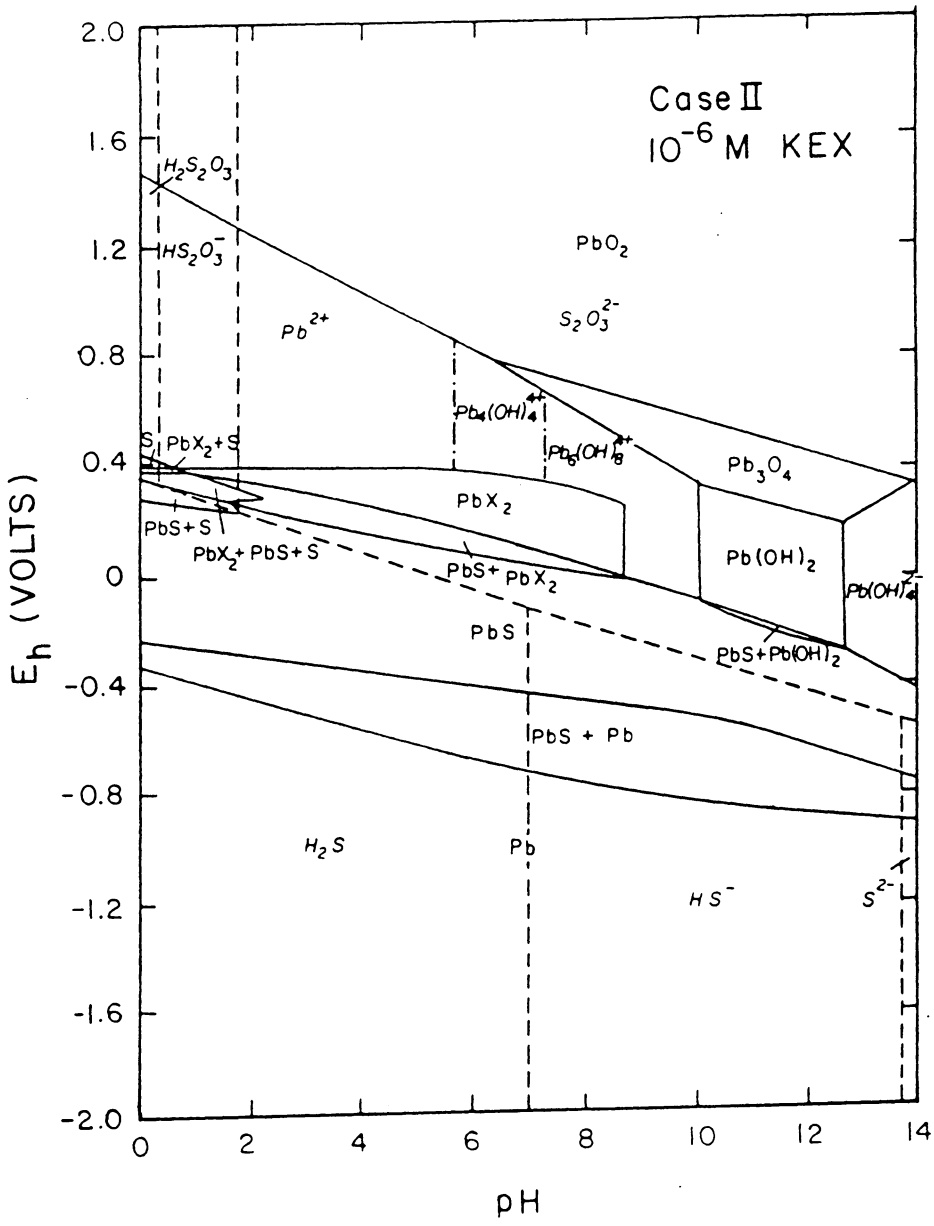


Figure 2.8 E_h-pH diagram of the PbS-KEX-H_2O system for Case II at a collector addition of 10-6 M KEX, T = 298°K and P = 1 atm.

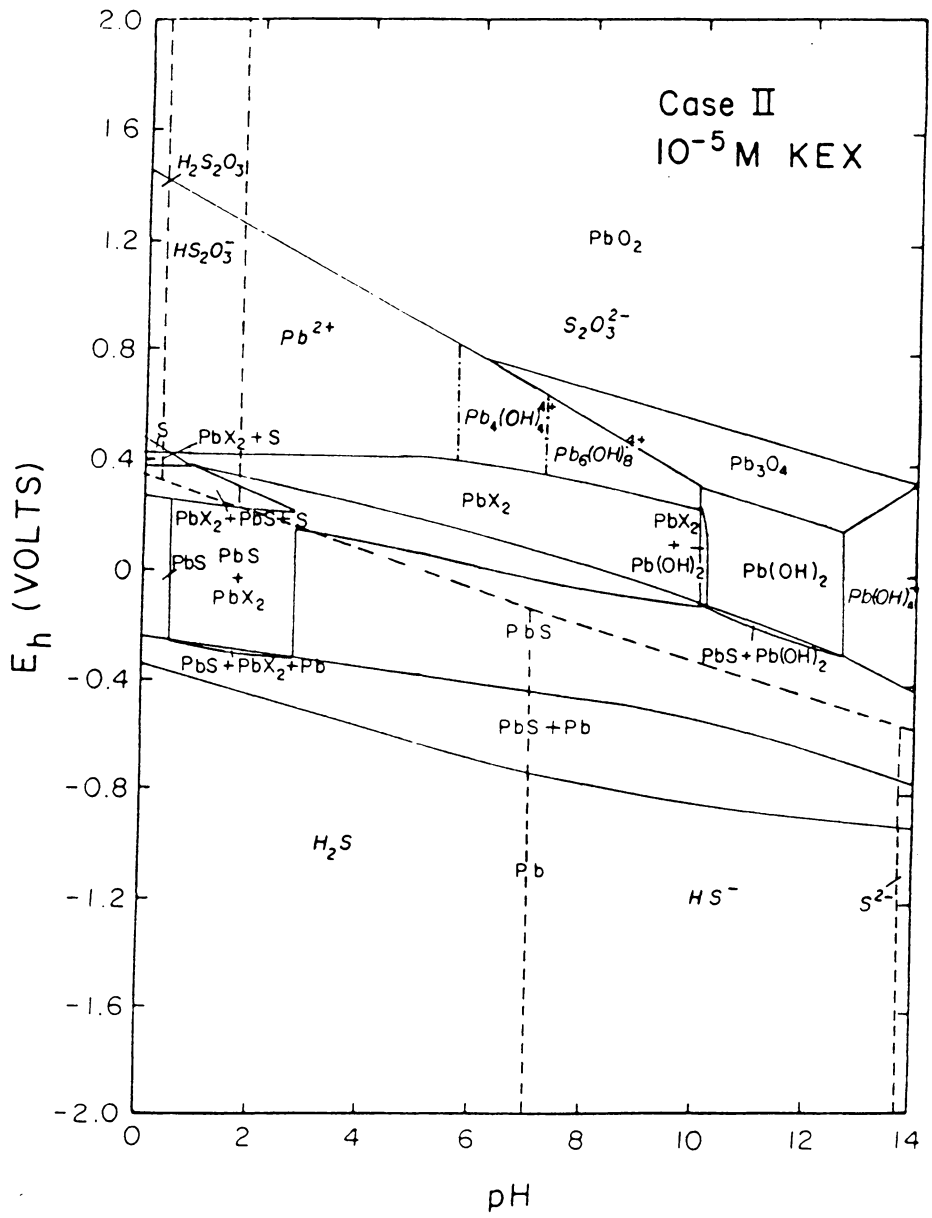


Figure 2.9 E_h-pH diagram of the PbS-KEX-H_2O system for Case II at a collector addition of 10^{-5} M KEX, T = 298°K and P = 1 atm.

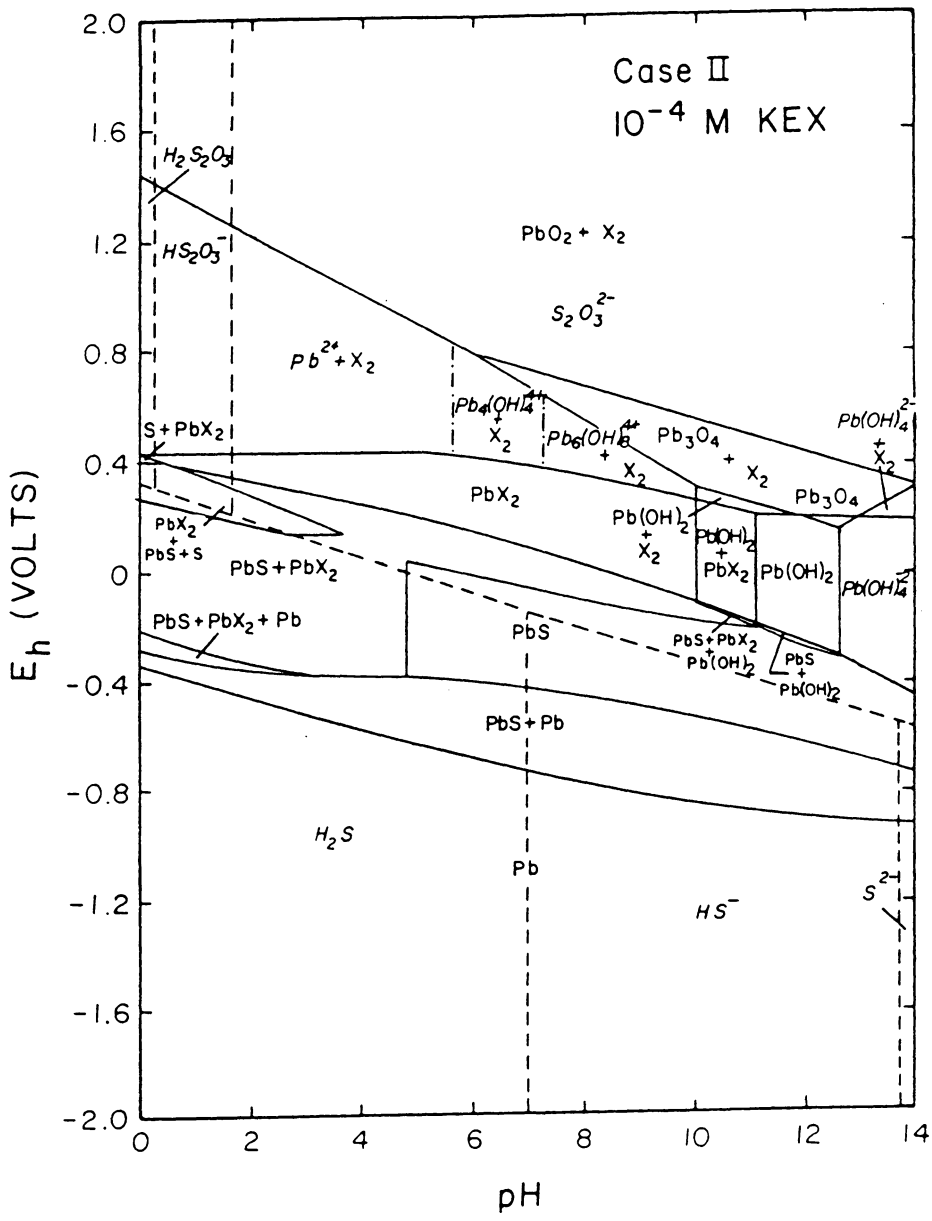


Figure 2.10 E_h-pH diagram of the PbS-KEX-H_2O system for Case II at a collector addition of 10^{-4} M KEX, T = 298°K and P = 1 atm.

enough that it is present along with PbS and Pb^o at low pH.

The xanthate concentration is also now high enough that $X_2(l)$ becomes stable above about 420 mv up to a pH of 6.0. Beyond this, the upper potential limit for $X_2(l)$ stability decreases and levels off at about 200 mv above pH 11.0.

c. Case III:

O M KEX: According to Case III (Figure 2.11), galena is oxidized via reactions:

$$PbS \longrightarrow Pb^{2+} + S^o + 2e \qquad [2.13] \qquad pH < 5.7$$

$$PbS + H_2O \longrightarrow PbOH^+ + S^o + H^+ + 2e \qquad [2.34] \qquad 7.1 < pH < 10.2$$

$$4PbS + 4H_2O \longrightarrow Pb_4(OH)_4^{4+} + 4S^o + 4H^+ + 8e \qquad [2.35] \qquad 5.7 < pH < 7.2$$

$$6PbS + 8H_2O \longrightarrow Pb_6(OH)_8^{4+} + 6S^o + 8H^+ + 12e \qquad [2.36]$$

$$7.2 < pH < 10.1$$

$$PbS + 2H_2O \longrightarrow Pb(OH)_2 + S^o + 2H^+ + 2e \qquad [2.37] \qquad 10.1 < pH < 12.7$$

$$PbS + 4H_2O \longrightarrow Pb(OH)_4^{2-} + S^o + 4H^+ + 2e \qquad [2.30] \qquad pH > 12.7$$

The same reduction reactions apply here as in the previous two cases. It should be noted that polysulfides are the predominant soluble sulfur-bearing species at high pH and potentials since oxidation to SO_4^{2-} or $S_2O_3^{2-}$ is not allowed. As in Case II, the polynuclear species, $Pb_4(OH)_4^{4+}$ and $Pb_6(OH)_8^{4+}$, are the most abundant lead species at intermediate pH and at moderately oxidizing potentials.

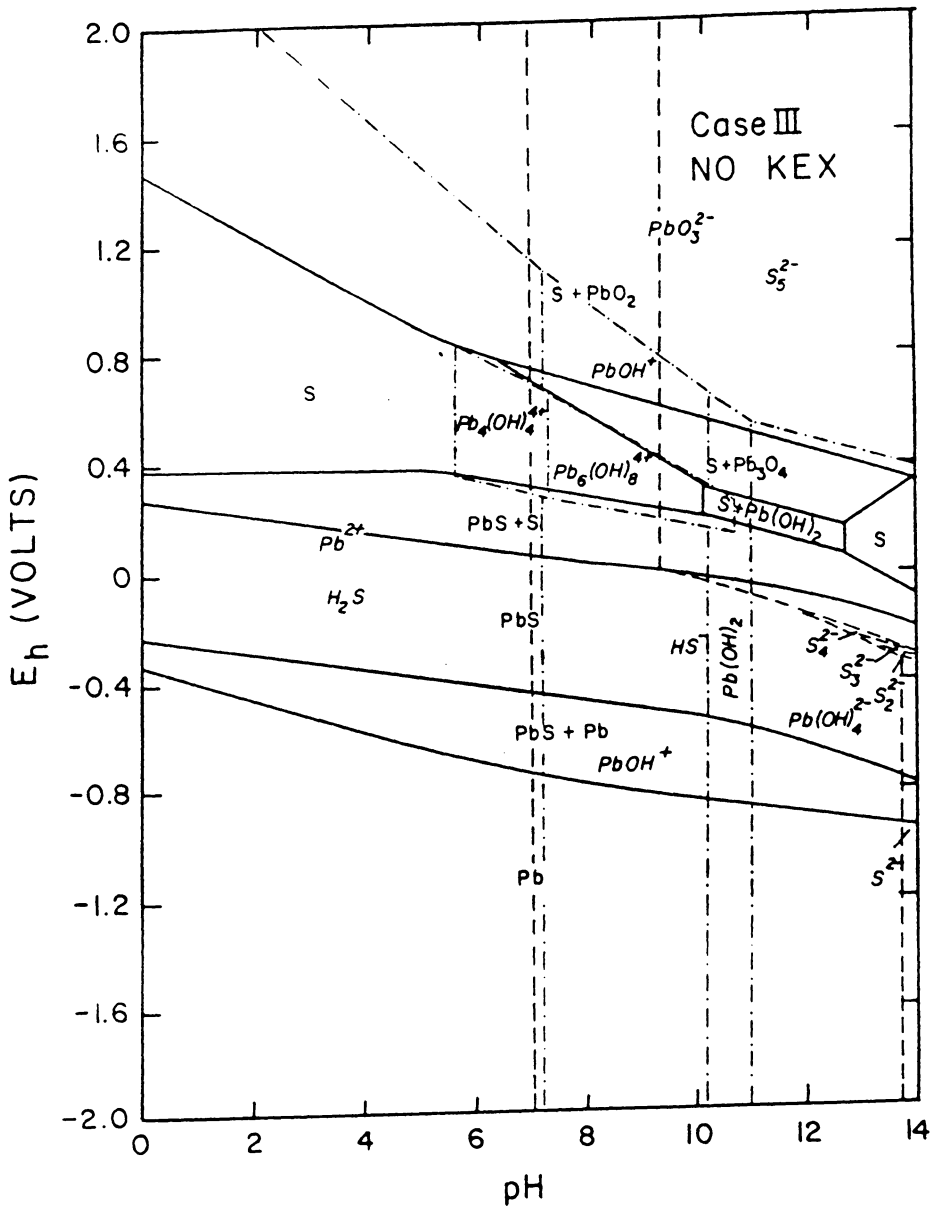


Figure 2.11 E_h-pH diagram of the PbS-H_2O system for Case III at T^o= 298^{o}K and P = 1 atm.

10^{-7} M KEX: The system is not as soluble as in Case II under the conditions that are most favorable for PbX_2 formation (i.e., at E_h ~ 300-400 mv and pH < 8) and, consequently, PbX_2 does not appear at this collector level.

10^{-6} M KEX: With an increase in the xanthate addition to 10^{-6} M, PbX_2 is found to be stable over an E_h region that is narrower than in the other two cases for the same collector level (Figure 2.12). The solid phases that can co-exist with PbX_2 are PbS and S^o through reaction:

$$PbS + 2X^- \longrightarrow PbX_2 + S^o + 2e. \qquad [2.39]$$

10^{-5} M KEX: Increasing the collector addition ten-fold enlarges the E_h-pH regions in which PbX_2 can form (Figure 2.13). The upper limit rises from 8.6 to 10.2 and the lower potential limit (above pH 2.8) has dropped from about 300 mv to 200 mv. In addition, there is a region between pH 0.5 and 2.8 in which PbX_2 co-exists only with PbS. This was also found in Cases I and II. This stability of PbX_2 can be attributed to the fact that galena is quite soluble under these conditions and that Pb^{2+} is the predominant soluble lead-bearing species. At pH ~ 10.0, PbX_2 also appears in a tiny region in which $Pb(OH)_2$ and S^o are also formed from the oxidation of PbS, i.e.,

$$2PbS + 2H_2O + 2X^- \longrightarrow Pb(OH)_2 + PbX_2 + 2S^o + 2H^+ + 4e. \qquad [2.40]$$

10^{-4} M KEX: Similar trends to those found in the previous two cases are also found in this one when 10^{-4} M KEX is added (Figure 2.14).

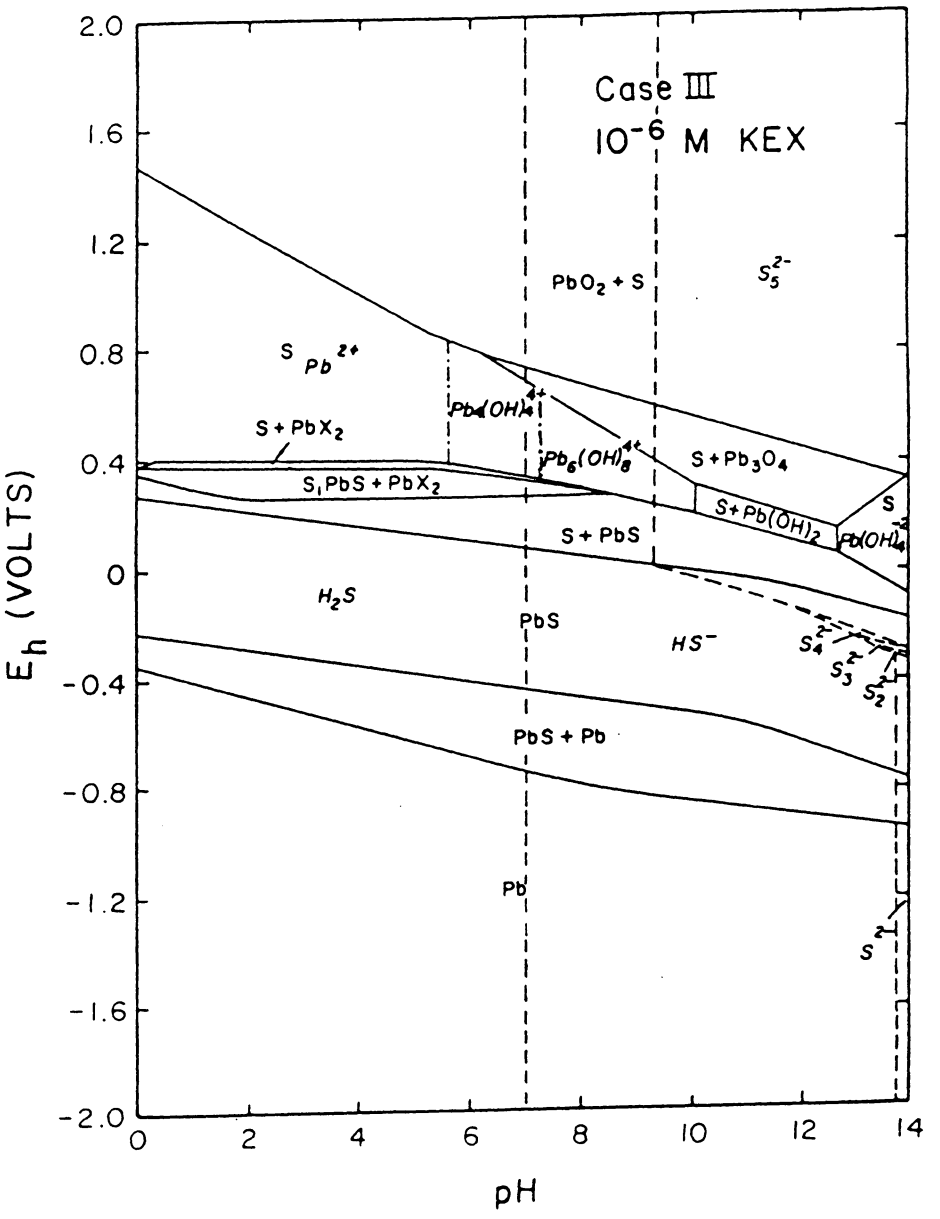


Figure 2.12 E_h-pH diagram of the PbS-KEX-H_2O system for Case III at a collector addition of 10^{-6} M KEX, T = 298°K and P = 1 atm.

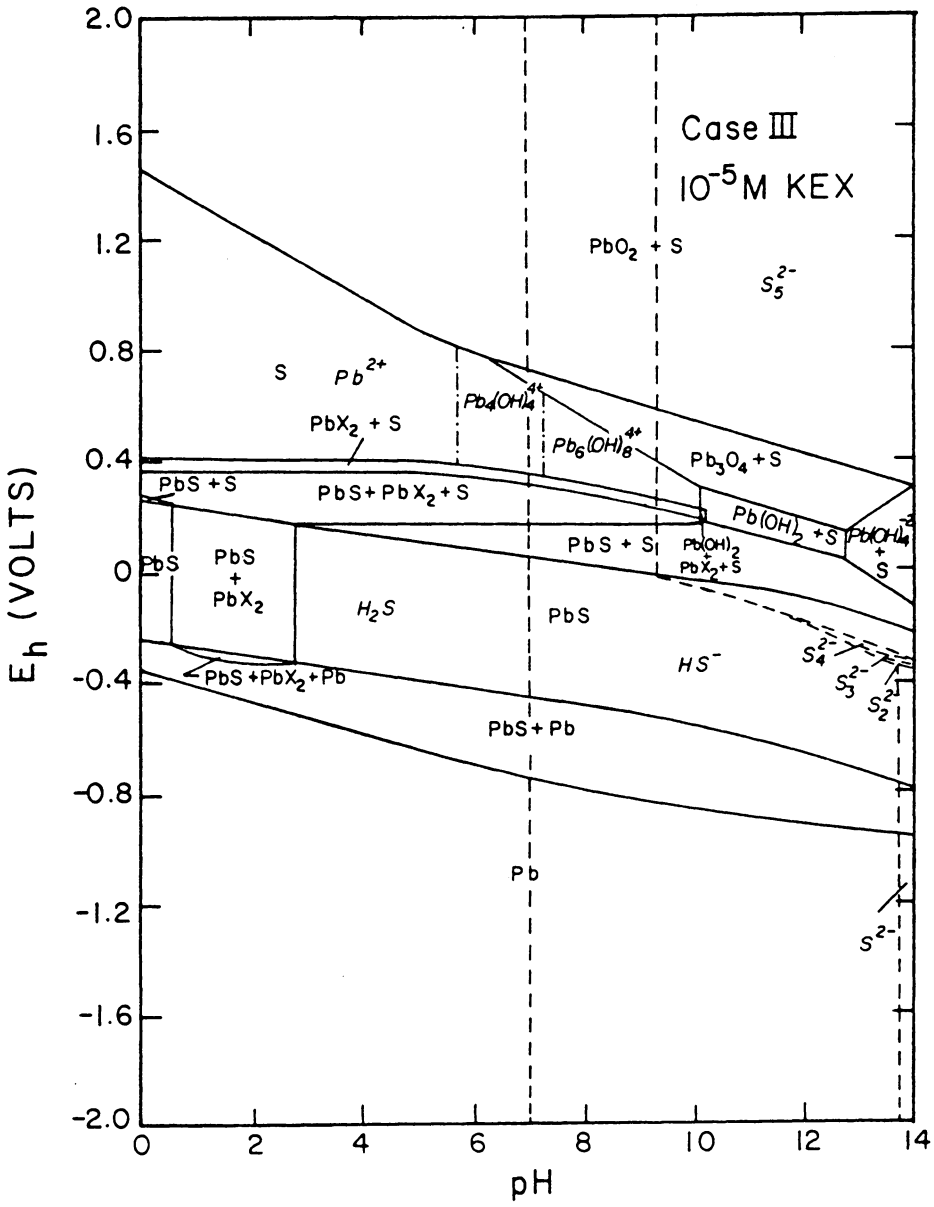


Figure 2.13 E_h-pH diagram of the PbS-KEX-H_2O system for Case III at a collector addition of 10^{-5} M KEX, T = 298°K and P = 1 atm.

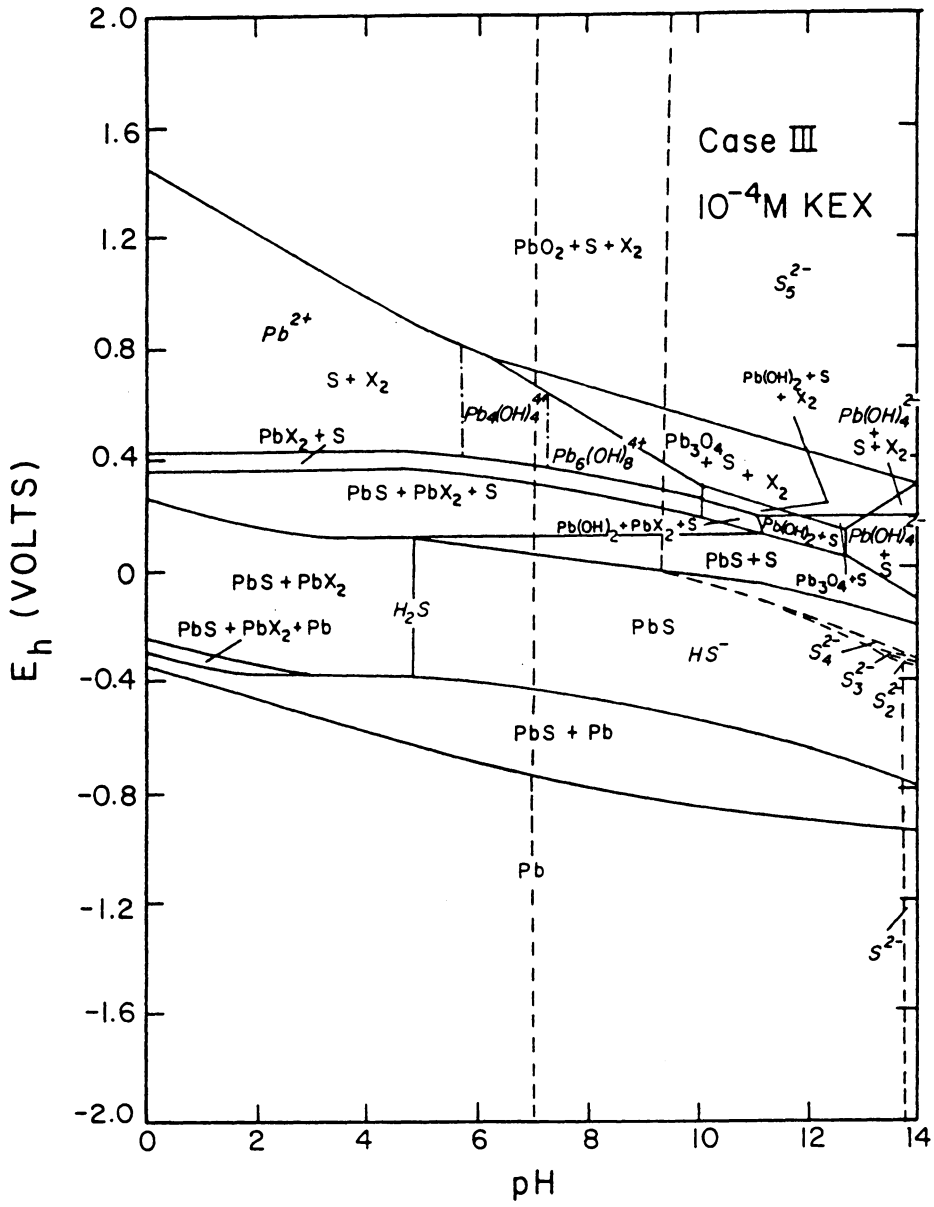


Figure 2.14 E_h-pH diagram of the PbS-KEX-H_2O system for Case III at a collector addition of 10^{-4} M KEX, T = 298°K and P = 1 atm.

The upper pH limit reaches to about 11.0 and the region in which PbS and PbX_2 co-exist at low pH also has grown. Ethyl dixanthogen also becomes stable under oxidizing conditions across the entire pH range.

2.4 Discussion

2.4.1 Oxidation and Collectorless Flotation of Galena

There has been a considerable amount of controversy concerning the nature of the oxidation products on galena and, consequently, a great deal of research has been directed in this area. Poling and Leja (1963) and Reuter and Stein (1957) reported the oxidation product to be PbS_2O_3, whereas Greenler (1962), Hagihara (1952), Manocha and Park (1977), and Steger and Desjardins (1980) concluded that it was $PbSO_4$. To add to the uncertainty, Plante and Sutherland (1949) found that in alkaline solutions both thiosulfate and sulfate were present in significant amounts. In addition, the work by Eadington and Prosser (1969) demonstrated that elemental sulfur was the primary product in acid solutions, lead sulfate in the neutral range, and lead thiosulfate beyond this.

These discrepancies may be related to the difficulties encountered in analyzing the surface species, the different histories of the samples, variations in surface stoichiometry, the various conditions under which oxidation was allowed to proceed and also to the complexity of the sulfide oxidation mechanism.

All of the findings noted above were based on ex-situ measurements of the reaction products. It is possible that changes to the mineral surface may have occurred during the transfer and preparation of the samples for surface analysis. Furthermore, it is now generally agreed that the mechanism for the aqueous oxidation of galena involves electron transfer. This introduces an additional variable, i.e., the potential at the mineral surface, into the description of what reactions are taking place. Since none of the above work included the control or monitoring of the potential, this may also contribute to the differences in the observed oxidation products.

Recently, there has been more emphasis on using electrochemical techniques to study the oxidation of galena in aqueous conditions. It should be noted that this approach has an important advantage over the previous ones in that the analysis is carried out in-situ. However, it suffers from the disadvantages that only electron transfer reactions can be directly monitored and that the nature of the reaction products can only be indirectly inferred from the data. From what appears in the literature, there appears to be a far greater degree of unanimity among electrochemists with regard to galena oxidation than among those cited previously. Brodie (1969), Skewes (1972), Johnson et al. (1978), Paul et al. (1978), and Gardner and Woods (1979b) concluded that reaction [2.13] is the primary oxidation reaction in acidic solutions. Furthermore, evidence for the formation of $PbSO_4$ only appeared when potentials of about 1000 mv SHE were reached. Comparison of this with what is expected on the basis of the thermodynamically most favored case

(i.e., Case I, Figure 2.2) indicates that there is an overvoltage of approximately 700 mv associated with the oxidation of PbS to $PbSO_4$. These workers also reported no evidence that thiosulfate was being generated, as would be anticipated from Case II. Although Case III would, therefore, appear to best describe what is observed up to a potential of about 100 mv, it obviously cannot account for the presence of $PbSO_4$ above 1000 mv. In this region, Case I might be more appropriate. However, the fact that the results of a single set of calculations do not apply a priori over the entire potential range points up a limitation of thermodynamics, even when metastable species are considered.

The most comprehensive work concerning galena oxidation over a range of pH values was the voltammetric study of Gardner and Woods (1979b). Generally, they found that even at neutral and alkaline pH, elemental sulfur was the initial sulfur-bearing oxidation product generated. With further oxidation, thiosulfate began to be detected, particularly as the pH or the applied potential was raised. These findings have recently been corroborated by Lamache et al. (1984), who electrolyzed a bed of galena particles at pH 9.2 for 2 to 3 hours and then analyzed the mineral surface and the solution for the reaction products. Although the presence of S^o is predicted by the calculations of Case III and that of $S_2O_3^{2-}$ by Case II, neither case by itself can provide a complete description of what was observed by Gardner and Woods (1979b).

Until recently, not much research has been concerned with the initial stages of the sulfide oxidation process in relation to flotation. Although Eadington and Prosser (1969) had proposed a reaction mechanism for this (which they termed the induction period) in their excellent study of the oxidation of lead sulfide, it was not seized upon with great interest by flotation chemists. The situation changed drastically, however, when it was demonstrated by several workers (Boyce et al., 1970; Lepetic, 1974; Heyes and Trahar, 1977; Yoon, 1981; Luttrell and Yoon, 1982) that galena and chalcopyrite could be successfully floated from actual ores without adding any collector. Some researchers believed that a "clean" sulfide surface was hydrophobic, while others contended that elemental sulfur formed by reaction [2.37] was responsible for the floatability. This debate has led to a flurry of research activity in this area in the last few years (Gardner and Woods, 1979a; Luttrell and Yoon, 1982, 1984, 1985; Buckley and Woods, 1984a,b; Hamilton and Woods, 1981, 1984; Guy and Trahar, 1984; Heyes and Trahar, 1984; Hodgson and Agar, 1984). The result of this is that there is now some consensus on a reaction mechanism for the initial stage of oxidation and collectorless flotation, which, as it turns out, is quite similar to the one originally proposed by Eadington and Prosser (1969).

Oxidation can be viewed as a process which involves the breaking of metal-sulfur bonds in the mineral lattice and the strengthening of sulfur-sulfur bonds. Metal species are removed from the sulfide structure either as soluble ions (at low pH) or as an oxide (at high

pH), leaving behind a sulfide phase which has become metal-deficient. This reaction can be generalized as:

$$MeS + xH_2O \longrightarrow Me_{1-x}S + xMeO + 2xH^+ + 2xe \qquad [2.41]$$

or

$$MeS \longrightarrow Me_{1-x}S + xMe^{2+} + 2xe, \qquad [2.42]$$

where $0 < x < 1$. With further oxidation, the sulfide phase will become deficient enough in metal that elemental sulfur can nucleate and form a separate phase (i.e., when $x = 1$). From this point on, oxidation can proceed by reactions [2.17], [2.29] or [2.37].

The floatability of sulfides during this initial period of oxidation is explained by the formation of the metal-deficient sulfide phase. Metal ions can be more easily hydrated than sulfide anions since they can form hydrogen bonds and can undergo ion/dipole interactions with water. Consequently, the formation of a metal-deficient sulfide should increase the hydrophobicity of the mineral surface for two reasons. Firstly, it removes metal from the surface layer; secondly, it leaves behind sulfur which increasingly resembles elemental sulfur (which is highly hydrophobic) as oxidation continues.

Reactions such as equations [2.41] and [2.42] cannot be handled using bulk thermodynamics. However, another way to view a metal-deficient sulfide is as a metal polysulfide. Luttrell and Yoon (1982, 1984, 1985) suggested that collectorless flotation of chalcopyrite may be attributed to metal polysulfides formed under oxidizing conditions. Polysulfide ions, S_x^{2-}, (where $x = 2,3,4,5$) are formed during the

oxidation of sulfide ions in aqueous solutions and have been observed under conditions typical of flotation pulps (Chen and Morris, 1972; Chen and Gupta, 1973; Hamilton and Woods, 1983). As mentioned previously, these were considered in the thermodynamic calculations for Case III, although metal polysulfides were not. Nevertheless, the conditions at which polysulfides are abundant would also likely be where metal polysulfides would form.

Guy and Trahar (1984) recently conducted flotation tests on a synthetic galena-quartz mixture at pH 8.0 in the absence of a collector. In Figure 2.15, the flotation recoveries of galena obtained as a function of potential measured on a platinum electrode are compared with some of the results of the calculations for Case III of this study. Included in this diagram are the percentage distributions of the soluble sulfur-bearing species computed as a function of potential and the potential ranges for the stable solid phases. All the polysulfides have been combined together and denoted as S_x^{2-}.

As can be seen, the potentials at which the polysulfides are most abundant coincide with those where elemental sulfur is stable. Furthermore, the best flotation is achieved when both sulfur and the polysulfides are present. Thus, the onset of flotation may be related to their presence, although it is impossible to conclude on the basis of these calculations if one or the other or both are required.

The drop-off in recovery above 300 mv falls in the region where PbS is no longer stable. It is possible that the decomposition of galena with the formation of lead hydroxyl complexes, such as $Pb_6(OH)_8^{4+}$, may

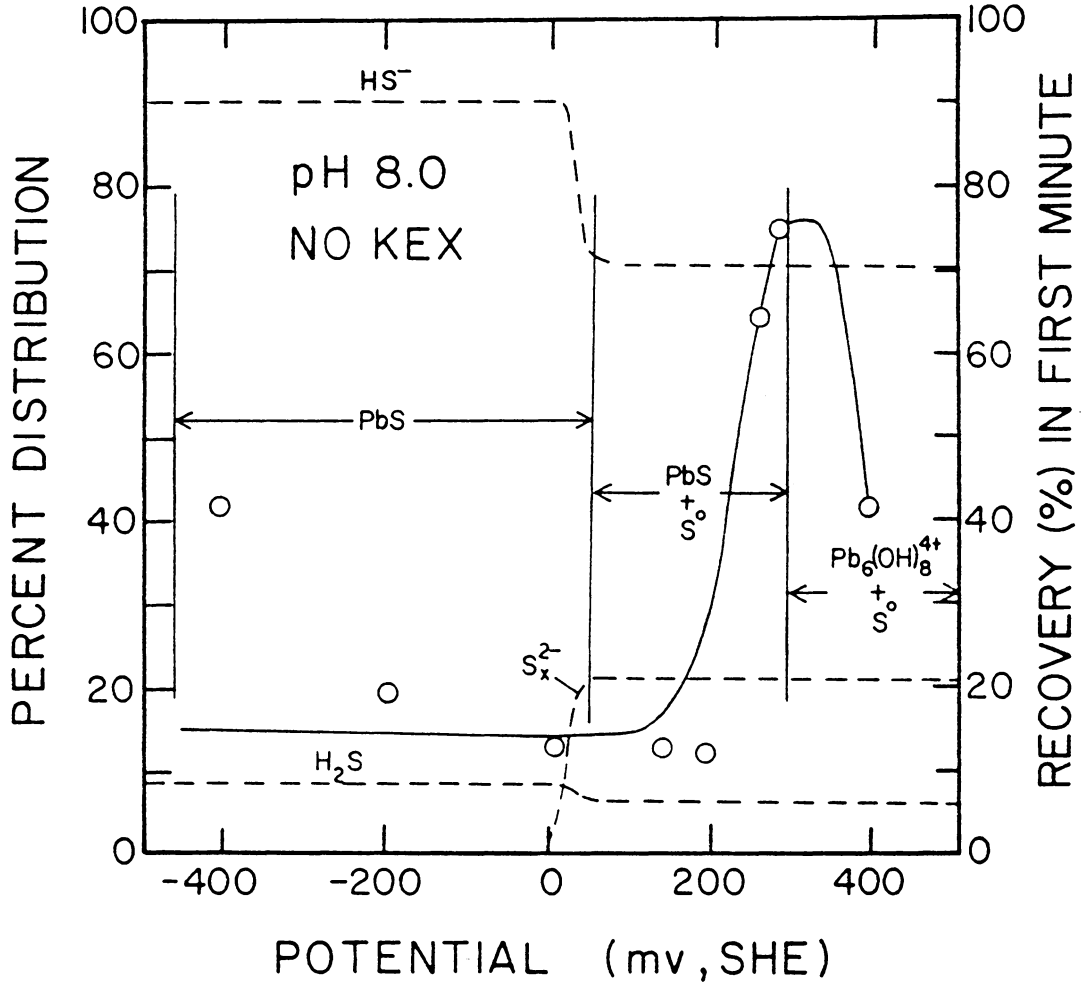


Figure 2.15 Comparison of the effect of E_h at pH 8.0 on the natural floatability of galena (—o—) and the percent distribution (---) of various sulfur-bearing species from the calculations of Case III. The flotation data are reproduced from Guy and Trahar (1984). The solid vertical lines show the upper and lower potential limits of the stability for the indicated phases.

make the mineral surface more hydrophilic. One difficulty with this explanation is that hydrophobic elemental sulfur is still present.

Another possible explanation for the drop in recovery stems from the experimental findings of Gardner and Woods (1979) that thiosulfate becomes increasingly favored over sulfur as an oxidation product at higher potentials. However, on the basis of the E_h-pH diagram for Case II (Figure 2.6), thiosulfate should have already become predominant at a potential as low as approximately -160 mv. This discrepancy is evidence of the existence of an overpotential associated with the formation of thiosulfate, which, of course, cannot be taken into account by thermodynamics.

Guy and Trahar (1984) also carried out a set of experiments that were identical to those mentioned above, with the exception that they also added 10^{-2} M Na_2S while the mineral mixture was being ground. Since such a high level of sulfide was added, a fair comparison cannot be made between the flotation results and those of the calculations that have been discussed to this point (which are based on a 1:1 lead-to-sulfur stoichiometry for the entire system). Consequently, a specific series of calculations for this situation was undertaken.

The voltammetric studies of Hamilton and Woods (1984) on a galena electrode indicate that in the presence of 10^{-4} M HS^-, these ions dominate the electrode reactions and that the mineral surface acts only as an electrocatalyst. Therefore, only the sulfur-water system was considered in this new set of calculations. As before, the computations were performed within the constraint that the total amount of material,

whether it be soluble or insoluble, in the system is fixed (in this case, 10^{-2} M). Two cases are considered: i) oxidation proceeds as far as the formation of elemental sulfur and ii) oxidation proceeds only as far as the formation of polysulfides.

The results are superimposed with the flotation data of Guy and Trahar in Figures 2.16 and 2.17. Comparison of the flotation recoveries in the absence and in the presence of sodium sulfide (See Figures 2.15 and 2.16) shows that this reducing agent shifts the lower flotation edge in the negative direction, but does not alter the upper limit. Hamilton and Woods (1984) observed a similar effect on the potential at which anodic current begins to flow during their voltammetry experiments. It is also evident that the potential where HS^- ions disappear and elemental sulfur (Figure 2.16) and polysulfides (Figure 2.17) appear coincides very closely with where flotation begins. As in the previous case, thermodynamics reasonably predicts the conditions for the onset of flotation, but not the suppression with further oxidation. It is also impossible to determine whether the presence of sulfur or polysulfides on the mineral surface renders galena floatable on the basis of these calculations.

Interpretation of rest potential data by means of thermodynamics may or may not be valid depending on the reversibility of the system in question. The measured open-circuit potential may correspond to the mixed potential of irreversible anodic and cathodic reactions proceeding at the same rate. In this case, it is not a thermodynamic property. This is particularly true when the rest potentials of sulfide electrodes

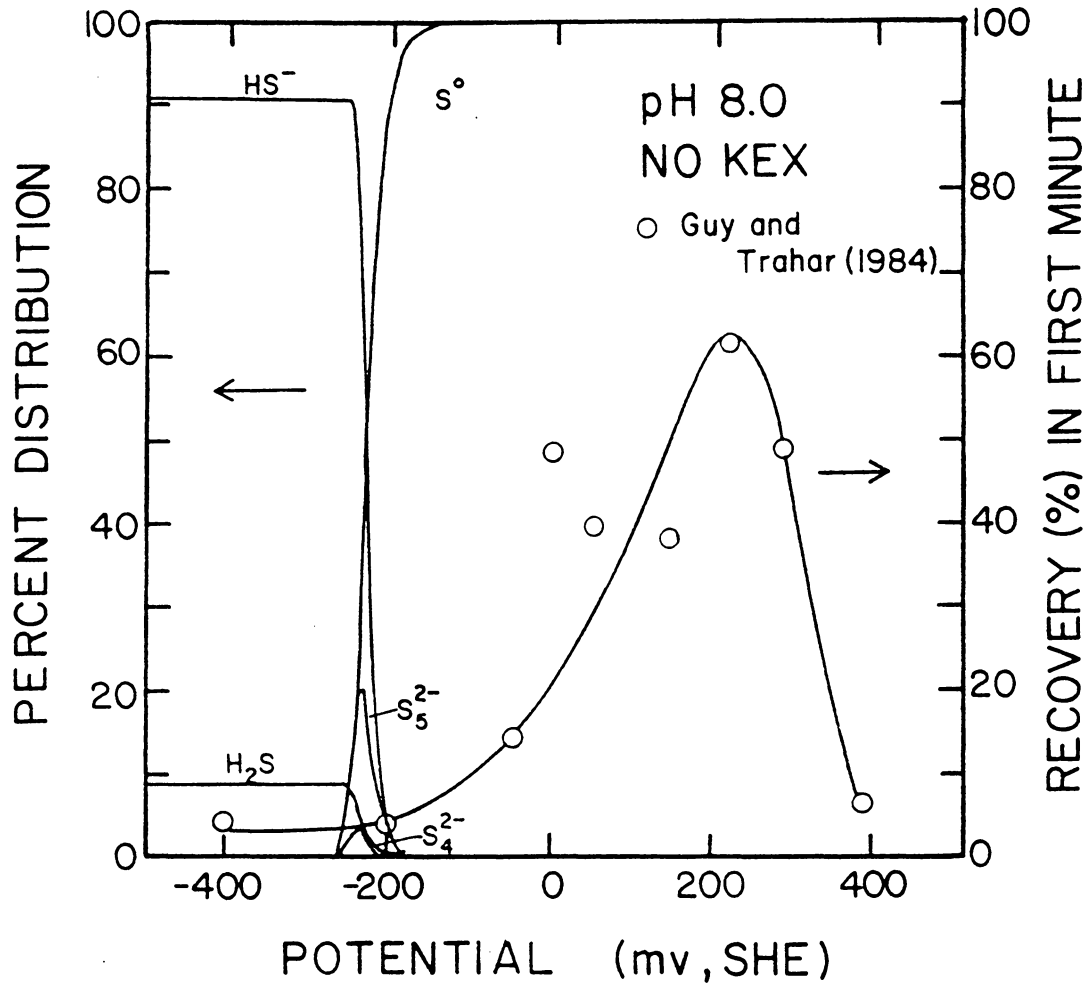


Figure 2.16 Comparison of the effect of E_h at pH 8.0 and a 10^{-2} M Na_2S addition on the floatability of galena (—o—) and the calculated percent distribution (——) of various sulfur-bearing species. The flotation data are reproduced from Guy and Trahar (1984). The calculations are based on the assumption that oxidation can proceed as far as the formation of S°.

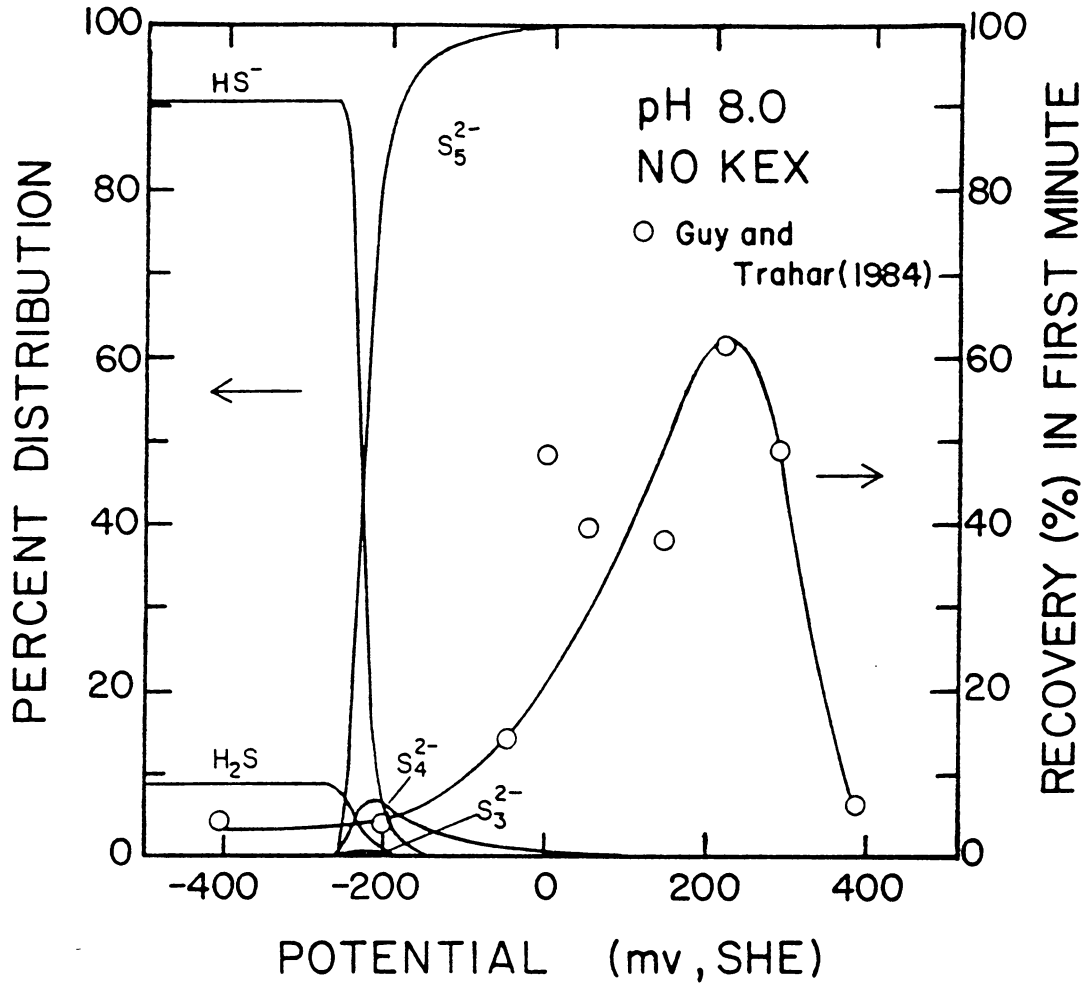


Figure 2.17 Comparison of the effect of E_h at pH 8.0 and a 10^{-2} M Na_2S addition on the floatability of galena (—o—) and the calculated percent distribution (——) of various sulfur-bearing species. The flotation data are reproduced from Guy and Trahar (1984). The calculations are based on the assumption that oxidation can proceed only as far as the formation of polysulfide.

are measured in solutions containing dissolved oxygen. In such a system, oxygen reduction, i.e.,

$$O_2 + 2H_2O + 4e \longrightarrow 4OH^- \text{ (in alkaline media)} \qquad [2.43]$$

readily occurs and the resulting electrode potential can be a mixed potential between this reaction and the oxidation of the mineral (e.g., reaction [2.37]). However, the rest potential for a reversible system should correspond to the equilibrium potential of the potential-determining reaction. A comparison of measured rest potentials with Nernst potentials can be used as an indicator of the reversibility of the system, provided that the potential-determining reaction is known.

Several rest potential studies on the galena-water system have been reported and show a wide distribution of results. Using freshly polished galena electrodes in deoxygenated solutions, Tolun and Kitchener (1964) found a value of -380 mv at pH 9.1, Yarar et al. (1969) measured -260 mv at pH 9.2, and Toperi and Tolun (1969) observed -80 mv at pH 8.0. One would expect these values to fall in a domain on the E_h-pH diagram in which PbS is still stable. Matching them with the diagram for Case I in Figure 2.2, one can see that the first two fall in the PbS stability region, whereas the latter lies in the $PbSO_4$ domain. On the other hand, all three are found in the PbS domain in Cases II and III (Figures 2.6 and 2.11). This difference is consistent with the previous discussion that oxidation of galena in neutral and alkaline pH solutions involves the formation of S^o and $S_2O_3^{2-}$, but not SO_4^{2-}.

2.4.2 Reduction of Galena

Since Cases I, II, and III only differ with regard to the highest oxidation state that sulfur can attain, they are identical when the reduction of galena is considered. As mentioned previously, the mineral is reduced according to reactions [2.19, [2.20] and [2.21], depending on the pH. Relatively little work has been reported in the literature concerning this aspect of galena chemistry. For the most part, galena reduction has been found to obey the behavior predicted by thermodynamics. Brodie (1969) cathodically polarized a galena electrode immersed in a 1 M $HClO_4$ solution (pH 0) and found that the stoichiometry of the resulting reduction reaction agreed with that of the expected reaction [2.19]. Furthermore, a cathodic current began to flow at a potential of about -350 mv, which is close to the $PbS/Pb^{o}+PbS$ boundary line in Figure 2.2.

More recently, Nicol et al. (1978) obtained linear sweep voltammograms and polarization curves on a rotating PbS disk electrode over the entire pH range from 0 to 14. Their data was consistent with what was expected for reactions [2.19], [2.20] and [2.21] (i.e., the shift in the potential at which cathodic current began to flow with increasing pH was in agreement with the thermodynamic predictions).

2.4.3 Relation Between Solution Chemistry and Electrokinetics of the Galena-Water System

When a partially soluble mineral is immersed in water, hydroxo-complexes $M(OH)_n^{z-n}$ are generated in solution. One of the mechanisms that has been proposed (Parks and deBruyn, 1962; Parks, 1965, 1967) to

explain the origin of the surface charge that is generated on the mineral surface when it is immersed involves the adsorption of these complexes from solution. Assuming that the surface reactivities of the various species are equal, then it follows that the isoelectric point of the solution (i.e., the situation when the net charge of the positive complexes is equal to that of the negative complexes) and, hence, point-of-zero charge (pzc) of the oxide correspond to the point of minimum solubility of the solid.

Principally because the adsorption of collectors, such as xanthates or dithiophosphates, onto sulfides has generally been considered to involve chemisorption, relatively little work has been done in studying the electrokinetics of these systems. Healy and Moignard (1976) have published the most extensive review of the literature in this area. They reported a number of studies done on galena, using microelectrophoresis and electro-osmosis as the experimental techniques. With only one exception, the point of zero zeta-potential was found in all the studies to occur at a pH in the vicinity of 3.0, although very little information concerning the conditioning of the samples was given. In the absence of specific adsorption of foreign ions, the point of zero zeta-potential (also called the iso-electric point of solid) corresponds to the pzc.

In order to evaluate how well the minimum solubility theory applies in the prediction of the pzc for galena, the pH corresponding to a minimum in the total concentration of dissolved lead-bearing species for a given E_h has been determined from the thermodynamic calculations for

Case III. The results have been superimposed on the E_h-pH diagram in Figure 2.18. As is evident, the behavior of the minimum solubility is rather complex and often follows some of the phase changes. Under reducing conditions, the minimum occurs over a range of pH values between 0 and 6. At approximately -500 mv, it jumps to pH 8.8, as indicated by the dashed line, and remains there as the E_h increases within the PbS stability domain. A further increase in the potential causes the oxidation of galena to begin and the iep at the solution to drop again to between 0 and 6.2 until $E_h \sim 300$ mV is reached. At this point, the pH of minimum solubility rises abruptly to a value of 11, where S^o and Pb_3O_4 are the stable solid phases. It decreases once again above 460 mv, closely following the boundary lines between PbO_3^{2-} and the dissolved Pb(II) species (the boundary lines are not shown on this diagram, but are on the E_h-pH diagram in Figure 2.11).

As discussed previously, Gardner and Woods (1979b) concluded from their voltammetry work that reaction [2.13] is the primary oxidation reaction up to a pH of at least 6.8. In many of the studies compiled by Healy and Moignard (1976), little attention was paid to preventing or controlling the oxidation of galena. It is quite possible, therefore, that the particles were being oxidized according to reaction [2.13], while the electrophoretic measurements were being made. On the basis of what is shown in Figure 2.18, the observed point of zero zeta-potential of 3.0 falls within the region of minimum solubility that is predicted when this reaction is occurring.

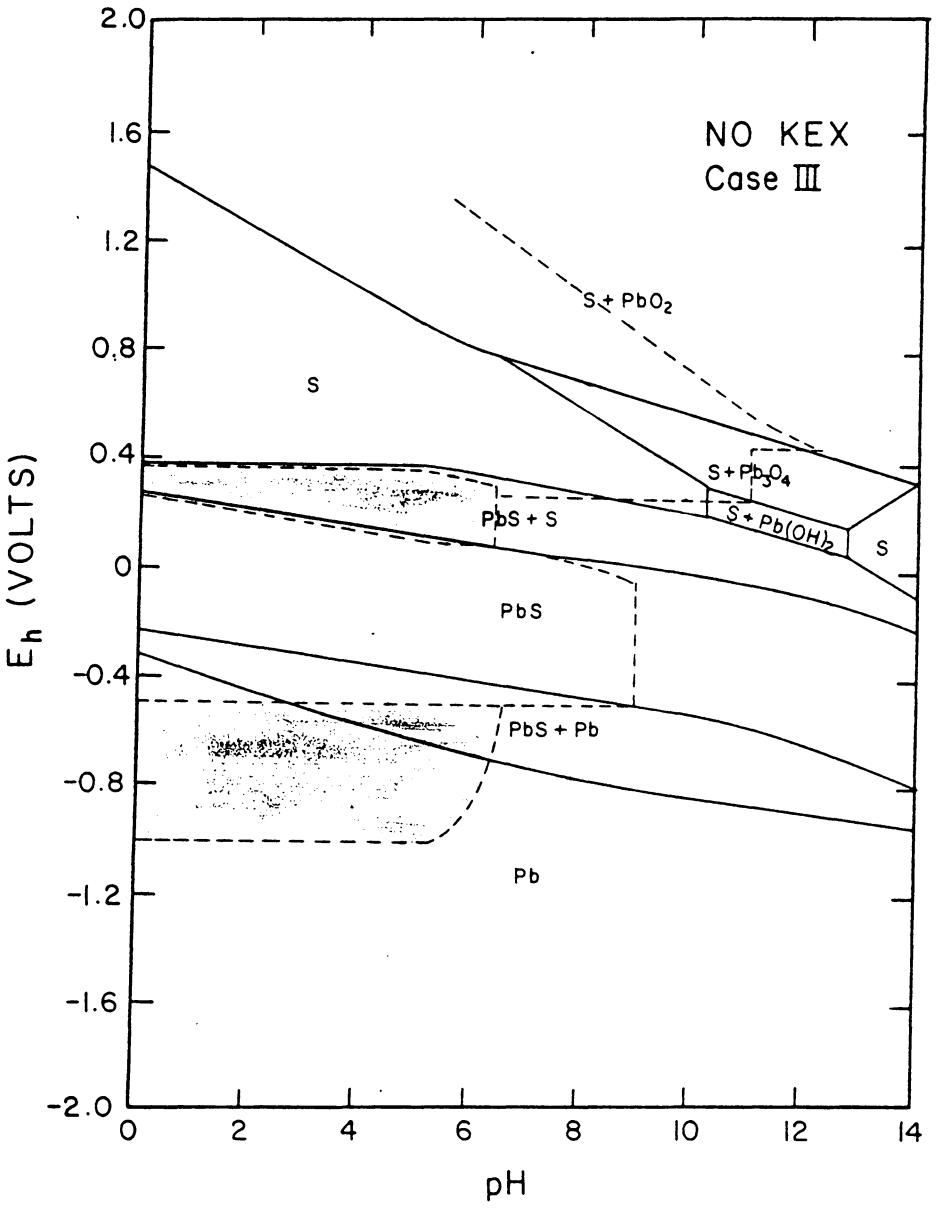


Figure 2.18 E_h-pH diagram showing the regions of minimum lead solubility (---) calculated for Case III in the absence of collector. The solubility remains constant at a minimum over a range of E_h and pH values in the two shaded regions.

Moignard et al, (1977) have determined the point of zero zeta-potential of elemental sulfur to occur at pH 2.0, which is close to the experimental points of zero zeta-potential of galena. This correspondence may suggest that elemental sulfur is an oxidation product of the mineral. A similar argument has been used by Moignard et al. (1977) to explain their electrokinetic data for ZnS and NiS. The fact that a pzc of pH 3.0 recurs again and again for these and most other sulfides (Healy and Moignard, 1976) lends support to the notion that it is due to the presence of elemental sulfur (which is an oxidation product on most sulfides).

2.4.4 Effect of E_h, pH, and Xanthate Addition on the Formation of PbX_2 and X_2

Although an E_h-pH diagram does yield useful information concerning the conditions under which a particular phase is stable, it does not say anything about how much of that phase there is. One advantage of the way in which these calculations have been done is that the weight of the solid phase(s) present is a direct output of the computations. In order to relate the thermodynamics of the flotation behavior of the galena-ethyl xanthate system, it will be interesting to look at how E_h, pH and xanthate concentration affect the amount of PbX_2 that is produced.

The quantity chosen to represent this is the percentage of the number of moles of KEX initially added that ends up as PbX_2:

$$\% PbX_2 = 2n_{PbX_2}/N_X \times 100\%$$

$$= 2(N_X - [X^-] - [HX] - 2[X_2(aq)])/N_X \times 100\%. \quad [2.44]$$

Since PbX_2 is considered to be the reaction product that renders a sulfide mineral hydrophobic, this quantity may be directly correlated with flotation results.

a. Effect of E_h: In Figures 2.19-2.28, % PbX_2 is plotted as a function of E_h at various pH values for KEX additions of 10^{-7}, 10^{-6}, 10^{-5}, and 10^{-4} M in Cases I, II and III. The general shapes of the curves are similar to those that have been observed experimentally by others (Heyes and Trahar, 1977; Gardner and Woods, 1979a; Luttrell and Yoon, 1982; Walker and Richardson, 1982) regarding the effect of potential (applied or open-circuit) on the floatability of sulfides with and without collector. As the potential is raised, % PbX_2 rises abruptly at a critical potential to a maximum, remains at this level for a certain interval, and then sharply drops to zero at another critical potential. As mentioned previously, the upper potential limit can be attributed to the decomposition of PbX_2, e.g.,

$$PbX_2 \longrightarrow Pb^{2+} + X_2(aq) + 2e \quad [2.32]$$

at low pH. It should be noted that when the KEX addition exceeds 2×10^{-5} M, $X_2(l)$ is formed under oxidizing conditions and can once again render flotation possible (see E_h-pH diagrams).

Other trends common to the three cases can be noted. As the xanthate concentration is raised, the maximum % PbX_2 attained increases

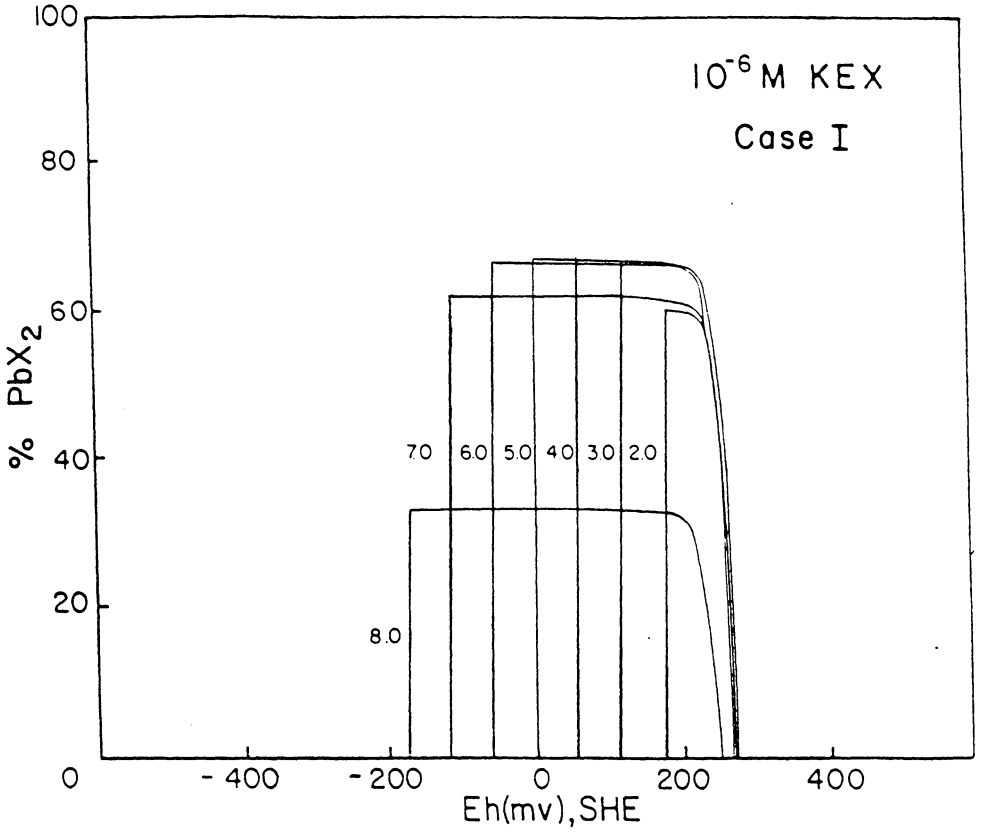


Figure 2.19 Effect of E_h on % PbX_2 for Case I and a collector addition of 10^{-6} M KEX. The number next to each curve denotes the pH.

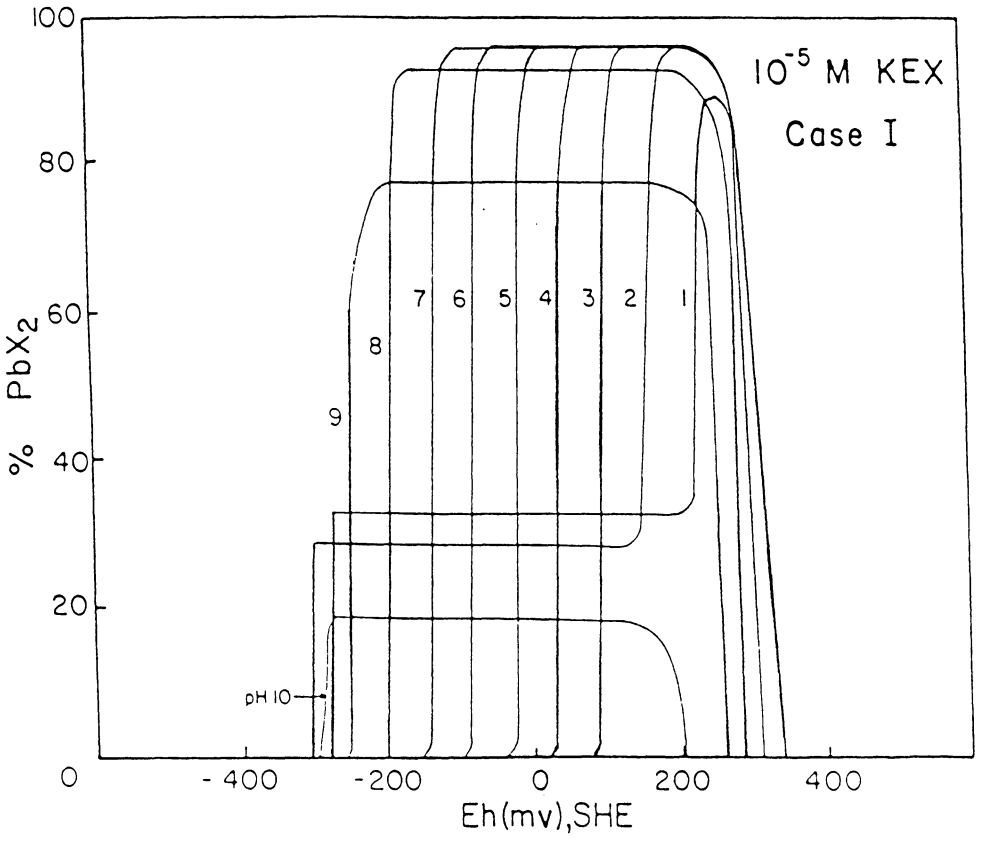


Figure 2.20 Effect of E_h on % PbX_2 for Case I and a collector addition of 10^{-5} M KEX. The number next to each curve denotes the pH.

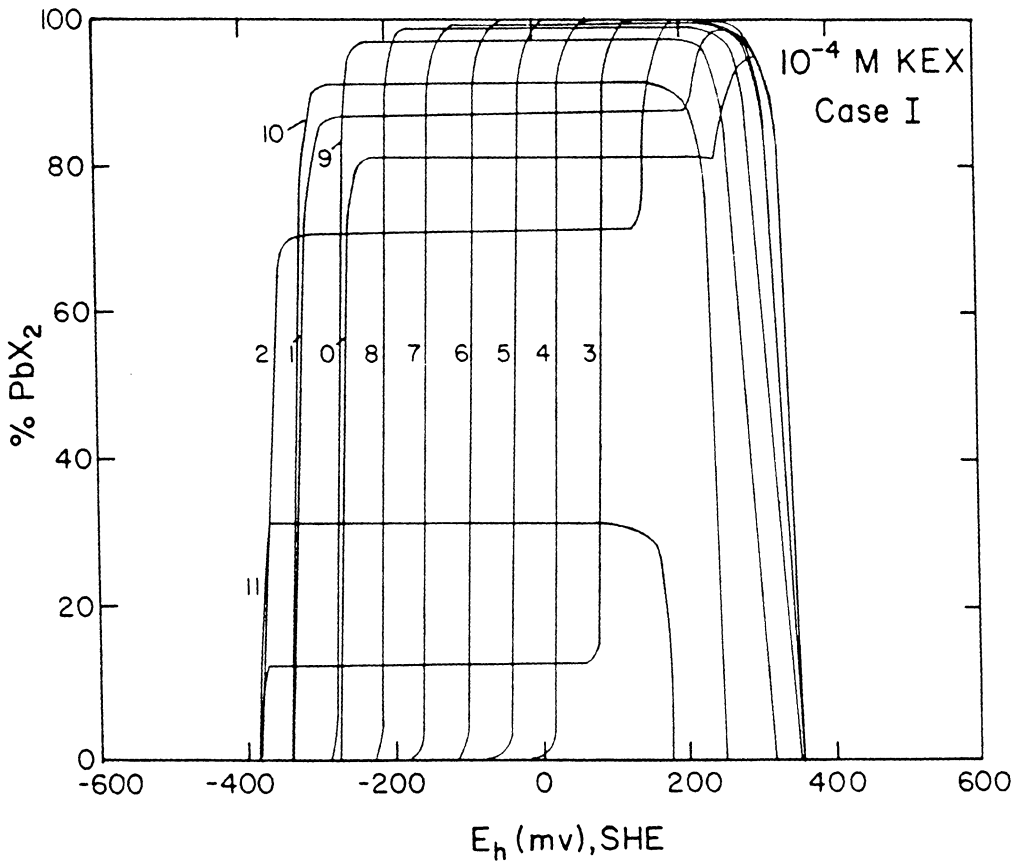


Figure 2.21 Effect of E_h on % PbX_2 for Case I and a collector addition of 10^{-4} M KEX. The number next to each curve denotes the pH.

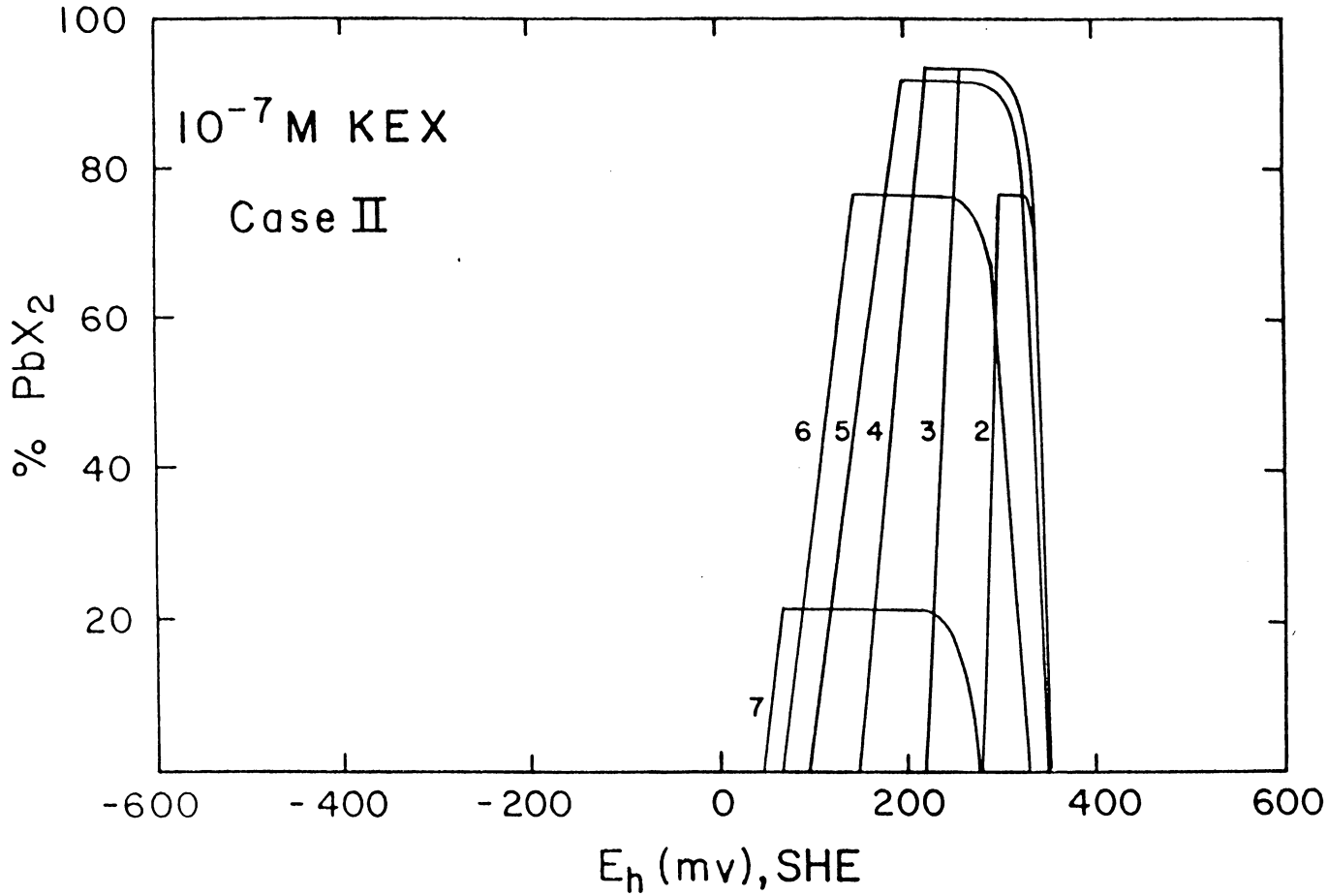


Figure 2.22 Effect of E_h on % PbX_2 for Case II and a collector addition of 10^{-7} M KEX. The number next to each curve denotes the pH.

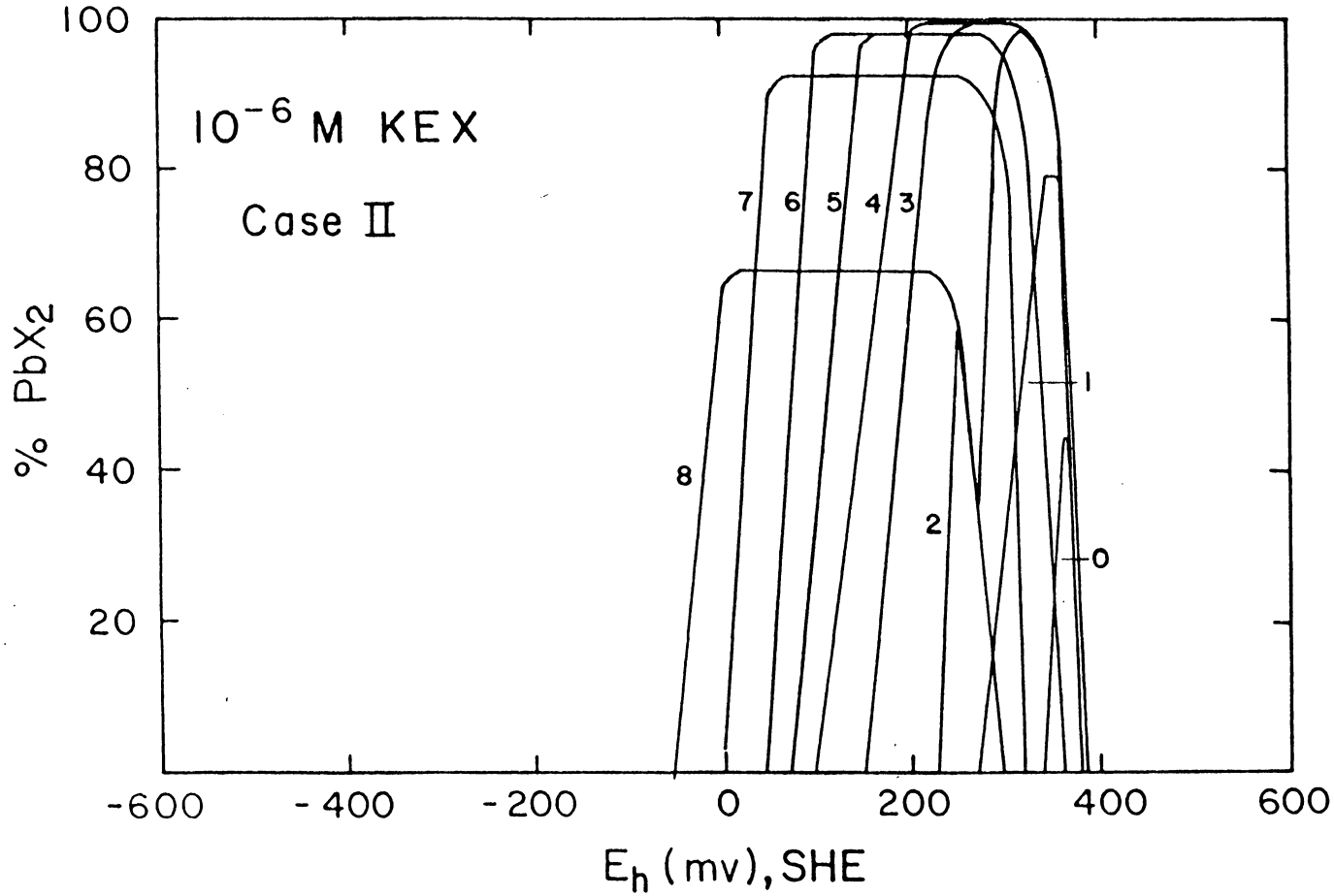


Figure 2.23 Effect of E_h on % PbX_2 for Case II and a collector addition of 10^{-6} M KEX. The number next to each curve denotes the pH.

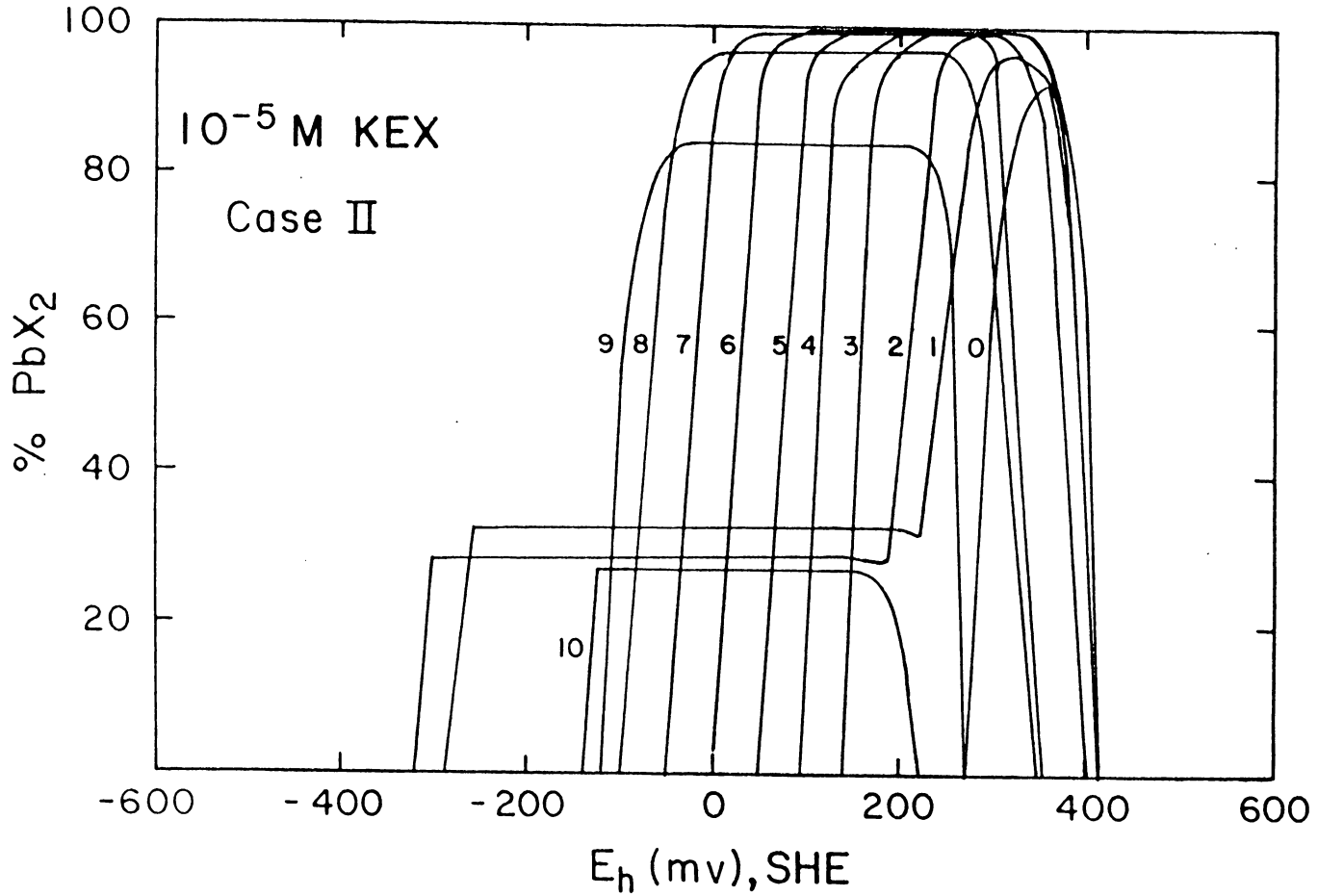


Figure 2.24 Effect of E_h on % PbX_2 for Case II and a collector addition of 10^{-5} M KEX. The number next to each curve denotes the pH.

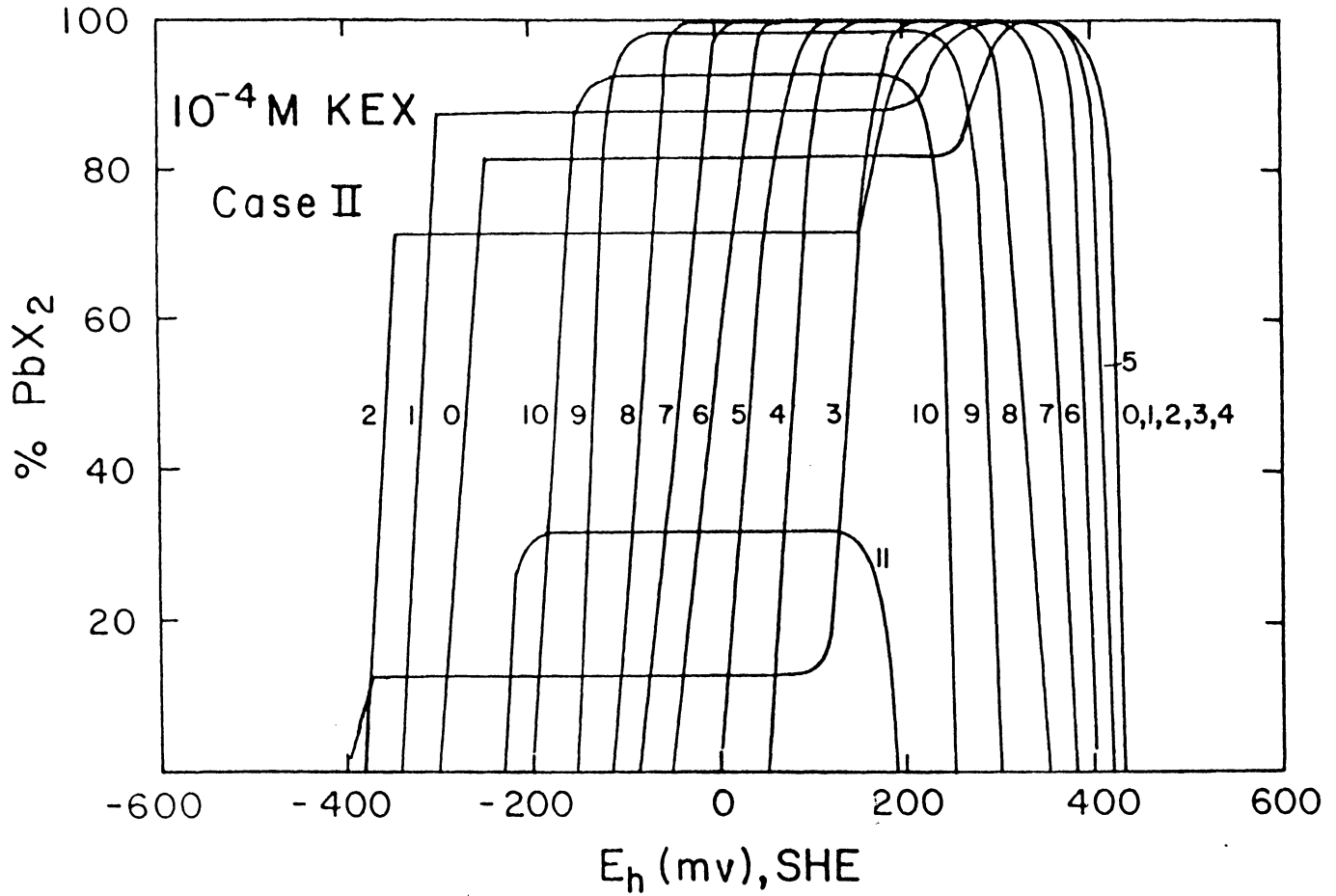


Figure 2.25 Effect of E_h on % PbX_2 for Case II and a collector addition of 10^{-4} M KEX. The number next to each curve denotes the pH.

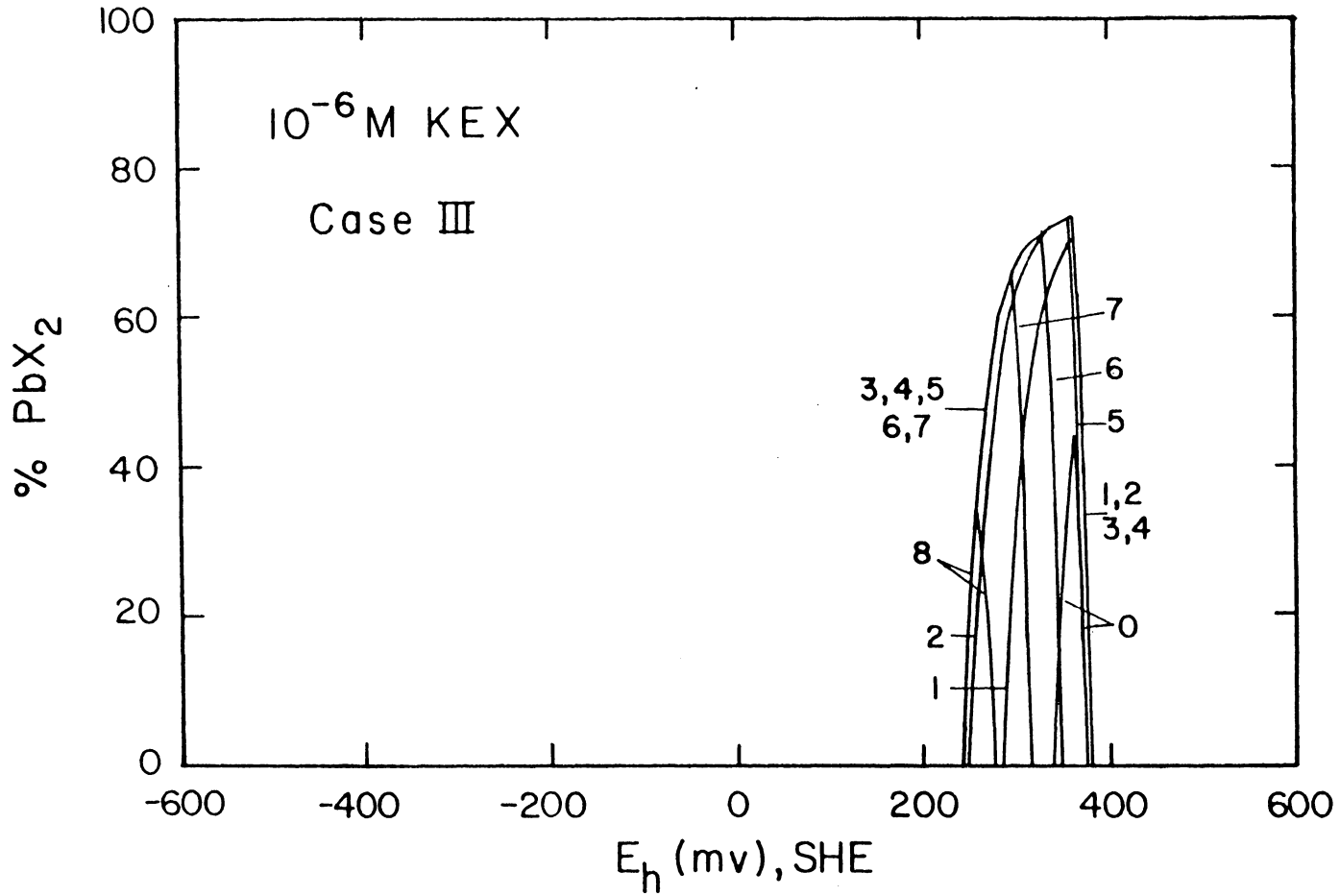


Figure 2.26 Effect of E_h on % PbX_2 for Case III and a collector addition of 10^{-6} M KEX. The number next to each curve denotes the pH.

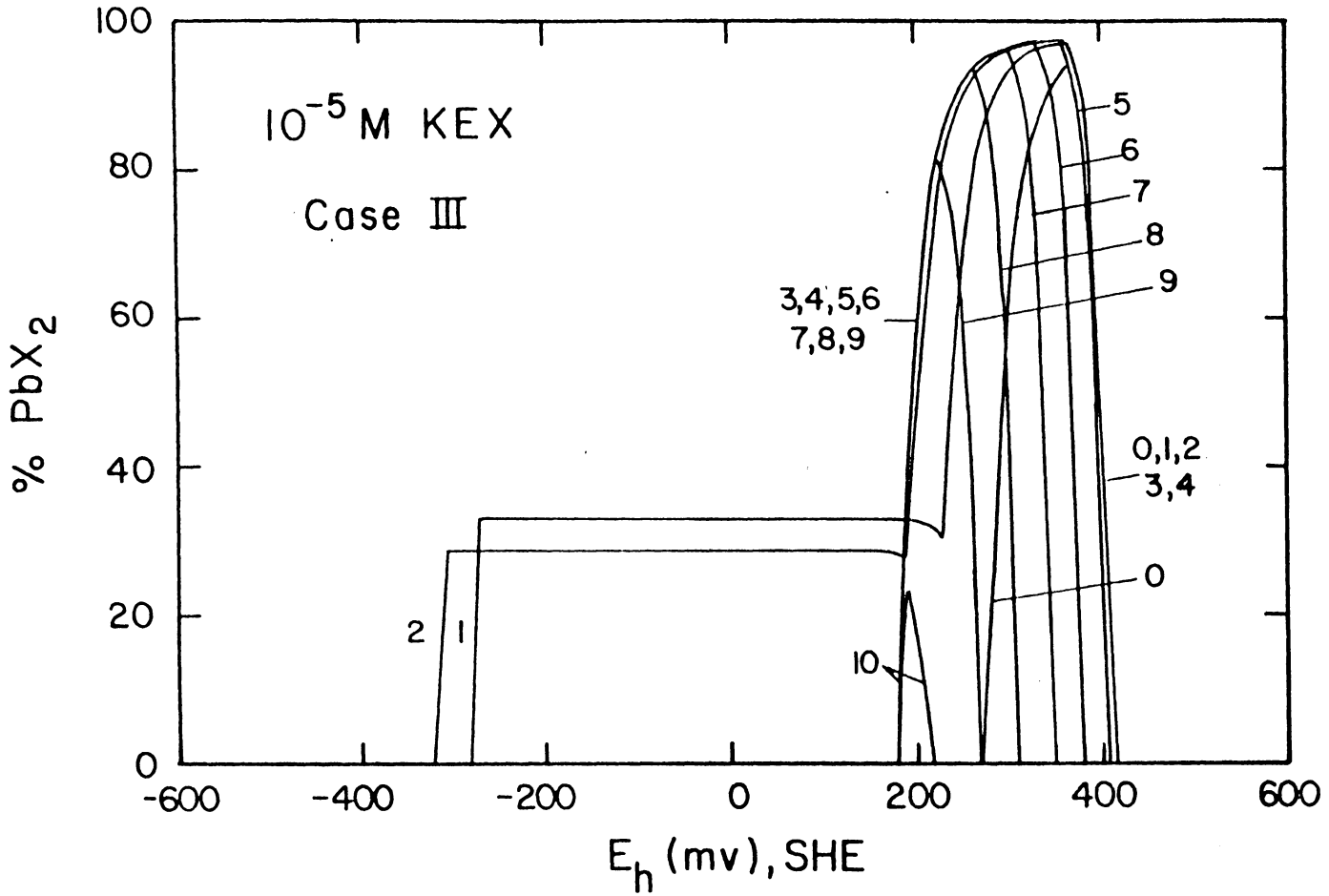


Figure 2.27 Effect of E_h on % PbX_2 for Case III and a collector addition of 10^{-5} M KEX. The number next to each curve denotes the pH.

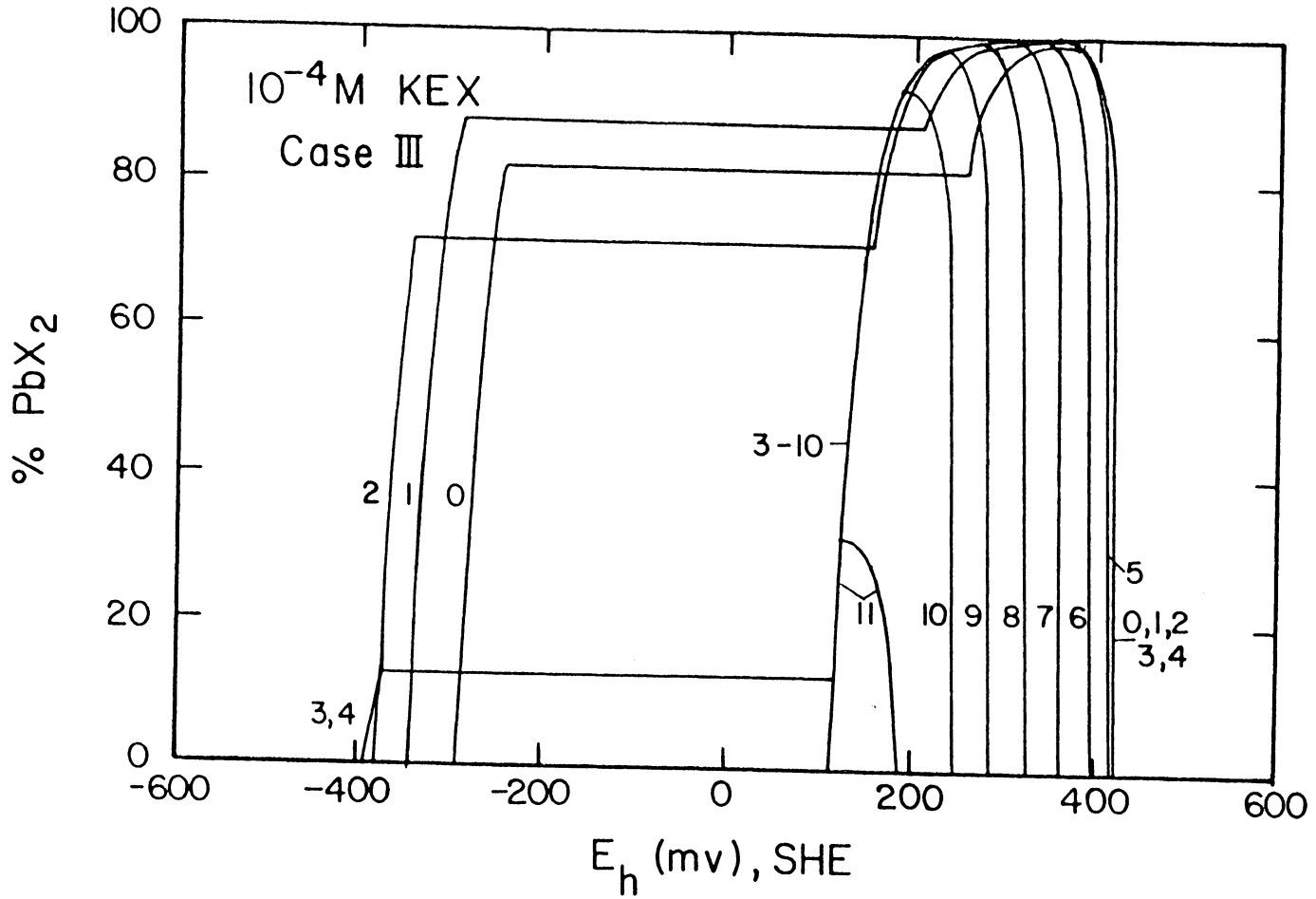


Figure 2.28 Effect of E_h on % PbX_2 for Case III and a collector addition of 10^{-4} M KEX. The number next to each curve denotes the pH.

and the stability range extends over a wider potential region at a given pH. Increasing the pH also enlarges the stability range until a pH of about 8 is reached, whereupon it begins to narrow.

Comparison of the calculations for the three cases shows that for 10^{-6} and 10^{-5} M KEX, in particular, the % PbX_2 is higher in Case II than in the other two. In addition, the stability range tends to be wider. This is due to the fact that the solubility of galena is higher in Case II so that the amount of xanthate required for PbX_2 to precipitate is lower.

Also, the PbX_2 stability range is extended to a higher potential in Cases II and III than in Case I. In the vicinity of the upper potential limit, $PbSO_4$ controls the solubility of the system in Case I, whereas all the lead-bearing species are dissolved in the other two. This reduces the amount of Pb^{2+} ions present in Case I compared to that of Case II and III and, therefore, the point where the xanthate requirement for the formation of PbX_2 cannot be met occurs at a lower potential.

In Figure 2.29, the results of the thermodynamic calculations for Cases I, II, and III are compared with the experimental data reported by Guy and Trahar (1984) for the batch flotation of a synthetic mixture of galena and quartz. Values of % PbX_2 are plotted as a function of E_h for a collector addition of 10^{-5} M KEX and pH 8.0. The flotation tests were conducted at pH 8.0 in a 3-liter modified Denver D-1 cell after adding 2×10^{-5} M KEX and the frother polypropylene glycol (PPG 400). The redox potential of the pulp was adjusted prior to each test by adding either

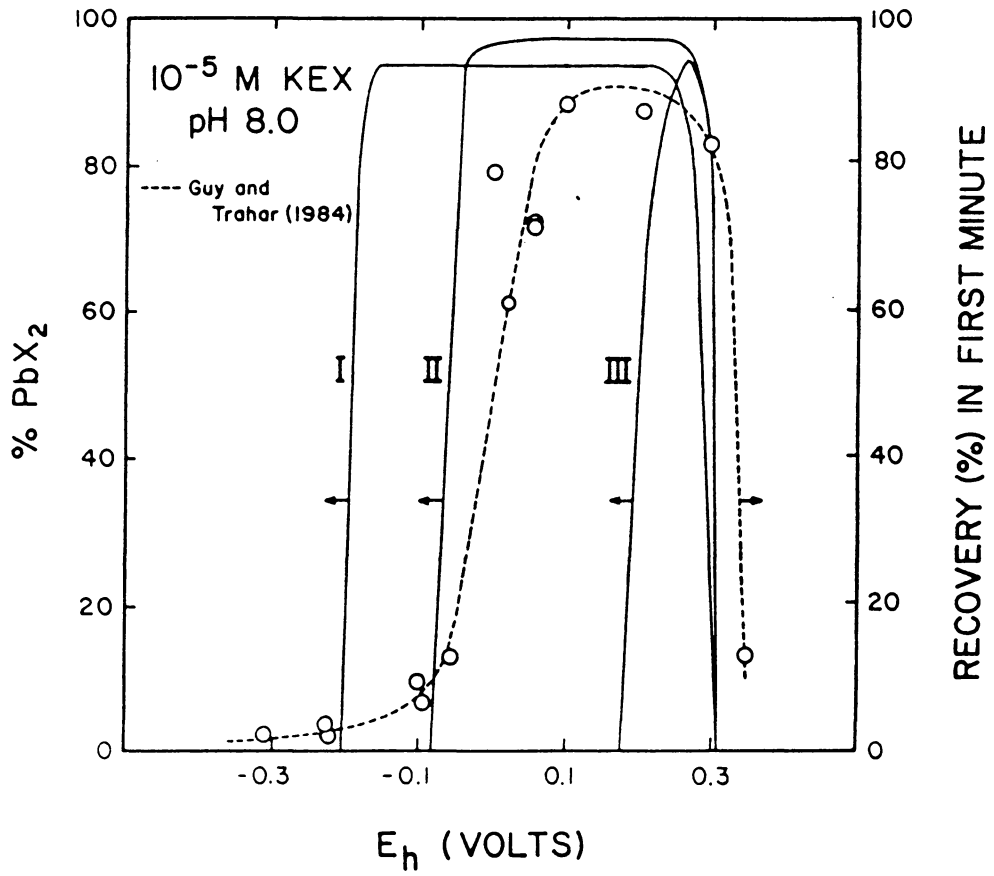


Figure 2.29 Comparison of the effect of E_h on the flotation recovery of galena (—o—) and on % PbX_2 (——) calculated for a collector addition of 10^{-5} M KEX and pH 8.0. The flotation data are the results reported by Guy and Trahar (1984) for a collector level of $2x10^{-5}$ M KEX and pH 8.0. The Roman numeral next to each solid curve denotes the case number.

sodium dithionate or hydrogen peroxide and then monitored with a platinum electrode.

As mentioned previously, the principal electrochemical reactions by which PbX_2 forms in Cases I, II and III are reactions [2.22], [2.31] and [2.39], respectively. The comparison in Figure 2.29 shows that the onset of flotation is most closely correlated to the onset of reaction [2.31] (i.e., Case II), although adsorption by reaction [2.39] (i.e., Case III) may also contribute above 200 mV. On the basis of this, one would conclude that PbX_2 formation occurs primarily by reaction [2.31]. This agrees with what Guy and Trahar (1984) themselves concluded.

However, the results of other studies suggest otherwise. Harris and Finkelstein (1975) used UV-spectrophotometry to study the adsorption of ethyl xanthate on 'sulfided' galena in the presence of oxygen. They found that as long as there were xanthate ions in solution, the thiosulfate peak at 214 nm did not appear. Only when all the xanthate was consumed could it be detected. From this, the authors concluded that thiosulfate was not being formed during the reaction between the collector and galena. As will be shown in Chapter IV, this agrees with the results of the voltammetry experiments at 10^{-3} M KEX.

Although the most widely accepted view (Granville et al., 1972; Allison et al., 1972; Finkelstein and Poling, 1977; Mielczarski et al., 1981) is that PbX_2 is the species responsible for flotation, evidence opposing this conclusion has been reported. Woods (1971) concluded from the results of chronoamperometry and linear sweep voltammetry experiments on a galena electrode immersed in a 9.5×10^{-3} M

KEX solution that the initial xanthate uptake occurs by an anodic chemisorption process:

$$X^- \longrightarrow X_{ads} + e. \qquad [2.45]$$

Gardner and Woods (1977) followed this up with contact angle and microflotation experiments, and observed that dixanthogen renders the mineral strongly hydrophobic but lead xanthate does not. Moreover, they concluded that the initial chemisorbed layer was the most important species for flotation.

Lamache et al. (1984) have recently reported results that dixanthogen is the principal hydrophobic species found on galena. They applied a voltage of 550 mv to 5 grams of a galena powder immersed in a deoxygenated ammonia buffer solution (pH 9.2) containing anywhere from about 3×10^{-4} M to about 2×10^{-3} M KEX. Analysis of the reaction products indicated that xanthate adsorption was occurring by two different processes: i) oxidation of xanthate to dixanthogen (i.e., reaction [2.23]) and ii) oxidation of PbS to S^o and $Pb(OH)_2$, followed by an ion-exchange between the hydroxyl groups in $Pb(OH)_2$ and xanthate anions to form PbX_2 on the surface. Very little thiosulfate was detected in the solution. Moreover, Lamache et al. presented evidence that adsorption by the second mechanism is slower than that by the other. In an electrolysis experiment lasting 2 to 3 hours, there was sufficient time for the ion exchange reaction to occur and, consequently, more PbX_2 than X_2 was formed on the surface. However, when voltammetric tests were carried out on a solid galena electrode in the same solutions, the

results suggested that only reaction [2.23] was occurring. The authors concluded that the duration of this experiment (on the order of one minute or so) was too short for the ion exchange reaction to have proceeded to any appreciable extent.

In considering the work by Lamache et al. (1984) and Gardner and Woods (1977), it is important to point out several important differences in the conditions during their electrochemical experiments and those of the flotation tests by Guy and Trahar (1984). For one thing, the xanthate levels were much higher in the electrochemical tests than in the flotation tests. As will be discussed later (Chapter III), the concentration of xanthate may have a significant effect upon the adsorption mechanism, particularly with respect to its reaction rates. For another, Lamache et al. applied a potential that is approximately 600 mv above the value corresponding to the onset of flotation. Under these conditions, additional adsorption reactions other than the one associated with the onset of flotation at -100 mv may now be possible. For example, it is not surprising that these workers detected dixanthogen on the galena surface, considering that the reversible potentials for reaction [2.23] vary between 100 and 150 mv for the collector levels used in their studies.

Another point concerning both the flotation and the electrochemical studies on galena powder should be stressed. In applying or monitoring the potential of a suspension or bed of particles, it is assumed that the particles attain the same potential as the working electrode (in this case, a platinum wire). Work in our laboratory and in others

(Richardson, 1984; Woods, 1984) has shown that even for a tightly packed bed of galena particles, potential control is difficult. The actual potential on the particle surfaces may vary according to how tightly the bed is packed, the particle size, the solution velocity, etc. Consequently, there may be a significant difference between the applied voltage and what actually exists on the mineral surface. In addition, the potentials reported for a particular system may not correspond to those for another.

Thus, there still exists some uncertainty concerning the identification of the primary xanthate adsorption reaction. What may help resolve this is an experiment in which the potential of a well-behaved packed-bed galena electrode is either controlled or monitored at the same time as the xanthate and thiosulfate concentrations are being measured. If this is followed by a flotation test, then it may be possible to more clearly see the relation between floatability and xanthate adsorption.

Guy and Trahar (1984) also conducted flotation tests on the galena-quartz mixture using 2×10^{-5} M KEX at pH 11.0. Their results, reproduced in Figure 2.30, show that flotation is effective between approximately -100 and 150 mv. Although the pH lies beyond the critical pH of 10.5 for galena flotation determined from the Barsky relationship (and beyond the upper limit of pH 10.2 on the basis of our calculations) (see Figure 2.9), these investigators concluded that xanthate still induces flotation.

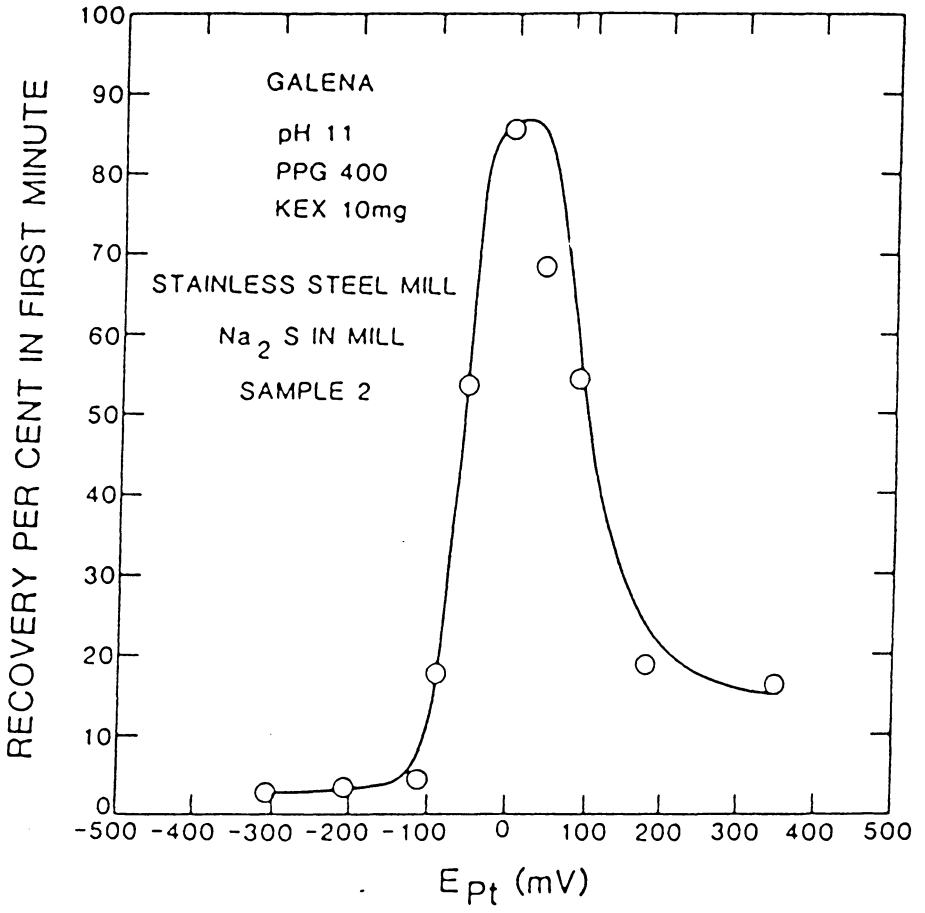


Figure 2.30 Effect of E_h on the flotation recovery of galena at a collector addition of 2×10^{-5} M KEX and pH 11.0 (from Guy and Trahar, 1984).

However, examination of Figure 2.11 may provide an alternative explanation. When the potential is raised to -50 mv, PbS is oxidized to $Pb(OH)_4^{2-}$ and S^o by reaction [2.38]. Gardner and Woods (1979) have shown that not only does S^o form in appreciable amounts at this pH, but that it does so at a faster rate than at pH 1 and 9.2. Possibly it is the presence of S^o on the mineral surface rather than xanthate which renders it hydrophobic. Until a potential of 150 mv is reached, this reaction continues and flotation is still possible. Beyond this, $S_2O_3^{2-}$ rather than S^o may become predominant and so the mineral may no longer be hydrophobic enough to be floated.

b. Effect of pH: The effect of pH on % PbX_2 for various E_h values in Cases I, II and III is shown in Figures 2.31-2.40. At a given potential, % PbX_2 increases abruptly at a critical pH and stays essentially constant until an upper pH limit is reached, whereupon it drops sharply. The upper edge is determined by the competition between xanthate ions and hydroxyl ions for lead. Pb^{2+} ions are not readily hydrolyzed at low and neutral pH so that PbX_2 can form. However, at alkaline pH, hydrolysis becomes predominant. The edge at low pH exists because at those conditions xanthic acid, HX, is the most abundant xanthate-bearing species. Only when the pH is raised so that the reaction,

$$HX \longrightarrow X^- + H^+, \qquad [2.46]$$

is shifted sufficiently to the right that there are enough free xanthate ions present, can PbX_2 become stable.

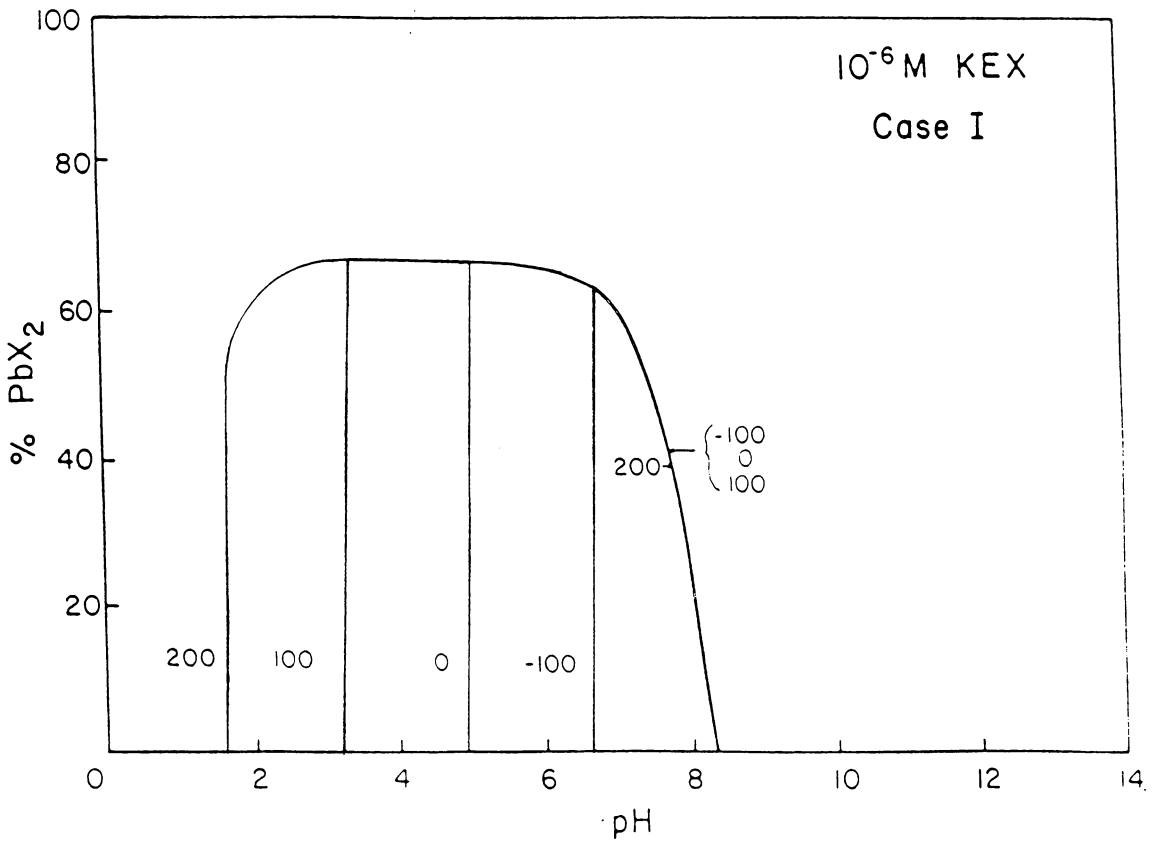


Figure 2.31 Effect of pH on % PbX_2 for Case I and a collector addition of 10^{-6} M KEX. The number next to each curve denotes the E_h (mv).

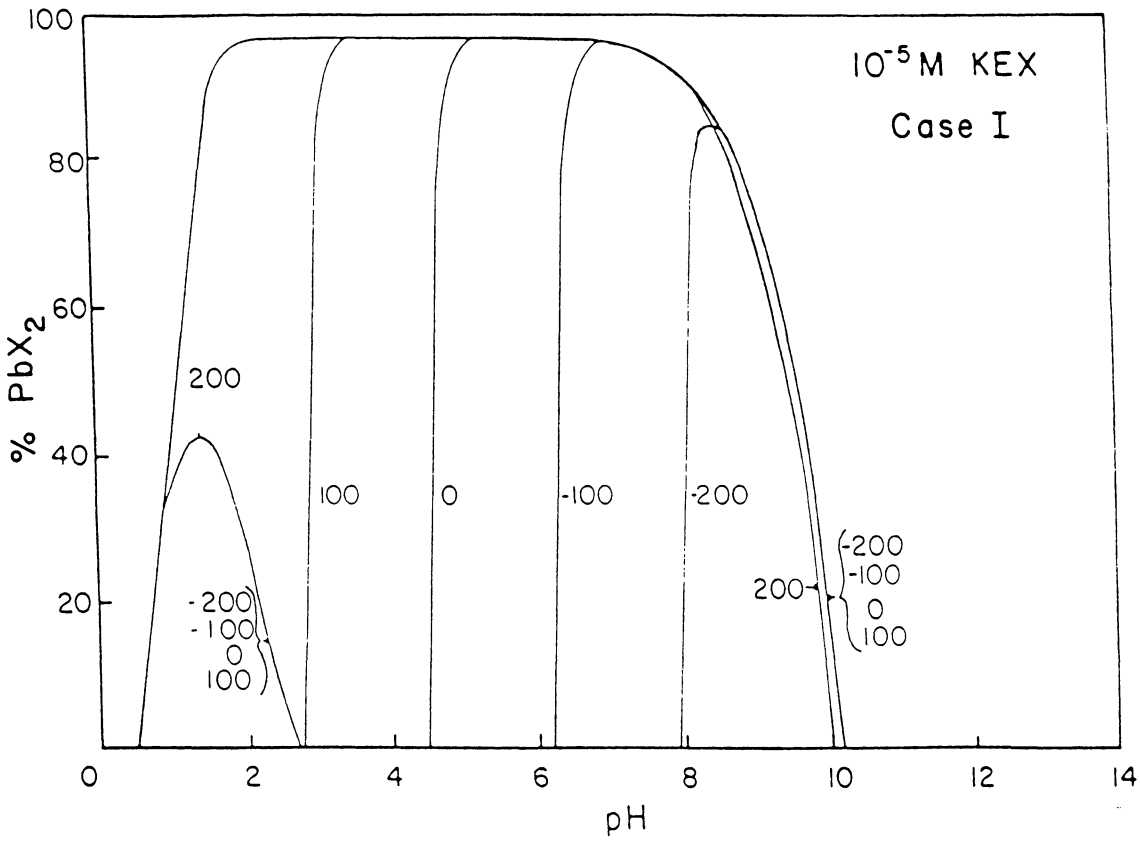


Figure 2.32 Effect of pH on % PbX_2 for Case I and a collector addition of 10^{-5} M KEX. The number next to each curve denotes the E_h (mv).

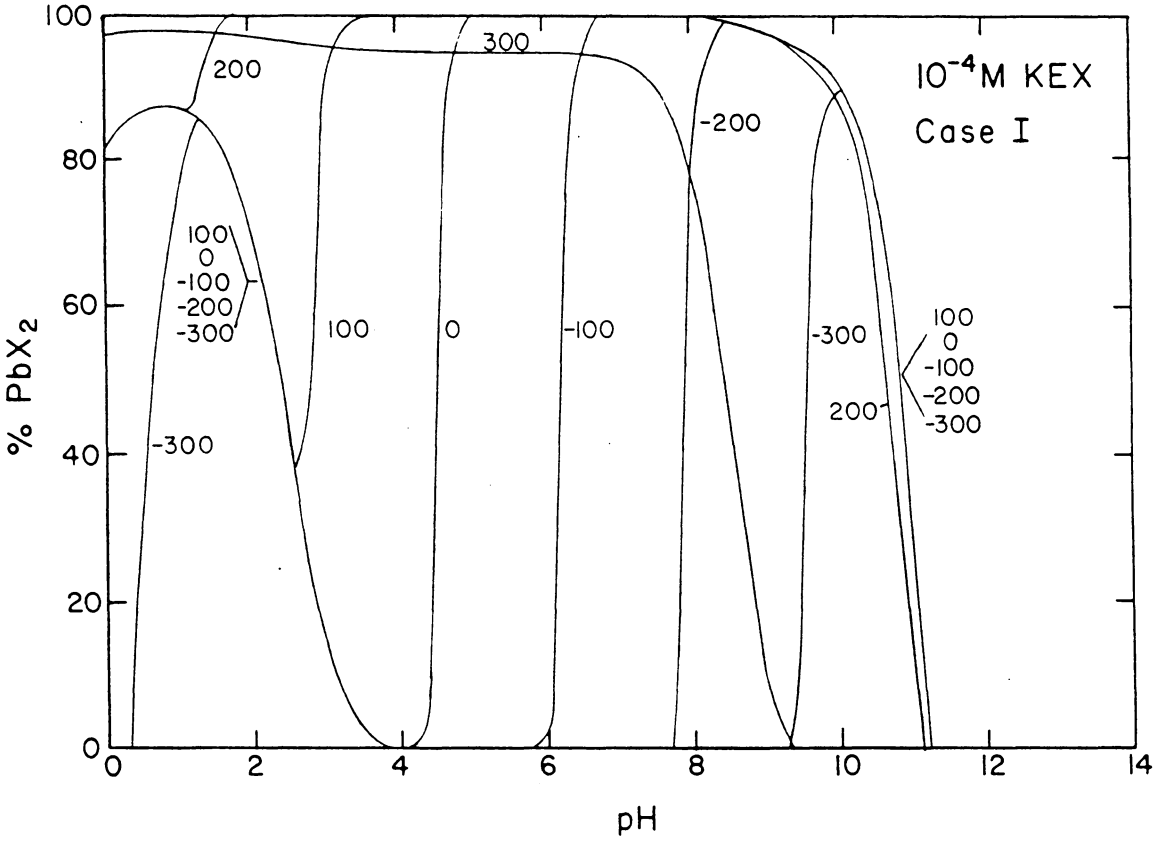


Figure 2.33 Effect of pH on % PbX_2 for Case I and a collector addition of 10^{-4} M KEX. The number next to each curve denotes the E_h (mv).

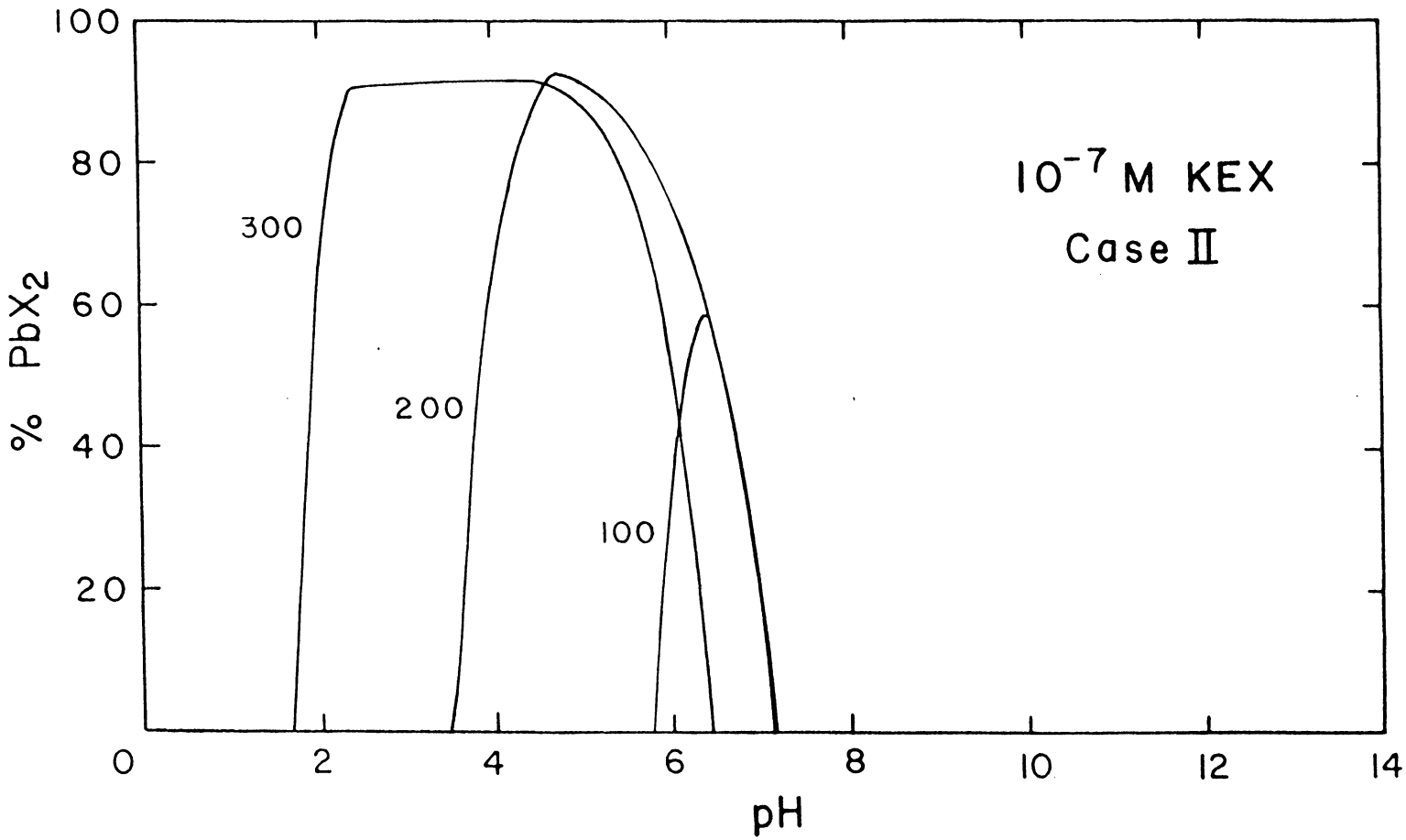


Figure 2.34 Effect of pH on % PbX_2 for Case II and a collector addition of 10^{-7} M KEX. The number next to each curve denotes the E_h (mv).

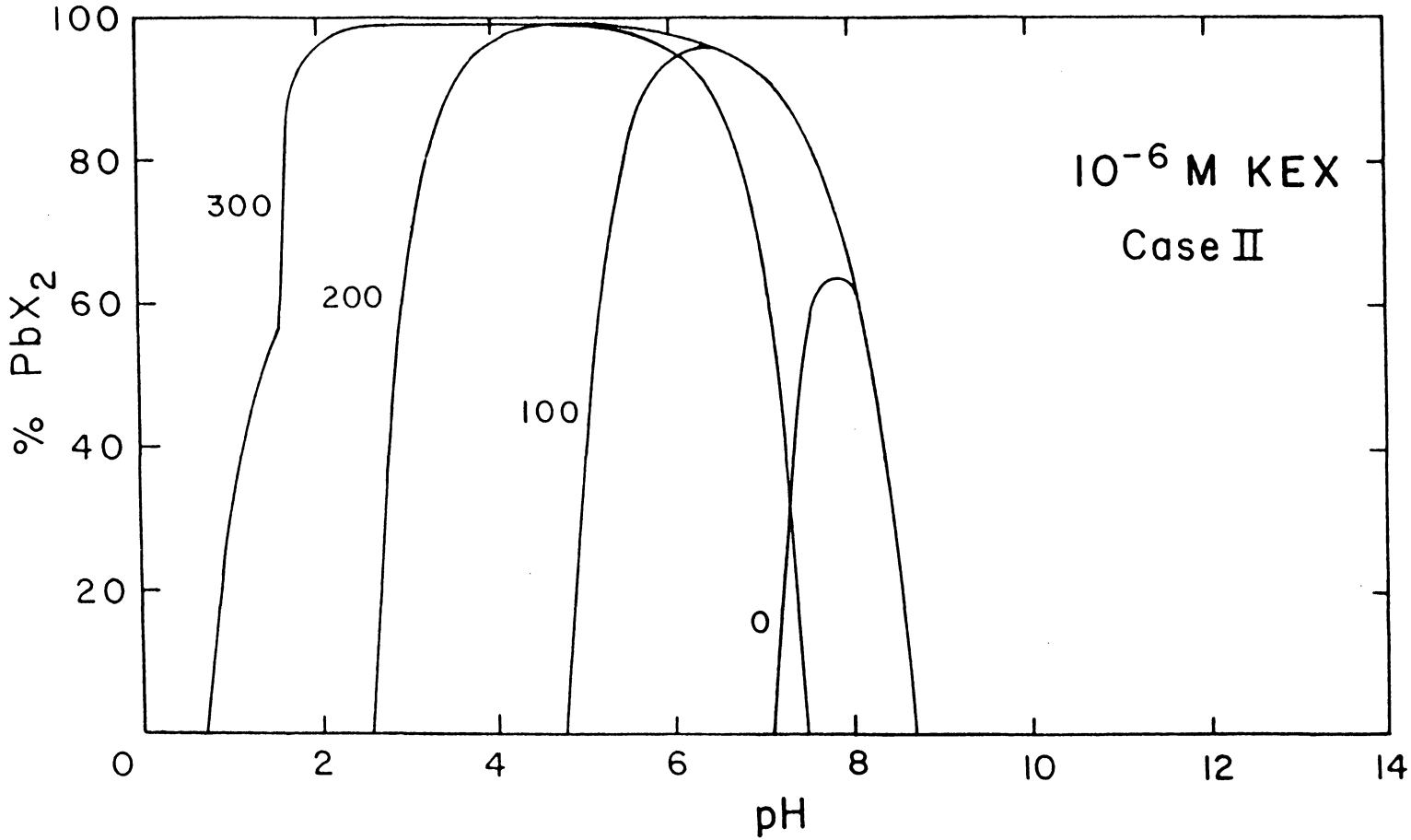


Figure 2.35 Effect of pH on % PbX_2 for Case II and a collector addition of 10^{-6} M KEX. The number next to each curve denotes the E_h (mv).

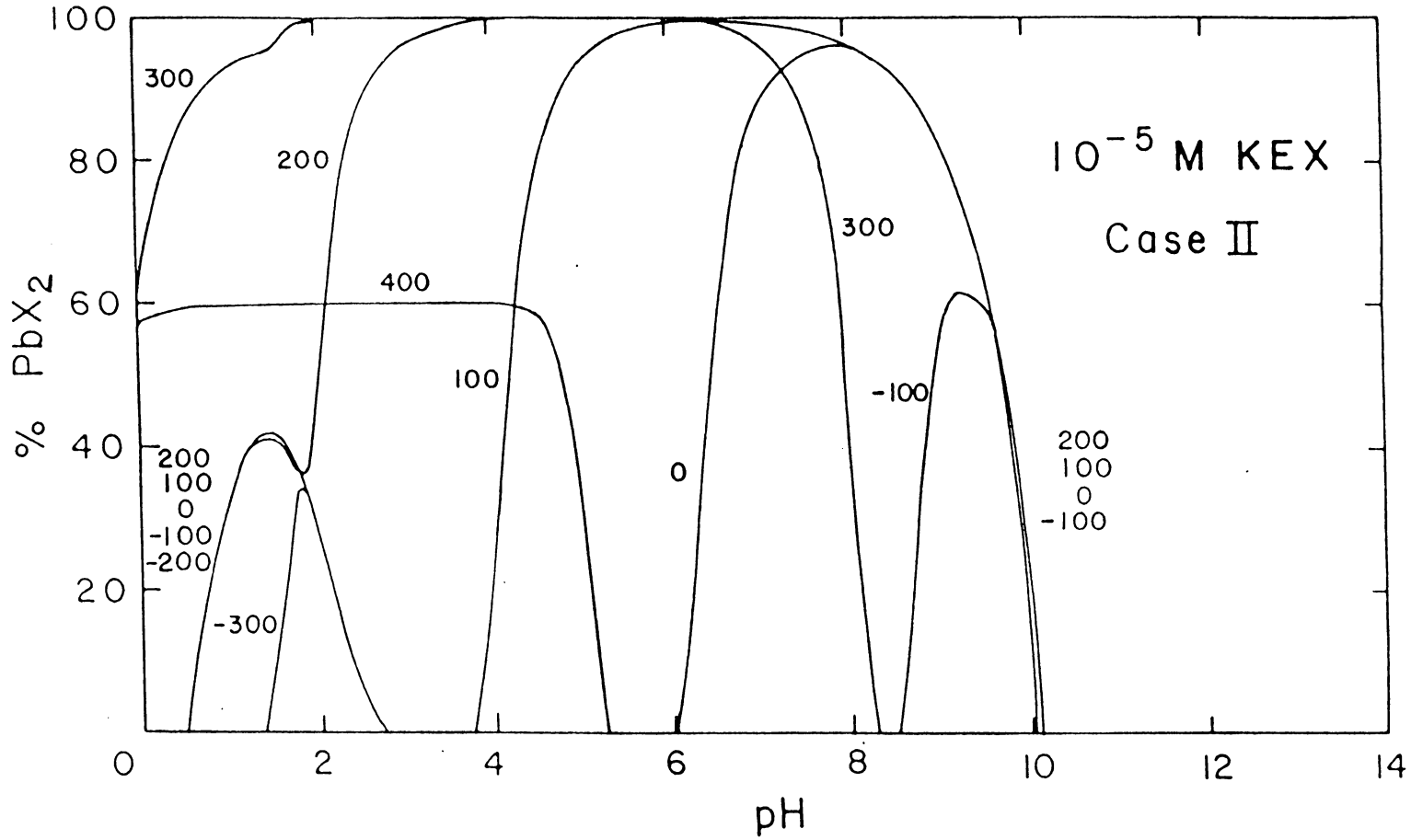


Figure 2.36 The effect of pH on % PbX_2 for Case II and a collector addition of 10^{-5} M KEX. The number next to each curve denotes the E_h (mv).

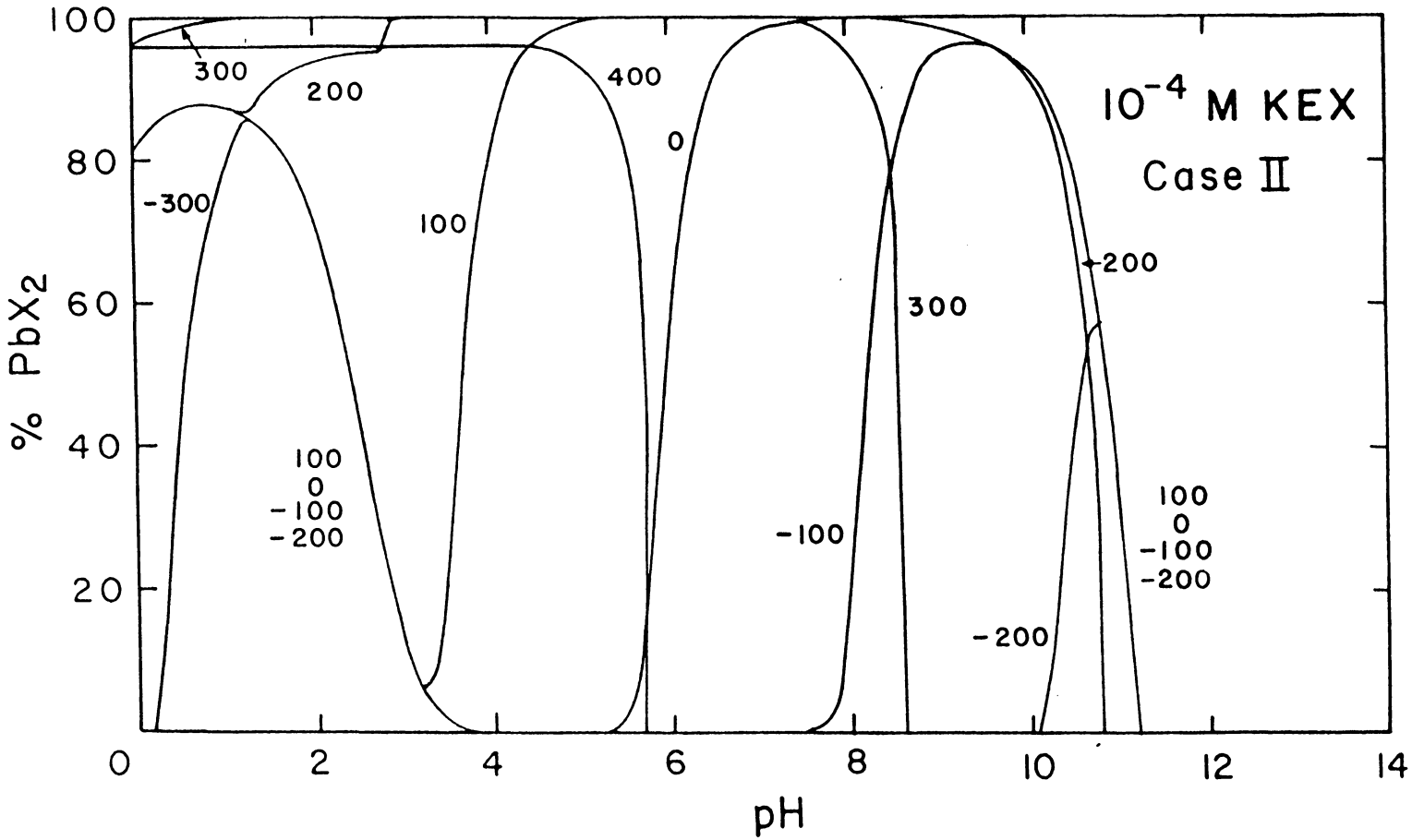


Figure 2.37 The effect of pH on % PbX_2 for Case II and a collector addition of 10^{-4} M KEX. The number next to each curve denotes the E_h (mv).

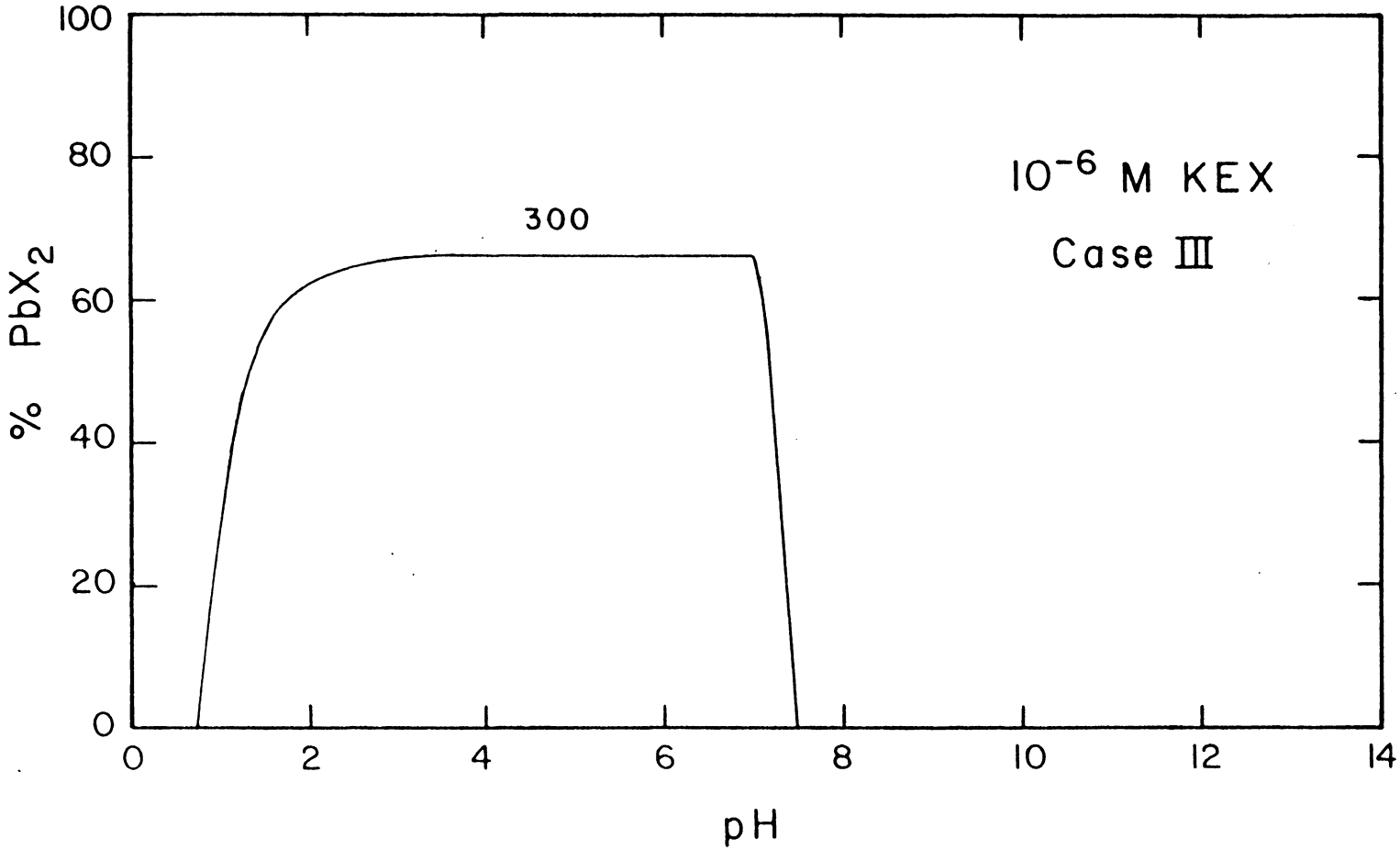


Figure 2.38 The effect of pH on % PbX_2 for Case III and a collector addition of 10^{-6} M KEX. The number next to each curve denotes the E_h (mv).

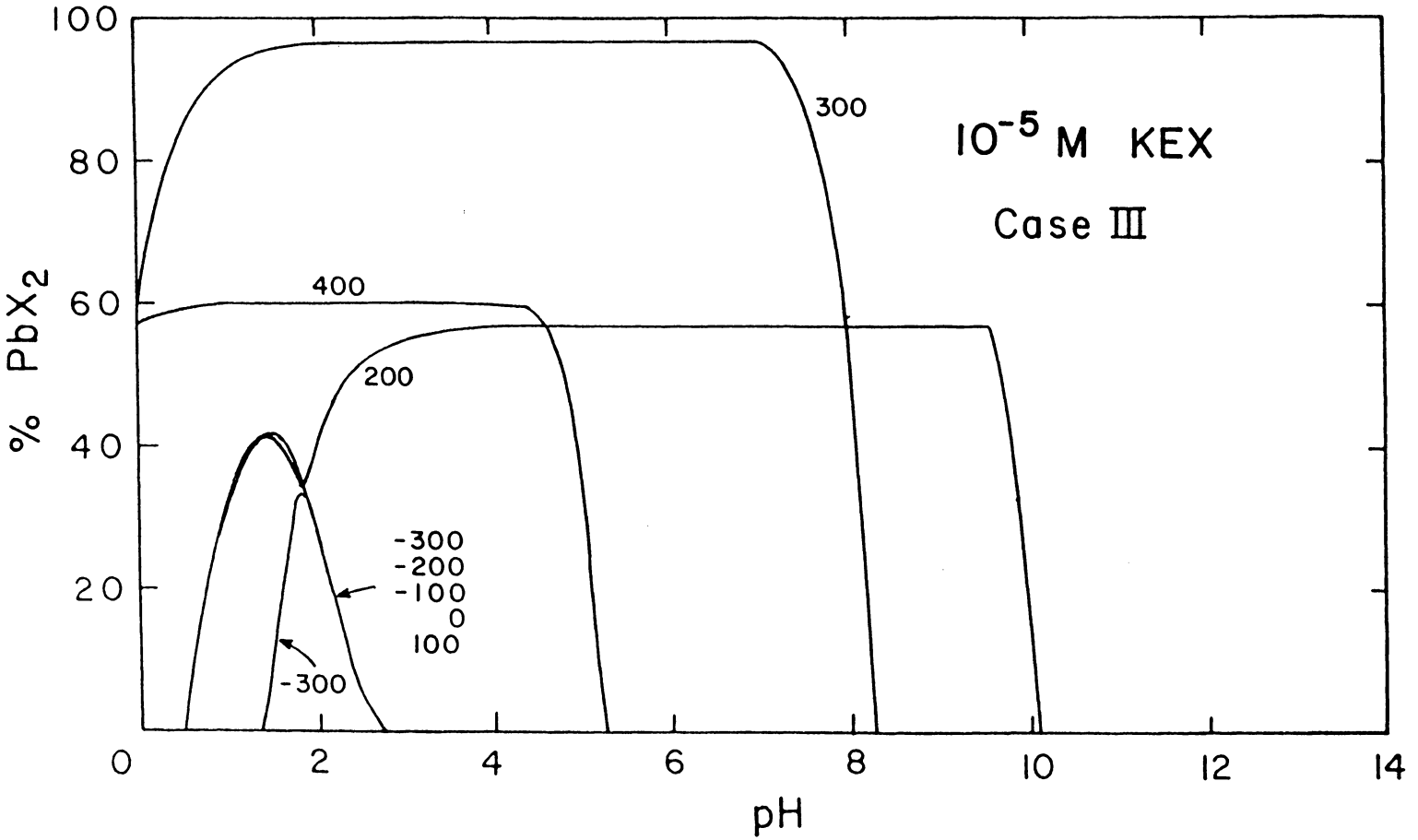


Figure 2.39 The effect of pH on % PbX_2 for Case III and a collector addition of 10^{-5} M KEX. The number next to each curve denotes the E_h (mv).

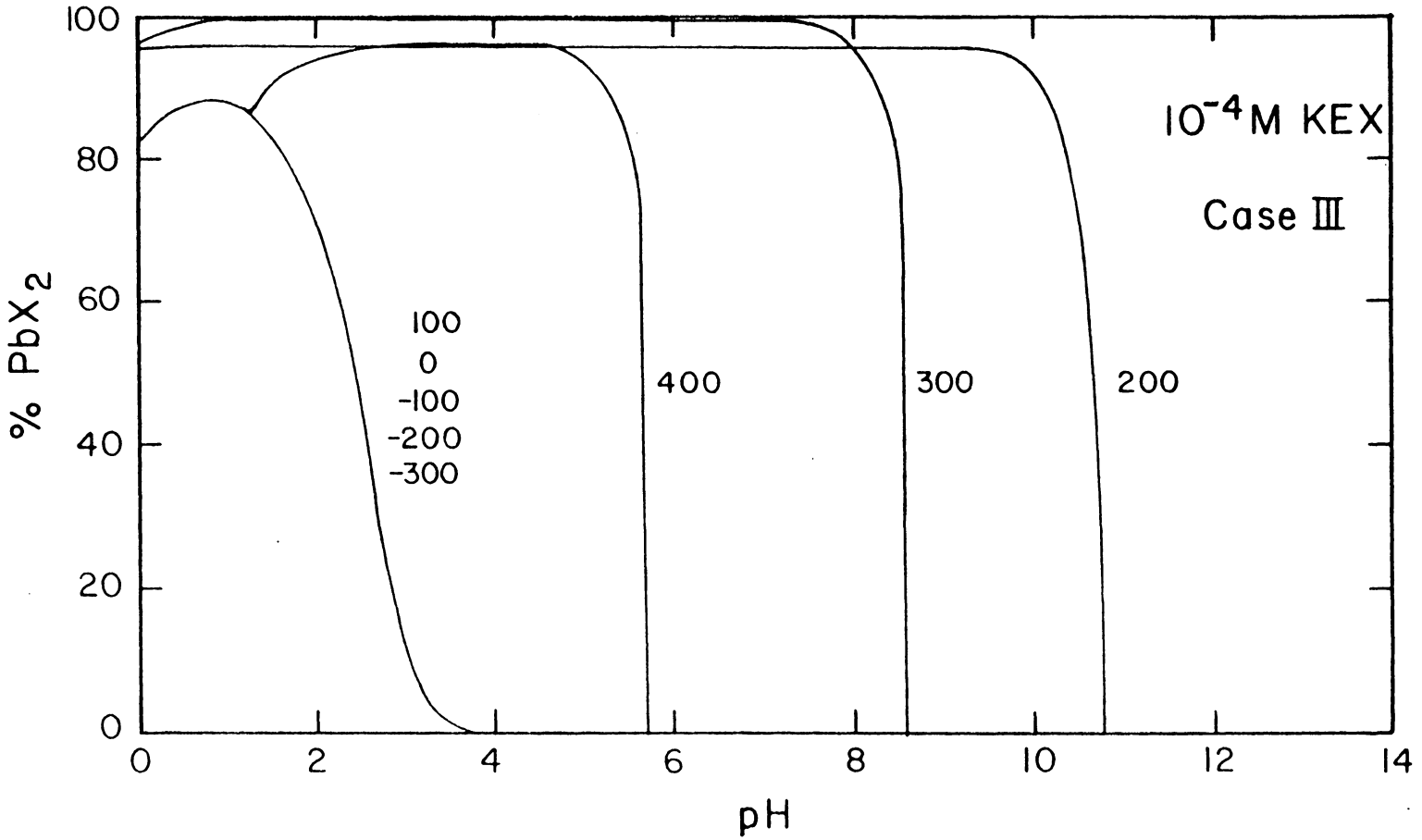


Figure 2.40 The effect of pH on % PbX_2 for Case III and a collector addition of 10^{-4} M KEX. The number next to each curve denotes the E_h (mv).

Some of the trends observed for Cases I and II are different from those noted for Case III. For the first two, the pH range in which PbX_2 is stable widens as the potential becomes more oxidizing. In addition, the lower pH limit tends to vary significantly with E_h, while the upper pH limit remains constant. However, in Case III, the upper limit also varies considerably with potential and the stability range widens only up to a potential of about 200 mv. A further increase in potential causes the range to begin to shrink.

The effect of pH on the formation of PbX_2 in Case III also differs from that of the other two in another respect at 10^{-5} and 10^{-4} M KEX. With the exception of the higher potentials, PbX_2 exists in two separate regions in Cases I and II, one at low pH and the other at higher pH, showing a gap between the two. A gap does not appear in Case III, however.

Shimoiizaka et al. (1976) showed that a "cleaned galena" sample floated well in both acidic and alkaline pH regions, but not at a neutral pH when using 2.1×10^{-5} M KEX. These results were obtained using fixed amounts of potassium dichromate which may have kept the potentials relatively constant and, therefore, may be comparable to the results of our calculations. Similar results have been reported by Fuerstenau et al. (1968) and Steininger (1968) based on their work with pyrite and copper-activated sphalerite, respectively. These investigators also found that the gap grew smaller as the xanthate concentration rose. Comparing the curves for 10^{-5} M and 10^{-4} M KEX in Cases I and II, similar trends are observed in the galena-xanthate system.

2.4.5 Contour Diagram and Three-Dimensional Plots

a. Lead solubility: In order to more clearly see the combined effect of E_h and pH on lead solubility and xanthate uptake, contour plots and three-dimensional block diagrams have been constructed through the use of the Surface II Graphics System developed by the Kansas Geological Survey (Sampson, 1978).

The basis for all operations in Surface II is to generate a rectangular grid of values from the (x,y,z) coordinates of the input data. From this grid, the software package can display the grid matrix either in the form of contour lines or as a block diagram. To draw contour lines, the program linearly interpolates between grid nodes to locate the points where a specified value of the z variable intersects the edge of a grid cell. The contour lines are then generated by joining the successive string of x and y coordinates with common z values. The construction of a block diagram is simpler since it only requires that each grid node be offset proportionally to the value of z so that no interpolation is necessary. However, at the same time, it is not easy to obtain accurate quantitative information from a block diagram, as can easily be done from a contour plot.

Contour plots and block diagrams showing the effect of E_h and pH on the concentration of Pb^{2+} ions in the absence of KEX for Cases I, II and III and presented in Figures 2.41-2.46. Since the equilibrium lead ion concentration is directly affected by the insoluble species present, the pattern of the contour lines (Figures 2.41, 2.43, 2.45) bears a resemblance to the stability domains of the E_h-pH diagrams (Figures 2.2,

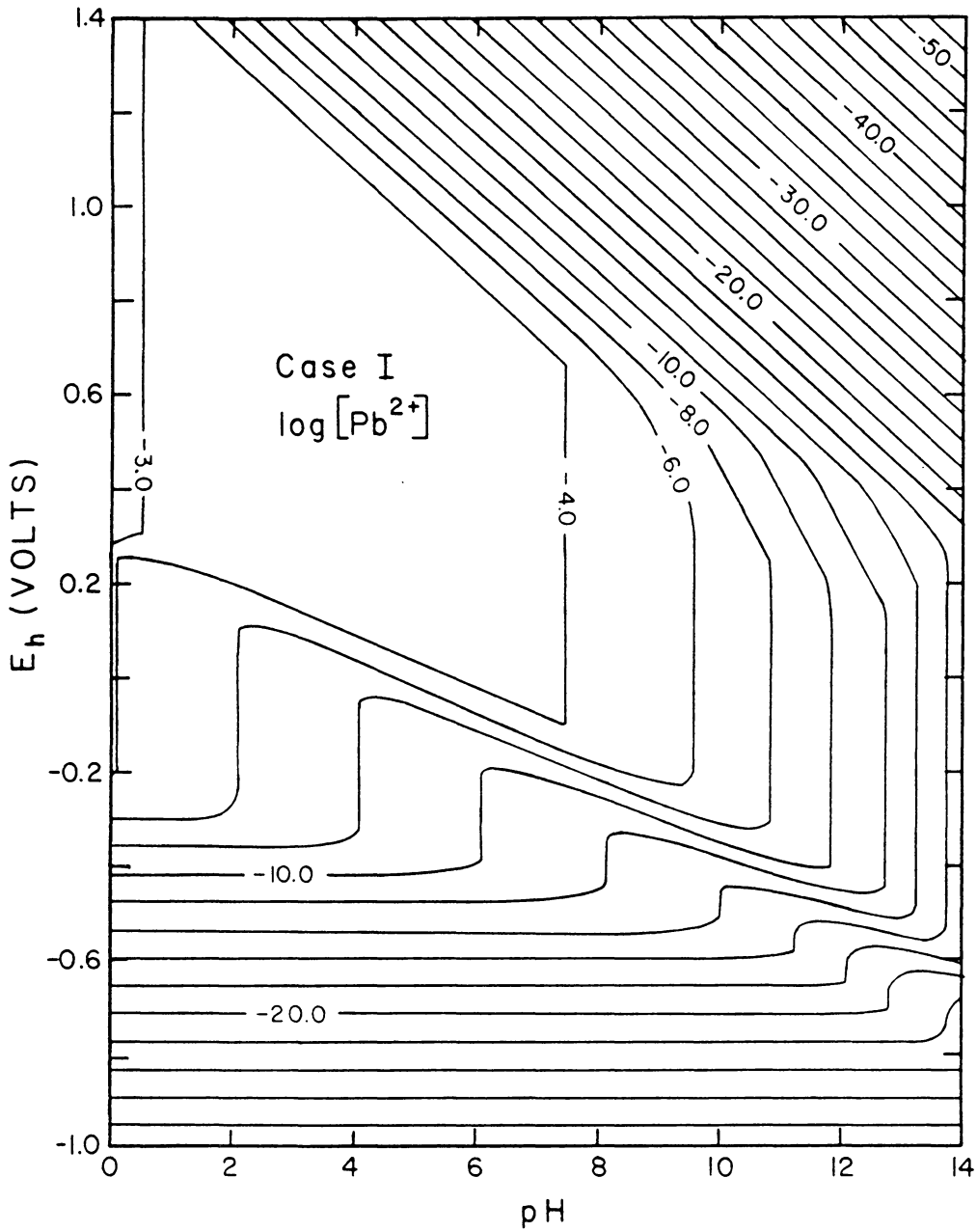


Figure 2.41 Contour plot showing the effect of E_h and pH on log $[Pb^{2+}]$ for Case I of the PbS-H_2O system.

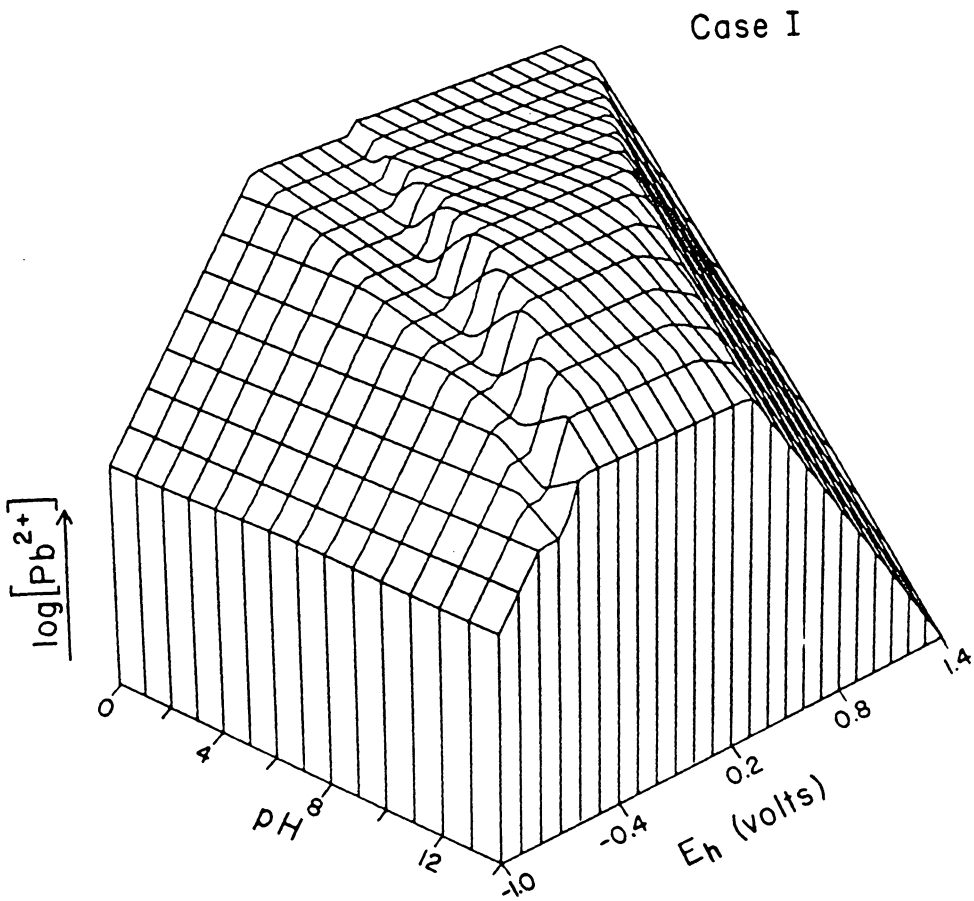


Figure 2.42 Three-dimensional block diagram showing the effect of E_h and pH on log $[Pb^{2+}]$ for Case I of the PbS-H_2O system.

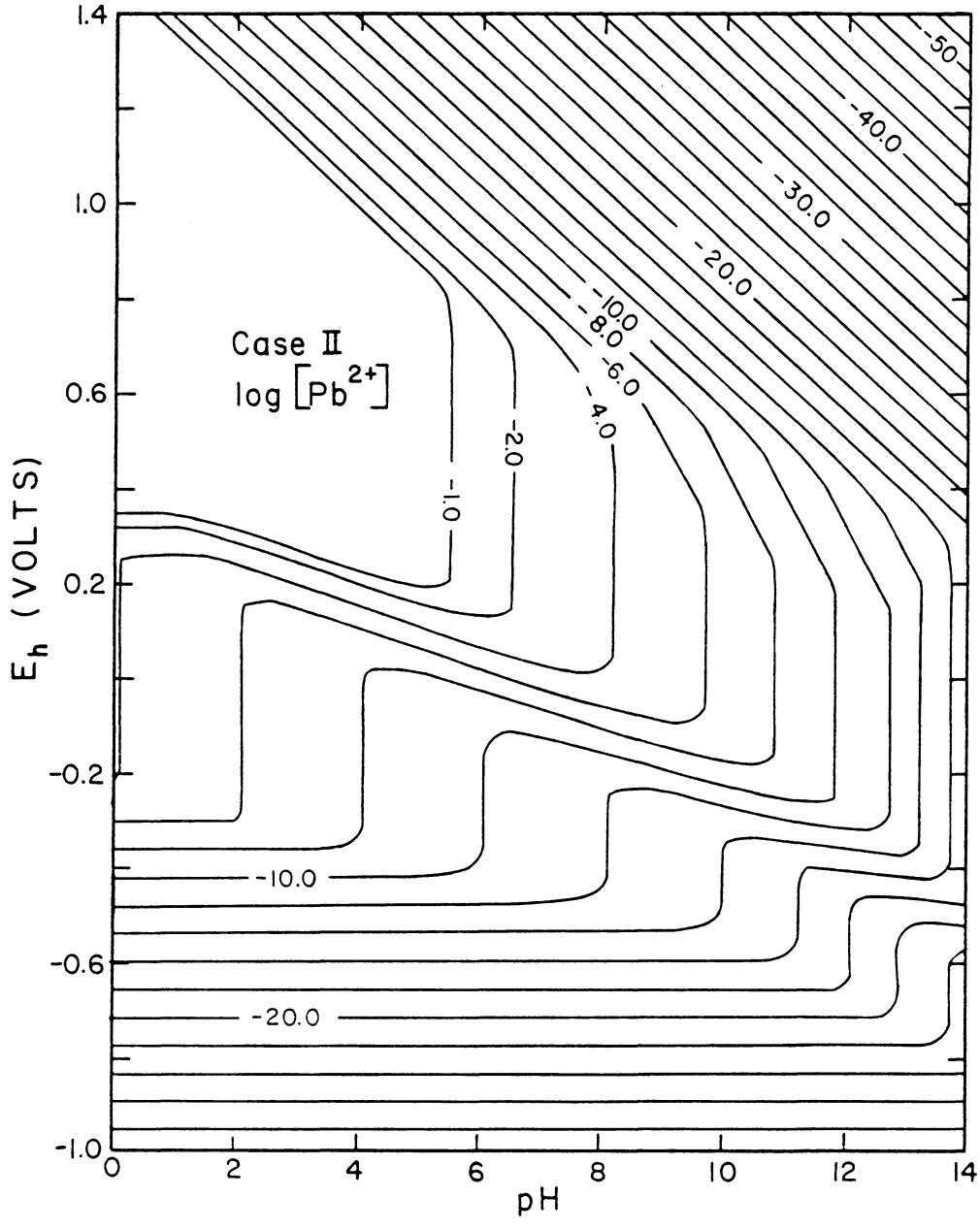


Figure 2.43 Contour plot showing the effect of E_h and pH on log $[Pb^{2+}]$ for Case II of the PbS-H_2O system.

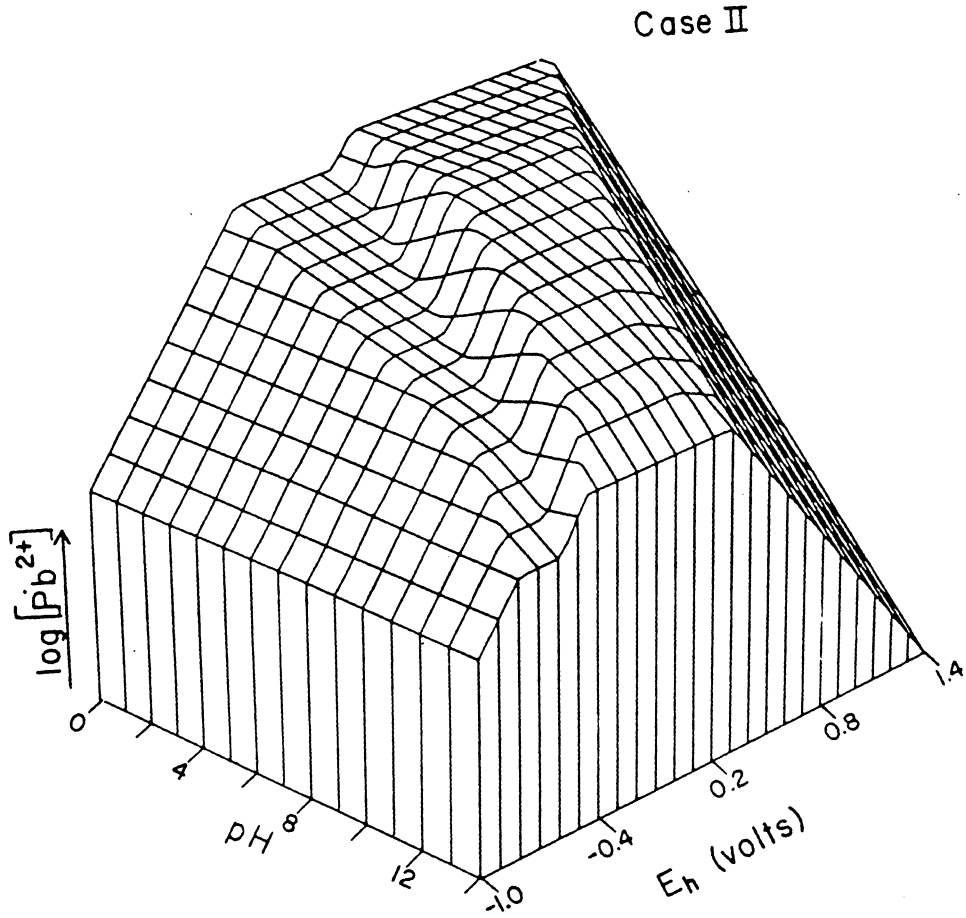


Figure 2.44 Three-dimensional block diagram showing the effect of E_h and pH on log $[Pb^{2+}]$ for Case II of the PbS-H_2O system.

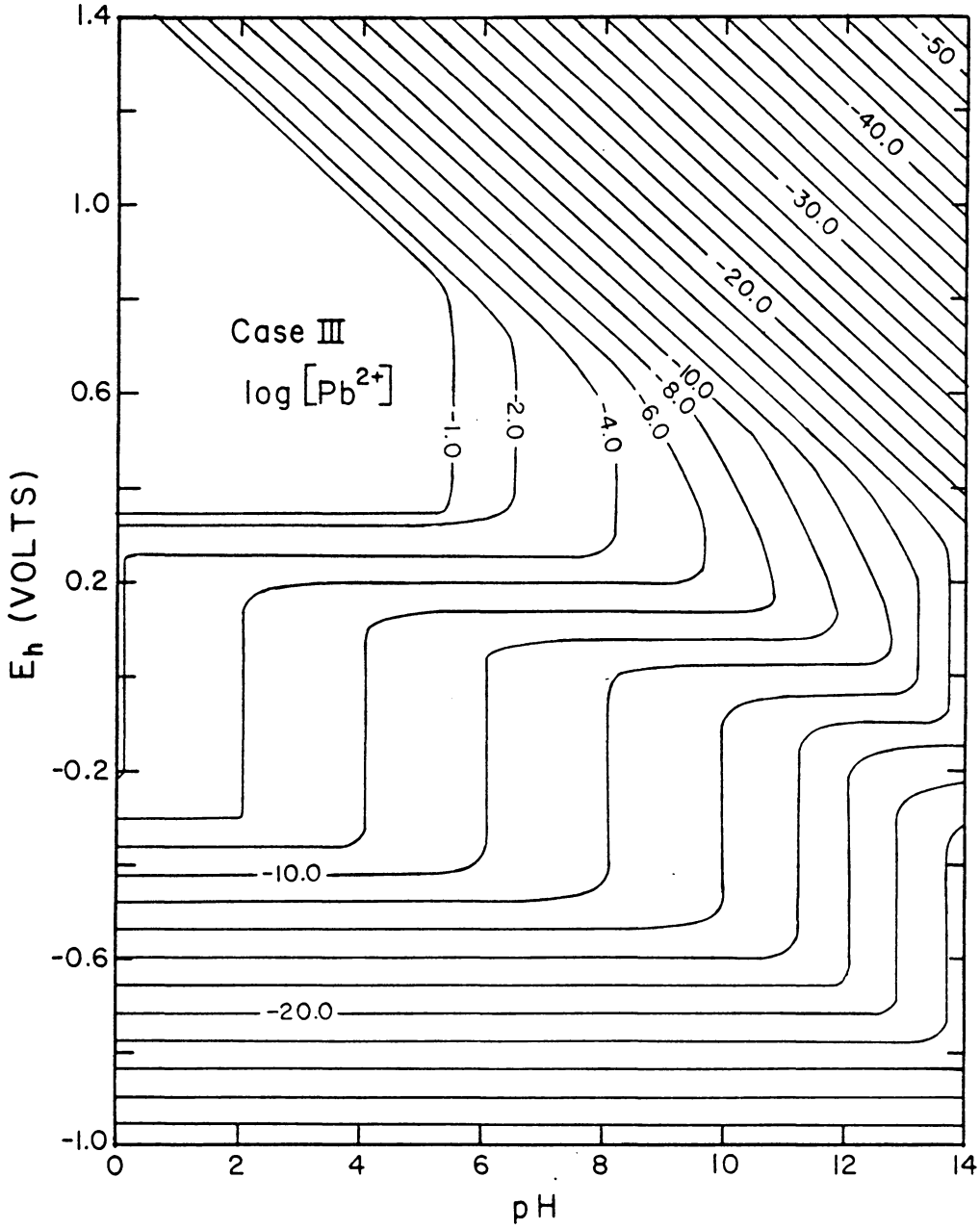


Figure 2.45 Contour plot showing the effect of E_h and pH on log $[Pb^{2+}]$ for Case III of the PbS-H_2O system.

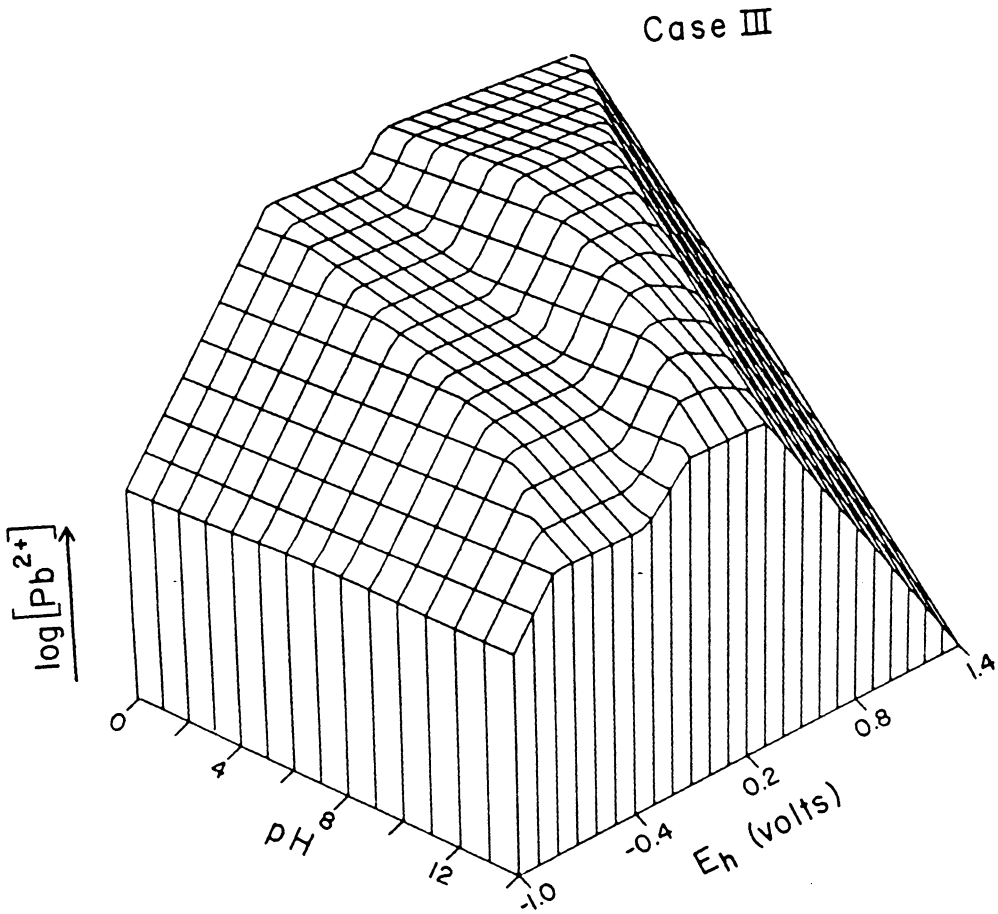


Figure 2.46 Three-dimensional block diagram showing the effect of E_h and pH on log $[Pb^{2+}]$ for Case III of the PbS-H_2O system.

2.6, 2.11). At high pH and E_h, PbO_2 is stable and, consequently, the lines are determined by the Nernst equation for the Pb^{2+}/PbO_2 couple. Under reducing conditions, the lines correspond to the Pb^{2+}/Pb^o couple and naturally are independent of pH. The lead concentration becomes more strongly dependent upon pH and less so with respect to potential in the region between these two. A very distinct transition in the contour lines occurs as the upper boundary for the PbS domain is crossed (see Figures 2.2, 2.6, 2.11). Although the lead concentration is independent of pH both above and below this boundary, the solubility is considerably lower at a given pH once PbS becomes stable. Consequently, as the potential is lowered to the boundary line, each contour line abruptly shifts to a more anodic pH.

Since the differences in Cases I, II and III lie in the nature of the sulfur-bearing species under consideration, the differences in the contour plots arise in the regions where $[Pb^{2+}]$ is affected by the concentration of sulfur species. These are, in particular, in the domains where PbS is stable. The diagrams also differ for conditions of low pH and high E_h. In Cases II and III, all lead-bearing species become soluble and, consequently, $[Pb^{2+}]$ reaches the maximum value of 0.45 M. However, when the presence of SO_4^{2-} is permitted in the calculations, the maximum value of $[Pb^{2+}]$ reaches only $10^{-2.7}$ because of the formation of $PbSO_4$.

Although a difference in the surfaces of the 3-D block diagrams for the three cases (Figures 2.42, 2.44, 2.46) is apparent in the region where PbS is stable, one can obtain only a qualitative sense of this.

However, at the same time, the diagrams do provide a clearer picture of the general effect of E_h and pH on log $[Pb^{2+}]$ than do the contour plots.

b. Xanthate uptake: Contour plots and block diagrams for xanthate uptake have been generated for the data of Cases II and III at 10^{-5} M KEX and are presented in Figures 2.47-2.50. They all show that there are two distinct regions for the formation of PbX_2. The first one occurs between pH 0.5 and 2.8 at potentials from about 300 to 200 mv. The contour lines here are fairly widely spaced and % PbX_2 reaches a maximum of only slightly above 40%. The second region occurs under more oxidizing conditions (as high as about 400 mv) and up to a pH of just beyond 10.

In Case III, the lower boundary of each of the contour lines in the second region is independent of pH, which reflects the fact that PbX_2 formation is controlled by reaction [2.39]. The boundary in Case II extends to considerably lower potentials and shows the strong pH dependence of reaction [2.31]. It is this pH dependence that brings about the gap in the formation of PbX_2 that was seen previously (Figure 2.36) as the pH is varied at constant potentials between about -150 and 150 mv.

2.4.6 Stability of Xanthate-Bearing Species

Because the thermodynamic data was not available in the literature, some of the species which are generated from reactions involving xanthate have not been included in these calculations. These can have a significant effect on flotation behavior since their very presence

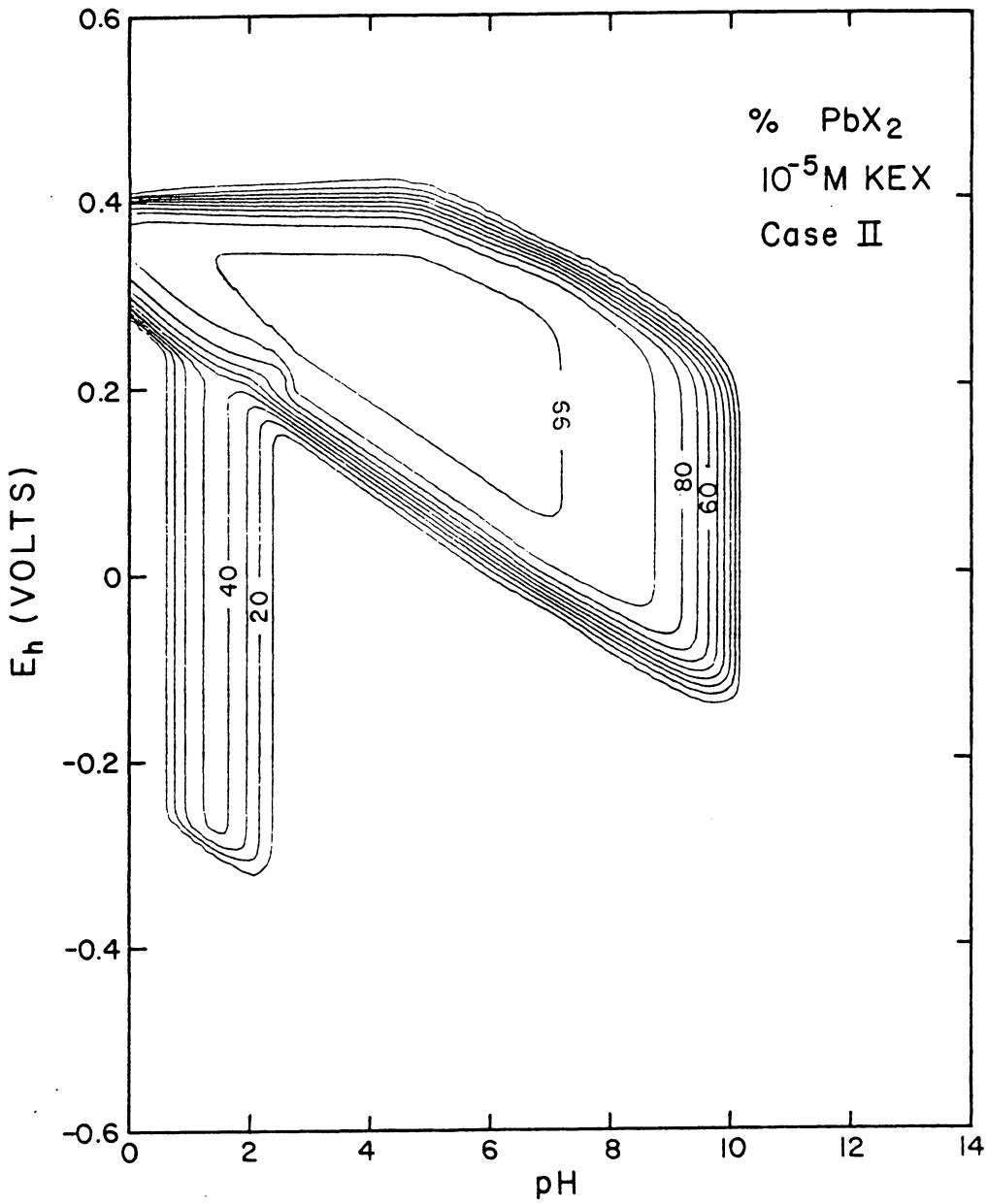


Figure 2.47 Contour plot showing the effect of E_h and pH on % PbX_2 for Case II and a collector addition of 10^{-5} M KEX.

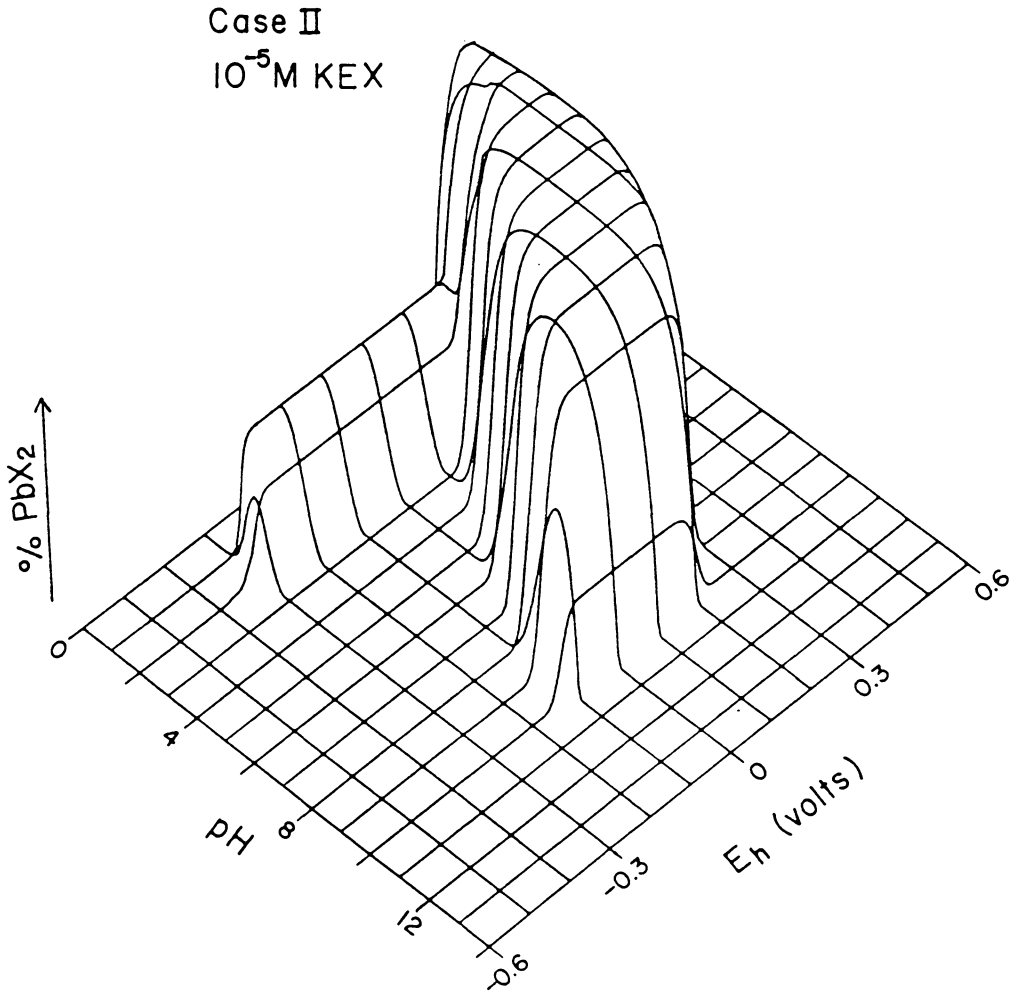


Figure 2.48 Three-dimensional block diagram showing the effect of E_h and pH on % PbX_2 for Case II and a collector addition of 10^{-5} M KEX.

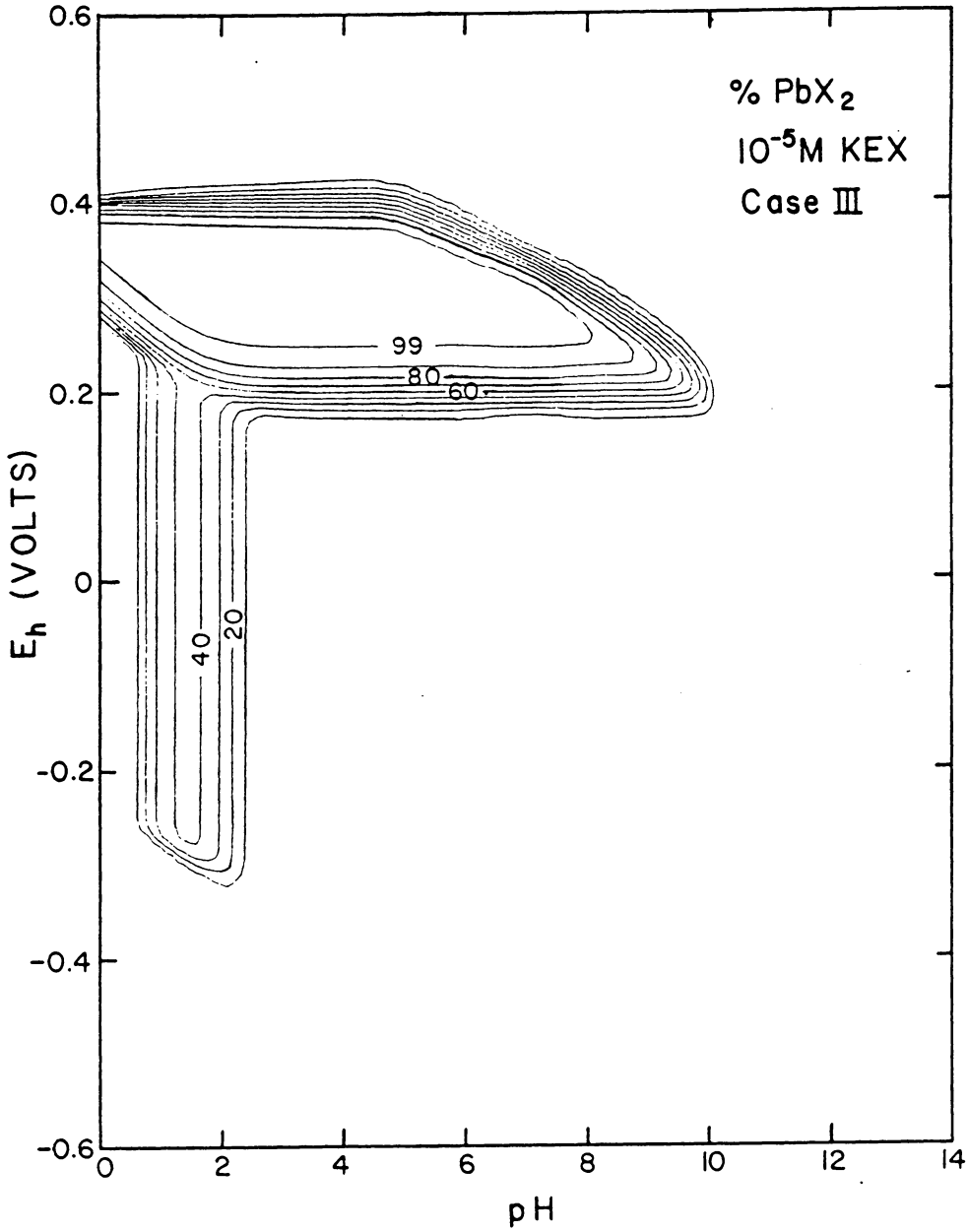


Figure 2.49 Contour plot showing the effect of E_h and pH on % PbX_2 for Case III and a collector addition of 10^{-5} M KEX.

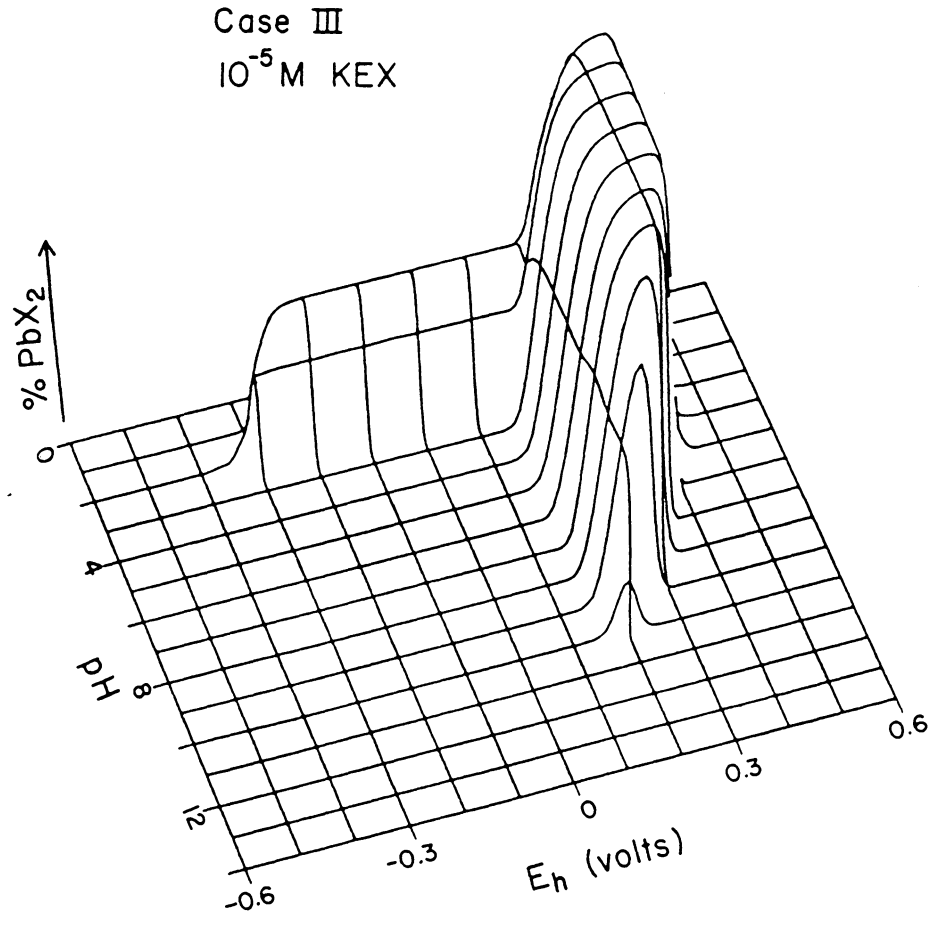


Figure 2.50 Three-dimensional block diagram showing the effect of E_h and pH on % PbX_2 for Case III and a collector addition of 10^{-5} M KEX.

arises from the decomposition of xanthate or dixanthogen. These reactions include:

i) decomposition of xanthic acid ($ROCS_2H$) to alcohol and carbon disulfide:

$$ROCS_2H \longrightarrow ROH + CS_2 \qquad [2.47]$$

ii) hydrolytic decomposition of xanthate to alcohol, carbon disulfide, carbonate, and trithiocarbonate:

$$6ROCS_2^- + 3H_2O \longrightarrow 6ROH + CO_3^{2-} + 3CS_2 + 2CS_3^{2-} \qquad [2.48]$$

iii) oxidation of xanthate to monothiocarbonate and elemental sulfur:

$$ROCS_2^- + 1/2\ O_2 \longrightarrow ROC(=O)S^- + S^o \qquad [2.49]$$

iv) oxidation of xanthate to perxanthate by peroxide:

$$ROCS_2^- + H_2O_2 \longrightarrow ROC(=S)SO^- + H_2O \qquad [2.50]$$

v) decomposition of aqueous dixanthogen to xanthate and peroxide:

$$(ROCS_2)_2 + 2OH^- \longrightarrow 2ROCS_2^- + H_2O_2 \qquad [2.51]$$

vi) decomposition of aqueous dixanthogen to monothiocarbonate, sulfur, and sulfide:

$$(ROCS_2)_2 + 4OH^- \longrightarrow 2RO_2CS^- + S^o + S^{2-} + 2H_2O \qquad [2.52]$$

In acid solutions, free xanthate is hydrolyzed to xanthic acid, which can subsequently decompose according to reaction [2.47]. Work by Iwasaki and Cooke (1958), Klein et al. (1960) and Tipman (1970) has indicated that reaction [2.47] is irreversible and fast at low pH. Tipman (1970) found from his UV work that xanthate has a half-life of only about 24 seconds at pH 2.0, but that it becomes considerably more stable with increasing pH. By pH 4.0, the half-life has reached about 32 minutes, which is comparable to residence times in typical flotation circuits.

Although the presence of xanthic acid has been considered in the thermodynamic calculations of this study, its decomposition by reaction [2.47] has not been included. Our calculations show that xanthic acid is the predominant aqueous xanthate-bearing species only below pH 1.6 and 280 mv. Furthermore, the molar ratio of HX to X^- is only 4.3×10^{-3} by pH 4.0. In view of the work by Tipman and others, the omission of reaction [2.47] is not significant at the pH conditions that are commonly encountered in sulfide flotation practice.

The decomposition of xanthate according to reaction [2.48] has been investigated by Wronski (1959) and Philipp and Fichte (1960) and found to be important only in highly alkaline solutions at pH 13.0.

Harris and Finkelstein (1975) have carried out extensive studies on the formation of monothiocarbonate ions (i.e., reaction [2.49]) after contacting galena with ethyl xanthate in the presence of oxygen at pH 9-10. They observed that monothiocarbonate was generated as long as the mineral was present and the solution contained oxygen or the mineral had

been pre-oxidized. On the basis of their kinetics experiments, it is estimated that as much as 20% of the initial KEX added is in the form of monothiocarbonate. Since this is an irreversible process, this represents a waste of collector added to a flotation circuit. However, monothiocarbonate formation would not be expected to prevent the flotation of galena since only a small surface coverage by adsorbed xanthate is sufficient for the recovery of the mineral.

It is important to realize that Harris and Finkelstein noted that the presence of oxygen or an oxidized mineral surface was needed in order for monothiocarbonate to form. This would be significant for an industrial flotation circuit since oxygen cannot be avoided. However, in the case of laboratory experiments where the solutions are deoxygenated, very little monothiocarbonate should be generated. Not including this species in the calculations will, then, have little effect on the correlation between the results of this type of experiment and of the computations. Even in situations where oxygen is present, the error is more likely to involve the magnitude of % PbX_2 rather than the determination of the upper and lower pH and E_h limits for PbX_2 stability.

Perxanthate resulting from reaction [2.50] has been detected by Jones and Woodcock (1978) in both plant solutions and in solutions resulting from the reaction of xanthate with hydrogen peroxide. As in the case of monothiocarbonate, the formation of perxanthate, which would waste collector, is possible only in solutions containing oxygen. This is due to the fact that hydrogen peroxide is found in flotation

solutions as an intermediate product during the reduction of oxygen on sulfide minerals.

Although, generally, dixanthogen is not likely to be found in large amounts in industrial flotation pulps, its occurrence may become significant if high xanthate additions are used or if xanthate is added during the grinding stage. In this case, the decomposition of dixanthogen to xanthate and monothiocarbonate by reactions [2.51] and [2.52] can be important. Jones and Woodcock (1983) observed that the rates of both reactions increases with pH; the time for all the dixanthogen to decompose is only a few minutes above pH 12, but over 20 hours at pH 9. Moreover, the relative rates of these two reactions is also affected by pH, with more monothiocarbonate than xanthate being produced at pH 12 and the reverse being true at pH 9. Jones and Woodcock also found that at high pH, some of the xanthate and peroxide from reaction [2.51], in turn, are converted to perxanthate and water (i.e., reaction [2.50]). Although the generation of xanthate is not a problem as far as reagent consumption is concerned, the formation of monothiocarbonate and perxanthate is.

According to the thermodynamic calculations for collector additions of 10^{-4} M KEX (see Figures 2.5, 2.10, 2.14), liquid dixanthogen is stable up to pH 14 above $E_h \sim 180$ mv. One would, therefore, still expect galena to be floatable under these conditions. Yet, the evidence shows that flotation recovery drops off at very high pH even at high collector additions. This discrepancy is, in part, likely due to the

fact that reactions [2.51] and [2.52] have not been considered in our calculations.

In laboratory experiments, particularly those of an electrochemical nature, the concentration of xanthate is often higher and the conditions more oxidizing than those encountered in industrial situations. Consequently, the omission of reactions [2.51] and [2.52] is probably more crucial when comparisons are made with the laboratory data. However, it should be kept in mind that most studies of galena flotation are conducted at pH values between 8 and 10. The data of Jones and Woodcock (1983) indicate that the decomposition of dixanthogen is already slow enough at these pH values that it probably is not much of a factor for most experiments.

In summary, some error may have been introduced into the calculations by the inability to consider reactions [2.47] - [2.52]. Nevertheless, in view of the preceding discussion, it is probably small, particularly when deoxygenated systems are being considered.

2.5 Summary

A detailed discussion of the approach taken in carrying out these calculations and the differences between this work and previous ones of this kind has been presented. Despite the more lengthy and expensive computations that are required, considerably more detailed and accurate information concerning the thermodynamics of the galena-ethyl xanthate system can be obtained.

Some of these data include a determination of the concentrations of all dissolved species as a function of E_h and pH and the conditions at which phase changes occur. This has enabled the following plots to be generated:

i) solubility diagrams showing the concentrations of soluble species as a function of pH at a given E_h,

ii) E_h-pH stability diagrams for each collector addition,

iii) xanthate uptake isotherms showing % PbX_2 as separate functions of E_h and pH, and

iv) contour plots and 3-dimensional block diagrams showing $[Pb^{2+}]$ and % PbX_2 as combined functions of E_h and pH.

A set of calculations has been done for three separate cases which differ in the extent to which sulfur-bearing species are allowed to be oxidized. The results have been compared with each other and with experimental data from the literature. It has been found that the flotation data of Guy and Trahar (1984) for a galena-quartz mixture obtained at pH 8.0 and 2×10^{-5} M KEX correlates well with the onset of the formation of PbX_2 and $S_2O_3^{2-}$ and, to a lesser extent, PbX_2 and S^o, as calculated in this study.

The question of the collectorless flotation of galena, which has received much attention recently, has also been addressed. On the basis of the thermodynamic calculations, the formation of elemental sulfur and/or polysulfides on the mineral surface is responsible for the

flotation of galena both in the absence and presence of excess sulfide ions.

CHAPTER III.

EXPERIMENTAL STUDIES REGARDING THE SOLUTION AND FLOTATION CHEMISTRY OF GALENA AT pH 6.8 AND 9.2

3.1 Introduction

3.1.1 General

The previous chapter dealt with a detailed study of the thermodynamics of the galena-ethyl xanthate system. Although some comparison was made between the calculated data and experimental data from the literature, the primary objective was to discuss the approach used in the calculations and to demonstrate various novel ways in which the results of this type of work can be presented. Chapter III will focus on the electrochemical experiments regarding the solution and flotation chemistry of galena at pH 6.8 and 9.2.

As will be shown in the literature review, there is considerable disagreement among researchers concerning the identity of the xanthate adsorption reaction(s). One of the main aims of conducting the electrochemical experiments will be to sort out some of the apparent discrepancies and to obtain a more comprehensive picture of the interaction of galena and xanthate.

Another area of contention has concerned the relative importance of kinetics and thermodynamics in understanding the oxidation and flotation of galena. Kinetic and mass transfer factors have been found to have a significant influence upon the aqueous chemistry of sulfide minerals.

Since these are the sorts of effects that can be detected by experimental techniques such as voltammetry, IGP and chronoamperometry, particular attention will be given to the similarities and differences between the experimental data presented in this chapter and the calculations of Chapter II.

3.1.2 Literature Review

As mentioned previously, galena has probably been the most widely studied sulfide mineral over the years. One reason for this continuing interest is that there exists a large body of knowledge and experience with which to compare new research. Another is that galena has proven to be very stubborn in revealing how it interacts with water and the various aqueous species it encounters during the flotation process.

Many of the early studies were concerned with characterizing the various reaction products using wet chemical methods, UV spectrophotometry, IR spectroscopy, diffuse reflectance spectroscopy, calorimetry and electron diffraction. Among the ones dealing with the oxidation of galena at neutral and alkaline pH in the absence of xanthate include those of Plante and Sutherland (1949), Hagihara (1952), Reuter and Stein (1957), Poling and Leja (1963), Eadington and Prosser (1966, 1969) and Steger and Desjardins (1980). Some of the work of this type for systems containing xanthate has been reported by Hagihara (1952), Greenler (1962), Leja et al. (1963), Mellgren and Subba Rau (1963), Burkin et al. (1964), Coleman and Powell (1965), Mellgren (1966), Abramov (1968), Finkelstein (1970), Klymowsky and Salman (1970), Allison and Finkelstein (1971) and Mielczarski et al.

(1981). Papers dealing directly with the flotation of galena using xanthate have been contributed by Bushell (1958), Cusack (1967), Woodcock and Jones (1970a,b), Shimoiizaka et al. (1976), Trahar (1976), Gutierrez and Martin-Poveda (1981) and Learmont and Iwasaki (1984).

X-ray photoelectron spectroscopy (XPS) has in recent years become a widely used tool for the surface analysis of many minerals. Most of this research with regard to galena has involved the oxidation of the mineral in air or water without a collector present (Manocha and Park, 1977; Zingg and Hercules, 1978; Hagstrom and Fahlman, 1978; Grandke and Cardona, 1980; Brion, 1980; Kar Chaudari et al., 1981; Evans and Raftery, 1982; Boissay et al., 1982; Buckley and Woods, 1984a,b). The few XPS studies of xanthate adsorption onto galena reported in the literature are those by Clifford et al. (1975) and Pillai et al. (1983).

In recent years, a great deal of attention has been focused on the electrochemical aspects of the galena-ethyl xanthate system. In the first reported work of this kind, Tolun and Kitchener (1964) used a steady-state polarographic technique to investigate the oxidation of ethyl xanthate at platinum, lead and galena electrodes. They found that under reducing conditions, no such reaction occurred on galena for a collector concentration of 10^{-3} M. When the electrode potential was raised to a value (150 mv) where dixanthogen can be formed, there was a strong contact between a bubble and the electrode. However, they observed only a feeble contact under conditions at which a lead xanthate film was produced.

This study was followed up by Toperi and Tolun (1969), who related

the hydrophobicity of a galena electrode obtained in 10^{-3} M KEX solutions at different pH values to measured rest potentials. Their results indicated that galena should be floatable under conditions where PbX_2, X^- and X_2 can co-exist.

Woods (1971) was the first to use linear sweep voltammetry to study the interaction between ethyl xanthate and galena. (More background information concerning this technique will be given in a later section of this chapter.) The voltammograms he obtained in a 0.1 M sodium tetraborate solution (pH 9.2) with and without 9.5×10^{-3} M KEX are shown in Figure 3.1. The initial rise in anodic current occurred at a potential below the reversible value for the formation of dixanthogen, i.e.,

$$2X^- \longrightarrow X_2 + 2e. \qquad [3.1]$$

Based on this and other experimental results, Woods concluded this initial rise was due to the chemisorption of a monolayer of xanthate by the one-electron transfer reaction:

$$X^- \longrightarrow X_{ads} + e. \qquad [3.2]$$

The second rise, which began at a potential close to the equilibrium potential for reaction [3.1], was attributed to the formation of dixanthogen. Bubble attachment to the galena became strong only when oxidation to dixanthogen was occurring.

Although some evidence has been presented since that time which supports this conclusion (Ahmed, 1978b), other evidence indicates that

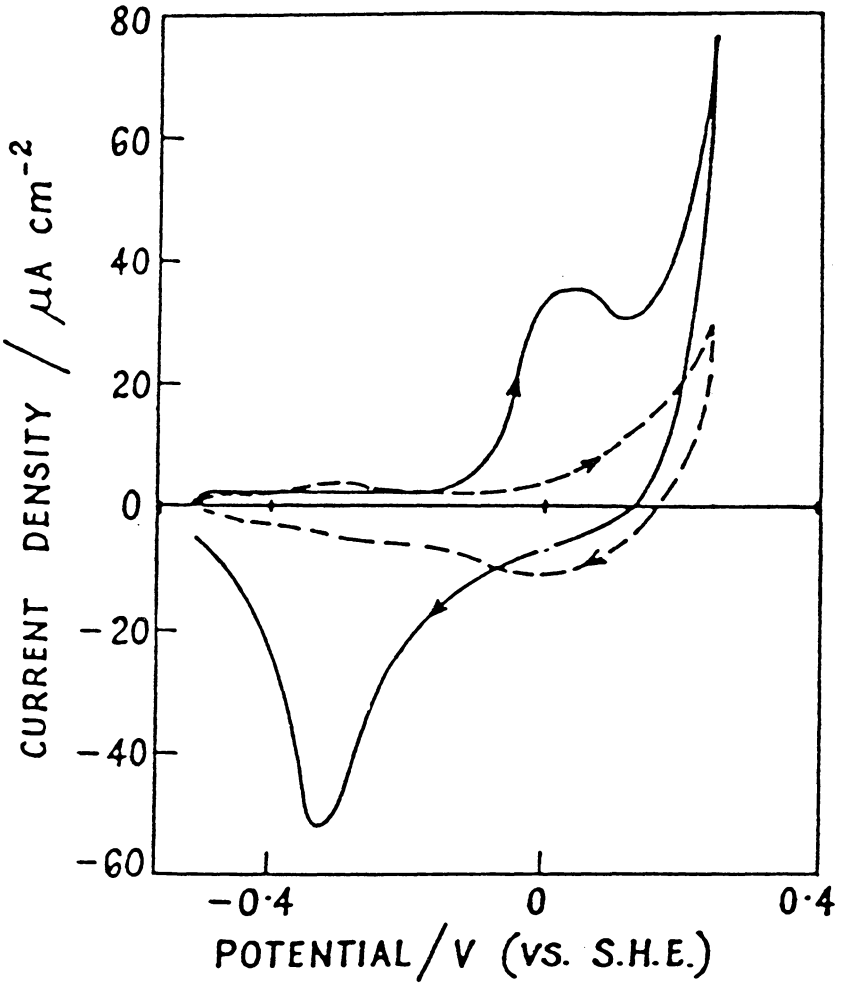


Figure 3.1 Linear sweep voltammograms of a galena electrode immersed in a 0.1 M $Na_2B_4O_7$ solution (pH 9.2) containing 0 M KEX (---) and 9.5×10^{-3} M KEX (—) (from Woods, 1971).

lead xanthate, rather than dixanthogen, forms and is the surface species responsible for flotation. Allison and Finkelstein (1971) reacted the collector with pure, ground mineral, extracted the reaction products in an organic solvent, and then analyzed for PbX_2 and X_2 using UV spectrophotometry and IR spectroscopy. Virtually only lead xanthate was detected. In another study, Allison et al. (1972) measured the rest potential of a galena electrode immersed in a 6.25×10^{-4} M KEX solution to be 60 mv. This value was below the reversible potential of 130 mv for reaction [3.1] and coincided almost exactly with the Nernst potential for reaction,

$$PbS + 2X^- \longrightarrow PbX_2 + S^o + 2e. \qquad [3.3]$$

Still other studies leave open the possibility that both lead xanthate and dixanthogen are the oxidation products. Gardner and Woods (1977) found that galena in a particular bed electrode began to float when a potential of 60 mv was applied. At the collector concentration of 6.2×10^{-3} M which was used, the reversible potentials of reactions [3.1] and [3.2] are 70 and 6 mv, respectively. Both are close enough to the value at which flotation began that the possibility of both reactions occurring cannot be ruled out. Recently, Lamache et al. (1984) conducted a very thorough analysis of the reaction products from the electrolysis of galena powder at fixed potentials at pH 9.2 in a specially designed electrochemical cell (Figure 3.2). They detected both dixanthogen and lead xanthate on the mineral surface in relative amounts that varied with the xanthate addition and the applied voltage.

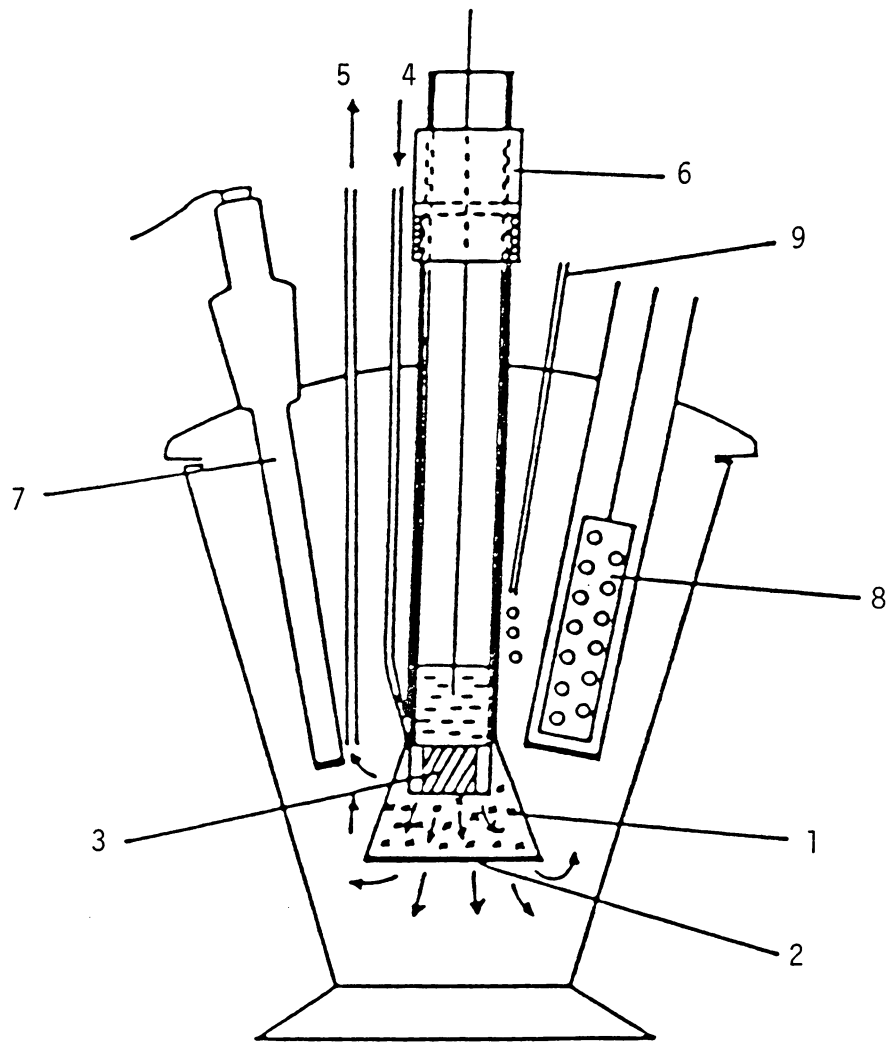


Figure 3.2 Electrochemical cell used by Lamache et al. (1984) in their studies on galena particle beds.

1 fluidized bed of galena particles
2 glass frit
3 galena contact
4 electrolyte inlet
5 electrolyte outlet
6 joint
7 reference electrode
8 platinum auxiliary electrode
9 argon

In all these electrochemical studies, the collector levels were considerably higher than concentrations of 10^{-5} M that are typically encountered in industrial flotation situations. Guy and Trahar (1984) have carried out more practical flotation experiments, using more realistic collector levels, larger mineral samples, and a mixture of galena and quartz. They found that under these conditions, the potential for the onset of flotation could best be correlated with the reversible potential for the reaction,

$$2PbS + 4X^- + 3H_2O \longrightarrow 2PbX_2 + S_2O_3^{2-} + 6H^+ + 8e. \qquad [3.4]$$

As shown previously in Section 2.4.4a, the calculations in this study also bear this out.

One of the principal aims of the experimental study to be described in this chapter will be to determine which of reactions [3.1], [3.2], [3.3] and [3.4] best describes xanthate adsorption for collector additions of 10^{-4} and 10^{-3} M at pH 9.2 and 6.8. Some of the results of these tests have been presented elsewhere (Pritzker and Yoon, 1984b; Pritzker et al., 1985). Although a great deal of work has been done at pH 9.2, very little has been reported for pH 6.8. It is hoped that such information will provide some insight into the effect of pH upon this system.

Linear sweep voltammetry (LSV), intermittent galvanostatic polarization (IGP) and chronoamperometry experiments have been conducted on a single fragment galena electrode immersed in deoxygenated buffer solutions. Since the conditions favorable for xanthate adsorption are

similar to those for oxidation of galena, particular attention has been paid to the electrochemistry of the mineral in the absence of collector. The effect of redox potential on the flotation of galena at pH 9.2 has been studied by treating ground samples in solutions at various oxidizing conditions and then floating them in a Partridge and Smith-type (1971) microflotation cell.

Although there is evidence that a mixed potential approach is more useful than thermodynamics in describing the adsorption of xanthate onto galena in an oxygenated system, this may not be so if oxygen is removed. Another important objective of these experiments is to look at this question more closely by comparing some of the resulting data to those of the thermodynamic calculations that were discussed in the previous chapter.

Before proceeding further to describe the experimental procedure followed in these tests, it will be instructive to include some background concerning the LSV and IGP techniques used in this study.

3.1.3 Linear Sweep Voltammetry

Linear sweep voltammetry (LSV) is a controlled potential technique in which the applied potential is varied linearly with time from an initial value, E_i, to a value, E_1. At E_1, the direction is reversed and the potential is scanned to E_2 (which may or may not be the same as E_i). When the sweep is repeated back and forth between the limits E_1 and E_2, this method is termed cyclic voltammetry. The starting potential, initial scan direction, upper limit, lower limit and the scan rate (v)

are controlled by a waveform generator that is connected to the potentiostat. A schematic diagram of the instrumentation for voltammetry is shown in Figure 3.3.

The shape of the resulting voltammogram (Figure 3.4b) can be explained as follows. Consider the case of an electrode immersed in a solution with concentration C_A^* of species A (curve 1, Figure 3.4a). A sweep begins in the anodic direction from an initial potential, E_i, that is below the reversible potential, E_r, for the anodic reaction,

$$A \longrightarrow B + ne. \qquad [3.5]$$

When the potential is above E_r, reaction [3.5] can begin to proceed and anodic current to flow. As the potential continues to rise, the rate of the reaction increases and so does the current. If the supply of A to the electrode surface cannot keep pace with the rate at which it is consumed, then the surface concentration will diminish until it falls to near zero (curves 2,3,4). Mass transport of A now entirely controls the rate and the diffusion layer becomes further depleted in A as the potential is further raised (curve 5). Since the current is proportional to the concentration gradient of A at the surface (Fick's Law), it will begin to drop, thereby producing a peak in the voltammogram. If the situation is such that A can always be supplied to the electrode fast enough to support the electrode reaction, then the current will continually rise as the potential is raised and no peak will appear.

When the scan is reversed at the upper limit, E_l, anodic current will still flow since the potential is still above E_r. It will continue

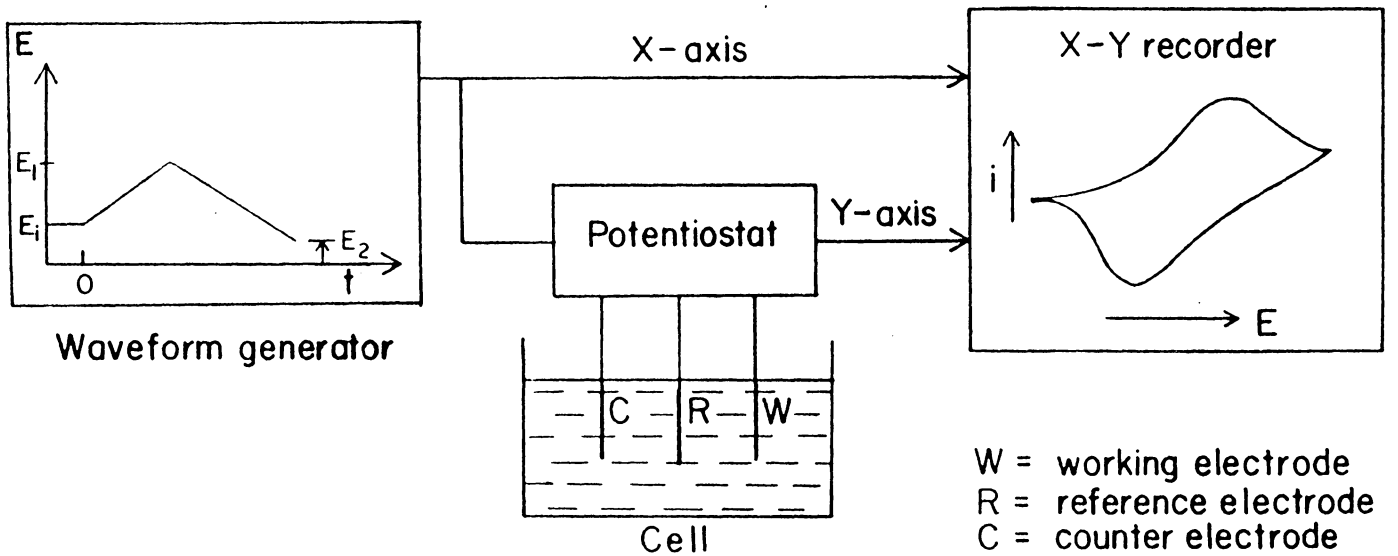


Figure 3.3 Schematic diagram of the instrumentation used for linear sweep voltammetry.

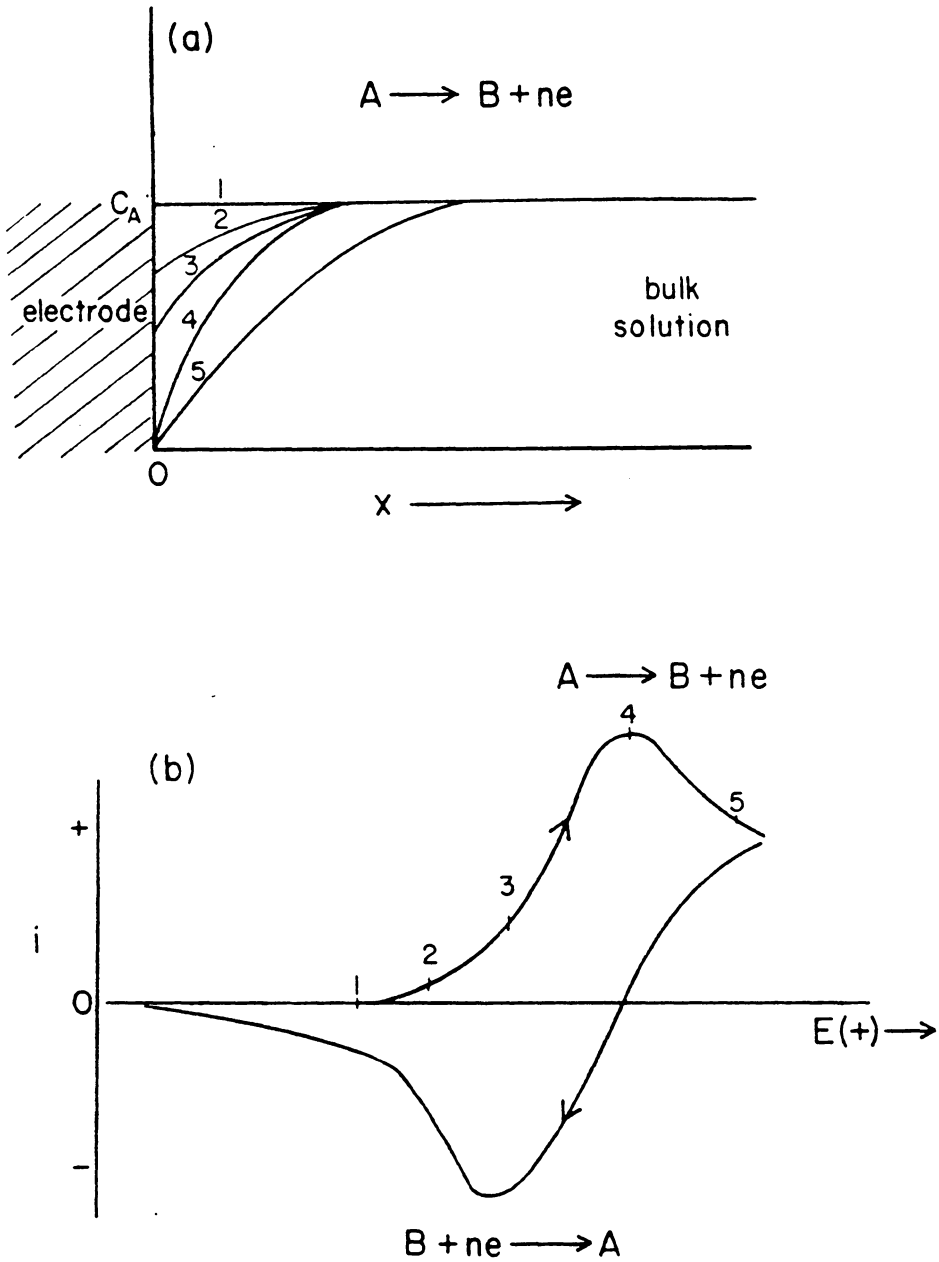


Figure 3.4 (a) Change in the concentration profile of species A which is being oxidized during an anodic scan.

(b) The shape of the voltammogram resulting from the depletion of A from the electrode surface during the anodic scan and of B during the reverse scan.

to decrease, however, as the diffusion layer is further depleted. As the anodic reaction has been proceeding, an accumulation of species B has built up near the electrode surface. Eventually, the potential will decrease below the reversible potential for reaction [3.5], the reduction of B back to A will begin to occur and cathodic current will flow. The shape of the remaining portion of the voltammogram is much like that for the anodic scan for essentially the same reasons.

Linear sweep voltammetry is very useful for systems in which a succession of anodic and/or cathodic reactions occurs since peaks corresponding to each one will appear. Furthermore, it is sensitive to reactions which proceed only to a small extent and to electrosorption of species in sub-monolayer amounts. Consequently, it has become an extremely popular experimental technique for the study of sulfides and their interactions with flotation reagents.

3.1.4 Intermittent Galvanostatic Polarization

The intermittent galvanostatic polarization (IGP) method is a modification of cyclic chronopotentiometry, in which a current is repeatedly applied to an electrode for a short duration and then turned off for, usually, an equal period of time. It has proven to be particularly useful in determining the reversible potentials of electrochemical reactions in aqueous systems. It was first applied by Nagel et al. (1957) in their studies of equilibrium potentials for electrochemical processes occurring in metal-water binary systems. Later, Horvath and Hackl (1965) used it successfully to verify calculated E_h-pH diagrams for metal-S-H_2O ternary

systems and to interpret the corrosion of metals in aqueous H_2S environments. More recently, Thornber (1982) used this technique and cyclic voltammetry to study the electrochemical reactions occurring at the surfaces of two nickel-iron sulfide minerals, pentlandite and violarite, at pH values from 0 to 8.

When a current is applied, the potential of the electrode will respond by increasing in the direction of the polarization until it reaches a level corresponding to an electron transfer reaction. When this happens, the electrode potential will begin to level off as the rate of the faradaic process is able to match the applied current. If for some reason, such as the reactant becoming depleted at the interface or the build-up of a product layer, the reaction can no longer keep up with the applied current, the potential will once again begin to change. The series of plateaus or arrests that appear on a recording of potential over time can be identified with the potentials for a sequence of reactions. However, the potentials must be measured at open-circuit in order for them to be related to equilibrium potentials. In order to do this and still continually polarize the electrode, the circuit is repeatedly opened and closed for short periods of time.

As the current pulses are applied, the electrode potential will be affected in two ways. The first is a rapid oscillation change as an immediate response to the current pulses (Figure 3.5). The second is a slower shift as the electrode goes through a succession of reactions. Since only the latter is of concern in this work, the potential is recorded at a slow speed, resulting in a continuous trace such as the

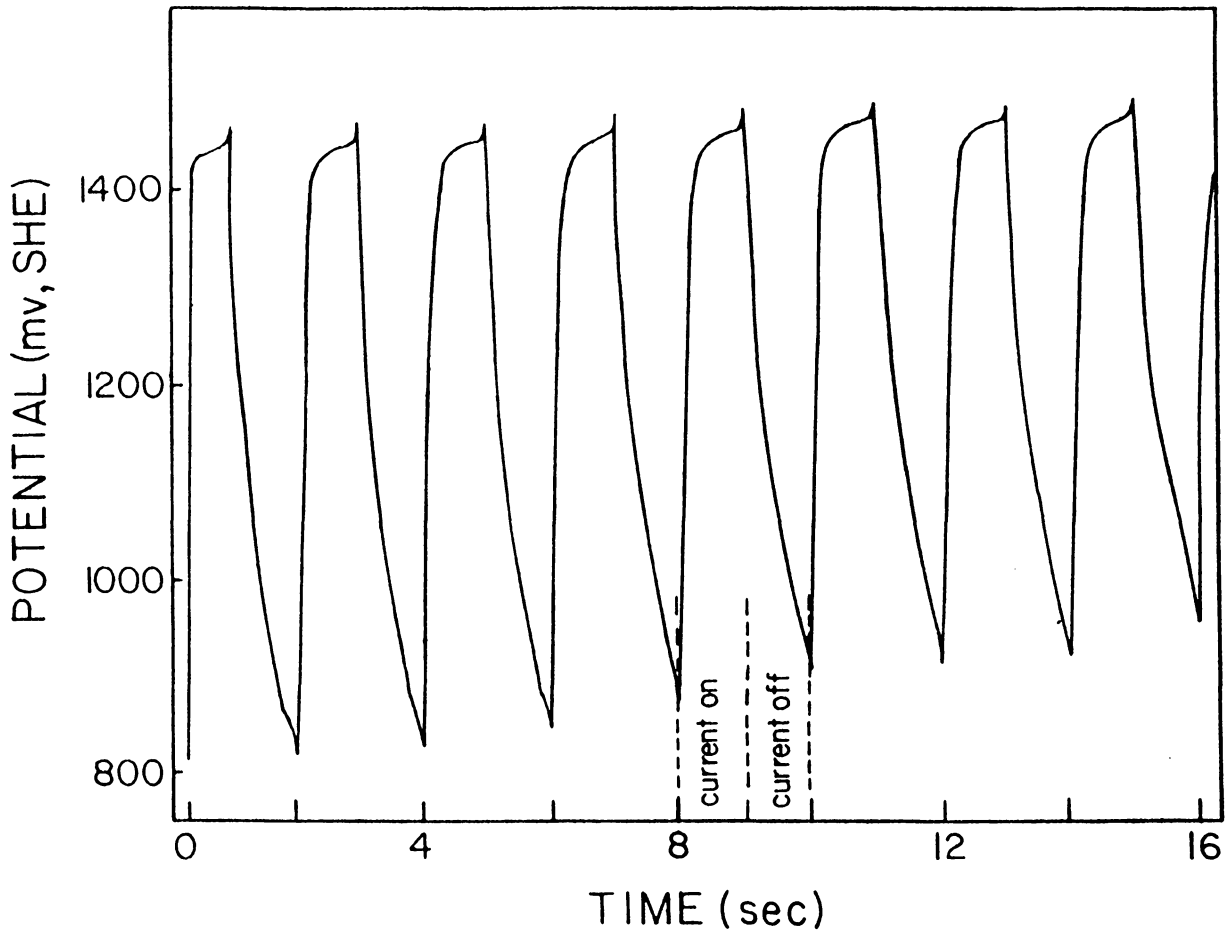


Figure 3.5 Typical response of the electrode potential to the application of short (1 second) on/off current pulses.

one appearing in Figure 3.6. The maximum for each excursion in the oscillation corresponds to the closed-circuit potential, while the minimum is the open-circuit potential.

Utilized in this way, the IGP technique is primarily a qualitative tool. A major reason for this is that a portion of the applied current is continually consumed by double-layer charging since the electrode potential is constantly changing with time. The magnitude of this effect will be influenced by a whole range of factors, such as the amplitude and duration of the current pulses, the instantaneous potential and the state of the electrode surface. Consequently, any attempt to quantify it will be extremely difficult.

3.2 Experimental

3.2.1 Materials

The galena used in the electrochemical and microflotation work was a research grade (> 99% pure) specimen obtained from Ward's Natural Science Establishment. It originated from the Brushy Creek Mine, Missouri.

The collector reagent was prepared by dissolving commercial grade potassium ethyl xanthate in acetone and recrystallizing it by adding petroleum ether. After repeating this three times, the purified crystals were kept immersed in the ether. When xanthate was needed, a small amount of the reagent was removed and the residual ether was driven off in a vacuum dessicator.

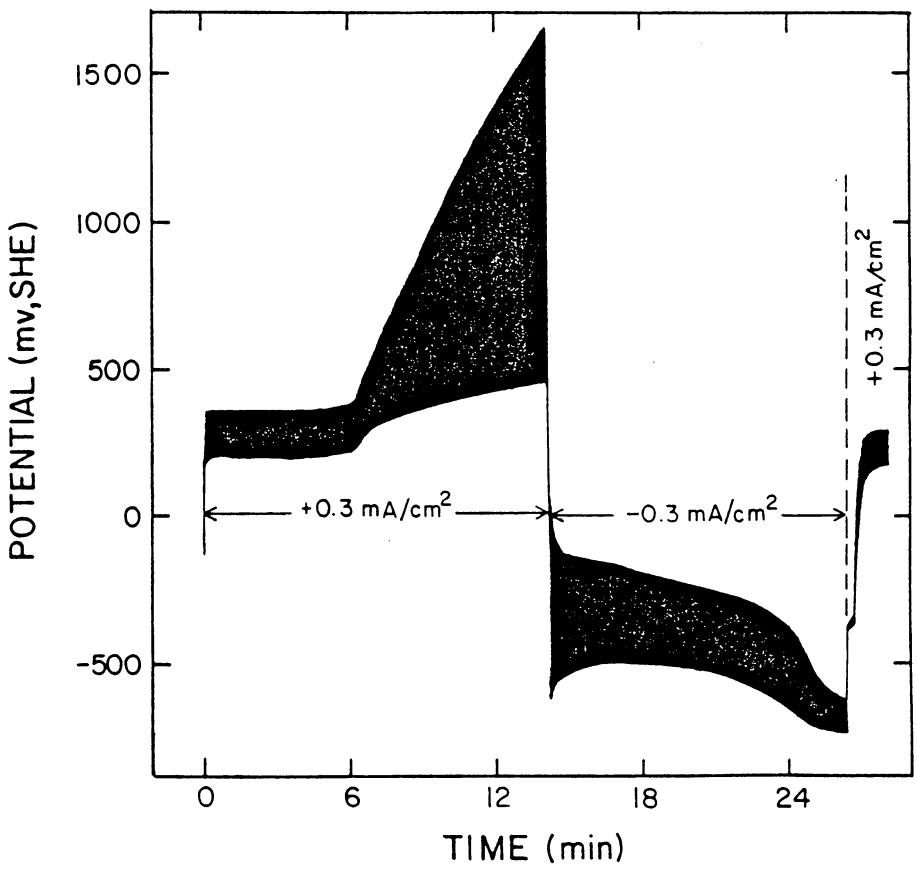


Figure 3.6 Typical IGP trace obtained after repeatedly applying short on/off current pulses and recording on a slow chart speed.

The electrochemical tests were conducted at pH 9.2 in 0.05 M $Na_2B_4O_7$ solutions and at pH 6.8 in 0.05 M KH_2PO_4/0.05 M Na_2HPO_4 solutions. Flotation tests were done only at pH 9.2. Fresh stock solutions of xanthate dissolved in the buffer solutions were prepared daily. The redox potential during microflotation was controlled by adding either hydrazine as a reducing agent or hydrogen peroxide as an oxidizing agent. All the chemicals were of A.C.S. reagent grade and all solutions were prepared with double-distilled water. Solutions were deoxygenated by purging with low-oxygen nitrogen gas (< 0.5 ppm O_2).

3.2.2 Preparation of Galena Electrode

A galena specimen about 1 cm in length with a rectangular cross-sectional area of 0.65 cm^2 was cut from a larger piece with a diamond saw. A copper lead was then fit into a small hole drilled into the back of the specimen and permanently attached with Electrodag 199, a carbon-based conducting cement. This assembly was then sealed in a glass holder with Buehler epoxy resin. The resistance of the electrode was measured at various times during its use and was always found to be between 5 and 10 ohms. Prior to each test run, the electrode surface was polished with 400- and 600-grit silicon carbide paper and then rinsed with distilled water.

3.2.3 Electrochemical Measurements

Prior to each experiment, 350 ml of the buffer solution was poured into the reaction vessel and then deoxygenated with nitrogen gas for one hour. Once the tests were begun, the gas sparger was raised above the

solution and nitrogen was continually introduced to maintain a positive pressure. Tests were conducted in the absence of xanthate and at collector concentrations of 10^{-4} and 10^{-3} M.

During the voltammetry and chronoamperometry experiments, a conventional three-electrode system was used. The electrode potential was controlled with a PAR Model 371 potentiostat/galvanostat and a PAR Model 175 Programmer; voltammograms were recorded on a Hewlett Packard 7004B X-Y recorder. The schematic diagram for this set-up is similar to the one shown in Figure 1.4. A saturated calomel electrode was used as the reference electrode, although all potentials reported here are expressed on the standard hydrogen scale. The determination of the areas under the current-voltage curves for the analysis of the voltammetry data was done with a Numonics electronic graphics calculator.

For the IGP experiments, the PAR 371 unit was operated in the galvanostatic mode and only a two-electrode system was needed (Figure 3.7). By placing a resistor across the controlled current binding posts on the potentiostat, voltage pulses from the programmer were converted to current pulses. A standard 470- or 1500-ohm resistor was used, depending on the desired currents. Each current pulse was applied for 1 second and then turned off for another second before being applied again. In order to monitor the change in electrode potential with time, the working electrode and reference electrode were connected across a Keithley Model 642 electrometer. The output was recorded on a Pedersen M27R strip chart recorder at a speed of 10 in/hr.

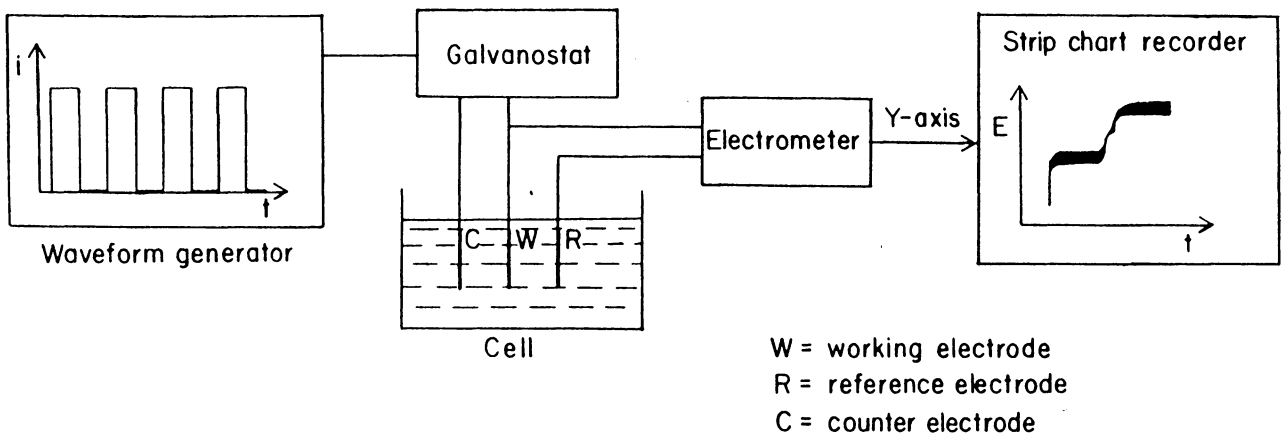


Figure 3.7 Schematic diagram of the instrumentation used for IGP experiments.

3.2.4 Microflotation Tests

In order to minimize oxidation, 1-gm flotation samples were prepared prior to each test by crushing a pure galena specimen with a porcelain mortar-and-pestle and screening out the -100+150 mesh size fraction.

Solutions were made by combining 80 ml of the borate buffer (pH 9.2) with 5 ml of the stock ethyl xanthate solution. The contents were deoxygenated by bubbling nitrogen through a sparger immersed in the solution. After 10 minutes, the ground galena was added and a small amount of hydrazine or peroxide was added to adjust the redox potential to the desired value. Then, the entire suspension was transferred to the flotation cell. To minimize possible oxidation, the preparation was done in such a way that the galena sample was introduced into the flask immediately after it was ground and the suspension was continually purged until it was transferred to the flotation cell.

As mentioned previously, a Partridge and Smith-type microflotation cell was used (Partridge and Smith, 1971). The redox potential of the solution was monitored with a platinum disk electrode and saturated calomel electrode connected to a Fisher Accumet Model 610 A potentiometer. This had been previously calibrated in a ZoBell solution, which has a known potential of 430 mv SHE. Flotation was initiated by passing nitrogen through a fine frit at the base of the cell and then continued for one minute. The floated and depressed portions were then collected, filtered, air-dried and then weighed.

3.3 Results and Discussion

3.3.1 In the Absence of Xanthate

a. Single sweep voltammetry at pH 9.2: The aqueous chemistry of galena at pH 9.2 was studied by conducting a series of voltammetry experiments on an electrode of this mineral in a 0.05 M $Na_2B_4O_7$ solution. Unless otherwise specified, the scans were begun from a potential of -355 mv at a speed of 20 mv/sec in the anodic direction. There was always the concern, despite the continual bubbling of nitrogen through the solution, that if the galena was immersed and kept at open-circuit conditions (i.e., not allowing any net current to flow) prior to the sweep, some oxidation would occur before it was desired. Consequently, a starting potential below the open-circuit value, which was typically between 0 and 100 mv, was chosen. In addition, holding the potential at -355 mv would remove oxidation products generated while the electrode was being polished and transferred to the cell. At the same time, the initial potential could not be too low to prevent galena from being reduced to lead metal.

Effect of anodic limit: In the first series of experiments, the effect of extending the scan to different anodic limits was investigated. Some of the voltammograms obtained in unstirred solutions are shown in Figure 3.8. All of these were single-cycle experiments in which the potential was scanned to the anodic limit, reversed down to a cathodic limit of -655 mv and then returned back in the anodic direction to a final potential of about -200 mv.

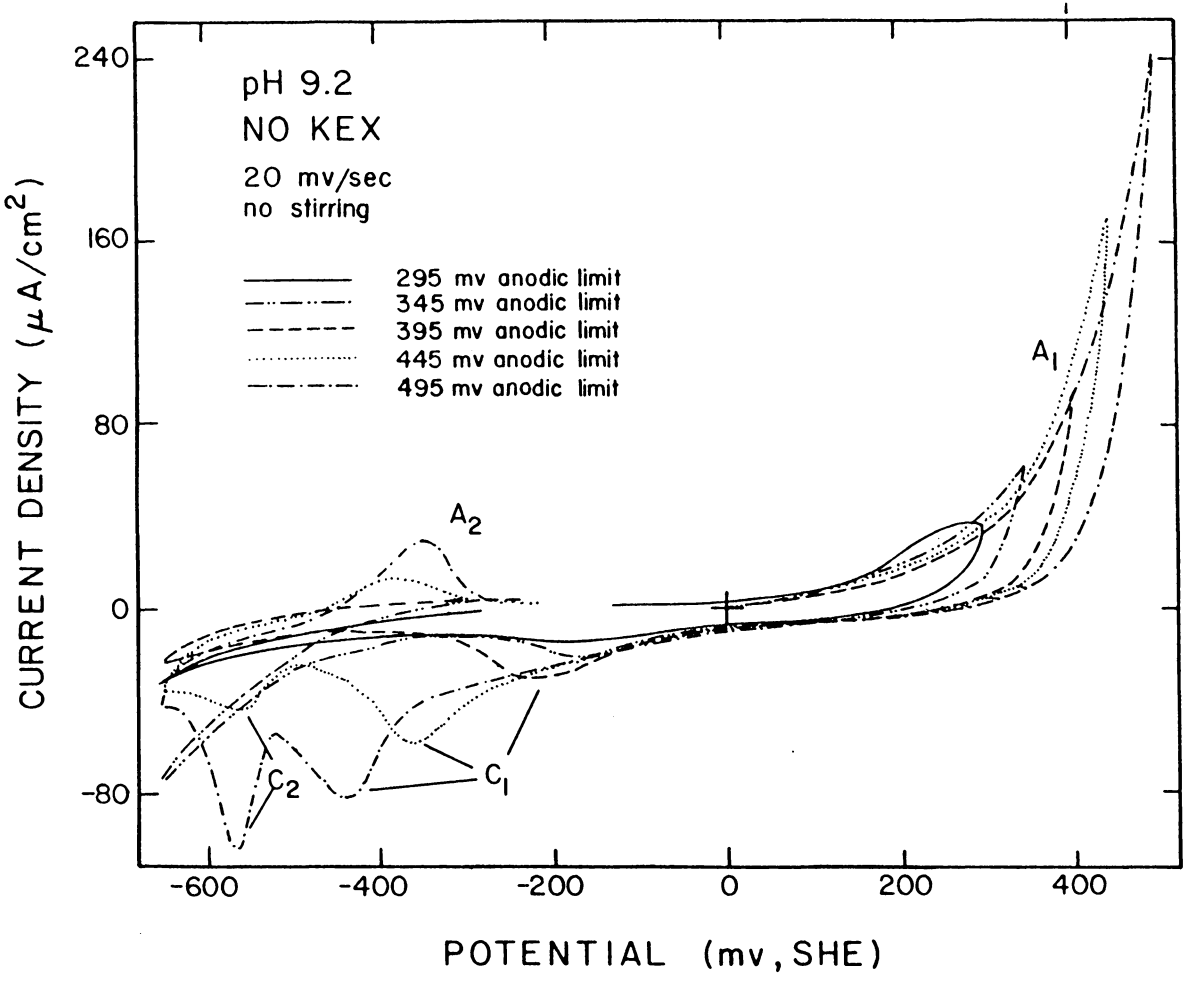


Figure 3.8 The effect of the anodic limit on the single sweep voltammograms for a galena electrode immersed in a 0.05 M $Na_2B_4O_7$ solution (pH 9.2). No stirring. Scan rate = 20 mv/sec.

Anodic current (denoted A_1) begins to flow at a potential of about 100 mv, which is close to what has been observed by others (Gardner and Woods, 1979b; Lamache et al., 1984). However, it is only when the anodic limit reaches 295 mv that a distinct cathodic peak (C_1) begins to appear during the reverse scan. With a further increase in the upper limit, the anodic current begins to rise sharply while the cathodic peak becomes more prominent and shifts toward more negative potentials. This shift indicates that it becomes increasingly difficult to remove the oxidation products as the anodic limit is extended. A second reduction peak (C_2) at approximately -550 mv, accompanied by a new oxidation peak (A_2) once the scan is reversed back in the positive direction, becomes visible in the voltammograms corresponding to anodic limits of 445 and 495 mv. Furthermore, the more negative cathodic peak C_2 grows in size relative to the other as the anodic limit is extended. The appearance of C_1 and C_2 for an anodic limit of 450 mv has also been observed by Gardner and Woods (1979b). Lamache et al. (1981) observed an additional reduction peak, but it should be noted that the anodic limit in their experiments was over 1000 mv.

Hamilton and Woods (1984) have proposed that the initial oxidation cannot be likened to any bulk reaction. Instead, it is a surface reaction involving the breakage of metal-sulfur bonds and the strengthening of sulfur-sulfur and metal-oxygen bonds. Eventually, bulk oxide and sulfur nucleate, at which point the overall reaction can be described as:

$$PbS + H_2O \longrightarrow PbO + S^o + 2H^+ + 2e. \qquad [3.6]$$

The voltammograms in Figure 3.8 show that the current begins to rise steeply above about 300 mv. Furthermore, a distinct peak, C_1, appears only when the anodic limit reaches 295 mv. These results suggest that this is the potential where the bulk phases first appear.

It is also apparent from Figure 3.8 that the current-voltage behavior is not exactly reproducible from one test to the next. In some instances, a pre-wave appears, whereas in other cases the current rise is much smoother. This apparent randomness primarily reflects the difficulty that is encountered in obtaining exactly reproducible data on the galena electrode from one test to the next. Apparently, oxidation of the galena is very sensitive to the sample preparation before immersion. It may proceed uniformly over the mineral surface, resulting in a complete initial monolayer of oxidation products that inhibits further oxidation. In this case, the voltammogram would show a pre-wave before the sharp current rise. If the oxidation products grow in clusters, then no distinction can be made between the completion of the first monolayer and the beginning of the second one. A smooth current rise would then result.

The appearance of C_1 and C_2 only after the galena is oxidized suggests that both can be associated with the reduction of species that are present because of the previous oxidation. Furthermore, C_2 is not observed each time that C_1 is, but only after the mineral is sufficiently oxidized. C_2 evidently involves the reduction of oxidation products associated with A_1 and not the further reduction of species

generated at C_1.

Effect of stirring: Examining the effect of stirring on a voltammogram can be an extremely useful tool in identifying reactions. Suppose that one of the products of an anodic reaction is soluble. If the solution is being stirred, then the soluble species will continually be dispersed away from the electrode surface. Now, when the scan direction is changed, the reverse of the anodic reaction will not occur since the soluble species is not present at the electrode. However, if the solution is quiescent, some of the soluble species will remain near the electrode and the cathodic reaction can proceed.

The effect of stirring on the voltammogram for galena is shown in Figure 3.9 and agrees well with what Gardner and Woods (1979b) have reported. Although there is a considerable difference in the relative sizes of C_1 and C_2 (more will be discussed concerning this later), it is significant that C_1, C_2 and A_2 all appear whether the solution is stirred or not. This is what is expected if all the reactions involve insoluble species.

Charge analysis of voltammetry peaks: Not only can a voltammogram indicate the potentials where faradaic reactions occur, but it can also provide direct information concerning the charge passed by them. This can be shown as follows: The coulombic charge, dQ, passed in the time interval, dt, when a current, $i(t)$ is flowing is given by:

$$dQ = i(t)\, dt. \qquad [3.7]$$

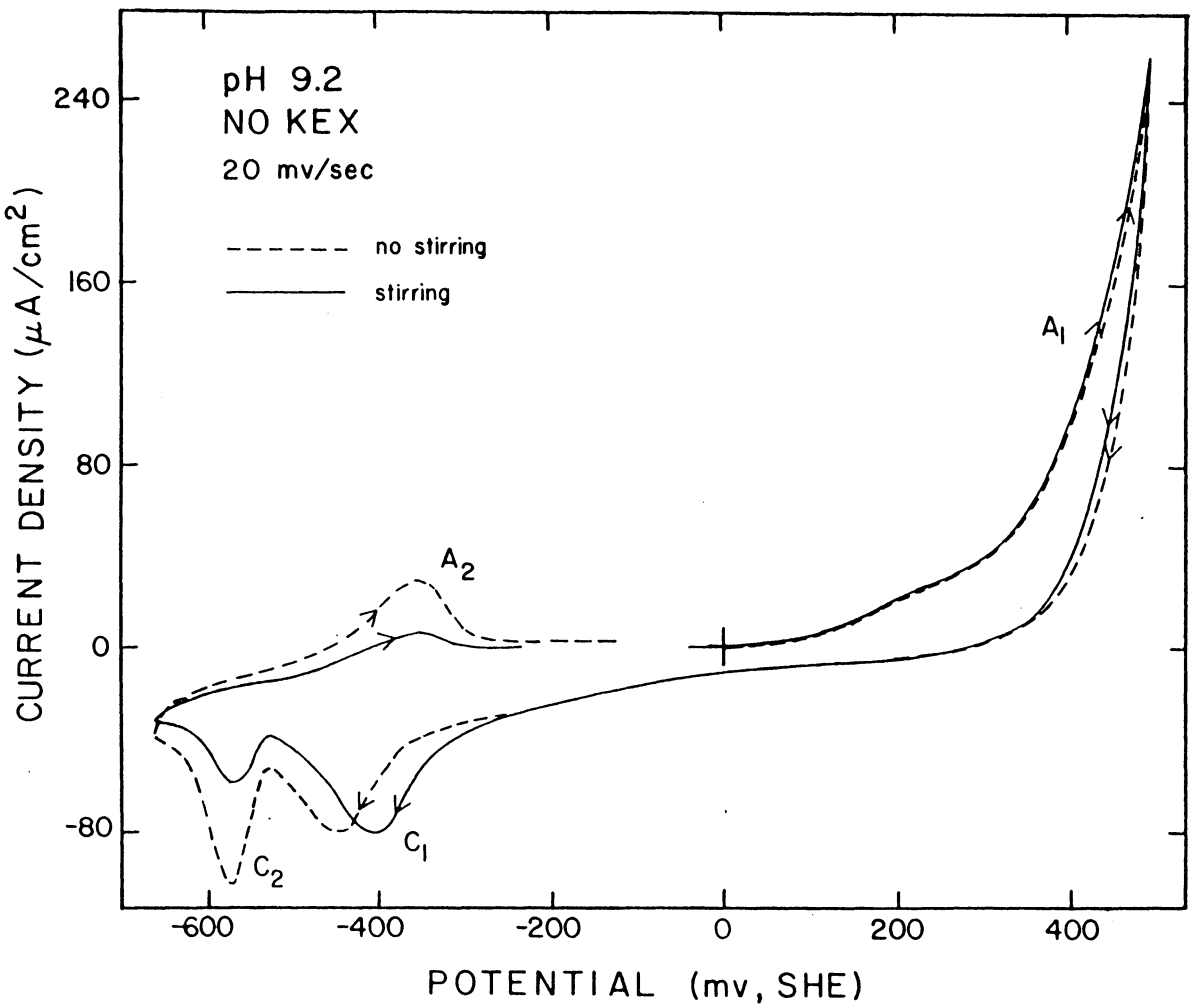


Figure 3.9 The effect of stirring on the single sweep voltammograms for a galena electrode immersed in a 0.05 M $Na_2B_4O_7$ solution (pH 9.2). Scan rate = 20 mv/sec.

Consequently, the total charge, Q, accumulated between t_1 and t_2 will be given by the integral,

$$Q = \int_{t_1}^{t_2} i(t)\, dt. \qquad [3.8]$$

However, in linear sweep voltammetry, it is more convenient to express Q in terms of current and potential. This can be achieved by recognizing that the potential, E, is a linear function of time:

$$E = E_i + vt, \qquad [3.9]$$

where E_i is the starting potential and v is the scan rate. Substituting Eq. [3.9] into Eq. [3.8] yields the expression:

$$Q = \frac{1}{v} \int_{E_1}^{E_2} i(E)\, dE, \qquad [3.10]$$

from which it can be seen that Q is proportional to the area under a voltammogram from E_1 to E_2. It thus becomes a straightforward matter to determine from a voltammogram the amount of charge associated with the various reactions.

It was shown previously that the reactions at C_1 and C_2 in the voltammograms of Figure 3.8 involved the reduction of the products of A_1. By assuming that all of these oxidation products are consumed by C_1 and C_2, it is possible to derive a relationship between the charges associated with A_1, C_1 and C_2 for a particular sequence of reactions. The most probable reaction sequences can then be determined by comparing the observed charge relationship with the theoretical ones for various proposed reactions. Such an analysis has been carried out on the

voltammograms in Figure 3.8 to gain more insight into the galena-water system.

Possible reaction schemes that have been considered are listed in Table 3.1, along with the theoretical relationships between Q_{A1}, Q_{C1} and Q_{C2}. In every case, each cathodic reaction involves at least one insoluble reactant in accordance with what has been concluded on the basis of the effect of stirring. The product of the reduction of $PbSO_4$ has been taken to be Pb^o rather than PbS based on what has been found to occur in lead-acid batteries (Gardner and Woods, 1979b). Also, oxidation reactions generating $S_2O_3^{2-}$ or SO_4^{2-} are considered irreversible, so that when the scan is reversed, these ions do not participate in any cathodic reactions. The derivation of the relationship between the charges for one sequence has been included in Appendix II as an example.

It should be emphasized that the charge determined by an area measurement can only be considered an approximate value. Since the electrode potential is continually changing during a sweep, a portion of the generated charge is associated with double-layer charging and not the faradaic processes. However, this double-layer charging is proportional to the scan rate and, consequently, should not be significant considering the relatively slow sweep rates employed in this study.

In the cases where two voltammetry peaks are separated but not entirely resolved (e.g., peaks C_1 and C_2 in Figure 3.9), the following assumption has been made. All the current on the C_1 side of the minimum between the two peaks is attributed to C_1 and the current on the other

Table 3.1

Possible Reaction Sequences in the Galena-Water System at pH 9.2

		Sequence	Charge Relationship
1.	A_1	$PbS + H_2O \longrightarrow PbO + S^o + 2H^+ + 2e$ $2PbS + 5H_2O \longrightarrow 2PbO + S_2O_3^{2-} + 10H^+ + 8e$	$\frac{Q_{A1} - Q_{C1}}{Q_{C2}} = 2$
	C_1	$PbO + S^o + 2H^+ + 2e \longrightarrow PbS + H_2O$	
	C_2	$PbO + 2H^+ + 2e \longrightarrow Pb^o + H_2O$	
2.	A_1	$PbS + H_2O \longrightarrow PbO + S^o + 2H^+ + 2e$ $PbS + 5H_2O \longrightarrow PbO + SO_4^{2-} + 10H^+ + 8e$	$\frac{Q_{A1} - Q_{C1}}{Q_{C2}} = 4$
	C_1	$PbO + S^o + 2H^+ + 2e \longrightarrow PbS + H_2O$	
	C_2	$PbO + 2H^+ + 2e \longrightarrow Pb^o + H_2O$	
3.	A_1	$PbS + H_2O \longrightarrow PbO + S^o + 2H^+ + 2e$ $PbS + H_2O \longrightarrow PbOH^+ + S^o + H^+ + 2e$	$\frac{Q_{A1} - Q_{C1}}{Q_{C2}} = 1$
	C_1	$PbO + S^o + 2H^+ + 2e \longrightarrow PbS + H_2O$	
	C_2	$PbOH^+ + S^o + H^+ + 2e \longrightarrow PbS + H_2O$	
4.	A_1	$PbS + H_2O \longrightarrow PbO + S^o + 2H^+ + 2e$ $PbS + H_2O \longrightarrow PbOH^o + S^o + 2H^+ + 2e$	$\frac{Q_{A1} - Q_{C1}}{Q_{C2}} = 1$
	C_1	$PbO + S^o + 2H^+ + 2e \longrightarrow PbS + H_2O$	
	C_2	$S^o + H^+ + 2e \longrightarrow HS^-$	
5.	A_1	$PbS + H_2O \longrightarrow PbO + S^o + 2H^+ + 2e$ $PbS + 5H_2O \longrightarrow PbOH^+ + SO_4^{2-} + 9H^+ + 8e$	$Q_{C1} = Q_{C2}$
	C_1	$S^o + H^+ + 2e \longrightarrow HS^-$	
	C_2	$PbO + 2H^+ + 2e \longrightarrow Pb^o + H_2O$	
6.	A_1	$PbS + H_2O \longrightarrow PbO + S^o + 2H^+ + 2e$ $2PbS + 5H_2O \longrightarrow 2PbOH^+ + S_2O_3^{2-} + 8H^+ + 8e$	$Q_{C1} = Q_{C2}$
	C_1	$S^o + H^+ + 2e \longrightarrow HS^-$	
	C_2	$PbO + 2H^+ + 2e \longrightarrow Pb^o + H_2O$	
7.	A_1	$PbS + H_2O \longrightarrow PbO + S^o + 2H^+ + 2e$	$Q_{A1} = Q_{C1} = Q_{C2}$
	C_1	$S^o + H^+ + 2e \longrightarrow HS^-$	
	C_2	$PbO + 2H^+ + 2e \longrightarrow Pb^o + H_2O$	

8. A_1 $PbS + H_2O \longrightarrow PbO + S^o + 2H^+ + 2e$
$PbS + 4H_2O \longrightarrow PbSO_4 + 8H^+ + 8e$

C_1 $PbO + S^o + 2H^+ + 2e \longrightarrow PbS + H_2O$
C_2 $PbSO_4 + 2e \longrightarrow Pb^o + SO_4^{2-}$

$$\frac{Q_{A1} - Q_{C1}}{Q_{C2}} = 4$$

9. A_1 $PbS + H_2O \longrightarrow PbO + S^o + 2H^+ + 2e$
$PbS + 4H_2O \longrightarrow PbSO_4 + 8H^+ + 8e$

C_1 $PbO + S^o + 2H^+ + 2e \longrightarrow PbS + H_2O$
C_2 $PbSO_4 + 9H^+ + 10e \longrightarrow Pb^o + HS^- + 4H_2O$

$$\frac{Q_{A1} - Q_{C1}}{Q_{C2}} = 0.8$$

10. A_1 $PbS + H_2O \longrightarrow PbO + S^o + 2H^+ + 2e$
$2PbS + 5H_2O \longrightarrow 2PbO + S_2O_3^{2-} + 10H^+ + 8e$

C_1 $S^o + H^+ + 2e \longrightarrow HS^-$
C_2 $PbO + 2H^+ + 2e \longrightarrow Pb^o + H_2O$

$$\frac{Q_{A1} + Q_{C1}}{Q_{C2}} = 2$$

11. A_1 $PbS + H_2O \longrightarrow PbO + S^o + 2H^+ + 2e$
$PbS + 5H_2O \longrightarrow PbO + SO_4^{2-} + 10H^+ + 8e$

C_1 $S^o + H^+ + 2e \longrightarrow HS^-$
C_2 $PbO + 2H^+ + 2e \longrightarrow Pb^o + H_2O$

$$\frac{Q_{A1} + 3Q_{C1}}{Q_{C2}} = 4$$

12. A_1 $PbS + H_2O \longrightarrow PbOH^+ + S^o + H^+ + 2e$
$2PbS + 5H_2O \longrightarrow 2PbO + S_2O_3^{2-} + 10H^+ + 8e$

C_1 $S^o + H^+ + 2e \longrightarrow HS^-$
C_2 $PbO + 2H^+ + 2e \longrightarrow Pb^o + H_2O$

$$\frac{Q_{A1} - Q_{C1}}{Q_{C2}} = 2$$

13. A_1 $PbS + H_2O \longrightarrow PbOH^+ + S^o + H^+ + 2e$
$2PbS + 5H_2O \longrightarrow 2PbO + S_2O_3^{2-} + 10H^+ + 8e$

C_1 $PbO + S^o + 2H^+ + 2e \longrightarrow PbS + H_2O$
C_2 $PbO + 2H^+ + 2e \longrightarrow Pb^o + H_2O$

$$\frac{Q_{A1} - 3Q_{C1}}{Q_{C2}} = 2$$

14. A_1 $PbS + H_2O \longrightarrow PbOH^+ + S^o + H^+ + 2e$
$2PbS + 5H_2O \longrightarrow 2PbO + S_2O_3^{2-} + 10H^+ + 8e$

C_1 $PbOH^+ + S^o + H^+ + 2e \longrightarrow PbS + H_2O$
C_2 $PbO + 2H^+ + 2e \longrightarrow Pb^o + H_2O$

$$\frac{Q_{A1} - Q_{C1}}{Q_{C2}} = 2$$

15. A_1 $PbS + H_2O \longrightarrow PbOH^+ + S^o + H^+ + 2e$
$2PbS + 5H_2O \longrightarrow 2PbO + S_2O_3^{2-} + 10H^+ + 8e$

C_1 $PbOH^+ + S^o + H^+ + 2e \longrightarrow PbS + H_2O$
C_2 $PbO + S^o + 2H^+ + 2e \longrightarrow PbS + H_2O$

$$\frac{Q_{A1} - Q_{C1}}{Q_{C2}} = 3$$

16. A_1 $PbS + H_2O \longrightarrow PbOH^+ + S^o + H^+ + 2e$
$2PbS + 5H_2O \longrightarrow 2PbO + S_2O_3^{2-} + 10H^+ + 8e$

C_1 $PbO + S^o + 2H^+ + 2e \longrightarrow PbS + H_2O$
C_2 $S^o + H^+ + 2e \longrightarrow HS^-$

$$\frac{Q_{A1} - 3Q_{C1}}{Q_{C2}} = 1$$

17. A_1 $PbS + H_2O \longrightarrow PbOH^+ + S^o + H^+ + 2e$
$PbS + 5H_2O \longrightarrow PbO + SO_4^{2-} + 10H^+ + 8e$

C_1 $S^o + H^+ + 2e \longrightarrow HS^-$
C_2 $PbO + 2H^+ + 2e \longrightarrow Pb^o + H_2O$

$$\frac{Q_{A1} - Q_{C1}}{Q_{C2}} = 4$$

18. A_1 $PbS + H_2O \longrightarrow PbOH^+ + S^o + H^+ + 2e$
$PbS + 5H_2O \longrightarrow PbO + SO_4^{2-} + 10H^+ + 8e$

C_1 $PbO + S^o + 2H^+ + 2e \longrightarrow PbS + H_2O$
C_2 $PbO + 2H^+ + 2e \longrightarrow Pb^o + H_2O$

$$\frac{Q_{A1} - 5Q_{C1}}{Q_{C2}} = 4$$

19. A_1 $PbS + H_2O \longrightarrow PbOH^+ + S^o + H^+ + 2e$
$PbS + 5H_2O \longrightarrow PbO + SO_4^{2-} + 10H^+ + 8e$

C_1 $PbOH^+ + S^o + H^+ + 2e \longrightarrow PbS + H_2O$
C_2 $PbO + 2H^+ + 2e \longrightarrow Pb^o + H_2O$

$$\frac{Q_{A1} - Q_{C1}}{Q_{C2}} = 4$$

20. A_1 $PbS + H_2O \longrightarrow PbOH^+ + S^o + H^+ + 2e$
$PbS + 5H_2O \longrightarrow PbO + SO_4^{2-} + 10H^+ + 8e$

C_1 $PbOH^+ + S^o + H^+ + 2e \longrightarrow PbS + H_2O$
C_2 $PbO + S^o + 2H^+ + 2e \longrightarrow PbS$

$$\frac{Q_{A1} - Q_{C1}}{Q_{C2}} = 5$$

21. A_1 $PbS + H_2O \longrightarrow PbOH^+ + S^o + H^+ + 2e$
$PbS + 5H_2O \longrightarrow PbO + SO_4^{2-} + 10H^+ + 8e$

C_1 $PbO + S^o + 2H^+ + 2e \longrightarrow PbS + H_2O$
C_2 $S^o + H^+ + 2e \longrightarrow HS^-$

$$\frac{Q_{A1} - 5Q_{C1}}{Q_{C2}} = 1$$

22. A_1 $PbS + H_2O \longrightarrow PbOH^+ + S^o + H^+ + 2e$
$PbS + 4H_2O \longrightarrow PbSO_4 + 8H^+ + 8e$

C_1 $S^o + H^+ + 2e \longrightarrow HS^-$
C_2 $PbSO_4 + 2e \longrightarrow Pb^o + SO_4^{2-}$

$$\frac{Q_{A1} - Q_{C1}}{Q_{C2}} = 4$$

23. A_1 $PbS + H_2O \longrightarrow PbOH^+ + S^o + H^+ + 2e$
$PbS + 4H_2O \longrightarrow PbSO_4 + 8H^+ + 8e$

C_1 $S^o + H^+ + 2e \longrightarrow HS^-$
C_2 $PbSO_4 + 9H^+ + 10e \longrightarrow Pb^o + HS^- + 4H_2O$

$$\frac{Q_{A1} - Q_{C1}}{Q_{C2}} = 0.8$$

24. A_1 $PbS + 4H_2O \longrightarrow PbSO_4 + 8H^+ + 8e$

C_1 $PbSO_4 + 9H^+ + 10e \longrightarrow Pb^o + HS^- + 4H_2O$

C_2 $PbSO_4 + 2e \longrightarrow Pb^o + SO_4^{2-}$

$$\frac{Q_{A1} - 0.8Q_{C1}}{Q_{C2}} = 4$$

side to C_2.

Integration under the voltammograms for different anodic limits gives the results shown in Table 3.2. Only at limits of 445, 495 and 545 mv is the C_2 peak large enough for reliable values of Q_{C2}/Q_{A1} to be determined. In these cases, the experimental values of $(Q_{A1} - Q_{C1})/Q_{C2}$ are 2.10, 2.04 and 1.94, respectively. Comparison of these with the theoretical ones in Table 3.1 indicates that the data coincide very closely with what is expected for reaction sequences 1, 12 and 14. No others fit nearly as well.

The oxidation reactions for these three cases are quite similar and result in the formation of PbO, S^o and $S_2O_3^{2-}$ on the galena surface. The only difference is that according to sequences 12 and 14, some of the PbO goes into solution as $PbOH^+$ ions. Recalling the E_h-pH diagrams for the PbS-H_2O system in the previous chapter (Figures 2.2, 2.6, 2.11), it becomes apparent that there are considerable differences between what is predicted and what seems to be observed. For one thing, neither Case II nor Case III alone can accomodate the co-existence of S^o and $S_2O_3^{2-}$ at this pH. This is clearly due to the sluggish kinetics of sulfur oxidation. For another, the thermodynamic calculations predict that PbO should not be stable until the pH reaches 10.1. Two possible reasons for the discrepancy between this and what the voltammograms indicate are that i) bulk free energy data have been used for these surface reactions and ii) there may be a considerable difference between the surface concentrations and the bulk concentrations of soluble species. One of the assumptions of these calculations is that mass transfer is so

Table 3.2

Charge Ratios Q_{C1}/Q_{A1} and Q_{C2}/Q_{A1} from the Single Sweep Scans as a Function of Anodic Limit

Anodic Limit (mv)	Q_{C1}/Q_{A1}	Q_{C2}/Q_{A1}
195	0.64	---
245	0.72	---
295	0.74	---
345	0.67	---
395	0.65	---
445	0.66	0.16
495	0.53	0.23
545	0.30	0.36

rapid that surface concentrations can be equated with bulk concentrations. It is possible that significant concentration gradients exist and that the surface activity of $PbOH^+$ or the local pH is high enough that PbO can form at the electrode surface. The effect of stirring that has been shown previously in Figure 3.9 does seem to bear this out. Agitation of the solution causes a significant diminution of the C_2 peak, which in all three sequences of 1, 12 and 14 involves the reduction of PbO to Pb^o. This is likely due to the fact that some of the PbO formed during the anodic scan has dissolved away by the time the scan reaches the C_2 peak. Apparently, the dissolution of PbO to $PbOH^+$ is limited by the supply of H^+ ions to the electrode surface.

It is noteworthy that Lamache et al. (1984) directly determined the oxidation products generated on galena after electrolyzing the mineral at pH 9.2 and found them to be S^o, $S_2O_3^{2-}$ and Pb(II) species. They concluded that PbO and Pb(OH)Cl were the likely Pb(II) species since they were thermodynamically favored under the conditions of their experiment. (The buffer they used was 0.5 M NH_4OH/0.5 M NH_4Cl.) Gardner and Woods (1979b) also concluded that S^o, $S_2O_3^{2-}$ and PbO were being formed on the basis of a similar treatment of their voltammograms as in the present study.

The reversible potentials for reaction [3.6] and for reaction,

$$2PbS + 5H_2O \longrightarrow 2PbO + S_2O_3^{2-} + 10H^+ + 8e, \qquad [3.11]$$

in A_1 of sequences 1, 12 and 14 are 234 and 135 mv (for $[S_2O_3^{2-}] = 10^{-6}$ M), respectively. The fact that current in the voltammograms in

Figures 3.8 and 3.9 begins to rise at potentials considerably lower than these values adds credence to the proposal of Hamilton and Woods (1984) that the initial stages of oxidation cannot be described by a bulk reaction. Instead, between about 0 and 300 mv (see Figures 3.8 and 3.9), a metal-deficient sulfide is being formed by reaction [2.41]. When 300 mv is reached, enough metal has been lost from the sulfide lattice at the surface that elemental sulfur nucleates. At this point, the current begins to rise more sharply, as can be seen in Figures 3.8 and 3.9, and oxidation can be described in terms of such bulk reactions as [3.6] and [3.11].

The values of Q_{A1}, Q_{C1} and Q_{C2} can be used to calculate the relative amounts of elemental sulfur and thiosulfate produced by the oxidation of the mineral. From the assumption that all of the oxidation products generated under A_1 are consumed by C_1 and C_2 in each cycle, it follows that all of the elemental sulfur present will be reduced by any of the C_1 reactions in sequences 1, 12 and 14. Thus, the charge associated with C_1 can be used as a measure of the amount of sulfur without knowing the exact identity of the reaction. It can be shown (see Appendix II) that the molar ratio of $S_2O_3^{2-}$ to S^o in all three cases is given by the expression,

$$\frac{n_{S_2O_3^{2-}}}{n_{S^o}} = \frac{1}{4}\,\frac{1 - Q_{C1}/Q_{A1}}{Q_{C1}/Q_{A1}} \qquad [3.12]$$

where n is the number of moles of $S_2O_3^{2-}$ or S^o. This ratio does not depend on the C_2 peak so that it can be determined even for the

voltammograms in Figure 3.8 where the peak does not appear.

The results listed in Table 3.3 indicate that up to approximately 500 mv, the amount of thiosulfate produced is constant and small compared to the amount of sulfur. However, beyond this potential, oxidation to thiosulfate increases rapidly and soon becomes dominant.

This entire analysis is based on the assumption that all of the oxidation products PbO and S^o are reduced by C_1 and C_2. An argument can be made that this is not valid, particularly if oxidation has been considerable. In this case, a value of Q_{C1}/Q_{A1} less than unity will not necessarily mean that an oxy-sulfur anion is being formed. Furthermore, this ratio should also be affected by the scan rate if removal of oxidation products is difficult since the time allowed for this would vary. However, analysis of the data shows that all the Q_{C1}/Q_{A1} values are between 0.58 and 0.68 for a series of experiments in which the scan rate was varied from 5 to 60 mv/sec and the anodic limit was held at 345 mv. These results support the conclusion that thiosulfate is indeed being formed. In addition, it is difficult to come to another conclusion considering that the ratios $(Q_{A1} - Q_{C1})/Q_{C2}$ in Table 3.2 are so close to the ideal value of 2.

Although the choices for the cathodic reaction, C_2, are identical in the reaction sequences 1, 12 and 14, i.e.,

$$PbO + 2H^+ + 2e \longrightarrow Pb^o + H_2O, \qquad [3.13]$$

those for C_1 are different in each case. They turn out to be:

Table 3.3

Molar Ratios $S_2O_3^{2-}/S^o$ Resulting from the Oxidation of Galena During Single Sweep Scans to Different Anodic Limits

Anodic Limit (mv)	$n_{S_2O_3^{2-}}/n_{S^o}$
195	0.14
245	0.10
295	0.09
345	0.12
395	0.13
445	0.13
495	0.22
545	0.58

Sequence 1 $PbO + S^o + 2H^+ + 2e \longrightarrow PbS + H_2O$ [3.14]

Sequence 12 $S^o + H^+ + 2e \longrightarrow HS^-$ [3.15]

Sequence 14 $PbOH^+ + S^o + H^+ + 2e \longrightarrow PbS + H_2O.$ [3.16]

Gardner and Woods (1979b) proposed the first one, although it is not certain that they ever considered the other two.

Identification of A_2 peak: It was mentioned previously with regard to the voltammograms in Figure 3.8, that the A_2 peak appears only once C_2 does. This suggests that it involves the oxidation of at least one of the products of reaction C_2, presumably Pb^o. In the reaction sequences 1 and 14, no other species that are generated in C_1 or C_2 are likely to be oxidized with Pb^o. In this case, the choice of a reaction for A_2 may be the oxidation of Pb^o to PbO or $PbOH^+$, i.e.,

$$Pb^o + H_2O \longrightarrow PbO + 2H^+ + 2e \quad [3.17]$$

$$Pb^o + H_2O \longrightarrow PbOH^+ + H^+ + 2e. \quad [3.18]$$

In the case of sequence 12, HS^- ions are also available from the reduction of S^o, and so another reaction in addition to those above is possible:

$$Pb^o + HS^- \longrightarrow PbS + H^+ + 2e. \quad [3.19]$$

The Nernst potentials for reactions [3.17], [3.18] and [3.19] (assuming $[PbOH^+] = [HS^-] = 10^{-6}$ M) at pH 9.2 are -266 mv, -366 mv and -661 mv, respectively. From the curves in Figures 3.8 and 3.9, current due to A_2 begins to flow at approximately -450 mv in an unstirred

solution. If reaction [3.17] or [3.18] is attributed to A_2, then this requires that there be a considerable underpotential in either case. Hamilton and Woods (1984) also noted a similar situation with this peak in their voltammetric studies. Based on some XPS work done on the same mineral sample (Buckley and Woods, 1984a,b), they speculated that the peak they were observing was due to the oxidation of an impurity, antimony, to its oxide. However, even in this event, they should still have observed a Pb^o/PbO peak.

One explanation for this discrepancy may be that the pH in the surface region may be significantly higher than the value of 9.2 in the bulk. Both the reactions C_1 and C_2 during the cathodic sweep consume H^+ ions and this may bring about their depletion at the galena surface. Since the scan direction is reversed almost immediately upon the completion of C_2 during these experiments, there may not be sufficient time for the surface concentration of H^+ ions to be replenished. This would have the effect of reducing the potential at which reaction [3.17] or [3.18] begins compared to the reversible potential based on the bulk pH.

If the oxidation of Pb^o proceeds by reaction [3.19], then there is no problem concerning any underpotential. However, even in an unstirred solution, some of the HS^- produced by reaction [3.15] will have diffused away from the electrode by the time A_2 is reached. This will create an excess of Pb^o over HS^- at the surface, with the result that not all the lead can be removed by reaction [3.19]. A separate reaction, such as [3.17] or [3.18], will then be required to remove the excess Pb^o and, consequently, two anodic peaks should be visible in the

voltammogram. However, from Figures 3.8 and 3.9, it can be seen that only one appears. This suggests that reaction [3.17] or [3.18] is the more likely choice for A_2 whether the solution is being stirred or not. Up to this point in the discussion, the possibility that the borate electrolyte itself may be reacting with the electrode surface has been ignored. Khairy et al. (1966b) and Abdul Azim and Anwar (1969) have studied the anodic passivation of lead metal over a range of pH values and also found evidence for an anodic reaction at a potential of about -370 mv in a 0.1 M $Na_2B_4O_7$ solution of pH 9.1. However, they attributed it to the oxidation of Pb^o to $Pb(BO_2)_2$ and not to PbO. They supported this conclusion with the fact that the reversible potential of -400 mv for the formation of lead borate at pH 9.2 is very close to where the reaction is observed to begin. In addition, they observed another anodic reaction at -250 mv, which is almost identical to that for the oxidation of Pb^o to PbO (i.e., reaction [3.17]). Assigning the A_2 peak in Figures 3.8 and 3.9 to the formation of $Pb(BO_2)_2$ would eliminate the difficulty of the existence of an underpotential, as is the case for the formation of PbO or $PbOH^+$ via reactions [3.17] and [3.18].

b. Cyclic voltammetry at pH 9.2:

Identification of C_1 peak: In order to look at the C_1 peak more closely, experiments in which the cathodic limit was raised were carried out. Figure 3.10 shows the voltammograms obtained in a stagnant solution by repeatedly cycling the potential between -455 and 345 mv. According to sequence 12, HS^- ions should be produced by the reaction at

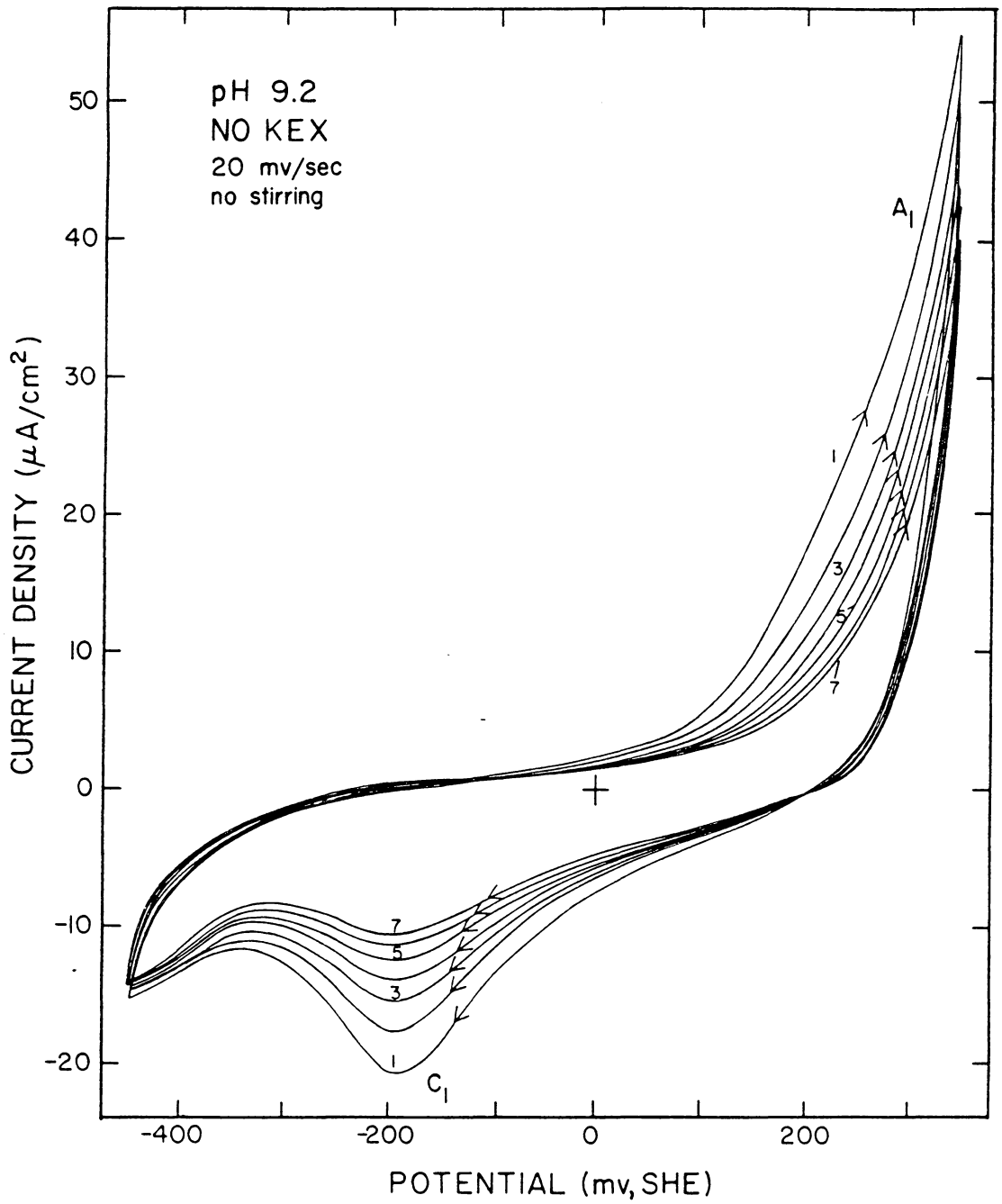


Figure 3.10 Cyclic voltammograms of a galena electrode in a 0.05 M $Na_2B_4O_7$ solution (pH 9.2) for potential sweeps between -455 and 345 mv. No stirring. Scan rate = 20 mv/sec. The number next to each curve denotes the cycle number.

A_1 = $PbS/PbO,S^0$ + $PbS/PbO,S_2O_3^{2-}$

C_1 = $PbO,S^0/PbS$ or S^0/HS^-

C_1. One might expect them to be oxidized back to S^o when the scan is reversed back in the anodic direction. However, no new anodic peak that might correspond to this is evident on the voltammogram. The reversible potential for the HS^-/S^o redox couple at pH 9.2, assuming that the surface concentration of HS^- ions is 10^{-6} M, is equal to -160 mv. Although this is close to where PbS itself begins to be oxidized, a separate peak or a shoulder for the oxidation of HS^- would still be expected.

However, the failure of a peak corresponding to the HS^-/S^o couple to appear does not necessarily eliminate sequence 12 as a valid choice. At pH 9.2, the equilibrium for reaction,

$$PbO + HS^- \longrightarrow PbS + OH^-, \qquad [3.20]$$

is shifted very strongly to the right and so it is very possible that all the HS^- near the electrode surface is consumed in this way. A voltammogram, of course, is not able to detect such a process.

Both of the C_1 reactions in sequences 1 and 14 involve the formation of PbS and, consequently, no additional anodic peak should appear when the scan direction is reversed. Therefore, it is not possible to rule out any of the three sequences on the basis of this experiment.

Effect of cycling on oxidation: An interesting observation concerning the cyclic voltammograms in Figure 3.10 is that the ratio Q_{C1}/Q_{A1} during each scan remains constant at about 0.71 (Table 3.4) although the total amount of mineral being oxidized decreases. This value is close to that of 0.67 obtained in the single-scan experiment

Table 3.4

Charge Ratios Q_{C1}/Q_{A1} and Q_{CT}/Q_{A1} Obtained During Cyclic Scans Between -455 and 345 mv

Cycle Number	Q_{C1}/Q_{A1}	Q_{CT}/Q_{A1}
1	0.70	0.97
2	0.72	1.07
3	0.72	1.08
4	0.72	1.11
5	0.72	1.14
6	0.70	1.14
7	0.69	1.17

for the same anodic limit of 345 mv (Figure 3.8, Table 3.2). This shows that repeated cycling does not significantly change the relative amounts of S^o and $S_2O_3^{2-}$ formed during oxidation. Using Eq. [3.12], $n_{S_2O_3^{2-}}/n_{S^o}$ is calculated to average about 0.10 throughout the experiment. In addition, the ratio of the total cathodic charge to the anodic charge passed (i.e., Q_{CT}/Q_{A1}) increased from 0.97 in the first cycle to 1.17 in the last one. Apparently, the removal of oxidation products is not inhibited by the continuous sweeping. The decline in the current rise at A_1 with each cycle indicates that the electrode is becoming passivated. This may partly be caused by the fact that the cathodic limit of -455 mv in these scans is too high for all the PbO to be removed by reaction [3.13].

With the small potential range scanned in this experiment, it is difficult to conclude anything concerning the effect of the cycling on the formation and reduction of PbO. The upper and lower limits were, therefore, extended to 445 and -555 mv so that the C_2 and A_2 peaks would appear. The resulting voltammogram (Figure 3.11) shows that both A_1 and C_1 diminish with the continuous cycling (as noted previously), whereas C_2 and A_2 grow. Gardner and Woods (1979b) also observed a similar trend in their studies of galena.

It is also observed that after one cycle the current associated with the reduction of PbO to Pb^o (i.e., C_2) is larger when the scan is in the anodic-going direction than when it is proceeding cathodically. Furthermore, the difference increases with each cycle. This phenomenon is characteristic of a reaction that occurs by a nucleation and growth

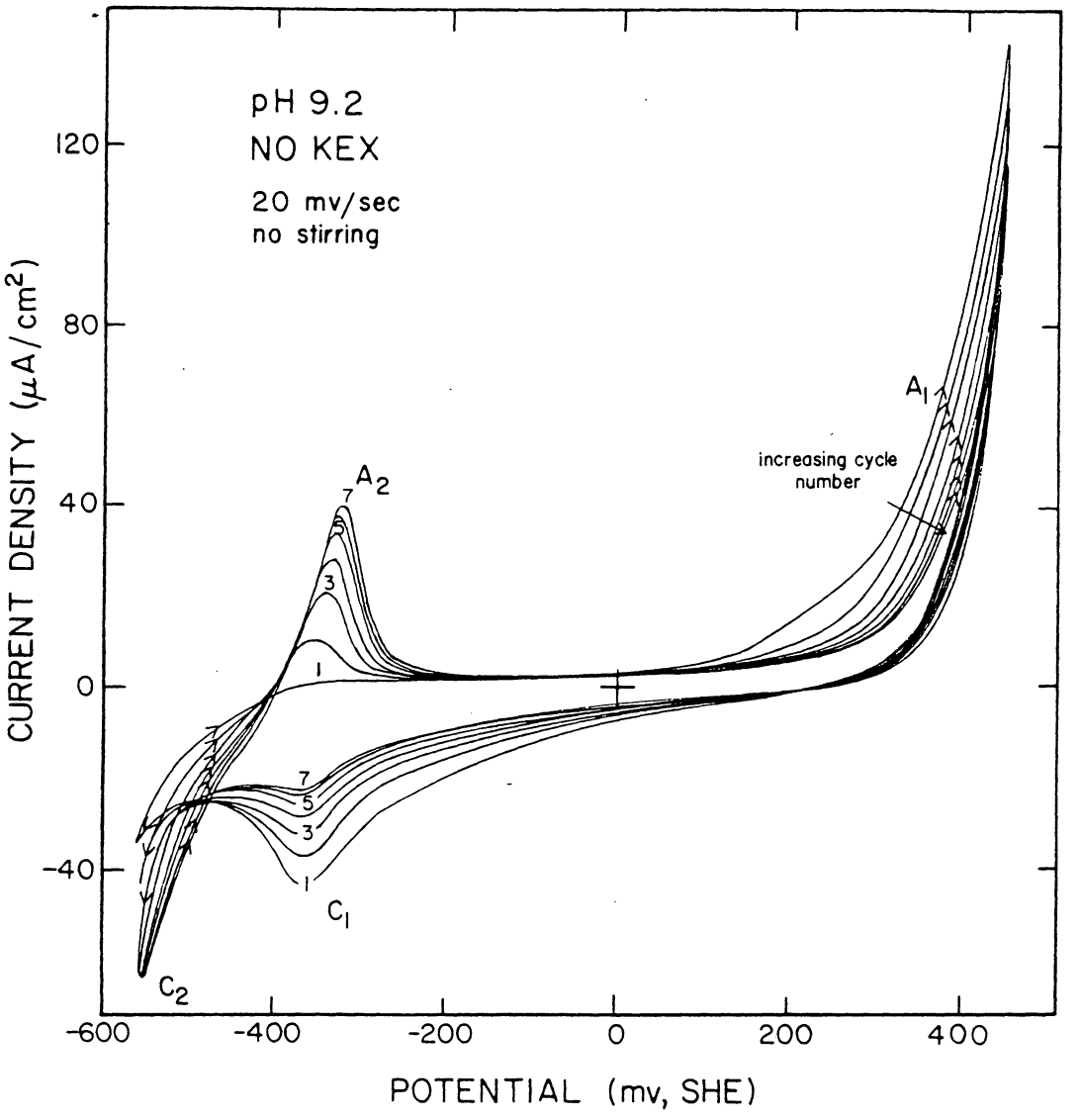


Figure 3.11 Cyclic voltammograms of a galena electrode in a 0.05 M $Na_2B_4O_7$ solution (pH 9.2) for potential sweeps between -555 and 445 mv. No stirring. Scan rate = 20 mv/sec. The number next to each curve denotes the cycle number.

A_1 = $PbS/PbO,S^0$ + $PbS/PbO,S_2O_3^{2-}$

A_2 = Pb^0/PbO or $Pb^0/Pb(BO_2)_2$

C_1 = $PbO,S^0/PbS$ or S^0/HS^-

C_2 = PbO/Pb^0

mechanism.

The process associated with reaction [3.13] entails not only the reduction of PbO to Pb^{o} on the mineral surface, but also the subsequent deposition of the elemental lead into a particular lattice site. According to theories developed by such workers as Brandes (1929), Erdey-Gruz and Volmer (1931), Lorenz (1953, 1954), Fischer (1954) and Gerischer (1958), the steps involved in deposition include: i) a charge-transfer reaction leaving a reduced species on the electrode surface; ii) surface diffusion of the reduced species to a lattice site; and iii) incorporation of the species into the lattice site.

Different models have been developed to determine the manner in which a metal is deposited on a substrate. The nucleation and growth mechanism has proven to be one of the most popular such models (Kolmogorov, 1937; Avrami, 1939; Evans, 1945; Bewick et al., 1962; Rangarajan, 1973a,b). It involves the formation of a nuclei, each containing a few atoms, which then become centers for growth by further deposition. In some cases, models based on two-dimensional growth of these nuclei have been very successful (Toschev and Mutaftschiew, 1964; Kaischew and Budevski, 1967), whereas in others, three-dimensional growth has worked better (Fleischmann and Thirsk, 1959; Davison and Harrison, 1973; Bindra et al., 1973).

Based on a two-dimensional model principally developed by Evans (1945) and Milchev and Stoyanov (1976), Angerstein-Kozlowska et al. (1978) carried out a computer simulation of the kinetic behavior of a nucleation and growth process driven by a linear potential sweep. They

demonstrated that reversing a sweep before a current peak is complete results in the behavior observed in Figure 3.11, in which the current on the reverse scan is greater than that on the forward scan.

Analysis of the charges associated with the various peaks on this voltammogram reveals some interesting behavior concerning the amount of PbO formed during oxidation and the amount reduced during reduction in each cycle. Assuming that A_2 is due to reaction [3.17], and that the reduction of galena itself,

$$PbS + H^+ + 2e \longrightarrow Pb^o + HS^-, \qquad [3.21]$$

makes no contribution to C_2, it can be shown (Appendix III) that the total number of moles of PbO produced during each pass is

$$(n_{PbO})_A = \frac{Q_{A1} + Q_{C1} + 2Q_{A2}}{4F}, \qquad [3.22]$$

and the amount consumed is

$$(n_{PbO})_C = \frac{Q_{C1} + Q_{C2}}{2F}. \qquad [3.23]$$

The ratios of these two quantities and that of $n_{S_2O_3^{2-}}$ to n_{S^o} generated during each cycle are listed in Table 3.5. Keeping in mind the approximate nature of the determination of these charges, the relative amounts of S^o and $S_2O_3^{2-}$ produced does not change significantly with the repeated scanning and is very close to that from the single-scan experiment for the same anodic limit (Table 3.3). However, at the same

Table 3.5

Molar Ratios $n_{S_2O_3^{2-}}/n_{SO}$ and $(n_{PbO})_A/(n_{PbO})_C$

Obtained During Cyclic Scans Between -555 mv and 445 mv

Cycle No.	$n_{S_2O_3^{2-}}/n_{SO}$	$(n_{PbO})_A/(n_{PbO})_C$
1	0.14	0.98
2	0.12	0.87
3	0.15	0.85
4	0.17	0.81
5	0.16	0.74
6	0.17	0.72
7	0.17	0.73

time, the results indicate that, except for the first cycle, there is more PbO being reduced than is being generated by reactions [3.6] and [3.11]. Furthermore, this effect becomes more pronounced with each successive sweep, although it seems to reach a steady state by the fifth one.

One reason for this may be that a significant amount of PbO is being formed as a result of the reverse of reaction [3.20]. This PbO can then be reduced via reaction [3.13] to Pb^o and, in so doing, makes an additional contribution to Q_{C2} and Q_{A2}. It is not exactly clear why this should increase in the first few cycles. The continual formation and removal of the oxidation products may roughen up the mineral surface and increase its surface area. However, the most likely reason is that a portion of the cathodic current near the lower limit is due not only to the reduction of PbO, but also to the reduction of galena itself.

Figure 3.12 shows the results of another continuous scan in which the upper limit was held constant at 245 mv while the lower limit was continually decreased. The previous analysis has shown that at this anodic limit, the C_2 peak does not appear although a small amount of thiosulfate is being produced during oxidation. As the lower limit is reduced below -400 mv, the cathodic current begins to increase indicating that a faradaic process is taking place. Since clearly more cathodic than anodic charge has been passed by this time, this electron transfer reaction can be attributed to the reduction of galena (reaction [3.21]).

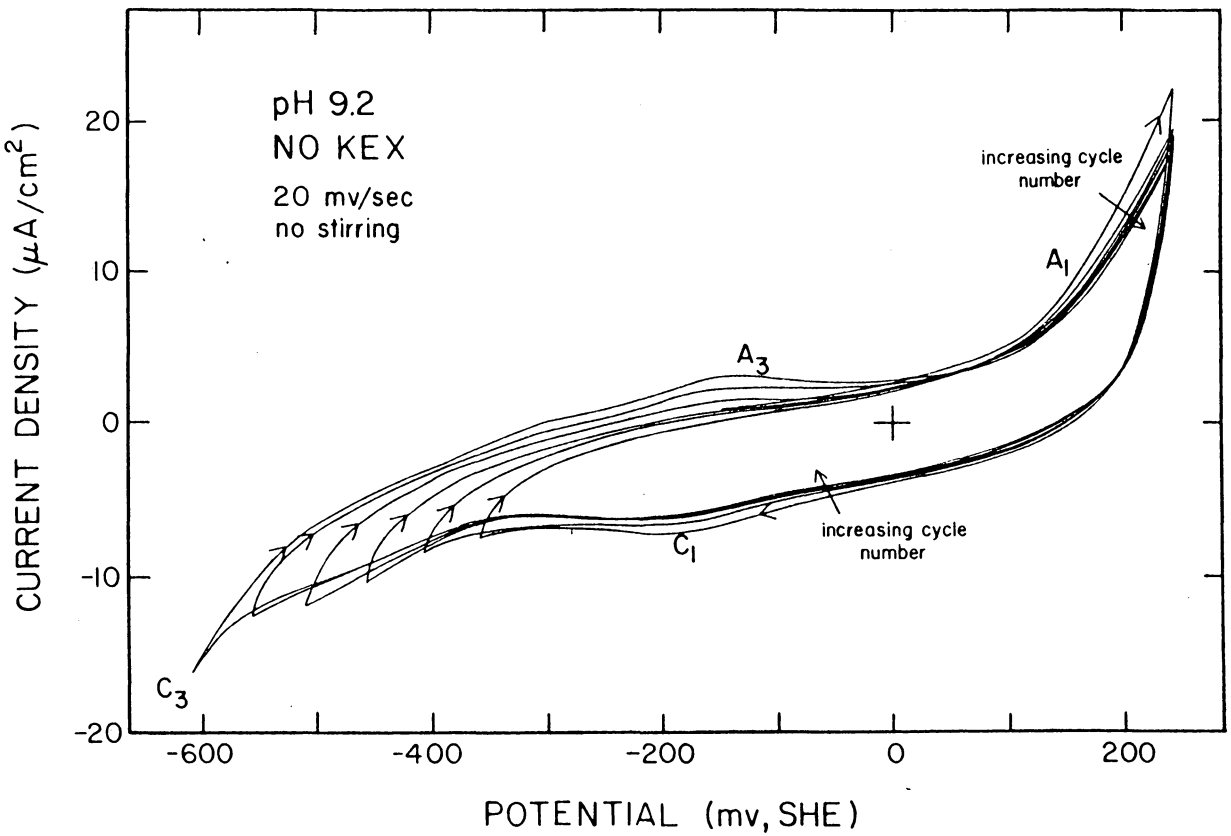


Figure 3.12 Effect of lowering the cathodic limit during the cyclic scan of a galena electrode in a 0.05 M $Na_2B_4O_7$ solution (pH 9.2). Anodic limit held at 245 mv. No stirring. Scan rate = 20 mv/sec.

$A_1 = PbS/PbO, S^0 + PbS/PbO, S_2O_3^{2-}$

$A_3 = HS^-/S^0$

$C_1 = PbO, S^0/PbS$ or S^0/HS^-

$C_3 = PbS/Pb^0, HS^-$

At the same time, a small anodic peak, A_3, that has not been observed to this point, appears at approximately -200 mv. This potential is very close to the Nernst potential of -160 mv for the reaction,

$$HS^- \longrightarrow S^o + H^+ + 2e, \qquad [3.24]$$

for $[HS^-] = 10^{-6}$ M. Furthermore, Hamilton and Woods (1984) observed an anodic peak at the same potential (although it was considerably larger) during their voltammetric study of galena in the presence of sulfide ions. They also assigned reaction [3.24] to this peak.

The results indicate that whereas the removal of the oxidation products during the cathodic scan tends to be complete, the oxidation of the species that replace them is not nearly as extensive. For example, although some elemental lead is being produced by reaction [3.21] during the scans in Figure 3.12, the A_2 peak is not observed. Even when it does appear (see Figures 3.8 and 3.9), it is smaller than C_2. A considerable amount of HS^- is also likely to have been released by reaction [3.21]. Yet, only a small fraction of it has been oxidized judging from the small size of A_3 compared to C_2. This reinforces the earlier contention that reaction [3.15] cannot be excluded as a possibility for C_1 simply because A_3 does not appear in the cyclic scan in Figure 3.10.

c. IGP experiments at pH 9.2: Current pulses of 0.05 mA/cm^2 were applied to a polished galena electrode in an unstirred borate solution for 0, 2, 3 and 6 minutes and then were reversed in order to reduce the

oxidation products. The results are shown in Figure 3.13. When galena is reduced without first oxidizing (Figure 3.13a), the open-circuit potential quickly drops until it reaches a plateau at -720 mv. (It should be noted that the open-circuit potential corresponds to the minimum along a trace when anodic current is being applied and to the maximum when the electrode is being cathodically polarized.) The onset of this plateau may be attributed to the reduction of galena (reaction [3.21]), which has a Nernst potential of -660 mv for $[HS^-] = 10^{-6}$ M and pH = 9.2.

When the freshly polished galena electrode is oxidized, a potential arrest begins at about 100 mv and develops into a well-defined plateau (Figure 3.13b). The oxidation process occurring is analogous to that which corresponds to A_1 (oxidation of PbS) in the voltammograms of Figures 3.8 and 3.9. The open-circuit potential along the plateau increases slowly with time, reaching approximately 300 mv after 6 minutes of polarization (see Figure 3.13d). This range coincides well with the Nernst potential for reaction [3.6] at this pH. It should be noted that at the applied current density of 0.05 mA/cm^2, bulk oxidation of PbS to PbO and S^o is occurring by the time the plateau appears.

Anodically polarizing the mineral for about 2 minutes causes the open-circuit potential to reach 250 mv and the closed-circuit value 350 mv (Figure 3.13b). When the current is reversed, a small arrest begins to appear at an open-circuit potential of about -100 mv and reaches its broadest at -150 mv. This is in excellent agreement with where cathodic current begins to flow and where the C_1 peak occurs in the voltammogram

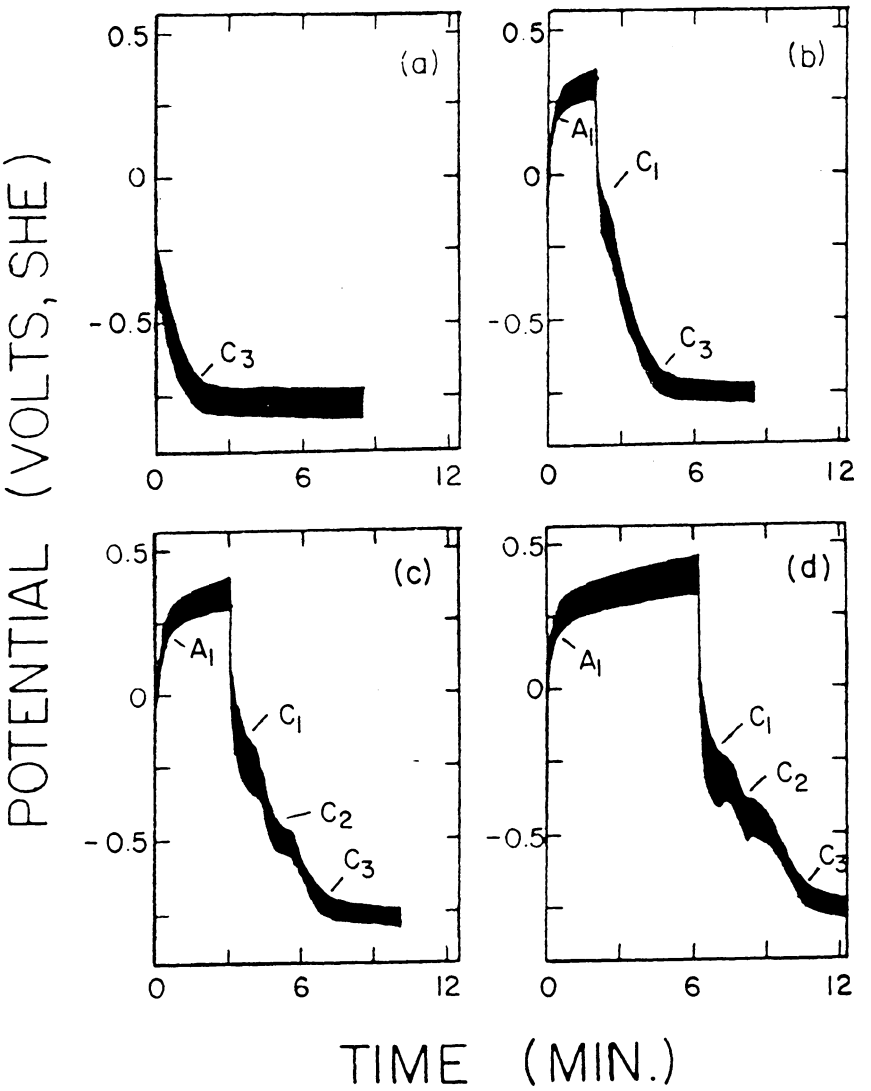


Figure 3.13 IGP diagrams obtained after applying current pulses of 0.05 mA/cm^2 to a galena electrode immersed in an unstirred 0.05 M $Na_2B_4O_7$ solution (pH 9.2). Anodic pulses applied initially for 0 (a), 2 (b), 3 (c) and 6 (d) minutes before reversal of current.

A_1 = $PbS/PbO,S^0$ + $PbS/PbO,S_2O_3^{2-}$

C_1 = $PbO,S^0/PbS$ or S^0/HS^-

C_2 = PbO/Pb^0

C_3 = $PbS/Pb^0,HS^-$

(Figure 3.8) obtained for an anodic limit of 345 mv. The charge analysis of the voltammograms (Section 3.3.1a) has indicated that the C_1 peak can be attributed to either the recombination of PbO (or $PbOH^+$) and S^o to PbS (reaction [3.14] or [3.16]) or to the reaction of S^o to HS^- (reaction [3.15]). The reversible potential for the latter at pH 9.2 is -160 mv, which is quite close to where the broadening in the potential-time diagram in Figure 3.13b occurs. On the other hand, reactions [3.14] and [3.16] have Nernst potentials of 234 and 135 mv, respectively, both of which are considerably more anodic. This suggests that the reduction of S^o to HS^- (reaction [3.15]) is the best choice for C_1.

With further cathodic polarization beyond this point, no plateau appears until PbS itself begins to decompose via reaction [3.21]. Apparently, the potential has not become high enough at the end of 2 minutes of anodic polarization for the PbO/Pb^o reaction plateau to appear. It has been shown in Figure 3.8 that the C_2 peak appears in the corresponding voltammogram only when the anodic limit has reached 445 mv.

Extending the duration of anodic polarization to 3 and 6 minutes (Figures 3.13c and 3.13d) causes the C_1 arrest to broaden. In addition, the C_2 plateau appears at -400 mv and becomes more distinct as the extent of oxidation increases. This is also consistent with what has been found in the voltammetry experiments.

The appearance of the PbO/Pb^o arrest indicates that thiosulfate is also being produced during oxidation. Comparison of the IGP diagrams in

Figure 3.13 shows that less time (and hence charge) is required to remove the oxidation products than it takes to produce them. Furthermore, the difference grows as the duration of the anodic polarization increases. This is an indication that the amount of thiosulfate being formed increases with the duration of anodic polarization.

Although these results do suggest that both $S_2O_3^{2-}$ and S^o are being produced, only one arrest for the oxidation of PbS appears in any of the potential-time diagrams. This may be explained as follows: When anodic current is flowing, oxidation to both species can take place; however, when the circuit is opened, the potential can only be controlled by the reaction which can proceed in both directions. Since the oxidation of galena to PbO and $S_2O_3^{2-}$, i.e., reaction [3.11], is irreversible, the open-circuit potential will be controlled by oxidation to PbO and S^o (reaction [3.6]) only.

The effect of stirring on the IGP diagram for galena when pulses of 0.05 mA/cm^2 are applied is shown in Figure 3.14. After 6 minutes of anodic polarization, the difference between the open- and closed-circuit potentials is about 50 mv less when the solution is being agitated than when it is stagnant. This is of interest because the potential to which an applied current drives an electrode while a faradaic process is underway is determined by the rate of that process.

When an anodic current is applied to an electrode by an external source, the influx of positive charge will cause the electrode potential to rise. It will continue to do so uninterrupted until an oxidation

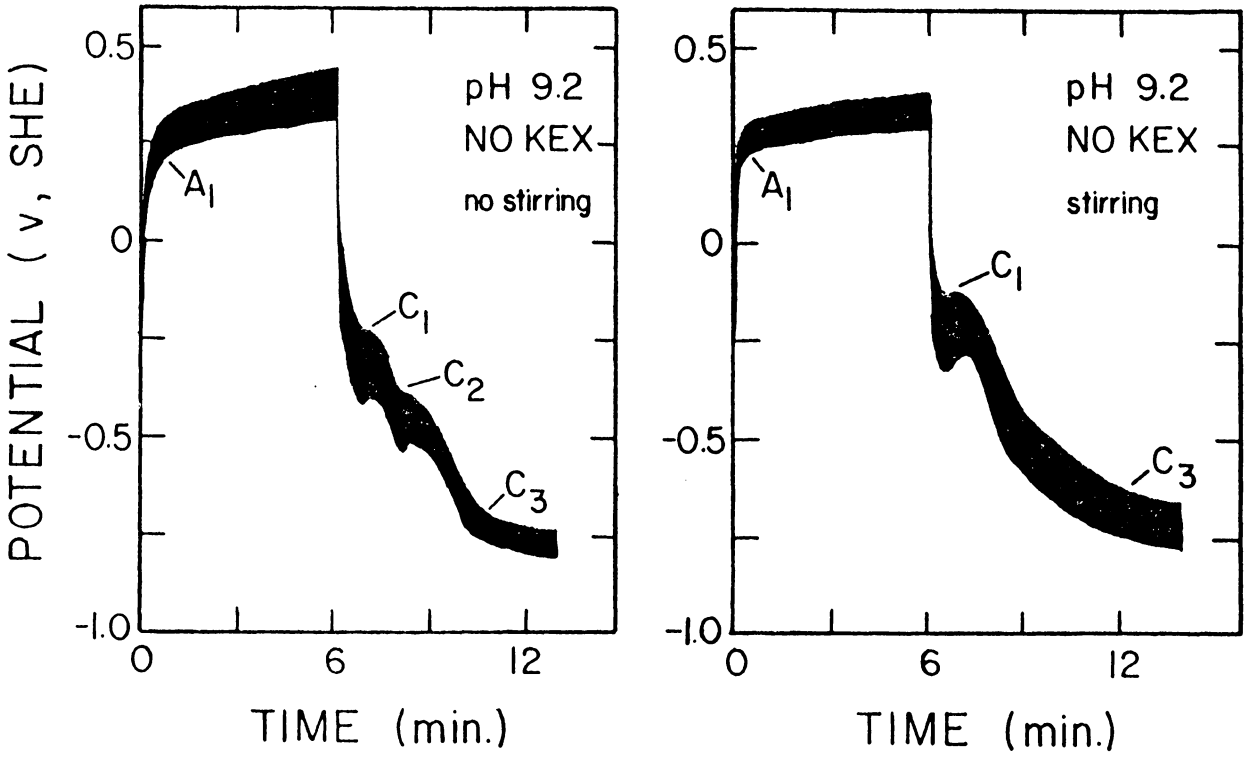


Figure 3.14 Effect of stirring on IGP diagrams obtained by applying a current pulse of 0.05 mA/cm^2 to a galena eelctrode immersed in a 0.05 M $Na_2B_4O_7$ solution (pH 9.2).

A_1 = $PbS/PbO,S^o$ + $PbS/PbO,S_2O_3^{2-}$

C_1 = $PbO,S^o/PbS$ or S^o/HS^-

C_2 = PbO/Pb^o

C_3 = $PbS/Pb^o,HS^-$

reaction begins, whereupon the rate of increase will slow down. If a point is reached where the rate at which electrons are evolved by the oxidation reaction becomes equal to the flow of current, then the potential will stop rising altogether. Thus, in an IGP experiment, the smaller the difference between the open-circuit and closed-circuit potentials, the faster the rate of the electron transfer reaction.

With this in mind, the results in Figure 3.14 indicate that the kinetics of galena oxidation is more facile when the solution is stirred than when it is not. However, this is in contrast to the previous observation in the voltammograms of Figure 3.9 that stirring has little effect upon the anodic current up to a potential of 445 mv. This discrepancy may be related to the difference in the period of oxidation in the two cases. Whereas galena is being oxidized for 30-40 seconds during the linear sweep experiment, it is being polarized for as long as 3 minutes (1/2 of the 6-minute polarization time) in the IGP test. During the initial stages of oxidation, the reaction may be activation-controlled and therefore relatively unaffected by stirring. However, in the later stages, the mass transfer of H^+ ions from the electrode may become the rate-determining process.

When the current is reversed in the cathodic direction, further differences in the two potential-time diagrams in Figure 3.14 can be observed. Firstly, the C_1 arrest occurs at a potential about 100 mv more anodic in the stirred case than in the unstirred one. Secondly, the C_2 plateau does not appear whatsoever when the solution is being agitated, although it is quite prominent when it is stagnant. These two

effects are similar to what has been observed in the voltammetry experiments (Figure 3.8).

The effects of stirring become even more pronounced when the current density is increased to 0.10 mA/cm^2 (Figure 3.15). There is a noticeable difference between the closed-circuit potentials during oxidation in the two diagrams, particularly in the later stages of oxidation. Although the C_2 plateau does appear when the solution is stirred, it is not as broad as when the current density is 0.05 mA/cm^2.

Increasing the current density even further to 0.5 mA/cm^2 causes a dramatic change in the traces (Figure 3.16). During oxidation, there is a very large fluctuation in potential for the first 2.5 minutes as the circuit is opened and closed. Although a larger variation in the open- and closed-circuit potentials is expected at such a high current density, the observed behavior also indicates that the PbO layer may be growing thick enough to passivate the electrode. The current polarizes the electrode enough that a new oxidation reaction begins to occur after about 2.5 minutes.

With the onset of the new reaction, the difference between the closed- and open-circuit potential during each pulse cycle diminishes. This change in behavior suggests that an oxidation product which is a good conductor is now being formed. The most probable species would be lead dioxide. PbO_2 is an n-type semiconductor with a band gap of about 1.5 ev and a high conductivity, equivalent to that of the metal bismuth (Hampson, 1979).

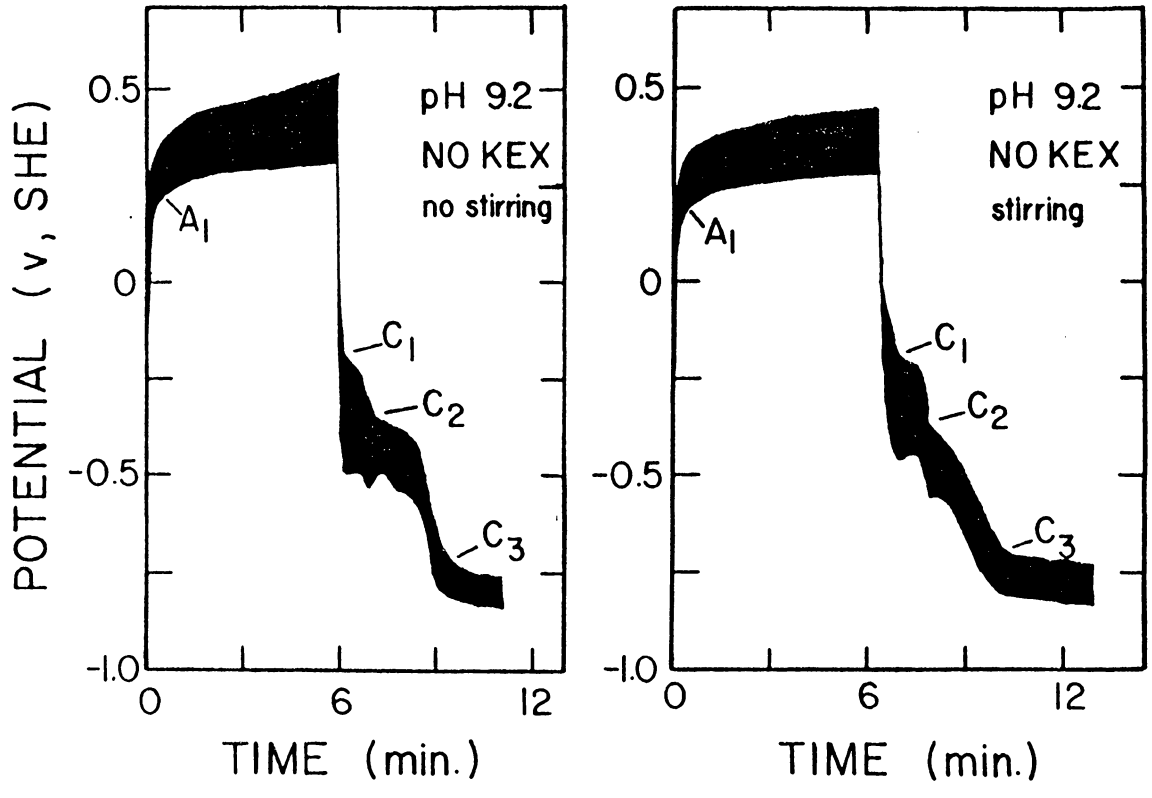


Figure 3.15 Effect of stirring on IGP diagram obtained by applying a current pulse of 0.10 mA/cm^2 to a galena electrode immersed in a 0.05 M $Na_2B_4O_7$ solution (pH 9.2).

A_1 = $PbS/PbO,S^o + PbS/PbO,S_2O_3^{2-}$

C_1 = $PbO,S^o/PbS$ or S^o/HS^-

C_2 = PbO/Pb^o

C_3 = $PbS/Pb^o,HS^-$

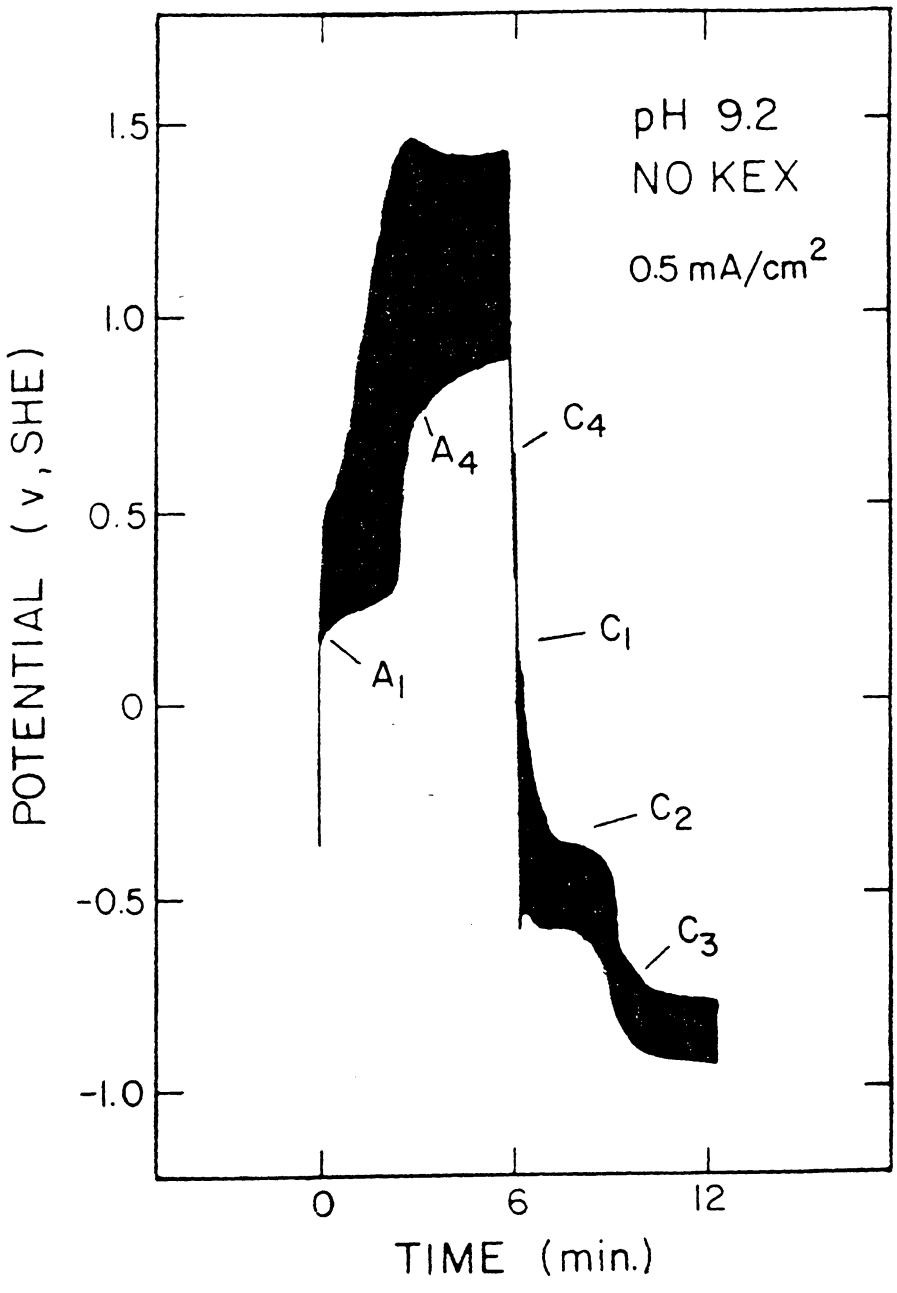


Figure 3.16 IGP diagram obtained after applying a current pulse of 0.5 mA/cm^2 to a galena electrode immersed in a stirred 0.05 M $Na_2B_4O_7$ solution (pH 9.2).

A_1 = $PbS/PbO,S^o$ + $PbS/PbO,S_2O_3^{2-}$

A_4 = $PbS/PbO_2,S_2O_3^{2-}$ or PbO/PbO_2

C_1 = $PbO,S^o/PbS$ or S^o/HS^-

C_2 = PbO/Pb^o

C_3 = $PbS/Pb^o,HS^-$

C_4 = PbO_2/PbO

Therefore, A_4 can be attributed to the oxidation of PbS to PbO_2 and $S_2O_3^{2-}$ and/or the oxidation of PbO to PbO_2. The reversible potentials for both of these reactions at pH 9.2, i.e., 100 mv and 502, respectively, are considerably lower than the open-circuit value of about 800 mv at which A_4 begins, as observed in Figure 3.16. A possible explanation for such a large overpotential is that both of these reactions would likely occur at the PbS/oxide interface since PbO is a poor electronic conductor. Since this interface would be far removed from the oxide/solution interface, the concentration of the reactant OH^- at the anodic sites would be considerably lower than the amount in the bulk electrolyte of pH 9.2. This lowering of the local pH would shift the Nernst potentials in the anodic direction.

When the current for the experiment shown in Figure 3.16 is reversed, a small cathodic plateau, C_4, appears at a potential of about 650 mv. Carr and Hampson (1971) conducted voltammetry studies on electrodeposited PbO_2 films in 4.7 M NaOH solutions and observed peaks for the reduction of PbO_2 to PbO at a potential of about 500 mv. It would seem, therefore, that PbO_2/PbO reduction is a reasonable choice for C_4.

With further cathodic polarization, the reduction of PbO to Pb^o (C_2) becomes predominant, indicating that oxidation is, for the most part, proceeding beyond the formation of elemental sulfur to that of oxy-sulfur species.

d. Chronoamperometry experiments at pH 9.2: In these experiments, the potential was stepped from an initial value of -345 mv to values of 45, 145, 245, 345 and 495 mv, and then held there while the current was monitored as a function of time. The results are shown in Figure 3.17.

At the lower applied potentials of 45, 145 and 245 mv, the current decays quickly to a steady value. The currents are considerably larger at the higher potentials for any given time and decay more slowly. This is not surprising since the potentials of 345 and 495 mv are considerably higher than the reversible potentials for the bulk reactions [3.6] and [3.11].

The fact that an appreciable amount of oxidation occurs even at potentials below the reversible potential for reaction [3.6] further substantiates the notion that oxidation begins with the formation of a metal-deficient sulfide (i.e., reaction [2.41]). One would therefore expect the total amount of charge passed at a potential of 145 mv, for example, to be the equivalent of a few monolayers of PbO and S^o generated by reaction [3.6]. Although the current-time plot for 145 mv in Figure 3.17 only covers the first 20 seconds, the actual experiment was continued until current could no longer be detected. The total charge passed in this time is approximately 1100 $\mu C/cm^2$. Assuming a charge density of 184 $\mu C/cm^2$ for an entire (100) plane of galena to be converted to PbO and S^o (Gardner and Woods, 1979b) and a roughness factor of 1.5, it is estimated that four monolayers of oxidation products have been formed.

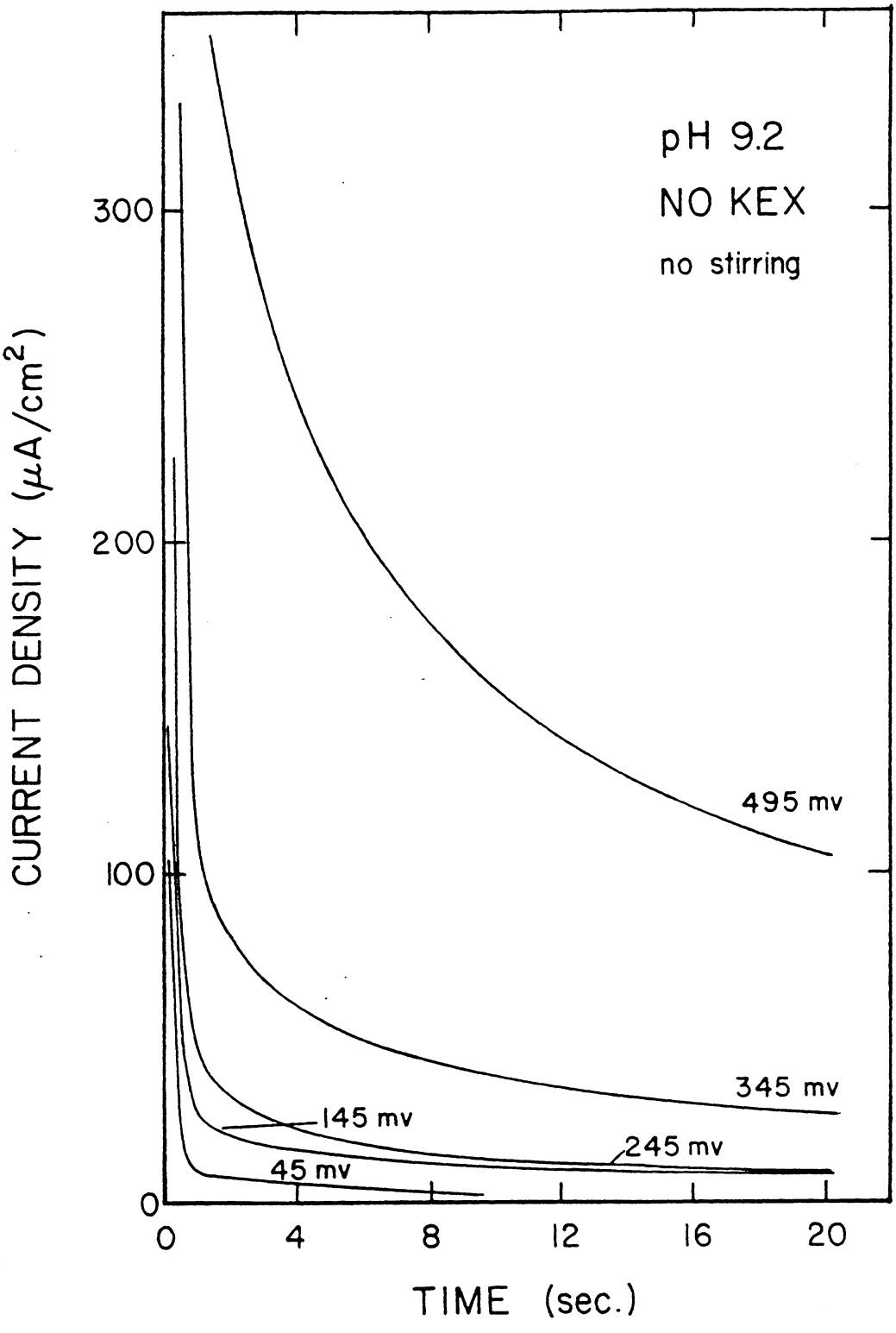


Figure 3.17 Current-time curves obtained after applying potentials of 45, 145, 245, 345 and 495 mv to a galena electrode immersed in an unstirred 0.05 M $Na_2B_4O_7$ solution (pH 9.2).

e. Single sweep voltammetry at pH 6.8: As in the work done at pH 9.2, the starting potential and scan rate used in the voltammetry experiments at pH 6.8 were -355 mv and 20 mv/sec, respectively, unless otherwise indicated. Single-scan current-potential curves obtained for anodic limits of 245, 295 and 345 mv in both stirred and unstirred solutions are shown in Figures 3.18 and 3.19, respectively.

Identification of A_1, C_1 and C_2 peaks: In both cases, the oxidation of galena (A_1) begins at approximately 0 mv and rises sharply above 200 mv. When the potential is scanned to 245 and 295 mv, a single cathodic peak, C_1, is observed in the vicinity of -160 mv. Extending the limit to 345 mv causes the appearance of a second, larger reduction peak, C_2, which strongly overlaps with the first one. Other than slightly decreasing the hysteresis between the anodic currents obtained in the forward and reverse directions, stirring does not have much of an effect on the voltammograms. These results are quite different from those of Gardner and Woods (1979b), who found that C_1 and C_2 were situated farther apart and that stirring shrunk C_1 considerably while enlarging C_2.

When irreversible reactions generating $S_2O_3^{2-}$ and SO_4^{2-} occur, Q_{A1} will always exceed the sum of Q_{C1} and Q_{C2}. (Note, for example, the charge relationship corresponding to sequence 1 in Table 3.1). The analysis of the charges associated with A_1, C_1 and C_2 for the scans with the upper limit of 345 mv shows that the ratio $(Q_{C1} + Q_{C2})/Q_{A1}$ is 1.02 in the unstirred case and 0.98 in the other. This suggests that no oxy-sulfur ions are being generated during oxidation, at least up to a

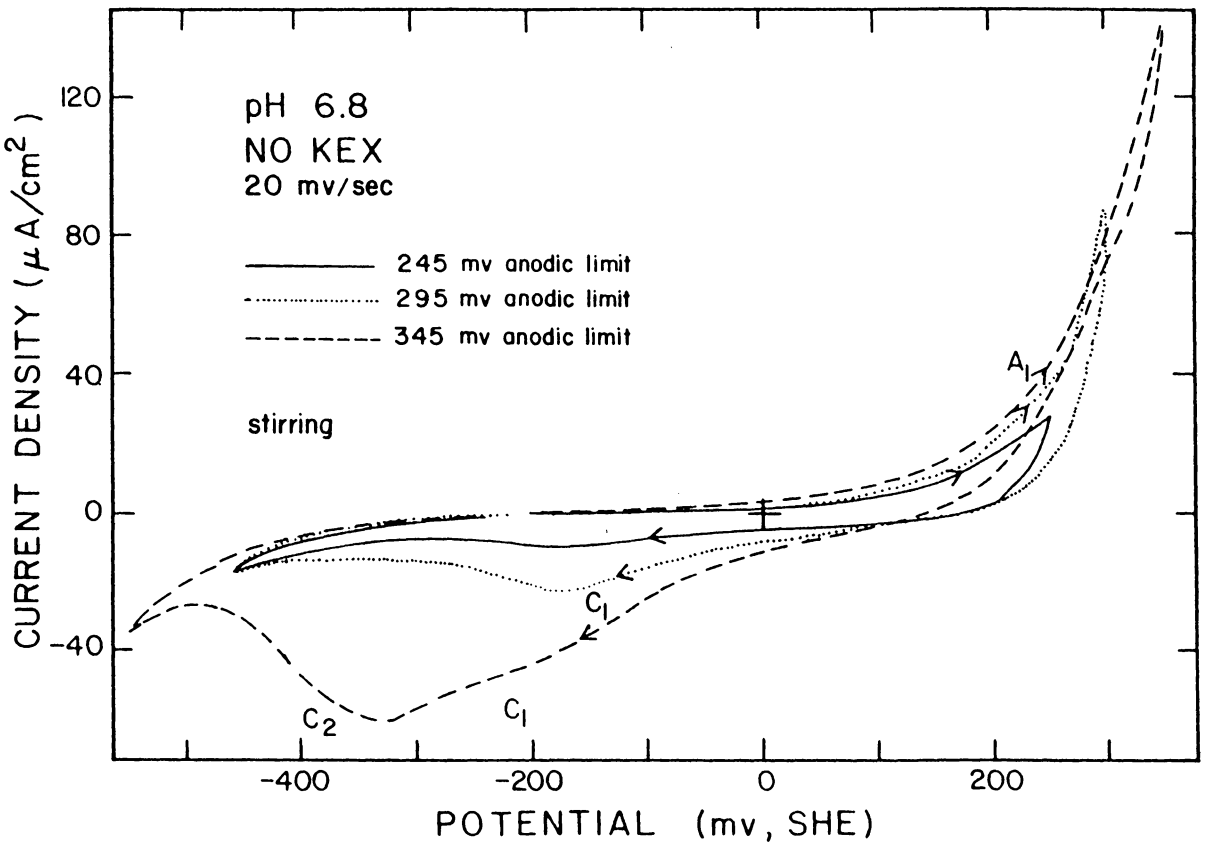


Figure 3.18 The effect of the anodic limit on the single sweep voltammograms for a galena electrode immersed in a stirred 0.05 M KH_2PO_4/0.05 M Na_2HPO_4 solution (pH 6.8). Scan rate = 20 mv/sec.

A_1 = $PbS/PbO,S^0 + PbS/PbOH^+,S^0$ C_1 = $PbO,S^0/PbS$ C_2 = S^0/HS^-

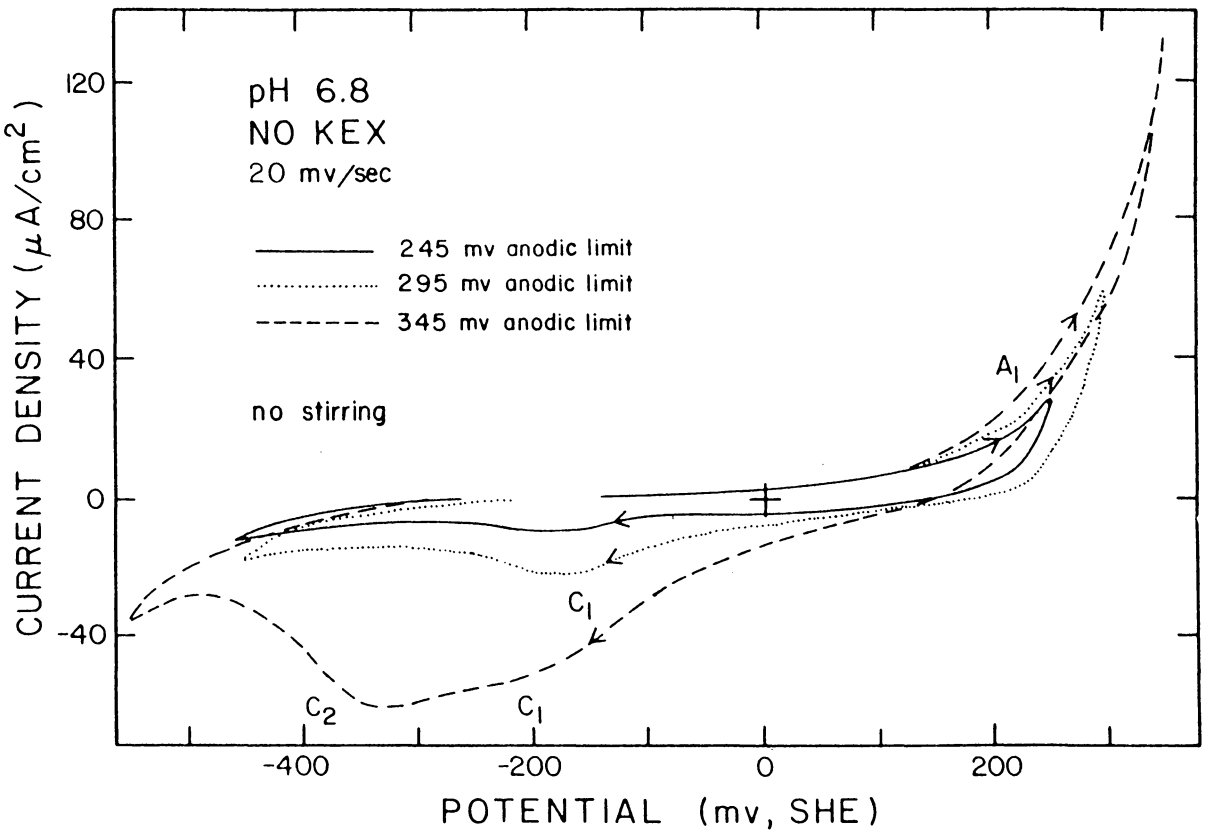


Figure 3.19 The effect of the anodic limit on the single sweep voltammograms for a galena electrode immersed in an unstirred 0.05 M KH_2PO_4/0.05 M Na_2HPO_4 solution (pH 6.8). Scan rate = 20 mv/sec.

A_1 = $PbS/PbO,S^o + PbS/PbOH^+,S^o$ C_1 = $PbO,S^o/PbS$ C_2 = S^o/HS^-

potential of 345 mv. It also follows that $(Q_{A1} - Q_{C1})/Q_{C2} = 1$, which is the same charge relationship as the ones for the reaction sequences 3 and 4 (Table 3.1). The oxidation reactions in either of these are the same and involve the formation of PbO and S^o by reaction [3.6] and $PbOH^+$ and S^o by reaction,

$$PbS + H_2O \longrightarrow PbOH^+ + S^o + H^+ + 2e. \qquad [3.25]$$

Once again, it can be seen that the experimental results indicate that PbO is being formed, although the thermodynamic calculations for Cases I, II and III do not predict this.

The C_1 peak is also attributed to the same reaction in both sequences, i.e., the recombination of PbO and S^o to PbS. Where the two differ, however, is in the choice of reaction C_2. Reaction [3.16] occurs according to scheme 3, whereas the reduction of S^o to HS^- (reaction [3.15]) takes place in the other.

It should be noted that sequence 3 is only possible in a stagnant solution. Since $PbOH^+$ is soluble, it will be dispersed away from the mineral when the solution is being stirred, thereby preventing it from recombining with S^o. The excess S^o at the galena surface can then only be directly reduced to HS^- (reaction [3.15]), which, of course, is the C_2 reaction in sequence 4.

Therefore, the possibility that the galena-water system obeys either of these sequences, depending upon whether the solution is being stirred or not, must be considered. In the case of sequence 3, stirring should cause a shift in the position of the C_2 peak. However,

comparison of Figures 3.18 and 3.19 shows that this peak is unaffected by stirring. This is, in fact, the behavior to be expected if the system follows only scheme 4.

Another difficulty concerning sequence 3 is that even under quiescent conditions, some of the $PbOH^+$ ions will diffuse away and, consequently, the direct reduction of S^o to HS^- should also be observed. There is no evidence of this in the voltammograms, however.

For these reasons, it can be concluded that sequence 4 best describes the chemistry of this system when the scan ranges from -545 to 345 mv. When the upper potential of the scan is limited to 295 mv, only one oxidation reaction is occurring. The only possible choices are reactions [3.6] and [3.25]. If $PbOH^+$ and S^o are formed via the latter reaction, one would expect to see C_2 rather than C_1 on the reverse scan in Figure 3.18. Since only C_1 appears, it is likely that PbO and S^o are the oxidation products up to 295 mv. Now, when the potential sweep is extended to 350 mv, $PbOH^+$ ions are also produced. This creates a sulfur-rich surface which can only be reduced by a combination of C_1 and C_2. It is interesting to note that Gardner and Woods (1979b) arrived at a similar conclusion although they found stirring to have a different effect from that observed in this study.

Figure 3.20 shows the single-scan current-potential curves obtained for an anodic limit of 445 mv and a cathodic limit of -655 mv. As can be seen, there is a tremendous rise in the current density from about 140 to about 1300 $\mu A/cm^2$ as the potential is scanned from 345 to 445 mv. Although the rate of galena oxidation in these voltammograms is slightly

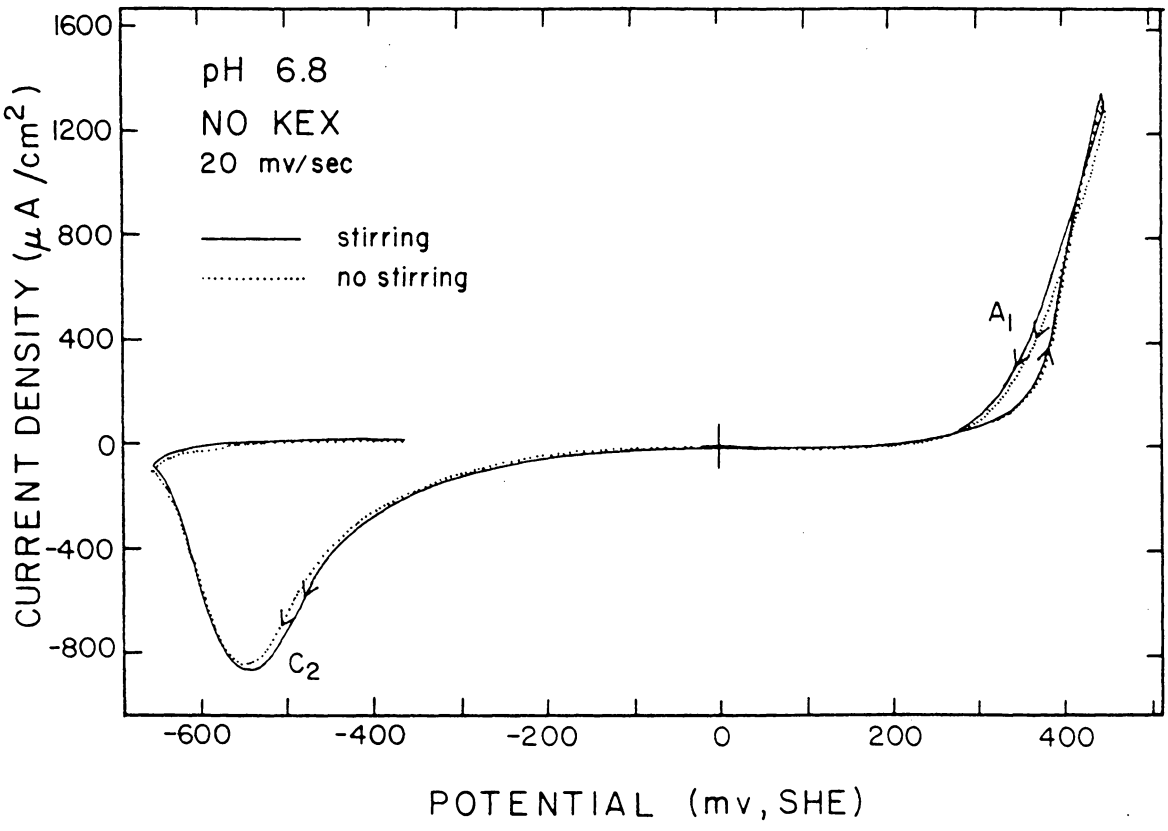


Figure 3.20 The effect of stirring on the single sweep voltammograms for a galena electrode immersed in a 0.05 M KH_2PO_4/0.05 M Na_2HPO_4 solution (pH 6.8). Scan rate = 20 mv/sec.

A_1 = $PbS/PbO,S^o$ + $PbS/PbOH^+,S^o$ C_2 = S^o/HS^-

higher when the solution is being stirred, the difference is small enough that it is difficult to conclude whether it is due to typical variations in electrode response from test to test or due to some kinetic effect. It is also observed that from about 275 to 425 mv, the current is greater when the potential is moving in the cathodic direction than when it is being increased anodically.

With the more severe oxidation of the mineral in this experiment compared to that for the lower anodic limits, only the C_2 peak is evident in the cathodic portion of these curves. It should be kept in mind, however, that the current scale is much larger in this figure than in the previous ones. Consequently, a small C_1 peak with a height of about 40 $\mu A/cm^2$ (the approximate height of C_1 in Figures 3.18 and 3.19) at about -200 mv may not be noticeable in Figure 3.20. In any event, the C_2 reaction is predominant.

Charge analysis reveals that for both the unstirred and stirred cases, there is still a balance between the number of faradays passed in the anodic process and the cathodic process. It is reasonable to conclude that oxidation follows sequence 4, but that above 395 mv, PbS is being converted primarily to $PbOH^+$ and S^o. Therefore, when the scan is reversed, the reduction of S^o to HS^- dominates.

It is interesting to note that although the reversible potential for the formation of $PbOH^+$ and S^o (206 mv) is lower than that for the formation of PbO and S^o (376 mv), the experimental data suggest that the latter occurs before the former does. However, once reaction [3.25] does begin, it becomes predominant. A possible explanation is that the

insoluble lead oxide film that forms initially does not do so according to the bulk reaction [3.6]. A more appropriate choice may be the formation of a metal-deficient sulfide (i.e., reaction [2.41]), as is observed at pH 9.2.

One series of reactions that is consistent with the voltammetry data is the following:

i) oxidation of galena to form a metal-deficient sulfide and a surface lead oxide up to a potential of about 345 mv.

ii) the accumulation of a few monolayers of these species leads to the nucleation of bulk S^o and PbO by the time the reversible potential for reaction [3.6] is reached (in the vicinity of 345 mv).

iii) the immediate dissolution of PbO to $PbOH^+$ ions.

Such a sequence is consistent with bulk thermodynamics which predicts that $PbOH^+$ is favored over PbO at this pH (see Figures 2.2, 2.6 or 2.11).

f. Cyclic voltammetry at pH 6.8: Figures 3.21 and 3.22 show the cyclic voltammograms of the galena electrode taken at pH 6.8. The upper limit was held at 345 mv while the lower limit was generally kept at -550 or -600 mv. There is a striking difference between these and the ones shown previously for pH 9.2 (Figures 3.10 and 3.11). Whereas repeated sweeping tends to passivate the galena surface at the higher pH, it apparently enhances oxidation at pH 6.8, particularly from the

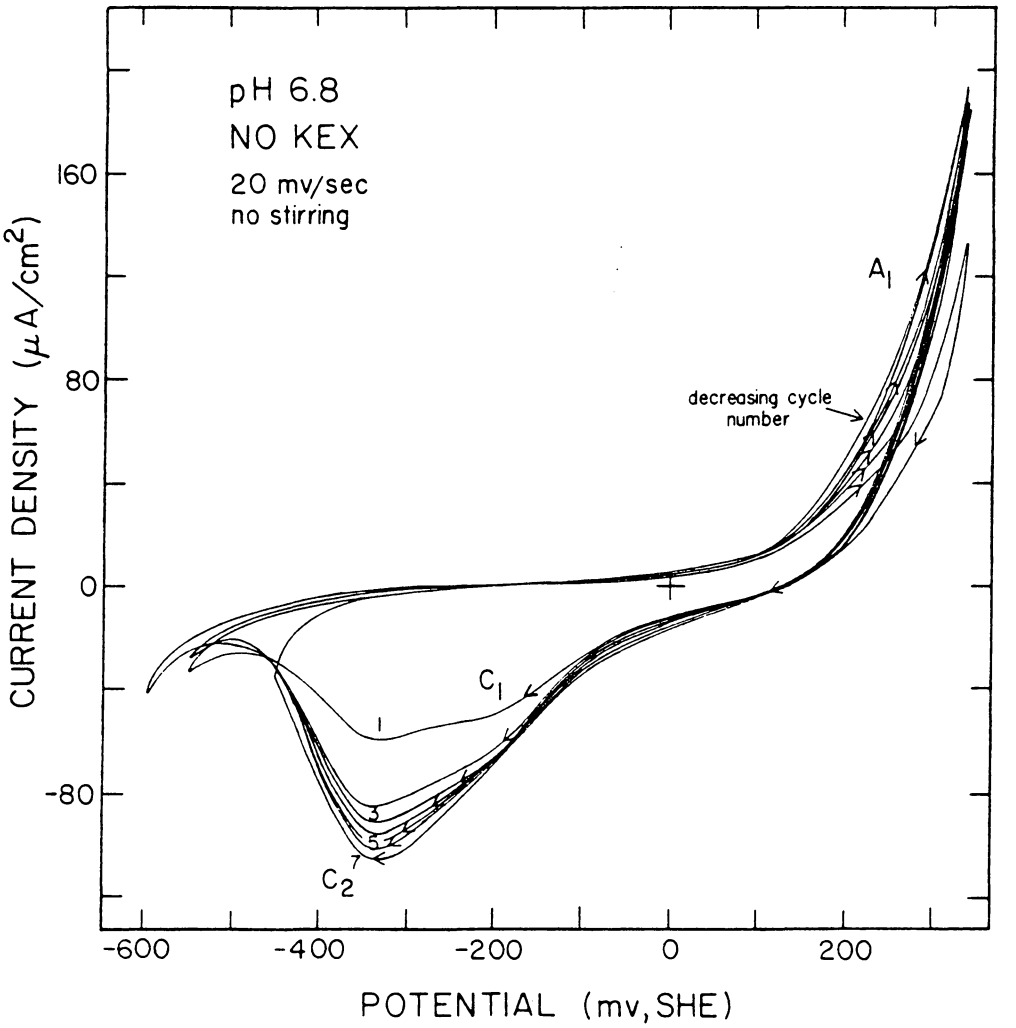


Figure 3.21 Cyclic voltammograms of a galena electrode in an unstirred 0.05 M KH_2PO_4/0.05 M Na_2HPO_4 solution (pH 6.8) for potential sweeps between -600 and 345 mv. Scan rate = 20 mv/sec. The number next to each curve denotes the cycle number.

A_1 = $PbS/PbO,S^o$ + $PbS/PbOH^+,S^o$

C_1 = $PbO,S^o/PbS$

C_2 = S^o/HS^-

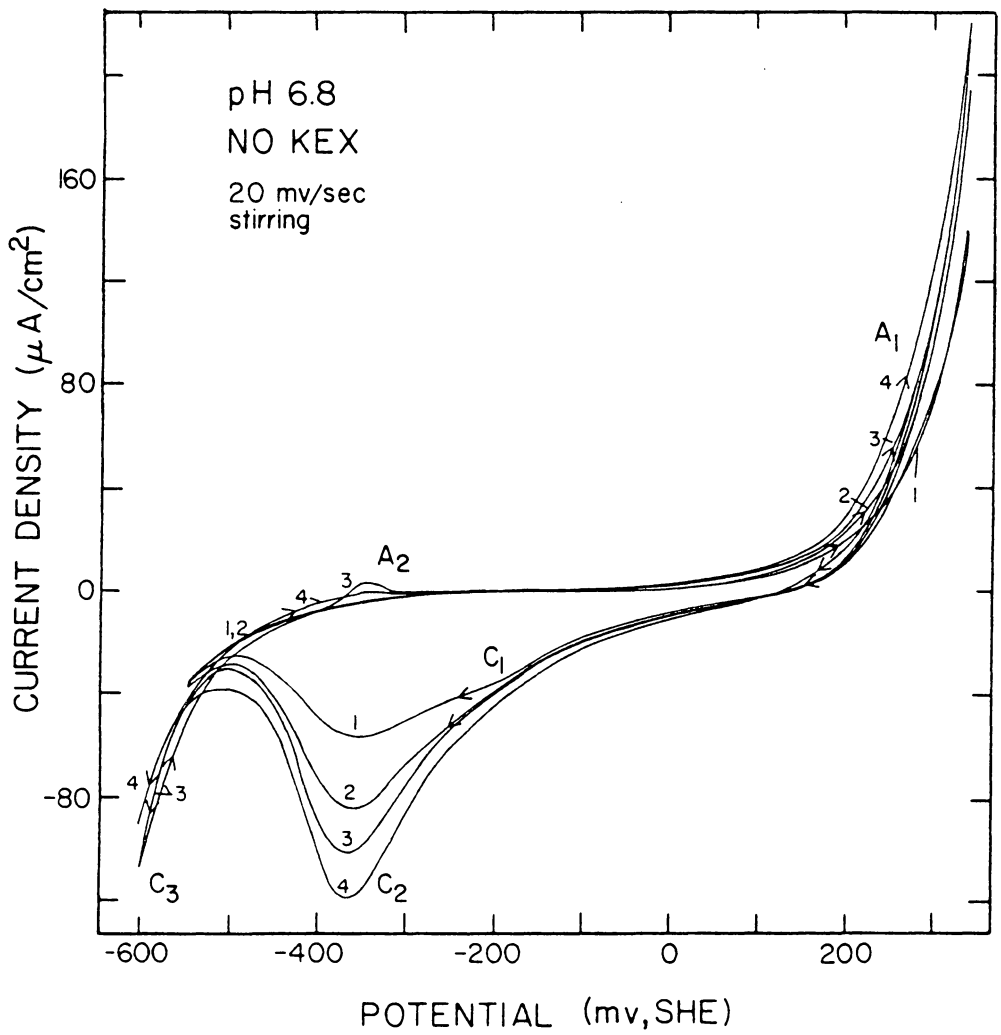


Figure 3.22 Cyclic voltammograms of a galena electrode in a stirred 0.05 M KH_2PO_4/0.05 M Na_2HPO_4 solution (pH 6.8) for potential sweeps between -600 and 345 mv. Scan rate = 20 mv/sec. The number next to each curve denotes the cycle number.

A_1 = $PbS/PbO,S^0 + PbS/PbOH^+,S^0$ C_1 = $PbO,S^0/PbS$

A_2 = Pb^0/PbO or $Pb^0,HPO_4^{2-}/PbHPO_4$ C_2 = S^0/HS^-

C_3 = $PbS/Pb^0,HS^-$

first to the second cycle. It is possible that the repeated formation and removal of oxidation products continuously roughens up and, hence, increases the surface area of the electrode. A balance between the anodic and cathodic charge is also observed in every sweep. This suggests that the reactions proceed via sequence 4 throughout the experiment and that cycling does not inhibit the removal of the oxidation products.

One feature of the voltammograms which cycling does affect is in the behavior of the current in the cathodic portion of the scan. The cathodic envelope grows in response to the increase in oxidation and becomes narrower as the C_2 peak is enlarged preferentially over C_1. In a stagnant solution (Figure 3.21), the shoulder due to C_1 can no longer be seen after the fourth cycle. Stirring promotes the dominance of C_2, as indicated by the fact that the envelope in this case is always narrower and that there is no evidence of C_1 after the first cycle (Figure 3.22).

One possible explanation for these trends is that continual sweeping causes some of the S^o to be reduced under C_2 rather than C_1. An important consequence of this is that some PbO should be left on the mineral after each cycle. This alternative is not likely, however. Since PbO is non-conducting, an accumulation of it on the surface would tend to passivate the electrode. This is not consistent with the observation that anodic current increases with each cycle.

It is more likely that both cycling and stirring promote the formation of $PbOH^+$ over PbO as an oxidation product. The effect of

stirring becomes clearer if the oxidation process in sequence 4 is viewed not as two separate electron transfer reactions, but as a single anodic reaction (i.e., oxidation of PbS to PbO and S^o) followed by the chemical dissolution of PbO to $PbOH^+$, i.e.,

$$PbO + H^+ \longrightarrow PbOH^+. \qquad [3.26]$$

Stirring should increase the rate at which PbO can be dissolved via this reaction since it speeds up the supply of H^+ ions to the galena surface and the removal of $PbOH^+$ ions away from the mineral.

From the cyclic scans in Figures 3.21 and 3.22, it is difficult to determine whether the C_1 peak is actually growing smaller or whether it is remaining the same size and only C_2 is becoming larger. The result obtained in Figure 3.23 shows quite clearly that it is the former that is occurring. The anodic limit is only 295 mv, and so C_1 is the principal cathodic reaction during the first cycle. However, during the next two sweeps, C_1 diminishes, while the C_2 peak appears and grows in size until it is larger. A steady state is reached by about the fourth cycle.

It is interesting to note that a small current rise, A_3, just prior to oxidation of galena, can be seen once the C_2 peak becomes visible. Evidently, this is due to the oxidation of HS^- ions generated by reaction C_2 (i.e., reaction [3.24]).

Figure 3.24 shows a cyclic voltammogram obtained after maintaining the upper limit at 345 mv while decreasing the lower limit from -455 to -655 mv. Since the results were found to be the same in quiescent and

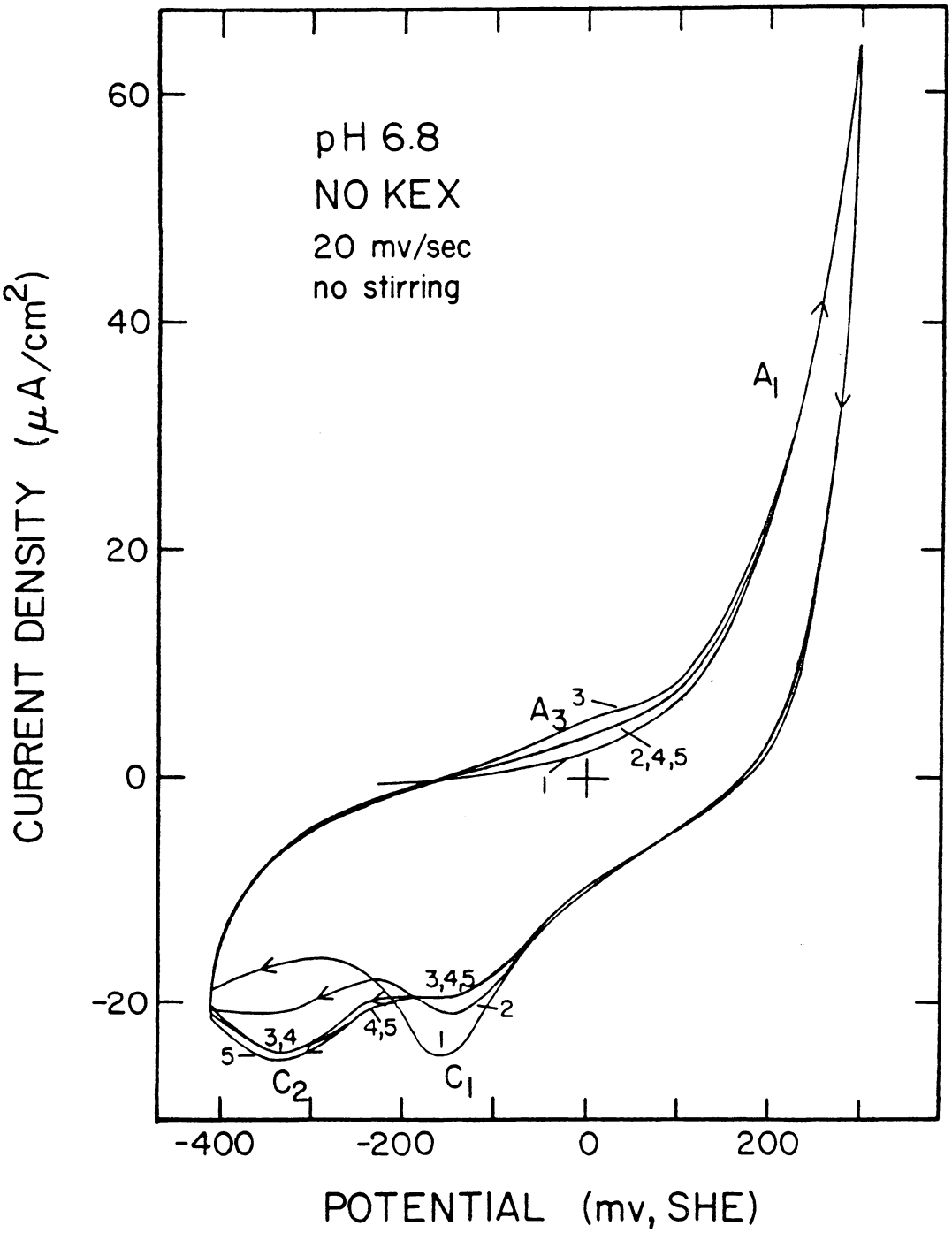


Figure 3.23 Cyclic voltammograms of a galena electrode in an unstirred 0.05 M KH_2PO_4/0.05 M Na_2HPO_4 solution (pH 6.8) for potential sweeps between -400 and 295 mv. Scan rate = 20 mv/sec. The number next to each curve denotes the cycle number.

A_1 = PbS/PbO,S^o A_3 = HS^-/S^o C_1 = PbO,S^o/PbS C_2 = S^o/HS^-

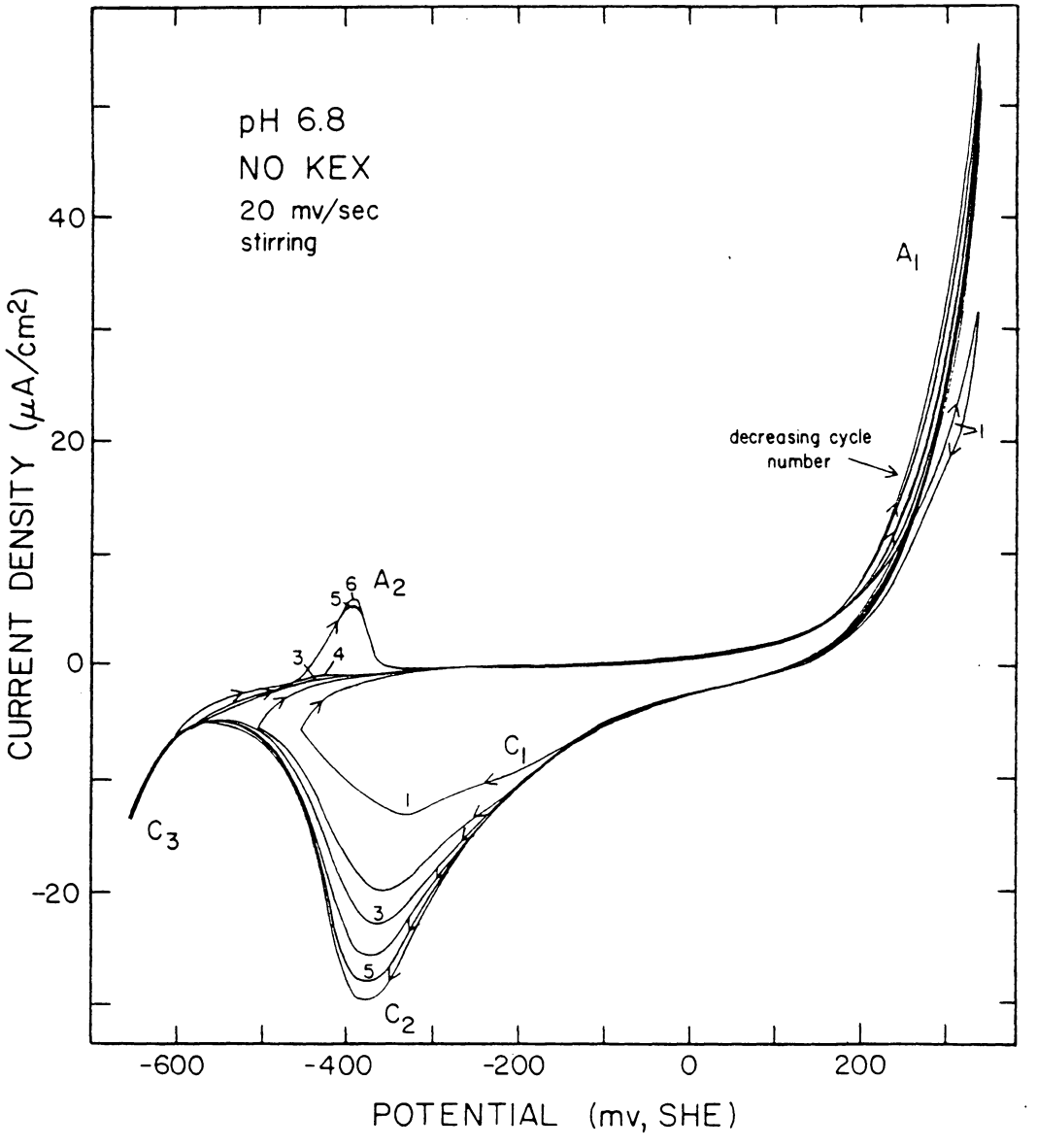


Figure 3.24 The effect of decreasing the cathodic limit during the cyclic scan of a galena electrode in a stirred 0.05 M KH_2PO_4/0.05 M Na_2HPO_4 solution (pH 6.8). Anodic limit held at 345 mv. Scan rate = 20 mv/sec.

A_1 = $PbS/PbO,S^0 + PbS/PbOH^+,S^0$ C_1 = $PbO,S^0/PbS$

A_2 = Pb^0/PbO or $Pb^0,HPO_4^{2-}/PbHPO_4$ C_2 = S^0/HS^-

C_3 = $PbS/Pb^0,HS^-$

stirred conditions, only one set of curves (stirred case) has been included. The features of the voltammograms are much the same as in the previous ones that have been discussed, except that an anodic peak, A_2, appears after the cathodic limit is lowered to -605 mv.

The reduction reaction occurring below -605 mv or so can be attributed to the cathodic decomposition of galena (reaction [3.21]), which has a Nernst potential of -590 mv at pH 6.8 ($[HS^-] = 10^{-6}$ M). The appearance of A_2 can then be attributed to the oxidation of Pb^o generated at the lower end of the cathodic sweep.

Two alternatives that can be considered for the reaction at A_2 are the oxidation of Pb^o to PbO (and subsequently to $PbOH^+$) and the oxidation of lead to lead phosphate ($PbHPO_4$). A major difficulty with the first choice is that it has a reversible potential of -125 mv, which is about 350 mv higher than where A_2 is observed to begin. The second possibility arises because of the use of a phosphate buffer at pH 6.8. Khairy et al. (1966a) and Abdul Azim and Anwar (1969) both noted a potential arrest at about -400 mv after anodically polarizing a Pb^o electrode immersed in a similar solution and attributed it to the formation of $PbHPO_4$. The Nernst potential for this reaction is -410 mv, which is very close to the position of the A_2 peak in Figure 3.24.

g. IGP experiments at pH 6.8: The results of IGP experiments, in which current pulses of 0.1 mA/cm^2 were applied to the galena electrode at pH 6.8, are depicted in the potential-time diagrams in Figure 3.25. Those shown were obtained by anodically polarizing the mineral for 0

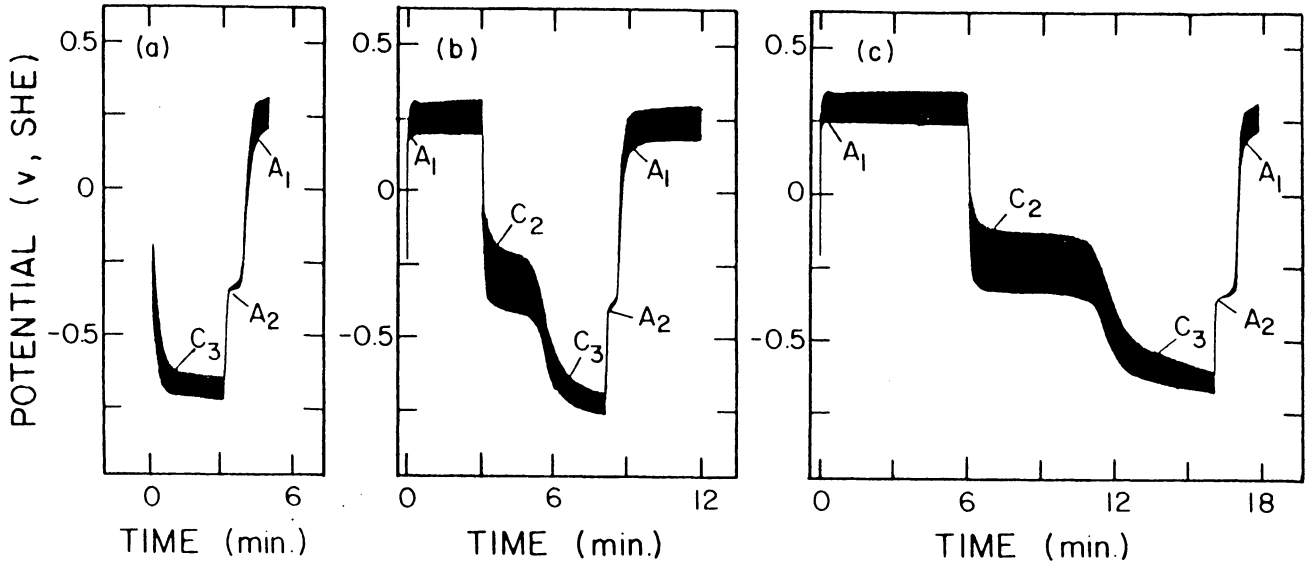


Figure 3.25 IGP diagrams obtained after applying current pulses of 0.1 mA/cm^2 to a galena electrode immersed in a stirred 0.05 M KH_2PO_4/0.05 M Na_2HPO_4 solution (pH 6.8). Anodic pulses applied initially for 0 (a), 3 (b) and 6 (c) minutes before reversal of current.

A_1 = $PbS/PbO,S^o + PbS/PbOH^+,S^o$

A_2 = Pb^o/PbO or $Pb^o,HPO_4^{2-}/PbHPO_4$

C_2 = S^o/HS^-

C_3 = $PbS/Pb^o,HS^-$

minutes (a), 3 minutes (b) and 6 minutes (c), and then reversing the polarity of the current to remove the oxidation products.

In the first case (Figure 3.25a) where the mineral is not initially polarized anodically, the applied cathodic current causes the electrode potential to drop quickly. This continues for about 30 seconds until the open-circuit reaches approximately -625 mv, where galena presumably begins to be reduced. This value is very close to the potential where the current due to C_3 in the voltammogram of Figure 3.24 begins to rise and is also close to the Nernst potential of -590 mv for the reduction of galena (reaction [3.21]).

After about 3 minutes of cathodic polarization, the polarity is reversed and, almost immediately, an anodic plateau appears at an open-circuit potential of -370 mv. This corresponds to the A_2 peak in Figure 3.24, although it occurs at a potential about 100 mv more positive than where A_2 begins in the voltammogram. It is noteworthy that the value from this experiment is closer to the reversible potential for the oxidation of Pb^o to PbO than is the one from the voltammogram, although it is still well below it. This is not surprising since much more charge is transferred during the IGP experiments and so the reactions are more bulk-like in nature. However, comparison of the length of time that the potential remains at the A_2 plateau with the length of time that the electrode has previously been cathodically polarized indicates that much less charge is associated with A_2 than with C_3. It should also be noted that A_2 may not be due to reaction [3.17], but to the oxidation of Pb^o to $PbHPO_4$, as has been discussed in Section 3.3.1e.

Further application of anodic current causes the potential to rise again to about 200 mv, where oxidation of galena itself (A_1) can begin.

When the galena is initially oxidized at 0.1 mA/cm^2 for 3 minutes (i.e., Figure 3.25b), the potential quickly rises to form an arrest between an open-circuit value of 220 mv and a closed-circuit one of 325 mv. With a reversal in the polarity of the current, the potential drops rapidly until an arrest begins to appear and has broadened into a well-defined plateau at an open-circuit potential of -150 mv. The change in potential along the plateau from -150 mv to a closed-circuit value of -400 mv between pulses coincides quite well with where the C_2 peak is found on the voltammograms (for example, Figures 3.18 and 3.19).

Extending the length of the initial anodic polarization to 6 minutes (Figure 3.25c) does not introduce any new features into the diagram. The C_2 plateau broadens in response to the increased amount of oxidation that has occurred. As in the previous diagram, there essentially is a balance in the charge associated with reaction C_2 and with the initial anodic polarization (A_1).

The IGP diagrams of galena immersed in a stagnant solution for the same applied current density are identical to the ones just shown and, consequently, are not included here.

The next series of experiments conducted was similar to the one discussed above, except that a current density of 0.2 mA/cm^2 was applied and the initial oxidation periods were 3, 6, 9.5 and 14 minutes (Figures 3.26 and 3.27). Oxidizing for only 3 minutes hardly changes the resulting potential-time diagram (Figure 3.26a) from the ones at the

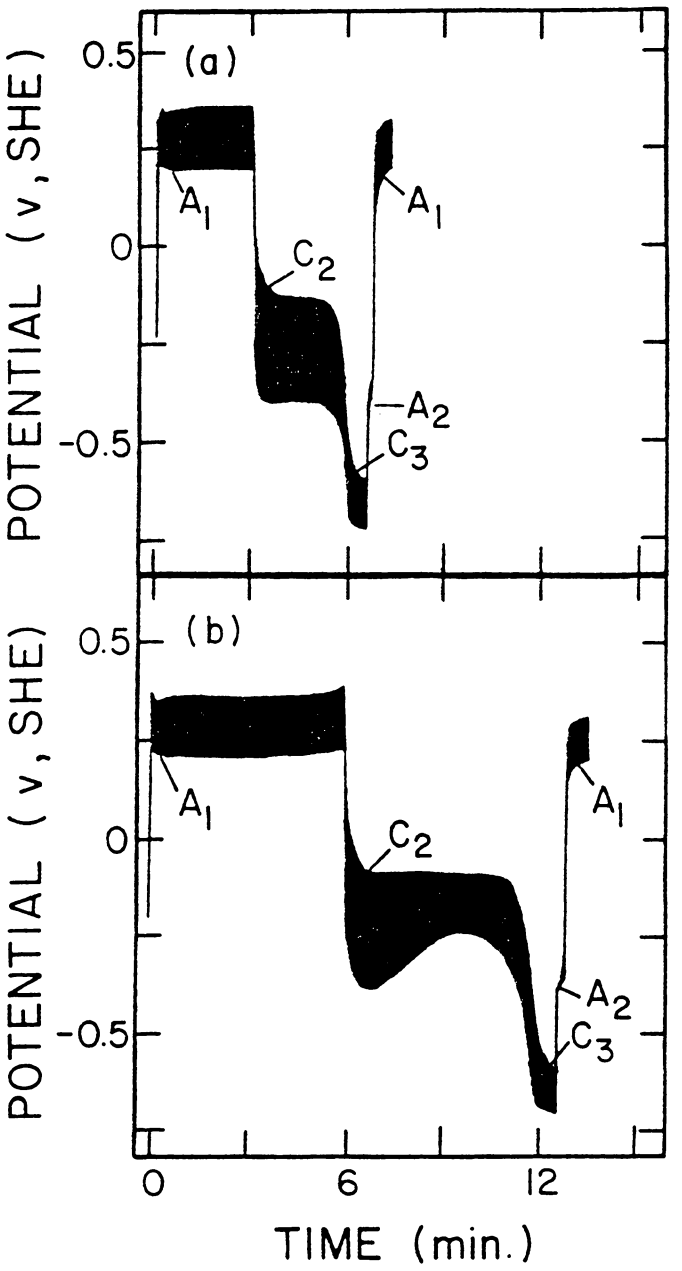


Figure 3.26 IGP diagrams obtained after applying current pulses of 0.2 mA/cm^2 to a galena electrode immersed in a stirred 0.05 M KH_2PO_4/0.05 M Na_2HPO_4 solution (pH 6.8). Anodic pulses applied initially for 3 (a) and 6 (b) minutes before reversal of current.

A_1 = $PbS/PbO,S^0 + PbS/PbOH^+,S^0$ C_2 = S^0/HS^-

A_2 = Pb^0/PbO or $Pb^0/HPO_4^{2-}/PbHPO_4$ C_3 = $PbS/Pb^0,HS^-$

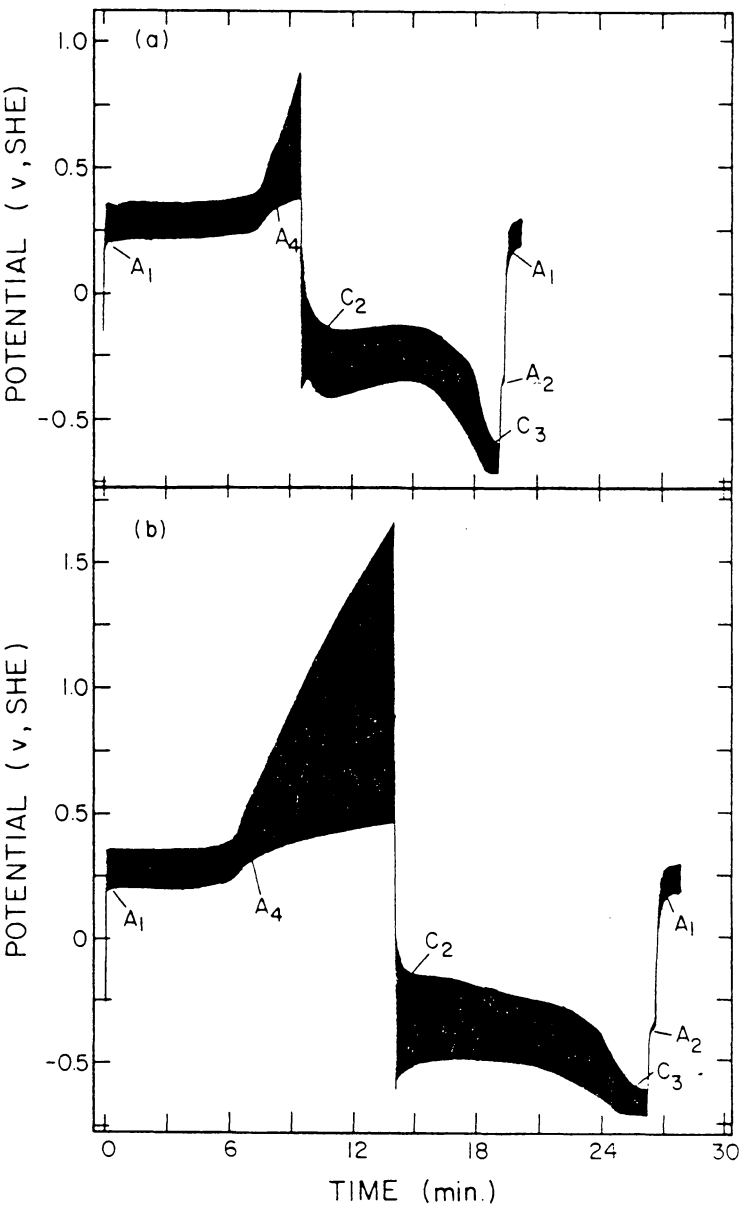


Figure 3.27 IGP diagrams obtained after applying current pulses of 0.2 mA/cm^2 to a galena electrode immersed in a stirred 0.05 M KH_2PO_4/0.05 M Na_2HPO_4 solution (pH 6.8). Anodic pulses applied initially for 9.5 (a) and 14 (b) minutes before reversal of current.

A_1 = $PbS/PbO,S^0$ + $PbS/PbOH^+,S^0$ C_2 = S^0/HS^-

A_2 = Pb^0/PbO or $Pb^0,HPO_4^{2-}/PbHPO_4$ C_3 = $PbS/Pb^0,HS^-$

A_4 = $PbS/PbOH^+,S_2O_3^{2-}$ or $PbS/PbO_2,S^0$

lower current density. However, when the period is increased to 6 minutes (Figure 3.26b), some differences are noticed. Just before the end of the anodic polarization, both the open-circuit and closed-circuit potentials of the galena electrode begin to rise. The C_2 plateau has shifted upward by about 50 mv to -100 mv, which is very close to the reversible potential of -90 mv for the reduction of S^o to HS^- (reaction 3.15]). Another new feature in Figure 3.26b is that the closed-circuit potential drops to -400 mv, as before, when cathodic current is first applied, but then begins to rise and reaches -260 mv after about 3 minutes. It is not clear why this should be the case.

The rise in the potential observed near the end of the six minutes of anodic polarization becomes very sharp when oxidation is continued for another 3.5 minutes (Figure 3.27a). The closed-circuit potential, in particular, rises very steeply, reaching 850 mv by the end of 9.5 minutes. Although the lower potential also increases, it does so much more slowly and levels off at approximately 350 mv. These observations suggest the onset of a new reaction, which is proceeding slowly and/or is passivating the mineral surface. One possibility is that some of the elemental sulfur is being oxidized to an oxy-sulfur anion such as thiosulfate or sulfate. Another is that PbO_2 is now being generated.

When the initial oxidation period is increased to 14 minutes, the closed-circuit potential during the anodic polarization reaches as high as 1700 mv, while the open-circuit potential reaches 450 mv. The amount of charge passed during oxidation is now greater than the amount associated with C_2. However, one difference from earlier results is

that the open-circuit potential along the C_2 plateau is no longer constant and now steadily drops.

One difficulty with the conclusion that elemental sulfur is being oxidized to thiosulfate or sulfate is that such reactions are irreversible and, consequently, should not directly affect the open-circuit potential. Yet, it appears from the diagrams in Figure 3.27 that the open-circuit potential after 6 minutes of anodic polarization is increasing. However, this may have more to do with the manner in which the experiment has been carried out than with something inherent to the galena system. After about 6 minutes of anodic polarization, the potential is rising so much while the circuit is closed during each pulse that there may not be enough time for it to fall to the true open-circuit value in one second when the current is turned off.

It can be recalled that at pH 9.2, thiosulfate is generated even when only 0.05 mA/cm^2 is applied (Figure 3.13). Even accepting the fact that thiosulfate or sulfate is being generated at pH 6.8, as much as 0.2 mA/cm^2 must be applied for this to be possible. Furthermore, it drives up the electrode potential tremendously in so doing. This clearly confirms that oxidation of sulfur to oxy-sulfur species becomes easier with increasing pH.

h. Chronoamperometry experiments at pH 6.8: Current-time plots for the oxidation of galena at pH 6.8 are presented in Figures 3.28 and 3.29. Up to a potential of 245 mv, the electrode response is similar to what has been observed at pH 9.2 (Figure 3.17). However, oxidation beyond this results in significantly higher currents at the lower pH.

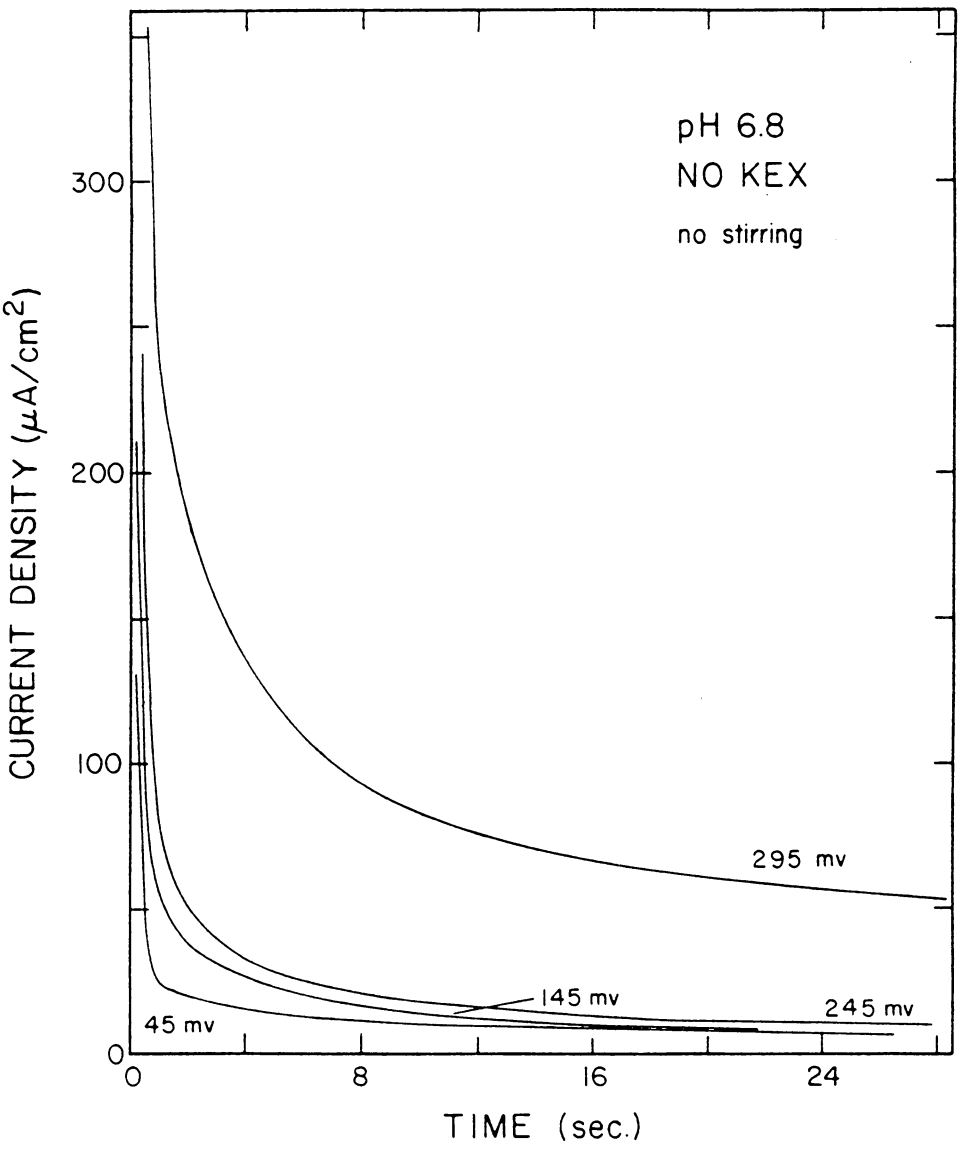


Figure 3.28 Current-time curves obtained after applying potentials of 45, 145, 245 and 295 mv to a galena electrode immersed in an unstirred 0.05 M KH_2PO_4/0.05 M Na_2HPO_4 solution (pH 6.8).

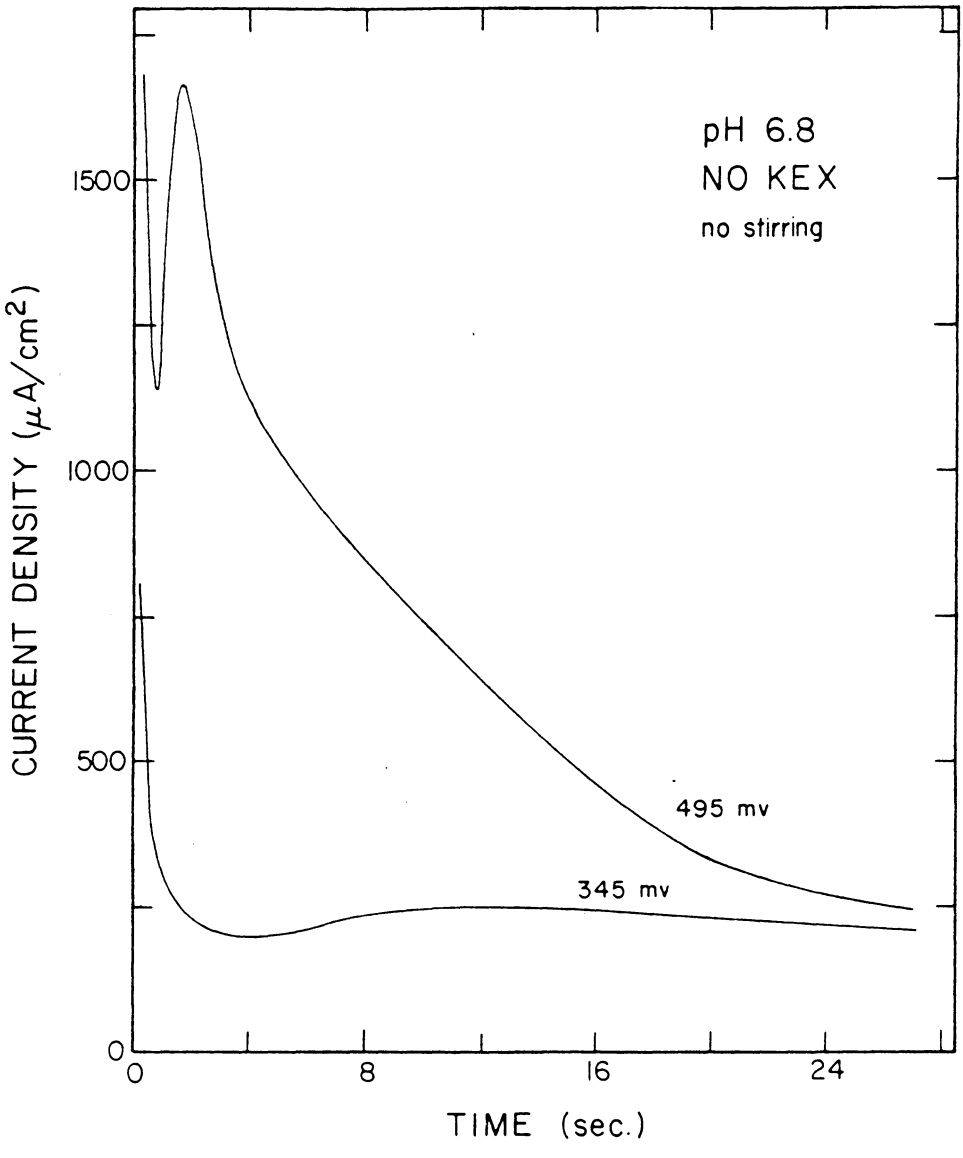


Figure 3.29 Current-time curves obtained after applying potentials of 345 and 495 mv to a galena electrode immersed in an unstirred 0.05 M KH_2PO_4/0.05 M Na_2HPO_4 solution (pH 6.8).

In addition, the curves for 345 mv, and particularly for 495 mv, appear quite differently in that after the initial relaxation of the electrode, the current begins to rise.

However, this behavior at 345 and 495 mv can be explained in terms of the sequence of reactions for the oxidation of galena at pH 6.8 that was proposed in Section 3.3.1e on the basis of the voltammetry data. According to this, oxidation proceeds initially by the formation of a metal-deficient sulfide and an insoluble lead oxide species. Such an oxide film would passivate the electrode surface and cause the current to drop sharply at the outset, as is observed in Figure 3.29. When enough of the product layer has accumulated, bulk-like S^o and PbO nucleate on the surface. At this pH, the PbO that forms immediately dissolves, thereby removing part of the passivating film. This should bring about the sudden rise in anodic current after the initial drop that is observed in Figure 3.29.

3.3.2 In the Presence of Xanthate

a. Single sweep voltammetry at pH 9.2:

Effect of xanthate concentration: Voltammograms on a galena electrode were obtained at a sweep rate of 20 mv/sec in unstirred 10^{-3} and 10^{-4} M KEX solutions. These are superimposed in Figure 3.30 with one obtained in the absence of collector. In the presence of 10^{-3} M KEX, the anodic current is increased significantly in the 0 to 200 mv range as compared to the case when no xanthate is present. This rise in current prior to the steeper current rise at approximately 200 mv is

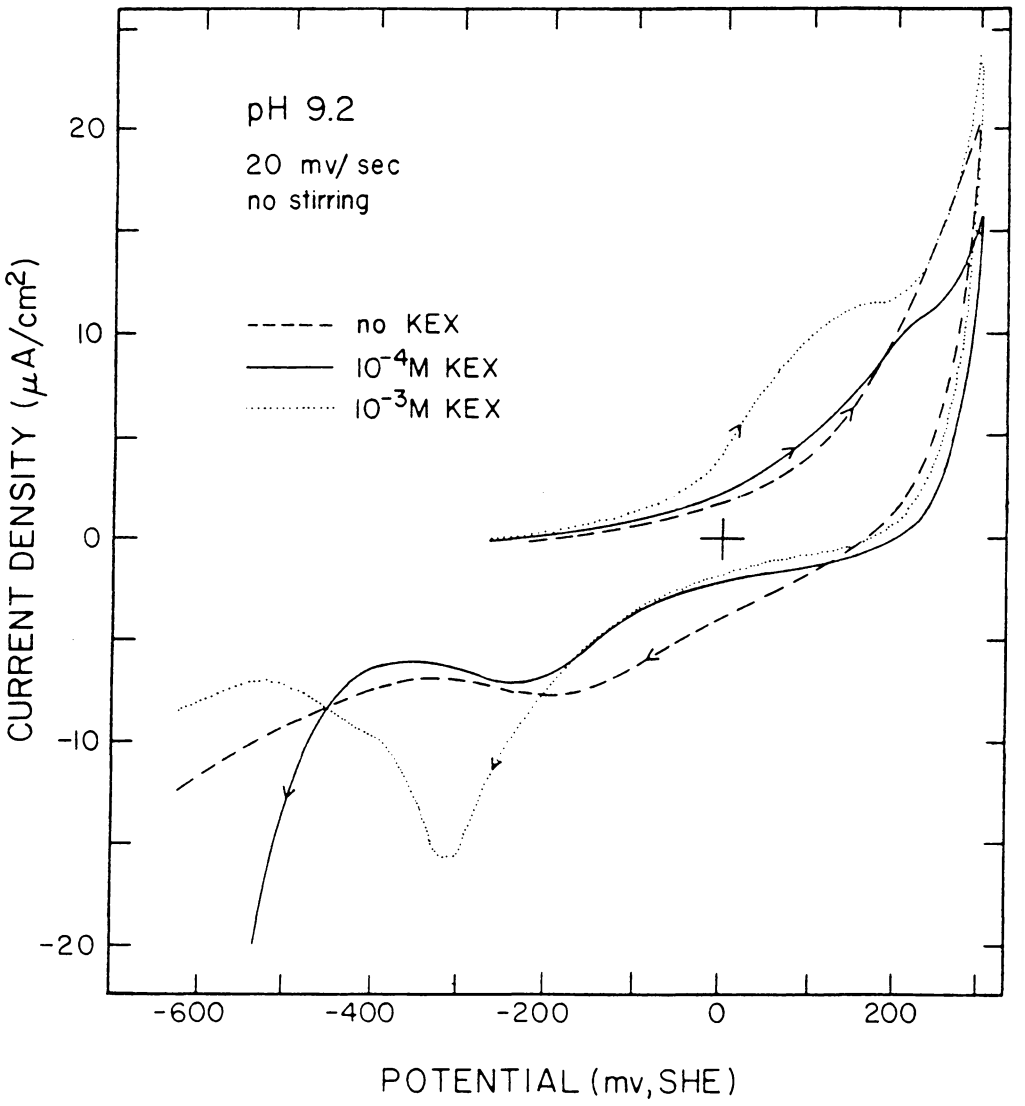


Figure 3.30 Single sweep voltammograms for a galena electrode immersed in a 0.05 M $Na_2B_4O_7$ solution (pH 9.2) containing 0 (---), 10^{-4} (—) and 10^{-3} (. . .) M KEX. No stirring. Scan rate = 20 mv/sec.

called a pre-wave and has been observed previously by Woods (1971) for a xanthate concentration of 9.5×10^{-3} M. On the reverse scan, a new peak, which is narrower and more cathodic than the one obtained in the absence of collector, appears. This peak is presumably due to the removal of xanthate from the galena surface.

When 10^{-4} M KEX is added, the resulting curve is somewhat intermediate to the other two. The anodic current is lower and the pre-wave is not nearly as distinct as at the higher concentration. Although the cathodic peak occurs at a potential cathodic to the one obtained in the absence of collector, it is not as sharp as the one for 10^{-3} M KEX.

A series of scans was performed on the galena electrode immersed in an unstirred 10^{-3} M KEX solution by varying the sweep rate between 10 and 50 mv/sec (Figure 3.31). Raising the scan rate increases the current, as expected, but it does not affect the position of the point of inflection between the anodic pre-wave and the steep rise portion of the curve. Pre-waves such as the ones in Figure 3.31 are often characteristic of a chemisorption process involving the transfer of electrons. Since the adsorption density for monolayer coverage in such a case is a function only of the geometry of the adsorbent and adsorbate, the corresponding quantity of charge passed should be independent of scan rate.

To determine whether xanthate chemisorption is responsible for the anodic pre-wave, the charge up to the point of inflection has been measured for each of the voltammograms in Figure 3.31. The results in Table 3.6 show that the charge passed is indeed independent of scan rate and averages about 110 $\mu C/cm^2$. This value is 1.5 times the theoretical

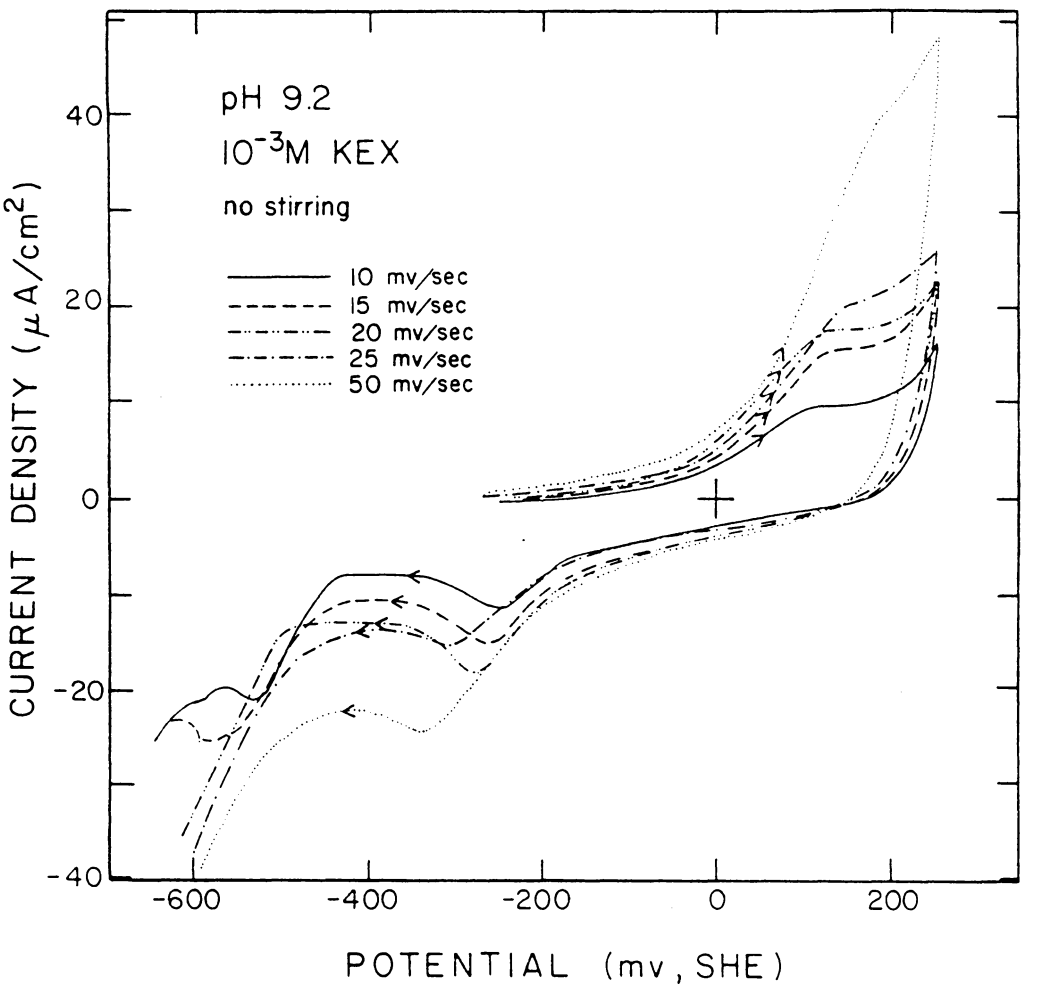


Figure 3.31 Effect of scan rate on the single sweep voltammograms for a galena electrode immersed in a 0.05 M $Na_2B_4O_7$ (pH 9.2) + 10^{-3} M KEX solution. No stirring.

Table 3.6

Effect of Scan Rate on the Charge Density of the Anodic Pre-Wave at pH 9.2 and 10^{-3} M KEX

Scan Rate (mv/sec)	Charge Density ($\mu C/cm^2$)
10	112
15	114
20	109
25	107
50	107

value since adsorption by a one-electron process would require 74 $\mu C/cm^2$ for monolayer coverage assuming that each xanthate ion occupies 21 $Å^2$ of the surface. The discrepancy likely arises from the fact that the actual surface area of the electrode is greater than the apparent one. Considering the relatively coarse polishing of the electrode before each test, a roughness factor of 1.5 may be quite reasonable.

The conclusion that xanthate initially adsorbs by an anodic reaction involving the transfer of one electron agrees with what Woods (1971) found. This process, which can be expressed as

$$X^- \longrightarrow X_{ads} + e, \qquad [3.2]$$

is a surface reaction, and so has not been considered in the calculations discussed in Chapter II. Only bulk thermodynamic data have been used for these calculations.

Once a complete monolayer of xanthate has formed on the mineral surface, further adsorption beyond 200 mv can occur by the formation of PbX_2 via reaction [3.3] and/or [3.4]. In view of the generally accepted view that xanthate adsorbs on galena as PbX_2 and not X_2, reaction [3.1] has been excluded as a possibility.

It is interesting to note that although xanthate chemisorption occurs separately from multi-layer adsorption, desorption seems to proceed all at once since only one single cathodic peak appears on the reverse scan. This has also been observed by Woods (1971) and Lamache et al. (1984).

Such behavior can be explained if the chemisorption reaction is considered to be the first step of the overall adsorption reaction:

$$PbS + 2X^- \longrightarrow PbX_2 + S^o + 2e. \qquad [3.3]$$

This first step (reaction [3.2]) would be followed by another (or more) in which a second xanthate ion and Pb^{2+} from the galena lattice combine with one of the chemisorbed xanthate atoms to form PbX_2. Once enough PbX_2 forms in this way, the original chemisorbed xanthate atoms might lose their identities and become indistinguishable from the xanthate in the other layers. Removal of the PbX_2 on the reverse scan would then occur as a single process.

Figure 3.32 shows the effect of scan rate for 10^{-4} M KEX. As mentioned previously (Figure 3.30), the anodic pre-waves are much less distinct at this xanthate level and, in fact, no point of inflection can be seen for the lower scan rates. The points of inflection at sweep speeds of 20 and 25 mv/sec occur at a potential of approximately 250 mv, which is about 50 mv higher than in the case of 10^{-3} M collector (Figure 3.31). This suggests that adsorption is slower at the lower xanthate concentration. Integrating under the voltammograms up to a potential of 250 mv reveals that charge now decreases with scan rate (Table 3.7). Moreover, the charge densities are considerably higher than those shown in Table 3.6 for 10^{-3} M KEX. One explanation for this behavior is that PbX_2 or X_2 begins to form before a monolayer of chemisorbed xanthate is completed. Another possibility is that other anodic reactions, such as the oxidation of galena itself, are also occurring simultaneously with

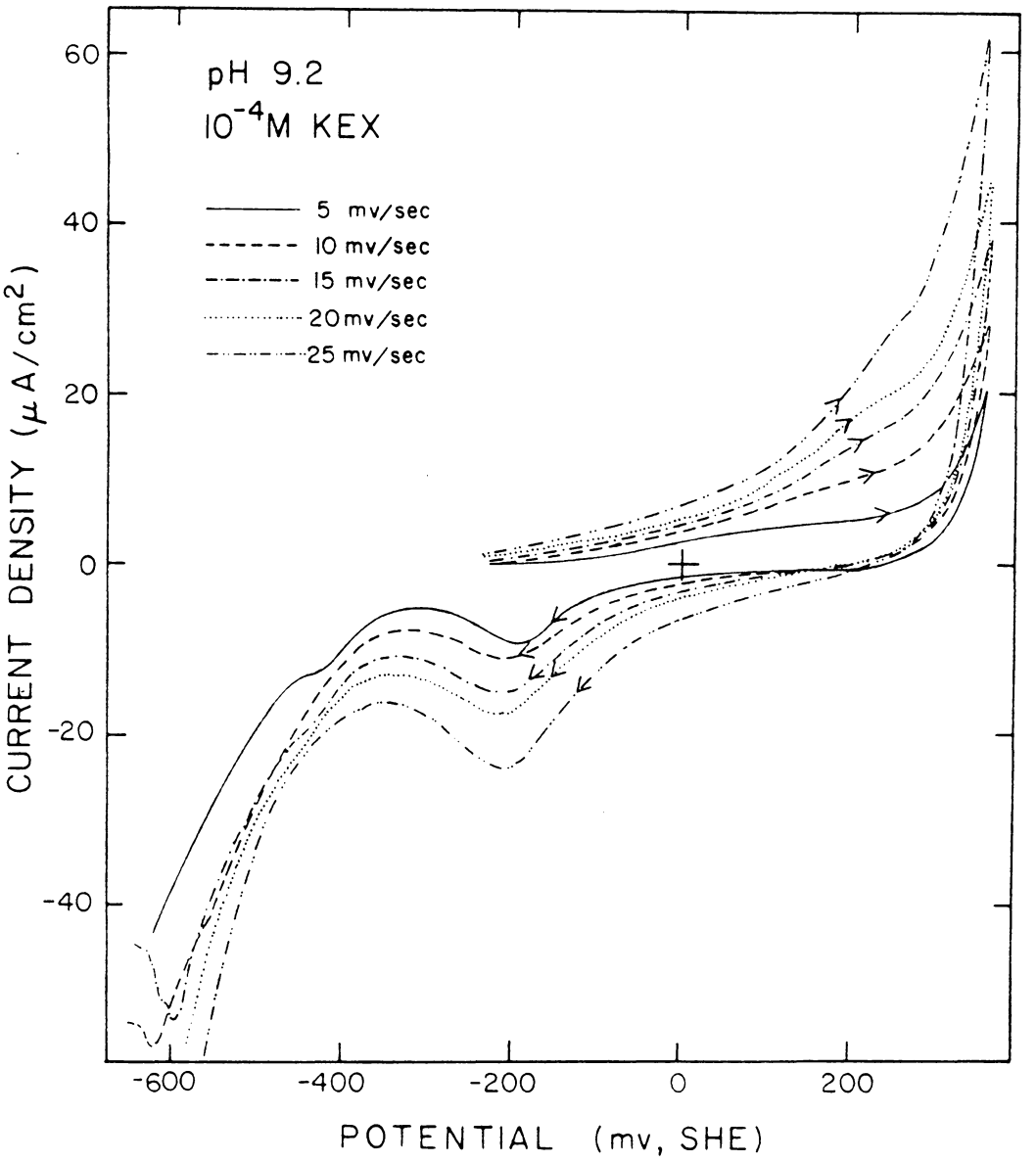


Figure 3.32 Effect of scan rate on the single sweep voltammograms for a galena electrode immersed in a 0.05 M $Na_2B_4O_7$ (pH 9.2) + 10^{-4} M KEX solution. No stirring.

Table 3.7

Effect of Scan Rate on the Charge Density of the Anodic Pre-Wave at pH 9.2 and 10^{-4} M KEX

Scan Rate (mv/sec)	Charge Density ($\mu C/cm^2$)
5	288
10	249
15	224
20	195
25	190

xanthate adsorption.

Effect of anodic limit at 10^{-3} M KEX: In order to gain a better understanding of the chemistry of the galena-xanthate system when adsorption proceeds beyond monolayer coverage, sweeps were carried out at a speed of 20 mv/sec with anodic limits varying from 45 to 545 mv. Some of the resulting voltammograms are shown in Figures 3.33 and 3.34.

From Figure 3.33, it is evident that the cathodic peak, C_1, at -300 mv begins to become prominent as the current at A_1 begins to rise sharply after the initial chemisorbed layer is complete. The growth of the C_1 peak is, therefore, likely associated with the removal of more and more PbX_2 as the anodic limit is increased.

Once the scan is extended beyond 295 mv, the current density rises very steeply (A_1) and becomes almost 500 $\mu A/cm^2$ by the time the potential reaches 545 mv (Figure 3.34). Increasing the anodic limit from 345 to 445 mv shifts the position of the cathodic peak from approximately -400 to -550 mv. However, the shift is likely due to the fact that there is a larger quantity of oxidation products to be reduced and not due to the onset of a new reaction. The rising portions of peaks associated with different reactions would not be expected to coincide, as the ones in Figure 3.34 do. (See Section 3.1.3 for the discussion concerning the origin and shape of a voltammogram.)

When the anodic limit is raised to 495 and 545 mv, two reduction peaks, C_2 and C_3, can be detected. The more anodic one, C_2, is found at much the same potentials as the one in the case of the 445 mv anodic

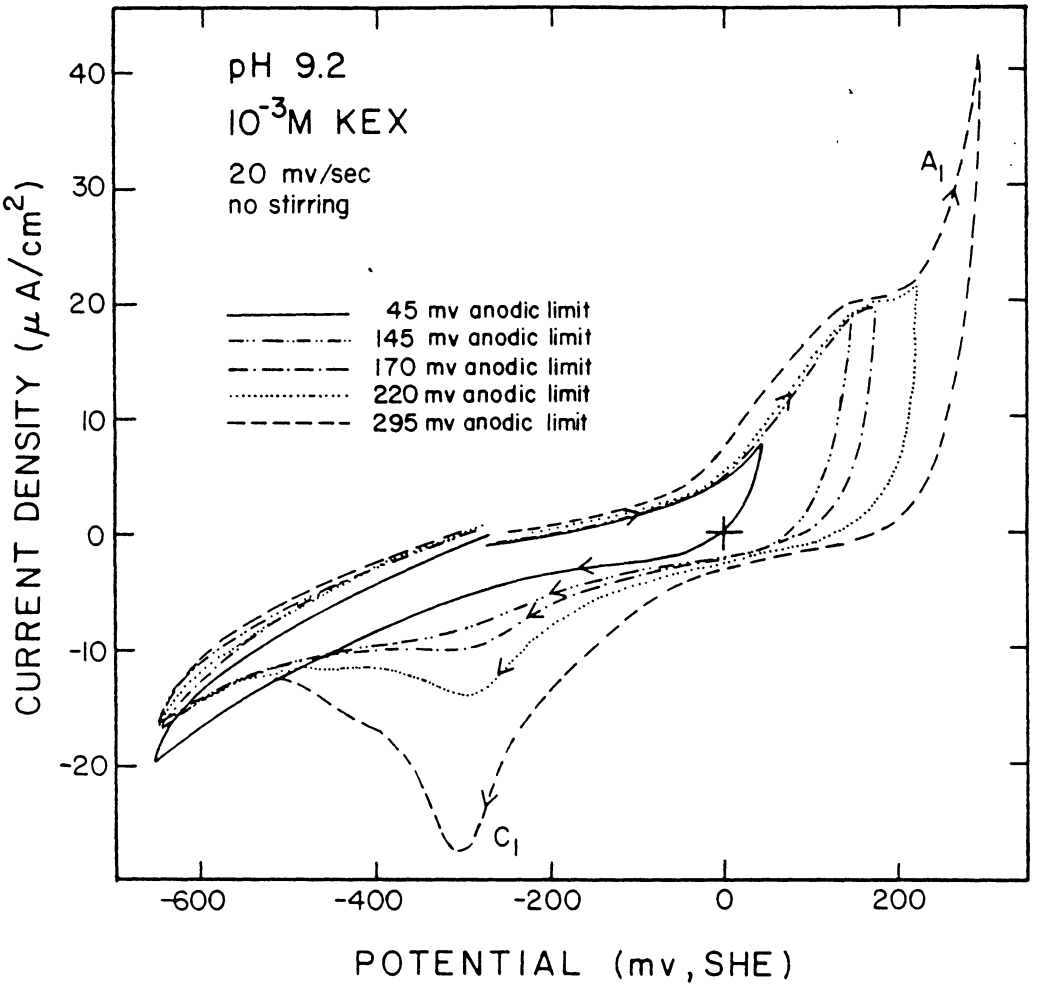


Figure 3.33 Effect of anodic limits between 45 and 295 mv on the single sweep voltammograms for a galena electrode immersed in a 0.05 M $Na_2B_4O_7$ (pH 9.2) + 10^{-3} M KEX solution. No stirring. Scan rate = 20 mv/sec.

$A_1 = PbS,X^-/PbX_2,S^0$ $\qquad$ $C_1 = PbX_2,S^0/PbS,X^-$

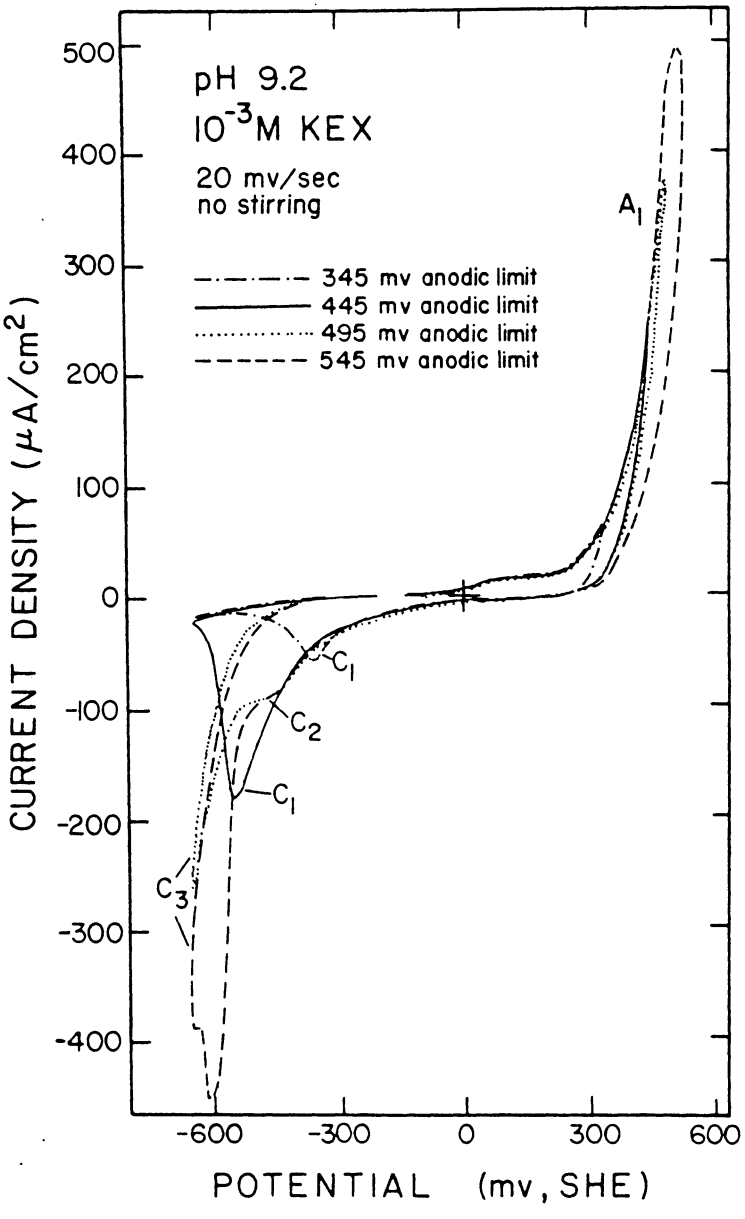


Figure 3.34 Effect of anodic limits between 345 and 545 mv on the single sweep voltammograms for a galena electrode immersed in a 0.05 M $Na_2B_4O_7$ (pH 9.2) + 10^{-3} M KEX solution. No stirring. Scan rate = 20 mv/sec.

345, 445 mv: $A_1 = PbS,X^-/PbX_2,S^0$ $C_1 = PbX_2,S^0/PbS,X^-$

495 mv: $A_1 = PbS,X^-/PbX_2,S^0 + PbX_2/PbO,X_2$

545 mv: $A_1 = PbS,X^-/PbX_2,S^0 + PbX_2/PbO,X_2 + S^0/S_2O_3^{2-}$

495, 545 mv: $C_2 = S^0/HS^-$ or X_2/X^- $C_3 = PbO/Pb^0$

limit, although the current is lower. This is followed soon after by a large increase in the cathodic current, C_3, signifying the onset of a second reaction.

Anodic limits up to 445 mv at 10^{-3} M KEX: The ratio of the charges associated with the anodic and cathodic portions of the voltammograms (i.e., Q_{CT}/Q_{A1}) in Figures 3.33 and 3.34 have been determined and are listed in Table 3.8. Except for the case of the highest anodic limit of 545 mv, a balance in the charges is observed. When xanthate is absent from the system, the situation is quite different in that an imbalance exists at a potential as low as 200 mv. An imbalance was the basis for the conclusion that thiosulfate is being generated during the oxidation of galena (Section 3.3.1a). Applying the same logic to the data obtained in the presence of 10^{-3} M KEX leads one to the conclusion that up to at least a potential of 495 mv, adsorption of xanthate is accompanied by the formation of S^o (reaction [3.3]) and not $S_2O_3^{2-}$ after monolayer coverage is reached via reaction [3.2]. It is, therefore, reasonable to assign the cathodic peak, C_1, which appears when the anodic limit is less than or equal to 445 mv, to the desorption of PbX_2 via the reverse of reaction [3.3].

As mentioned previously (see Section 3.12), Lamache et al. (1984) have come to the same conclusion on the basis of their work. However, at the same time, it should be recalled that the onset of flotation of galena at 2×10^{-5} M KEX, as reported by Guy and Trahar (1984), is best correlated to reaction [3.4] involving the formation of PbX_2 and $S_2O_3^{2-}$

Table 3.8

Charge Ratios Q_{CT}/Q_{Al} Obtained
From the Voltammograms for 10^{-3} M KEX at pH 9.2

Anodic Limit (mv)	Q_{CT}/Q_{Al}
245	0.96
295	1.02
345	1.01
445	0.99
495	1.01
545	0.60

(Figure 2.29). A discussion of the possible reasons for these differences will be included in Chapter V.

Anodic limit of 495 mv at 10^{-3} M KEX: Now, when the anodic limit is extended beyond 445 mv, at least one additional oxidation reaction likely occurs in view of the two reduction peaks appearing on the reverse scan (Figure 3.34). This upper limit (495 mv) is very close to the Nernst potential for the anodic decomposition of PbX_2, i.e.,

$$PbX_2 + H_2O \longrightarrow PbO + X_2 + 2H^+ + 2e. \qquad [3.27]$$

Accepting that PbX_2 is the xanthate-bearing species produced up to 445 mv, then this is a reasonable choice for the second anodic reaction.

Oxidation under A_1 can then be envisaged to proceed initially via

$$PbS + 2X^- \longrightarrow PbX_2 + S^o + 2e, \qquad [3.3]$$

and then

$$yPbX_2 + yH_2O \longrightarrow yPbO + yX_2 + 2yH^+ + 2ye, \qquad [3.28]$$

where y is the fraction of PbX_2 that is decomposed. Again, it should be emphasized that the chemisorption reaction [3.2] has not been explicitly written as one of the oxidation reactions since it is being viewed as part of the overall reaction [3.3]

On the reverse scan, the remaining PbX_2 is removed under C_1 by the process:

$$(1-y)PbX_2 + (1-y)S^o + 2(1-y)e \longrightarrow (1-y)PbS + 2(1-y)X^-. \qquad [3.29]$$

Once this is completed, y moles of PbO and y moles of S^o still remain on the galena surface. Possible reactions for C_3 are the reduction of PbO and/or S^o (i.e., reactions [3.13], [3.14] or [3.15]). Choosing for the moment the reduction of PbO to Pb^o, C_3 can be written as:

$$yPbO + 2yH^+ + 2ye \longrightarrow yPb^o + yH_2O. \qquad [3.30]$$

The total anodic and cathodic charges can then be obtained by summing up the individual charges:

$$Q_{AT} = 2F(1+y)N_{PbS} \qquad [3.31]$$

$$Q_{CT} = 2FN_{PbS} \qquad [3.32]$$

where N_{PbS} is the number of moles of PbS reacted. These can then be combined to yield the expression,

$$Q_{CT}/Q_{AT} = 1/(1+y), \qquad [3.33]$$

for the charge ratio. Inspection of Eq. [3.33] shows that a value of unity that is observed when the anodic limit is 495 mv can only be obtained when y = 0. However, this would nullify the entire reaction scheme since y = 0 means that reactions [3.28] and [3.30] do not occur. The same result is also reached if C_3 is attributed to reaction [3.14] or [3.15]. Therefore, these schemes can be rejected.

Another possible interpretation of the voltammograms for the upper limit of 495 mv is that <u>all</u> the PbX_2 that is produced by reaction [3.3] is subsequently decomposed by reaction [3.28]. Then, the more positive reduction peak (C_2) can be assigned to a reaction which is different

from that of C_1 which appears in the case of the lower anodic limits. In the absence of collector, one of the reduction reactions that is observed is the recombination of PbO and S^o. It is reasonable to propose that this reaction also occurs when xanthate is present. Accordingly, a sequence that can be considered is that some of the PbO and S^o generated at A_1 recombines via reaction [3.14] at C_2, while the remaining portion of one of these oxidation products is reduced at C_3. If PbO is reduced under C_3, then the scheme becomes:

A_1 $$PbS + 2X^- \longrightarrow PbX_2 + S^o + 2e \qquad [3.3]$$

$$PbX_2 + H_2O \longrightarrow PbO + X_2 + 2H^+ + 2e \qquad [3.27]$$

C_2 $$yPbO + yS^o + 2yH^+ + 2ye \longrightarrow yPbS + yH_2O \qquad [3.34]$$

C_3 $$(1-y)PbO + 2(1-y)H^+ + 2(1-y)e \longrightarrow (1-y)Pb^o + (1-y)H_2O. \qquad [3.35]$$

The charges associated with these are:

$$Q_{A1} = 4FN_{PbS}, \qquad [3.36]$$

$$Q_{C2} = 2yFN_{PbS}, \qquad [3.37]$$

$$Q_{C3} = 2(1-y)FN_{PbS}, \qquad [3.38]$$

for which a charge ratio,

$$(Q_{C2} + Q_{C3})/Q_{A1} = 0.5, \qquad [3.39]$$

is obtained. This is considerably different from the observed value of unity (see Table 3.8) and, consequently, it can be concluded that the occurrence of the above sequence is not likely. Replacing reaction [3.14] with [3.15] for C_3 leads to the same result. Therefore, it does not seem likely that PbO and S^o recombine at all under C_2 when the solution contains 10^{-3} M KEX.

One alternative to this is that S^o and PbO are reduced separately. The reaction sequence would then become:

A_1 $\quad PbS + 2X^- \longrightarrow PbX_2 + S^o + 2e$ [3.3]

$\quad PbX_2 + H_2O \longrightarrow PbO + X_2 + 2H^+ + 2e$ [3.27]

C_2 $\quad S^o + H^+ + 2e \longrightarrow HS^-$ [3.15]

C_3 $\quad PbO + 2H^+ + 2e \longrightarrow Pb^o + H_2O$ [3.13]

If all the S^o and PbO from A_1 are reduced by C_2 and C_3, respectively, then the anodic and cathodic charges will balance. On the basis of this analysis, this is the most likely sequence considered so far.

It is worth noting an interesting consequence of this sequence concerning the decomposition of PbX_2. Evidence from the voltammograms indicates that PbX_2 is still stable at a potential of 445 mv. However, when the scan is extended only by another 50 mv, all the PbX_2 has disappeared. Such a rapid decomposition is consistent with the flotation data of Guy and Trahar (1984), which shows a very sharp drop

in recovery above 300 mv at pH 8.0.

According to the above scheme, X_2 is being produced by reaction [3.27] under A_1. If the X_2 does not remain on the galena surface, then it will not be involved in any of the reduction reactions during the reverse sweep. However, if it does, then it may participate in the cathodic reactions.

One possibility is for C_2 to be attributed to the reduction of X_2, i.e.,

$$X_2 + 2e \longrightarrow 2X^-, \qquad [3.40]$$

and for C_3 to be assigned to the reduction of PbO and/or S^o (i.e., reactions [3.13], [3.14] or [3.15]). All of these sequences would have a Q_{CT}/Q_{AT} value of unity which is observed for the anodic limit of 495 mv. Therefore, these alternatives are also quite possible.

A sequence that involves the formation of X_2 which remains on the galena surface would be quite interesting in view of the results of the previous research on the galena-ethyl xanthate system. According to the above scheme, both PbX_2 and X_2 can be produced on a galena surface, but not at the same time. At potentials of 445 mv or below, only PbX_2 will exist; at 495 mv or beyond, only X_2 will be observed. This type of behavior is consistent with what has been reported in the literature. Some researchers claim that they have detected PbX_2, while others opt for X_2. Both groups may be correct, depending on the oxidizing conditions during their experiments.

Anodic limit of 545 mv at 10^{-3} M KEX: When the anodic limit is increased to 545 mv, a charge imbalance arises for the first time (see Table 3.8). A possible explanation is that a portion of the S^o produced by A_1 is further oxidized to $S_2O_3^{2-}$. This would modify the previously discussed sequence and the corresponding charges:

A_1 $$PbS + 2X^- \longrightarrow PbX_2 + S^o + 2e \qquad [3.3]$$

$$PbX_2 + H_2O \longrightarrow PbO + X_2 + 2H^+ + 2e \qquad [3.27]$$

$$yS^o + 3/2\ y\ H_2O \longrightarrow 1/2\ y\ S_2O_3^{2-} + 3yH^+ + 2ye \qquad [3.41]$$

C_2 $$(1-y)S^o + (1-y)H^+ + 2(1-y)e \longrightarrow (1-y)HS^- \qquad [3.42]$$

C_3 $$PbO + 2H^+ + 2e \longrightarrow Pb^o + H_2O \qquad [3.13]$$

$$Q_{A1} = (4 + 2y)FN_{PbS} \qquad [3.43]$$

$$Q_{C2} = 2(1-y)FN_{PbS} \qquad [3.44]$$

$$Q_{C3} = 2FN_{PbS}. \qquad [3.45]$$

In this case, the charge ratio would be:

$$(Q_{C2} + Q_{C3})/Q_{A1} = (4F - 2yF)/(4F + 2yF)$$

$$= (2 - y)/(2 + y). \qquad [3.46]$$

Using the observed ratio of 0.60 from Table 3.8, the fraction, y, of S^o that is converted to $S_2O_3^{2-}$ is calculated to be 0.5. The corresponding

value of 0.25 for $n_{S_2O_3^{2-}}/n_{S^o}$ is considerably less than the value of 0.58 obtained in the absence of xanthate for the same anodic limit (see Table 3.3).

As in the previous case, the C_2 peak can also be assigned to the reduction of X_2 to X^- (i.e., reaction [3.40]) and C_3 to one of the reactions involving the reduction of S^o and/or PbO.

Effect of anodic limit at 10^{-4} M KEX: The effect of the anodic limit on the voltammograms for the galena electrode immersed in an unstirred 10^{-4} M KEX solution has also been investigated. The results of experiments in which the upper limit was varied from 245 to 545 mv are shown in Figures 3.35 and 3.36. It is interesting to compare several of the aspects of these curves with those of the voltammograms shown previously for 0 and 10^{-3} M KEX.

The anodic currents are lower than those obtained when 10^{-3} M KEX is added (see Figures 3.33 and 3.34). At 10^{-4} M KEX, a cathodic peak, C_1, first begins to appear when the anodic limit reaches 295 mv, which is close to where the first cathodic peak occurs in the absence of collector, but about 150 mv higher than in the case of 10^{-3} M KEX. However, these differences may have more to do with the amount of oxidation during the anodic sweep than in the nature of the oxidation reaction.

Increasing the anodic limit shifts the cathodic peak in the negative direction and eventually causes a second peak to appear at approximately -550 mv. Although this behavior is observed at both 0 and

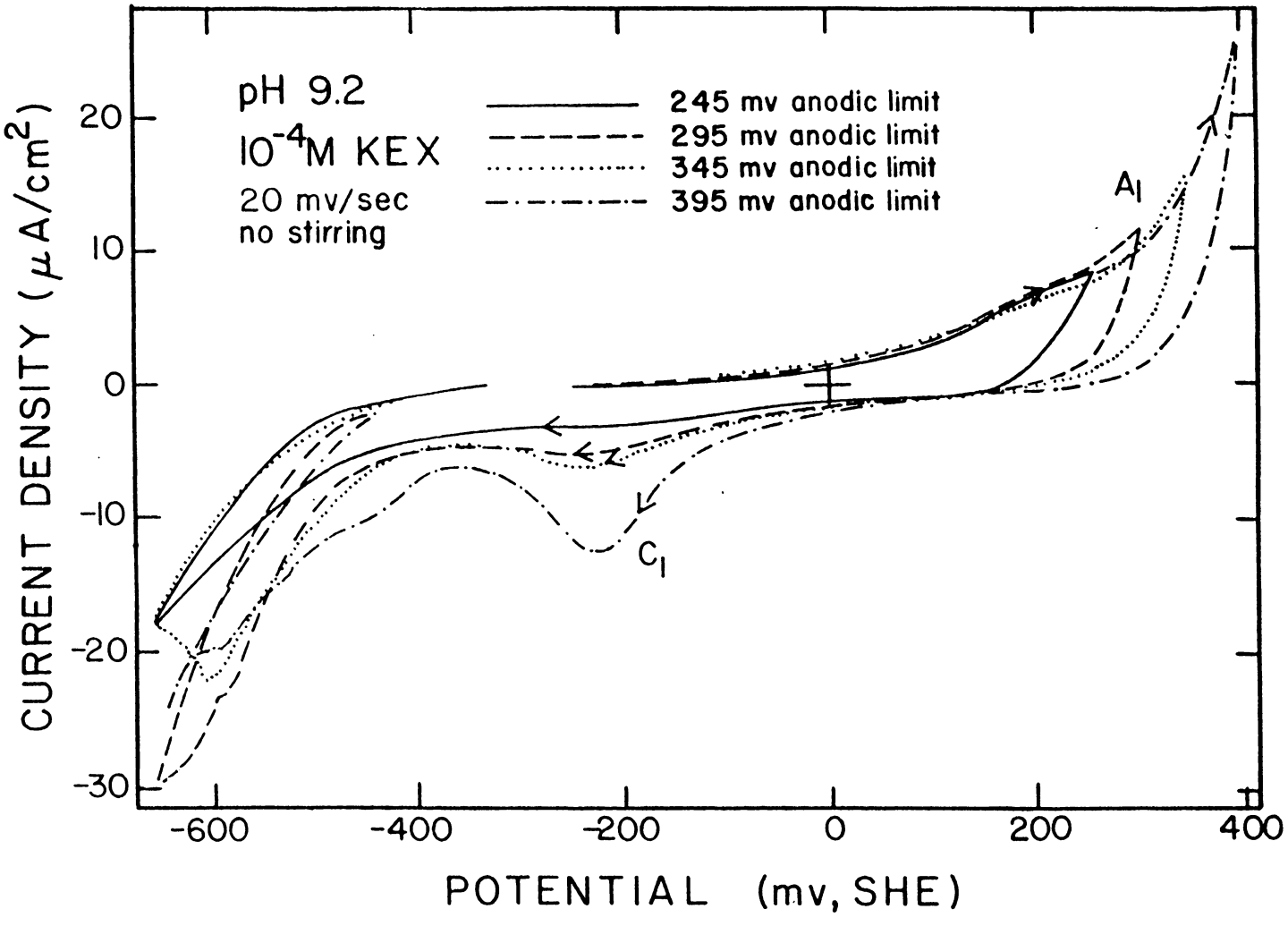


Figure 3.35 Effect of anodic limits between 245 and 395 mv on the single sweep voltammograms for a galena electrode immersed in a 0.05 M $Na_2B_4O_7$ (pH 9.2) + 10^{-4} M KEX solution. No stirring. Scan rate = 20 mv/sec.
A_1 = $PbS,X^-/PbX_2,S^o$ + $PbS,X^-/PbX_2,S_2O_3^{2-}$ C_1 = $PbX_2,S^o/PbS,X^-$ C_2 = $PbX_2/Pb^o,X^-$

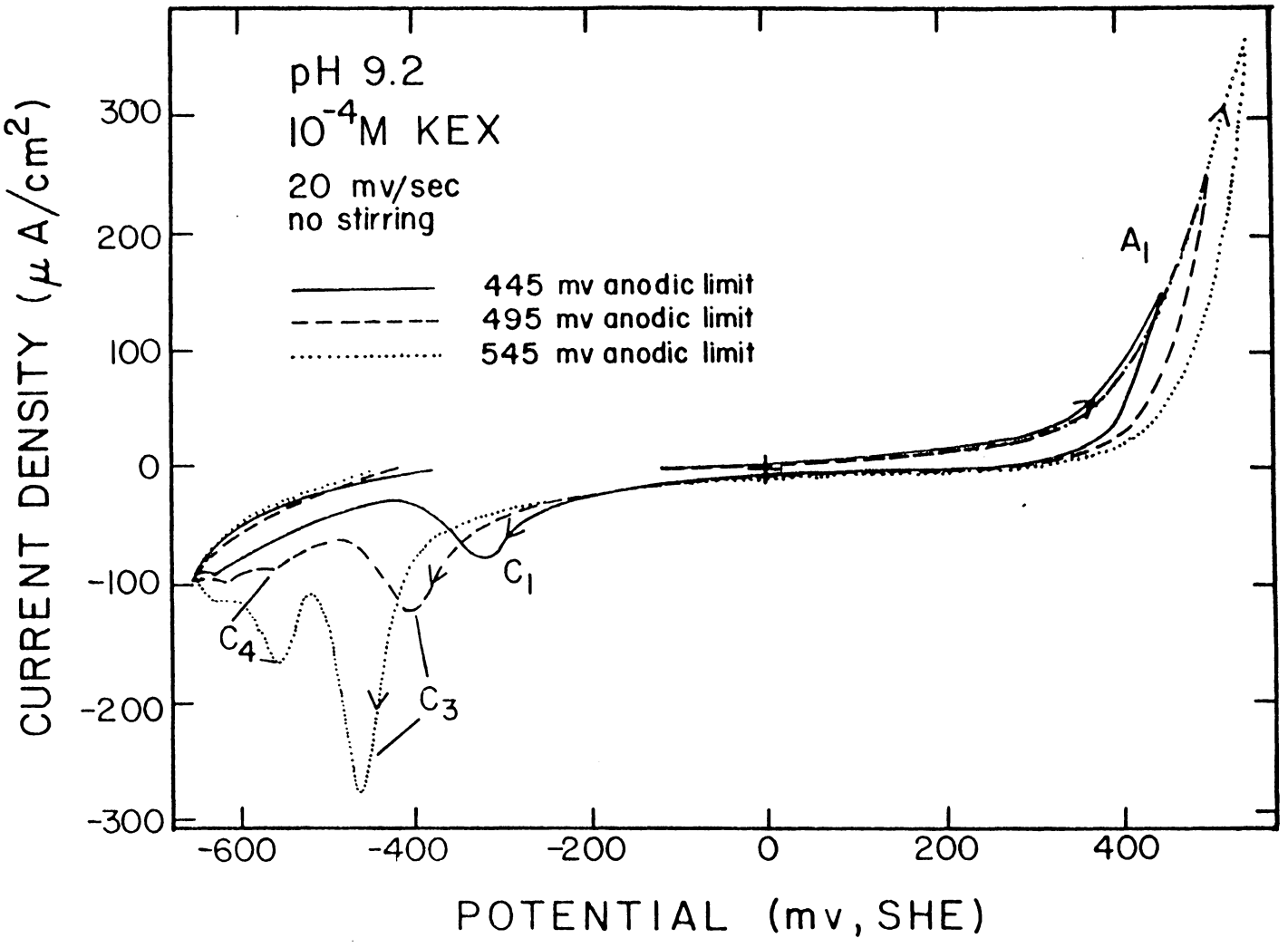


Figure 3.36 Effect of anodic limits between 445 and 545 mv on the single sweep voltammograms for a galena electrode immersed in a 0.05 M $N_2B_4O_7$ + 10^{-4} M KEX solution. No stirring. Scan rate = 20 mv/sec.

10^{-3} M KEX, the two peaks at 10^{-4} M KEX more closely resemble those occurring in the absence of xanthate in terms of shape and separation.

Anodic limits below 495 mv at 10^{-4} M KEX: The ratios of the charges associated with A_1 and C_1 are given in Table 3.9 for those curves in which the peak areas can be reliably measured. For every anodic limit beyond 245 mv, the values are less than unity and not much different from what is found in the absence of xanthate (Table 3.2). These results suggest that at 10^{-4} M KEX, thiosulfate is being generated during oxidation at a potential as low as 295 mv. This potential is about 250 mv lower than when thiosulfate first appears at a xanthate level of 10^{-3} M.

The formation of thiosulfate at such a low potential indicates that it occurs at the same time as PbX_2 at 10^{-4} M, rather than after PbX_2 has decomposed (as is the situation at 10^{-3} M KEX). One possible reaction sequence that can explain the current-potential behavior at the lower anodic limits (i.e., until PbX_2 decomposes) is:

A_1 $$yPbS + 2yX^- \longrightarrow yPbX_2 + yS^o + 2ye \qquad [3.47]$$

$$(1-y)PbS + 2(1-y)X^- + 3/2\ (1-y)H_2O \longrightarrow (1-y)PbX_2 + 1/2\ (1-y)S_2O_3^{2-} + 3(1-y)H^+ + 4(1-y)e \qquad [3.48]$$

C_1 $$yPbX_2 + yS^o + 2ye \longrightarrow yPbS + 2yX^- \qquad [3.49]$$

C_2 $$(1-y)PbX_2 + 2(1-y)e \longrightarrow (1-y)Pb^o + 2(1-y)X^- \qquad [3.50]$$

Table 3.9

Charge Ratios Q_{Cl}/Q_{Al} Obtained
as a Function of the Anodic Limit for 10^{-4} M KEX and pH 9.2

Anodic Limit (mv)	Q_{Cl}/Q_{Al}
295	0.71
345	0.63
395	0.65
445	0.63
495	0.58
545	0.54

where y is the fraction of reacted PbS that is oxidized according to reaction [3.46].

The charges associated with these reactions are:

$$Q_{A1} = 2yFN_{PbS} + 4(1-y)FN_{PbS} \quad [3.51]$$

$$Q_{C1} = 2yFN_{PbS} \quad [3.52]$$

$$Q_{C2} = 2(1-y)FN_{PbS} \quad [3.53]$$

$$Q_{C1}/Q_{A1} = y/(2-y). \quad [3.54]$$

Substituting the observed charge ratios from Table 3.9 into Eq. [3.54], values of y and the relative amounts of S^o and $S_2O_3^{2-}$ can be calculated. The ratios $n_{S_2O_3^{2-}}/n_{S^o}$ shown in Table 3.10 have not been determined for the anodic limits of 495 and 545 mv since PbX_2 presumably becomes unstable and the sequence above does not apply at such high potentials. Comparison of these ratios with those obtained in the absence of xanthate (Table 3.3) shows that the presence of 10^{-4} M KEX has little effect on the amount of thiosulfate produced.

Although the above sequence involves two reduction reactions, only one distinct peak is observed, except when the anodic limit is 395 mv (Figure 3.35). One explanation for this may be that C_2 does not occur to a large enough extent for it to be distinguished from the reduction of the mineral itself. This is borne out by the fact that Q_{C1}/Q_{C2} (= y/1-y) varies from 2.8 to 4.9 for the various anodic limits below 495 mv.

Table 3.10

Molar Ratios $n_{S_2O_3^{2-}}/n_{SO}$ Obtained During Oxidation at 10^{-4} M KEX and pH 9.2

Anodic Limit (mv)	$n_{S_2O_3^{2-}}/n_{SO}$
295	0.10
345	0.15
395	0.13
445	0.18

Anodic limits of 495 and 545 mv at 10^{-4} M KEX: When the anodic limit is raised to 495 and 545 mv, two distinct cathodic peaks appear. These are designated as C_3 and C_4 (see Figure 3.36) since, as will be shown, they are likely due to different reactions from the ones occurring for lower anodic limits. It should be recalled that at 10^{-3} M KEX, oxidation proceeds by the formation of PbX_2 initially, and then by its decomposition via reaction [3.27] above 445 mv. The cathodic sweep then involves the removal of PbO and S^o.

However, the charge analysis at 10^{-4} M KEX shows that a similar reaction scheme is not likely at the lower collector. For one thing, it predicts that Q_{C3}/Q_{C4} should not exceed unity, although the actual C_3 peaks in Figure 3.36 are considerably larger than C_4. For another, the maximum charge ratio, Q_{C3}/Q_{A1}, allowed by this scheme is 0.5, which is less than the values of 0.58 and 0.54 observed for anodic limits of 495 and 545 mv, respectively (see Table 3.9).

One possibility is that some of the PbO produced during the anodic scan dissolves as $PbOH^+$. If C_3 is assigned to the reduction of S^o (reaction [3.15]) and C_4 to the reduction of PbO (reaction [3.13]), then this would enable Q_{C3}/Q_{C4} to exceed unity, as has been observed. It should be recalled that a portion of the PbO does dissolve, according to one of the reaction schemes that fit the voltammetry data when no KEX is present (i.e., sequence 12 in Table 3.1).

This alternative, however, would not solve the problem that Q_{C3}/Q_{A1} cannot exceed a value of 0.5. Oxidation when the anodic scan reaches beyond 495 mv at the lower xanthate level of 10^{-4} M may become an even

more complicated process than that which has already been proposed. For example, once PbX_2 decomposes, the underlying PbS may itself begin to oxidize. This would be consistent with the idea that xanthate adsorption and galena oxidation are competitive reactions.

b. Cyclic voltammetry at 10^{-3} M KEX and pH 9.2: Figure 3.37 shows a cyclic sweep between -655 and 245 mv at 20 mv/sec in a solution containing 10^{-3} M KEX. During the first cycle (denoted as '1' on the figure), the voltammogram is very similar to the curve in Figure 3.33 with the same anodic limit. However, from the second cycle onward, two additional anodic waves, A_2 and A_3, and a new cathodic peak, C_5, appear.

Since the anodic limit is only 245 mv, all the PbX_2 and S^o generated on the galena surface under A_1 should be converted back to PbS and X^- at C_1. Consequently, the rise in cathodic current, C_3, as the potential approaches the lower limit during the first cycle must be due to the reduction of the mineral itself (i.e., reaction [3.21]). Both A_2 and A_3 appear only after this occurs and so it is likely that they involve the oxidation of the products of reaction [3.21]. However, the A_2 wave has a much different shape and begins at a potential about 100 mv higher than the Pb^o/PbO peak which appears in Figure 3.8. A more likely choice for A_2 is the reaction of X^- ions with Pb^o to form PbX_2, i.e.,

$$Pb^o + 2X^- \longrightarrow PbX_2 + 2e. \qquad [3.55]$$

A_3 resembles very closely the wave in Figure 3.12 which has been

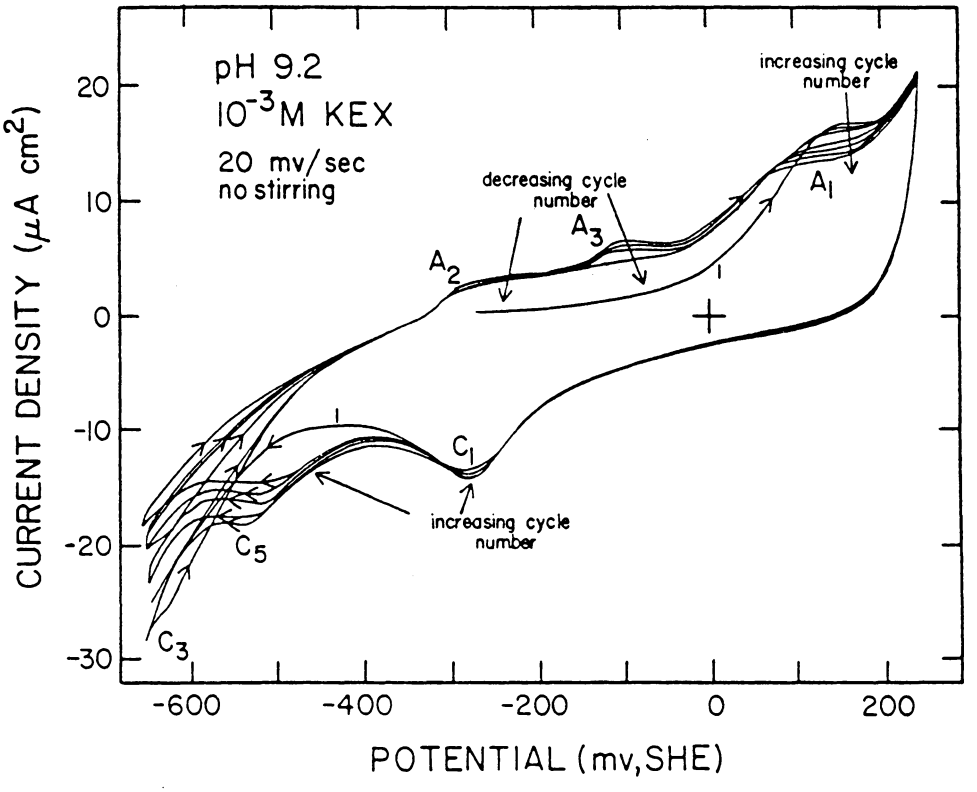


Figure 3.37 Cyclic voltammograms of a galena electrode in an unstirred 0.05 M $Na_2B_4O_7$ (pH 9.2) + 10^{-3} M KEX solution for potential sweeps between -655 and 245 mv. Scan rate = 20 mv/sec.

$A_1 = PbS,X^-/PbX_2,S^0$

$A_2 = Pb^0,X^-/PbX_2$

$A_3 = HS^-/S^0$

$C_1 = PbX_2,S^0/PbS,X^-$

$C_3 = PbS/Pb^0,HS^-$

$C_5 = PbX_2/Pb^0,X^-$

assigned to the oxidation of HS^- ions to S^o (reaction [3.24]). This reaction should occur just as easily whether or not collector has been added to the system.

A portion of the HS^- released by reaction [3.21] is likely to diffuse away from the electrode even in a stagnant solution. Therefore, more PbX_2 should be generated during each anodic sweep than S^o from the reactions at A_1 and A_3. Moreover, this excess should increase with each cycle. Since C_1 involves the reduction of equal moles of PbX_2 and S^o, the excess PbX_2 can only be removed by a new reaction, C_5, presumably the reverse of reaction [3.55]. This possibility is strengthened by the fact that the reversible potential for this reaction at $[X^-] = 10^{-3}$ M is calculated to be -432 mv, which lies between the current rise due to A_2 and C_5.

c. IGP experiments at pH 9.2: IGP diagrams obtained using unstirred borate solutions containing 0, 10^{-4} and 10^{-3} M KEX, are shown in Figure 3.38. In each case, current pulses of 0.02 mA/cm^2 have been applied for 3 minutes before being reversed in order to remove the oxidation products.

Comparison of the results shows that the presence of xanthate lowers the electrode potential of galena during anodic polarization. At 10^{-4} and 10^{-3} M KEX, the open-circuit potential is initially about 150 mv, rises quickly to approximately 150 mv, and thereafter begins to level off. At this applied current, the amount of charge passed by the time the potential begins to level off is well beyond what is required for monolayer coverage by xanthate via the one-electron chemisorption

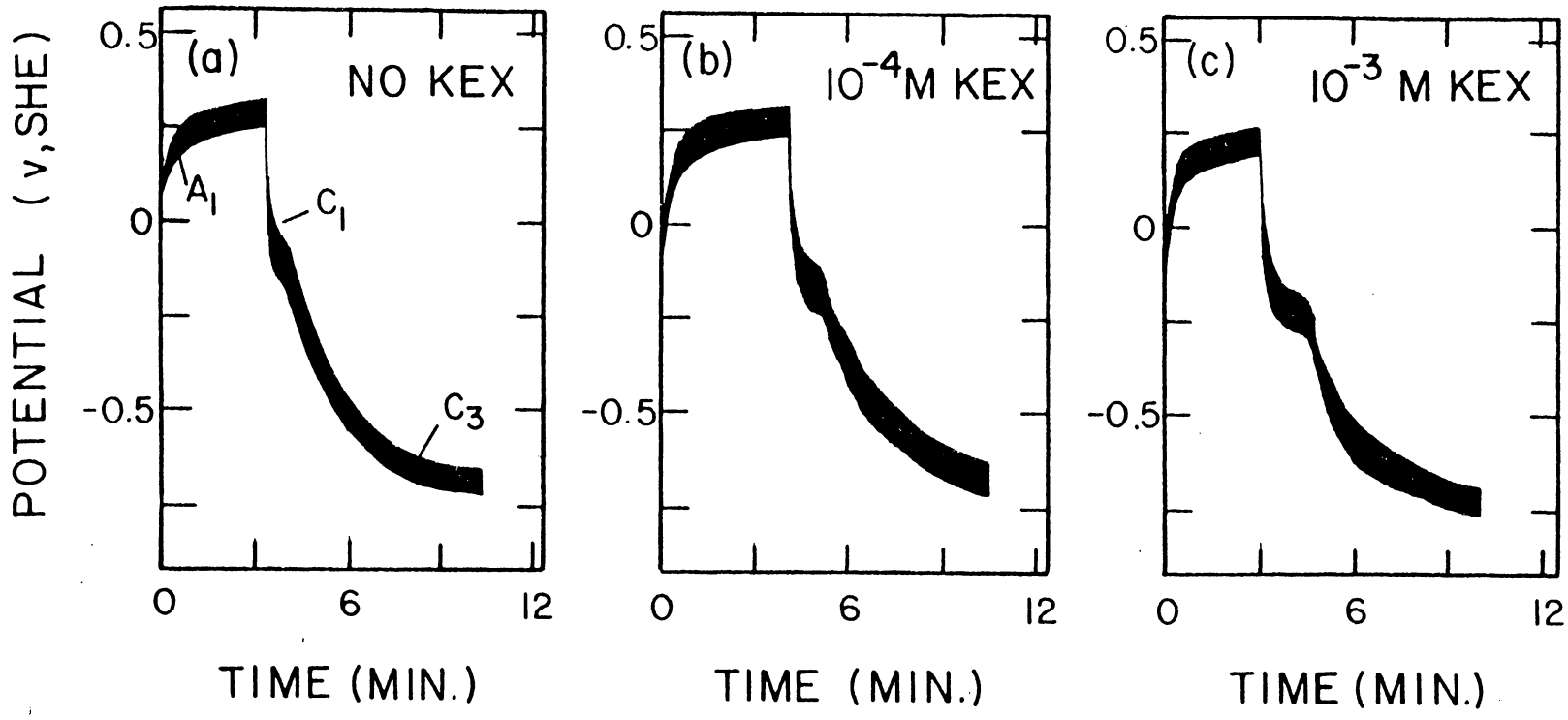


Figure 3.38 IGP diagrams obtained after applying current pulses of 0.02 mA/cm^2 to a galena electrode immersed in an unstirred solution containing 0.05 M $Na_2B_4O_7$ (pH 9.2) + 0 (a), 10^{-4} (b) and 10^{-3} (c) M KEX.

reaction [3.2]. Xanthate uptake will then be expected to involve the formation of bulk PbX_2.

The results of the voltammetry studies at 10^{-3} M KEX suggest that up to a potential of 495 mv, only PbX_2 and S^o are being formed during oxidation. The same should also hold true during the 3 minutes of anodic polarization in the IGP test (Figure 3.38c) since the maximum potential attained by the galena electrode is only 250 mv. It should be noted that the open-circuit potential of 150 mv is about 185 mv lower than the Nernst value calculated for reaction [3.3]. In fact, even the maximum potential reached by the mineral is less than the reversible value.

When the polarity of the pulses is switched negatively, an arrest begins to form at an open-circuit potential of about -100 mv and broadens into a plateau by about -200 mv. However, the charge consumed during this time is only half or so of what was passed while the galena was being oxidized. A similar, but larger, imbalance is noted in the diagram obtained in the absence of xanthate (Figure 3.38a). It should be recalled that this type of behavior has previously been used to support the notion that thiosulfate is being generated during oxidation. Yet, there is no evidence for the formation of thiosulfate at 10^{-3} M KEX from the voltammograms until the scan proceeds beyond 495 mv.

The results for 10^{-4} M KEX (Figure 3.38b) are similar to those of the higher concentration. There is less discrepancy with what is observed in the potential sweep experiments because the latter also show an imbalance between the anodic and cathodic charges.

d. Single sweep voltammetry at pH 6.8

Effect of xanthate concentration: In order to highlight the effect of xanthate at pH 6.8, voltammograms obtained in unstirred 0, 10^{-4} and 10^{-3} M KEX solutions at a scan rate of 20 mv/sec are superimposed in Figure 3.39. The curve for 10^{-3} M KEX is quite similar to the corresponding one at pH 9.2 in that it is characterized by a very distinct anodic pre-wave followed by a steep current rise and a single cathodic peak, C_2, in the vicinity of -270 mv. When the xanthate concentration is reduced to 10^{-4} M, the anodic current is lowered and no distinct pre-wave appears. Again, this has also been noted at pH 9.2. However, what has changed is that two peaks, C_1 and C_2, appear during the cathodic scan. The peak position of C_1 lies at approximately -150 mv and coincides closely with that of the lone reduction peak observed in the absence of xanthate, which has previously been attributed to the recombination of PbO and S^o to PbS (see Section 3.3.1f). The second peak, on the other hand, lines up with the one occurring at 10^{-3} M KEX. This strongly suggests that both xanthate adsorption and galena oxidation are taking place at the intermediate collector concentration.

Initial xanthate adsorption: The effect of scan rate at 10^{-3} and 10^{-4} M KEX has been investigated in a similar manner as to what was done at pH 9.2 (Figures 3.40, 3.41 and 3.42).

At 10^{-3} M KEX, the pre-wave extends up to a potential of approximately 150 mv at all the sweep rates from 5 to 50 mv/sec (Figures 3.40 and 3.41). Analysis of the charges associated with the pre-wave for the

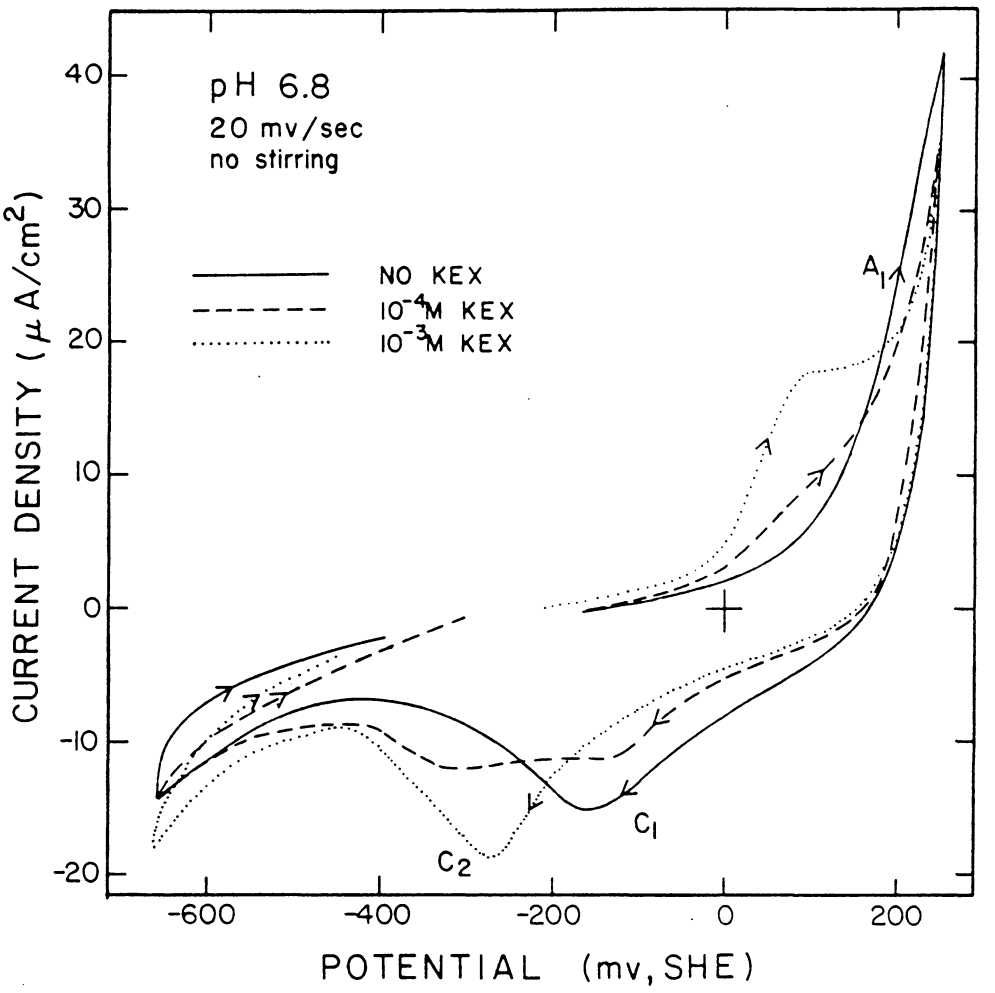


Figure 3.39 Single sweep voltammograms for a galena electrode immersed in a 0.05 M KH_2PO_4/0.05 M Na_2HPO_4 (pH 6.8) + 0 (a), 10^{-4} (b) and 10^{-3} (c) M KEX solution. No stirring. Scan rate = 20 mv/sec.

A_1 = PbS/PbO,S^o (no KEX)
PbS/PbO,S^o + PbS,X^-/PbX_2,S^o (10^{-4} M KEX)
PbS,X^-/PbX_2,S^o (10^{-3} M KEX)

C_1 = PbO,S^o/PbS

C_2 = PbX_2,S^o/PbS,X^-

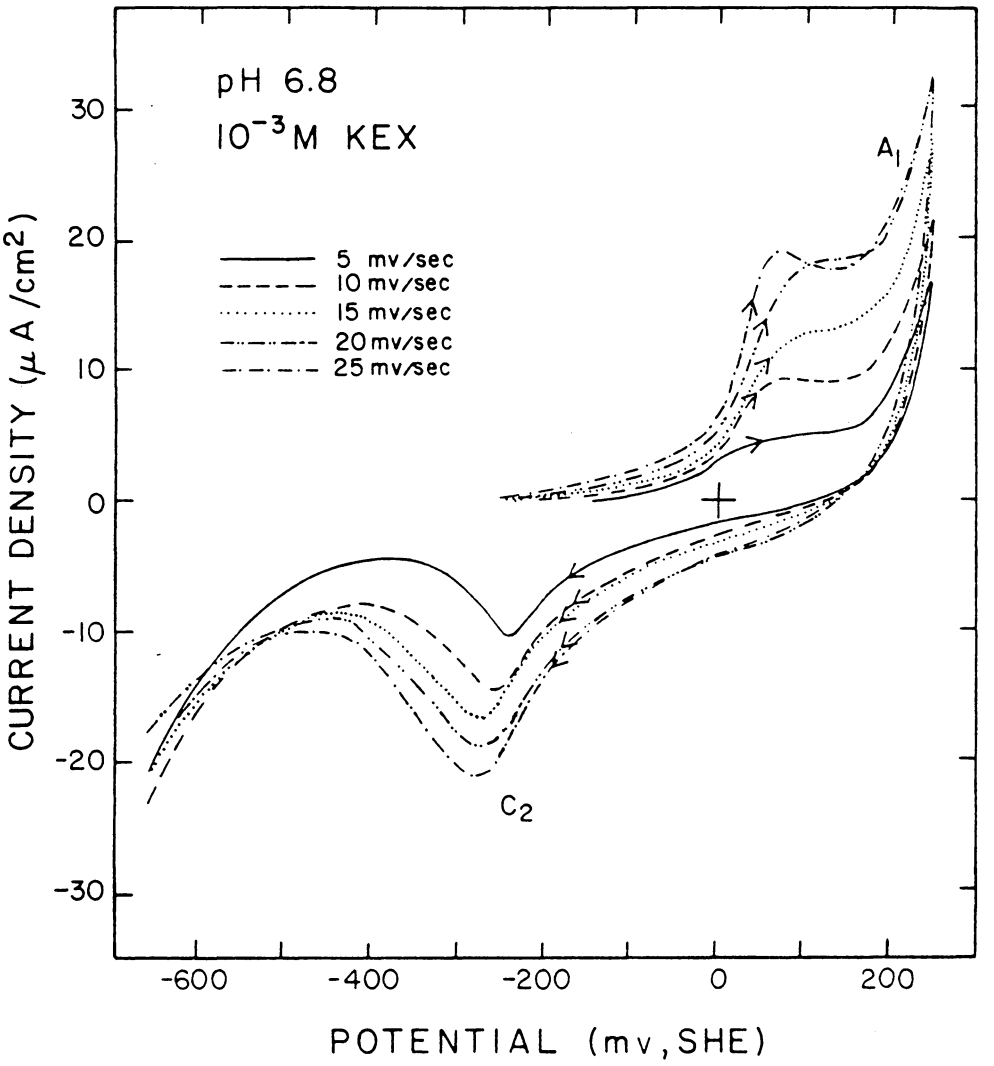


Figure 3.40 Effect of scan rate on the single sweep voltammograms for a galena electrode immersed in a 0.05 M KH_2PO_4/ 0.05 M Na_2HPO_4 (pH 6.8) + 10^{-3} M KEX solution. Scan rate varied from 5 to 25 mv/sec. No stirring.

$A_1 = PbS,X^-/PbX_2,S^o$ $\qquad$ $C_2 = PbX_2,S^o/PbS,X^-$

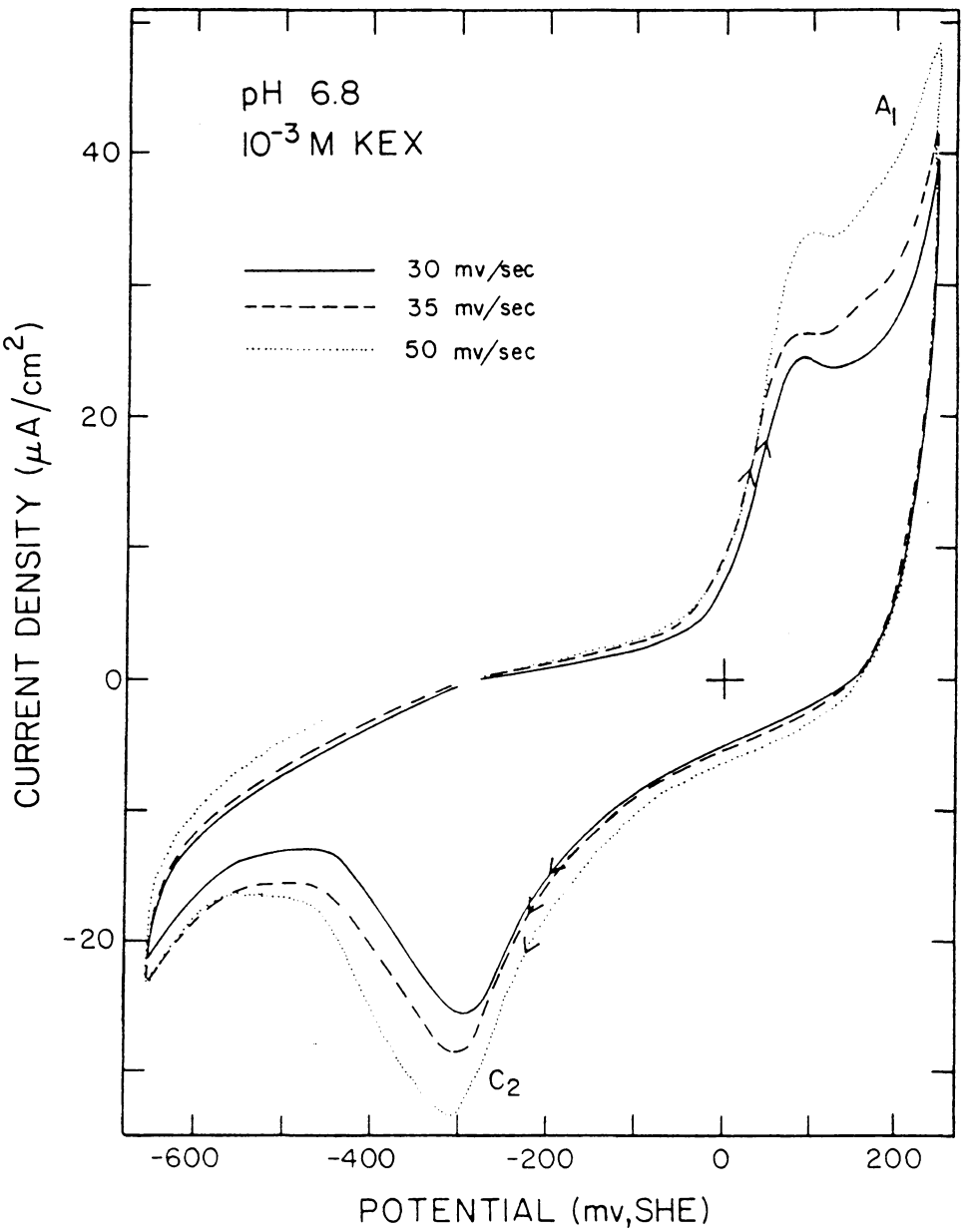


Figure 3.41 Effect of scan rate on the single sweep voltammograms for a galena electrode immersed in a 0.05 M KH_2PO_4/ 0.05 M Na_2HPO_4 (pH 6.8) + 10^{-3} M KEX. Scan rate varied from 30 to 50 mv/sec. No stirring.

$A_1 = PbS,X^-/PbX_2,S^o$ $C_2 = PbX_2,S^o/PbS,X^-$

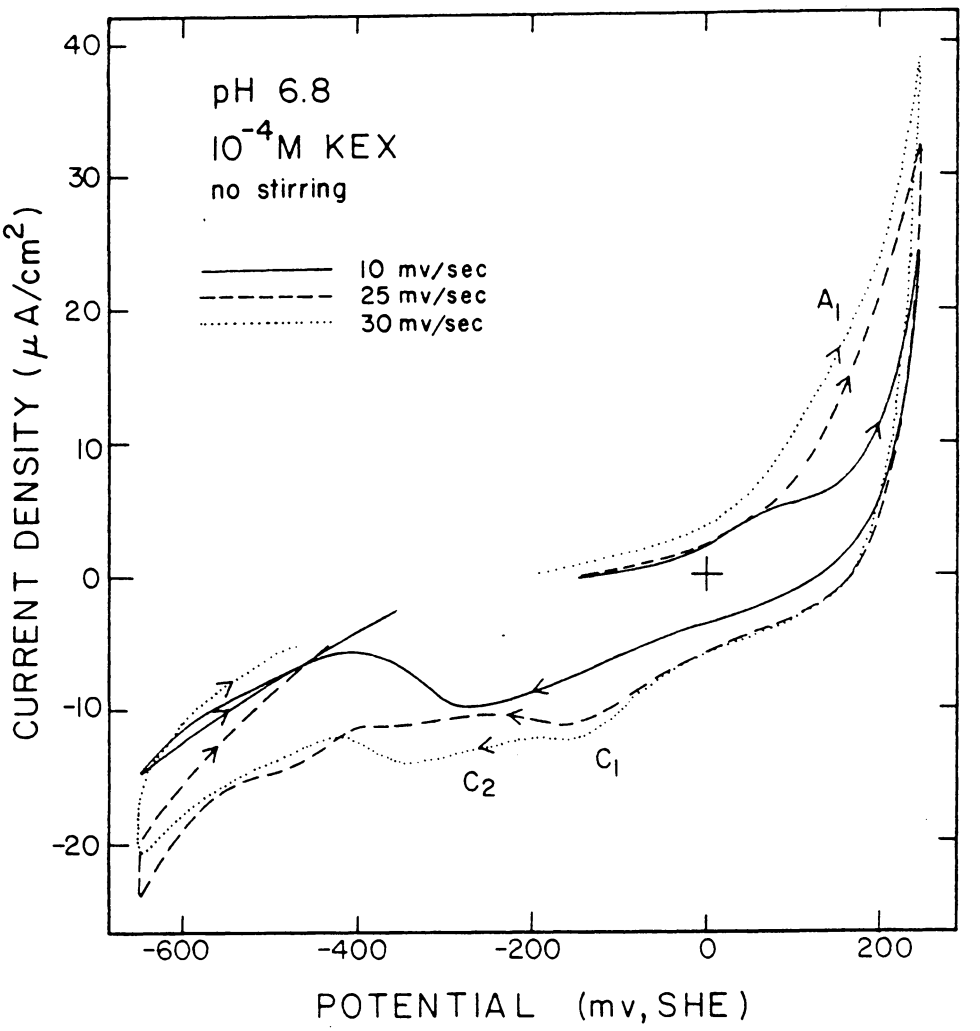


Figure 3.42 Effect of scan rate on the single sweep voltammograms for a galena electrode immersed in a 0.05 M KH_2PO_4/ 0.05 M Na_2HPO_4 (pH 6.8) + 10^{-4} M KEX. No stirring.

10 mv/sec: $A_1 = PbS,X^-/PbX_2,S^o$

25, 30 mv/sec: $A_1 = PbS,X^-/PbX_2,S^o + PbS/PbO,S^o$

$C_1 = PbO,S^o/PbS$

$C_2 = PbX_2,S^o/PbS,X^-$

different scan speeds (Table 3.11) yields results almost identical to what has been found at pH 9.2 (Table 3.6) as long as the scan speed does not exceed 25 mv/sec. Since only C_2 (see Figure 3.39) is observed on the cathodic portion of the curves, xanthate adsorption is presumably the sole process going on during oxidation. What is likely happening is that xanthate chemisorbs by reaction [3.2] until a monolayer is complete and then adsorbs in multilayers to form PbX_2 and S^o (reaction [3.3]).

Scanning the potential at a rate faster than 25 mv/sec causes a significant drop in the charge density associated with the pre-wave. Even so, only xanthate adsorption appears to be occurring since the C_1 peak is not observed. The chemisorption step (reaction [3.2]) evidently is not fast enough to keep up with the sweep rate and, consequently, a potential is reached where PbX_2 can begin to form on top of chemisorbed xanthate before a monolayer of it has formed.

Whereas the scan rate does not seem to affect what reactions are occurring when 10^{-3} M KEX is present, the same is not true at the lower collector level (Figure 3.42). The pre-wave is very distinct and C_2 appears to be the principal cathodic reaction when the potential is scanned at a speed of 10 mv/sec. However, increasing the ramp speed causes the pre-wave to disappear and C_1 to grow in size relative to C_2. Such behavior is to be expected if both xanthate is being adsorbed and galena itself is being oxidized. What seems to be occurring at 10 mv/sec is very similar to what takes place in the presence of 10^{-3} M KEX at scan speeds above 25 mv/sec. PbX_2 begins to proceed after only about 27 $\mu C/cm^2$ of anodic charge (one-fourth of the amount corresponding to a

Table 3.11

Effect of Scan Rate on the Charge Density of the Anodic Pre-Wave at pH 6.8 and 10^{-3} M KEX

Scan Rate (mv/sec)	Charge Density ($\mu C/cm^2$)
5	115
10	111
15	111
20	110
25	102
30	39
35	33
50	31

complete monolayer) has been passed as a result of the chemisorption reaction.

The appearance of the C_1 peak in the current-potential curves in Figure 3.42 for scan speeds of 25 mv/sec and 30 mv/sec indicates that galena itself is also being oxidized. Evidently, xanthate adsorption does not proceed quickly enough at 10^{-4} M KEX to prevent the oxidation of galena itself from also occurring during the anodic scan.

Anodic limits up to 345 mv at 10^{-3} M KEX: Figure 3.43 shows the voltammograms obtained after sweeping the potential of the galena electrode immersed in an unstirred 10^{-3} M KEX solution to different anodic limits. The anodic current is characterized by a pre-wave up to a potential of about 150 mv, as mentioned previously, followed by a very steep rise above 250 mv.

Only the C_2 peak appears on the cathodic portion of the curves when the upper limit is less than or equal to 295 mv. Although a reliable measurement of the area under the C_2 peak is not possible for the lower two anodic limits, analysis of the third (295 mv) reveals that the charges associated with the anodic and cathodic processes balance each other. From this, it can be concluded that S^o and not $S_2O_3^{2-}$ is being generated during oxidation. This is not surprising since the previous results in Section 3.3.1e indicate that $S_2O_3^{2-}$ is not even being produced in the absence of collector at pH 6.8.

Anodic limit of 345 mv at 10^{-3} M KEX: Extending the sweep to 345 mv results in the appearance of two reduction peaks during the reverse

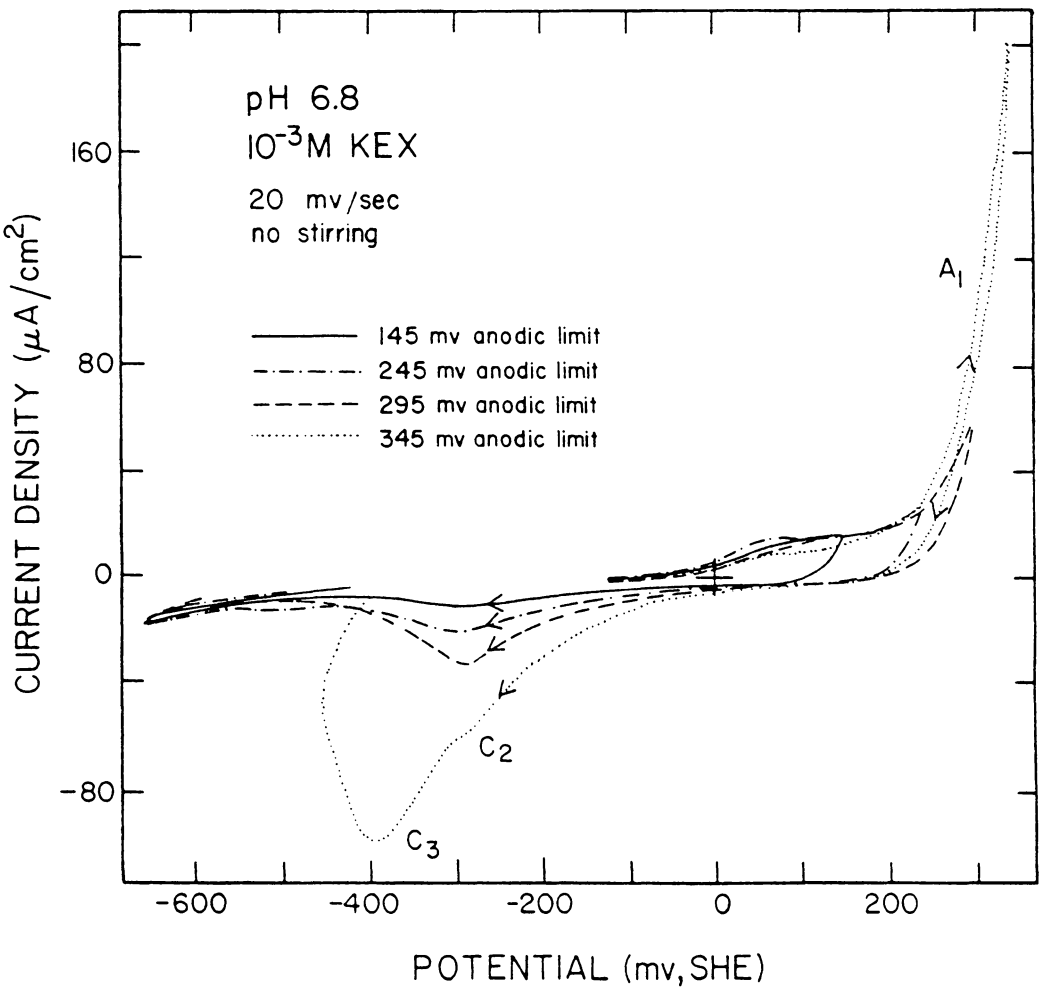


Figure 3.43 Effect of anodic limit on the single sweep voltammograms for a galena electrode immersed in a 0.05 M KH_2PO_4/0.05M Na_2HPO_4 (pH 6.8) + 10^{-3} M KEX solution. No stirring. Scan rate = 20 mv/sec.

145-295 mv: $A_1 = PbS,X^-/PbX_2,S^0$

345 mv: $A_1 = PbS,X^-/PbX_2,S^0 + PbS/PbO,S^0$

$C_2 = PbX_2,S^0/PbS,X^-$

$C_3 = S^0/HS^-$

scan - the first one at a potential close to where C_2 occurs and the second one, C_3, which is much larger, at a potential of about -400 mv. This suggests that a second anodic reaction is occurring somewhere between 295 and 345 mv. It should also be noted that even at such a high potential there is a balance between the anodic and cathodic charges.

Two possible choices for this reaction are the decomposition of the PbX_2 and the oxidation of galena itself (reaction [3.6] and/or [3.25]). It turns out that if the first alternative is considered, then the resulting possible schemes predict either that the charge ratio should be less than unity or that the C_2 peak should be as large as the C_3 peak. In view of Figure 3.43, this is hardly the case. Moreover, the upper limit of 345 mv is lower than the reversible potential for the decomposition of PbX_2 at pH 6.8. It is likely that the second anodic reaction involves the oxidation of the mineral.

One possible sequence can be as follows:

A_1 $$yPbS + 2yX^- \longrightarrow yPbX_2 + yS^o + 2ye \qquad [3.56]$$

$$zPbS + zH_2O \longrightarrow zPbO + zS^o + 2zH^+ + 2ze \qquad [3.57]$$

$$(1-y-z)PbS + (1-y-z)H_2O \longrightarrow (1-y-z)PbOH^+ + (1-y-z)S^o + (1-y-z)H^+ + 2(1-y-z)e \qquad [3.58]$$

C_2 $$yPbX_2 + yS^o + 2ye \longrightarrow yPbS + 2yX^- \qquad [3.59]$$

C_3 $$(1-y)S^o + (1-y)H^+ + 2(1-y)e \longrightarrow (1-y)HS^-, \quad [3.60]$$

$$(Q_{C2} + Q_{C3})/Q_{A1} = 1. \quad [3.61]$$

It can be seen that the charge ratio is always equal to the observed value of unity regardless of what y and z are.

The occurrence of this sequence for an anodic limit of 345 mv indicates that the simultaneous adsorption of xanthate and the oxidation of galena begins at a lower potential than is the case at pH 9.2.

Anodic limits up to 245 mv at 10^{-4} M KEX: The effect of varying the anodic limit was also studied for the electrode immersed in a 10^{-4} M KEX solution. Figure 3.44 presents the resulting curves for upper limits of 145 and 245 mv.

When the potential is increased only as far as 145 mv, only a small peak corresponding to C_2 is visible. This indicates that the principal oxidation process is likely the chemisorption of xanthate (reaction [3.2]) with a small contribution from the formation of PbX_2 via reaction [3.3].

At some potential beyond 145 mv, galena itself also begins to be oxidized since the C_1 is quite evident in the voltammogram for the 245 anodic limit. As mentioned previously, this peak has already been attributed to recombination of lead oxide and S^o (reaction [3.14]) on the basis of the work done in the absence of collector (Section 3.3.1e). The reaction sequence for the galena-xanthate system, at least up to 245 mv, at a collector concentration of 10^{-4} M can, thus, be written as:

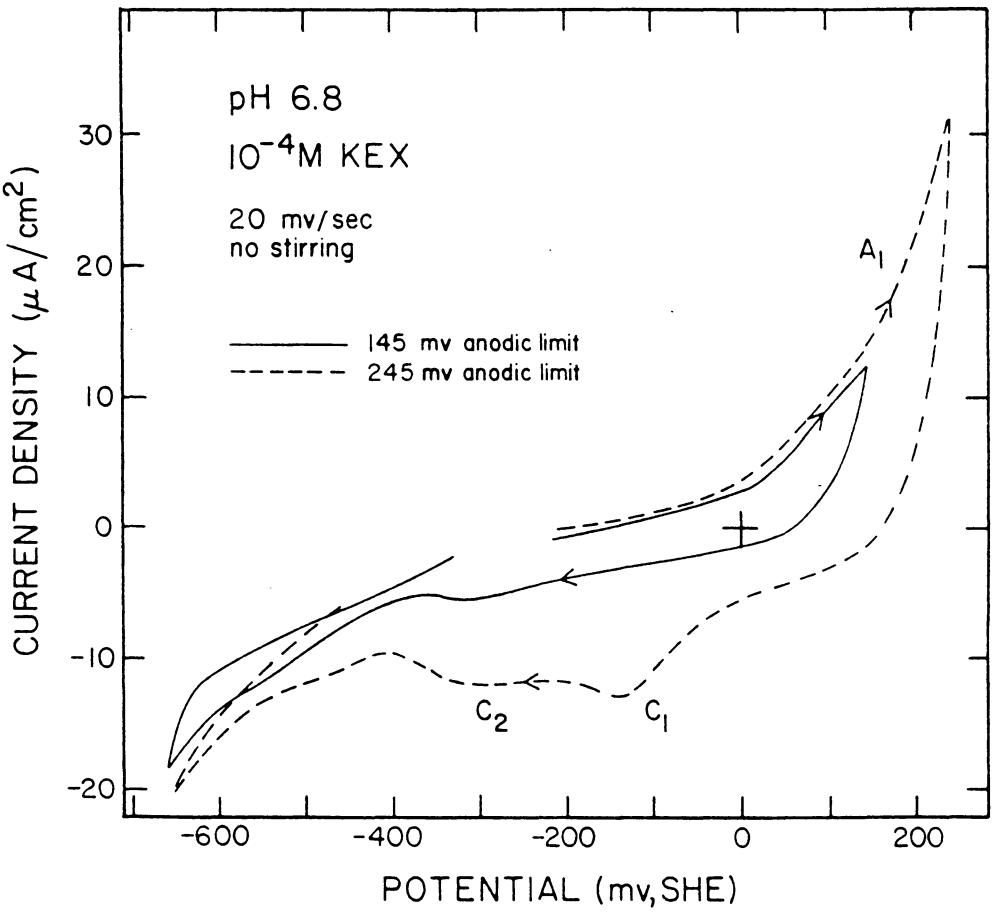


Figure 3.44 Effect of anodic limit on the single sweep voltammograms for a galena electrode immersed in a 0.05 M KH_2PO_4/0.05 M Na_2HPO_4 (pH 6.8) + 10^{-4} M KEX solution. No stirring. Scan rate = 20 mv/sec.

145 mv: $A_1 = X^-/X_{ads}$

245 mv: $A_1 = PbS,X^-/PbX_2,S^o + PbS/PbO,S^o$

$C_1 = PbO,S^o/PbS$

$C_2 = PbX_2,S^o/PbS,X^-$

A_1 $yPbS + 2yX^- \longrightarrow yPbX_2 + yS^o + 2ye$ [3.56]

$(1-y)PbS + (1-y)H_2O \longrightarrow (1-y)PbO + (1-y)S^o$

$+ 2(1-y)H^+ + 2(1-y)e$ [3.62]

C_1 $(1-y)PbO + (1-y)S^o + 2(1-y)H^+ + 2(1-y)e \longrightarrow$

$(1-y)PbS + (1-y)H_2O$ [3.63]

C_2 $yPbX_2 + yS^o + 2ye \longrightarrow yPbS + 2yX^-$ [3.59]

(It was previously concluded that bulk lead oxide does not form until a potential of 345 mv is reached. The species 'PbO' appears in the C_1 reaction of this sequence more as a simplification than to imply that a bulk species is being produced.) It should be noted that the system is showing essentially the same behavior whether 10^{-4} or 10^{-3} M KEX has been added. The difference in the reaction sequences for the two cases arises because of the effect of xanthate in retarding the oxidation of the mineral. At the lower concentration, the formation of PbO and S^o by reaction [3.6] begins to proceed at much the same potentials as in the absence of collector. Since $PbOH^+$ was shown previously not to appear until a potential of 345 mv is reached, the first reduction reaction expected to occur on the cathodic scan should be the recombination of PbO and S^o (reaction [3.14]).

Increasing the xanthate concentration to 10^{-3} M raises the potential at which reaction [3.6] can occur to somewhere between 295 and 345 mv. As has already been shown in Section 3.3.1e, this is

precisely where $PbOH^+$ rapidly takes over from PbO as an oxidation product. Therefore, it is not surprising that C_3 (reduction of S^o to HS^-) rather than C_1 (reduction of PbO and S^o to PbS) is the cathodic reaction to be observed once reaction [3.6] begins in the presence of 10^{-3} M KEX.

e. IGP experiments at pH 6.8: In Figure 3.45, a comparison is made between the IGP diagrams obtained in unstirred solutions containing 0 and 10^{-3} M KEX by applying current pulses of 0.1 mA/cm^2 to the galena electrode. The most important effect xanthate seems to have is in the portion during which the mineral is being polarized cathodically. In the absence of collector, the maximum and minimum potentials along the plateau remain essentially constant. When xanthate has been added, they continually decrease with time, thereby resulting in a plateau that slopes downward. It should be pointed out that since the maximum potential reached by the electrode during oxidation in Figure 3.45b is about 330 mv, one would expect reaction [3.3] to be the principal anodic process. Therefore, the downward-sloping plateau may be characteristic of the desorption of PbX_2. The presence of a heterogeneous PbX_2 layer on the surface may cause the open-circuit potential to steadily drop along the plateau.

In the next series of experiments, 0.2 mA/cm^2 pulses were applied to the mineral in a 10^{-3} M KEX solution. The IGP diagrams obtained in stirred solution after 3 and 6 minutes of anodic polarization are shown in Figures 3.46a and 3.46b. After 3 minutes of oxidation, the closed-circuit potential of the electrode reaches about 360 mv, and so the

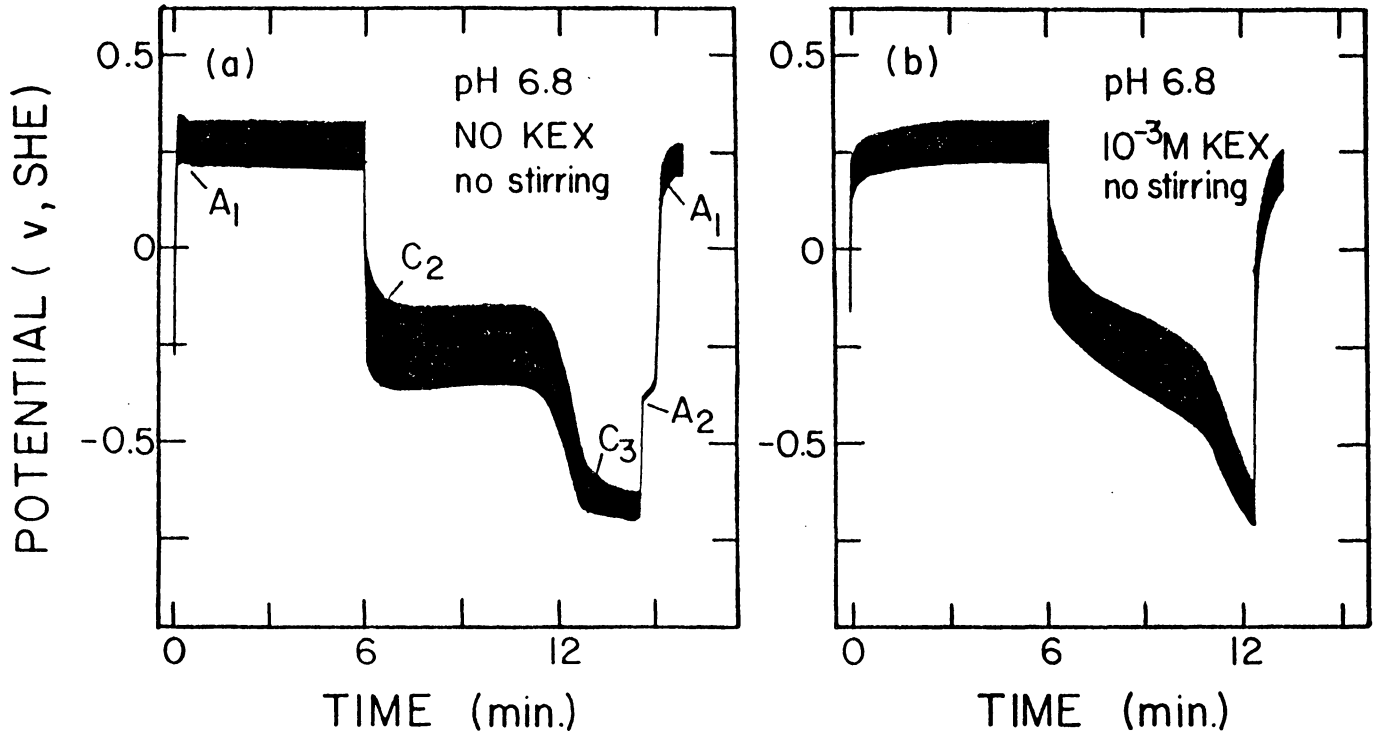


Figure 3.45 IGP diagrams obtained after applying current pulses of 0.1 mA/cm^2 to a galena electrode immersed in an unstirred solution containing 0.05 M KH_2PO_4/0.05 M Na_2HPO_4 (pH 6.8) + 0 (a) and 10^{-3} (b) M KEX.

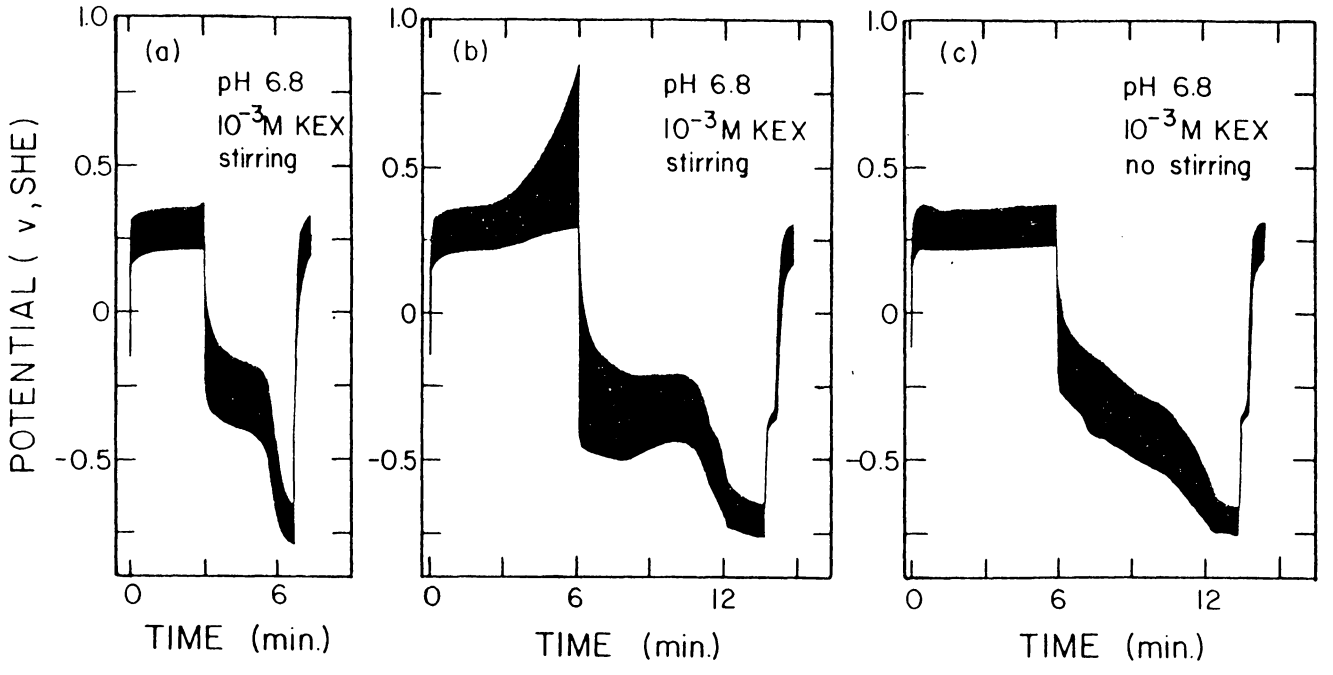


Figure 3.46 IGP diagrams obtained after applying current pulses of 0.2 mA/cm^2 to a galena electrode immersed in a solution containing 0.05 M KH_2PO_4/0.05 M Na_2HPO_4 (pH 6.8) + 10^{-3} M KEX. Anodic pulses applied initially for:
(a) 3 minutes while stirred;
(b) 6 minutes while stirred; and
(c) 6 minutes while unstirred
before current reversal.

formation of PbX_2 and S^o (reaction [3.3]) should still be predominant. This is supported by the observation that the plateau formed during the subsequent cathodic polarization slopes downward and appears different from the one obtained in the absence of collector (see Figure 3.26).

When the galena is anodically polarized for 6 minutes (Figure 3.46b), the potential begins to rise sharply in a manner similar to what has been observed when no xanthate has been added (see Figure 3.27). The arrest that results when the polarity of the pulses is reversed has also become closer in appearance to the one obtained in the absence of xanthate than the one obtained with 0.1 mA/cm^2 pulses at 10^{-3} M KEX (Figure 3.45b). The dominance of the 'xanthate-free' nature of the diagram is not that surprising since the potential of 850 mv reached by the mineral during oxidation is sufficient for any PbX_2 to have decomposed.

Comparison of the IGP diagram obtained at 0.2 mA/cm^2 current density in a stirred solution (Figure 3.46b) with the corresponding one in a quiescent solution (Figure 3.46c) shows that agitation has a significant effect. The maximum potential reached by the electrode during 6 minutes of anodic polarization remains constant at about 350 mv if the solution is stagnant. Consequently, one would expect xanthate adsorption to be the primary anodic reaction. This is supported by the fact that the portion of the diagram generated after the current polarity is reversed cathodically has the appearance characteristic of xanthate desorption (Figure 3.45b).

Apparently, stirring promotes the oxidation of galena at the expense of PbX_2 formation. This indicates that the former is probably more strongly controlled by mass transport than the latter. Such behavior is not surprising when it is considered that galena oxidation involves the transfer of hydroxyl ions, which have a bulk concentration of only ~ 10^{-7} M at this pH, to the mineral surface. On the other hand, the bulk xanthate concentration of 10^{-3} M is quite high so that it is not likely that the diffusion layer would become depleted of the collector.

f. Chronoamperometry experiments at 10^{-3} M KEX and at pH 6.8 and 9.2: In order to learn more about the dynamic aspects of xanthate adsorption, chronoamperometry experiments were also conducted on the mineral in the presence of 10^{-3} M KEX at pH 6.8 and 9.2 (Figures 3.47 and 3.48). Comparison of the results in the two cases shows that the electrode responses are quite similar as long as the applied potential is not above 245 mv. Above this level, the currents become larger at pH 6.8. It should be recalled that a similar trend is observed in the absence of collector (Figures 3.17 and 3.29).

Xanthate seems to have a different effect on the current for a potential of 345 mv depending on the pH. The collector tends to significantly lower the current at the lower pH, whereas it causes a small increase at pH 9.2. The decrease in current at pH 6.8 is probably due to the fact that insoluble products (i.e., S^o, PbX_2) that tend to passivate the surface are formed during the oxidation. In the absence of collector, $PbOH^+$ is being produced and, consequently, passivation

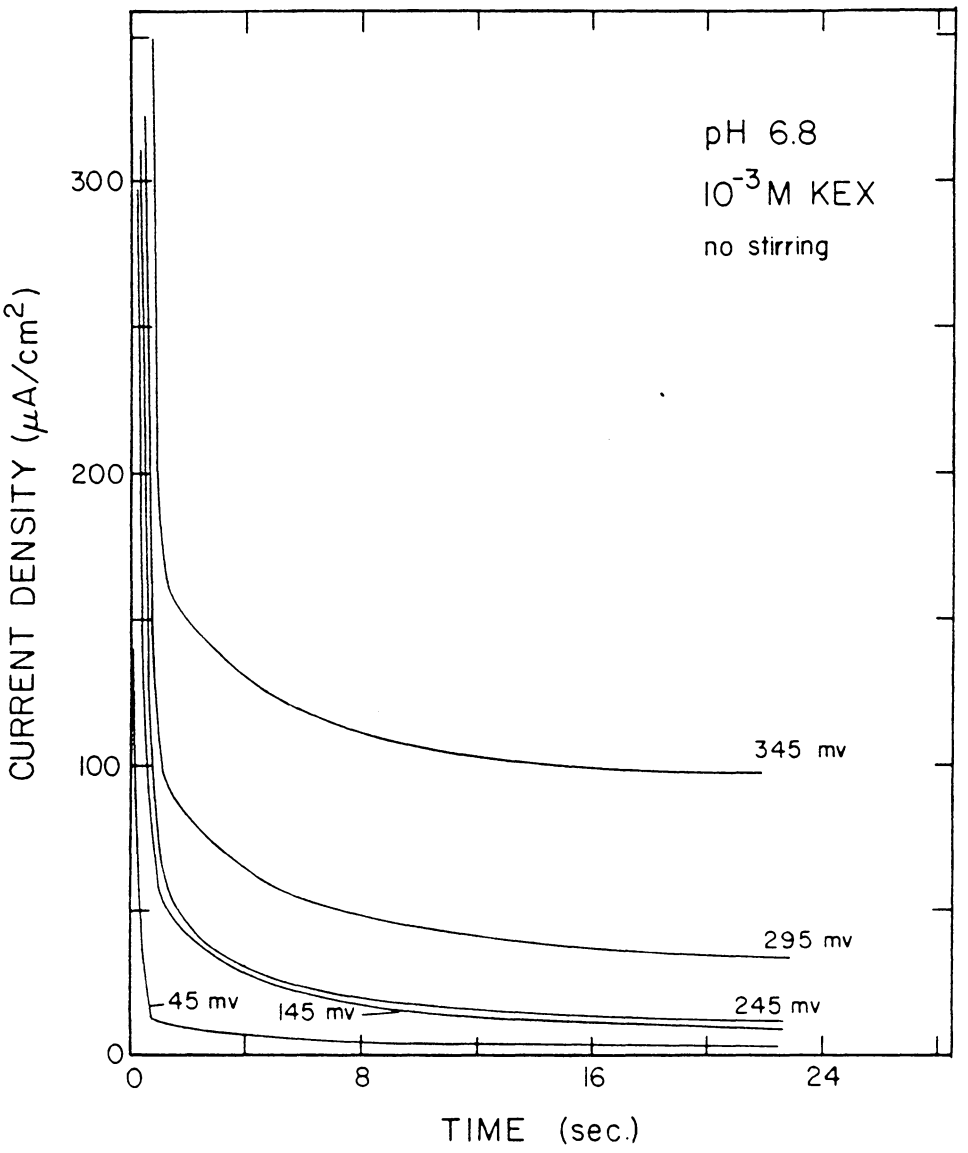


Figure 3.47 Current-time curves obtained after applying potentials of 45, 145, 245, 295 and 345 mv to a galena electrode immersed in a 0.05 M KH_2PO_4/0.05 M Na_2HPO_4 (pH 6.8) + 10^{-3} M KEX solution. No stirring.

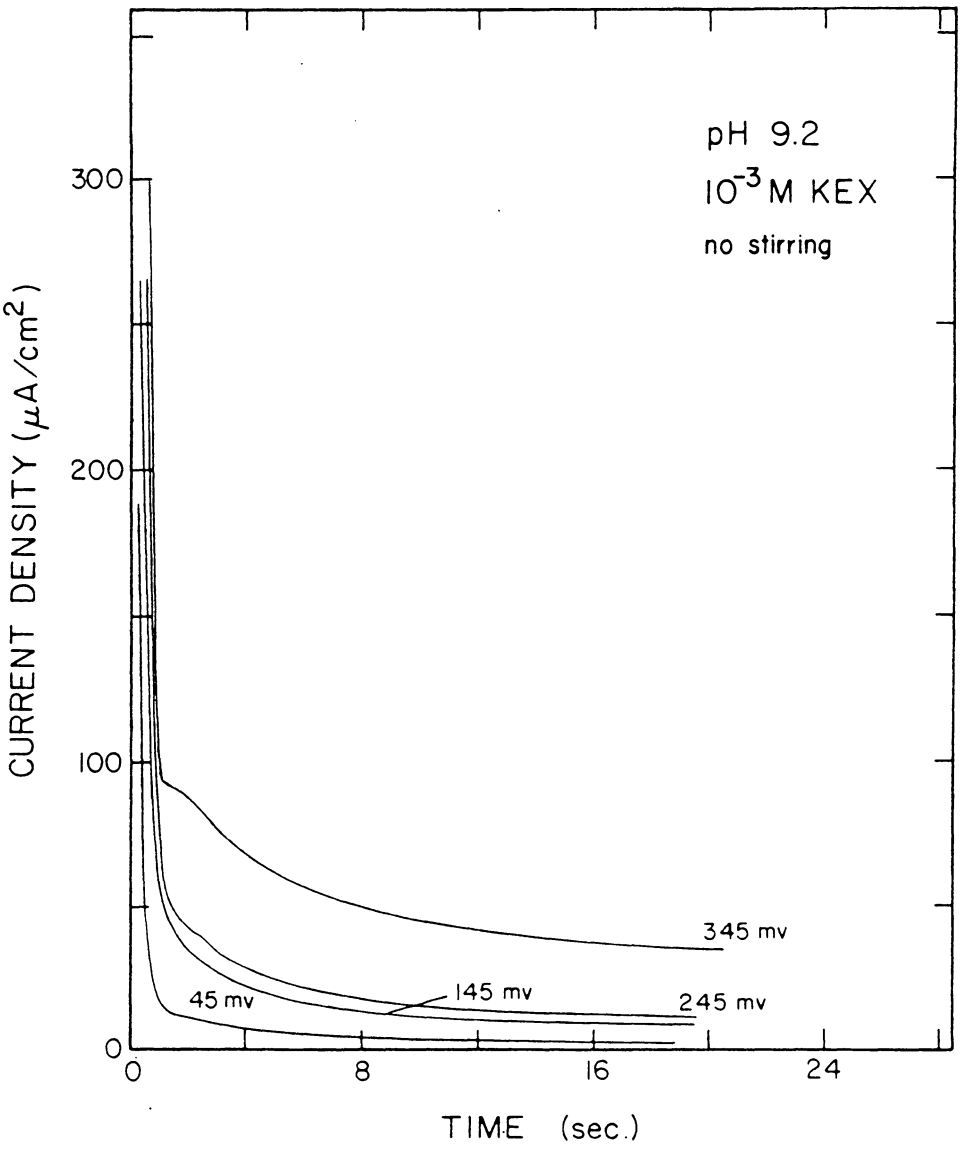


Figure 3.48 Current-time curves obtained after applying potentials of 45, 145, 245 and 345 mv to a galena electrode immersed in a 0.05 M $Na_2B_4O_7$ (pH 9.2) + 10^{-3} M KEX solution. No stirring.

should not be as severe.

g. Microflotation tests at pH 9.2: The effect of the redox potential on the recovery of galena obtained from the microflotation tests done in the absence of KEX is shown in Figure 3.49. The results indicate that the sample exhibits some natural floatability, particularly at a potential of about -60 mv, where about 50% recovery is achieved.

Comparison of these results with the voltammograms in Figures 3.8 and 3.9 indicates that this flotation behavior may be related to the different stages of oxidation that galena undergoes. The region of maximum floatability at -60 mv coincides with where anodic current in the voltammograms first begins to rise. As discussed previously (Section 3.3.1a), the initial oxidation of galena will result in the weakening of Pb—S bonds and the strengthening of S—S and Pb—O bonds. As oxidation continues, regions in the surface structure will become more and more similar to hydrophobic S^o and to hydrophilic PbO. The combination of these opposing tendencies may impart a certain degree of floatability to the mineral.

However, one would expect the oxide-like portions to be oriented more toward the solution than the sulfur-like portions. Consequently, one would expect the hydrophobicity of the surface to decrease as the potential increases above -60 mv. Once bulk PbO and S^o nucleate at a potential of about 300 mv, the oxide so dominates the surface region that no flotation will be possible. The flotation recoveries in Figure

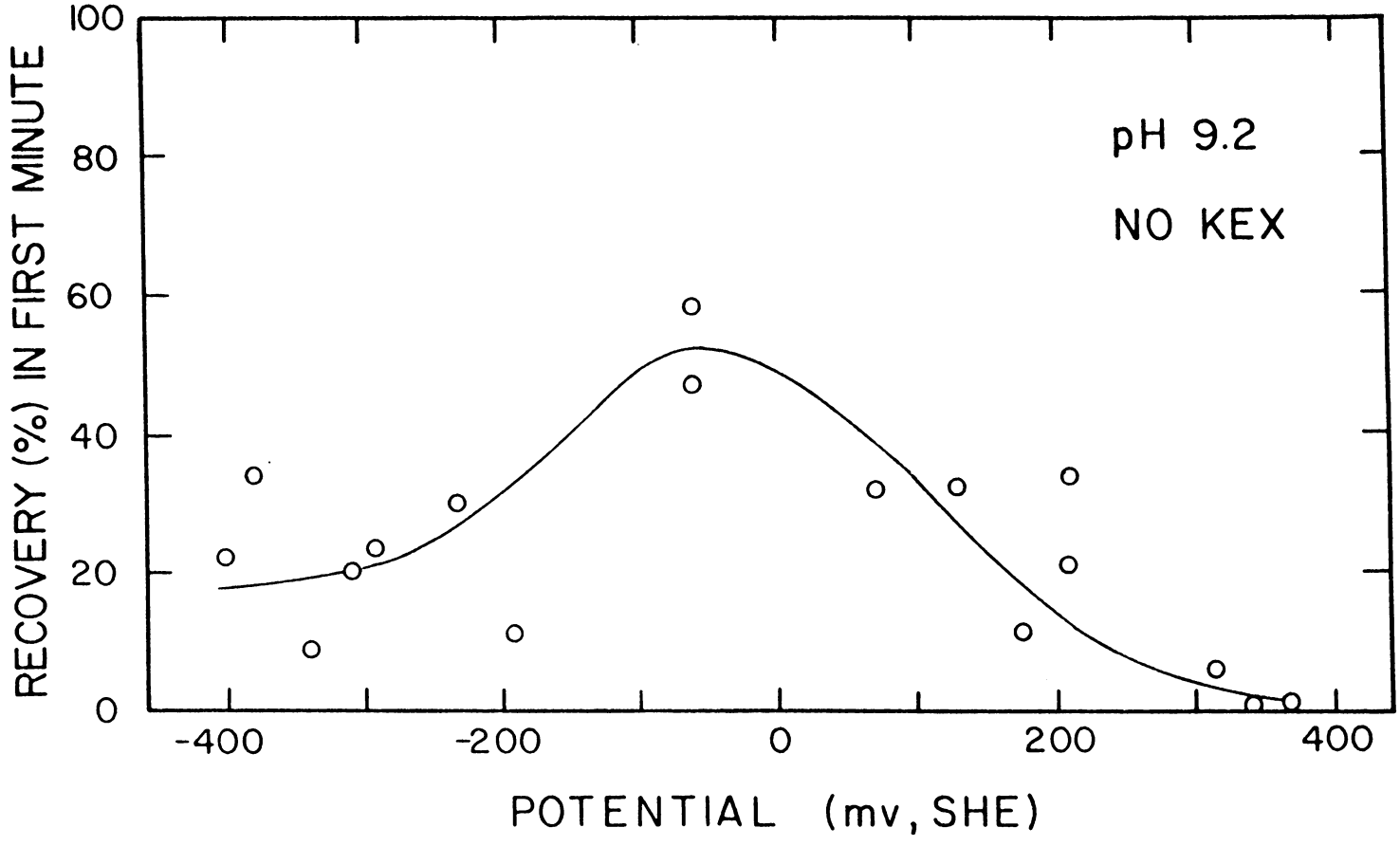


Figure 3.49 Effect of E_h on the galena recovery obtained after 1 minute of microflotation in a 0.05 M $Na_2B_4O_7$ solution (pH 9.2).

3.49 follow this trend. This explanation is further strengthened by the XPS spectra of Evans and Raftery (1982) and Hamilton and Woods (1984), which show that the oxidation products segregate into PbO at the outermost surface and S^o beneath.

The results of the microflotation tests done at 10^{-5} M KEX are presented in Figure 3.50, along with the values of % PbX_2 from the computer calculations of Chapter II. The flotation recovery is almost 100% at potentials between -300 and 200 mv, but then quickly drops as the potential is varied beyond this range.

There is good agreement between the calculated upper potential limits for PbX_2 stability and the potential where flotation begins to be suppressed. This provides strong support that the drop in recovery is due to the anodic decomposition of PbX_2. Furthermore, the upper limit can be predicted by thermodynamics. It should be recalled that a similar conclusion was previously reached from a comparison between flotation data of Guy and Trahar (1984) at pH 8.0 and the thermodynamic calculations (see Section 2.4.4a).

Under reducing conditions, on the other hand, the agreement between the thermodynamic predictions and the experimental data is not nearly as good. Flotation is observed at a potential about 200 mv less than the lower limit based on the calculations for Case II.

This discrepancy may be related to the manner in which the experiments were carried out and the kinetics of xanthate desorption. The procedure followed in these experiments was to add the galena particles to a deoxygenated xanthate solution <u>prior</u> to adding hydrazine.

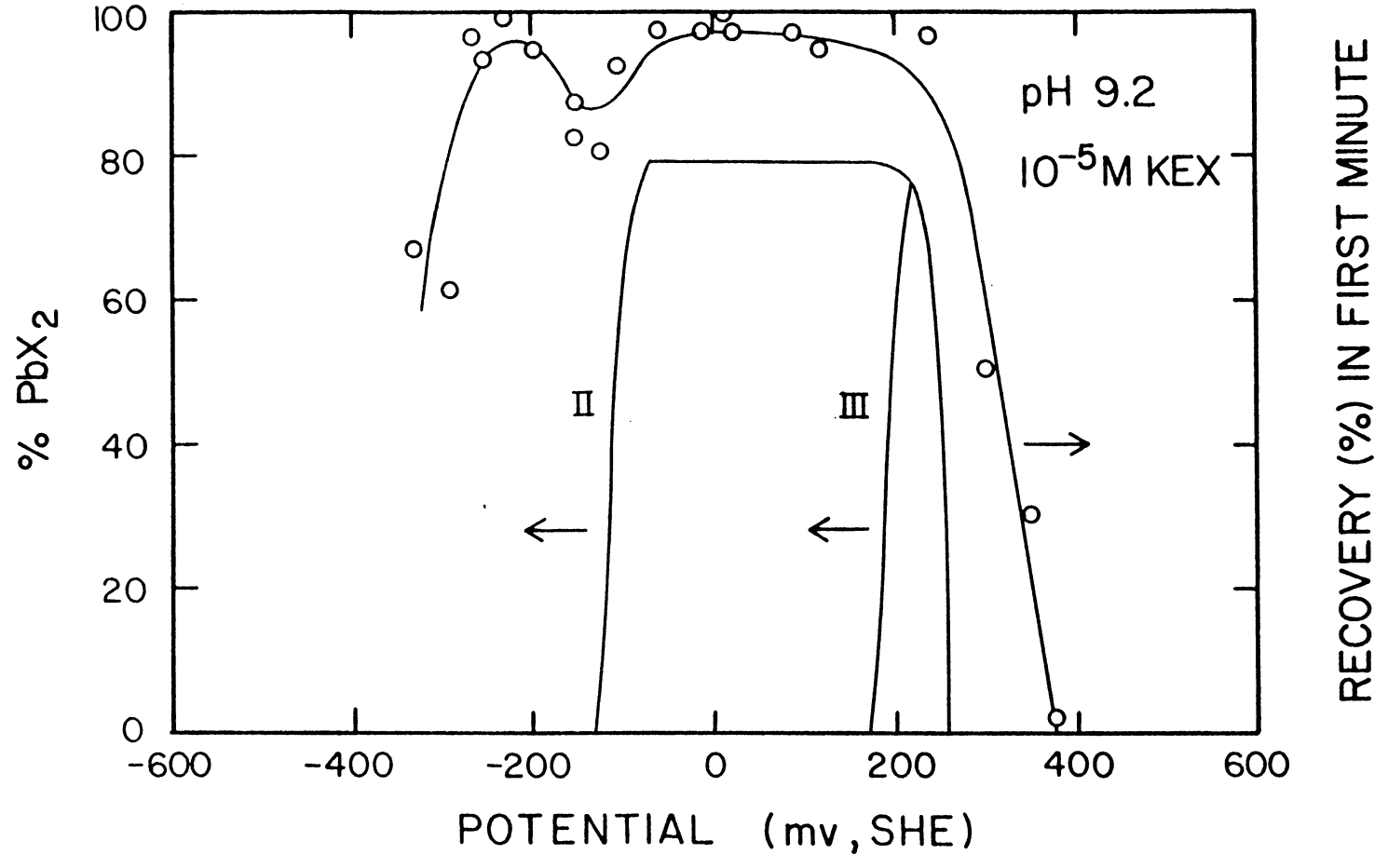


Figure 3.50 Comparison of the effect of E_h on the microflotation recovery of galena (—o—) and on the calculated % PbX_2 (—) at a collector addition of 10-5 M KEX and pH 9.2. The Roman numeral next to each curve for % PbX_2 denotes the case number.

When the mineral and collector first came into contact, the redox potential typically had a value of 240 mv. On the basis of the voltammograms in Figure 3.35, xanthate should have immediately adsorbed onto the galena. The subsequent addition of hydrazine dropped the potential and brought about the removal of some of the adsorbed xanthate. Obviously, one would expect flotation to no longer be possible when the potential was lowered sufficiently to desorb all the collector. Previously, the C_1 peak in Figure 3.35 was attributed to the removal of adsorbed xanthate by the reaction,

$$PbX_2 + S^o + 2e \longrightarrow PbS + 2X^-. \qquad [3.64]$$

It appears from this figure that when the potential falls to somewhere between -350 and -400 mv, all the xanthate will have been desorbed. This is precisely the potential where the galena recovery in Figure 3.50 is observed to decline.

The discrepancy between the calculated and observed lower limits is therefore related to hysteresis between xanthate adsorption and desorption. Since it becomes energetically more difficult to desorb xanthate than it is to adsorb it, the lower limit that is observed is more cathodic than the value predicted by equilibrium thermodynamics.

3.4 Summary

The voltammetry and IGP experiments indicate that the principal oxidation products of galena at pH 9.2 in the absence of xanthate are PbO, S^o and $S_2O_3^{2-}$. The formation of thiosulfate becomes more and more

favored over that of elemental sulfur as the potential and the time of oxidation are increased. It has also been found that some PbO, which should not be present at this pH on the basis of thermodynamics, dissolves off the surface, particularly in a stirred solution.

At pH 6.8, the data suggest that galena oxidation begins with the formation of a metal deficient sulfide, as has been observed by others at pH 9.2. An insoluble lead oxide, a few monolayers thick, builds up until a potential of about 345 mv is reached. At this point, bulk lead oxide forms and then immediately dissolves. Oxidation is restricted to the formation of sulfur at this pH, and no evidence for the formation of $S_2O_3^{2-}$ or SO_4^{2-} has been detected.

The initial monolayer of xanthate adsorbs via a one-electron transfer chemisorption step. Xanthate adsorbing onto this first layer does so in the form of PbX_2. At collector concentrations of 10^{-3} M KEX and lower scan speeds, the chemisorbed monolayer is completed before PbX_2 begins to form. However, when the concentration is lower and the sweep rate is faster, PbX_2 is observed before xanthate has completely covered the initial monolayer.

The experiments conducted in the presence of KEX also suggest that xanthate adsorption and galena oxidation are competitive reactions. At 10^{-3} M KEX and pH 9.2, PbX_2 and S^o are the only oxidation products until PbX_2 decomposes at a potential near 445 mv. Charge analysis of the voltammograms indicates that $S_2O_3^{2-}$ begins to form only when the anodic limit extends beyond 495 mv, whereas it is present at potentials as low as 195 mv in the absence of collector. When the xanthate addition is

decreased to 10^{-4} M, there is apparently not enough xanthate to suppress the further oxidation of sulfur, and consequently $S_2O_3^{2-}$ is produced along with PbX_2 and S^o.

Decreasing the pH to 6.8 has a similar effect as dropping the xanthate concentration in that it makes galena oxidation more competitive with collector adsorption. Although PbX_2 and S^o are the first products formed at a collector level of 10^{-3} M KEX, PbO (and $PbOH^+$) begins to appear when the potential reaches about 300 mv. At 10^{-4} M KEX, the potential at which the oxide begins to form is lowered to somewhere between 145 and 245 mv.

Microflotation tests conducted on a ground sample in a borate solution indicate that the galena exhibits some natural floatability under moderately oxidizing conditions. This may be attributed to the formation of a metal-deficient sulfide on the mineral surface during the initial stages of oxidation. In the presence of 10^{-5} M KEX, almost complete flotation is possible between -300 and 200 mv. Suppression of flotation under highly oxidizing conditions can be predicted from thermodynamics to be due to the anodic decomposition of PbX_2. The lower potential limit for flotation was likely determined by the desorption of PbX_2 and could not be accurately predicted by the thermodynamic calculations.

CHAPTER IV.

ELECTROCHEMICAL STUDIES OF GALENA AT pH 1.1 AND 4.6

4.1 Introduction

4.1.1 General

Partly because of the wide interest in the flotation of galena, more research has been reported concerning the chemistry of the $PbS-H_2O$ system in alkaline solutions than in acidic solutions. Another reason for this is that, unlike most other base metals, lead is commercially produced by an entirely pyrometallurgical process and, consequently, there has not been the same impetus to study the solution chemistry of galena as there has been for some other sulfides.

The present practice of extracting lead from the galena flotation concentrate involves air roasting the sulfide to an oxide sinter, followed by reduction to the metal in a blast furnace. There are major difficulties associated with this approach. Firstly, it is not very effective in treating low-grade or complex ores. Secondly, the roasting step releases large quantities of sulfur dioxide which must be removed from the gas stream before it is discharged to the atmosphere. The usual way this second problem is handled is to design high stacks and closed-loop circuits in the roasting operations and to produce sulfuric acid from the SO_2.

It is generally believed that the most desirable way of dealing with both of these problems would be to eliminate the roasting step

altogether. Therefore, efforts have been made to devise alternative processes utilizing hydrometallurgical or electrometallurgical techniques (Forward and Warren, 1960; Ito et al., 1961; Brodie, 1969; Bratt and Pickering, 1970; Skewes, 1972; Queneau and Schuhmann, 1974; Moriss and Fernandez, 1974). None of these methods have been able to supplant the conventional process, however, partly because many of the fundamental aspects of galena chemistry in an acidic environment are not completely understood. This has spurred hydrometallurgists to conduct further research in this area.

The conditions found when a mineral is immersed in an acidic solution may be conducive to the system reaching thermodynamic equilibrium since reaction rates and solubilities tend to be high. It would, thus, be very interesting to compare some of the predictions based on the calculations of Chapter II to the results of electrochemical experiments conducted on the galena electrode in an acidic environment.

Accordingly, a detailed study of the galena-water system has been undertaken at pH 1.1 and 4.6, using several electrochemical techniques. The methods chosen for this study include chronoamperometry, linear sweep voltammetry and intermittent galvanostatic polarization. These techniques have been described in the previous chapter (Section 3.1). An additional set of experiments has also been conducted to determine the relationship between the open-circuit potential of the galena electrode and the dissolution of the mineral. This data will also be compared to the results of the thermodynamic calculations.

4.1.2 Literature Review

Most of the electrochemical studies have dealt with the anodic dissolution of galena, in part to determine whether direct leaching of the flotation concentrate is a feasible process. The most favored oxidation reaction on the basis of thermodynamics is:

$$PbS + 4H_2O \longrightarrow PbSO_4 + 8H^+ + 8e. \qquad [4.1]$$

Yet, the conclusion from virtually all of the reported work (Brodie, 1969; Eadington and Prosser, 1969; Skewes, 1972; Paul et al., 1978; Johnson et al., 1978; Gardner and Woods, 1979b; Lamache et al., 1981) is that the reaction actually observed at acidic pH is:

$$PbS \longrightarrow Pb^{2+} + S^o + 2e. \qquad [4.2]$$

Furthermore, the data indicate that $PbSO_4$ only begins to form when the potential is raised at least 700 mv above the reversible potential for reaction [4.1]. This is fortunate from the standpoint of leaching since it is desirable to generate a soluble product.

Paul et al. (1978) went further in their study of the dissolution of galena and found that the reaction mechanism that best fit their experimental data involved two single electron-transfer steps:

$$PbS \underset{k-1}{\overset{k_1}{\rightleftharpoons}} Pb^{2+} + S^- + e \qquad [4.3]$$

$$S^- \xrightarrow{k_2} S^o + e, \qquad [4.4]$$

where S^- is a sulfur intermediate. They determined that the oxidation

of this intermediate to elemental sulfur was rate-controlling.

Since galena is a semiconductor, there has also been a considerable amount of interest in examining the effect of point defects on the reactivity of the mineral. Lead sulfide has a structure which can contain cation vacancies and cation interstitials in the crystal lattice, as well as electronic defects. Consequently, it may behave either as an n-type (conduction by movements of electrons) or a p-type (conduction by movement of holes) semiconductor, depending on the stoichiometry and impurity content.

The earliest reported study of this kind was conducted by Simkovich and Wagner (1963), who investigated the kinetics of the dissolution of synthetic PbS as a function of the lead/sulfur stoichiometry and the amount of the doping addition of Ag_2S and Bi_2S_3. When galena was immersed in concentrated nitric acid, the leaching rate was very sensitive to the defect structure of the sulfide and increased with a rise in its p-type character. However, similar experiments in hydrochloric acid showed that there was much less difference between the dissolution rates of the doped and undoped crystals.

This difference in behavior is related to the fact that the leaching mechanism in the presence of one acid is not the same as in the other. In nitric acid solutions, dissolution involves the transfer of electrons via reaction [4.2] since HNO_3 is also an oxidizing agent. Hydrochloric acid, on the other hand, is not oxidizing, so lead sulfide is leached by the chemical reaction,

$$PbS + 2H^+ \longrightarrow Pb^{2+} + H_2S. \qquad [4.5]$$

This result is significant because it shows that the semiconducting properties can affect a reaction on the solution side of the solid/liquid interface when it involves the transfer of electrons.

Further research by others has led to some confusion concerning whether dissolution is faster for n-type or p-type PbS. Although Eadington and Prosser (1969) also found that p-type (sulfur-rich) PbS oxidized faster than n-type (lead-rich) in an $HClO_4$ solution at pH 1.5, Eadington (1973) observed the opposite to be the case in a 10^{-5} M HNO_3 solution. It is possible that this discrepancy can be attributed to the fact that the type of acid and pH were different in these two sets of experiments. To further add to the debate, Springer (1970) conducted experiments on n-type galena rather than on a synthetic sample and could not detect any effect that its semiconducting properties had on anodic or cathodic polarization.

Although not studied as extensively as anodic dissolution, mineral reduction is another aspect of the galena-water system that has received some attention. At low pH, galena is expected to be reduced according to the reaction,

$$PbS + 2H^+ + 2e \longrightarrow Pb^o + H_2S, \qquad [4.6]$$

beginning at approximately -300 mv (see Figure 2.2). Brodie (1969) carried out experiments to determine the current efficiency for this reaction by polarizing the electrode at constant potentials in the range from -300 mv to -1000 mv, and then doing analysis to determine the

amount of H_2S gas that was evolved. The current efficiencies were found to be 80-90% above -500 mv and then to increase to a constant value of about 95% as the potential was further lowered. From this, two conclusions were drawn: i) reaction [4.6] did, indeed, begin to proceed at a potential close to its reversible value, and ii) a second reduction reaction was making a minor contribution to the total cathodic current at all the applied potentials. On the basis of previously published data concerning the hydrogen overvoltage on lead (Latimer, 1952), Brodie concluded that the second cathodic reaction could be attributed to the evolution of H_2, i.e.,

$$2H^+ + 2e \longrightarrow H_2. \qquad [4.7]$$

Nicol et al. (1978) employed linear sweep voltammetry on a rotating PbS disk electrode in their study of the reduction of galena in acidic media. When the mineral was reduced at different pH values without first being oxidized, a very steep cathodic current was observed to begin at potentials close to the Nernst values for reaction [4.6]. Furthermore, the observed current-potential data was found to best fit a mechanism in which the reduction of an intermediate S^- to HS^- was rate-controlling, i.e.,

$$PbS + e \rightleftharpoons Pb^o + S^- \qquad [4.8]$$

$$S^- + H^+ + e \longrightarrow HS^- \qquad [4.9]$$

$$HS^- + H^+ \rightleftharpoons H_2S. \qquad [4.10]$$

Interest in the electrochemistry of galena has also been generated because of its geological, as well as metallurgical, implications. Local intense potential gradients and certain solution and reprecipitation effects near lead/zinc and lead/iron deposits (Sivenas and Beales, 1982a,b; Sivenas, 1981) have been tentatively attributed to local galvanic cells associated with interactions between the sulfide minerals. Recently, Sivenas and Foulkes (1984) conducted an extensive voltammetric study of the cathodic reactions of galena in 1 M perchloric acid. They found that the electrochemical behavior was very complex and could identify seven cathodic reactions occurring between the potential limits of 345 and -1000 mv, depending on the conditions of the experiment.

4.2 Experimental

Details concerning the galena sample, the preparation of the electrode and the electrical set-up for the electrochemical experiments have been described in the previous chapter and, consequently, will not be included here.

The electrolytes used consisted of 0.1 M $HClO_4$ at pH 1.1 and 0.5 M CH_3COOH/0.5 M CH_3COONa at pH 4.6. Analysis of the dissolved lead concentrations for the chronoamperometry and open-circuit potential experiments was conducted with a plasma emission spectrometer (Spectrospan IV).

For the most part, the procedure for the open-circuit potential tests followed the one described by Brodie (1969) for a similar set of

experiments done at pH 0. The galena electrode (0.42 cm^2 area) was immersed in 400 ml of stirred, deoxygenated electrolyte and cathodically polarized for 70 minutes at an applied current of -0.6 mA to build up a layer of lead metal. Once this was done, anodic current was applied for a short period of time and then turned off in order to monitor the resulting open-circuit potential using the Keithley Model 642 electrometer. When a steady potential was obtained, a 5-ml aliquot of the electrolyte was removed for lead analysis. This cycle of applying anodic current, opening the circuit and then taking a sample was repeated over and over again in order to cover a wide range of open-circuit potentials.

4.3 **Results and Discussion**

4.3.1 Electrochemical Experiments at pH 1.1

a. Chronoamperometry: On the basis of the thermodynamic calculations that have been carried out for the three cases in Chapter II, three possible reactions for the oxidation of galena at pH 1.1 can be written:

Case I: $$PbS + 4H_2O \longrightarrow Pb^{2+} + SO_4^{2-} + 8H^+ + 8e \qquad [4.11]$$

Case II: $$2PbS + 3H_2O \longrightarrow 2Pb^{2+} + S_2O_3^{2-} + 6H^+ + 8e \qquad [4.12]$$

Case III: $$PbS \longrightarrow Pb^{2+} + S^o + 2e. \qquad [4.2]$$

A fourth reaction that involves the dissolution of PbS, but not its

oxidation, is:

$$PbS + 2H^{+} \longrightarrow Pb^{2+} + H_2S. \qquad [4.5]$$

One of the ways in which these reactions differ is in the ratio of the number of Faradays of charge transferred to the number of moles of Pb^{2+} ions produced (hereupon referred to as Q/M). Since both the charge and the amount of lead ions dissolved can readily be measured at this pH, this ratio offers a very useful way to determine which reaction(s) predominates at a given potential. A Q/M ratio of 8:1, 4:1, 2:1 or 0:1 indicates that reaction [4.11], [4.12], [4.2] or [4.5], respectively, is occurring.

Accordingly, a series of experiments was conducted in which the polished galena electrode was immersed in a stirred, deoxygenated 0.1 M $HClO_4$ solution and a constant potential was applied to it. The current was monitored on a strip chart recorder throughout the course of the test run. Once the mineral was polarized long enough for a detectable amount of lead to dissolve (usually about 2 hours), the experiment was terminated and a sample of the electrolyte was removed for lead analysis. The charge that had been passed was determined by integrating under the current-time curve.

The results obtained for potentials of 545, 645, 945, 1045 and 1245 mv are given in Figures 4.1 and 4.2 and in Table 4.1. The Q/M values in Table 4.1 show quite clearly that Pb^{2+} and S^{o} are the principal oxidation products in this potential range. This agrees with what has been found from previous electrochemical work done on galena at this pH

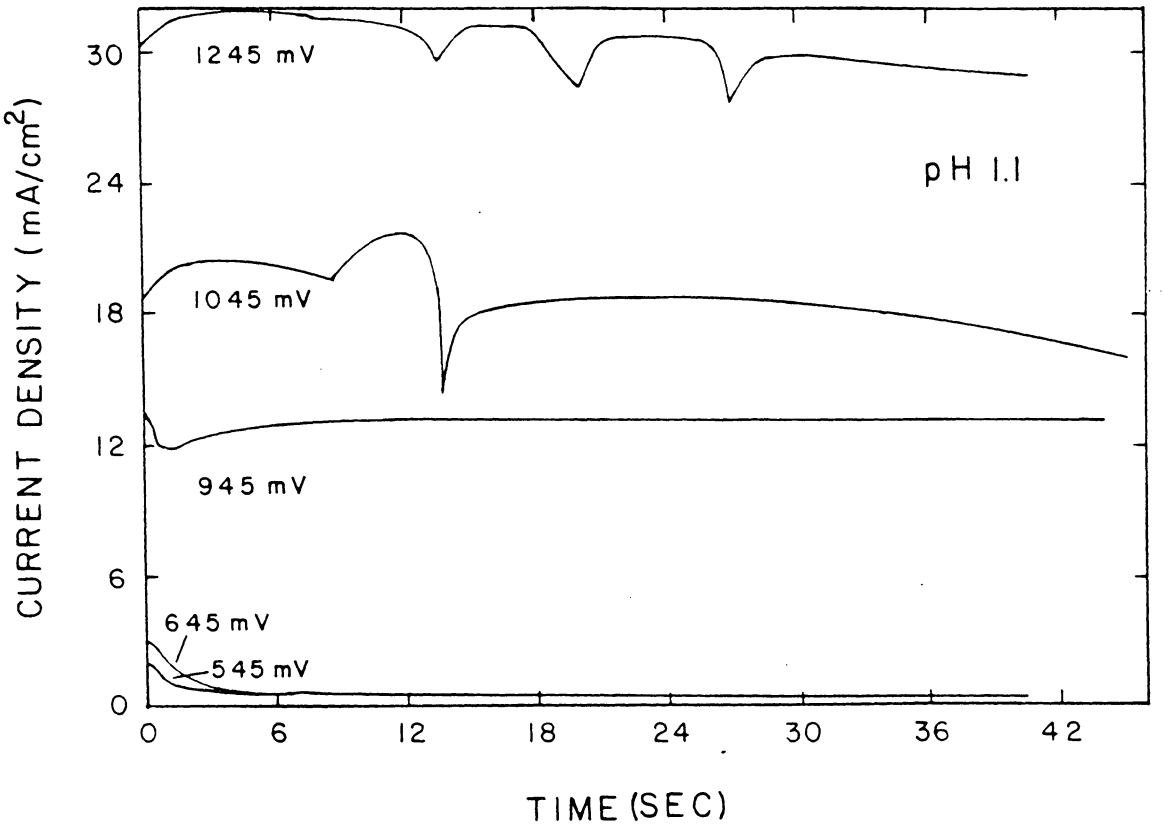


Figure 4.1 Current-time curves for the initial stages of oxidation after applying potentials of 545, 645, 945, 1045 and 1245 mv to a galena electrode immersed in a 0.1 M $HClO_4$ solution (pH 1.1). Solution stirred.

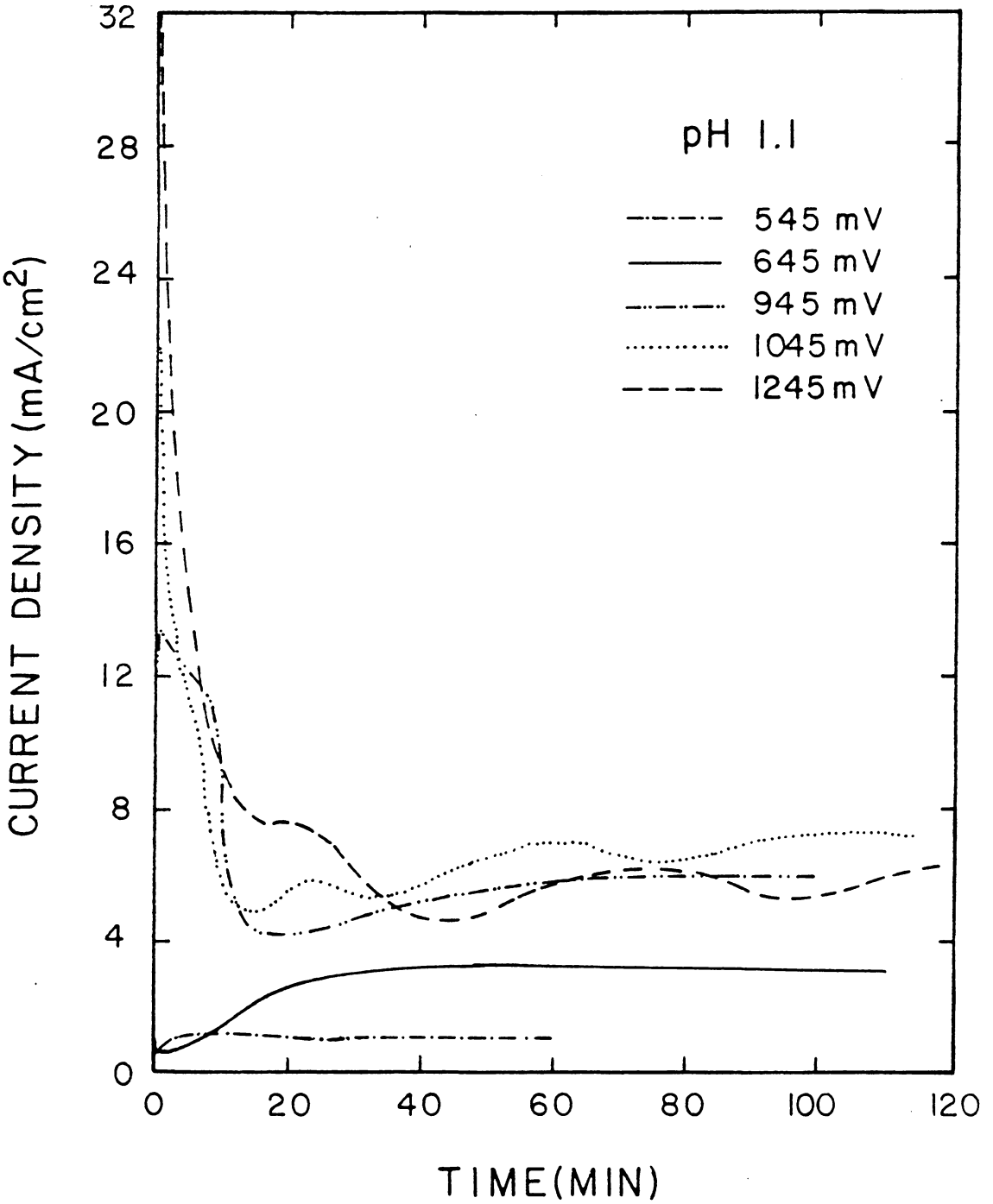


Figure 4.2 Current-time curves obtained over a longer duration applying potentials of 545, 645, 945, 1045 and 1245 mv to a galena electrode immersed in a 0.1 M $HClO_4$ solution (pH 1.1).

Table 4.1

Measured Q/M Ratios for a Galena Electrode Held at Different Potentials at pH 1.1

Potential (mv)	Q/M
545	1.8
645	1.9
945	1.9
1045	1.9
1245	2.1

(Brodie, 1969; Skewes, 1972; Paul et al., 1978; Johnson et al., 1978; Gardner and Woods, 1979b). From the E_h-pH diagrams for Cases I and II (Figures 2.2 and 2.6), oxidation to SO_4^{2-} and $S_2O_3^{2-}$ should begin to proceed at potentials of about 300 and 400 mv, respectively. Apparently, the oxidation of sulfide to the thermodynamically more favored species is sluggish and requires an overvoltage of at least 800 or 900 mv.

Several other observations concerning the current-time curves can be made. Figure 4.1 shows that in the first 40 seconds, the transient behavior of the currents for 945, 1045 and 1245 mv is quite irregular. The behavior observed at 945 mv is similar to that reported by Gardner and Woods (1979b) for galena at this same pH. In both cases, the current drops very quickly until about 10 mC/cm^2 of charge has been passed and then begins to increase. This type of transient curve is often found for nucleation and growth processes (Nicol et al., 1978). It is possible that the initial sulfur product layer inhibits further oxidation, but as it builds up, becomes porous enough that oxidation becomes promoted. Another contributing factor may be that there is an initial build up of Pb^{2+} ions at the electrode surface, which is eventually dispersed away by stirring. The presence of Pb^{2+} ions would also tend to retard reaction [4.2].

The curves for 1045 and 1245 mv are even more unusual in that the current first increases with time and then intermittently over the first 30 seconds or so quickly drops and rises. The second effect may be due to fluctuations in the resistance and/or porosity of the sulfur layer.

In Figure 4.2, the current over the entire duration of the experiment has been plotted in order to examine longer-term oxidation behavior. Even over long periods of time, the current at the higher potentials fluctuates considerably. Also, the higher the potential, the more sharply the current diminishes during the first stages of the polarization. This may suggest that the initial oxidation rate has an important effect on the resistance and porosity of the sulfur layer. The results also indicate that by the end of two hours, the current at 1045 mv is greater than at 1245 mv.

This type of behavior is often observed on electrodes covered with insulating surface films (Vijh, 1973). The presence of such a layer imposes an additional barrier which dissipates a portion of the applied potential and fundamentally changes the nature of the electrocatalytic surface. Furthermore, the surface layer tends to inhibit the transport of reactants and products to and from the reaction sites.

b. Single sweep voltammetry:

Identification of A_1, C_1 and C_2 peaks: In order to further study the PbS-H_2O system at pH 1.1, a series of voltammetry experiments was carried out in 0.1 M $HClO_4$ solution. In most cases, the freshly polished galena electrode was immersed in the deoxygenated buffer solution and the scan was begun in the anodic direction at a sweep rate of 20 mv/sec.

Figure 4.3 shows the effect of stirring and of extending the anodic limit from 545 to 645 mv. In all instances, anodic current (A_1) begins to flow when a potential of about 300 mv is reached, although it does

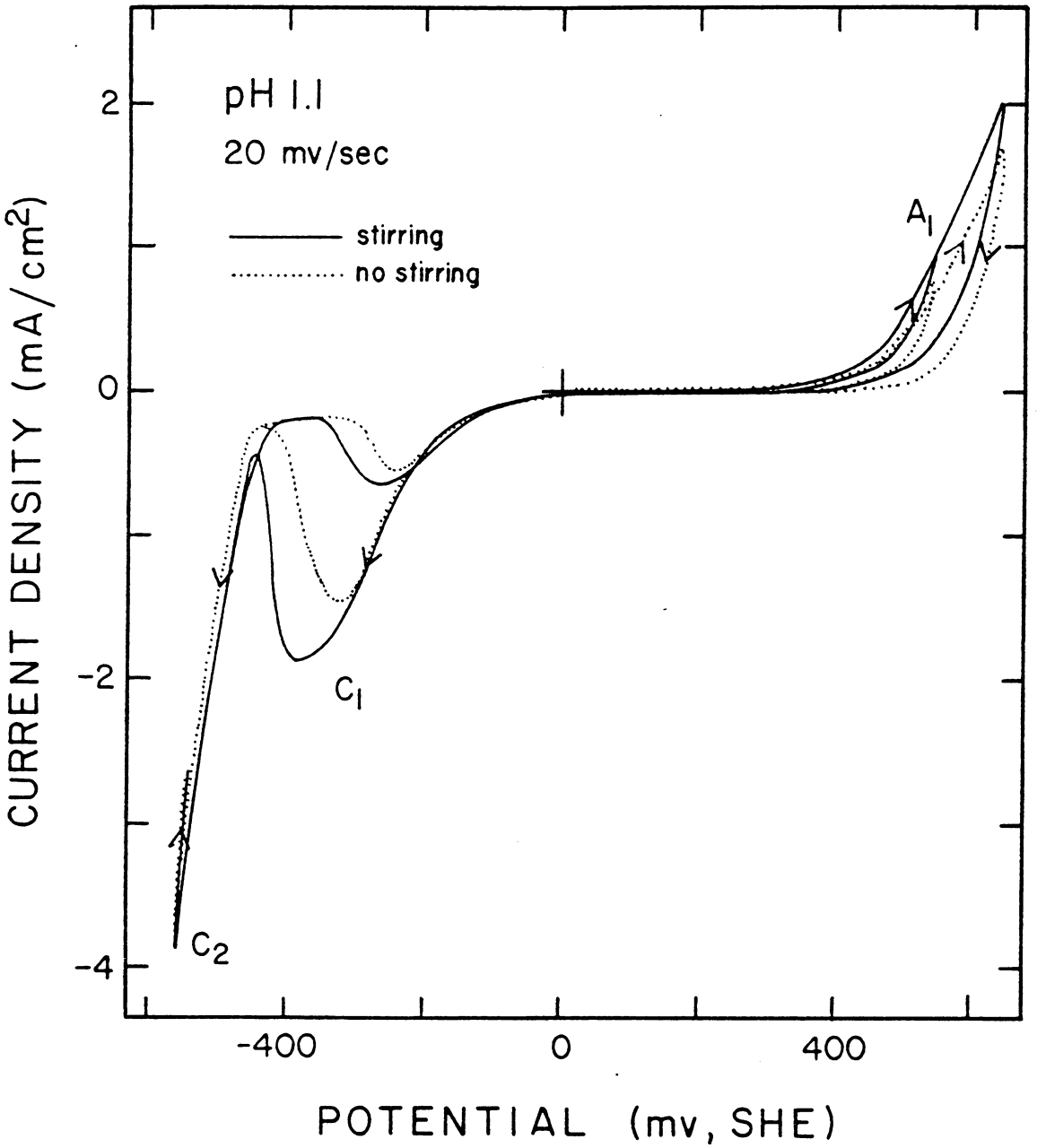


Figure 4.3 The effect of stirring and of extending the anodic limit from 545 to 645 mv on the single sweep voltammograms for a galena electrode in a 0.1 M $HClO_4$ solution (pH 1.1). Scan rate = 20 mv/sec.

$A_1 = PbS/Pb^{2+},S^0$ $C_1 = S^0/H_2S$ $C_2 = PbS/Pb^0,H_2S$

not begin to rise sharply until about 425 mv. Once the scan direction is reversed and the potential is lowered below 0 mv, a cathodic peak, C_1 is observed, presumably due to the removal of the products from the anodic scan. A further lowering of the potential to below -400 mv brings about the appearance of a second reduction peak, C_2, likely due to the decomposition of PbS via reaction [4.6]. The voltammograms are much the same as the ones obtained during a similar study by Gardner and Woods (1979b). On the other hand, they differ somewhat from those reported by Nicol et al. (1978), in which two peaks rather than one are associated with the reduction of oxidation products.

Referring back to the E_h-pH diagrams in Figures 2.2, 2.6 and 2.11, a potential of 300 mv, where the anodic current in the voltammograms begins to flow, corresponds closely to what is expected for any of reactions [4.11], [4.12] and [4.2]. However, in view of the previous findings of this study and others, oxidation to produce Pb^{2+} and S^o is the likely reaction. This is further substantiated by measurement of the area under the four sets of curves in Figure 4.3, which shows that the charges associated with A_1 and C_1 balance each other. As is the case at higher pH values, reactions such as [4.11] and [4.12], which produce $S_2O_3^{2-}$ and SO_4^{2-} anions, are irreversible and should cause an imbalance between the anodic and cathodic charges.

The voltammograms in Figure 4.3 also show that stirring increases the oxidation rate of galena at pH 1.1. Presumably, flowing electrolyte prevents Pb^{2+} ions from accumulating at the electrode surface and inhibiting oxidation. Two possible mechanisms are consistent with this

behavior: 1) if dissolution is activation-controlled, an accumulation of Pb^{2+} ions at the electrode increases the backward rate of reaction [4.2]; and 2) diffusion of Pb^{2+} ions away from the electrode is rate-controlling. Nicol et al. (1978) also observed similar behavior for galena in a 1 M $HClO_4$ solution and explained it in terms of the effect of the Pb^{2+} concentration on the rate of the backward reaction.

The cathodic peaks in the stirred cases are obviously larger than the ones obtained under quiescent conditions. However, other than that, there does not appear to be a significant difference. This suggests that C_1 involves the reduction of an insoluble oxidation product. Given the nature of the oxidation process, the reaction,

$$S^o + 2H^+ + 2e \longrightarrow H_2S, \qquad [4.13]$$

is the only reasonable choice.

Another interpretation of how the oxidation products are removed has been proposed by Gardner and Woods (1979b). According to their view, two cathodic reactions occur when the solution is not being stirred. The first involves the recombination of Pb^{2+} and S^o to form PbS by the reverse of reaction [4.2], i.e.,

$$Pb^{2+} + S^o + 2e \longrightarrow PbS. \qquad [4.14]$$

Some Pb^{2+} will manage to diffuse away from the galena surface even under stagnant conditions and, in so doing, cause a stoichiometric excess of S^o. This excess can then be removed by reaction [4.13]. When the solution is stirred, all of the Pb^{2+} ions will be swept away and only

reaction [4.13] will proceed.

It should be noted that although two reactions may be involved in the cathodic process, only one peak, C_1, has been observed in the voltammograms of Gardner and Woods and of the present study. Gardner and Woods explained this by the fact that the reversible potentials for reactions [4.13] and [4.14] are within about 60 mv of each other at this pH, although they are somewhat anodic with respect to where C_1 is observed to begin on the voltammograms. One difficulty with this hypothesis is that even though these reactions occur at similar potentials, one would still expect the C_1 peak to become narrower in a stirred solution. However, this does not appear to be borne out by the curves in Figure 4.4.

As pointed out previously, the voltammogram presented by Nicol et al. (1978), obtained for a rotating PbS disk electrode at pH 1, is different from the ones of this study and of Gardner and Woods (1979b). For convenience, it is reproduced in Figure 4.4. (It should be noted that Nicol et al. reported the electrode potential on the saturated calomel scale.)

As can be seen, for an anodic limit of 350 mv (SCE) (or 600 mv SHE), the reduction of oxidation products from A_1 occurs at two separate peaks (which Nicol et al. designated C_1 and C_2) instead of at a single one. Furthermore, these authors observed that C_1 disappeared if the anodic sweep was extended beyond 400 mv (SCE), and that C_2 appeared only if the anodic sweep went beyond 300 mv (SCE). They postulated that oxidation produced two types of sulfur: i) an "easily reducible" form

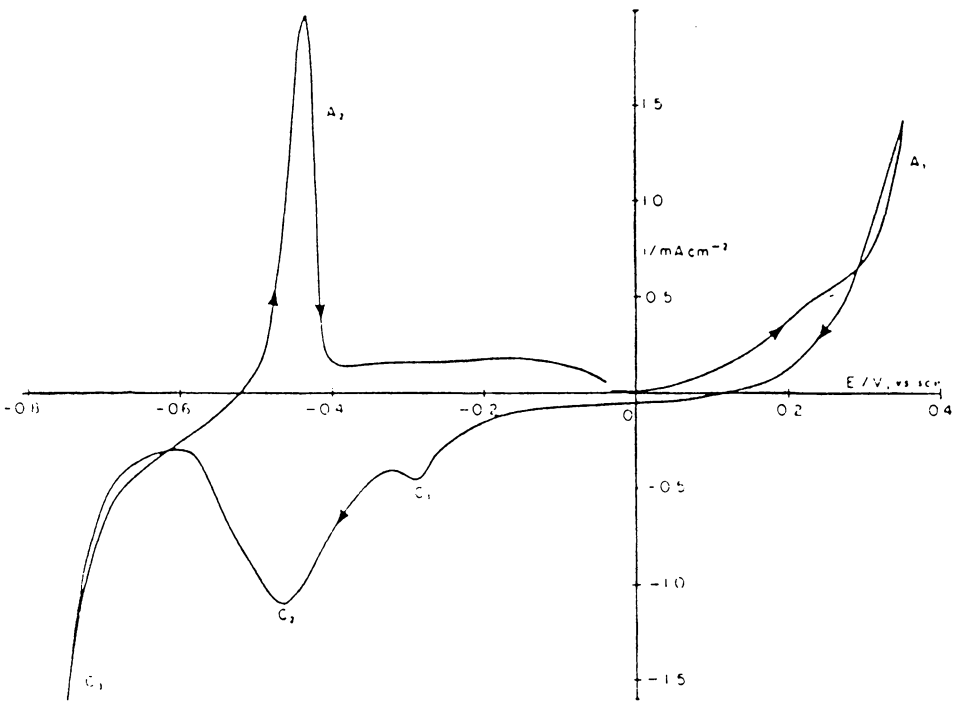


Figure 4.4 Voltammogram obtained for a rotating galena disk electrode in a solution of pH 1 (reproduced from Nicol et al., 1978).

generated near the PbS/S^o interface, and ii) a less active bulk form. The removal of these products would occur at C_1 and C_2, respectively. Excessive oxidation would convert the easily reducible type to the bulk type and, so, result in the disappearance of C_1.

Although two peaks corresponding to C_1 and C_2 have not been found in the voltammograms of this study, examination of the galena electrode after each of the tests suggested that the nature of the anodic film changes in a manner consistent with the hypothesis proposed by Nicol et al. The film appears light in color and can easily be wiped off if oxidation is only moderate. More severe oxidation causes it to turn dull gray, however, and to become strongly adherent. Brodie (1969) has also reported a similar phenomenon.

Figure 4.5 shows two voltammograms obtained under quiescent conditions. In the first one, the potential was raised only to 345 mv during the anodic scan and then reversed to a lower limit of -755 mv before being returned once again to the upper limit. The second test was identical, except that the anodic limit was increased to 745 mv.

In the first sweep, very little oxidation occurs by the time the 345 mv limit is reached, so that no peak corresponding to C_1 (reduction of S^o to H_2S) appears on the reverse reaction. Only when PbS is reduced according to reaction [4.6] does any cathodic current flow.

When the scan direction is again reversed anodically, a small pair of peaks (A_2) and a much larger one (A_3) appear in the vicinity of -300 and 200 mv, respectively. The fact that these are essentially the same whether galena is oxidized during the first sweep (as in the case of

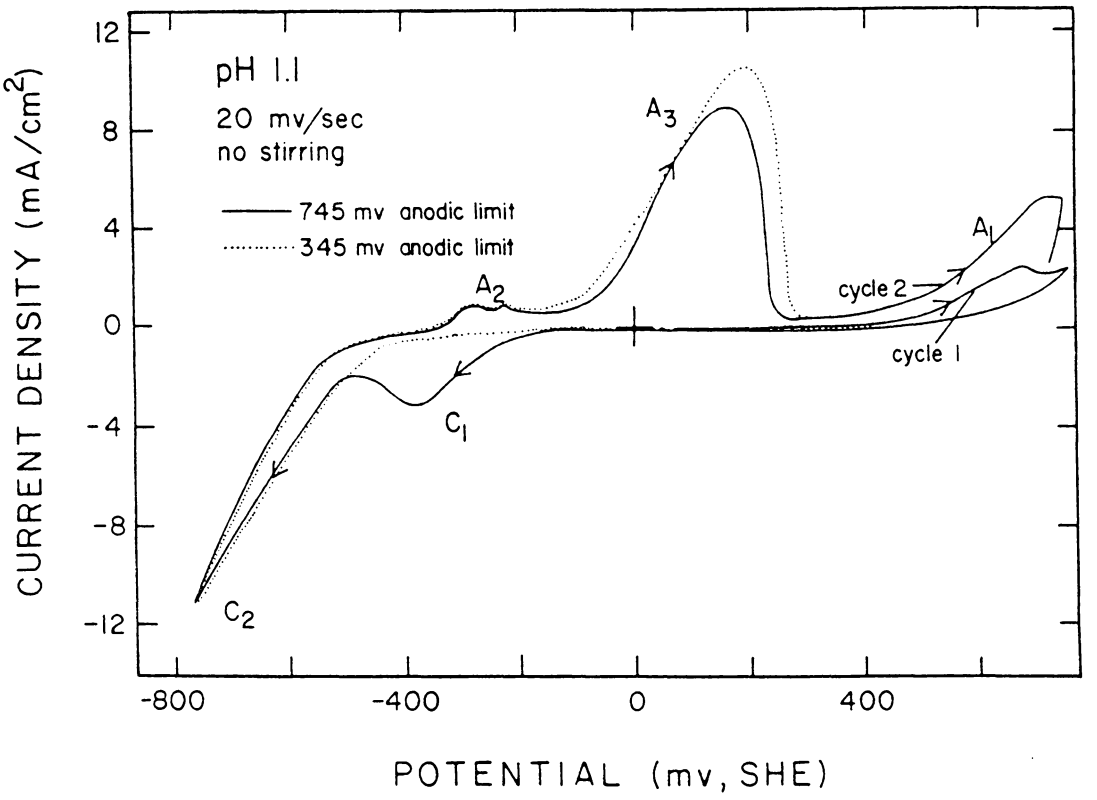


Figure 4.5 Effect of extending the anodic limit from 345 to 745 mv on the voltammograms for a galena electrode immersed in a 0.1 M $HClO_4$ solution (pH 1.1). No stirring. Scan rate = 20 mv/sec.

$A_1 = PbS/Pb^{2+},S^0$ $\quad A_2 = Pb^0,H_2S/PbS$ $\quad A_3 = Pb^0/Pb^{2+}$

$C_1 = S^0/H_2S$ $\quad C_2 = PbS/Pb^0,H_2S$

sweeping to the 750 mv anodic limit) or not indicates that they involve the oxidation of the products of the cathodic reduction of PbS. This will subsequently be discussed further.

When the anodic limit is extended to 745 mv, the current begins to rise at approximately 300 mv and reaches a maximum at 650 mv before dipping slightly beyond this. Paul et al. (1978) and Gardner and Woods (1979b) also found a similar peak in their voltammograms at 550 mv. In this study, the charge consumed up to the peak at 650 mv is about 13 mC/cm^2, which is quite close to the charge passed up to the minimum in the current-time curve at 945 mv (see Figure 4.1). Once again, there is evidence of the inhibition of oxidation by the initial product layer of sulfur on the electrode. Just after the initial amount of sulfur is formed, the oxidation rate drops off even though the potential is becoming increasingly positive. Only after the potential has been increased by about 50 mv does the current begin to increase again.

The remainder of the voltammogram is similar to the one for the lower anodic limit, except that the reduction peak, C_1, appears. It should also be noted that on the second anodic-going sweep, the current rise, A_1, is greater than in the first scan. Apparently, the sequence of oxidizing galena, removing the oxidation products, then reducing galena, and finally removing the reduction products has roughened up the electrode surface.

When the anodic limit is extended even further to 1245 mv, the voltammograms in Figures 4.6 and 4.7 are obtained. Peaks are again observed at a potential of approximately 700 mv under both quiescent and

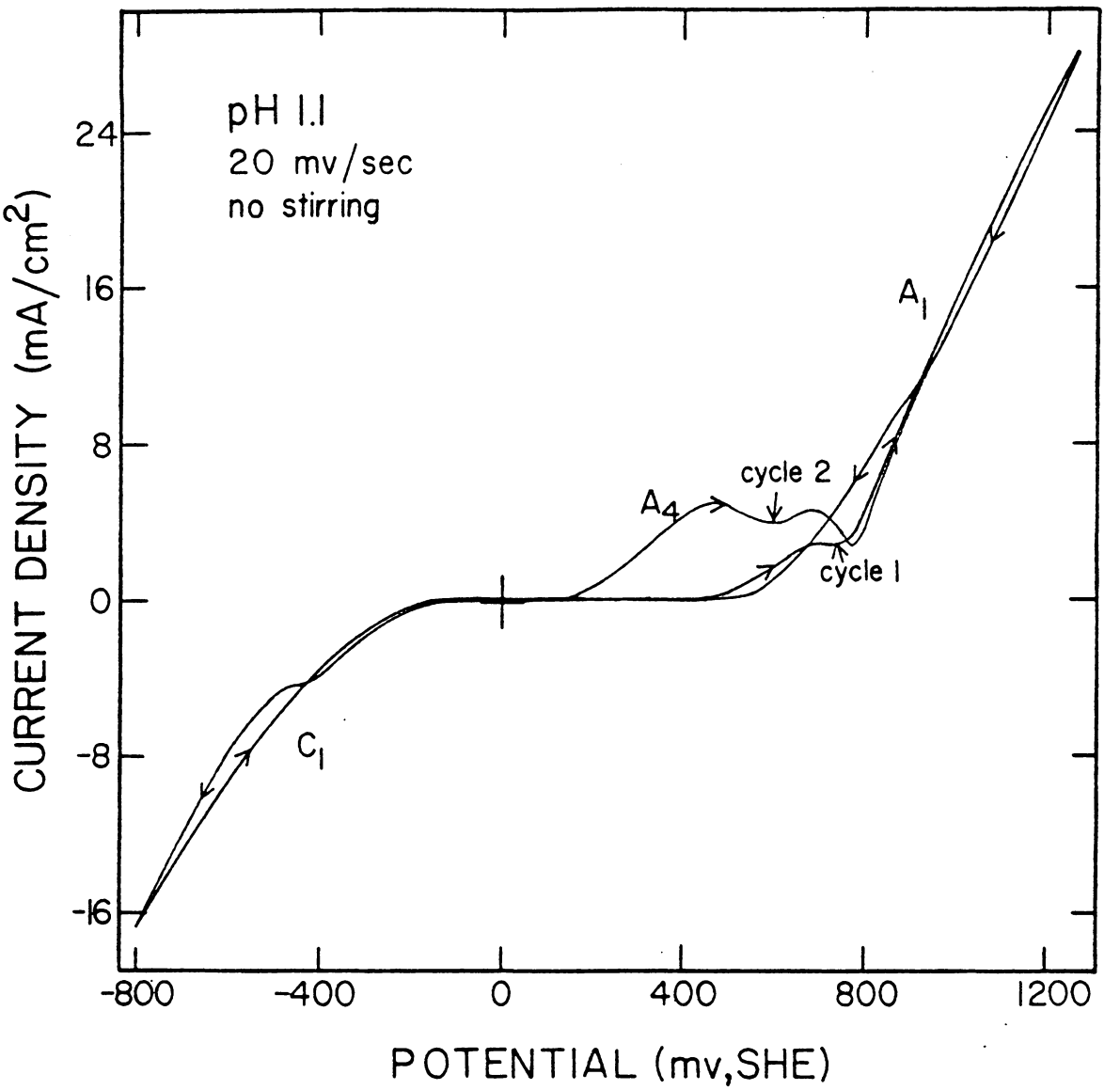


Figure 4.6 Single sweep voltammogram for a galena electrode in an unstirred 0.1 M $HClO_4$ solution (pH 1.1) after scanning between -800 and 1245 mv. Scan rate = 20 mv/sec.

$A_1 = PbS/Pb^{2+},S^o$ $C_1 = S^o/H_2S$ $A_4 = H_2S/S^o$

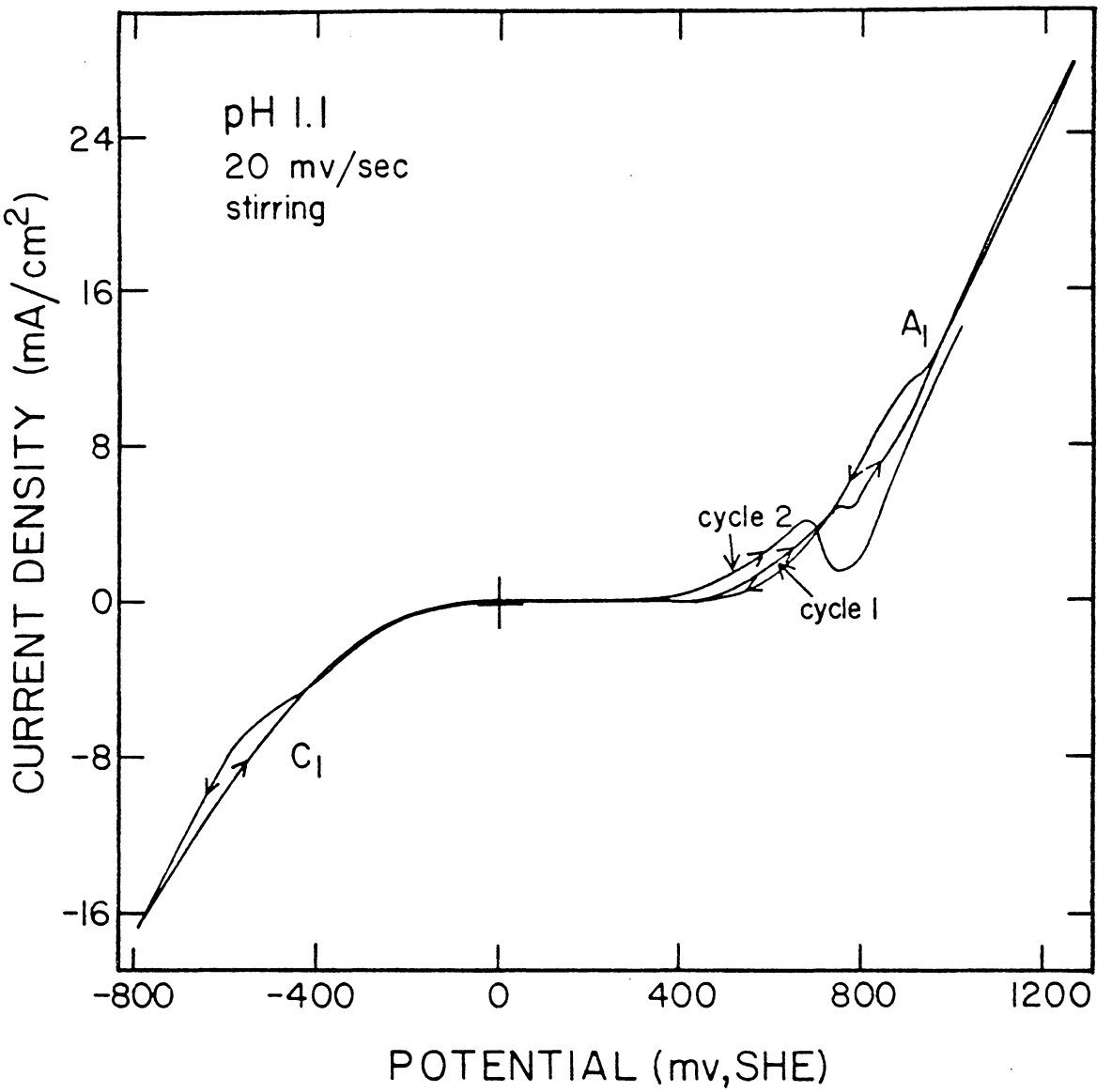


Figure 4.7 Single sweep voltammogram for a galena electrode in a stirred 0.1 M $HClO_4$ solution (pH 1.1) after scanning between -800 and 1245 mv. Scan rate = 20 mv/sec.

$$A_1 = PbS/Pb^{2+},S^o \qquad C_1 = S^o/H_2S$$

stirred conditions and during both the first and second anodic-going scans. Stirring also enhances the dissolution of galena at potentials below 900 mv in both scan directions. Above 900 mv, the current density is essentially unaffected by any agitation.

It can also be seen that between 650 and 900 mv the current is greater along the reverse scan than along the forward scan, something which is indicative of a nucleation and growth mechanism. Below 650 mv, the currents cross over and the amount in the anodic-going direction becomes greater. Once again, evidence appears that suggests that some transition in the nature of the oxidation product layer occurs near a potential of about 650 mv. It should be recalled that the shape of the current-time plots (Figures 4.1 and 4.2) changes as the electrode potential is increased above 650 mv. Furthermore, a peak along the anodic rise, A_1, in the voltammograms of Figures 4.5, 4.6 and 4.7 occurs at the same potential. This is also where Nicol et al. (1978) proposed that the sulfur product layer was being converted from an easily reduced form to a bulk-like form. A more detailed discussion concerning the apparent change in the mechanism of the oxidation reaction will be included in Chapter V.

In the cathodic region, the results are identical for the stirred and non-stirred solutions. When the sweep is again anodic-going and the potential reaches approximately 150 mv, however, a new peak, A_4, begins to appear only in the unstirred case (Figure 4.6). Integration of the area under the voltammograms reveals that more anodic charge than cathodic charge is passed during the first cycle. Therefore, not all of

the oxidation products are removed by the time the cathodic limit of -800 mv is reached and the potential is increased back to 150 mv. Furthermore, the anodic peaks, A_2 and A_3, that appear in Figure 4.5 are not present in this voltammogram. Since these involve the products from the cathodic decomposition of galena, this suggests that the reduction of galena has not begun by the time the lower limit reaches -800 mv. This behavior shows clearly that the more extensive the oxidation, the more difficult it becomes to remove the oxidation products. In the previous experiments (Figures 4.3 and 4.5), the oxidation products were completely removed by the time the potential was lowered to -500 mv during the cathodic-going excursion.

Since A_4 appears only under quiescent conditions, it must involve the oxidation of a dissolved species. Now, considering that the only dissolved species generated at C_1 is H_2S, the anodic reaction beginning at 150 mv in Figure 4.6 is likely to be just the reverse of reaction [4.13], i.e.,

$$H_2S \longrightarrow S^o + 2H^+ + 2e. \qquad [4.15]$$

This conclusion is further supported by the fact that the Nernst potential for this reaction at pH 1.1 and $[H_2S] = 10^{-6}$ M is 147 mv.

Identification of A_2 and A_3 peaks: In order to learn more about the reactions corresponding to peaks A_2 and A_3, several experiments were specifically carried out. For the voltammograms shown in Figure 4.8, the following scan was used. Beginning at open-circuit (220 mv), the

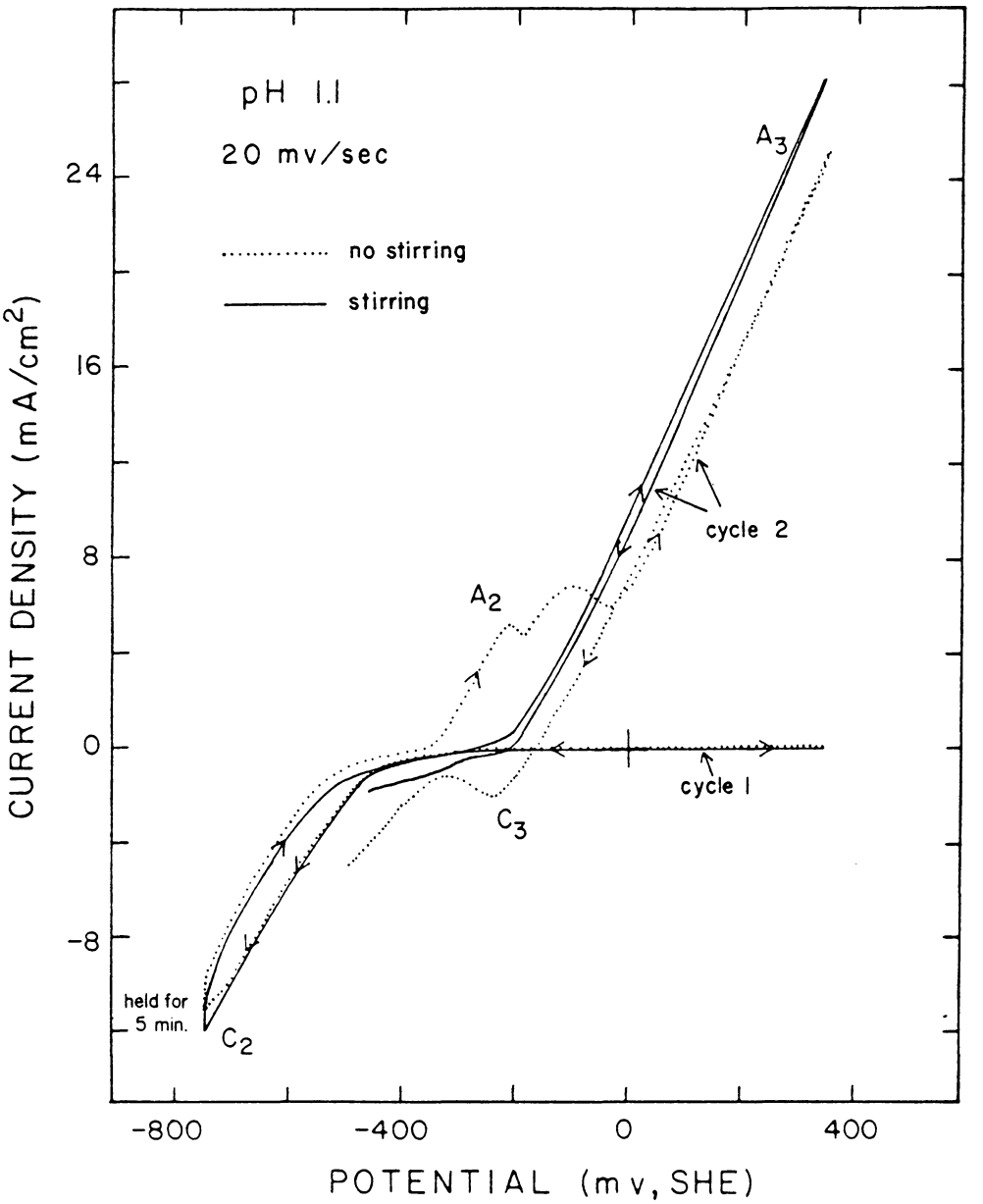


Figure 4.8 Effect of stirring on the voltammogram for a galena electrode in a 0.1 M $HClO_4$ solution (pH 1.1) after holding its potential at -755 mv for 5 minutes.

$A_2 = Pb^0, H_2S/PbS$ $\quad C_2 = PbS/Pb^0, H_2S$

$A_3 = Pb^0/Pb^{2+}$ $\quad C_3 = Pb^{2+}/Pb^0$

potential was increased at 20 mv/sec up to 345 mv, then reversed to -760 mv and held there for 5 minutes. After this, it was cycled back up to 345 mv before being reversed for the final scan to -500 mv.

As noted in earlier experiments, no current rise is observed during the first excursion to 345 mv under both stirred and quiescent conditions and, consequently, peak C_1 does not appear when the scan is reversed. After the potential is held at -760 mv for 5 minutes, a difference is observed in the anodic currents depending upon whether the solution is stirred or not. In the unstirred case, the two peaks at A_2 and the current rise, A_3, have grown considerably compared to what has been observed previously (Figure 4.5); in the stirred case, the peaks at A_2 do not appear at all and the current associated with A_3 is greater than when the solution is not stirred.

On the basis of this, it would appear that the process occurring at A_2 involves the oxidation of a soluble product from the reduction of galena (C_2). A reasonable choice is:

$$Pb^o + H_2S \longrightarrow PbS + 2H^+ + 2e. \qquad [4.16]$$

It is not clear whether this accounts for both peaks at A_2 or for only one of them.

The oxidation process that occurs at A_3 occurs in both stirred and unstirred solutions and, thus, is likely to involve the oxidation of the Pb^o left on the surface, i.e.,

$$Pb^o \longrightarrow Pb^{2+} + 2e. \qquad [4.17]$$

This would also explain the observation that more charge is associated with A_3 in the stirred case. Since reaction [4.16] does not occur when the solution is flowing, more Pb^o will be available for oxidation to Pb^{2+} ions.

After the potential reaches the upper limit of 345 mv and is reversed, a cathodic peak (C_3) appears in close proximity to A_3 only when the solution is quiescent. It is likely that this corresponds to the reverse of reaction [4.17], i.e.,

$$Pb^{2+} + 2e \longrightarrow Pb^o. \qquad [4.18]$$

Stirring the solution will disperse Pb^{2+} ions away from the electrode and make it impossible for it to occur. To determine whether the two peaks at A_2 involve a single reaction or separate ones, a further series of experiments in unstirred solutions was conducted. These were similar to the previous one, except that after the potential was held at -760 mv for 5 minutes, it was increased to different anodic limits (-300, -150, -30 mv). The voltammograms so obtained are presented in Figure 4.9.

When the potential limit during the second anodic-going scan reaches -300 mv, a new reduction peak, C_4, at approximately -450 mv appears immediately after the potential is reversed in the cathodic direction. As the anodic limit is extended to -150 and -30 mv, it grows in size. In fact, there is an exact balance between the anodic charge associated with A_2 and the cathodic charge along C_4. This suggests that the single reaction [4.16] (i.e., oxidation of Pb^o and H_2S to PbS) is responsible for both peaks at A_2 and that the current flow at

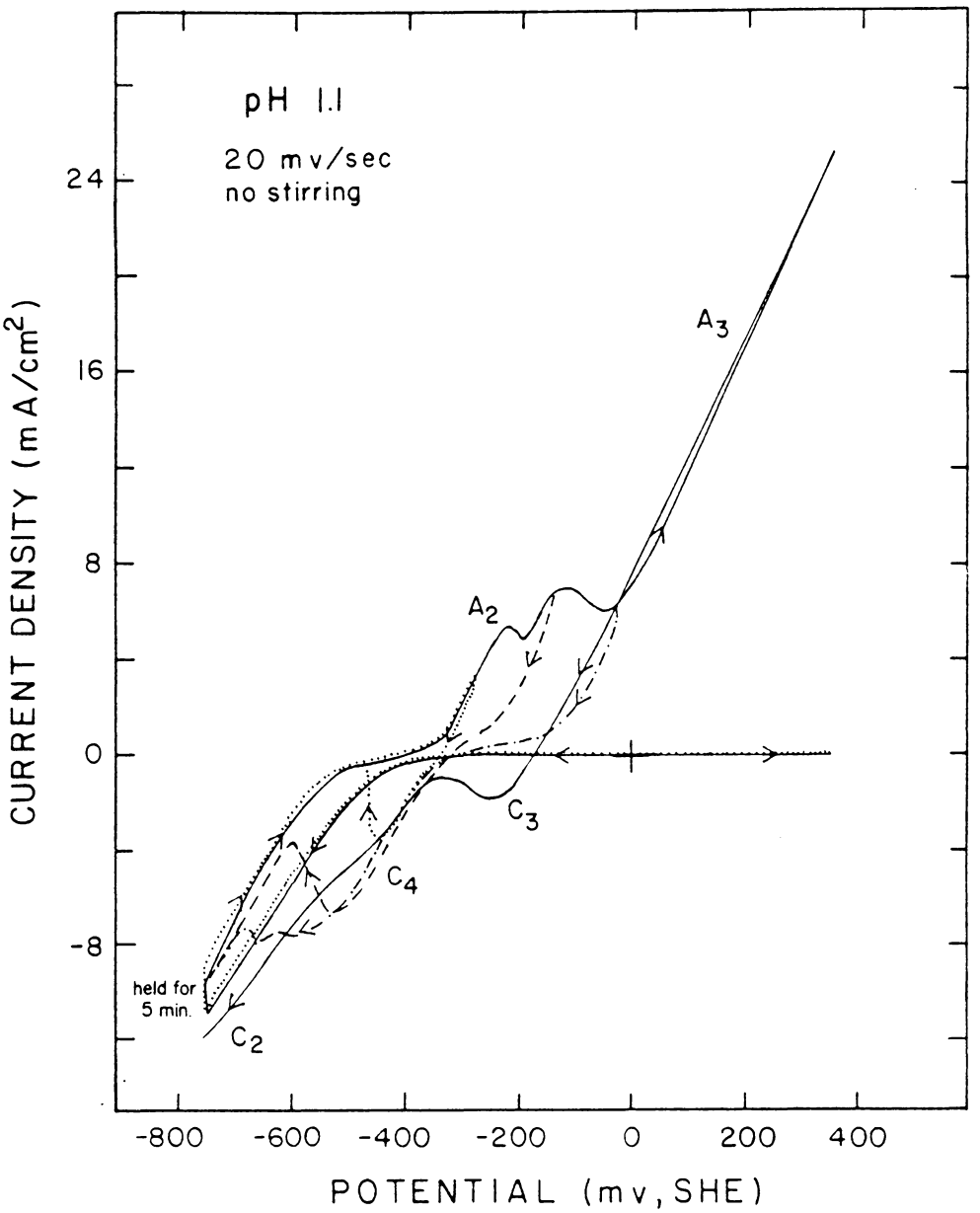


Figure 4.9 Effect of anodic limit on the voltammograms for a galena electrode in a 0.1 M $HClO_4$ solution (pH 1.1) after holding its potential at -755 mv for 5 minutes. No stirring. Scan rate = 20 mv/sec.

$A_2 = Pb^0, H_2S/PbS$ $\quad C_2, C_4 = PbS/Pb^0, H_2S$

$A_3 = Pb^0/Pb^{2+}$ $\quad C_3 = Pb^{2+}/Pb^0$

C_4 is brought about by the reversal of this reaction.

An interesting aspect of the current-potential curve obtained for an anodic limit of -300 mv is that just after the cathodic current reaches a maximum at -450 mv, it quickly drops to almost zero. This is what one might expect if the reaction involved the removal of a thin layer of PbS that is produced by the anodic reaction corresponding to A_2. Once the thin layer is removed, the current cannot be sustained and so it quickly drops to zero.

c. Intermittent galvanostatic polarization: As mentioned previously, the intermittent galvanostatic polarization technique is a particularly useful tool for the study of electrochemical reactions that occur extensively on an electrode surface. The preceding potentiostatic and voltammetry experiments on galena at pH 1.1 showed that the rates of the reactions observed are indeed high and, consequently, the IGP method should complement the other techniques used very well.

IGP diagrams obtained by applying current density pulses of 3.9 mA/cm^2 to the electrode in both stirred and unstirred solutions are presented in Figure 4.10. In these experiments, the freshly polished mineral was polarized cathodically for approximately 9 minutes before being oxidized.

In the first part of both diagrams, the electrode potential quickly drops until it reaches a value where galena begins to be reduced (C_2). Thereupon, the open-circuit potential becomes constant at about -390 mv in the stirred case and about -420 mv in the unstirred case. Both of

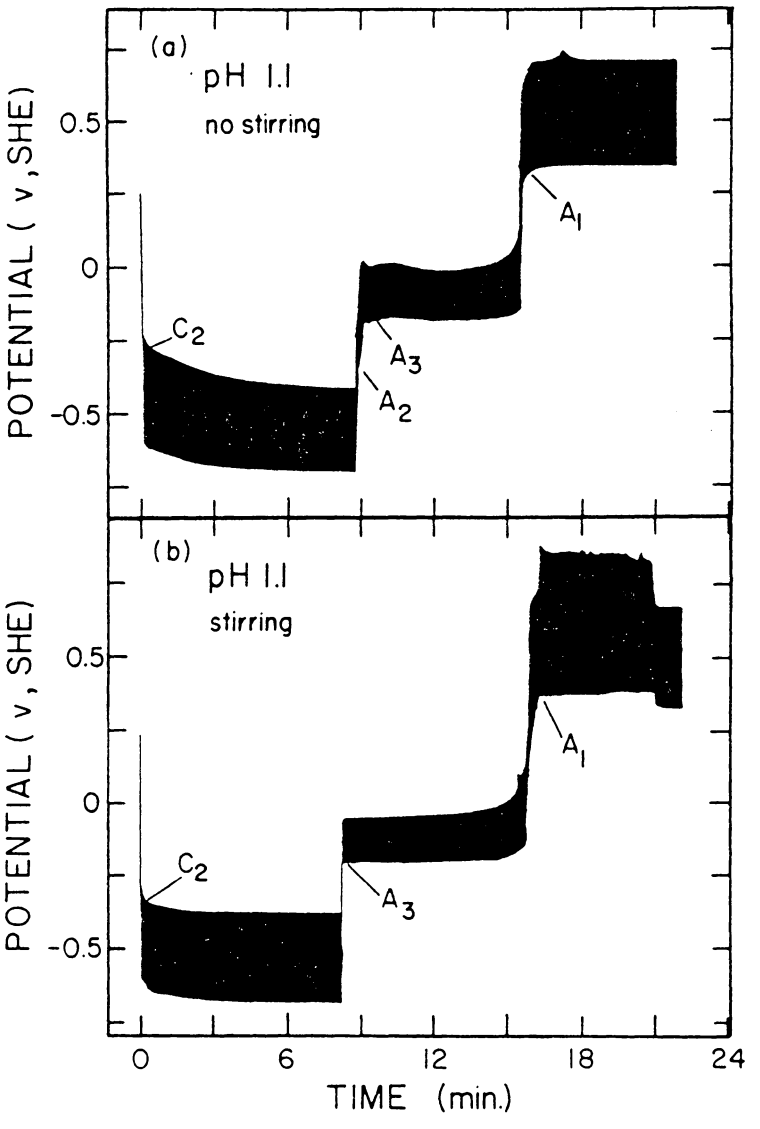


Figure 4.10 IGP diagrams obtained after applying current pulses of 3.9 mA/cm^2 to a galena electrode immersed in an unstirred (a) and stirred (b) 0.1 M $HClO_4$ solution (pH 1.1).

$A_1 = PbS/Pb^{2+},S^o$ $\quad A_2 = Pb^o,H_2S/PbS$ $\quad A_3 = Pb^o/Pb^{2+}$

$C_2 = PbS/Pb^o,H_2S$

these are in close agreement with the Nernst potential for the reduction of galena (reaction [4.6]) and the potential on the voltammograms in Figures 4.3 and 4.5, where this reaction begins to occur. It can be seen that not only is the open-circuit potential lower under quiescent conditions, but that it also takes longer to reach steady state. This can be explained in terms of the law of mass action for this reaction. Stirring continually sweeps away the reaction product, H_2S, from the electrode surface so that the surface concentration of this species quickly becomes constant and is always less than in the unstirred case. Consequently, the potential at which the forward and backward rates are equal will be more anodic. Furthermore, when the solution is quiescent, there will be a build-up of H_2S at the electrode surface during the first part of the cathodic polarization, which will cause the surface concentration of H_2S and, hence, the open-circuit potential to take longer to stabilize.

When the polarity of the pulses is reversed, the open-circuit potential for the stirred solution rises immediately to -200 mv and stays at this level for almost as long as the electrode has previously been cathodically polarized. This potential is very close to where peak A_3 on the voltammogram first begins to appear and so it is reasonable to assign this plateau to the same reaction (i.e., oxidation of Pb^o to Pb^{2+}). Once this reaction is complete, the potential rises to about 370 mv, where galena itself is oxidized (A_1).

The diagram for the unstirred case is similar except for a small arrest, A_2, between plateaus C_2 and A_3 at approximately -360 mv. Again,

this matches the onset of a peak in the voltammograms obtained in unstirred solution (Figure 4.5). Furthermore, the smallness of the arrest compared to the A_3 plateau is similar to the relative sizes of the corresponding peaks in the voltammograms. This reflects that the recombination of Pb^o and H_2S to PbS (reaction [4.16]) occurs to a far less extent than does the oxidation of Pb^o to Pb^{2+} (reaction [4.17]). It also indicates that reaction [4.16] is not very reversible. This can be attributed to sluggish kinetics and/or the diffusion of most of the H_2S produced by the cathodic decomposition of galena away from the electrode even under quiescent conditions.

Another slight difference between the two IGP diagrams in Figure 4.10 is that the Pb^o/Pb^{2+} plateau in the unstirred case is about 15-20 mv higher and not as flat as in the stirred case. The same reasoning that has been used to explain the differences in the C_2 plateaus can also be applied in this instance.

Figure 4.11 shows the results of two experiments in which anodic pulses of 3.9 mA/cm^2 were first applied for slightly over 7 minutes, and then the polarity was reversed in order to remove the oxidation products. In both cases shown, the solution was not being stirred and the only difference was that in the second one, the electrode was not reduced for a long enough time to remove all of the oxidation products before positive pulses were again applied.

The potential rises immediately (A_1) after the anodic pulsing is begun, and eventually levels off. For the experiment in Figure 4.12a, the open-circuit potential remains constant for slightly less than 6

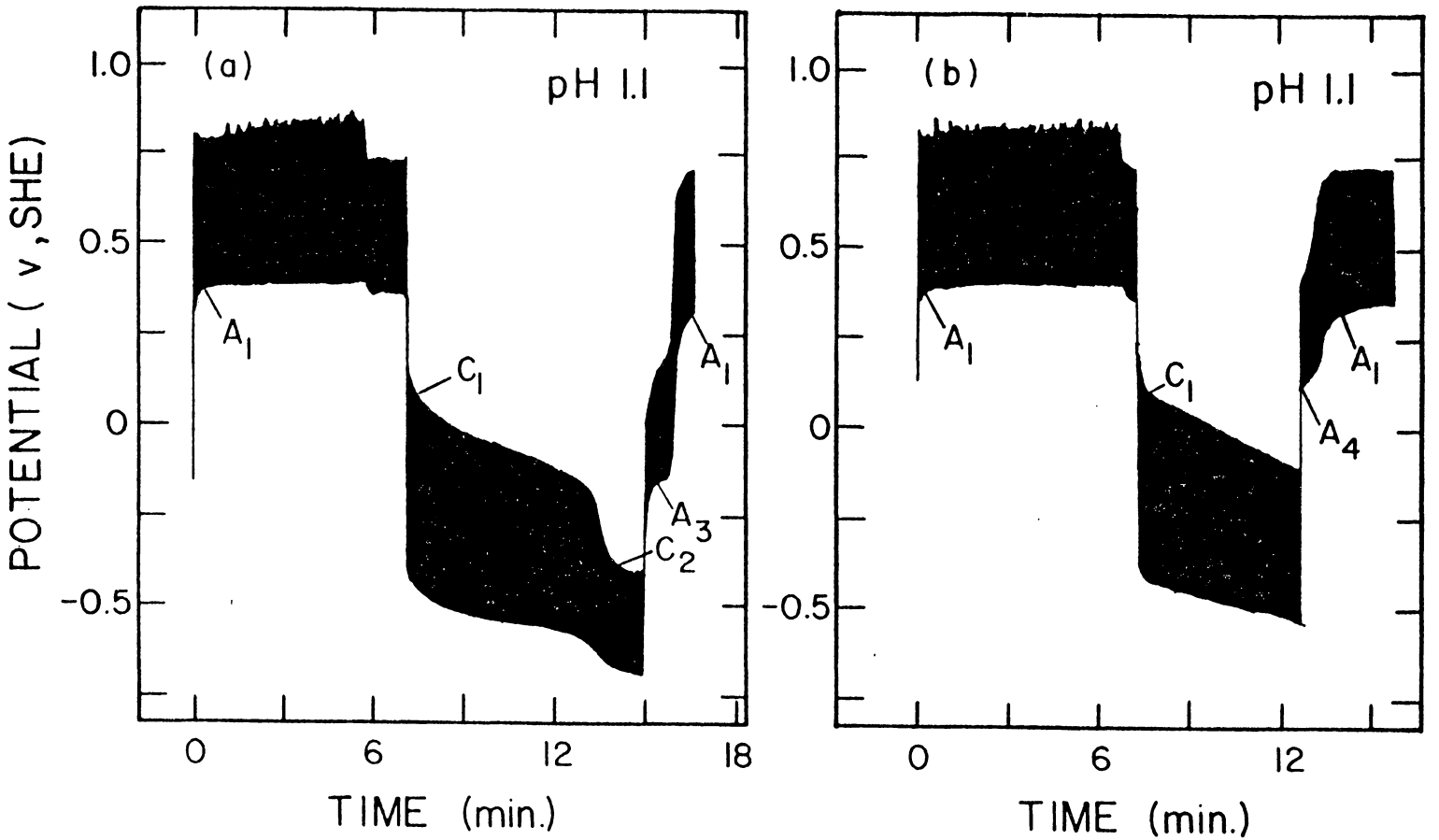


Figure 4.11 IGP diagrams obtained after applying current pulses of 3.9 mA/cm^2 to a galena electrode immersed in an unstirred 0.1 M $HClO_4$ solution (pH 1.1). The difference in the two cases is that after initial anodic pulses (7 minutes), (a) cathodic polarization maintained long enough to remove all oxidation products and (b) cathodic polarization terminated before all oxidation products removed.

$A_1 = PbS/Pb^{2+},S^o$ $A_3 = Pb^o/Pb^{2+}$ $A_4 = H_2S/S^o$ $C_1 = S^o/H_2S$ $C_2 = PbS/Pb^o,H_2S$

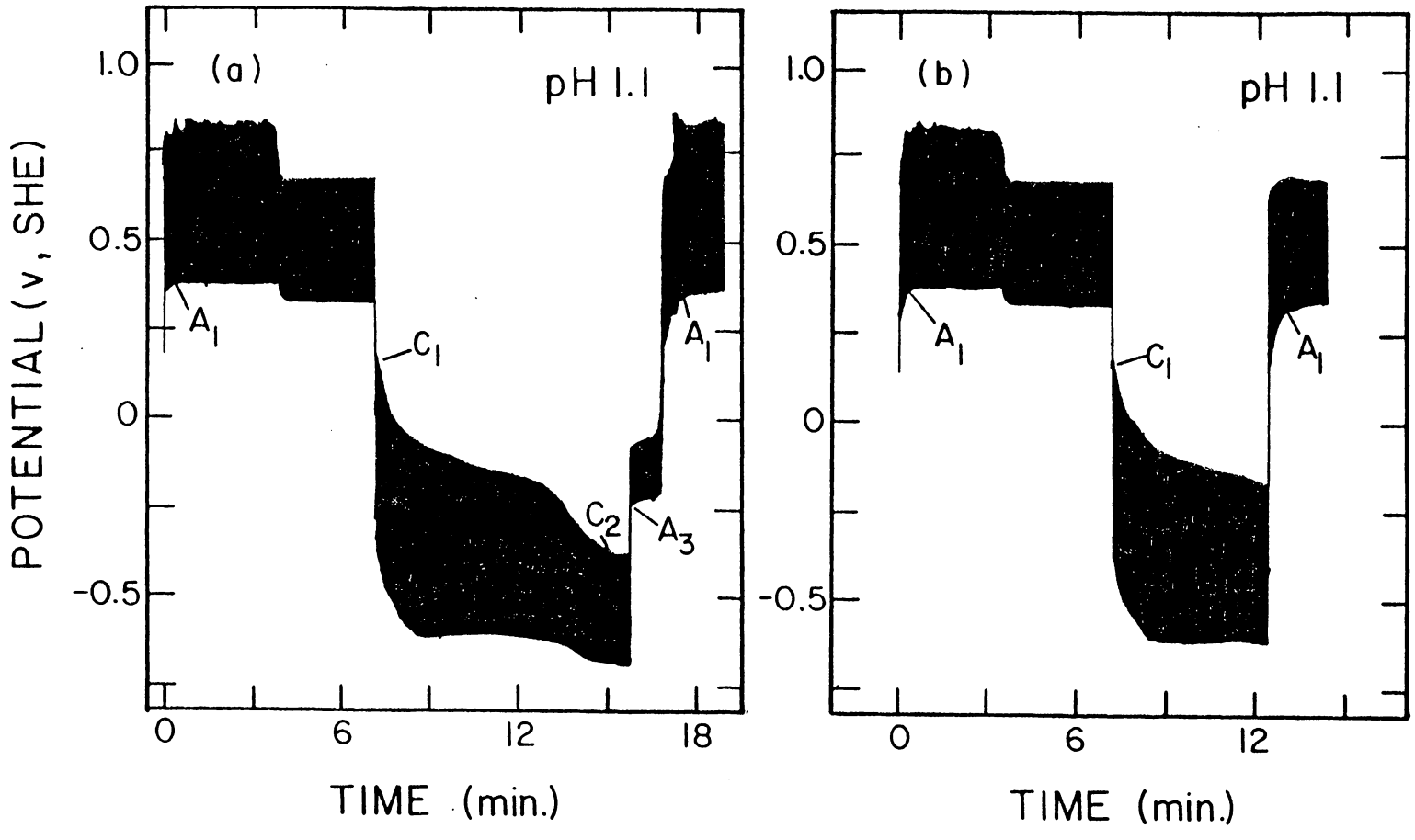


Figure 4.12 IGP diagrams obtained after applying current pulses of 3.9 mA/cm^2 to a galena electrode immersed in a stirred 0.1 M $HClO_4$ solution (pH 1.1). The difference in the two cases is that after initial anodic pulses (7 minutes), (a) cathodic polarization maintained long enough to remove all oxidation products and (b) cathodic polarization terminated before all oxidation products removed.

$A_1 = PbS/Pb^{2+},S^o$ $A_3 = Pb^o/Pb^{2+}$ $C_1 = S^o/H_2S$ $C_2 = PbS/Pb^o,H_2S$

minutes at a value of 375 mv, which is close to where the current rise for reaction [4.12] is observed to begin in the voltammograms (Figures 4.3 and 4.5). At the same time, the maximum potential attained during each pulse cycle continually fluctuates, possibly due to variations in the porosity and resistance of the sulfur product layer. After about 6 minutes, there is a sudden decrease in the open-circuit potential to 350 mv and in the maximum potential to 720 mv. It was noted previously that various changes in the voltammograms (Figures 4.6 and 4.7) and current-time curves (Figures 4.1 and 4.2) occur at about the same potential of 650 mv. What causes this may also be responsible for the abrupt drop in the potential observed in the A_1 plateau of Figure 4.12a. In the second experiment shown in Figure 4.12b, a similar transition occurs, but only after a longer time has elapsed.

Once the current is reversed in both cases, the potential decreases and a plateau, C_1, that is not observed in Figure 4.10 soon appears. Presumably, this can be attributed to the removal of oxidation products via reactions [4.13] and/or [4.14]. This is supported by the fact that the amount of charge passed along the cathodic plateau is fairly close to that passed during the initial oxidation. The open-circuit potential drops continually along the plateau from about 165 to -200 mv because of the depletion of Pb^{2+} ions from the surface region and/or a heterogeneity of the sulfur oxidation layer. As a result of this heterogeneity, the easiest-to-remove sulfur will be reduced first, leaving behind what will be progressively more difficult to remove as polarization proceeds.

In the case where all the oxidation products are removed (Figure 4.11a), the potential drops to -400 mv and the mineral itself begins to be reduced at C_2. When the polarity is reversed back in the anodic direction, arrest A_2 does not appear, presumably because reaction [4.16] is too sluggish to be detected at this applied current. Only plateaus A_3 and A_1 are observed during the subsequent oxidation.

The behavior of the electrode when the second anodic polarization is begun before all the oxidation products are removed (Figure 4.11b) is considerably different from that in the corresponding stage in Figure 4.11a. Since no Pb^o is produced during the cathodic polarization, arrests A_2 and A_3 do not appear. Instead, a plateau, A_4, due to the oxidation of H_2S to S^o (reaction [4.15]) is observed at approximately 125 mv. Previous evidence for this reaction appeared in the voltammogram presented in Figure 4.7.

Although this work has focused on the electrochemical reactions related to the solution and flotation chemistry of galena, consideration must also be given to reactions that do not involve electron transfer. These can be important not only for a more complete description of galena chemistry, but also for their influence upon the electrochemical reactions. One such reaction is the non-oxidative dissolution of galena to Pb^{2+} and H_2S (i.e., reaction [4.5]). Although the results of this study and others indicate that this does not contribute appreciably to the leaching of galena, at least in the environment of these tests, it is possible that the backward reaction may be significant. In fact, its occurrence may explain why reaction [4.15] is observed in certain

situations, but not in others.

As noted previously, reaction [4.15] is not observed when the reduction of PbS to Pb^o takes place even if the solution is unstirred. The reduction of PbS is the only way that lead metal enters the system. Furthermore, when the potential is in the vicinity of the lower limit, Pb^{2+} ions can only be generated via the reduction of galena [4.17]. Consequently, if the potential never reaches a value low enough for PbS to be reduced, then no Pb^{2+} ions will be present near the electrode surface. H_2S, then, can only be consumed by reaction [4.15] once the polarity of the current is reversed back in the anodic direction during the IGP tests or once the sweep is reversed again in the anodic direction during the voltammetry tests.

If the reduction of PbS to Pb^o and H_2S does take place, however, and this is followed by the oxidation of Pb^o to Pb^{2+}, the reverse of reaction [4.5] can proceed since Pb^{2+} and H_2S are now available. This reaction does not involve the transfer of electrons and so its occurrence is not directly visible on the voltammograms or the IGP diagrams. Nevertheless, it may remove all the H_2S from the electrode surface, thereby preventing reaction [4.15]. This would explain why the A_4 peak never appears when the A_3 peak does.

Figure 4.12 shows IGP diagrams for galena obtained under identical conditions to those of Figure 4.11, except that the solution was stirred. One major effect of stirring is that the point where the sudden drop in potential occurs during anodic polarization takes place earlier. Another is that the A_4 plateau does not appear in Figure

4.12b, as expected, since the flowing solution has swept all of the H_2S away from the electrode.

4.3.2 Voltammetry Experiments at pH 4.6:

The E_h-pH diagrams for Cases I, II and III (Figures 2.2, 2.6 and 2.11) indicate that the initial oxidation products of galena should be the same at pH 4.6 as at pH 1.1 In order to examine this and other aspects of the solution chemistry of PbS at pH 4.6, a series of voltammetry experiments were conducted on the electrode immersed in 0.5 M sodium acetate/0.5 M acetic acid buffer solutions.

Identification of peaks: Figure 4.13 shows the voltammograms obtained in stirred and unstirred solutions for an anodic limit of 645 mv and a cathodic limit of -755 mv. As is found at pH 1.1, stirring increases the oxidation rate of galena. Determination of the area under both curves in Figure 4.13 indicates that a balance between the anodic and cathodic charges exists. This observation supports the notion that galena is being oxidized to Pb^{2+} and S^o (reaction [4.2]). Charge analysis by Gardner and Woods (1979b) of their voltammograms has shown a similar result. Furthermore, Lamache et al. (1981) electrolyzed galena at a potential of 750 mv and determined the charge-to-metal ratio to have the value of 2 expected for reaction [4.2].

Upon reversal of the scan in the cathodic direction, a small peak, C_1, at -400 mv in addition to a much larger one at -600 mv appears only under quiescent conditions. Gardner and Woods (1979b) also observed this and attributed the small peak to the recombination of Pb^{2+} and S^o

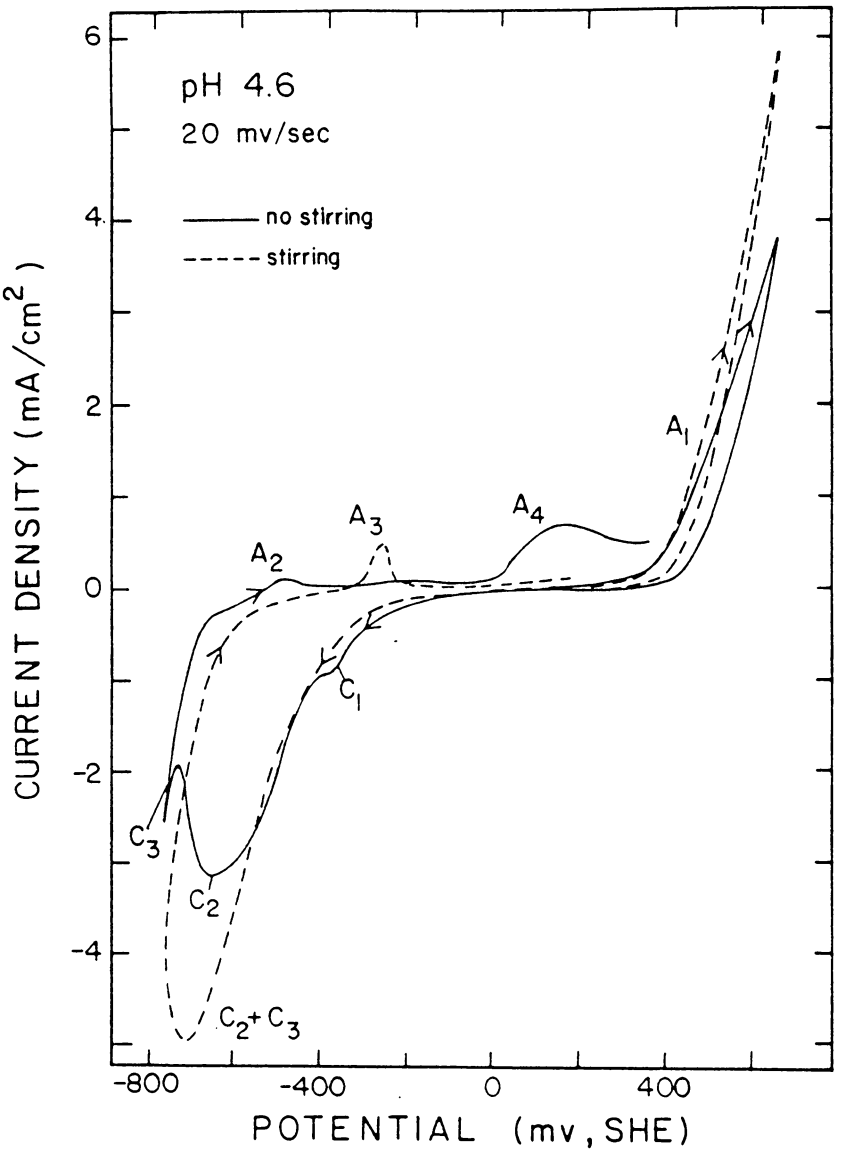


Figure 4.13 Effect of stirring on the single sweep voltammograms for a galena electrode immersed in a 0.5 M CH_3COOH/0.5 M CH_3COONa solution (pH 4.6). Potential scan between -755 and 645 mv. Scan rate = 20 mv/sec.

$A_1 = PbS/Pb^{2+},S^0$
$A_2 = Pb^0,H_2S/PbS$
$A_3 = Pb^0/Pb^{2+}$
$A_4 = H_2S/S^0$

$C_1 = Pb^{2+},S^0/PbS$
$C_2 = S^0/H_2S$
$C_3 = PbS/Pb^0,H_2S$

to form PbS (reaction [4.14]) and the larger one, C_2, to the reduction of S^o to H_2S (reaction [4.13]). Although these are the same reactions that they proposed for pH 1.1, the peaks become separated at pH 4.6 because the reversible potential of reaction [4.13] shifts with a pH change (59.1 mv/pH), whereas that of reaction [4.14] does not.

Beyond these peaks, the reduction of PbS via reaction [4.6] (C_3) occurs. In the unstirred case, there is some separation between the current rise for this reaction and that for C_2. However, when the solution is stirred, there is so much oxidation of the mineral that C_2 and C_3 probably overlap.

Again, as in the case of pH 1.1, stirring has a significant effect on the voltammogram during the second anodic-going sweep. Peaks A_2 and A_4 due to reactions [4.16] and [4.15], respectively, appear when there is no stirring, whereas only A_3 (reaction [4.17]) is detected under stirred conditions. The oxidation of Pb^o and H_2S to PbS (reaction [4.16]) begins at a potential of -540 mv compared to about -320 mv at pH 1.1 (see Figure 4.6). The difference of 220 mv agrees almost exactly with the value of 207 mv calculated on the basis of the Nernst equation for this reaction. Again, as is noted at pH 1.1, A_3 and A_4 do not appear on the same curve. It is interesting that there is no evidence of the oxidation of Pb^o to Pb^{2+} (reaction [4.17]) in the unstirred case, although some Pb^o has been generated by the reduction of PbS during the preceding cathodic sweep. Instead, a constant current flow of about 0.1 mA/cm^2 is observed in the potential region where A_3 would appear..

Because of the separation between C_3 and the other two cathodic peaks in the quiescent case, it is possible to estimate the cathodic charge associated with the removal of the oxidation products from the first anodic scan and compare it to the anodic charge passed. From the voltammogram shown in Figure 4.13, it has been determined that 45.5 mC/cm^2 of charge is passed during oxidation, whereas 45.0 mC/cm^2 is consumed during reduction. This is consistent with what would be anticipated if [4.2], [4.13] and [4.14] are, indeed, the reactions involved.

In order to estimate the charges in the stirred case, a different approach has been taken because of the overlap of the reduction peaks. If all of the Pb^o produced by the reduction of PbS is oxidized to Pb^{2+} at A_3 (it should be recalled, however, that this is generally not the case at pH 9.2), then the anodic charge associated with the latter reaction can be used as a measure of how much of the cathodic charge is associated with C_3. Since all the reactions involve the transfer of two Faradays of charge per gmole of lead reacted, then the charge for C_2 should be equal to the difference between the total cathodic charge passed (including the anodic-going portion) and the anodic charge due to A_3. Analysis of the voltammogram using this approach indicates that the charge due to C_2 is 72.6 mC/cm^2, compared to a value of 71.2 mC/cm^2 for the oxidation of PbS on the first scan. Considering some of the inaccuracies with this method, it can be seen that a charge balance exists.

The appearance of a peak (C_1) that can be attributed to reaction [4.14] at pH 4.6 may be one reason to suspect that it also proceeds at pH 1.1, in spite of the fact that no direct indication for this has been found at the lower pH. There is no obvious reason why this reaction should proceed at pH 4.6 but not at pH 1.1.

Previously, Gardner and Woods (1979b) had proposed that the direct reduction of S^o to H_2S occurs because there is always an excess of S^o over Pb^{2+} near the electrode surface whether the solution is being agitated or not. Thus, the complete disappearance of the C_1 peak under stirred conditions at pH 4.6 (Figure 4.13) results from the total removal of Pb^{2+} ions from the mineral surface. However, it can be argued that this disappearance is due to a change in the oxidation reaction occurring during the anodic scan. An experiment described below has been conducted to evaluate which of the two is more likely. The potential was swept to an upper limit of 545 mv before being reversed and brought down to about -625 mv in order to completely remove all the oxidation products. The electrolyte was left unstirred throughout this scan. This was followed by a second scan which was identical to the first in every respect except that stirring was begun when the potential reached a value of about 50 mv during the cathodic-going portion of the sweep.

As can be seen in Figure 4.14, stirring causes the C_1 peak to disappear, although the conditions under which galena has been oxidized (and the resulting current) are exactly the same in both scans. Therefore, the interpretation put forth by Gardner and Woods (1979b)

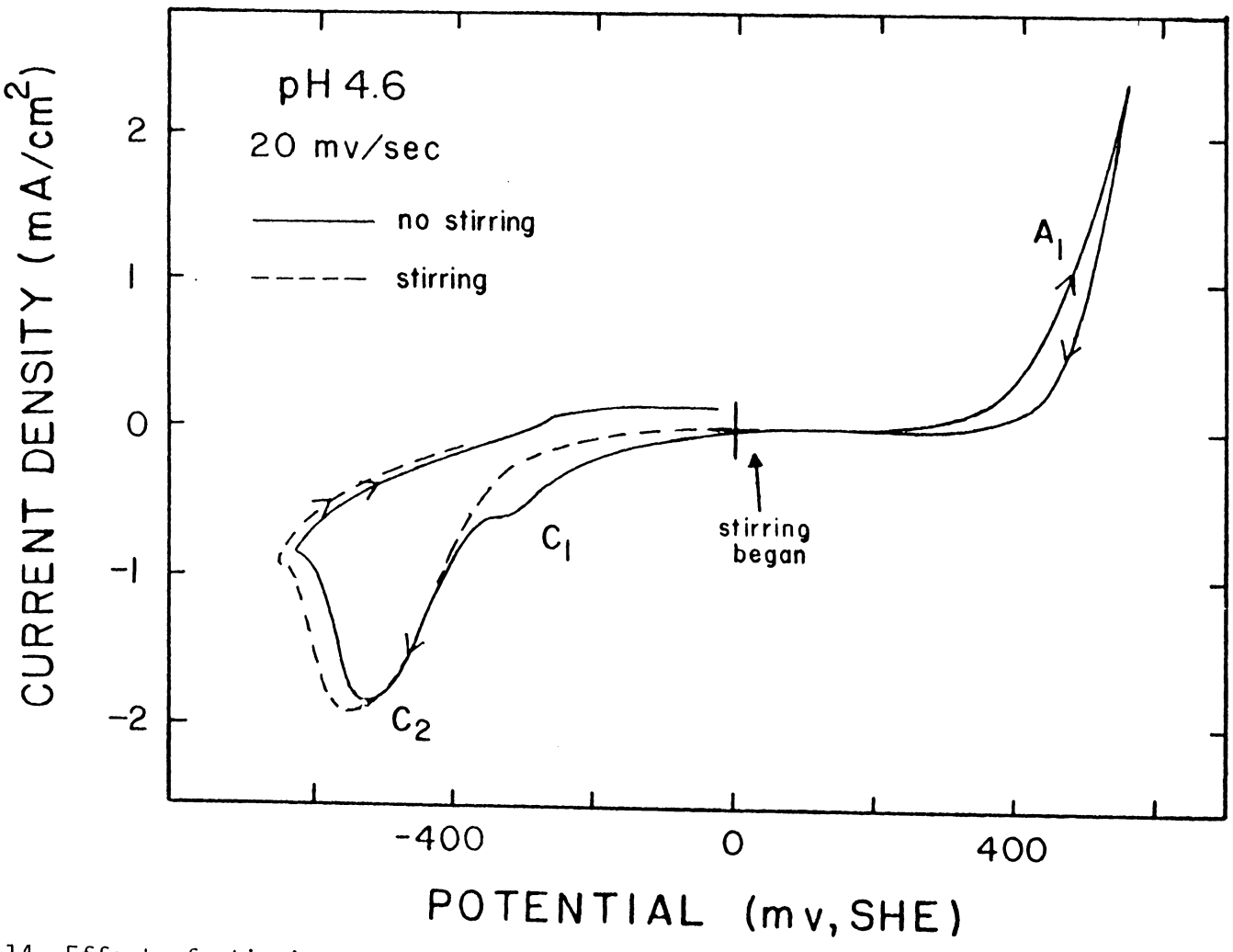


Figure 4.14 Effect of stirring on the cathodic portion of the single sweep voltammograms for a galena electrode immersed in a 0.5 M CH_3COOH/0.5 M CH_3COONa solution (pH 4.6). Potential scan between -625 and 545 mv. Scan rate = 20 mv/sec.

$A_1 = PbS/Pb^{2+},S^o$ $C_1 = Pb^{2+},S^o/PbS$ $C_2 = S^o/H_2S$

appears to be the correct one. Integration of the voltammograms indicates that the loss of 1.2 mC resulting from the disappearance of C_1 in the stirred case is exactly compensated by a 1.2 mC enlargement of C_2.

The information obtained from this experiment can also be used to estimate the relative amounts of current consumed by reactions [4.13] and [4.14] under quiescent conditions. The charge passed during the oxidation of the mineral is determined to be 7 mC. Assuming that all the oxidation products are removed by the time the cathodic limit is reached, then the fraction of the current due to reaction [4.14] is 1.2/7.0 or 0.17. This shows that even under relatively quiescent conditions, the reduction of S^o to H_2S (reaction [4.13]) is the predominant cathodic reaction. Evidently, a considerable amount of Pb^{2+} ions has diffused away by the time reduction commences and/or the kinetics of reaction [4.14] are slower than those of reaction [4.13].

Effect of anodic limit: The effect on the voltammograms of varying the anodic limit from 445 to 845 mv is shown in Figure 4.15. These experiments were carried out at a scan rate of 20 mv/sec in a stirred solution. The cathodic limit in each case was extended far enough to ensure that all the oxidation products were removed.

At the two highest anodic limits, a peak in the anodic rise at A_1 appears at approximately 650 mv, followed by a minimum at about 700 mv. Similar behavior has been observed at pH 1.1 (see Figure 4.7). Once again, it appears that the initial sulfur layer inhibits further oxidation. Enough has accumulated by 650 mv to cause the current to

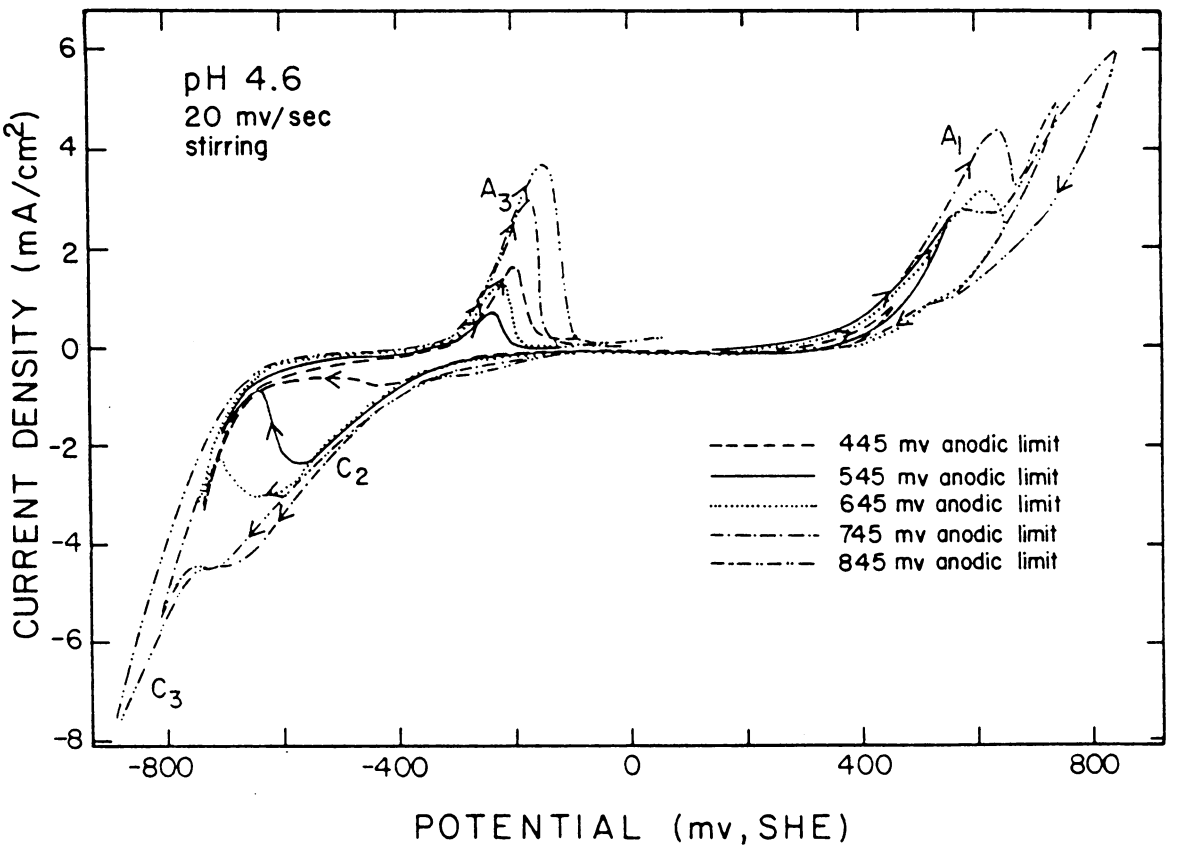


Figure 4.15 Effect of the anodic limit on the single sweep voltammograms for a galena electrode immersed in a stirred 0.5 M CH_3COOH/0.5 M CH_3COONa solution (pH 4.6). Scan rate = 20 mv/sec.

$A_1 = PbS/Pb^{2+}, S^o$ $\quad C_2 = S^o/H_2S$

$A_3 = Pb^o/Pb^{2+}$ $\quad C_3 = PbS/Pb^o, H_2S$

drop until the potential is raised another 50 mv.

Although the amount of oxidation increases with a rise in the anodic limit, the current rise from one test run to the next, particularly during the initial portion, is not as reproducible as in previous cases. This may be due to the fact that the initial oxidation is critically dependent upon the state of the electrode surface produced by polishing. Once some elemental sulfur covers the mineral, the effect may no longer be felt as strongly.

The integrated charges show that even at a potential as high as 845 mv, there is still a balance between the anodic and cathodic charges. This indicates that at pH 4.6, $S_2O_3^{2-}$ or SO_4^{2-} are not readily produced by the oxidation of galena.

Effect of scan rate: The effect of scan rate has also been investigated and the resulting voltammograms and integrated charges are presented in Figure 4.16 and Table 4.2. For the most part, increasing the scan rate increases the current densities. Furthermore, it tends to smooth out the maximum at about 600-650 mv during the anodic rise and shift it toward higher potentials.

It is not possible to separate the reduction of the oxidation products from that of the mineral itself on these curves. As has been done at pH 1.1, the anodic peak, A_3, due to the oxidation of Pb^o to Pb^{2+}, has been included in the charge analysis to determine how much of the cathodic charge can be attributed to C_2. (It should be noted that C_1 does not appear since the electrolyte is being stirred in this experiment.) The results of this analysis, given in Table 4.2, show

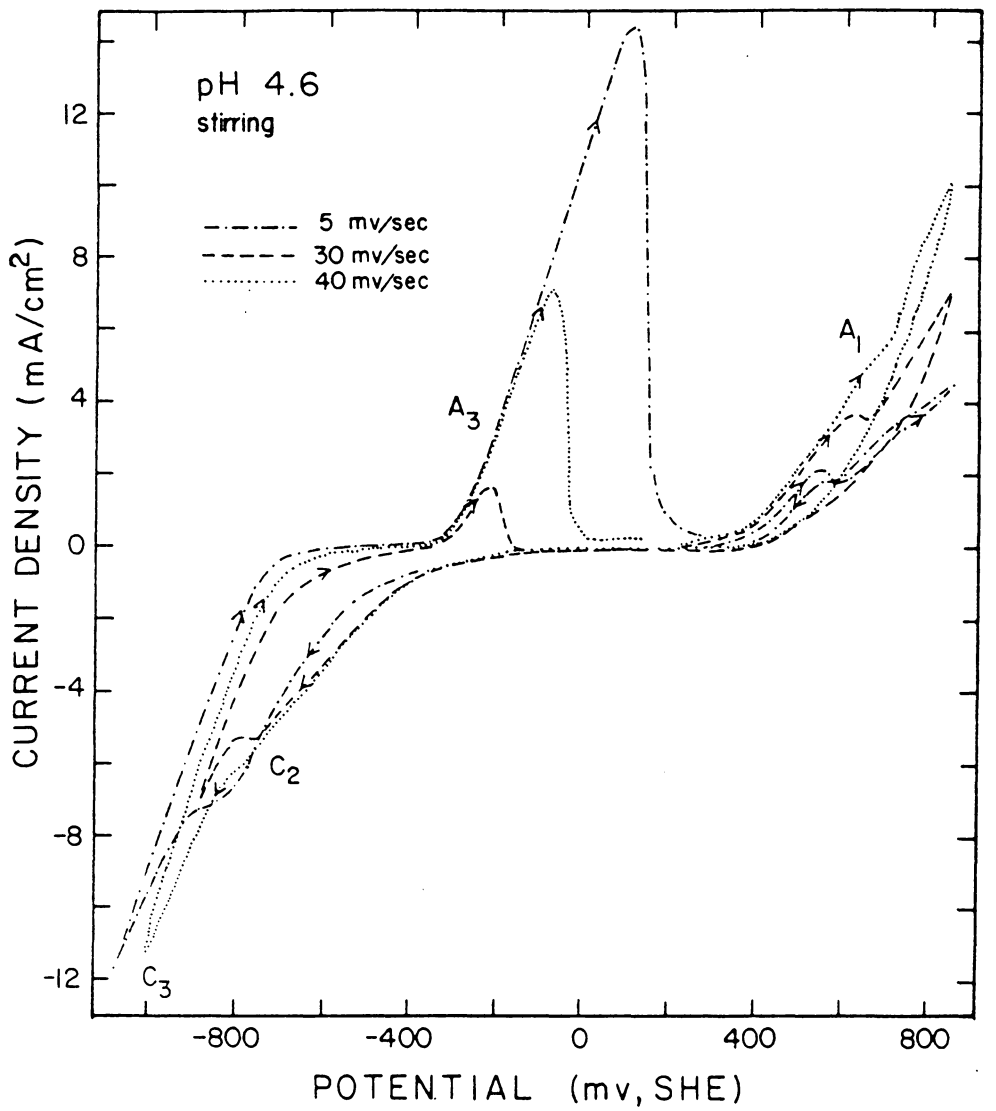


Figure 4.16 Effect of scan rate on the single sweep voltammograms for a galena electrode immersed in a stirred 0.5 M CH_3COOH/0.5 M CH_3COONa solution (pH 4.6).

$A_1 = PbS/Pb^{2+},S^o$ $C_2 = S^o/H_2S$

$A_3 = Pb^o/Pb^{2+}$ $C_3 = PbS/Pb^o,H_2S$

Table 4.2

The Effect of Scan Rate on the Anodic and Cathodic Charges at pH 4.6

Scan Rate (mv/sec)	Q_{A1} (mC/cm^2)	Q_{C2+C3} (mC/cm^2)	Q_{A3} (mC/cm^2)	Q_{C2} (mC/cm^2)
5	424.1	1123.1	701.9	421.2
10	237.1	457.9	218.8	239.1
20	118.8	142.1	23.6	118.5
30	90.0	89.5	5.2	84.3
40	94.3	124.5	29.0	95.5
50	67.1	76.2	7.4	68.8

that Q_{C2} remains equivalent to Q_{A1} regardless of the scan rate. Evidently, A_1 and C_2 can still be associated with reactions [4.2] and [4.13], respectively. The almost exact charge balance also strengthens the assumption that all the Pb^o generated by the reduction of galena at this pH is removed by the oxidation process at A_3.

The data in Table 4.2 also show that while the current density during the anodic sweep increases with scan rate, the amount of charge passed steadily diminishes. One reason for this behavior may be that the faster the potential is swept, the higher the initial rate of deposition and the less porous and more passivating the sulfur film becomes. Another reason may be that dissolution of galena is not rapid enough to keep up with the decrease in time permitted for oxidation as the sweep rate increases.

Another interesting observation concerning the voltammograms in Figure 4.16 is that at the slowest speed (5 mv/sec), the current is greater during the negative-going portion of the anodic scan than during the positive-going part. The reverse is true for the higher sweep rates. Gardner and Woods (1979b) noticed the same phenomenon at pH 1.1 and attributed it to a change in the nature of the sulfur deposition process. This will be discussed in more detail in Chapter V.

Effect of Pb^{2+} concentration: In a typical industrial leaching situation where the surface area of the galena is as high as is feasible, there will be a gradual build-up of the dissolved lead concentration as the process continues. Consequently, it is important

to study the effect of dissolved lead upon the solution chemistry of galena. Accordingly, experiments have been conducted in 10^{-3} and 10^{-2} M lead acetate solutions.

Figures 4.17 and 4.18 show current-potential curves for anodic limits of 545 and 645 mv obtained in both unstirred and stirred 10^{-3} M Pb^{2+} solutions. The addition of lead appears to have several important consequences. Comparison of the current densities in these figures with those in Figure 4.14 indicates that the oxidation rate of galena is lowered in the presence of Pb^{2+} ions. This is consistent with what has previously been reported by Paul et al. (1978).

A second observation is that stirring no longer increases the anodic current, regardless of whether the potential is swept up to 545 or 645 mv. In these experiments, the surface concentration of Pb^{2+} will always be at least 10^{-3} M whether the solution is stirred or not. As has just been mentioned, the presence of these ions retards the oxidation rate. However, it would be expected that increasing the concentration beyond a certain level will no longer inhibit oxidation any further. If 10^{-3} M is greater than this critical amount, then the effect of stirring in removing excess Pb^{2+} from the surface will no longer be felt.

Another effect of the presence of dissolved lead is that the C_1 peak appears in both stirred and unstirred cases. This provides further support that this peak should be identified with the reaction between Pb^{2+} and S^o to form PbS.

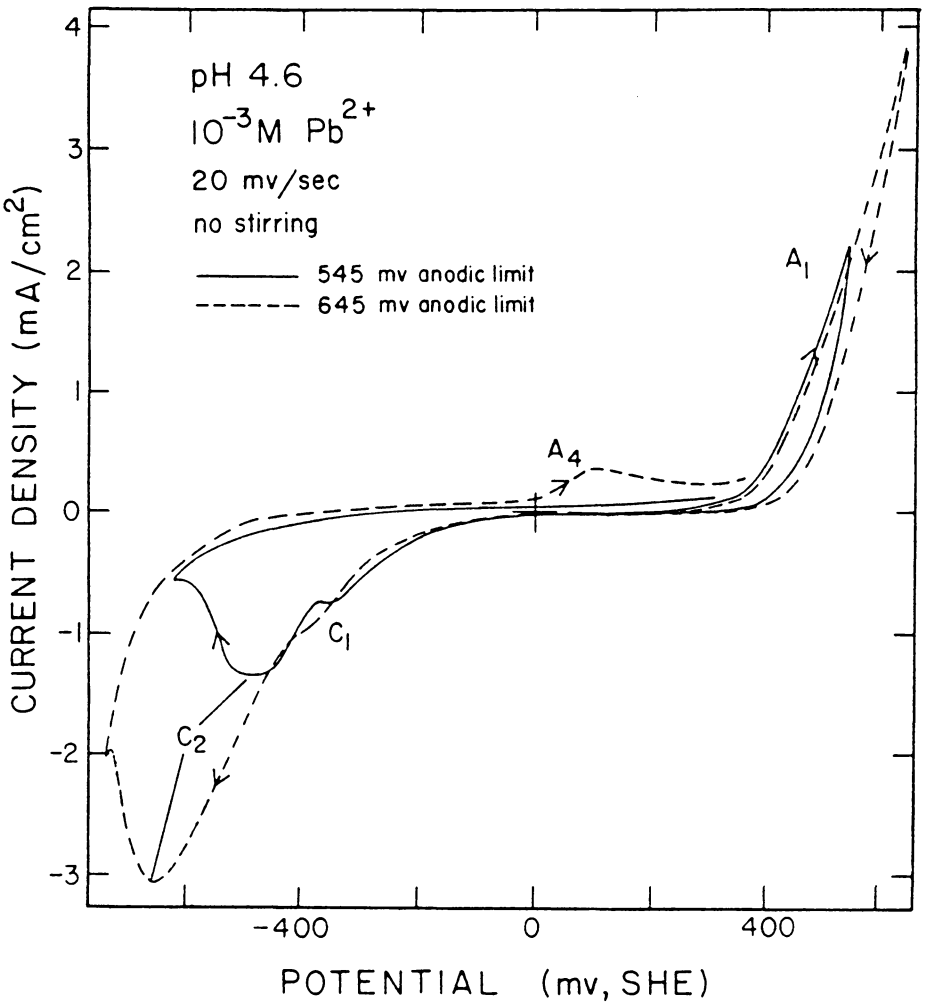


Figure 4.17 Effect of anodic limit on the single sweep voltammograms for a galena electrode immersed in an unstirred 0.5 M CH_3COOH/0.5 M CH_3COONa (pH 4.6) + 10^{-3} M Pb^{2+} solution. Scan rate = 20 mv/sec.

$A_1 = PbS/Pb^{2+},S^o$ $\quad$ $C_1 = Pb^{2+},S^o/PbS$

$A_4 = H_2S/S^o$ $\quad$ $C_2 = S^o/H_2S$

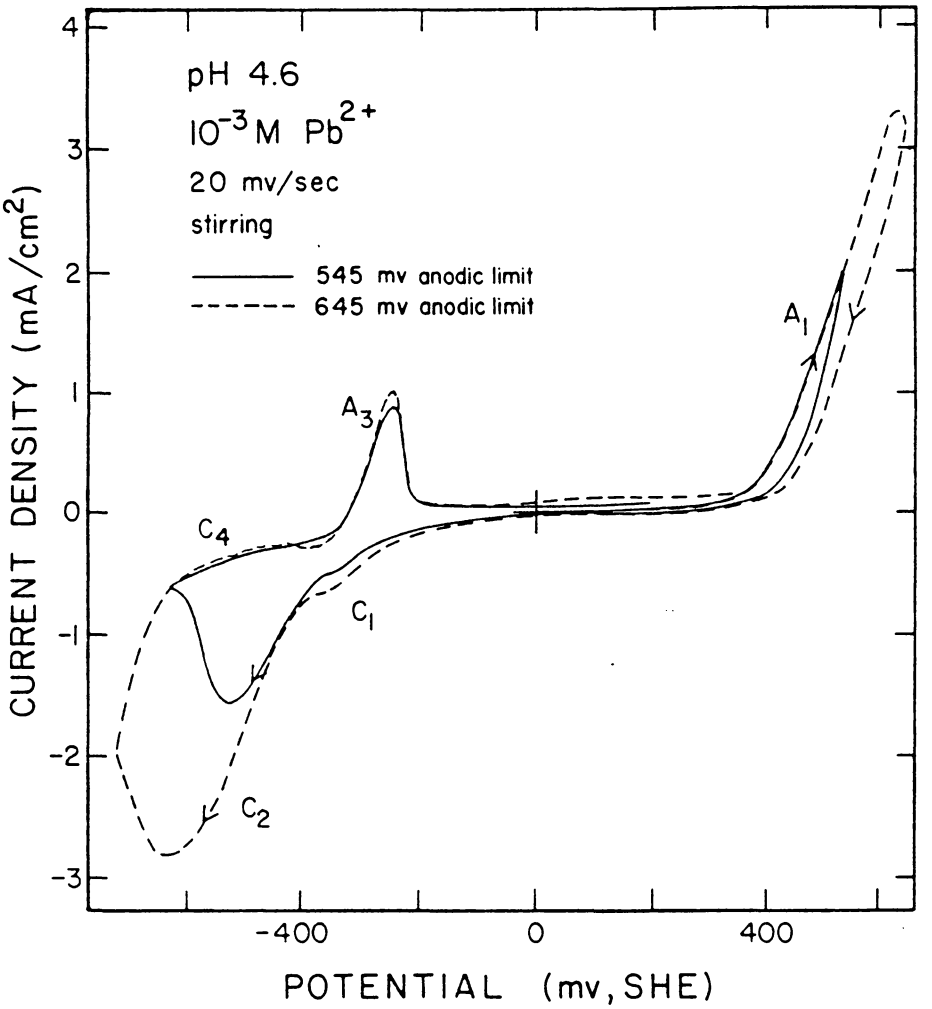


Figure 4.18 Effect of anodic limit on the single sweep voltammograms for a galena electrode immersed in a stirred 0.5 M CH_3COOH/0.5 M CH_3COONa (pH 4.6) + 10^{-3} M Pb^{2+} solution. Scan rate = 20 mv/sec.

$A_1 = PbS/Pb^{2+},S^0$

$A_3 = Pb^0/Pb^{2+}$

$C_1 = Pb^{2+},S^0/PbS$

$C_2 = S^0/H_2S$

$C_4 = Pb^{2+}/Pb^0$

Once the lower potential limit is reached and the scan direction is reversed, there is a difference in the behavior of the current in the potential range from -550 to -200 mv, depending on whether the solution is being stirred or not. In the case of the stagnant solution (Figure 4.17), little cathodic current flows from approximately -550 to -330 mv and the Pb^{o}/Pb^{2+} anodic peak does not appear above -330 mv. However, when the solution is agitated, a virtually constant current density of about -0.4 mA/cm^2 is observed until about -330 mv, whereupon the current rises sharply to form the Pb^{o}/Pb^{2+} peak. There are several reasons to believe that the elemental lead being oxidized does not originate from the reduction of galena, but from a cathodic reaction, C_4, occurring from -550 to -330 mv on the second anodic-going sweep. For one thing, measurement of the charges associated with the anodic and cathodic current rises on the voltammograms in Figures 4.17 and 4.18 shows that by the time the lower potential limit is reached, galena reduction has not yet occurred to an appreciable extent. For another, the amount of charge associated with the Pb^{o}/Pb^{2+} peak (~ 1.2 mC) is virtually the same as the amount passed between -550 and -330 mv.

The most likely cathodic reaction that occurs at C_4 is the deposition of the added plumbous ions as lead metal (i.e., reaction [4.18]). It is also significant that the current signal for this reaction is noisy when the solution is being stirred, but smooth when the solution is stagnant. This is indicative of a reaction that is diffusion-controlled. Stirring will continually replenish the Pb^{2+} ions at the electrode, resulting in a current that, on the average, is

constant but periodically fluctuates. In the absence of any agitation, the supply of Pb^{2+} ions to the mineral surface will not be fast enough to sustain the reaction at an appreciable rate. Consequently, the current density will diminish to zero, as is observed in Figure 4.17.

The results of the voltammogram for 10^{-3} M Pb^{2+} in Figure 4.18 can be used to estimate the diffusion boundary layer thickness for the deposition of lead onto galena. Assuming that the process is entirely mass transfer-controlled and that the boundary layer thickness remains constant, then the limiting current density, i_d, for the deposition can be expressed as:

$$i_d = \frac{nFD_{Pb}\, C_{Pb}^*}{\delta}, \qquad [4.19]$$

where n = number of electrons transferred

F = Faraday constant

D_{Pb} = diffusion coefficient of Pb^{2+} ions

C_{Pb}^* = bulk Pb^{2+} concentration

δ = diffusion boundary layer thickness.

This equation can be used to calculate δ once i_d, n, D_{Pb} and C_{Pb}^* are known. In this case, n and C_{Pb}^* are equal to 2 and 10^{-3} M, respectively. Diffusion coefficients for ions in aqueous solutions are typically on the order of 10^{-5} cm^2/sec (Geiger and Poirier, 1973). A value of 0.4 mA/cm^2 can be used for i_d on the basis of the constant current density obtained for the deposition of lead from the voltammogram in Figure 4.18. Substituting these parameters into equation [4.19], $\delta \sim 0.5$ microns is obtained. Such a boundary layer

thickness is reasonable for flowing systems (Vetter, 1967).

It is also interesting to note that the deposition of lead only begins after the elemental sulfur oxidation product is removed during the cathodic-going scan. Since sulfur is passivating, Pb^{2+} ions would have to diffuse through this layer to the unreacted PbS core in order to be reduced to elemental lead. This process is certain to be slow and, consequently, will only commence once the oxidation products have been removed.

One would expect that the reversible potential for the Pb^{o}/Pb^{2+} couple should correspond to the potential on the voltammogram where the current abruptly changes from cathodic to anodic flow on the second anodic-going scan. However, the value obtained from Figure 4.18, i.e., -320 mv, is about 110 mv more negative than the Nernst potential of -210 mv calculated for $[Pb^{2+}] = 10^{-3}$ M.

The H_2S/S^{o} oxidation peak, A_4, appears in one of the voltammograms obtained in a stagnant solution (i.e., the one with a cathodic limit of -750 mv), but not in the other (i.e., -600 mv cathodic limit). In light of the previous discussion concerning this reaction, it is surprising that the behavior of these two is different. The previous results from the voltammetry and IGP experiments have shown that when Pb^{2+} ions are produced from the oxidation of elemental lead, the oxidation of H_2S to S^{o} does not occur (section 4.3.1b). Consequently, one would expect the A_4 peak to be suppressed when the electrolyte contains 10^{-3} M Pb^{2+}.

In order to look more closely at the effect of the state of the mineral surface on the deposition of elemental lead on galena,

voltammograms were obtained both in the presence and absence of 10^{-3} M Pb^{2+} when the limit during the first anodic-going scan was only 345 mv (Figure 4.19). Comparison of these results with those in Figure 4.18 clearly shows that the presence of oxidation products on galena suppresses deposition. When little or no oxidation is allowed to take place prior to reduction, elemental lead begins to be deposited as soon as the potential drops below about -300 mv during the cathodic-going scan. When the electrode is oxidized prior to the cathodic scan, deposition only begins after elemental sulfur has been removed from the surface.

It should also be noted that the reduction of galena itself commences at -600 mv no matter whether there is dissolved lead in solution or not. Apparently, the occurrence of reaction [4.18] does not interfere with reaction [4.6] at this Pb^{2+} concentration.

When the dissolved lead concentration is raised to 10^{-2} M, the results given in Figure 4.20 are obtained. The oxidation of galena is not enhanced by agitation, as was found for 10^{-3} M Pb^{2+}. Furthermore, the anodic current is essentially the same as at the lower lead concentration. Both these observations are consistent with the previous discussion that the bulk concentration of Pb^{2+} ions is high enough that there might be no further inhibition of reaction [4.2].

With a reversal of the scan direction, the current-potential curves are drastically different from what has appeared previously. The cathodic peak due to the Pb^{2+},S^{o}/PbS reaction is observed at approximately -350 mv, as in the case of 10^{-3} M Pb^{2+}, in all three

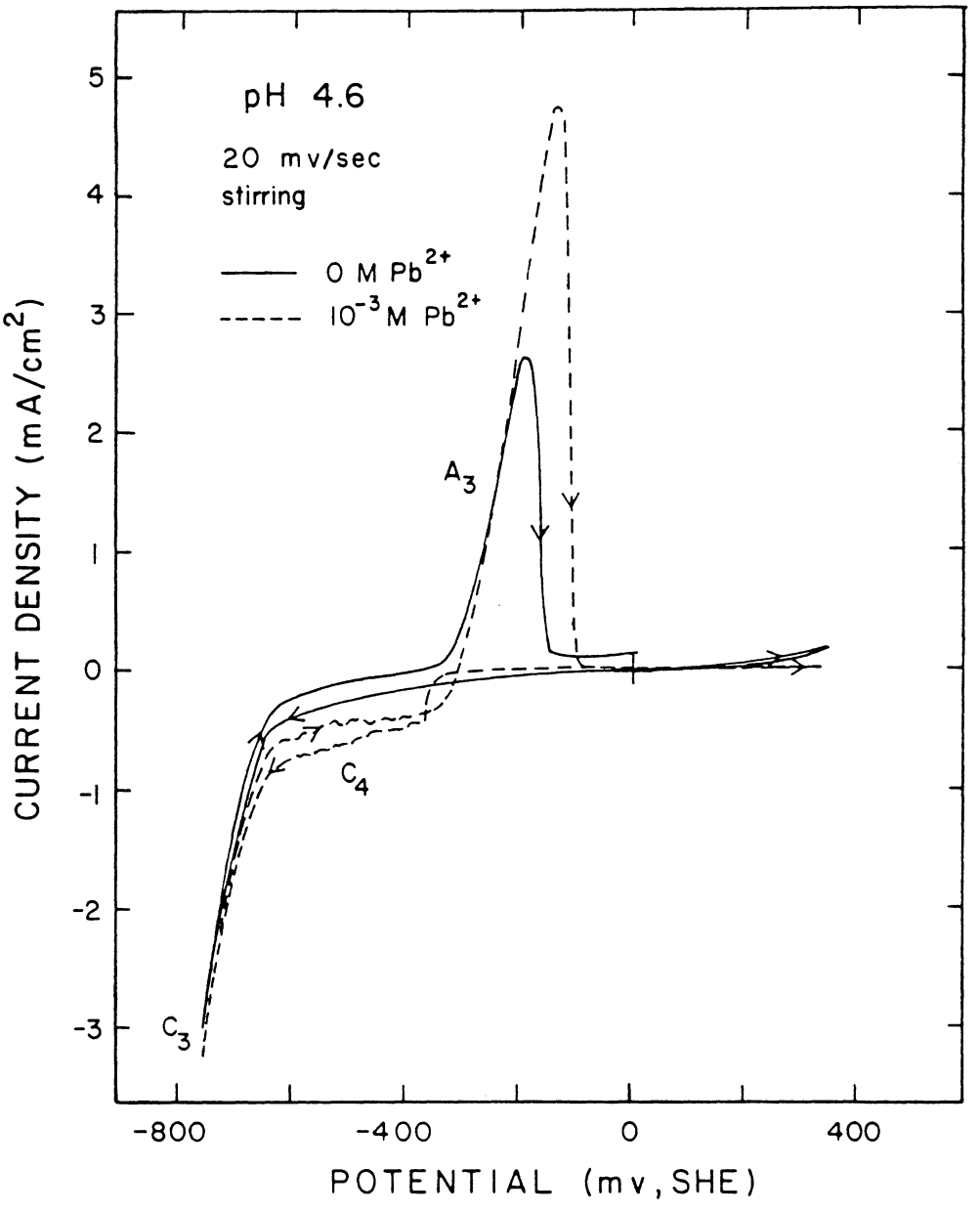


Figure 4.19 Effect of Pb^{2+} ion addition on the cathodic portion of the single sweep voltammograms for a galena electrode immersed in a stirred 0.5 M CH_3COOH/ 0.5 M CH_3COONa solution (pH 4.6). Scan rate = 20 mv/sec.

$A_3 = Pb^0/Pb^{2+}$ $C_3 = PbS/Pb^0, H_2S$ $C_4 = Pb^{2+}/Pb^0$

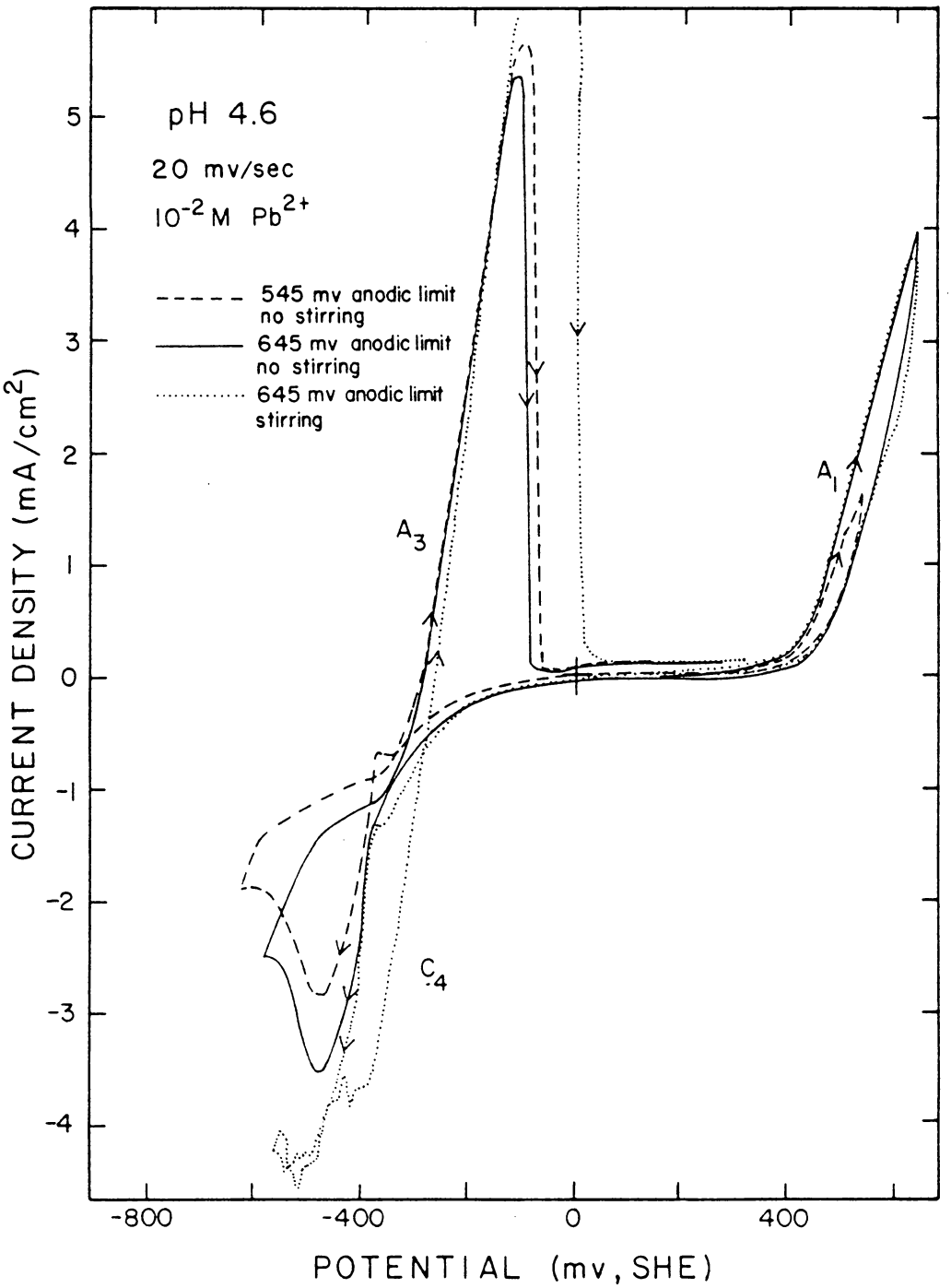


Figure 4.20 Effect of anodic limit and stirring on the single sweep voltammograms for a galena electrode immersed in a 0.5 M CH_3COOH/0.5 M CH_3COONa (pH 4.6) + 10^{-3} M Pb^{2+} solution. Scan rate = 20 mv/sec.

$A_1 = PbS/Pb^{2+},S^0$ $\quad A_3 = Pb^0/Pb^{2+}$ $\quad C_4 = Pb^{2+}/Pb^0$

voltammograms in Figure 4.20. However, just beyond this, the cathodic current rises sharply, although in quite a different manner depending on whether the solution is stagnant or not. The current density in the stirred case is greater and displays a noisy signal as the potential drops below -400 mv. Also, when the potential is reversed back in the anodic-going direction, the current is greater than it is in the first direction. This behavior is strongly suggestive of the diffusion-controlled deposition of lead under stirred conditions. Without stirring, the cathodic current increases to a maximum at about -500 mv before diminishing as the potential approaches the lower limit. The shape of these curves is very characteristic of that obtained for diffusion-controlled reactions under stagnant conditions. Further evidence that lead is being deposited is that there is a tremendous growth in the A_3 peak when the scan is reversed back in the anodic direction.

Unlike what is noted at 10^{-3} M Pb^{2+}, the deposition of lead apparently begins before all the sulfur from the preceding oxidation is removed since no separate peak, C_2, for the reduction of S^o to H_2S is visible. Apparently, the concentration of lead ions is high enough to overcome the diffusional barrier of the sulfur layer. It is also possible that the reduction of the oxidative products from the anodic scan is occurring simultaneously with deposition, although this is not obvious from the voltammograms.

4.3.3 Effect of Open-Circuit Potential on the Dissolution of Galena:

a. In 1 M $HClO_4$ solution (pH 0): One of the interesting aspects of the work by Brodie (1969) was his investigation of the relation between the rest potential of the galena electrode and the amount of Pb^o and S^o on the mineral surface and the dissolved lead concentration.

A galena electrode was electrolyzed cathodically at a current density of 1 mA/cm^2 for about one hour. This reduced galena and left a layer of lead metal on the mineral surface. The electrode was then transferred to a fresh, deaerated 1 M $HClO_4$ solution and electrolyzed anodically at 1 mA/cm^2. The current was periodically switched off and both the rest potential and the dissolved Pb^{2+} concentration were monitored over time. Brodie's results are shown in Figure 4.21.

In the early stages of the electrolysis, the rest potential remained almost constant in the range of -270 to -240 mv, while the Pb^{2+} concentration increased from 2.5 to 20 ppm. Beyond this point, the rest potential began to rise sharply as the lead concentration levelled off at about 28 ppm (or 1.3×10^{-4} M). This continued until a potential of about 200 mv was reached, whereupon $[Pb^{2+}]$ began to increase sharply again with small changes in the rest potential. Brodie was able to match the flat portions of the curve with the equilibrium potentials for the reactions,

$$PbS = Pb^{2+} + S^o + 2e, \qquad [4.2]$$

above E_h = 240 mv, and

$$Pb^o = Pb^{2+} + 2e \qquad [4.17]$$

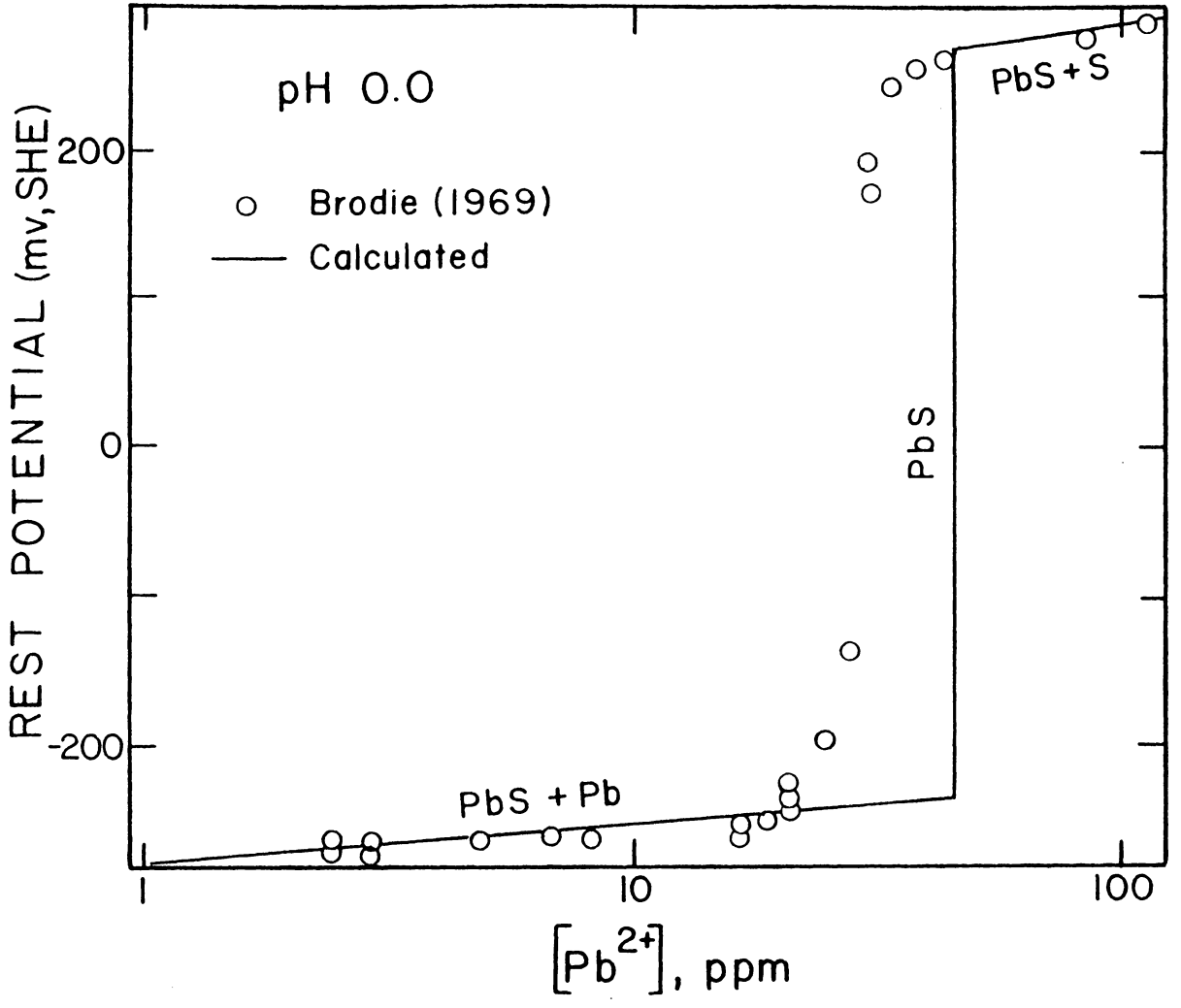


Figure 4.21 Relation between the open-circuit potential and dissolved lead concentration obtained for a galena electrode immersed in a stirred 1 M $HClO_4$ solution (pH 0.0). Experimental data (o) reproduced from Brodie (1969). Calculated curve (—) determined from the computations of this study.

below E_h = -240 mv.

Furthermore, Brodie concluded that the rapid change in rest potential between these potential limits is due to slight changes in the amounts of elemental sulfur and lead on the galena surface as the mineral is anodized. At -240 mv, the surface is saturated with lead (a_{Pb^o} = 1) and reaction [4.17] is potential-determining. As anodic current continues to be applied, the lead is depleted and this causes a_{Pb^o} to drop rapidly and the rest potential to rise steeply. As this is happening, a_{S^o} increases sharply as minute amounts of elemental sulfur are formed due to reaction [4.2], until it becomes unity when E_h = 240 mv. Brodie pointed out that this can occur at an essentially constant Pb^{2+} concentration because a lead (or sulfur) variation of only about 10^{-6} mole percent in composition of galena represents the difference between sulfur saturation and lead saturation.

Since one of the output variables from the thermodynamic calculations done in this study (Chapter II) is the Pb^{2+} concentration, the relationship between E_h and the predicted $[Pb^{2+}]$ can be compared to that determined experimentally. However, in conducting his test, Brodie altered the lead-sulfur stoichiometry when he removed the galena electrode from the original solution after cathodically polarizing it. Consequently, the mass balance calculations must be modified from the ones done in Chapter II to take into account the change in stoichiometry.

The lead and sulfur mass balance equations can be written as:

$$\text{lead:} \quad n_{PbS} + \Sigma(Pb) = N_{Pb} \qquad [4.20]$$

$$\text{sulfur:}\quad n_{PbS} + \Sigma(S) = N_S. \qquad [4.21]$$

Subtracting one from the other yields the relation:

$$\Sigma(Pb) - \Sigma(S) = N_{Pb} - N_S. \qquad [4.22]$$

The right-hand side of this expression is no longer equal to zero, but instead is equivalent to the number of moles of PbS, X_{Pb}, that has been converted to Pb^o during the cathodic polarization. The solution of Eq. [4.22] is simplified considerably when it is realized that at pH 0, Pb^{2+} and H_2S are the predominant lead- and sulfur-bearing dissolved species, respectively:

$$[Pb^{2+}] - [H_2S]_{aq} - [H_2S]_g = X_{Pb}. \qquad [4.23]$$

Substitution of the equilibrium relationship between $[Pb^{2+}]$ and $[H_2S]$ for reaction

$$Pb^{2+} + H_2S = PbS + 2H^+ \qquad [4.5]$$

results in the expression,

$$[Pb^{2+}] - \frac{1.828\times10^{-8}}{[Pb^{2+}]} = X_{Pb}, \qquad [4.24]$$

which can readily be solved if X_{Pb} is known. According to his experimental procedure, Brodie cathodically polarized the galena electrode at 1 mA/cm^2 for one hour. Assuming a current efficiency of

100% for the reduction of galena, a value of 1.27×10^{-4} gmoles/liter for X_{Pb} is estimated. Equation [4.24] is then solved to obtain a value of $[Pb^{2+}]$ of 2.1×10^{-4} M or 44.1 ppm when PbS is the lone stable solid. It should be noted that the amount of dissolved lead remains constant throughout this region.

The calculated relation between E_h and $[Pb^{2+}]$ is plotted in Figure 4.21, along with the experimentally determined one. Although the theoretical curve is consistent with the experimental data in that it shows a potential range from about -240 to 240 mv where galena is electrochemically inactive, it predicts the mineral solubility to be about twice as large as it actually is. Some factor other than thermodynamics is apparently controlling the concentration at which the open-circuit potential begins to rise steeply.

Just what this factor is becomes more obvious when it is noted that this concentration coincides closely with the value of X_{Pb}. Dissolution of galena under the conditions of the experiment is likely occurring in the following manner. As long as elemental lead is present on the mineral surface, the application of anodic current causes it to dissolve reversibly according to the Pb^{o}/Pb^{2+} couple. When the final amount of lead is just removed, the newly exposed PbS surface will be at a potential much too low for oxidation. Any further anodic polarization will cause the electrode potential to rise quickly until it reaches a value where another faradaic process that generates electrons, i.e., reaction [4.2], can begin. Apparently, the non-oxidative dissolution reaction [4.5] does not occur fast enough for $[Pb^{2+}]$ to reach the

thermodynamically predicted value of 44.1 ppm in the time it takes the electrode potential to reach 240 mv. The match between the calculated line and the data points obtained by Brodie beyond 240 mv indicates that reaction [4.2] proceeds reversibly.

b. In 0.1 M $HClO_4$ solution (pH 1.1): An experiment similar to that performed by Brodie was conducted on the galena electrode immersed in a 0.1 M $HClO_4$ solution at pH 1.1. The procedure followed in this study was modified, however, in an effort to preserve the lead-sulfur stoichiometry in the system. By doing this, it would be appropriate to compare the subsequent experimental data with the results of the thermodynamic calculations described in Chapter II. After immersing the mineral in a stirred, deoxygenated 400-ml solution, sparging with N_2 was discontinued in order to minimize any leaks of H_2S gas to the atmosphere. The galena was then cathodically polarized with a current of -0.6 mA for 75 minutes. Once this was done, periodic anodic pulses were applied in the same manner as described in the previous section. However, unlike the earlier case, the electrode was kept immersed in the same electrolyte in which it had been cathodically polarized.

An "open" test, in which sparging was continued throughout, was also performed. It was thought that comparison of open- and closed-system data might provide insight into the nature of the potential-determining reactions involved in the dissolution of lead at this pH.

The results of the calculations for Cases I, II and III and the electrochemical experiments are superimposed in Figure 4.22. Although there is qualitative agreement between the experimental and the

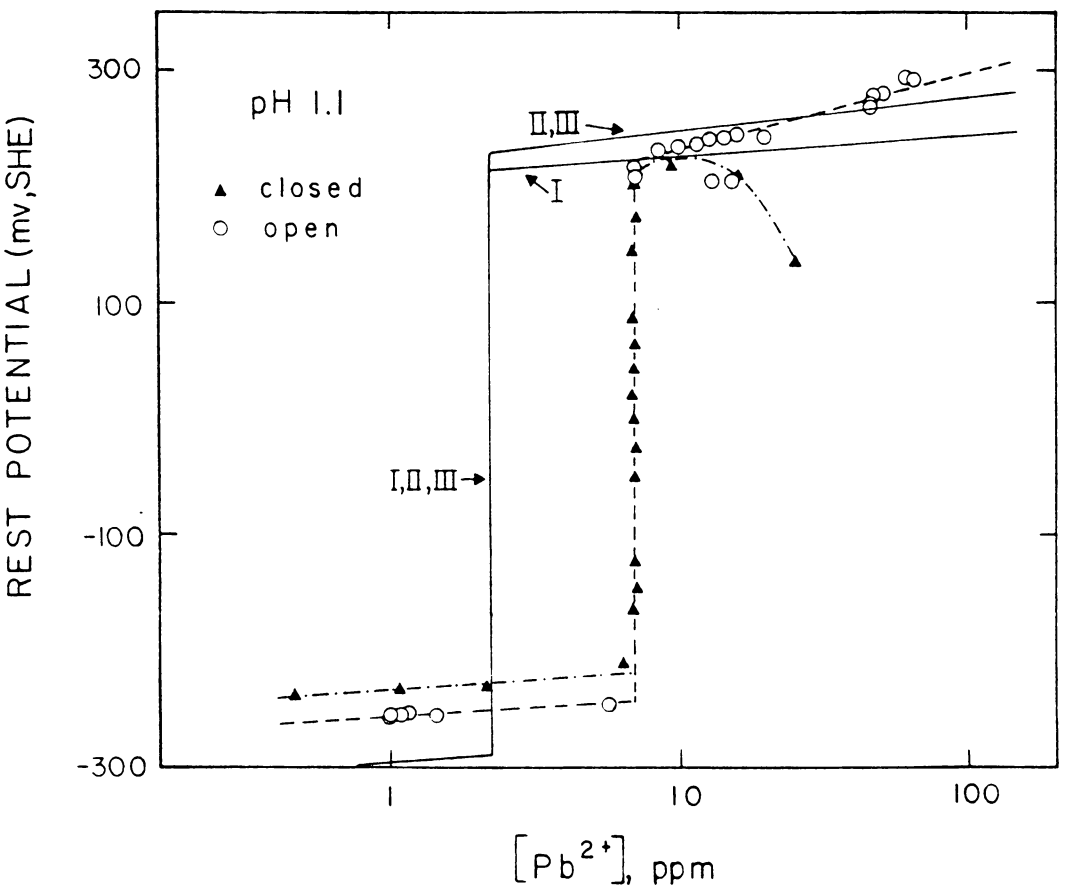


Figure 4.22 Relation between the open-circuit potential and dissolved lead concentration obtained for a galena electrode immersed in a stirred 0.1 M $HClO_4$ solution (pH 1.1). Cell contents either closed (▲) or open (o) to atmosphere during experiments. Roman numeral next to each solid curve denotes the case number for the corresponding calculations.

calculated curves, there is less quantitative agreement than in the case at pH 0.0. The electrode potential is lower than the value predicted by the calculations when Pb^{o} is on the mineral surface. Furthermore, along the vertical portion of the curve from -250 to 225 mv, the theoretical lead concentration of 2.2 ppm is more than three times smaller than that of the closed test. Agreement is good between 225 and 250 mv, but beyond this, the difference begins to increase again.

The amount of charge that has been consumed during the cathodic polarization of the electrode at -0.6 mA for 75 minutes corresponds to 2.7 coulombs. Assuming once again that all this charge goes into the reduction of galena, then $[Pb^{2+}]$ should be 7.3 ppm when the entire lead layer on the galena has been dissolved away by the anodic polarization. This agrees well with the observed concentration along the vertical portion of the curve, as is the case at pH 0.0. Apparently, dissolution proceeds by a similar mechanism as at the lower pH, i.e., the electrode behaves entirely as a lead electrode as long as any lead is present on the surface and then quickly (and spontaneously) reverts to its galena character when the final amount of metal has been removed.

One thing that the results of this test indicate is that the relation between E_h and $[Pb^{2+}]$ when reaction [4.2] or [4.17] is occurring cannot be described as Nernstian nearly as well at pH 1.1 as at the lower pH. It is also interesting that the data obtained from the open test are closer to the theoretical values along the lower portion of the curves in Figure 4.22 than are those of the closed test. One reason for this is that the electrolyte was not sparged during the

closed test and some oxygen may have leaked into the system. This would result in the anodic shift in the open-circuit potentials for this test that is observed.

c. In 0.5 M CH_3COOH/0.5 M CH_3COONa solution (pH 4.6): The experimental results for an open test done at pH 4.6 are shown in Figure 4.23 and are compared with those of the computations in Table 4.3. As can be seen, the measured concentrations are orders of magnitude higher than the calculated ones in the potential range studied.

The curve indicates that as lead is dissolving, the potential remains constant at approximately -340 mv. This behavior differs from that for pH 0.0 and 1.1 where an increase in potential is observed during this stage of oxidation. Since the electrode was cathodically polarized for one hour with an applied current of -0.65 mA, a dissolved lead concentration of 6.3 ppm would be expected, assuming 100% current efficiency for reaction [4.6]. However, from the curve in Figure 4.23, it can be seen that the solubility reaches only 4.8 ppm. This discrepancy can likely be attributed to the fact that another reduction reaction, e.g.,

$$2H^+ + 2e \longrightarrow H_2, \qquad [4.7]$$

is occurring along with galena reduction during the cathodic polarization. At pH 0 and 1.1, the reduction of galena may proceed fast enough that hydrogen evolution does not interfere. However, increasing the pH to a value of 4.6 may slow the rate sufficiently that

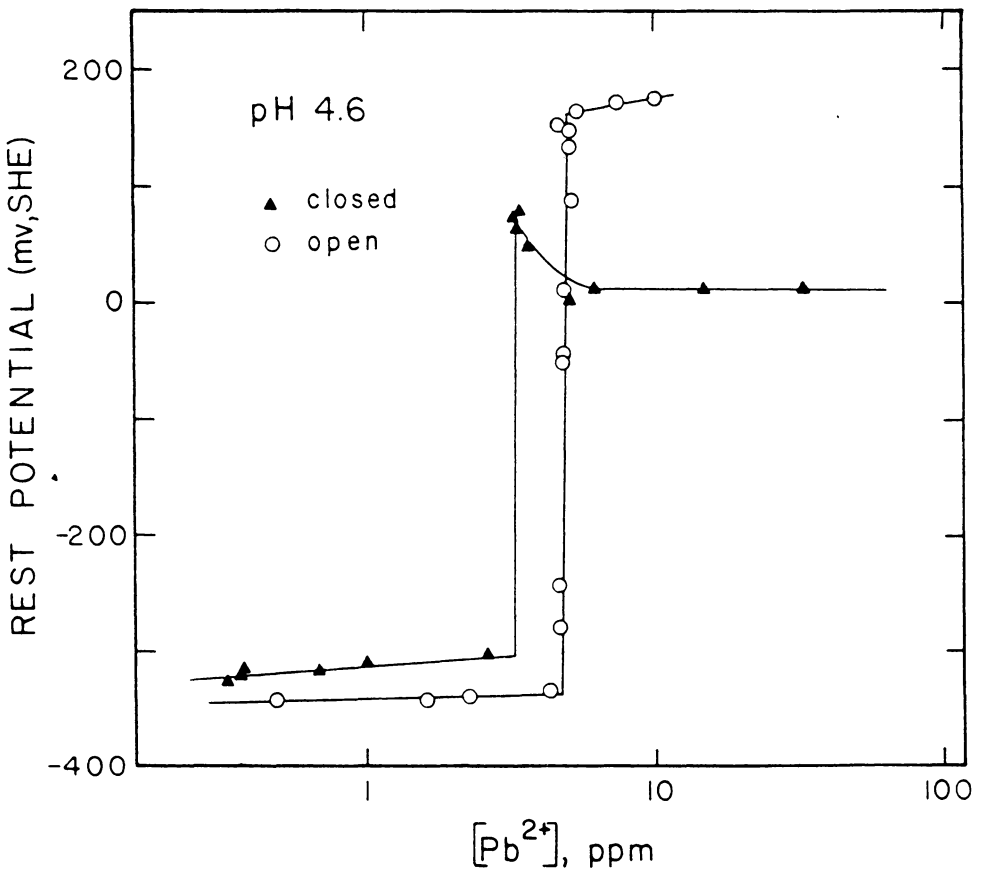


Figure 4.23 Experimental relation between the open-circuit potential and the dissolved lead concentration obtained for a galena electrode immersed in a stirred 0.5 M CH_3COOH/ 0.5 M CH_3COONa solution (pH 4.6). Cell contents either closed (▲) or open (o) to atmosphere during experiments.

Table 4.3

Dissolved Lead Concentration as a Function of Rest Potential at pH 4.6

Potential (mv, SHE)	Observed $[Pb^{2+}]$ (ppm)	Calculated $[Pb^{2+}]$ (ppm)
-342	0.48	7.1×10^{-4}
-342	1.62	7.1×10^{-4}
-339	2.28	7.1×10^{-4}
-334	4.34	7.1×10^{-4}
-280	4.63	7.1×10^{-4}
-244	4.59	7.1×10^{-4}
- 50	4.79	7.1×10^{-4}
- 40	4.88	7.1×10^{-4}
11	4.81	7.1×10^{-4}
89	5.20	
133	5.05	
149	5.03	5.0×10^{-3}
154	4.58	
157	4.78	
163	5.51	
172	7.34	2.4×10^{-2}
175	10.00	
200		0.25
250		12.26

about 25% of the applied current is consumed by reaction [4.7].

Comparison of Figure 4.23 with 4.22 shows that there is a cathodic shift in the lines corresponding to reactions [4.2] and [4.17] by about 80 mv to 100 mv with an increase in pH from 1.1 to 4.6. Essentially no shift is observed from pH 0.0 to 1.1. Any pH dependence is somewhat surprising since no protons are involved in either of these reactions. It should be recalled, however, that the possibility that oxygen reduction is also occurring to a certain extent has been mentioned in the previous section. Such a reaction might impart a pH dependence to the open-circuit potential.

4.4 Summary

At pH 1.1 and 4.6, the oxidation of galena results in the formation of only Pb^{2+} and S^o, at least up to a potential of 845 mv. There is strong evidence that the mechanism for dissolution changes at about 650 mv. No evidence for the presence of the thermodynamically more favored $S_2O_3^{2-}$ or SO_4^{2-} has been found at either pH.

The pH does seem to affect which reactions occur to remove the species generated during the anodic polarization. At pH 1.1, the voltammograms suggest that only one cathodic reaction, the reduction of S^o to H_2S, proceeds even when the solution is stagnant. At pH 4.6, however, two cathodic reactions are observed under quiescent conditions: the recombination of Pb^{2+} and S^o to PbS and the reduction of S^o to H_2S.

The addition of 10^{-3} or 10^{-2} M Pb^{2+} to the electrolyte at pH 4.6 slows the rate at which galena is oxidized. Furthermore, the Pb^{2+} ions

that are introduced will begin to be reduced to lead metal and to deposit on the mineral surface when the potential falls below about -330 mv. At 10^{-3} M Pb^{2+}, this will begin only after any elemental sulfur from previous oxidation is removed first; at 10^{-2} M Pb^{2+}, this process can begin before all the sulfur has disappeared, however.

The experiments designed to determine the relation between the open-circuit potential and the dissolved lead concentration indicate that the system deviates farther and farther from reversible behavior as the pH is increased from 0 to 4.6. Whereas the oxidation of Pb^{o} to Pb^{2+} and of PbS to Pb^{2+} and S^{o} obeys the Nernst equation quite closely at pH 0, the observed and calculated lead concentrations are orders of magnitude apart by pH 4.6. Furthermore, as long as any lead metal is present on the galena surface, the surface seems to act as a lead electrode and does not seem to be affected by the PbS beneath or the H_2S in solution.

CHAPTER V.

POSSIBLE MECHANISMS FOR GALENA OXIDATION AND XANTHATE ADSORPTION

5.1 Introduction

5.1.1 General

It was mentioned in Section 1.1 that one thing in common between the flotation and leaching of sulfides is that both involve oxidation reactions. Although other aspects of galena chemistry are important, these anodic processes are of greatest interest to flotation chemists and hydrometallurgists. The emphasis that has been placed on oxidation throughout the present work reflects this point of view.

As a way of highlighting some of the main findings of this study, Chapter V will include a discussion of possible mechanisms of galena oxidation and xanthate adsorption at pH 9.2 and 6.8 on the basis of data gathered here and elsewhere. Much of this section will be based upon a quantitative analysis of the data obtained from the chronoamperometry experiments that have been described in Chapter III (Sections 3.3.1d, 3.3.1h and 3.3.2f).

This section will be followed by another that deals with the oxidation of galena at low pH. The discussion will be of a more qualitative nature than the previous one.

5.1.2 Electronic Properties of Galena

As in the case of the other transition metal sulfides, the chemical bonding between lead and sulfur in galena is primarily covalent in

character. Although natural galena usually exhibits n-type semiconducting properties, it can remain stable over rather wide ranges of non-stoichiometry, and so p-type samples are not too uncommon (Vaughan and Craig, 1978). PbS also has a narrow band gap, which is generally accepted to be 0.41 ev (Vaughan and Craig, 1978), and usually has a high concentration of charge carriers. Richardson and O'Dell (1984) have recently conducted Hall effect measurements on a galena specimen from the same deposit as the one used in this study (i.e., Brushy Creek, Missouri). They reported that this sample was highly n-type and had a high carrier concentration of 2×10^{18} cm^{-3}.

These properties give galena its relatively low resistivity of 1×10^{-5} - 7×10^{-6} ohm-m (Shuey, 1975). The high carrier concentration also reduces the thickness of the space charge layer within the mineral to a very narrow region beneath the surface (Tributsch and Gerischer, 1976). Consequently, it becomes possible for the mineral surface to assume a potential very close to the value applied to the bulk of the electrode. Furthermore, narrowing the space charge layer increases the probability that electrons can tunnel across the solid/liquid interface from the electron-donor to the electron-acceptor. It is this effect which enables electron transfer reactions to occur on a semiconductor surface since tunneling is the only way in which electrons can cross the interface at room temperature. An applied electrode potential can therefore raise or lower the Fermi level in the solid and become the driving force for these reactions.

5.2 Galena Oxidation and Xanthate Adsorption at pH 9.2 and 6.8

5.2.1 Galena Oxidation at pH 9.2

Chronoamperometry and voltammetry are techniques that complement each other very well. Although voltammetry is very effective for delineating possible reaction steps and detecting reaction intermediates, it does not lend itself easily to mathematical analysis. The mathematical treatment of chronoamperometry, on the other hand, is considerably more straightforward. Consequently, it can be useful for testing mechanisms that have been suggested by another technique such as voltammetry.

The main objective of this section will be to propose a reaction mechanism for the oxidation of galena at pH 9.2 on the basis of the results of the chronoamperometry experiments described in Section 3.3.1d. Most attention will be focused on the initial stages of oxidation. At the outset, it should be emphasized that the amount of data on which this analysis is based is not large. Consequently, the conclusions that will be drawn should be considered as tentative and should be subject to further evaluation.

The results of the voltammetry and IGP experiments indicate that PbO, S^o and $S_2O_3^{2-}$ are the bulk oxidation products formed at pH 9.2. At the same time, the data also suggest that below a potential of 500 mv, oxidation of sulfur predominantly proceeds to the formation of S^o. Since the primary interest of this discussion is in the initial stages of oxidation, the quantitative analysis will consider only the formation of PbO and S^o.

a. Mechanism for initial stages of galena oxidation: One reaction mechanism for the initial stages of oxidation under closed circuit conditions that can then be envisaged involves the anodic adsorption of OH^- ions onto surface lead sites:

$$PbS + OH^- \underset{k-1}{\overset{k_1}{\rightleftharpoons}} \overline{Pb\text{—}(OH)S} + e \qquad [5.1]$$

$$\overline{Pb\text{—}(OH)S} + OH^- \underset{k-2}{\overset{k_2}{\rightleftharpoons}} \overline{PbO} + \bar{S}^o + H_2O + e \qquad [5.2]$$

The bar indicates that the species is still part of the PbS lattice and not a separate phase. The electronic structure of these species will be somewhere between that of PbS and of PbO and S^o.

The electrons released by steps [5.1] and [5.2] will originate from the highest energy states in the valence band. Correlation of XPS spectra data (McFeely et al., 1973) with molecular orbital cluster calculations (Hemstreet, 1975) shows that these energy states come primarily from S_{3p} atomic energy levels. A decrease in the charge density associated with these orbitals will cause the Pb—S bonds to weaken and, at the same time, enable sulfur atoms to overlap more strongly with each other. Viewed this way, oxidation at pH 9.2 is a process that involves the continual weakening of Pb—S bonds and the strengthening of Pb—O and S—S bonds.

Bulk $\overline{PbO}$ and $\bar{S}^o$ will nucleate when clusters of PbO and S^o reach critical sizes n_1 and n_2, i.e.,

$$(\overline{PbO})_{n_1} \longrightarrow n_1 PbO \qquad [5.3]$$

$$(\overline{S^o})_{n_2} \longrightarrow n_2 S^o \qquad [5.4]$$

Combination of reactions [5.1] - [5.4] yields the overall reaction:

$$PbS + 2OH^- \longrightarrow PbO + S^o + H_2O + 2e. \qquad [5.5]$$

It should be emphasized that the $\overline{PbO}$ and $\overline{S^o}$ are not static entities. As the clusters grow in size, the electronic charge distributions around the atoms will approach that of the bulk phases PbO and S^o.

Although the proposed reactions appear differently from the one proposed by Hamilton and Woods (1984) for the formation of a metal-deficient sulfide (reaction [2.41]), the mechanisms are actually quite similar. However, it is more convenient to express the process in the form of equations [5.1] - [5.3] for the purpose of doing a quantitative kinetic analysis.

Anodic adsorption of oxygen and some organic species onto platinum has often been found to obey the Elovich rate equation (Feldberg et al., 1963; Gilman, 1964; Bagotskii and Vasiliev, 1964; Biegler and Koch, 1967; Reddy et al., 1968; Vetter and Schultze, 1972a,b; Gilroy, 1976). It has been shown (Biegler and Koch, 1967) that an Elovich-type equation can be derived by making a simplification of a rate expression corresponding to Temkin adsorption behavior. When a species chemisorbs onto a surface, the free energy of adsorption often decreases with coverage. The Temkin model takes this into account by assuming that the

surface is uniform, but that the standard free energy of adsorption is a linear function of coverage. Since reactions [5.1] and [5.2] that have been proposed for the initial oxidation of galena are adsorption processes, it will be interesting to determine if the oxidation below 300 mv follows Elovich behavior.

Expressions for the current densities of reactions [5.1] and [5.2] for Elovich conditions can be written as follows:

$$i_1 = Fk_1C_{OH} \exp\left(\frac{\beta_1 FE}{RT}\right) \exp\left(-\alpha_1 f_1 \theta_1\right) -$$

$$F\, k_{-1} \exp\left[\frac{-(1-\beta_1)FE}{RT}\right] \exp\left[(1-\alpha_1)\, f_1 \theta_1\right] \qquad [5.6]$$

$$i_2 = Fk_2C_{OH} \exp\left(\frac{\beta_2 FE}{RT}\right) \exp\left(\alpha_1 F_1 \theta_1\right) \exp\left(-\alpha_2 F_2 \theta_2\right) -$$

$$Fk_{-2} \exp\left[\frac{-(1-\beta_2)FE}{RT}\right] \exp\left[-(1-\alpha_1) f_1 \theta_1\right] \exp\left[(1-\alpha_2)\, f_2 \theta_2\right] \qquad [5.7]$$

where k_1, k_{-1}, k_2, k_{-2} = rate constant

β_1, β_2 = transfer coefficient

α_1, α_2 = symmetry factor

f_1, f_2 = heterogeneity factor

C_{OH} = concentration of OH^- ion at electrode

E = electrode potential

θ_1, θ_2 = fraction of surface occupied by $\overline{\text{Pb–(OH)S}}$ and $\overline{\text{PbO}}$, respectively, at time t.

The heterogeneity factors, f_1 and f_2, are proportionality constants between the free energies of adsorption for reactions [5.1] and [5.2], respectively, and the corresponding surface coverages.

The use of the Elovich model assumes that the oxidation is entirely activation-controlled and not limited by mass transfer. Furthermore, if it can be assumed that reaction [5.1] is the slow step and that the backward rate of this reaction is much smaller than the forward rate, then the total current density, i, becomes:

$$i = 2i_1 = 2Fk_1C_{OH} \exp\left(\frac{\beta_1 FE}{RT}\right) \exp\left(-\alpha_1 f_1 \theta_1\right). \qquad [5.8]$$

Equation [5.8] is not in a convenient form to be applied to chronoamperometry since i is not an explicit function of t. However, Biegler and Koch (1967) have derived an expression equivalent to this in which 1/i is a linear function of t, i.e.,

$$\frac{1}{i} = \frac{1}{2Fk_1C_{OH} \exp\left(\frac{\beta_1 FE}{RT}\right)} + \frac{\alpha_1 f_1 t}{2q_s} \qquad [5.9]$$

where q_s = saturation coverage by $\overline{Pb\text{—}(OH)S}$ (mC/cm^2). A plot of 1/i versus t can, therefore, be used as a test for this mechanism. Furthermore, if a linear relationship is found to exist, then numerical values for the kinetic parameters can be determined. $\alpha_1 f_1$ can be determined directly from the slope, β_1 from the potential dependence of the intercept and k_1 also from the intercept once β_1 is known.

In Figure 5.1, 1/i is plotted versus t from the data obtained for potential steps to 145, 245, 345 and 495 mv. In all cases, the experimental points fall along a straight line for values of t above about 1 second. The deviation below t = 1 sec is not that surprising since a large portion of the initial current is due to double layer charging, and not to the faradaic process. In addition, the accuracy of the data obtained during this period when the current is changing so rapidly is limited by the response of the strip chart recorder. Therefore, no attempt has been made to interpret the initial electrode response. Although not shown in Figure 5.1, the points also begin to deviate from linearity above about t = 10 sec. Apparently, after some time, oxidation no longer proceeds as a surface reaction and/or mass transfer becomes significant.

Straight lines have been drawn through points using a least-squares fit. The slopes and intercepts of the lines are listed in Table 5.1, along with the regression coefficients. According to equation [5.9], the straight lines should be parallel since the slope $m = \alpha_1 f_1/2q_s$ is independent of potential. Although this is true for the data at 145 and 245 mv, the lines at the higher potentials are much flatter. The difference in the slopes probably reflects that the reaction mechanism is no longer the same at these potentials.

The fact that the lines for 145 and 245 mv are parallel suggests that oxidation at these two potentials can be described by equation [5.9]. From the slope and the intercepts of these plots, the kinetic parameters are determined to be:

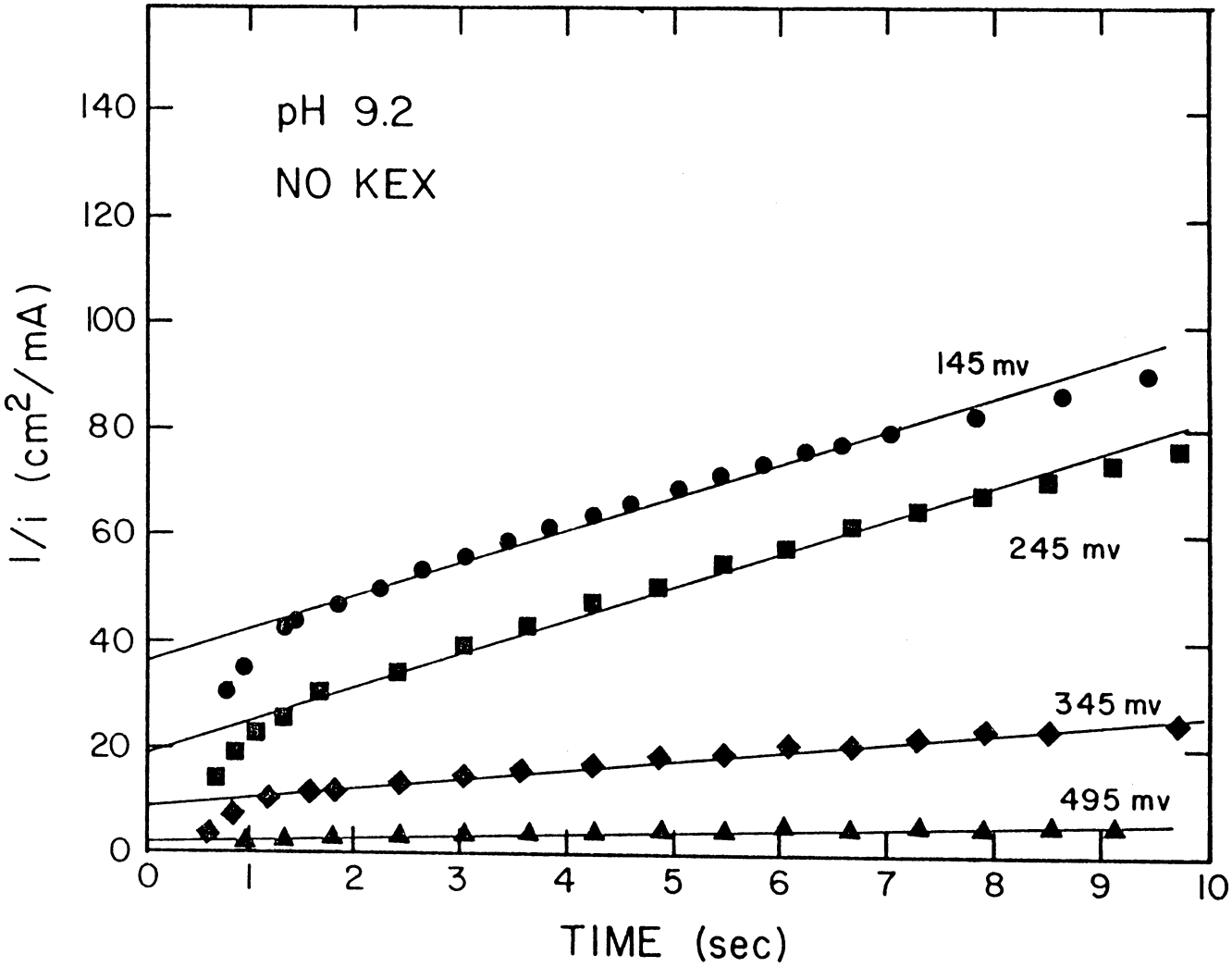


Figure 5.1 Plot of 1/i versus time for the chronoamperometry data obtained for the galena electrode in an unstirred 0.05 M $Na_2B_4O_7$ solution (pH 9.2).

Table 5.1

Fit of Chronoamperometry Data for Galena Oxidation at pH 9.2
According to an Equation of the Form 1/i = mt + b

Potential (mv, SHE)	m (cm^2/mC)	b (cm^2/mA)	r
145	6.32	36.10	0.993
245	6.51	18.61	0.998
345	1.82	8.77	0.993
495	0.43	2.31	0.997

$k_1 = 3.47 \times 10^{-3}$ cm/sec; $\beta_1 = 0.17$; and $\alpha_1 f_1/q_s = 12.83$ cm^2/mC.

A transfer coefficient of $\beta_1 = 0.17$ is considerably lower than the value of 0.5 that is customarily assumed. However, values of about 0.2-0.3 have commonly been observed for reactions involving crystallization and dissolution (Vetter, 1967) and for reactions occurring on oxide-covered electrodes (Vijh, 1973). Recently, McMillan et al. (1982) have reported similar values for the anodic dissolution of n- and p-type chalcopyrite.

The most successful explanation of anomalously low β values is the dual-barrier model proposed by Meyer (1960). If an insulating film is present on an electrode, a portion of the applied potential operates across the film and, hence, is not available to drive the charge transfer reaction. Meyer (1960) took this into account by considering that two activation barriers exist: i) the electric field due to the double layer on the solution side of the interface (this is the one encountered in all electron transfer reactions), and ii) the electric field due to the potential drop across the film.

As mentioned previously, the mechanism proposed for galena oxidation involves the adsorption of an OH^- ion and the discharge of an electron from the PbS lattice. However, the transport of the electron back into the bulk of the electrode will be retarded as $\overline{PbO}$ and $\bar{S}^o$ (and eventually PbO and S^o) form on the surface. This will reduce the apparent transfer coefficient, β_1, from the value corresponding to an unoxidized surface. Meyer (1960) derived an expression for β_1 for steady state conditions, which for single-charge carriers becomes:

$$\beta_1 = \frac{\beta_f \beta_s}{\beta_f + \beta_s} , \qquad [5.10]$$

where β_f is the transfer coefficient for electron transport through the oxidized layer and β_s is the transfer coefficient for the transport of OH^- ions through the solution double layer. This equation predicts that the observed β_1 will generally be smaller than either β_f or β_s.

b. Formation of bulk oxidation products: The voltammograms in Figure 3.9 show that the current rises slowly up to a potential of about 300 mv and then begins to rise much more sharply thereafter. A sudden increase in the amount of $S_2O_3^{2-}$ being produced would have such an effect since its formation involves the transfer of 4 Faradays/gmole PbS. However, the charge analysis in Table 3.3 indicates that no such increase in the amount of $S_2O_3^{2-}$ is occurring. It is more likely that the increase in the current can be attributed to the nucleation of bulk PbO and S^o phases. Once bulk phases have formed, subsequent oxidation should likely occur at a faster rate since it involves the incorporation of the oxidation products into existing PbO and S^o lattices.

The decrease in the slopes of the lines for 345 and 495 mv may therefore be related to the fact that bulk PbO and S^o phases are being formed. One model that has been proposed for the growth of oxide films on metals is the place-exchange mechanism (Lanyon and Trapnell, 1955; Reddy et al., 1968; Vetter and Schultze, 1972b; Angerstein-Kozlowska et al., 1973). According to this model, some of the oxygens (or hydroxyls) exchange positions with the metal beneath them, resulting in

an alternating structure (Figure 5.2b) rather than the one with a regular array (Figure 5.2a). It is believed that this rearrangement lowers the energy of the surface structure and makes it more difficult to remove. A similar mechanism may also apply for the oxidation of galena at 345 and 495 mv since it also predicts the linear relationship between 1/i and t that is observed in Figure 5.1.

An argument against the comparison of the oxidation of PbS with that of Pb^0 can be raised since it ignores the presence of sulfur. It should be pointed out, however, that bulk PbO and S^0 are likely to nucleate and grow in patches on the surface, as was mentioned previously. Consequently, sulfur may not have a significant influence on the growth of the PbO clusters.

c. Thiosulfate formation: Recently, there has been a great deal of interest in determining whether thiosulfate is being formed during the oxidation of galena, both in the absence and presence of xanthate (Pritzker and Yoon, 1984b; Lamache et al., 1984; Guy and Trahar, 1984). Aqueous sulfur chemistry is very complicated and only partially understood at the present time.

Two paths exist for the oxidation of sulfide sulfur to thiosulfate:

i) conversion of the elemental sulfur resulting from the initial oxidation of galena via a reaction such as:

$$2S^0 + 3OH^- \longrightarrow S_2O_3^{2-} + 3H^+ + 4e, \qquad [5.11]$$

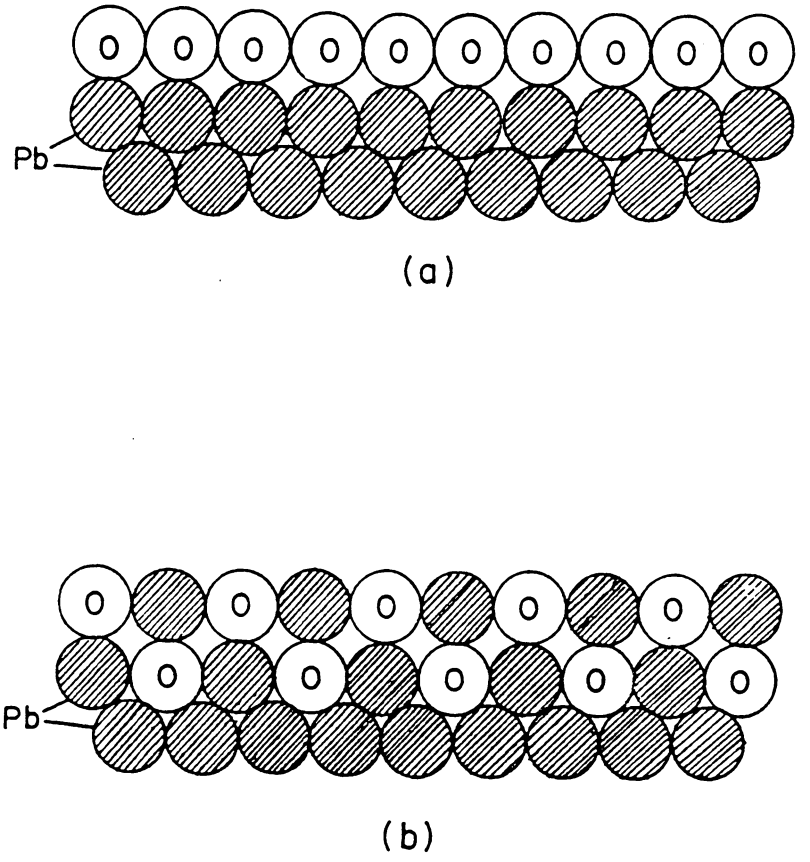


Figure 5.2 Possible arrangement of oxygen on the lead surface after oxidation:
(a) Regular array in which oxygens are on the same side of the interface;
(b) Alternating array after some oxygens have exchanged places with lead cations.

ii) direct oxidation of sulfide from the galena lattice via a reaction such as:

$$2PbS + 5OH^- \longrightarrow 2PbO + S_2O_3^{2-} + 5H^+ + 8e. \qquad [5.12]$$

The charge analysis of the voltammograms in Chapter III is not affected by which path oxidation proceeds because the overall amount of charge that is transferred remains the same in both cases.

Numerous investigations have shown that once elemental sulfur is present, it is not easily oxidized to any oxy-sulfur species (Avrahami and Golding, 1968; Najdeker and Bishop, 1973; Tributsch and Gerischer, 1976; Wiersè et al, 1978; Hamilton and Woods, 1983). Therefore, it is more likely that thiosulfate will be formed directly from sulfide (reaction [5.12]) than from elemental sulfur unless high overpotentials are applied.

It should be recalled that the charge analysis of the voltammograms in Section 3.3.1a has shown that the $n_{S_2O_3^{2-}}/n_{S^o}$ ratio remains constant at about 0.1 until a potential of 500 mv is reached. Beyond this potential, the amount of thiosulfate increases rapidly. This is not the type of behavior that can be easily explained if thiosulfate is being generated by a single reaction mechanism. However, it can be understood if thiosulfate is being produced by two independent reactions, such as [5.11] and [5.12]. Below 500 mv, oxidation can proceed by the direct attack of PbS (reaction [5.12]); above 500 mv, it can occur by both oxidation of S^o and direct attack of PbS.

The separation of thiosulfate formation according to these two reactions might also explain why $n_{S_2O_3^{2-}}/n_{S^o}$ is independent of potential below 500 mv. If reaction [5.11] is occurring, then this ratio will be expected to increase with potential. However, if S^o and $S_2O_3^{2-}$ are being formed by parallel and independent reactions [5.5] and [5.12], then the ratio will remain constant as long as the reaction rates have a similar potential dependency.

One important consequence of PbS being directly oxidized to PbO and $S_2O_3^{2-}$ via reaction [5.12] is that S^o cannot be formed as an intermediate since this would practically stop the reaction. Tributsch and Gerischer (1976) have pointed out that this is only possible if at least one reaction that does not involve electron transfer participates in the overall process. Presently, very little is understood concerning the nature of the mechanism, and so any discussion of this is rather speculative. It might involve the chemisorption of OH radicals onto surface sulfur atoms to form oxy-sulfur intermediates which, in turn, are further oxidized to $S_2O_3^{2-}$.

Avrahami and Golding (1968) have observed that molecular oxygen can rapidly oxidize HS^- ions to $S_2O_3^{2-}$ and SO_4^{2-}. It is possible that O_2 is responsible for the direct oxidation of PbS to PbO and $S_2O_3^{2-}$. Although the solution was constantly being deoxygenated during these experiments, there might have been enough dissolved oxygen present for this to occur.

5.2.2 Galena Oxidation at pH 6.8

On the basis of some of the experimental results of this study and others, the oxidation of galena at pH 6.8 differs from that at pH 9.2 in

two important respects: lead oxide that is formed readily dissolves and neither thiosulfate nor sulfate is produced. Nevertheless, a reaction mechanism that is similar to the one proposed for pH 9.2 can be postulated:

$$PbS + H_2O \underset{k_{-3}}{\overset{k_3}{\rightleftharpoons}} \overline{\overline{Pb\text{–}(OH)S}} + H^+ + e \qquad [5.13]$$

$$\overline{\overline{Pb\text{–}(OH)S}} \underset{k_{-4}}{\overset{k_4}{\rightleftharpoons}} \overline{PbO} + \bar{S}^o + H^+ + e \qquad [5.14]$$

$$(\overline{PbO})_{n_1} \longrightarrow n_1 PbO \qquad [5.3]$$

$$(\bar{S}^o)_{n_2} \longrightarrow n_2 S^o \qquad [5.4]$$

$$PbO + H^+ \rightleftharpoons PbOH^+. \qquad [5.15]$$

At pH 6.8, the OH^- concentration is low enough that the adsorption steps are more likely to proceed by the dissociative adsorption of water. This will result in the formation of lattice $\overline{PbO}$ and $\bar{S}^o$, as before, which will nucleate into bulk phases when the clusters reach a critical size. Once bulk PbO begins to appear at a potential of about 345 mv, it dissolves according to reaction [5.15]. At pH 6.8, the equilibrium of this reaction is shifted far to the right, so the PbO will tend to disappear completely.

If reaction [5.13] is assumed to be rate-controlling and mass transfer effects are ignored, the relationship between i and t should be

of the same form as equation [5.9], i.e.,

$$\frac{1}{i} = \frac{1}{2Fk_3 \exp\left(\frac{\beta_3 FE}{RT}\right)} + \frac{\alpha_3 f_3 t}{2q_s}, \qquad [5.16]$$

where k_3, β_3 and f_3 are the kinetic parameters for reaction [5.13]. The results of a plot of 1/i versus t for potentials of 45, 145, 245 and 295 mv are shown in Figure 5.3 and Table 5.2. As can be seen, a linear relationship is found in each of the cases. Furthermore, the lines are reasonably parallel for the two lower potentials, but become less steep for the higher potentials. This trend is similar to what has been observed for pH 9.2.

On the basis of this, it can be inferred that reaction [5.13] is the rate-controlling step at potentials of 45 and 145 mv. The kinetic parameters for this potential range are then determined to be

$k_3 = 9 \times 10^{-11}$ gmole/cm^2-sec, $\beta_3 = 0.23$ and $\alpha_3 f_3 / q_s = 11.5$ cm^2/mC.

An average value of the slope, m, (see Table 5.2) has been used to calculate $\alpha_3 f_3 / q_s$.

The situation is somewhat more troublesome when it comes to potentials of 245 and 295 mv. The lower slopes in these cases cannot be attributed to a mechanism associated with a bulk oxidation product since other data from this study suggest that bulk phases form only above about 345 mv.

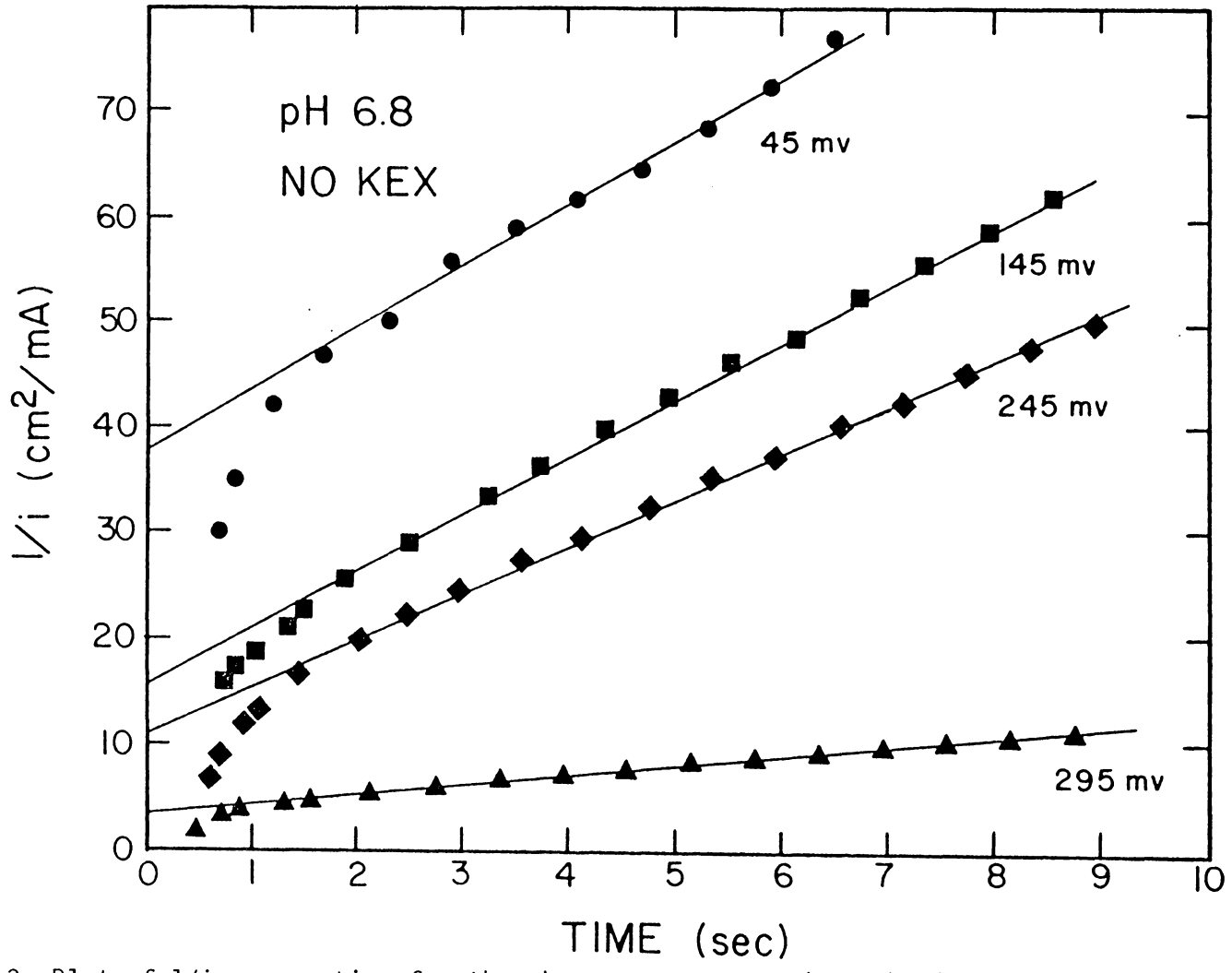


Figure 5.3 Plot of 1/i versus time for the chronoamperometry data obtained for the galena electrode in an unstirred 0.05 M KH_2PO_4/0.05 M Na_2HPO_4 solution (pH 6.8).

Table 5.2

Fit of Chronoamperometry Data for Galena Oxidation at pH 6.8
According to an Equation of the Form $1/i = mt + b$

Potential (mv, SHE)	m (cm^2/mC)	b (cm^2/mA)	r
45	5.71	38.30	0.998
145	5.44	15.77	0.999
245	4.40	11.46	0.999
295	0.90	3.65	0.998

One possible explanation is that as the potential is raised, the rate-controlling step for oxidation changes from reaction [5.13] to reaction [5.14]. Increasing the potential may increase the rate of the first reaction enough that the second one is the slow step at 245 mv. If it is assumed that reaction [5.13] is at quasi-equilibrium and that reaction [5.14] is rate-limiting, then it can be shown that i is related to t by the expression:

$$\frac{1}{i} = \frac{1}{2Fk_4 \left(\frac{k_3}{k_{-3}}\right)^{\alpha_3} \left(\frac{1}{C_{H^+}}\right)^{\alpha_3} \exp\left[\left(\frac{\alpha_3+\beta_4}{RT}\right)FE\right]} + \frac{\alpha_4 f_4 t}{2q_s}, \qquad [5.17]$$

where k_4, β_4, α_4 and f_4 are the previously described kinetic parameters for reaction [5.14].

This equation shows that 1/i should also be a linear function of t, but with a slope and intercept different than when reaction [5.13] is the slow step. Such a result supports the possibility that reaction [5.14] becomes the rate-determining step at 245 mv.

On the other hand, straight lines are also expected if a place-exchange reaction between Pb and OH is rate-controlling. This might equally explain the current-time behavior for potentials of 245 and/or 295 mv. Clearly, more experimental work needs to be done in order to be more certain of the reaction mechanisms at these two potentials.

5.2.3 Chemisorption of Xanthate at pH 9.2 and 6.8

The analysis of the voltammograms obtained in the presence of 10^{-3} M KEX at pH 9.2 and 6.8 (Sections 3.3.2a and 3.3.2d) confirms previously

reported results (Woods, 1971) that the first monolayer of xanthate adsorbing onto galena does so by a chemisorption reaction,

$$X^- \xrightarrow{k_5} X_{ads} + e. \qquad [5.18]$$

Moreover, there is also evidence that only after the first monolayer is completely laid down (at a potential of about 150 - 200 mv) does PbX_2 begin to form.

During his study on the PbS-KEX system, Woods (1971) found that his chronoamperometry data for the oxidation of galena in a 7.1×10^{-3} M KEX solution at pH 9.2 could be fit by an expression of the form of equation [5.9], i.e.,

$$\frac{1}{i} = \frac{1}{k_5 F C_x \exp\left(\frac{\beta_5 FE}{RT}\right)} + \frac{\alpha_5 f_5 t}{q_s'}, \qquad [5.19]$$

where k_5, β_5, and $\alpha_5 f_5$ are the kinetic parameters for reaction [5.18], C_x is the xanthate concentration and q_s' is the charge corresponding to monolayer coverage by xanthate.

Plots of 1/i versus t have been drawn for the data obtained in this study at 10^{-3} M KEX (Figures 3.47 and 3.48). The results in Figure 5.4 and Table 5.3 show that at both pH 9.2 and 6.8, the data can be fit to relations of the form of equation [5.19]. Potentials above 145 mv have not been included since this would correspond to values beyond the pre-wave in the voltammograms of Figures 3.31 and 3.40.

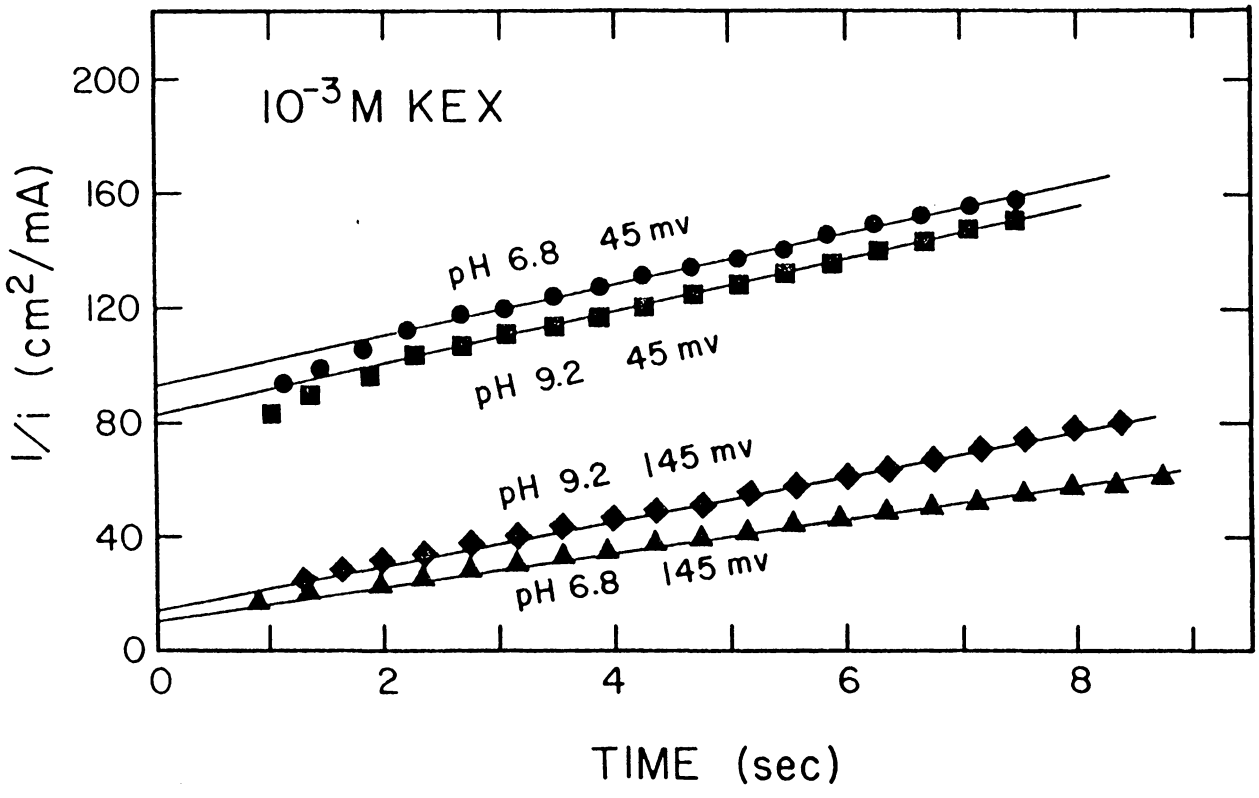


Figure 5.4 Plot of 1/i versus time for the chronoamperometry data obtained for the galena electrode immersed in unstirred 0.05 M $Na_2B_4O_7$ (pH 9.2) + 10^{-3} M KEX and unstirred 0.05 M KH_2PO_4/ 0.05 M Na_2HPO_4 (pH 6.8) + 10^{-3} M KEX solutions.

Table 5.3

Fit of Chronoamperometry Data for Xanthate Adsorption at pH 9.2 and 6.8 According to an Equation of the Form $1/i = mt + b$

pH	Potential (mv, SHE)	m (cm^2/mC)	b (cm^2/mA)	r
6.8	45	8.81	93.5	0.998
6.8	145	7.21	9.63	0.999
9.2	45	8.59	83.47	0.997
9.2	145	8.18	12.53	0.998

The kinetic parameters for the adsorption reactions have been evaluated from the slopes and intercepts of the lines obtained from the least-squares fit (Table 5.3):

pH 9.2: $\alpha_5 f_5/q_s' = 16.77\ cm^2/mC$; $\beta_5 = 0.49$; $k_5 = 5.29 \times 10^{-5}$ cm/sec

pH 6.8: $\alpha_5 f_5/q_s' = 16.02\ cm^2/mC$; $\beta_5 = 0.58$; $k_5 = 3.99 \times 10^{-5}$ cm/sec.

Although the overall reaction rates are fairly similar at pH 9.2 and 6.8, some difference in the values of the kinetic parameters is observed, however. Some of the difference can undoubtedly be attributed to the difficulties of reproducibility inherent to these systems and to the relatively small amount of data on which this analysis is based. Nevertheless, it may also be due to an effect that pH is having on the adsorption process itself.

In the case of the adsorption of an organic species such as xanthate, the displacement of the solvent at the solid/liquid interface by the adsorbent can be extremely important. Gileadi and Stoner (1971) have derived a rate equation for Temkin conditions that takes this into account. Although their expression has the same functional form as equation [5.19], both the parameters, β and α, are strongly influenced by the water structure at the electrode surface. There might be some difference in this structure when the pH is 9.2 than when it is 6.8.

Before leaving this section, one important comment should be made. It was previously estimated from voltammetry (Sections 3.3.2a and 3.3.2d) that the apparent charge density transferred in adsorbing a single monolayer of xanthate onto galena was 110 $\mu C/cm^2$. However,

integration under the entire current-time curves of Figures 3.47 and 3.48 yields charge densities that are considerably higher than this value. This suggests that even at potentials as low as 45 mv and 145 mv, PbX_2 begins to form once the initial chemisorbed layer is filled. It should be recalled that the voltammograms obtained in this study indicate that PbX_2 does not yet form at these potentials. The difference is probably related to the fact that xanthate adsorption has only occurred for about 10 seconds by the time a potential of 145 mv is reached during the voltammetry experiments.

5.2.4 Xanthate Adsorption and Sulfide Oxidation as Competitive Processes

As briefly touched upon in Chapter III, one thing that is very apparent from this study is that xanthate adsorption and galena oxidation are in competition with each other for the mineral surface. It should be mentioned that this idea was first proposed by Wark (1938), although it was not looked upon in terms of electrochemical reactions. For example, at pH 9.2 and 10^{-4} M KEX, $S_2O_3^{2-}$ begins to appear along with PbX_2 and S^o at a potential quite close to where it is first observed in the absence of collector. However, when the collector concentration is increased to 10^{-3} M, the oxidation of sulfur is suppressed sufficiently enough that $S_2O_3^{2-}$ does not appear at all as long as PbX_2 is stable.

Although this study has been restricted to the galena system, the notion that the adsorption of xanthate is competing with the oxidation of the mineral itself should apply to other sulfides and metals as well.

With this in mind, a general mechanism can be postulated.

In Sections 5.2.1 and 5.2.2, it was shown that the data for the initial stages of oxidation in the absence of xanthate were consistent with what is expected for the anodic adsorption of OH^- ions (at pH 9.2) and H_2O (at pH 6.8). This process is shown schematically in Figure 5.5a. Eventually, when oxidation becomes extensive enough, bulk oxidation products will nucleate.

As has been shown in the previous sections, the initial phases of galena oxidation and xanthate adsorption have both been found to fit the behavior for single-step one-electron transfer chemisorption reactions. Since bulk metal xanthate (MeX_2) or dixanthogen is more likely to grow on top of X_{ads} sites and bulk metal oxide on top of OH_{ads} sites, the way in which the first monolayer is filled is crucial to the fate of the mineral.

At exceedingly low collector concentrations, the rate of adsorption will still be considerably slower than the rate of mineral oxidation and the situation will remain the same as in Figure 5.5a. If the concentration is raised sufficiently that the adsorption rate becomes comparable to the oxidation rate, then both X_{ads} and OH_{ads} can occupy the first monolayer (Figure 5.5b). One can envisage that with further anodic polarization, patches of metal xanthate (or dixanthogen) and metal oxide will form on the electrode surface. Increasing the xanthate level even further will cause collector adsorption to dominate the electrode surface (Figure 5.5c). Under these conditions, chemisorbed xanthate will occupy the entire first monolayer and, consequently, only metal

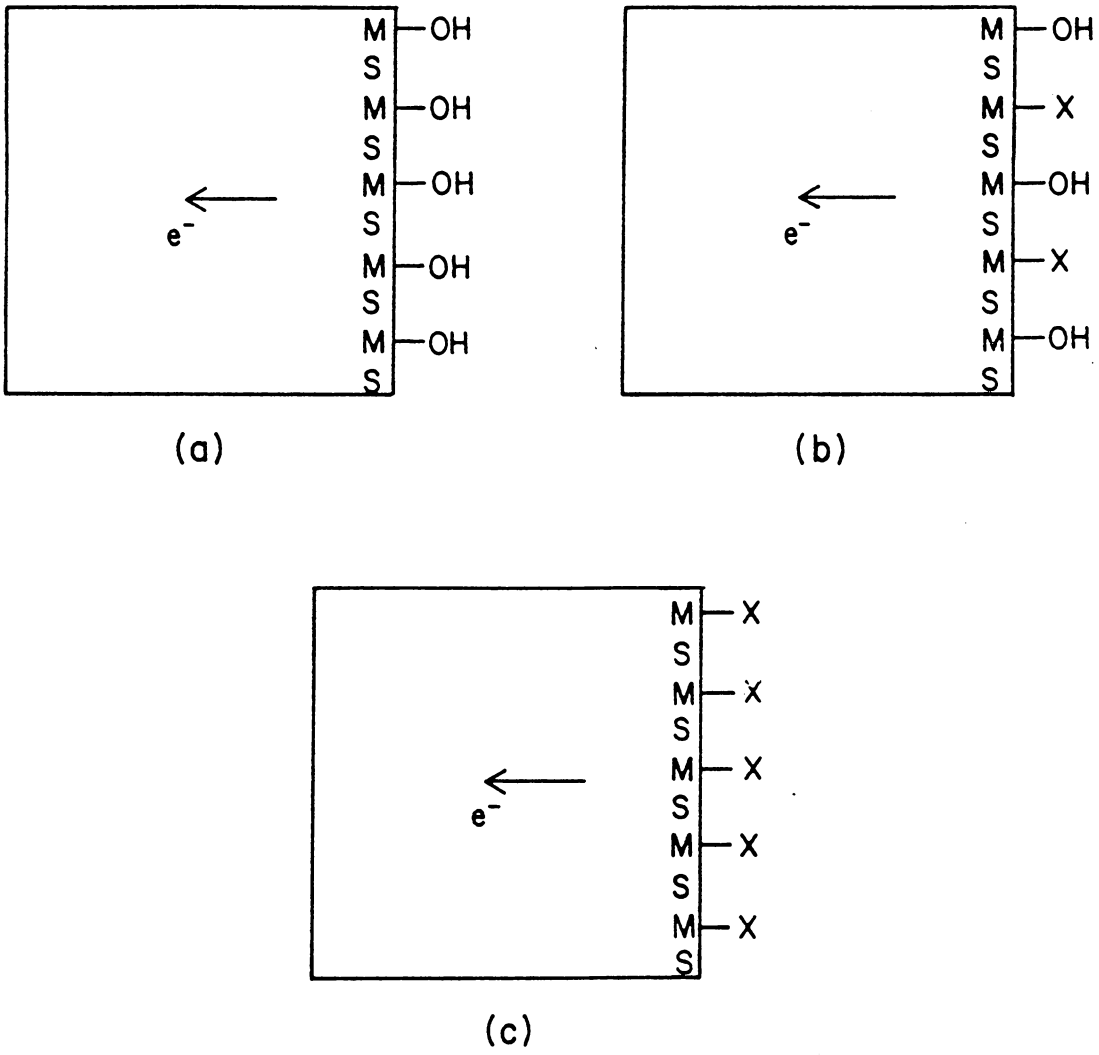


Figure 5.5 Competition of X^- and OH^- anions for the galena surface during oxidation:
(a) Total oxide layer when little or no xanthate is added.
(b) Mixed oxide-xanthate surface when intermediate concentrations of xanthate are added.
(c) Total xanthate surface when high concentrations of xanthate are added.

xanthate or dixanthogen (but no metal oxide) will be able to form on top of this. Whether or not MeX_2 or X_2 appear before the chemisorbed layer has been completely laid down will depend on the xanthate concentration. The voltammetry experiments of this study indicate that at 10^{-3} M KEX, the bulk products will appear only after the first monolayer is filled, but by 10^{-4} M KEX they begin to form before the first layer is complete.

In order for the mineral to become floatable, it may not be necessary for xanthate to occupy its entire surface. At intermediate xanthate levels where both the collector and hydroxyl groups can adsorb, both xanthate and oxide clusters will form on the surface. The resulting hydrophobicity of the mineral will be determined by the relative proportions of the two types of sites. It follows that at some critical xanthate concentration in this range, the mineral behavior will change from non-floatable to floatable. Determining this critical value will be extremely important from a practical point of view since this is where industrial flotation operators will want to set their xanthate levels.

The electrochemistry experiments done in this study suggest that at pH 9.2, xanthate adsorption dominates over galena oxidation when the collector concentration is 10^{-3} or 10^{-4} M. Presumably, a lower addition, say 10^{-5} M, is required for a mixed oxide-xanthate surface to result. Based on the discussion in the previous paragraph, this should also be close to the minimum collector requirement for flotation. It may, therefore, be no coincidence that a level of 10^{-5} - 10^{-4} M KEX is typically used in industrial galena flotation circuits.

The voltammetry experiments at pH 6.8, on the other hand, have shown that a mixed surface is produced at both 10^{-4} and 10^{-3} M KEX (Section 3.3.2d). Differences in the oxidation rate of galena are probably responsible for this pH effect. Analysis of the current-time data obtained in the absence of xanthate has revealed that mineral oxidation proceeds more rapidly at the lower pH (Sections 5.2.1a and 5.2.2). At the same time, the pH has been found not to have much of an effect on the adsorption of collector in solutions containing 10^{-3} M KEX (Section 5.2.4). One would therefore expect the xanthate requirement for flotation to be higher at pH 6.8 than at pH 9.2.

Much of the research concerning the interactions between xanthate and sulfides (and metals) has focused on determining whether metal xanthate (MeX_2) or dixanthogen (X_2) is being formed. Although it is generally agreed that PbX_2 is being formed in the case of galena (Allison and Finkelstein, 1971; Finkelstein et al., 1975; Finkelstein and Poling, 1977; Guy and Trahar, 1984), some recent electrochemical studies have indicated that dixanthogen is a product of xanthate oxidation (Ahmed, 1978b; Thi et al., 1981; Schuhmann et al., 1983; Lamache et al., 1984). These results are conflicting only if one assumes that one or the other is being produced, but not both.

The overall process by which MeX_2 or X_2 can be incorporated into the product layer is composed of several steps:

i) removal of the Me cation from the lattice of the substrate

ii) transport of the Me cation to the site of MeX_2 formation

iii) transport of X^- ions to the site of MeX_2 or X_2 formation

iv) Me–X or X–X bond formation.

In the case of base metals that do not have a strong affinity for xanthate (e.g., iron) and noble metals, only X_2 will be formed. However, in the case where base metals, such as lead and copper, can readily form complexes with xanthate, none of the steps required for MeX_2 are severely impeded. The xanthate concentration will then become crucial in determining whether MeX_2 or X_2 is produced.

In the discussions concerning whether PbX_2 or X_2 is forming on galena, very little attention has been paid to the amount of xanthate that was used during the experiments. It is possible that at concentrations below, say, about 10^{-3} M KEX, PbX_2 is the dominant species being produced. However, if the concentration is increased beyond this, the rate at which xanthate anions approach the reaction interface may become great enough that a mixture of PbX_2 and X_2 or X_2 alone can form in the product layer.

In recent years, there has been some disagreement over whether PbX_2 forms by the reaction,

$$PbS + 2X^- \longrightarrow PbX_2 + S^o + 2e, \qquad [5.20]$$

or

$$2PbS + 4X^- + 3H_2O \longrightarrow 2PbX_2 + S_2O_3^{2-} + 6H^+ + 8e. \qquad [5.21]$$

Lamache et al. (1984) found that only X_2, S^o and PbX_2 were generated after electrolyzing galena-bed electrodes for several hours in solutions ranging from 3×10^{-4} to 2×10^{-3} M KEX. Very little thiosulfate was detected. Guy and Trahar (1984) conducted batch flotation tests on a

synthetic galena-quartz at a much lower collector level of $2x10^{-5}$ M KEX and found that the start of flotation could best be correlated with the formation of PbX_2 and $S_2O_3^{2-}$ via reaction [5.21]. The thermodynamic calculations carried out in this study (Section 2.4.4a) have given a similar result.

Pritzker and Yoon (1984b) speculated, without any direct proof, that both groups might be correct and that this apparent discrepancy was only a manifestation of the effect of xanthate concentration. The results of the voltammetry experiments in this study support this hypothesis. Furthermore, the difference in the extent of oxidation of the sulfur-bearing species in these two cases becomes understandable if one adopts the view that galena oxidation and xanthate adsorption are competitive processes. The more xanthate that is present, the less the mineral surface itself is oxidized and the less likely oxidation of sulfur will proceed as far as the formation of oxy-sulfur anions.

There is an important consequence to attributing the flotation of galena at $2x10^{-5}$ M KEX, as observed by Guy and Trahar (1984), to reaction [5.21]. That reaction implies that $S_2O_3^{2-}$ and not S^o is the principal sulfur-bearing oxidation product. On the surface, this contradicts the results of the present electrochemical study which indicate that S^o is the predominant species formed whether or not xanthate has been added. However, what may be responsible for this difference is that Guy and Trahar (1984) carried out their experiments under open-circuit conditions and used hydrogen peroxide to obtain oxidizing potentials. As has been pointed out by Tributsch and

Gerischer (1976), H_2O_2 is a strong enough oxidizing agent to promote the oxidation of metal sulfides to oxy-sulfur species by the direct route (see Section 5.2.1c). It is quite possible that at the relatively low concentration of $2x10^{-5}$ M KEX used in the flotation tests, there is not enough collector present to suppress the action of peroxide in promoting the formation of thiosulfate.

5.3 Galena Oxidation at pH 1.1 and 4.6

5.3.1 Mechanism Change with the Extent of Reaction

As mentioned previously in Section 4.3, experimental results of this study and of others show that under acidic conditions galena oxidation, below at least 1000 mv, proceeds via the reaction,

$$PbS \longrightarrow Pb^{2+} + S^{o} + 2e. \qquad [5.22]$$

At the same time, however, there are indications that the mechanisms for this reaction may change as the amount of oxidation becomes extensive enough.

The potential-step and voltammetry data in Figures 4.1 and 4.3 for the cases where the potential does not exceed 650 mv are typical of what would be expected if dissolution is proceeding as a surface reaction restricted to a few monolayers. In this case, the instantaneous rate of reaction is determined by the number of sites still left unreacted in the monolayer, the potential and an activation energy of adsorption which varies with the extent of the reaction. Dissolution occurs at

discrete, isolated sites and does not proceed by the formation of nuclei of a few reacted sites and the subsequent growth of these reaction centers.

However, when the potential is increased beyond 650 mv or oxidation is allowed to continue long enough, the behavior of the system changes quite noticeably. At 945, 1045 and 1245 mv, the current varies in a very complex manner as the reaction proceeds (Figures 4.1 and 4.2) and actually increases with time at various stages. Even when the potential is only 545 and 645 mv, the current eventually begins to increase (Figure 4.2) after the initial decay (Figure 4.1). The voltammograms in Figures 4.6 and 4.7 show that when the anodic limit becomes high enough, the oxidation current is greater along the reverse scan than it is along the forward scan as long as the potential exceeds 650 mv. Moreover, Nicol et al. (1978) proposed, on the basis of their voltammetry experiments, that the elemental sulfur produced above about 650 mv is of a different, more bulk-like and difficult-to-reduce form than that generated below 650 mv.

These observations are typical of what is found for reactions controlled by a nucleation and growth mechanism. Both electrocrystallization and electrodissolution can be described by such a model since one process is just the reverse of the other. This mechanism involves two processes: i) the formation of nuclei containing either small clusters of deposited material or small holes due to the removal of electrode material; and ii) the growth of these nuclei as material is either incorporated or removed from the perimeters of these expanding

centers.

The change in the mechanism of galena oxidation from a random surface process to one controlled by nucleation and growth as the reaction becomes extensive is strongly supported by direct observations of the electrode surface during this study and that of Brodie (1969). Examination of the electrode after it had been polarized to less than about 600 mv showed that the anodic film was yellow in color and that it could be easily wiped off. Apparently, a relatively uniform sulfur product layer was being left behind under these conditions. After a potential above 600 mv was applied, however, the surface turned dark gray and the film became strongly adherent. Brodie (1969) carried out an X-ray analysis of such a film and observed that both S^o and unreacted PbS were present. This is what is expected if nuclei are forming within a region near the electrode surface and coalescing as oxidation continues.

5.3.2 Dissolution by a Random Surface Process

The initial dissolution of galena might occur essentially as a surface reaction, similarly to what has been observed in the case of the adsorption of hydrogen and oxygen onto noble metals (e.g., Will and Knorr, 1960; Conway and Gileadi, 1962; Parsons, 1961; Bockris and Reddy, 1970; Tilak et al., 1973; Angerstein-Koslowska et al., 1977). As shown previously in this study (Section 5.2), the initial oxidation of galena and adsorption of xanthate onto galena at higher pH have also been found to obey the kinetics for this type of reaction.

One possible mechanism for the overall reaction [5.22] may involve the two single-electron steps:

$$PbS + H_2O \longrightarrow Pb\text{—}(OH)_{ads}S + H^+ + e \qquad [5.23]$$

$$Pb\text{—}(OH)_{ads}S \longrightarrow Pb^{2+} + OH^- + S^o + e. \qquad [5.24]$$

This is analogous to the reactions proposed for the dissolution of iron at low pH (Bignold and Fleischmann, 1974). It is also similar to the sequence presented previously (reactions [5.13] and [5.14]) for the oxidation of galena at pH 6.8. The only difference is that lead oxide is the final stable product at neutral pH, whereas plumbous ions are generated at low pH. It should be emphasized that the choice of reactions [5.23] and [5.24] must be considered to be tentative at this point. More research is required in order to evaluate this mechanism.

Reaction [5.23] involves the adsorption of OH radicals on the minerals surface and, in the most general case, its rate (assuming activation control) can be expressed in terms of a Butler-Volmer equation, i.e.,

$$i = k\,(1-\theta_{OH})\,\exp\left(\frac{\beta FE}{RT}\right)\exp\left(-\alpha g(\theta)\right) - k'\theta_{OH}\exp\left[\frac{-(1-\beta)FE}{RT}\right]\exp\left[(1-\alpha)\,g\,(\theta)\right], \qquad [5.25]$$

where θ_{OH} is the fractional surface coverage of adsorbed OH, g (θ) is a function describing the change in the activation energy of adsorption with surface coverage and the other parameters have their usual meaning. Under conditions where the second term can be ignored, Temkin behavior

is obeyed (i.e., $g(\theta) = f\theta$) and a change in θ_{OH} influences the exponential factor, $\exp(-\alpha g(\theta))$, much more strongly than the pre-exponential factor $(1-\theta_{OH})$, equation [5.25] simplifies to an Elovich rate expression.

An important consequence of a relation of this type is that at constant E, the current will decrease as θ_{OH} increases. In this case, one would therefore expect the current monitored during a potential-step experiment to continually decrease with time. The results obtained for the initial stages of oxidation at 545 and 645 mv (Figure 4.1) follow this behavior.

Angerstein-Koslowska et al. (1977) have carried out computer simulations of the kinetic behavior of a reaction governed by an equation such as [5.25] when it is driven by a linear potential sweep. They found that the current after the sweep reversal was always less than that along the forward scan no matter the choice of the Temkin factor, f, and the upper potential limit. The voltammograms in Figure 4.3 show that the same trend is observed for anodic limits of 545 and 645 mv. Once again, the experimental results support the notion that the initial stage of dissolution of galena at lower overpotentials proceeds as a surface reaction.

The results of this study also indicate that mass transfer may have an important influence upon the dissolution rate during the surface reaction phase of the process. For example, the current passed during the anodic scans in Figure 4.3 (pH 1.1) and Figure 4.13 (pH 4.6) is greater when the electrolyte is stirred than when it is not. This is

presumably due to the fact that agitation disperses Pb^{2+} ions, which tend to inhibit reaction [5.23], away from the electrode surface. Other evidence of the importance of mass transfer can be seen in the current-time curves for potentials of 545 and 645 mv in Figure 4.1. Although the current is initially greater at 645 mv, it drops to the same level as in the case of the lower potential after only a few seconds and remains there for the next 40 seconds or so. The independence of the current from the potential over this time suggests that the reaction rate has become limited by either the transport of Pb^{2+} ions through the product layer or the transport of Pb^{2+} ions through the solution away from the mineral surface.

5.3.3 Dissolution by a Nucleation and Growth Mechanism

As has been mentioned previously, it appears that the mechanism of the dissolution of galena changes to one involving nucleation and growth after oxidation has become extensive enough. Although a great deal of theoretical and experimental research has been conducted in this area, it has primarily dealt with the deposition and dissolution of metals. The dissolution of galena is likely to be more complex since it involves both the removal of lead from the mineral lattice and the formation of a solid sulfur phase on the mineral surface. Nevertheless, a brief discussion of some of the recent contributions to the theory of nucleation and growth processes may be helpful in explaining some of the experimental results of this study.

Two approaches have been taken in describing this phenomenon:

1) the nucleation of two-dimensional centers on a substrate and the subsequent growth along a plane parallel to the surface (Figure 5.6a); and
2) the nucleation of three-dimensional centers on a substrate and the subsequent growth in directions parallel and perpendicular to the surface (Figure 5.6b).

In the case of the two-dimensional process, a three-dimensional deposit or pit is formed by successive layer-by-layer nucleation and growth.

Regardless of the geometry of the nuclei, an important aspect that must be taken into account is that the expanding centers eventually coalesce and cease to grow at the mutual areas of contact. The Avrami model (1939), which relates the actual area of the nuclei to that which would arise if no overlap is occurring, has been most commonly adopted for this purpose. It assumes that nucleation occurs at random sites and is most strictly applicable when the number of growth centers is large.

Abyaneh and Fleischmann (1981, 1982) have recently derived a general current-time equation for two-dimensional nucleation and growth under the condition that the reaction rate is controlled by the incorporation of material into a deposit or removal of material from a pit (i.e., activation control). Two limiting cases for this expression are worth noting for the purpose of the present discussion. When nucleation is fast (i.e., all the centers form instantaneously) compared to growth, the current due to deposition or dissolution in the first monolayer is given by:

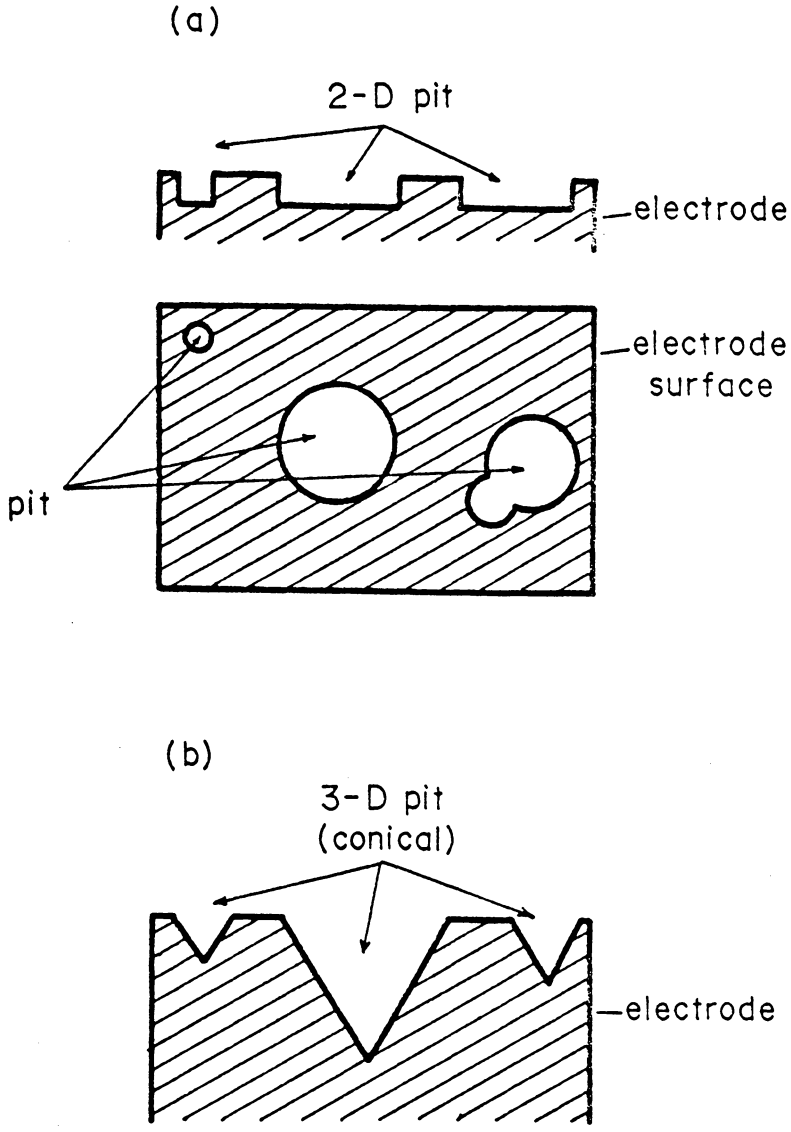


Figure 5.6 Schematic diagrams showing two types of nucleation and growth:
(a) Side and plan view of two-dimensional pits growing in a plane parallel to the electrode surface;
(b) Side view of a three-dimensional pit with the geometry of a right circular cone growing across and into the electrode surface.

$$i = At \exp(-Bt^2), \qquad [5.26]$$

where A and B are constants determined by the nature of the reacting material and the kinetics of nucleation. At the other extreme when nucleation is very slow (this is termed progressive nucleation), the expression becomes:

$$i = A't^2 \exp(-B't^3). \qquad [5.27]$$

These functions have the characteristic shapes shown in Figure 5.7a,b. (It should be noted that these limiting cases were first derived many years earlier by Bewick et al. (1962).) The build-up of a three-dimensional deposit or pit by the growth of successive monolayers has been treated by several researchers (e.g., Fleischmann and Thirsk, 1964; Armstrong and Harrison, 1969). A typical result is shown in Figure 5.7c.

Three-dimensional models have been found to be useful when the spreading of two-dimensional layers is inhibited by a heterogeneous substrate. When the expanding centers have the geometry of a right circular cone, the current-time relationships for the same limiting cases considered above have been shown (Armstrong et al., 1966; Abyaneh and Fleischmann, 1982) to have the form:

$$i = C\,[1 - \exp(-Dt^2)] \quad \text{(instantaneous nucleation)} \qquad [5.28]$$

and

$$i = C\,[1 - \exp(-D't^3)] \quad \text{(progressive nucleation)} \qquad [5.29]$$

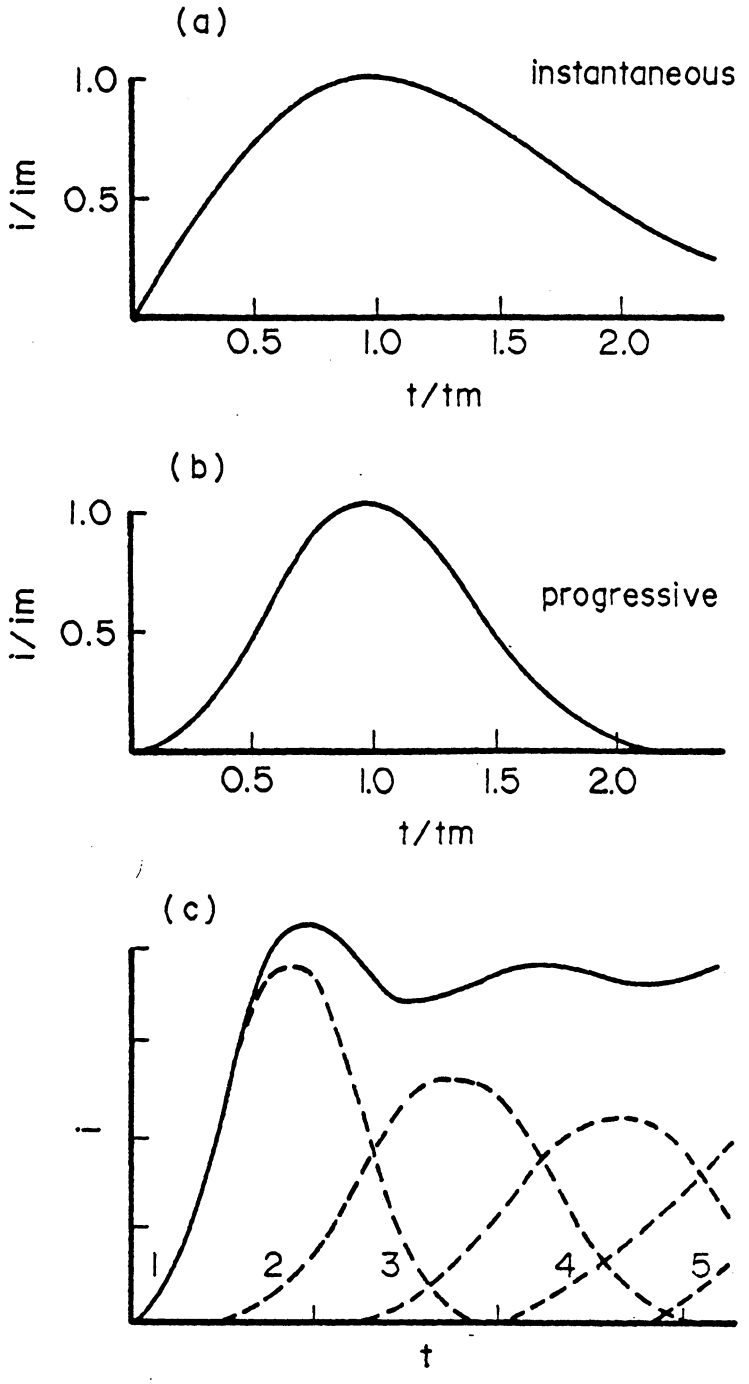


Figure 5.7 Theoretical current-time transients for two-dimensional instantaneous nucleation and growth according to Eq. [5.26] (a); two-dimensional progressive nucleation and growth according to Eq. [5.27] (b); and successive layer-by-layer growth of two-dimensional centers for progressive nucleation (Armstrong and Harrison, 1969) (c). (c).

where C, D and D' are constants. Equation [5.29] is shown schematically in Figure 5.8.

The curves in Figures 5.7 and 5.8 do display some of the essential features of the current-time data which have been observed in this study for the dissolution of galena at pH 1.1 (Figure 4.1 and 4.2). Most importantly, all of the theoretical relations show that the current should increase with time during some stage of oxidation. This is characteristic of the nucleation and growth process. Furthermore, the experimental data for oxidation of galena at 545 and 645 mv over a time period of 1 or 2 hours (Figure 4.2) bear a strong resemblance to the curve in Figure 5.8 for the case of three-dimensional nucleation and growth. The oscillating nature of the current-time transients for potentials of 945, 1045 and 1245 mv is also quite similar to that observed in the theoretical calculation for successive layer-by-layer growth of two-dimensional nuclei (Figure 5.7c).

As was pointed out previously in Section 5.3.1, observations in this study and in that by Brodie (1969) indicate that the applied potential has a significant effect on the nature of the electrode deposit. The presence of unreacted PbS in the product layer at high overpotentials suggests that the rate of nucleation becomes increasingly favored over the rate of growth as the potential is increased. This may be explained by the following argument.

Oxidation during the growth phase will proceed by the consumption of PbS surrounding the nuclei, the incorporation of sulfur onto the periphery of the expanding centers and the transport of Pb^{2+} ions toward

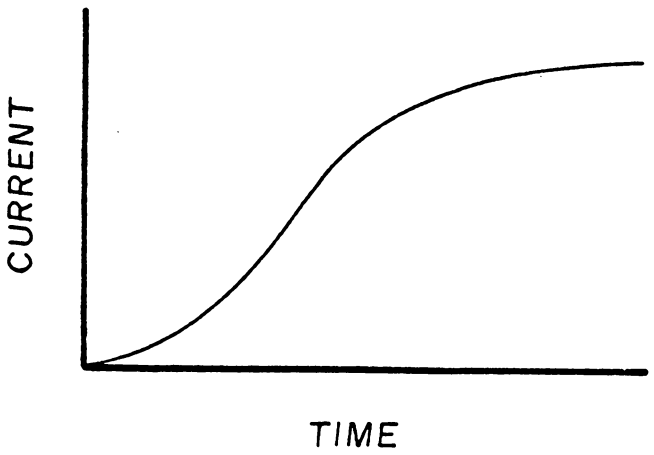


Figure 5.8 Theoretical current-time curve for three-dimensional nucleation and growth of right circular cones according to Eq. [5.29] (Armstrong et al., 1966).

the solution. Eventually, these centers will begin to overlap and to encapsulate pockets of unreacted PbS. Once these pockets become isolated from the bulk of the galena electrode, further reaction there becomes more difficult since elemental sulfur is a poor electronic conductor. At this point, it may become energetically more favorable for oxidation to continue by the formation of new nuclei in the portion of the mineral still in electrical contact with the potentiostat. The resulting product layer will then tend to become thick and contain unreacted PbS.

The steady-state rate of nucleation, J, has been shown to be related to the overpotential, η, by the relation:

$$J = K_1 \exp(-K_2/\eta^2), \qquad [5.30]$$

according to the classical theory (Bindra et al., 1973), and by the relation:

$$J = K'_1 \exp(K'_2\eta), \qquad [5.31]$$

according to the atomistic theory (Milchev and Stoyanov, 1976). Here, K_1, K_2, K'_1 and K'_2 are constants independent of η. Without going into any details concerning these theories, it suffices for the present purpose to note that the nucleation rate should increase with η. At the same time, the limit to the growth of the expanding centers resulting from the isolation of the unreacted PbS pockets should not be affected by the potential. This should then result in the increasing predominance of nucleation over growth that has been observed as the oxidation

potential is raised.

The results of this study and of others (Paul et al., 1978; Gardner and Woods, 1979) have also revealed other important characteristics of the dissolution of galena. These are the apparently random fluctuations in the electrode response during the course of potentiostatic experiments (e.g., the potential-time curves for 1045 and 1245 mv in Figure 4.1) and the difficulty in achieving reproducibility of the electrode response from one test to the next.

Paul et al. (1978) attributed this behavior to fluctuations in the Pb^{2+} concentration at the electrode surface due to the presence of the sulfur product layer. As more and more sulfur forms, it becomes more difficult for the Pb^{2+} ions to diffuse through the layer to the solution. The Pb^{2+} concentration and the local pH at the reaction interface therefore rise, eventually leading to the precipitation of lead thiosulfate and basic lead sulfate. Since these species are passivating, the oxidation current drops. However, all the while, the Pb^{2+} ions in the product layer continue to diffuse through to the solution. This works against the process of raising the local pH and tends to promote the dissolution of the thiosalts. When enough of these thiosalts have been removed, the galena electrode becomes reactivated and the cycle of rising and then falling current can then be repeated.

However, there are some difficulties with this explanation. For one thing, since the rather slow process of solid-state diffusion is involved, one would not expect the sharp fluctuations in the current that are observed during the initial polarization of galena at 1045 and

1245 mv (see Figure 4.1). Another problem is that fluctuations are not observed when a potential of 945 mv is applied, although nearly as much charge is passed over a period of 2 hours (see Figure 4.2) as in the case of 1045 and 1245 mv. One would therefore expect the same amount of elemental sulfur to be formed and the same sort of fluctuations caused by the difficulties in the transport of Pb^{2+} ions through the product layer.

The fluctuations and the lack of reproducibility that have been observed in the transient behavior may not be caused by changes in the Pb^{2+} concentration and pH at the reaction interface, but instead may be an inherent part of the nucleation and growth process. By their very nature, electrodeposition and electrodissolution are highly stochastic phenomena.

The two variables that are required to describe nucleation are the number of growth centers that are formed and their spatial distribution. Most researchers have assumed that the distribution is random and can be characterized by a Poisson distribution (e.g., Barradas and Porter, 1980; Abyaneh and Fleischmann, 1981, 1982). However, as Barradas et al. (1979) have pointed out, there are many kinds of randomness that can be considered. For example, the nuclei may be distributed along line defects, grain boundaries or scratches. The stochastic nature of the process will then arise not only from the use of a Poisson distribution for each line, but also from variations in the position, length and number of such lines. Some of the difficulty in this study associated with achieving reproducibility from one test to the next may be

attributed to this, particularly in view of the relatively coarse polishing of the galena electrode.

Nucleation is probabilistic with respect to time in addition to space. Moreover, Bindra et al. (1973) have shown theoretically that the fluctuations in current observed during a potential-step experiment should become larger as the potential is increased. The current-time data in Figures 4.1 and 4.2 show a trend which is consistent with the theoretical prediction.

Although crystal growth has been assumed to be deterministic in most theoretical treatments, it also is a stochastic process. For one thing, it is strongly affected by nucleation which, as has just been noted, is itself probabilistic. For another, the overlap of centers will cause growth to cease at the points of contact. Under these conditions, the geometry and rate of growth changes and becomes very complex. Furthermore, the individual centers can no longer be considered to grow independently of each other. The process must then be approached as a multi-center problem.

CHAPTER VI.

SUMMARY AND CONCLUSIONS

6.1 Introduction

As mentioned earlier, one of the primary objectives of the present study has been to examine the roìe of equilibrium thermodynamics in describing the electrochemistry of the PbS-H_2O and PbS-H_2O-KEX systems. Chapter II has dealt with the results of comprehensive thermodynamic calculations, whereas Chapters III, IV and V have focused on the data obtained from electrochemical experiments. Throughout, comparisons have been made between what is observed and what is predicted, principally for the purpose of identifying reactions. However, no attempt has yet been made to draw these comparisons together and to make any general observations concerning the conditions when this mineral system may or may not behave reversibly. This question will now be addressed in this chapter.

Following that discussion, the dissertation will conclude with a summary of the major findings of this work and recommendations for future research.

6.2 Role of Thermodynamics in Describing Galena Aqueous Chemistry

6.2.1 In the Absence of Xanthate

Because of its central role in both flotation and leaching, the oxidation process with and without ethyl xanthate at a variety of pH

values has been investigated more closely than any other aspect of galena electrochemistry during the course of this study. The experimental results of this study and of others indicate that S^o is the primary sulfur-bearing oxidation product formed between pH 0 and 9.2, and that the primary lead-bearing species generated changes from Pb^{2+} to $PbOH^+$ to PbO as the pH increases. Thiosulfate has been detected in smaller amounts at pH 9.2 and only begins to become prominent at potentials above about 500 mv.

Comparison with the results of the thermodynamic calculations indicates that agreement between the observed and predicted behavior becomes better as the pH is lowered. At pH 0, the species that form (i.e., Pb^{2+} and S^o) are the same as the ones expected from thermodynamics, regardless of whether oxidation is allowed to proceed to the formation of S^o, $S_2O_3^{2-}$ or SO_4^{2-}. Furthermore, the amount of lead that is dissolving is roughly close to the amount expected on the basis of the calculations. However, as the pH is raised, the predicted solubility becomes much lower than the observed one.

The oxidation of lead-bearing species tends to follow expected behavior more closely than that of the sulfur species, at least in a qualitative sense. One noticeable exception, however, arises at pH 9.2 where PbO should not be forming under equilibrium conditions, yet has been observed to be the predominant oxidation product.

Whereas there are problems associated with using thermodynamic calculations to predict what species are produced, better results are achieved if one starts from the premise that the oxidation reaction is

known and then uses the Nernst equation to estimate the potential for the onset of this reaction. This is particularly true if S^o is one of the oxidation products. The IGP and rest potential measurements of this study have shown that for the most part, the oxidation reactions begin at potentials close to their reversible values at all the pH values studied.

Undoubtedly, this stems from the fact that S^o, which is the initial bulk oxidation product, forms quite rapidly but resists subsequent conversion to $S_2O_3^{2-}$ and SO_4^{2-}. PbS is also a good electronic conductor and so does not retard the transport of electrons that are released during oxidation. In addition, other factors such as mass transfer of reactants and products to and from the electrode surface and the formation of a solid product layer, which might bring about a significant overpotential, are not important during the initial stages of oxidation.

Kinetic effects can be included, to some extent, in thermodynamic calculations by putting restrictions on the species considered in the system. An attempt has been made in the present study to account for the sluggishness of sulfur oxidation by considering three separate cases in which it is permitted to proceed to the formation of sulfate (Case I), thiosulfate (Case II) and elemental sulfur (Case III). Although this is certainly a much more realistic approach for aqueous sulfide systems, it has a severe limitation in that it cannot consider two of these cases together at the same time. Using equilibrium free energy data, there is no way that calculations can show S^o and $S_2O_3^{2-}$, for

example, to be present at the same time, although there is experimental evidence at pH 9.2 to indicate that this indeed occurs.

Recently, however, Peters (1984) has presented a novel approach to account for the slow kinetics of sulfur oxidation that can be used in thermodynamic calculations. He estimated that the addition of 75 kcal/mole to the free energy of formation of SO_4^{2-} would account for the overpotential observed for its appearance in the Cu-S-H_2O system. The resulting E_h-pH stability diagram was in closer agreement with what is actually observed than was the one obtained using the conventional approach.

Another question concerning thermodynamic calculations of the type done in this study is how to include surface reactions. As has been shown in Chapter V, these play an important role in galena chemistry, particularly in the initial stages of the oxidation of the mineral. What would be required to include a surface species into the system are its standard free energy of adsorption, ΔG^o_{ads}, and the surface area of the mineral. Although obtaining ΔG^o_{ads} for xanthate adsorption and galena oxidation may not be a simple matter, it should be possible to do so from polarization curves.

Whereas certain aspects of the oxidation of galena can be reasonably described by thermodynamics, the reduction of the oxidation products is somewhat more problematical. The system exhibits some degree of reversibility in the sense that the solid oxidation products, S^o and PbO, can be removed by cathodic polarization. In fact, this observation has been used as the basis for the charge analysis of the

voltammograms presented in this study. Bard and Faulkner (1980) have termed this behavior "chemical reversibility".

On the other hand, other species that are formed during oxidation are not so easily removed. The reactions which produce oxy-sulfur anions are so irreversible that any $S_2O_3^{2-}$ or SO_4^{2-} that is formed is essentially lost from the system. At most, only a portion of species such as Pb^{2+} and $PbOH^{+}$ participate in the cathodic reactions because they are soluble and usually present in vanishingly small amounts in the bulk solution. When the solution is being stirred, these cations are completely dispersed away from the electrode surface; even when the solution is quiescent, a considerable fraction diffuses into the solution and, consequently, is not available for an electron-transfer reaction.

Another observation from the voltammograms and IGP diagrams that cannot be explained by equilibrium thermodynamics is the hysteresis between the potentials at which oxidation products are formed and then removed. Whereas oxidation is usually found to begin at a potential close to the Nernst value, most of the reduction occurs at potentials that are considerably cathodic with respect to the reversible value. Furthermore, this overpotential increases with the extent of oxidation.

There may be several reasons for this behavior. Firstly, at all the pH values studied, oxidation results in the formation of an insulating product layer - either S^{o} alone or S^{o} and PbO together. The cathodic reduction of PbO and S^{o} must then occur at the PbS/oxidation product interface. Consequently, H^{+} ions which also participate in

these reactions must diffuse through the product layer to this interface in order for reduction to proceed. This may lead to an overpotential.

Secondly, once the product layer forms, it may also rearrange itself into a more stable structure which is more difficult to remove. PbO and S^o may segregate from each other and crystallize into bulk-like forms when oxidation becomes extensive enough. In the case of PbO, this may involve the place-exchange (see Section 5.2.1b) between lead and oxygen.

Segregation of PbO from S^o at pH 9.2 may also cause the observed cathodic reactions to be different from the ones that are expected. From a thermodynamic point of view, one would expect reduction to occur via the reverse of the oxidation reaction, i.e., the recombination of PbO and S^o back to PbS. Yet, there is evidence from some of the electrochemical experiments of this study that S^o and PbO do not react with each other, but instead are reduced separately to HS^- and Pb^o, respectively.

6.2.2 In the Presence of Xanthate

As has been discussed in Chapters III and V, the first stage in the interaction between xanthate and galena involves the chemisorption of the collector via a single electron-transfer oxidation reaction Eq. [3.2]. Since this is not a bulk reaction, it has not been included in the thermodynamic calculations presented in this study. It should be possible, however, to incorporate it into the framework of these calculations in much the same way as has been mentioned concerning the

initial stage of galena oxidation (see Section 6.2.1).

One of the most important results of this study has been the direct evidence from the voltammetry experiments that hydroxyl ions compete with xanthate anions for the galena surface. Furthermore, the presence of xanthate tends to suppress the oxidation of sulfide so that at higher collector additions, no thiosulfate has been found to form.

The notion that xanthate adsorption and sulfide oxidation are competitive processes is not a new one. It has long been known from both industrial and laboratory experience that for a given xanthate concentration, there is a definite upper pH beyond which flotation does not occur. The relation between the collector concentration and the maximum pH is given by the Barsky equation:

$$pH_{max} = K + \log [X^-] \qquad [6.1]$$

where K is a constant that depends upon the mineral.

Although it originated empirically, equation [6.1] can also be derived from thermodynamics by considering the equilibrium conditions for the stability of PbX_2. This is also reflected in the appearance of distinct upper pH limits in the plots of % PbX_2 versus pH that are shown in Figures 2.31-2.40.

The competition between X^- and OH^- for adsorption onto the first monolayer was discussed in the previous chapter, but not in a quantitative manner. Nevertheless, it can be shown (Appendix IV) that if both adsorb according to a Temkin isotherm, then the ratio in the number of sites occupied by xanthate and by hydroxyl at equilibrium is given by:

$$\frac{\theta_X}{\theta_{OH}} = K_1 \frac{C_X}{C_{OH}} \exp\left[-K_2'(\theta_X + \theta_{OH})\right], \qquad [6.2]$$

where θ_X, θ_{OH} = fraction of sites occupied by X^- and OH^-, respectively,

C_X, C_{OH} = bulk concentrations of X^- and OH^-, respectively, and

K_1 and K_2' are constants.

Under the conditions where the first monolayer is complete (i.e., $\theta_X + \theta_{OH} = 1$), the ratio becomes:

$$\frac{\theta_X}{\theta_{OH}} = K_2 \frac{C_X}{C_{OH}}, \qquad [6.3]$$

where $K_2 = K_1 \exp(-K_2')$. This equation clearly shows the competitive aspect of adsorption since raising the collector concentration or decreasing the pH will increase the value of θ_X/θ_{OH}. Therefore, it can be seen that this competitive aspect can also be described by equilibrium thermodynamics.

The suppression of the oxidation of sulfide due to the presence of xanthate is also a manifestation of the competition between collector adsorption and galena oxidation. However, it is not something that can be explained by thermodynamics. The oxidation of sulfur to thiosulfate can be written as:

$$2S^o + 3H_2O \longrightarrow S_2O_3^{2-} + 6H^+ + 4e. \qquad [6.4]$$

It is clear from this equation that the equilibrium amount of $S_2O_3^{2-}$ that is generated is unaffected by the quantity of xanthate in the

system. Instead, the inhibition of sulfide oxidation is more likely caused by an increase in the rate of the anodic adsorption of xanthate relative to that of galena oxidation as the collector concentration is raised. At a sufficiently high xanthate concentration, the mineral surface becomes protected enough that sulfide oxidation cannot proceed to the formation of thiosulfate.

6.3 Contributions from the Present Study

6.3.1 Thermodynamic Calculations

Contributions to the study of the aqueous and flotation chemistry of galena from the thermodynamic calculations of this work can be summarized as follows:

1. Thermodynamic calculations based on comprehensive mass balance equations for lead-bearing, sulfur-bearing and xanthate-bearing species have been carried out for the PbS-KEX-H_2O system for collector additions of 0, 10^{-7}, 10^{-6}, 10^{-5} and 10^{-4} M. Three sets of calculations, in which oxidation of sulfide is allowed to proceed to the formation of i) sulfate (Case I), ii) thiosulfate (Case II) and iii) elemental sulfur (Case III), have been carried out to include metastable species within the scope of this work. The results yield information concerning the equilibrium concentrations of all soluble species and the weights of all solid phases over the E_h and pH range from -2000 to 2000 mv and from 0 to 14, respectively. In addition, they have been used to generate E_h-pH stability

diagrams for each xanthate addition.

2. The calculations are more comprehensive than earlier ones of this kind in several important respects:

   i) Insoluble species, as well as soluble ones, have been included in the mass balances, whereas only dissolved species were considered until now.

   ii) In previous work, the total concentrations of soluble metal-bearing, sulfur-bearing and xanthate-bearing species have been fixed at arbitrary levels and have been assumed to remain unchanged over the entire E_h-pH range. The approach taken in the present study, on the other hand, requires that only the total amount of material, both soluble and insoluble, in the system be fixed and not the dissolved concentrations alone. Consequently, the amount of material in solution will vary according to the E_h and pH, which is what would be expected to be the case in a real system.

   iii) Whereas most previous work has been restricted to determining only the phase boundaries on an E_h-pH diagram, the calculations of the type in this study can be carried out for any given E_h and pH.

3. In order to demonstrate other useful information that thermodynamics can provide, several novel ways of displaying the results of the calculations have been presented. These include two-dimensional plots showing the effect of E_h or pH on the xanthate uptake (% PbX_2) and three-dimensional contour plots and block diagrams showing the effect of both E_h and pH on % PbX_2. Comparison of these diagrams

with observed flotation behavior has proven to be very useful in determining the reactions responsible for the onset and termination of flotation.

4. Comparison of the observed and calculated effect of potential on the flotation recovery of galena obtained in the presence of 10^{-2} M Na_2S (no KEX) indicates that the lower flotation edge coincides well with the formation of either elemental sulfur or polysulfides.

5. The shapes of the calculated plots showing the effect of E_h or pH are quite similar to those of the typical experimental curves showing the effect of E_h or pH on flotation recovery. These are characterized by the % PbX_2 or flotation recovery remaining constant at a maximum within certain E_h or pH limits and then sharply dropping to zero at both ends of the range.

6. Comparison of the experimental flotation data obtained by Guy and Trahar (1984) for galena at pH 8 and $2x10^{-5}$ M KEX with the calculations of this study indicates that the bulk reaction which most closely predicts the onset of flotation is:

$$2PbS + 4X^- + 3H_2O \longrightarrow 2PbX_2 + S_2O_3^{2-} + 6H^+ + 8e. \qquad [6.5]$$

7. Although most of the emphasis in the calculations has been placed on flotation, the results of this type of work are also of use to hydrometallurgists. For example, the effect of E_h and pH on the mineral solubility, which can be easily extracted from the computed

data, can provide invaluable information concerning leaching.

6.3.2 Electrochemical Experiments at pH 9.2 and 6.8

Some of the significant findings of the electrochemical work done on the galena electrode at pH 9.2 and 6.8 are:

1. The IGP technique, which until now has rarely been used in electrochemical studies of sulfides, has been shown to be a very valuable tool in the study of the aqueous chemistry of galena.

2. Below about 300 mv at pH 9.2 and 345 mv at pH 6.8, oxidation of galena in the absence of xanthate is not extensive enough for any bulk products yet to be formed on the mineral. Instead, it may occur by a surface process which involves the electrosorption of OH^- ions by a one-electron transfer reaction that leads to the formation of a metal-deficient sulfide and an insoluble lead oxide. The adsorption kinetics over the first 10 seconds have been found to obey an Elovich-type rate equation.

3. At pH 9.2, the principal bulk oxidation products formed on galena are PbO, S^o and $S_2O_3^{2-}$. Under extremely oxidizing conditions, PbO_2 may also be produced. There is also evidence that a fraction of the PbO may dissolve, presumably in the form of $PbOH^+$.

4. Thiosulfate produced at pH 9.2 has been found only in relatively small amounts compared to S^o when the potential is kept below 500 mv. Above 500 mv, the quantity of $S_2O_3^{2-}$ rises more sharply. The

formation of $S_2O_3^{2-}$ may occur by two distinct reaction paths: i) the direct attack of PbS probably as soon as oxidation begins, and ii) the conversion of S^o generated during the previous stage of oxidation only when the potential increases beyond about 500 mv.

5. Cycling the potential of the galena electrode between fixed cathodic and anodic limits at pH 9.2 does not affect the relative amount of S^o and $S_2O_3^{2-}$ produced. However, the amount of current passed diminishes with each successive cycle.

6. At pH 6.8, an increase in the potential above 345 mv causes the surface lead oxide to nucleate into a bulk form, most of which rapidly dissolves as $PbOH^+$. Elemental sulfur is also formed at the same time. No evidence for the presence of $S_2O_3^{2-}$ or SO_4^{2-} has been detected at this pH.

7. The solubility of PbO at pH 6.8 leaves the oxidized surface sulfur-rich. Consequently, the reduction of the oxidation products proceeds via two reactions: the recombination of PbO and S^o to PbS and the reduction of S^o to HS^-.

8. Stirring the solution promotes the dissolution of PbO at pH 9.2 and 6.8, which suggests that this process is controlled by the supply of H^+ ions to the surface.

9. The electrode response during cyclic sweeps is different at pH 6.8 than at pH 9.2 in that the anodic current is found to increase with

each successive scan.

10. Microflotation tests at pH 9.2 in the absence of xanthate indicate that galena exhibits some natural floatability in the potential range where polysulfides or a metal-deficient sulfide surface can be formed. Once the potential is increased to about 300 mv, collectorless flotation is no longer possible, presumably due to the formation of PbO.

11. The initial monolayer of xanthate adsorbs onto galena via a one-electron transfer chemisorption reaction:

$$X^- \longrightarrow X_{ads} + e. \qquad [6.6]$$

It has been found that the kinetics of this reaction obeys the Elovich equation in the initial stages. Multi-layers of xanthate result from the formation of PbX_2 on top of the chemisorbed layer.

12. At collector concentrations of 10^{-3} M KEX and lower scan speeds, the chemisorbed monolayer is laid down completely before PbX_2 begins to form. However, if only 10^{-4} M KEX is added or if the sweep rate becomes high enough, PbX_2 appears before the completion of the chemisorbed layer.

13. Xanthate adsorption and galena oxidation are parallel anodic reactions, competing on the mineral surface. Consequently, the occurrence of one tends to inhibit that of the other.

When 10^{-3} M KEX is added to a solution of pH 9.2, $S_2O_3^{2-}$ and PbO are not produced until PbX_2 becomes unstable and the potential has been increased above 495 mv. When no xanthate is present, $S_2O_3^{2-}$ is detected as soon as bulk oxidation begins at 300 mv. At 10^{-4} M KEX, the adsorption rate becomes slow enough that sulfide oxidation is not suppressed and $S_2O_3^{2-}$ forms along with PbX_2 and S^o at potentials as low as it does in the absence of collector.

At pH 6.8, galena oxidizes more rapidly than at pH 9.2 and, consequently, PbO can form along with PbX_2 in both 10^{-4} and 10^{-3} M KEX solutions.

14. Almost complete flotation recovery of galena is possible in the potential range from -300 to 200 mv at pH 9.2 and a 10^{-5} M KEX addition. The upper potential limit is accurately predicted by the thermodynamic calculations of this study and can be attributed to the anodic decomposition of PbX_2. The lower limit, on the other hand, is about 200 mv more negative than the closest predicted value for any of the bulk reactions. However, it may be associated with the chemisorption of xanthate by reaction [6.6] rather than with the formation of bulk PbX_2.

6.3.3 Electrochemical Experiments at pH 1.1 and 4.6

On the basis of the experiments conducted in electrolytes at pH 1.1 and 4.6, the following results have been obtained:

1. At both pH 1.1 and 4.6, the oxidation of galena results in the formation of only Pb^{2+} and S^o, at least below a potential of 845 mv.

2. The mechanism for oxidative dissolution appears to change once the reaction becomes extensive enough. At potentials below 650 mv, the electrode response in the early stages of oxidation is characteristic of a random surface process. After a certain time, however, the behavior changes to what is typical of reactions controlled by a nucleation and growth mechanism. When the applied potential is greater than 650 mv, dissolution occurs by nucleation and growth immediately after the start of the reaction.

3. At pH 1.1, only a single cathodic reaction seems to occur to remove the oxidation products whether the solution is stirred or not, i.e., the reduction of S^o to H_2S.

4. At pH 4.6, the reduction of oxidation products occurs via two reactions under quiescent conditions, i.e., the recombination of Pb^{2+} and S^o to PbS and the reduction of S^o to H_2S. Less than 20% of the cathodic charge can be attributed to the first reaction. Of course, only the second reaction is observed when the solution is being agitated.

5. The reduction of PbS to Pb^o and H_2S begins at potentials close to the Nernstian values at both pH 1.1 and 4.6. If the electrode is then anodically polarized, these reduction products are oxidized via two reactions, i.e., the recombination of Pb^o and H_2S to PbS only under quiescent conditions and the dissolution of Pb^o to Pb^{2+} under all conditions.

6. The addition of 10^{-3} or 10^{-2} M Pb^{2+} to the electrolyte at pH 4.6 decreases the current passed during the anodic dissolution of galena. It is likely that the accumulation of Pb^{2+} ions at the electrode increases the rate of the reverse of the dissolution reaction.

7. When 10^{-3} or 10^{-2} M Pb^{2+} is added to the electrolyte at pH 4.6, these ions are reduced to lead metal and deposit on the galena surface when the potential is lowered to below about -330 mv.

8. Comparison of the observed relation between the open-circuit potential and the dissolved lead concentration with that predicted from the thermodynamic calculations indicates that the system deviates farther from reversibility as the pH is increased from 0 to 4.6. At pH 0, the oxidation of Pb^{o} to Pb^{2+} and PbS to Pb^{2+} and S^{o} closely follows Nernstian behavior; at pH 4.6, however, the differences between the predicted and observed concentrations are orders of magnitude apart.

9. As long as lead metal is present on the galena surface, it seems to dominate the electrode response. Only after all the metal has dissolved will the open-circuit potential rise to the value expected for a galena electrode.

6.4 Recommendations for Future Research

On the basis of the research that has been conducted during this investigation, the following areas for future research are suggested:

1. Thermodynamic calculations should be carried out extending the approach introduced by Peters (1984) to account for the sluggishness of sulfide oxidation by raising the free energy of formation of the sulfate ion. As has been shown, thiosulfate is an important oxidation product of galena at high pH. Accordingly, an appropriate change in the free energy of thiosulfate should be made and then incorporated, along with the one for sulfate, into the mass balance calculations.

2. Thermodynamic calculations of the type done in this study should be extended to include the chemisorption reactions by which the initial stages of xanthate adsorption and galena oxidation have been observed to occur at pH 9.2 and 6.8.

3. Further experiments should be carried out to verify some of the reactions that have been proposed in this study primarily on the basis of voltammetry. These should include work on both polished galena electrodes and galena particle beds.

   Possible experiments on a small polished electrode would include:

   i) sweeping the potential to different points along a voltammogram and then removing the electrode for surface analysis by ESCA, FTIR, mass spectrometry and/or SEM.

ii) using a cell similar to the one designed by Mielczarski et al. (1979) which permits in-situ IR spectroscopic analysis of electrode surfaces at the same time that electrochemical experiments are being carried out.

The relation between potential and the appearance or disappearance of such species as S^o, $S_2O_3^{2-}$, SO_4^{2-}, Pb^{2+}, $PbOH^+$, HS^- and H_2S can best be examined by conducting electrochemical experiments on galena particle beds or suspensions and then analyzing the mineral surfaces and solutions for these species. UV spectrophotometry, ESCA, potentiometry, gravimetry and titrimetry are techniques that can be used for this analysis. The amount of oxidation products formed can be checked against the charge that is measured during the reaction.

4. A study should be carried out to more clearly delineate the mechanism associated with oxidation of sulfide to S^o, $S_2O_3^{2-}$ and SO_4^{2-} on a galena surface. Particular attention should be directed toward verifying whether the formation of thiosulfate and sulfate occurs via the two paths discussed in Chapter V. It should be possible to distinguish the direct oxidation path from the one involving the oxidation of intermediate S^o since the former is believed to involve the reaction of dissolved O_2 or H_2O_2 with the galena surface via a non-electron transfer reaction. Consequently, the direct reaction should be largely independent of potential. In addition, the amount of thiosulfate formed by the direct oxidation of sulfide is probably much more strongly dependent upon the oxygen

partial pressure under closed-circuit conditions than is the amount produced by the other route.

The effect of the substrate on sulfide oxidation is also another factor that should be examined. Not only the kinetics of oxidation, but also the nature of the oxidation products, has been found to vary, depending upon whether the electrode in question is, for example, galena, pyrite, chalcocite or platinum.

5. Although it was not examined in any detail during this study, how oxidation evolves over time is a very important aspect that needs further research. This can be studied on a polished mineral electrode by carrying out a series of experiments in which the potential is stepped to some oxidizing value, held there for varying lengths of time and then scanned back linearly in the cathodic direction to remove the oxidation products. The reduction peaks that appear on the reverse scan serve as fingerprints to identify the oxidation products. In addition, the solution and mineral surface can be analyzed for oxidation products if the reaction has been extensive enough or if the mineral has a large enough surface area.

6. A detailed study of the current-time behavior for the dissolution of galena at acidic pH should be undertaken with the objective of fitting the data to quantitative models based on the random surface and nucleation and growth mechanisms that were proposed in Chapter V. These experiments should be carried out on a rotating PbS disk

electrode to promote reproducibility since such an experimental set-up has well-controlled hydrodynamics. This electrochemistry work should be accompanied by an SEM study of the morphology of the electrode surface after different stages of oxidation.

7. Study of the effect of potential on the microflotation of galena should be extended from what has been done in this study (pH 9.2, 10^{-5} M KEX) to cover a range of pH values and collector additions. This should be accompanied by a measurement of the amount of xanthate adsorbed and S^o and $S_2O_3^{2-}$ produced as a result of the interaction between the collector and the mineral. This may provide direct evidence as to what reactions are responsible for the upper and lower potential limits for flotation.

8. Experiments should be specially designed to directly test the premise suggested here that the presence of xanthate tends to inhibit the oxidation of the mineral itself. For example, this might include a measurement of the amount of thiosulfate released during galena oxidation as a function of the xanthate concentration.

9. It has been suggested in Chapter V of this study that both PbX_2 and X_2 may form on a galena surface, depending upon the xanthate addition. Although there have been many previous attempts to analyze for these two using IR and UV spectroscopy, very little attention was paid to the xanthate concentration and the surface potential. It may be useful to carry out a systematic study in

which xanthate is adsorbed under controlled collector additions and oxidizing conditions and then the particle surfaces are analyzed for PbX_2 and X_2.

10. Some preliminary kinetic studies of galena oxidation and xanthate adsorption at pH 9.2 and 6.8 were conducted during this study and resulted in some useful information concerning the initial stages of these processes. This work should be followed up with a more thorough investigation under carefully controlled hydrodynamic conditions for the purpose of developing a kinetic model describing the competition between galena oxidation and xanthate adsorption.

11. Many of the phenomena discussed in this work, e.g., the competition between galena oxidation and xanthate adsorption and the way the mechanism for the dissolution of galena at low pH changes from a surface process to a nucleation and growth process, are ones that should also be observed in other sulfide systems. Therefore, work similar to what has been recommended in this section should also be done on other sulfides. The experimental results should be interpreted from the point of view of testing some of what has been proposed in the present study and of drawing some general conclusions concerning the solution and flotation chemistry of sulfides.

12. Although oxygen is always found in real flotation and hydrometallurgical systems, it was not included in this study since its presence tends to complicate the interpretation of experimental

results. However, once enough of the work that has been outlined in this section has been done and the chemistry of galena itself is understood well enough, it will be of great value to carry out tests in which oxygen is introduced into the system. One of the aims would be to develop quantitative models for the mixed potential behavior of xanthate adsorption and sulfide oxidation and leaching.

REFERENCES

Abdul Azim, A.A. and Anwar, M.M., 1969. Anodic passivation of Pb in various media. Corrosion Science, 9:245-260.

Abramov, A.A., 1968. Method for the quantitative determination of the sorption forms of solvents on mineral surfaces. Sov. Min. Sci., 384-389.

Abyaneh, M.Y. and Fleischmann, M., 1981. The electrocrystallisation of nickel. I. Generalised models of electrocrystallisation. J. Electroanal. Chem., 119:187-195.

Abyaneh, M.Y. and Fleischmann, M., 1982. The role of nucleation and of overlap in electrocrystallisation reactions. Electrochim. Acta, 27:1513-1518.

Adam, K. and Iwasaki, I., 1984. Grinding media - sulfide mineral interaction and its effect on flotation. In: P.E. Richardson, S. Srinivasan and R. Woods (Editors), Proceedings of the International Symposium on Electrochemistry in Mineral and Metal Processing. The Electrochemical Society, Pennington, NJ, 84-10:66-80.

Agar, G.E., Kipkie, W.B. and Wells, P.F., 1982. The separation of chalcopyrite and pentlandite from INCO Metals' Sudbury area ores. XIV International Mineral Processing Congress, Toronto, Canada, Paper IV-1.

Ahmed, S.M., 1978a. Electrochemical studies of sulphides: I. The electrocatalytic activity of galena, pyrite and cobalt sulphide for oxygen reduction in relation to xanthate adsorption and flotation. Int. J. Miner. Process., 5:163-174.

Ahmed, S.M., 1978b. Electrochemical studies of sulphides: II. Measurement of the galvanic currents in galena and the general mechanism of oxygen reduction and xanthate adsorption on sulphides in relation to flotation. Int. J. Miner. Process., 5:175-182.

Allison, S.A. and Finkelstein, N.P., 1971. Study of the products of reaction between galena and aqueous xanthate solutions. Trans IMM, 80:C235-239.

Allison, S.A., Goold, L.A., Nicol, M.J. and Granville, A., 1972. A determination of the products of reaction between various sulfide minerals and aqueous xanthate solution, and a correlation of the products with electrode rest potentials. Metall. Trans., 3:2613-2618.

Angerstein-Kozlowska, H., Conway, B.E. and Sharp, W.B.A., 1973. The real condition of electrochemically oxidized platinum surfaces. I. Resolution of component processes. J. Electroanal. Chem., 43:9-36.

Angerstein-Kozlowska, H., Klinger, J. and Conway, B.E., 1977. Computer simulation of the kinetic behavior of surface reactions driven by a linear potential sweep. I. Model 1-electron reaction with a single adsorbed species. J. Electroanal. Chem., 75:45-60.

Angerstein-Kozlowska, H., Conway, B.E. and Klinger, J., 1978. Computer simulation of the kinetic behavior of surface reactions driven by a linear potential sweep. III. Monolayer formation by a nucleation and growth mechanism, J. Electroanal. Chem., 87:301-320.

Armstrong, R.D., Fleischmann, M. and Thirsk, H.R., 1966. The anodic behavior of mercury in hydroxide ion solutions. J. Electroanal. Chem., 11:208-223.

Armstrong, R.D. and Harrison, J.A., 1969. Two-dimensional nucleation in electrocrystallisation. J. Electrochem. Soc., 116:328-331.

Avrahami, M. and Golding, R.M., 1968. The oxidation of the sulphide ion at very low concentrations in aqueous solutions. J. Chem. Soc. (London), A:647-651.

Avrami, M., 1939. Kinetics of phase change. J. Chem. Phys., 7:1103-1112.

Bagotskii, V.S. and Vasiliev, Yu.B., 1964. Some characteristics of oxidation reactions of organic compounds on platinum electrodes. Electrochim. Acta, 9:869-882.

Bard, A.J. and Faulkner, L.R., 1980. Electrochemical Methods. Fundamentals and Applications. John Wiley and Sons, New York, pp. 44-46.

Barradas, R.G., Bowie-Reed, R., Fletcher, S. and Porter, J.D., 1979. Some statistical aspects of the growth of crystals in passivation, metal deposition and anodic film formation. J. Electroanal. Chem., 103:165-178.

Barradas, R.G. and Porter, J.D., 1980. Studies in electrocrystallisation. IV. Experimental investigation of two-dimensional nucleation-growth processes in terms of surface coverages derived from transient measurements. J. Electroanal. Chem., 110:159-180.

Bewick, A., Fleischmann, M. and Thirsk, H.R., 1962. Kinetics of the electrocrystallization of thin films of calomel. Trans. Farad. Soc., 58:2200-2216.

Biegler, T. and Koch, D.F.A., 1967. Adsorption and oxidation of methanol on a platinum electrode. J. Electrochem. Soc., 114:904-909.

Bignold, G.J. and Fleischmann, M., 1974. Identification of transient phenomena during the anodic polarisation of iron in dilute sulphuric acid. Electrochim. Acta, 19:363-374.

Bindra, P., Fleischmann, M., Oldfield, J.W. and Singleton, D., 1973. Nucleation. Faraday Discuss. Chem. Soc. (London), 56:180-198.

Bockris, J.O'M., Drazic, D. and Despic, A.R., 1961. The electrode kinetics of the deposition and dissolution of iron. Electrochim. Acta., 4:325-361.

Bockris, J.O'M. and Reddy, A.K.N., 1970. Modern Electrochemistry, Vol. 2. Plenum Press, New York.

Boissay, S., Cecile, J.-L. and Bloise, R., 1982. Etude electrochimique de l'effet inhibiteur des ions sulfite et chromate sur la galene et la chalcopyrite. Ind. Miner. [Ser.] Tech., 3:214-224.

Bold, W. and Breiter, M.W., 1961. Untersuchung des anodischen aufbauo und der kathodischen reduktion der sauerstoff-belegungan glatten Pt-elektroden. Electrochim. Acta, 5:145-160.

Boyce, J.R., Venter, W.J. and Adam, J., 1970. Beneficiation practice at the Tsumeb concentration. In D.O. Rausch and B.C. Mariacker (Editors), World Symposium on Mining and Metallurgy of Lead and Zinc. AIME, New York, 542-570.

Brandes, H., 1929. Z. Physik. Chem., 142:97.

Bratt, G.C. and Pickering, R.W., 1970. Production of lead via ammoniacal ammonium sulfate leaching. Met. Trans., 1:2141-2149.

Brion, D., 1980. Etude par spectroscopie de photoelectrons de la degradation superficielle de FeS_2, $CuFeS_2$, ZnS et PbS a l'air et dans l'eau. Appl. Surf. Sci., 5:133-152.

Brion, D., Hayer, J. and Predali, J.J., 1980. Characterization by ESCA of surface compounds of fine pyrite during the flotation process. In: P. Somasundaran (Editor), Fine Particles Processing. AIME, New York, 544-557.

Brodie, J.B., 1969. Electrochemical Dissolution of Galena. M.Sc. Thesis, University of British Columbia, Canada.

Buckley, A.N. and Woods, R., 1984a. An x-ray photoelectron spectroscopic study of the oxidation of galena. Appl. Surf. Sci., 17:401-414.

Buckley, A.N. and Woods, R., 1984b. An x-ray photoelectron spectroscopic investigation of the surface oxidation of sulfide minerals. In: P.E. Richardson, S. Srinivasan and R. Woods (Editors), Proceedings of the International Symposium on Electrochemistry in Mineral and Metal Processing. The Electrochemical Society, Pennington, NJ, 84-10:286-302.

Burkin, A.R., Rogers, M.J. and Hazel, G.J.E., 1964. Adsorption and reaction of xanthates at galena-liquid interfaces. Proceedings, 7th Int. Miner. Process. Congr., New York, 337-345.

Bushell, C.H.G., 1958. Behavior of xanthates in flotation. Trans. CIM, 61:65-77.

Carr, J.P. and Hampson, N.A., 1971. Differential capacitance and linear sweep voltammetry studies on polycrystalline lead and electrodeposited lead dioxide. J. Electrochem. Soc., 118:1262-1268.

Castro, S. and Larrondo, J., 1981. An electrochemical study of depression and flotation of chalcocite by cyanide and iron-cyanide complexes. J. Electroanal. Chem., 118:317-326.

Chander, S. and Fuerstenau, D.W., 1975. Electrochemical reaction control of contact angles on copper and synthetic chalcocite in aqueous potassium diethyldithiophosphate solutions. Int. J. Miner. Process., 2:333-352.

Chen, K.Y. and Morris, J.C., 1972. Kinetics of oxidation of aqueous sulfide by O. Enviro. Sci. Tech., 6:529-537.

Chen, K.Y. and Gupta, S.K., 1973. Formation of polysulfide in aqueous solution. Env. Letters, 4:187.

Clifford, R.K., Purdy, K.L. and Miller, J.D., 1975. Characterization of sulfide mineral surfaces in froth flotation systems using electron spectroscopy for chemical analysis. AIChE Symp. Ser., 150:138-147.

Coleman, R.E. and Powell, H.E., 1965. Infrared spectroscopy studies of a xanthate-galena system. USBM RI 6816.

Conway, B.E. and Gileadi, E., 1962. Kinetic theory of pseudo-capacitance and electrode reactions at appreciable surface coverage. Trans. Faraday Soc., 58:2493-2509.

Cook, M.A. and Nixon, J.C., 1950. Theory of water-repellent films on solids formed by adsorption from aqueous solutions of heteropolar compounds. J. Phys. Colloid Chem., 54:445-459.

Cusack, B.L., 1967. Some aspects of the role of oxygen in sulphide mineral flotation. Proc. Australas. IMM, 224:1-7.

Davison, W. and Harrison, J.A., 1973. The electrochemical growth of three-dimensional nuclei during a potentiostatic pulse - a simulation. J. Electroanal. Chem., 44:213-219.

DuRietz, C., 1957. Xanthate analysis by means of potentiometric titration: some chemical properties of the xanthates. Svensk. Kem. Tidskr., 69:310-327.

DuRietz, C., 1976. Chemisorption of collectors in flotation. Proc. 11th Int. Miner. Process. Congr., Cagliari, 1975, 375-403.

Eadington, P., 1973. Leaching of illuminated lead sulphide with nitric acid as a function of the solid state electronic properties. Trans. IMM, 82:C158-C161.

Eadington, P. and Prosser, A.P., 1966. Surface oxidation products of lead sulphide. Trans. IMM, 75:C125.

Eadington, P. and Prosser, A.P., 1969. Oxidation of lead sulphide in aqueous suspensions. Trans. IMM, 78:C74-C82.

Elgillani, D.A. and Fuerstenau, M.C., 1968. Mechanisms involved in cyanide depression of pyrite. Trans. AIME, 241:437-445.

Erdey-Gruz, T. and Volmer, M., 1931. Z. Physik. Chem., A157:165.

Evans, U.R., 1945. The laws of expanding circles and spheres in relation to the lateral growth of surface films and the grain size of metals. Trans. Farad. Soc., 41:365-374.

Evans, S. and Raftery, E., 1982. Electron spectroscopic studies of galena and its oxidation by microwave-generated oxygen species and by air. J. Chem. Soc., Faraday Trans. I, 78:3545-3560.

Feldberg, S.W., Enke, C.G. and Bricker, C.E., 1963. Formation and dissolution of platinum oxide film: Mechanism and kinetics. J. Electrochem. Soc., 110:826-834.

Finkelstein, N.P., 1970. Quantitative aspects of the role of oxygen in the interaction between xanthate and galena. Sep. Sci., 5:227-256.

Finkelstein, N.P., Allison, S.A., Lovell, V.M. and Stewart, B.V., 1975. Natural and induced hydrophobicity in sulfide mineral systems. AIChE Symp. Ser., 71(150):165-175.

Finkelstein, N.P. and Poling, G.W., 1977. The role of dithiolates in the flotation of sulphide minerals. Miner. Sci. Eng., 9:177-197.

Fischer, H., 1954. Electrolytische Abscheidung und Elektrokristallisation von Metallen (Electrolytic Separation and Electrolytic Crystallization of Metals). Springer, Berlin, pp. 118ff and 323ff.

Fleischmann, M. and Thirsk, H.R., 1959. The potentiostatic study of the growth of deposits on electrodes. Electrochim. Acta, 1:146-160.

Fleischmann, M. and Thirsk, H.R., 1964. Electrochemical kinetics of formation of monolayers of solid phases. Electrochim. Acta, 9:757-771.

Forward, F.A. and Warren, 1960. Met. Rev., 5:137-164.

Fuerstenau, M.C., Kuhn, M.C. and Elgillani, D.A., 1968. The role of dixanthogen in xanthate flotation of pyrite. Trans. AIME, 241:148-156.

Gardner, J.R. and Woods, R., 1973. The use of a particulate bed electrode for the electrochemical investigation of metal and sulfide flotation. Aust. J. Chem., 26:1635-1644.

Gardner, J.R. and Woods, R., 1977. An electrochemical investigation of contact angle and of flotation in the presence of alkylxanthates. II. Galena and pyrite surfaces. Aust. J. Chem., 30:981-991.

Gardner, J.R. and Woods, R., 1979a. An electrochemical investigation of the natural floatability of chalcopyrite. Int. J. Miner. Process., 6:1-16.

Gardner, J.R. and Woods, R., 1979b. A study of the surface oxidation of galena using cyclic voltammetry. J. Electroanal. Chem., 100:447-459.

Gaudin, A.M., 1957. Flotation, 2nd Edition. McGraw-Hill, New York, ch. 9.

Gaudin, A.M. and Finkelstein, N.P., 1965. Interactions in the system galena-potassium ethyl xanthate-oxygen. Nature, 207:389-391.

Geiger, G.H. and Poirier, D.R., 1973. Transport Phenomena in Metallurgy. Addison-Wesley, Reading, Mass., p. 463.

Gerischer, H., 1958. Z. Elektrochem., 62:256.

Gileadi, E. and Stoner, G.E., 1971. The effect of competition with water on the kinetic parameters in electrode reactions. J. Electrochem. Soc., 118:1316-1319.

Gilman, S., 1964. Electrochemical surface oxidation of platinum. Electrochim. Acta, 9:1025-1046.

Gilroy, D., 1976. Oxide growth at platinum electrodes in H_2SO_4 at potentials below 1.7 V. J. Electroanal. Chem., 71:257-277.

Gilroy, D. and Conway, B.E., 1965. Kinetic theory of inhibition and passivation in electrochemical reactions. J. Phys. Chem., 69:1259-1267.

Goldstick, T.K., 1959. Electrochemical investigations of ethyl xanthate. M.Sc. Thesis, Massachusetts Institute of Technology, Boston, Massachusetts.

Grandke, T. and Cardona, M., 1980. Electronic properties of clean and oxygen-covered (100) cleaved surfaces of PbS. Surf. Sci., 92:385-392.

Granville, A., Finkelstein, N. and Allison, S.A., 1972. Review of Reactions in the flotation system galena-xanthate-oxygen. Trans IMM, 81:C1-C30.

Greenler, R.G., 1962. An infrared investigation of xanthate adsorption by lead sulphide. J. Phys. Chem., 66:879-883.

Gutierrez, C. and Martin-Proveda, F., 1981. Flotation of galena, influence of grain size of pulp deoxygenation and of cleaning with ammonium acetate. Int. J. Miner. Process., 8:111-123.

Guy, P.J. and Trahar, W.J., 1984. The influence of grinding and flotation environments on the laboratory batch flotation of galena. Int. J. Miner. Process., 12:15-38.

Hagihara, H., 1952. Mono- and multilayer adsorption of aqueous xanthate on galena surfaces. J. Phys. Chem., 56:616-621.

Hagstrom, A.L. and Fahlman, A., 1978. The interaction between oxygen and the lead chalcogenides at room temperature studied by photoelectron spectroscopy. Appl. Surf. Sci., 1:455-470.

Hamilton, I.C. and Woods, R., 1981. An investigation of surface oxidation of pyrite and pyrrhotite by linear potential sweep voltammetry. J. Electroanal. Chem., 118:327-343.

Hamilton, I.C. and Woods, R., 1983. An investigation of the deposition and reactions of sulfur on gold electrodes. J. Appl. Electrochem., 13:783-794.

Hamilton, I.C. and Woods, R., 1984. A voltammetric study of the surface oxidation of sulfide minerals. In: P.E. Richardson, S. Srinivasan and R. Woods (Editors), Proceedings of the International Symposium on Electrochemistry in Mineral and Metal Processing. The Electrochemical Society, Pennington, NJ, 84-10:259-285.

Hampson, N.A., 1979. The aqueous system Pb^{4+}/Pb^{2+}: Electrochemical aspects. In A.T. Kuhn (Editor), The Electrochemistry of Lead. Academic Press, New York, pp. 29-63.

Harris, P.J. and Finkelstein, N.P., 1975. Interactions between sulfide minerals and xanthates. I. The formation of monothiocarbonate at galena and pyrite surfaces. Int. J. Miner. Process., 2:77-100.

Healy, T. W. and Moignard, M.S., 1976. A review of electrokinetic studies of metal sulphides. In M.C. Fuerstenau (Editor), Flotation, A.M. Gaudin Memorial Volume, AIME, New York, 1:275-297.

Hemstreet, L.A., 1975. Cluster calculations of the effects of single vacancies of the electronic properties of PbS. Phys. Rev., 11B:2260-2270.

Hepel, T. and Pomianowski, A., 1977. Diagrams of electrochemical equilibria of the system copper-potassium ethylxanthate-water at 25°C. Int. J. Miner. Process., 4:345-361.

Heyes, G.W. and Trahar, W.J., 1977. The natural floatability of chalcopyrite. Int. J. Miner. Process., 4:317-344.

Heyes, G.W. and Trahar, W.J., 1979. Oxidation-reduction effects in the flotation of chalcocite and cuprite. Int. J. Miner. Process., 6:229-252.

Heyes, G. W. and Trahar, W.J., 1984. The flotation of pyrite and pyrrhotite in the absence of conventional collectors. In: P.E. Richardson, S. Srinivasan and R. Woods (Editors), Proceedings of the International Symposium on Electrochemistry in Mineral and Metal Processing. The Electrochemical Society, Pennington, NJ, 84-10:219-232.

Hodgson, M. and Agar, G.E., 1984. An electrochemical investigation into the natural flotability of pyrrhotite. In: P.E. Richardson, S. Srinivasan and R. Woods (Editors), Proceedings of the International Symposium on Electrochemistry in Mineral and Metal Processing. The Electrochemical Society, Pennington, NJ, 84-10:185-201.

Hopstock, D.M., 1968. Chemical Properties of Xanthates and Dithiocarbamates. M.Sc. Thesis, University of Minnesota, Minneapolis.

Horvath, J. and Hackl, L., 1965. Check of the potential/pH equilibrium diagrams of different metal-sulphur-water ternary systems by intermittent galvanostatic polarization method. Corr. Sci., 5:525-538.

Ito, H., Yanagase, T. and Higashi, K.J., 1961. J. Min. Met. Inst. Jap., 77:579.

Iwasaki, I. and Cooke, S.R.B., 1958. The decomposition of xanthate in acid solution. J. Am. Chem. Soc., 80:285-288.

Janetski, N.D., Woodburn, S.I. and Woods, R., 1977. An electrochemical investigation of pyrite flotation and depression. Int. J. Miner. Process., 4:227-239.

Johnson, J.W., Chang, J., Narasagoudar, R.A. and O'Keefe, T.J., 1978. Anodic dissolution of galena concentrate in perchloric acid. J. Appl. Electrochem., 8:25-32.

Jones, M.H. and Woodcock, J.T., 1978. Perxanthates - A new factor in the theory and practice of flotation. Int. J. Miner. Process., 5:285-296.

Jones, M.H. and Woodcock, J.T., 1983. Decomposition of alkyl dixanthogens in aqueous solution. Int. J. Miner. Process., 10:1-24.

Kaischew, R. and Budevski, E., 1967. Surface processes in electrocrystallization. Contemp. Phys., 8:489-516.

Kakovskii, I.A. and Arashkevich, V.M., 1969. The investigation of the properties of organic disulphides. Proceedings of the 8th International Congress of Mineral Processing, 2:300-314

Kar Chaudari, S.N., Chang, F.C. and Cheng, K.L., 1981. Determination of the surface composition of lead electrode membranes by electron spectroscopy for chemical analysis. Anal. Chem., 53:2048-2053.

Khairy, E.M., Abdul Azim, A.A. and El-Sobki, K.M., 1966a. The effect of antimony and different anions on the potential of lead. J. Electroanal. Chem., 12:27-35.

Khairy, E.M., Abdul Azim, A.A. and El-Sobki, K.M., 1966b. Polarisation phenomena manifested by Pb-Sb alloys at low current densities. J. Electroanal. Chem., 11:282-290.

Klein, E., Bosarge, J.K. and Norman, I., 1960. Spectrophotometric determination of fast xanthate decomposition kinetics. J. Phys. Chem., 64:1666-1670.

Klymowsky, I.B. and Salman, T., 1970. The role of oxygen in xanthate flotation of galena, pyrite and chalcopyrite. CIM Bull., 63:683-688.

Kolmogorov, A.N., 1937. Izv. Akad. Nauk SSSR, Otd. Matem. Estestv. Nauk, 9:355.

Lamache, M., Bauer, D. and Pegouret, J., 1981. Comportement electrochimique de la galene (PbS) dans les conditions de pH proches de celles de la flotation. Electrochim. Acta, 26:1845-1850.

Lamache, M., Lam, O. and Bauer, D., 1984. Electrochemical oxidation of galena and ethylxanthate. In: P.E. Richardson, S. Srinivasan and R. Woods (Editors), Proceedings of the International Symposium on Electrochemistry in Mineral and Metal Processing. The Electrochemical Society, Pennington, NJ, 84-10:54-65.

Lanyon, A.H. and Trapnell, B.M.W., 1955. The interaction of oxygen with clean metal surfaces. Proc. Roy. Soc., Ser. A, 227:387-399.

Latimer, W.M., 1952. Oxidation Potentials. Prentice-Hall, Englewood Cliffs, N.J.

Learmont, M.E. and Iwasaki, I., 1984. The effect of grinding media on flotation of galena. 113th AIME Annual Meeting, Los Angeles, California, February 26-March 1, 1984; Preprint No. 84-84.

Leja, J., Little, L.H. and Poling, G., 1963. Xanthate adsorption using infrared spectroscopy. 1 - Oxidized and sulphidized copper substrates. 2 - Evaporated lead sulfide, galena and metallic lead substrates. Trans. IMM, 72:407-423.

Leonov, S.B. and Badenikov, V. Ya., 1973. Redox potential of flotation pulp as a generalized and controllable parameter of flotation. Fiz.-Khim. I. Tekhnol. Issled. Protsessov Pererabotki Polezn. Iskop., 12.

Lepetic, V.M., 1974. Flotation of chalcopyrite without collector after dry autogenous grinding. CIM Bull., June:71-77.

Lorenz, W., 1953. Z. Physik Chem., 202:275.

Lorenz, W., 1954. Z. Naturforsch, 99:716.

Luttrell, G.H. and Yoon, R.H., 1982. Collectorless flotation of sulfide ores. Presented at 111th AIME Annual Meeting, Dallas, Texas, February 14-18, 1982.

Luttrell, G.H. and Yoon, R.H., 1984. The collectorless flotation of chalcopyrite ores using sodium sulfide. Int. J. Miner. Process., 13:271-283.

Luttrell, G.H. and Yoon, R.H., 1985. Surface studies of the collectorless flotation of chalcopyrite. Colloids and Surfaces, 12(3/4):239-254.

Majima, H., 1961. Fundamental studies on the collection of sulphide minerals with xanthic acid. Sci. Rep. Res. Inst. Tohuku Univ., Ser. A., 13:433-447.

Manocha, A.S. and Park, R.L., 1977. Flotation related ESCA studies on PbS surfaces. Appl. Surf. Sci., 1:129-141.

McFeely, F.R., Kowalczyk, S., Ley, L., Pollack, R.A., Shirley, D.A., 1973. High-resolution x-ray-photoemission spectra of PbS, PbSe and PbTe valence bands. Phys. Rev., 7B:5228-5237.

McMillan, R.S., MacKinnon, D.J. and Dutrizac, J.E., 1982. Anodic dissolution of n-type and p-type chalcopyrite. J. Appl. Electrochem., 12:743-757.

Mellgren, O., 1966. Heat of adsorption and surface reactions of potassium ethyl xanthate on galena. Trans. AIME, 235:46-60.

Mellgren, O. and Subba Rau, M.G., 1963. Adsorption of ethyl xanthate on galena. Trans. IMM, 72:425-443.

Meyer, R.E., 1960. Cathodic processes on passive zirconium. J. Electrochem. Soc., 107:847-853.

Mielczarski, J., Nowak, P., Strojek, J.W. and Pomianowski, A., 1981. Investigations of the products of ethyl xanthate sorption on sulphides by IR-ATR spectroscopy. In J. Laskowski (Editor), Proceedings, Thirteenth Int. Miner. Process. Congr., Warsaw, June, 1979, Elsevier, Amsterdam, pp. 110-133.

Milchev, A. and Stoyanov, S., 1976. Classical and atomistic models of electrolytic nucleation - comparison with experimental data. J. Electroanal. Chem., 72:33-43.

Moignard, M.S., Dixon, D.R. and Healy, T.W., 1977. Electrokinetic properties of the zinc sulphide-water and nickel sulphide-water interfaces. Proc. Aust. IMM, 263:31-38.

Moriss, A.E. and Fernandez, R., 1974. A new process for the direct smelting of lead concentrates. Presented at 111th AIME Annual Meeting, Dallas, Texas, February 14-18, 1982.

Nagel, K., Ohse, R. and Lange, E., 1957. Z. Electrochem., 61:75.

Najdeker, E. and Bishop, E., 1973. The formation and behavior of platinum sulphide on platinum electrodes. J. Electroanal. Chem., 73:79-87.

Natarajan, K.A. and Iwasaki, I., 1973. Practical implications of E_h measurements in sulfide flotation circuits. Trans. AIME/SME, 254:323-328.

Navarro, A. and Gutierrez, A., 1980a. Elimination of oxygen from electrolytes by gas bubbling. J. Electroanal. Chem., 109:361-364.

Navarro, A. and Gutierrez, C., 1980b. Influence of the semiconducting character of a bed of galena particles on its potential during flotation. J. Colloid Interface Sci., 81:390-395.

Nicol, M.J., Paul, R.L. and Diggle, J.W., 1978. The electrochemical behaviour of galena (lead sulphide). II. Cathodic reduction. Electrochim. Acta, 23:635-639.

O'Dell, C.S., Dooley, R.K., Walker, G.W. and Richardson, P.E., 1984. Chemical and electrochemical reactions in the chalcocite-xanthate system. In: P.E. Richardson, S. Srinivasan and R. Woods (Editors), Proceedings of the International Symposium on Electrochemistry in Mineral and Metal Processing. The Electrochemical Society, Pennington, NJ, 84-10:81-95.

Parks, G.A., 1965. The isoelectric points of solid oxides, solid hydroxides and aqueous hydroxo complex systems. Chem. Rev., 65:177-198.

Parks, G.A., 1967. Aqueous surface chemistry of oxides and complex oxide minerals. Advan. Chem. Ser., 67:121-160.

Parks, G.A. and deBruyn, P.L., 1962. The zero point of charge of oxides. J. Phys. Chem., 66:967-973.

Parsons, R., 1961. In: P. Delahay (Editor), Advances in Electrochemistry and Electrochemical Engineering, Vol. 1. Interscience Publishers, New York, ch.1, pp. 1-64.

Partridge, A.C. and Smith, G.W., 1971. Small-sample flotation testing: a new cell. Trans IMM, 80:C199.

Paul, R.L., Nicol, M.J., Diggle, J.W. and Saunders, A.D., 1978. The electrochemical behaviour of galena (lead sulphide). I. Anodic dissolution. Electrochim. Acta, 23:625-633.

Peters, E., 1984. Electrochemical mechanisms for decomposing sulphide minerals. In: P.E. Richardson, S. Srinivasan and R. Woods (Editors), Proceedings of the International Symposium on Electrochemistry in Mineral and Metal Processing. The Electrochemical Society, Pennington, NJ, 84-10:341-361.

Phillip, B. and Fichte, C., 1960. Kinetic studies on the decomposition of xanthate. Fraserforsch Text-Tech., 11:118-124; 172-179.

Pillai, K.C., Young, V.Y. and Bockris, J.O'M., 1983. XPS studies of xanthate adsorption of galena surfaces. Appl. Surf. Sci., 16:322-344.

Plaksin, I.N. and Bessonov, S.V., 1957. Role of gases in flotation reactions. Proc. 2nd Int. Congr. Surface Act., Butterworths, London, 3:361-367.

Plante, E.C. and Sutherland, K.L., 1949. Effects of sulphide minerals on their flotation properties. Trans. AIME, 183:160-188.

Poling, G.W. and Leja, J., 1963. Infrared study of xanthate adsorption on vacuum deposited films of lead sulfide and metallic copper under conditions of controlled oxidation. J. Phys. Chem., 67:2121-2126.

Pomianowski, A. and Leja, J., 1963. Spectrophotometric study of xanthate and dixanthogenate solutions. Can. J. Chem., 41:2219-2230.

Pourbaix, M., 1966. Atlas of Electrochemical Equilibria. Gauthiers-Villars, Paris.

Pritzker, M.D. and Yoon, R.H., 1984a. Thermodynamic calculations on sulfide flotation systems. I. Galena-ethyl xanthate system in the absence of metastable species. Int. J. Miner. Process., 12:95-125.

Pritzker, M.D. and Yoon, R.H., 1984b. Thermodynamic calculations and electrochemical studies on the galena-ethyl xanthate system. In: P.E. Richardson, S. Srinivasan and R. Woods (Editors), Proceedings of the International Symposium on Electrochemistry in Mineral and Metal Processing. The Electrochemical Society, Pennington, NJ, 84-10:26-53.

Pritzker, M.D., Yoon, R.H., Basilio, C.I. and Choi, W.Z., 1985. Solution and flotation chemistry of sulfide minerals. Can. Met. Quarterly, (submitted for publication).

Pryor, W.A., 1960. The kinetics of the disproportionation of sodium thiosulfate to sodium sulfide and sulfate. J. Am. Chem. Soc., 82:4794-4797.

Queneau, P.E. and Schuhmann, R., 1974. The Q-S oxygen process. J. Metals, 26:14-16.

Rand, D.A.J. and Woods, R., 1984. E_h measurements in sulphide mineral slurries. Int. J. Miner. Process., 13:29-42.

Rangarajan, S.K., 1973a. Electrocrystallization: A stochastic theory of monolayer formation. J. Electroanal. Chem., 46:119-123.

Rangarajan, S.K., 1973b. Electrocrystallization: Multilayer formation and potentiostatic transients. J. Electroanal. Chem., 46:125-129.

Reddy, A.K.N., Genshaw, M.A. and Bockris, J.O'M., 1968. Ellipsometric study of oxygen-containing films on platinum anodes. J. Chem. Phys., 48:671-675.

Reuter, B. and Stein, R., 1957. Die Oxydation von Bleisulfid bei niedrigen Temperaturen. Z. Elektrochem., 61:440-454.

Richardson, P.E., 1984. Private communication.

Richardson, P.E. and O'Dell, C.S., 1984. Semiconducting characteristics of galena electrodes. In: P.E. Richardson, S. Srinivasan and R. Woods (Editors), Proceedings of the International Symposium on Electrochemistry in Mineral and Metal Processing. The Electrochemical Society, Pennington, NJ, 84-10:132-151.

Richardson, P.E., Stout, J.V., Proctor, C.L. and Walker, G.W., 1984. Electrochemical flotation of sulfides: Chalcocite-ethylxanthate interactions. Int. J. Miner. Process., 12:73-93.

Salamy, S.G. and Nixon, J.C., 1953. The application of electrochemical methods to flotation research. In: Recent Developments in Mineral Dressing. IMM, p. 503.

Sampson, R., 1978. Surface II Graphics System. Lawrence, Kansas.

Schuhmann, D., Guinard-Batiele, A.M. and Lamache, M., 1983. Sur l'electrosorption d'ethylxanthate au cours de la polarisation anodique d'electrodes de platine et de galene. Electrochim. Acta, 28:79-85.

Schultze, J.W., Lohrengel, M.M. and Ross, D., 1983. Nucleation and growth of anodic oxide films. Electrochim. Acta, 28:973-984.

Shimoiizaka, J., Usui, S., Matsuoka, I. and Sasaki, H., 1976. Depression of galena flotation by sulfite or chromate ion. In: M.C. Fuerstenau (Editor), Flotation, A.M. Gaudin Memorial Volume. AIME, New York. 1:393-413.

Shuey, R.T., 1975. Semiconducting Ore Minerals. Elsevier, New York.

Sillen, L.G. and Martell, A.E., 1964. Stability Constants of Metal-Ion complexes. Spec. Publ. No. 17, Chemical Society, London.

Simkovich, G. and Wagner, J.B., 1963. The influence of point defects on the kinetics of dissolution of semiconductors. J. Electrochem. Soc., 110:513-516.

Sivenas, P., 1981. Aspects of Electrochemistry Applied to the Study of Mississippi Valley Type Ore Deposits. Ph.D. Thesis, University of Toronto, Canada, p. 180.

Sivenas, P. and Beales, F.W., 1982a. J. Geochem. E., 17:123.

Sivenas, P. and Beales, F.W., 1982b. J. Geochem. E., 17:145.

Sivenas, P. and Foulkes, F.R., 1984. Cathodic reactions of natural galena in perchloric acid. 29:1215-1223.

Skewes, H.R., 1972. Electrowinning of lead directly from galena. Proc. Aust. Inst. Min. Met., 244:35-41.

Springer, G., 1970. Observations on the electrochemical reactivity of semiconducting minerals. Trans. IMM, 79:C11-C14.

Steger, H.F. and Desjardins, L.E., 1980. Oxidation of sulfide minerals. V. Galena, sphalerite and chalcocite. Can. Mineral., 18:365-372.

Steininger, J., 1968. The depression of sphalerite and pyrite by basic complexes of copper and sulphydryl flotation collectors. Trans. AIME, 24:34-42.

Sutherland, K.L. and Wark, I.W., 1955. Principles of Flotation. Aust. Inst. Min. Met., Melbourne.

Szeglowski, Z., 1960. Electric potential of local galvanic elements on the galena surface and their influence upon the adsorption of potassium xanthate. Proc. III Int. Congr. Surf. Act., Cologne, 2:110-111.

Taggart, A.F., del Giudice, G.R.M. and Ziehl, O.A., 1934. The case for the chemical theory of flotation. Trans. AIME, 112:348-381.

Thi, O.H., Lamache, M. and Bauer, D., 1981. Comportement electrochimique de l'ethylxanthate sur differents types d'electrodes: platine, or, galene, mercure. Electrochim. Acta, 26:33-44.

Thirsk, H.R. and Harrison, J.A., 1972. A Guide to the Study of Electrode Kinetics. Academic Press, New York, 115-135.

Thornber, M.R., 1982. Mineralogical and electrochemical stability of the nickel-iron sulphides - pentlandite and violarite. J. Appl. Electrochem., 13:253-267.

Tilak, B.V., Conway, B.E. and Angerstein-Kozlowska, H., 1973. The real condition of oxidation Pt electrodes. III. Kinetic theory of formation and reduction of surface oxides. J. Electroanal. Chem., 48:1-23.

Tipman, R.N., 1970. The Reactions of Potassium Ethyl Xanthate in Aqueous Solution. Ph.D. Thesis, University of British Columbia, Canada.

Tipman, R.N. and Leja, J., 1975. Reactivity of xanthate and dixanthogen in aqueous solutions at different pH. Colloid Polym. Sci., 253:1-12.

Tolun, R. and Kitchener, J.A., 1964. Electrochemical study of the galena-xanthate-oxygen flotation system. Trans. IMM, 73:313-322.

Toperi, D. and Tolun, R., 1969. Electrochemical study and thermodynamic equilibria of the galena-oxygen-xanthate flotation system. Trans. IMM, 78:C191-C197.

Tornell, B., 1966. Svensk Papperstidning, 69(19):658-663.

Toschev, S. and Mutaftschiew, B., 1964. On the activity of platinum electrodes during the process of electrolytic nucleation - I. Electrochim. Acta, 9:1203-1210.

Trahar, W.J., 1976. The selective flotation of galena from sphalerite with special reference to the effects of particle size. Int. J. Miner. Process., 3:151-166.

Trahar, W.J., 1983a. The influence of pulp potential in sulphide flotation. Presented at the Wark Symposium, Adelaide, Australia, July, 1983.

Trahar, W.J., 1983b. A laboratory study of the influence of sodium sulphide and oxygen on the collectorless flotation of chalcopyrite. Int. J. Miner. Process., 11:57-74.

Tributsch, H. and Gerischer, H., 1976. The oxidation and self-heating of metal sulphides as an electrochemical corrosion phenomenon. J. Appl. Chem. Biotechnol., 26:747-761.

Vaughan, D.J. and Craig, J.R., 1978. Mineral Chemistry of Metal Sulfides. Cambridge University Press, New York.

Vetter, K.J., 1967. Electrochemical Kinetics. Theoretical and Experimental Aspects. Academic Press, New York, pp. 189-193.

Vetter, K.J. and Schultze, J.W., 1972a. The kinetics of the electrochemical formation and reduction of monomolecular oxide layers on platinum in 0.5 M H_2SO_4. Part I. Potentiostatic pulse measurements. J. Electroanal. Chem., 34:131-139.

Vetter, K.J. and Schultze, J.W., 1972b. The kinetics of the electrochemical formation and reduction of monomolecular oxide layers on platinum in 0.5 M H_2SO_4. Part II. Galvanostatic pulse measurements and the model of oxide growth. J. Electroanal. Chem., 34:141-158.

Vijh, A., 1973. Electrochemistry of Metals and Semiconductors. Marcel Dekker, New York, Ch. 6, pp. 167-188.

Walker, G.W. and Richardson, P.E., 1982. Study of the electrochemical component of ethylxanthate-chalcocite reactions. Presented at the 56th Colloid and Surface Science Symposium, Blacksburg, Virginia, June, 1982.

Walker, G.W., Stout, J.V. and Richardson, P.E., 1984a. Electrochemical flotation of sulfides: Reactions of chalcocite in aqueous solution. Int. J. Miner. Process., 12:55-72.

Walker, G.W., Walters, C.P. and Richardson, P.E., 1984b. Correlation of the electrosorption of sulfur and thiol collectors with contact angle and flotation. In: P.E. Richardson, S. Srinivasan and R. Woods (Editors), Proceedings of the International Symposium on Electrochemistry in Mineral and Metal Processing. The Electrochemical Society, Pennington, NJ, 84-10:202-218.

Wark, I.W., 1938. Principles of Flotation. Aust. Inst. Min. Met., Melbourne, Australia.

Wierse, D.G., Lohrengel, M.M. and Schultze, J.W., 1978. Electrochemical properties of sulfur adsorbed on gold electrodes. J. Electroanal. Chem., 92:121-131.

Will, F. and Knorr, C.A., 1960. Z. Elektrochem., 64:270.

Woodcock, J.T. and Jones, M.H., 1970a. Chemical environment in Australian lead-zinc flotation plant pulps: I. pH, redox potentials and oxygen concentrations. Aust. Inst. Min. Met., 235:45-60.

Woodcock, J.T. and Jones, M.H., 1970b. Chemical environment in Australian lead-zinc flotation plant pulps: II. Collector residuals, metals in solution and other parameters. Aust. Inst. Min. Met., 235:61-76.

Woods, R., 1971. The oxidation of ethyl xanthate on platinum, gold, copper and galena electrodes. Relation to the mechanism of mineral flotation. J. Phys. Chem., 75:354-362.

Woods, R., 1972. The anodic oxidation of ethylxanthate on metal and galena electrodes. Aust. J. Chem., 25:2329-2335.

Woods, R., 1976. Electrochemistry of sulfide flotation. In: M.C. Fuerstenau (Editor), Flotation, A.M. Gaudin Memorial Volume. AIME, New York, 1:298-333.

Woods, R., 1984. Private communication.

Woods, R., 1984. Electrochemistry of sulphide flotation. In: M.H. Jones and J.T. Woodcock (Editors), Principles of Mineral Flotation. The Wark Symposium. Aust. Inst. Min. Met., Parkville, Victoria, Australia, pp. 91-115.

Wronski, M., 1959. Kinetics of decomposition of xanthogenates in sodium hydroxide solutions. Rocz. Chem., 33:1071-1080.

Yarar, B., Haydon, B.C. and Kitchener, J.A., 1969. Electrochemistry of the galena-diethyldithiocarbamate-oxygen flotation system. Trans. IMM, 78:C181-C184.

Yoon, R.H., 1981. Collectorless flotation of chalcopyrite and sphalerite ores by using sodium sulfide. Int. J. Miner. Process., 8:31-48.

Zingg, D.S. and Hercules, D.M., 1978. Electron spectroscopy for chemical analysis studies of lead sulfide oxidation. J. Phys. Chem., 82:1992-1995.

APPENDIX I.

Sample Computer Program

```
C
C
C      THIS COMPUTER PROGRAM DOES A THERMODYNAMIC-MASS BALANCE
C      CALCULATION FOR THE PBS-H2O-KEX SYSTEM IN THE CASE WHEN
C      OXIDATION OF SULFIDE IS ALLOWED TO PROCEED ONLY AS FAR
C      AS ELEMENTAL SULFUR.
C      EACH COMPUTER RUN DETERMINES THE FOLLOWING:
C                        1) THE EQUILIBRIUM CONCENTRATIONS OF ALL
C                           SOLUBLE SPECIES FOR PH VALUES BETWEEN
C                           0 AND 14 AT A GIVEN ELECTRODE POTENTIAL
C                        2) THE PH VALUES AT WHICH PHASE CHANGES
C                           OCCUR.
C                        3) THE PERCENTAGE OF XANTHATE ADDED THAT
C                           ENDS UP AS PBX2 (%PBX2) OR X2 (%X2)
C
C
C      THE PROGRAM VARIABLES ARE WRITTEN IN DOUBLE-PRECISION
C
C
       IMPLICIT REAL*8(A-H,O-Z)
       DIMENSION AH(1500),DS(1500),DPB(1500),D(1500),DX(1500)
       DIMENSION CAP(20)
       DIMENSION DPBT(1500),DST(1500),DXT(1500)
       DIMENSION H(150),PPB(150),PBOH(150),PBOH2(150),PBOH3(150)
      *,PB3OH4(150),PB4OH4(150),PB6OH8(150),PB4(150),PBO3(150),
      *PBO4(150),PB2OH(150),PBOH4(150)
       DIMENSION SS(150),HS(150),PH2S(150),H2S(150),S2(150),S3(150),
      *S4(150),S5(150)
       DIMENSION XAN(150),HXAN(150),XAN2(150),PERX1(150),PERX2(150)
       DIMENSION PBT(150),ST(150),XT(150)
       DIMENSION DISK(30,150)
C
C      SECTION 1 : INPUT AND INITIALIZATION

C
C      THE INPUT DATA IS INSERTED AT THIS POINT. THE FIRST STATEMENT
C      READS IN THE TITLE FOR THE TOP OF THE FIRST PAGE OF OUTPUT.
C      THE SECOND STATEMENT READS IN THE INPUT VARIABLES. ONLY FOUR
C      INPUT VARIABLES ARE REQUIRED:
C                        1) PH- INITIAL PH VALUE
C                        2) E - ELECTRODE POTENTIAL(SHE)
C                        3) XM- TOTAL AMOUNT OF METAL CATION (PB)
C                              IN SYSTEM (MOLES/LITER)
C                        4) XINIT- TOTAL AMOUNT OF XANTHATE
C                                  IN SYSTEM (MOLES/LITER)
C      IN THIS PROGRAM, ONLY A 1:1 STOICHIOMETRIC RATIO BETWEEN PB
C      AND S HAS BEEN CONSIDERED. IF A DIFFERENT RATIO IS DESIRED,
C      IT CAN BE EASILY CHANGED AT A LATER POINT IN THE PROGRAM,
C      WHICH WILL BE INDICATED.
C
```

```
C
      READ (31,333) (CAP(I),I=1,18)
 333  FORMAT(18A4)
      WRITE (6,334) (CAP(I),I=1,18)
 334  FORMAT(///2X,18A4)
      READ (31,3) PH,E,XM,XINIT
 3    FORMAT(4D10.4)
C
C     THE FOLLOWING SECTION INITIALIZES THE VARIOUS COUNTERS THAT
C     WILL BE USED. K KEEPS TRACK OF THE PH VALUES,WHICH ARE IN-
C     CREASED FROM 0 TO 14 AT INTERVALS OF 0.01. THE L VALUES KEEP
C     TRACK OF THE PH VALUES AT WHICH DIFFERENT PHASE CHANGES OCCUR.
C     AN L VALUE OF ZERO MEANS THAT A GIVEN PHASE CHANGE HAS NOT
C     OCCURRED. AN L VALUE OF ONE MEANS THAT THE CORRESPONDING
C     PHASE CHANGE HAS TAKEN PLACE. THIS WILL BE INDICATED IN THE
C     OUTPUT SECTION.
C
      K=0
      L0=0
      L1=0
      L2=0
      L3=0
      L5=0
      L6=0
      L7=0
      L8=0
      L9=0
      L10=0
      L11=0
      L12=0
      L13=0
      L14=0
      L15=0
      L16=0
      L17=0
      L18=0
      L19=0
      L20=0
      L21=0
      L22=0
      L23=0
      L24=0
      L25=0
      L26=0
      L27=0
      L28=0
      L29=0
      L30=0
      L31=0
      L32=0
```

```
      L33=0
      L34=0
      L35=0
      L36=0
      L37=0
      L38=0
      L39=0
      L40=0
      L41=0
      L42=0
      L43=0
      L44=0
      L45=0
      L46=0
      L47=0
      L48=0
      L49=0
      L50=0
      L51=0
      L52=0
      L53=0
      L54=0
      L55=0
      L56=0
      L57=0
      L58=0
      L59=0
      L60=0
      L61=0
      L62=0
      L63=0
      L64=0
      L65=0
      L66=0
      L67=0
      L68=0
      L69=0
      L70=0
      L71=0
C
C     N IS AN INDICATOR THAT LETS THE COMPUTER KNOW WHETHER PH 14
C     HAS BEEN REACHED. IF N=0, PH IS LESS THAN 14 AND THE PROGRAM
C     REMAINS IN THIS SECTION. IF N=1, PH 14 HAS BEEN REACHED AND
C     THE PROGRAM MOVES TO THE OUTPUT SECTION.
C
      N=0
      DXM=DLOG10(XM)
      DXINIT=DLOG10(XINIT)
      X2=XM
      DXCRIT=-(E+0.06D0)/0.059135928D0
```

```
C
C     SUBROUTINE UPDATE IS CALLED TO INCREASE THE PH BY 0.01 AND
C     THE COUNTER K BY 1.  PH IS ALSO CHECKED TO SEE IF IT EXCEEDS
C     14.
C
      CALL UPDATE(K,PH,D,AH,N)
C
C
C     SECTION 2 : MASS BALANCE- THERMODYNAMIC CALCULATIONS
C
C     THIS SECTION FORMS THE LARGEST PART OF THE PROGRAM.  IT IS
C     BROKEN UP INTO SMALL UNITS, EACH OF WHICH CORRESPONDS TO
C     THE CASE WHERE A DIFFERENT PHASE(S) IS(ARE) STABLE.  ONCE
C     THE APPROPRIATE EQUATION IS SOLVED, IT IS CHECKED TO SEE
C     WHETHER ANY OTHER PHASE IS MORE STABLE.  IF SO, THE PROGRAM
C     JUMPS TO THE UNIT FOR THE MORE STABLE PHASE.  THIS PROCEDURE
C     IS REPEATED UNTIL NO MORE PHASE CAN BE FOUND.  AT THIS POINT,
C     THE PROGRAM RETURNS TO SUBROUTINE UPDATE AND THE PH IS IN-
C     CREASED AGAIN.
C
C     THIS UNIT CONSIDERS THE CASE WHEN ONLY SOLUBLE SPECIES ARE
C     STABLE.  SUBROUTINES SULF AND XANTH SOLVE THE MASS BALANCE
C     EQUATIONS FOR SULFUR-BEARING AND XANTHATE-BEARING SPECIES,
C     RESPECTIVELY, UNDER THESE CONDITIONS.  SOLVE IS A SUBROUT-
C     INE WHICH SOLVES POLYNOMIAL EQUATIONS FOR SEVERAL CASES.
C     IN THIS ONE, THE MASS BALANCE EQUATION FOR LEAD-BEARING
C     SPECIES WHEN ALL ARE DISSOLVED IS HANDLED.
C
 6    CALL SULF (K,AH,E,DS,DXM,XM)
      LL=1
      CALL SOLVE (X2,AH,E,K,XM,PH,DPB,LL,XINIT)
      CALL XANTH (K,AH,E,XINIT,DX)
      IF(L27.NE.0) GO TO 26
 26   DPBCRT=(E+0.1260D0)/0.029567964D0
      IF(DPB(K).GT.DPBCRT) GO TO 7
      IF(L16.NE.0) GO TO 22
      DSCRT=-(E+0.4761D0)/0.029567964D0
      IF(DS(K).GT.DSCRT) GO TO 8
 22   IF(L9.NE.0) GO TO 17
      PBS=DPB(K)+DS(K)
      IF(PBS.GT.-28.7864D0) GO TO 9
      PBX2=DPB(K)+2.D0*DX(K)
      IF(PBX2.GT.-16.7D0) GO TO 24
 17   IF(L10.NE.0) GO TO 18
      DPBCRT=13.6348D0-2.D0*PH
      IF(DPB(K).GT.DPBCRT) GO TO 12
 18   IF(L11.NE.0) GO TO 19
      DPBCRT=-(E-2.0944D0+0.236544D0*PH)/0.08870389D0
      IF(DPB(K).GT.DPBCRT) GO TO 13
 19   DPBCRT=-(E-1.8056D0+0.177408D0*PH)/0.059135928D0
```

```
      IF(DPB(K).GT.DPBCRT) GO TO 14
      DPBCRT=-(E-1.4495D0+0.118272D0*PH)/0.029567964D0
      IF(DPB(K).GT.DPBCRT) GO TO 15
C
C     DXCRIT IS THE CRITICAL FREE XANTHATE ION CONCENTRATION
C     REQUIRED FOR LIQUID DIXANTHOGEN TO BE STABLE (IN THIS CASE,
C     L19 IS SET EQUAL TO 1)
C
      IF(DX(K).GT.DXCRIT.AND.L19.NE.0) GO TO 1600
      IF(DX(K).GT.DXCRIT) L19=L19+1
      IF(DX(K).GT.DXCRIT) P19=PH
 1600 IF(DX(K).GT.DXCRIT) DX(K)=DXCRIT
C
C     SSOL, PBSOL AND XSOL ARE FUNCTION SUBPROGRAMS WHICH DETERMINE
C     THE TOTAL DISSOLVED SULFUR-, LEAD-, AND XANTHATE-BEARING SPE-
C     CIES CONCENTRATIONS
C
      DST(K)=SSOL (K,E,AH,PH,DS)
      DPBT(K)=PBSOL (K,AH,E,PH,DPB)
      DXT(K)=XSOL (K,AH,E,DX)
      IF(L0.NE.0) GO TO 1601
      L0=L0+1
      P0=PH
C     THIS NEXT UNIT CONSIDERS THE CASE WHERE PB METAL IS STABLE.
C     THIS WILL ENTIRELY DETERMINE THE DISTRIBUTION OF LEAD-BEARING
C     SPECIES. SULF AND XANTH CALCULATE THE SULFUR AND XANTHATE
C     SPECIES CONCENTRATIONS.
C
 1601 CALL UPDATE(K,PH,D,AH,N)
      IF(N.EQ.1) GO TO 11
      GO TO 6
 7    IF(L1.NE.0) GO TO 1602
      L1=L1+1
      P1=PH
 1602 DPB(K)=(E+0.1260D0)/0.029567964D0
      CALL SULF (K,AH,E,DS,DXM,XM)
      DSCRT=-(E+0.4761D0)/0.029567964D0
      IF(DS(K).GT.DSCRT) GO TO 8
      CALL XANTH (K,AH,E,XINIT,DX)
      PBS=DPB(K)+DS(K)
      IF(PBS.GT.-28.7864D0) GO TO 9
      PBX2=DPB(K)+2.D0*DX(K)
      IF(PBX2.GT.-16.7D0) GO TO 24
      DPBCRT=13.6348D0-2.D0*PH
      IF(DPB(K).GT.DPBCRT) GO TO 12
      DPBCRT=-(E-2.0944D0+0.236544D0*PH)/0.08870389D0
      IF(DPB(K).GT.DPBCRT) GO TO 13
      DPBCRT=-(E-1.8056D0+0.177408D0*PH)/0.059135928D0
      IF(DPB(K).GT.DPBCRT) GO TO 14
      DPBCRT=-(E-1.4495D0+0.118272D0*PH)/0.029567964D0
```

```
      IF(DPB(K).GT.DPBCRT) GO TO 15
      DST(K)=SSOL (K,E,AH,PH,DS)
      DPBT(K)=PBSOL (K,AH,E,PH,DPB)
      DXT(K)=XSOL (K,AH,E,DX)
      CALL UPDATE(K,PH,D,AH,N)
      IF(N.EQ.1) GO TO 11
      GO TO 7
C
C     THIS UNIT CONSIDERS THE SITUATION WHEN ELEMENTAL SULFUR IS
C     PRESENT. SOLVE AND XANTH ARE USED TO DETERMINE THE LEAD AND
C     XANTHATE CONCENTRATIONS.
C
 8    IF(L2.NE.0) GO TO 1603
      L2=L2+1
      P2=PH
 1603 DS(K)=-(E+0.4761D0)/0.029567964D0
      LL=1
      IF(K.EQ.1) X2=10.D0**DPB(K)
      IF(K.GT.1) X2=10.D0**DPB(K-1)
      CALL SOLVE (X2,AH,E,K,XM,PH,DPB,LL,XINIT)
      CALL XANTH (K,AH,E,XINIT,DX)
      IF(L67.NE.0) GO TO 1705
      PBS=DPB(K)+DS(K)
      IF(PBS.GT.-28.7864D0) GO TO 9
 1705 IF(L66.NE.0.OR.L42.NE.0) GO TO 1701
      PBX2=DPB(K)+2.D0*DX(K)
      IF(PBX2.GT.-16.7D0) GO TO 24
 1701 DPBCRT=13.6348D0-2.D0*PH
      IF(DPB(K).GT.DPBCRT) GO TO 41
      DPBCRT=-(E-2.0944D0+0.236544D0*PH)/0.08870389D0
      IF(DPB(K).GT.DPBCRT) GO TO 42
      DPBCRT=-(E-1.8056D0+0.177408D0*PH)/0.059135928D0
      IF(DPB(K).GT.DPBCRT) GO TO 14
      DPBCRT=-(E-1.4495D0+0.118272D0*PH)/0.029567964D0
      IF(DPB(K).GT.DPBCRT) GO TO 43
      DST(K)=SSOL (K,E,AH,PH,DS)
C
C     IT IS NOW CHECKED TO SEE WHETHER THE TOTAL CONCENTRATION OF
C     SULFUR SPECIES EXCEEDS THE TOTAL AMOUNT OF SULFUR IN THE
C     SYSTEM. IF SO, THEN IT IS IMPOSSIBLE FOR ELEMENTAL SULFUR TO
C     EXIST.
C
      IF(DST(K).GT.DXM.AND.L16.NE.0) GO TO 1668
      IF(DST(K).GT.DXM) L16=L16+1
      IF(DST(K).GT.DXM) P16=PH
 1668 IF(DST(K).GT.DXM) GO TO 6
      DPBT(K)=PBSOL (K,AH,E,PH,DPB)
      IF(DX(K).GT.DXCRIT.AND.L20.NE.0) GO TO 1604
      IF(DX(K).GT.DXCRIT) L20=L20+1
      IF(DX(K).GT.DXCRIT) P20=PH
```

```
 1604 IF(DX(K).GT.DXCRIT) DX(K)=DXCRIT
      DXT(K)=XSOL (K,AH,E,DX)
      CALL UPDATE(K,PH,D,AH,N)
      IF(N.EQ.1) GO TO 11
      GO TO 8
C
C     THIS UNIT CONSIDERS THE CASE WHERE PBS IS THE STABLE PHASE.
C     SOLUTION OF THE APPROPRIATE MASS BALANCE EQUATION BY SUB-
C     ROUTINE SOLVE DETERMINES THE LEAD AND SULFUR DISTRIBUTIONS.
C
  9   IF(L3.NE.0) GO TO 1605
      L3=L3+1
      P3=PH
 1605 LL=2
      IF(K.EQ.1) X2=1.3519D-04
      CALL SOLVE (X2,AH,E,K,XM,PH,DPB,LL,XINIT)
      DS(K)=-28.7864D0-DPB(K)
      IF(L15.NE.0) GO TO 1708
      DPBCRT=(E+0.1260D0)/0.029567964D0
      IF(DPB(K).GT.DPBCRT) GO TO 21
      IF(DPB(K).LE.DPBCRT.AND.L14.NE.0) L15=L15+1
      IF(DPB(K).LE.DPBCRT.AND.L14.NE.0) P15=PH
 1708 CALL XANTH (K,AH,E,XINIT,DX)
  754 IF(L13.NE.0) GO TO 753
      DSCRT=-(E+0.4761D0)/0.029567964D0
      IF(DS(K).GT.DSCRT) GO TO 20
      IF(L38.NE.0) GO TO 755
  753 PBX2=DPB(K)+2.D0*DX(K)
      IF(PBX2.GT.-16.7D0.AND.L35.NE.0) GO TO 28
      IF(PBX2.GT.-16.7D0) GO TO 27
  755 DPBCRT=13.6348D0-2.D0*PH
      IF(DPB(K).GT.DPBCRT) GO TO 12
      DPBCRT=-(E-2.0944D0+0.236544D0*PH)/0.08870389D0
      IF(DPB(K).GT.DPBCRT) GO TO 13
      DPBCRT=-(E-1.8056D0+0.177408D0*PH)/0.059135928D0
      IF(DPB(K).GT.DPBCRT) GO TO 14
      DPBCRT=-(E-1.4495D0+0.118272D0*PH)/0.029567964D0
      IF(DPB(K).GT.DPBCRT) GO TO 15
      DST(K)=SSOL (K,E,AH,PH,DS)
      DPBT(K)=PBSOL (K,AH,E,PH,DPB)
      IF(DX(K).GT.DXCRIT.AND.L21.NE.0) GO TO 1607
      IF(DX(K).GT.DXCRIT) L20=L20+1
      IF(DX(K).GT.DXCRIT) P20=PH
 1607 IF(DX(K).GT.DXCRIT) DX(K)=DXCRIT
      DXT(K)=XSOL (K,AH,E,DX)
      CALL UPDATE(K,PH,D,AH,N)
      IF(N.EQ.1) GO TO 11
      GO TO 9
C     THIS UNIT HANDLES THE CASE WHEN PB(OH)2 IS STABLE. SULF AND
C     XANTH DETERMINE THE SULFUR AND XANTHATE SPECIES DISTRIBUTIONS.
```

```
C
 12   IF(L5.NE.0) GO TO 1608
      L5=L5+1
      P5=PH
 1608 DPB(K)=13.6348D0-2.D0*PH
      CALL SULF (K,AH,E,DS,DXM,XM)
      DSCRIT=-(E+0.4761D0)/0.029567964D0
      IF(DS(K).GT.DSCRIT) GO TO 41
      CALL XANTH (K,AH,E,XINIT,DX)
      PBS=DPB(K)+DS(K)
      IF(PBS.GE.-28.7864D0) GO TO 23
      IF(PBS.LT.-28.7864D0.AND.L17.NE.0.AND.L18.NE.0) GO TO 1610
      IF(PBS.LT.-28.7864D0.AND.L17.NE.0) L18=L18+1
      IF(PBS.LT.-28.7864D0.AND.L17.NE.0) P18=PH
 1610 DPBCRT=-(E-2.0944D0+0.236544D0*PH)/0.08870389D0
      IF(DPB(K).GT.DPBCRT) GO TO 13
      DPBCRT=-(E-1.8056D0+0.177408D0*PH)/0.059135928D0
      IF(DPB(K).GT.DPBCRT) GO TO 14
      DPBCRT=-(E-1.4495D0+0.118272D0*PH)/0.029567964D0
      IF(DPB(K).GT.DPBCRT) GO TO 15
      DST(K)=SSOL (K,E,AH,PH,DS)
      DPBT(K)=PBSOL (K,AH,E,PH,DPB)
C
C     THE PROGRAM NOW CHECKS TO SEE WHETHER THE TOTAL LEAD CONCEN-
C     TRATION IS GREATER THAN THE AMOUNT ALLOWABLE ON THE BASIS
C     OF THE QUANTITY OF MINERAL INITIALLY PUT INTO THE SYSTEM.
C
      IF(DPBT(K).GT.DXM.AND.L10.NE.0) GO TO 1611
      IF(DPBT(K).GT.DXM) L10=L10+1
      IF(DPBT(K).GT.DXM) P10=PH
 1611 IF(DPBT(K).GT.DXM) GO TO 6
      IF(DX(K).GT.DXCRIT.AND.L22.NE.0) GO TO 1609
      IF(DX(K).GT.DXCRIT) L22=L22+1
      IF(DX(K).GT.DXCRIT) P22=PH
 1609 IF(DX(K).GT.DXCRIT) DX(K)=DXCRIT
      DXT(K)=XSOL (K,AH,E,DX)
      CALL UPDATE(K,PH,D,AH,N)
      IF(N.EQ.1) GO TO 11
      GO TO 12
C
C     THE SITUATION WHEN PB3O4 IS STABLE IS NOW CONSIDERED.
C
 13   IF(L6.NE.0) GO TO 1612
      L6=L6+1
      P6=PH
 1612 DPB(K)=-(E-2.0944D0+0.236544D0*PH)/0.08870389D0
      CALL SULF (K,AH,E,DS,DXM,XM)
      DSCRIT=-(E+0.4761D0)/0.029567964D0
      IF(DS(K).GT.DSCRIT) GO TO 42
      CALL XANTH (K,AH,E,XINIT,DX)
```

```
      DPBCRT=-(E-1.8056D0+0.177408D0*PH)/0.059135928D0
      IF(DPB(K).GT.DPBCRT) GO TO 14
      DPBCRT=-(E-1.4495D0+0.118272D0*PH)/0.029567964D0
      IF(DPB(K).GT.DPBCRT) GO TO 15
      DST(K)=SSOL (K,E,AH,PH,DS)
      DPBT(K)=PBSOL (K,AH,E,PH,DPB)
      IF(DPBT(K).GT.DXM.AND.DX(K).GE.DXCRIT.AND.L41.NE.0) GO TO 1614
      IF(DPBT(K).GT.DXM.AND.DX(K).GE.DXCRIT) L41=L41+1
      IF(DPBT(K).GT.DXM.AND.DX(K).GE.DXCRIT) P41=PH
 1614 IF(DPBT(K).GT.DXM.AND.DX(K).GE.DXCRIT) GO TO 6
      IF(DPBT(K).GT.DXM.AND.L11.NE.0) GO TO 1615
      IF(DPBT(K).GT.DXM) L11=L11+1
      IF(DPBT(K).GT.DXM) P11=PH
 1615 IF(DPBT(K).GT.DXM) GO TO 6
      IF(DX(K).GT.DXCRIT.AND.L23.NE.0) GO TO 1613
      IF(DX(K).GT.DXCRIT) L23=L23+1
      IF(DX(K).GT.DXCRIT) P23=PH
 1613 IF(DX(K).GT.DXCRIT) DX(K)=DXCRIT
      DXT(K)=XSOL (K,AH,E,DX)
      CALL UPDATE(K,PH,D,AH,N)
      IF(N.EQ.1) GO TO 11
      GO TO 13
C
C     THIS UNIT CONSIDERS THE CASE WHEN PB2O3 IS THE ONLY INSOL-
C     SPECIES.
C
 14   IF(L7.NE.0) GO TO 1616
      L7=L7+1
      P7=PH
 1616 DPB(K)=-(E-1.8056D0+0.177408D0*PH)/0.059135928D0
      CALL SULF (K,AH,E,DS,DXM,XM)
      DPBCRT=-(E-1.4495D0+0.118272D0*PH)/0.029567964D0
      IF(DPB(K).GT.DPBCRT) GO TO 15
      DST(K)=SSOL (K,E,AH,PH,DS)
      DPBT(K)=PBSOL (K,AH,E,PH,DPB)
      DXT(K)=XSOL (K,AH,E,DX)
      CALL UPDATE(K,PH,D,AH,N)
      IF(N.EQ.1) GO TO 11
      GO TO 14
C
C     THIS PROCEDURE IS NOW DONE FOR THE CASE WHEN PBO2 EXISTS.
C
 15   IF(L8.NE.0) GO TO 1617
      L8=L8+1
      P8=PH
 1617 DPB(K)=-(E-1.4495D0+0.118272D0*PH)/0.029567964D0
      CALL SULF (K,AH,E,DS,DXM,XM)
      DSCRIT=-(E+0.4761D0)/0.029567964D0
      IF(DS(K).GT.DSCRIT) GO TO 43
      CALL XANTH (K,AH,E,XINIT,DX)
```

```
      DST(K)=SSOL (K,E,AH,PH,DS)
      DPBT(K)=PBSOL (K,AH,E,PH,DPB)
      IF(DX(K).GT.DXCRIT.AND.L24.NE.0) GO TO 1618
      IF(DX(K).GT.DXCRIT) L24=L24+1
      IF(DX(K).GT.DXCRIT) P24=PH
 1618 IF(DX(K).GT.DXCRIT) DX(K)=DXCRIT
      DXT(K)=XSOL (K,AH,E,DX)
      CALL UPDATE(K,PH,D,AH,N)
      IF(N.EQ.1) GO TO 11
      GO TO 15
C
C     WE ARE NOW AT THE PART OF THIS SECTION WHERE SITUATIONS IN
C     WHICH MORE THAN ONE INSOLUBLE SPECIES CO-EXITS ARE TAKEN
C     CARE OF. THE FIRST ONE INVOLVES ELEMENTAL SULFUR AND PBS
C     BEING PRESENT TOGETHER. XANTH IS ONCE AGAIN USED TO DETER-
C     MINE THE BREAKDOWN OF XANTHATE-BEARING SPECIES.
C
 20   IF(L12.NE.0) GO TO 1619
      L12=L12+1
      P12=PH
 1619 DS(K)=-(E+0.4761D0)/0.029567964D0
      DPB(K)=-28.7864D0-DS(K)
      CALL XANTH (K,AH,E,XINIT,DX)
      DPBCRT=13.6348D0-2.D0*PH
      IF(DPB(K).GT.DPBCRT) GO TO 41
      DST(K)=SSOL (K,E,AH,PH,DS)
      IF(DST(K).GT.DXM.AND.L13.NE.0) GO TO 1621
      IF(DST(K).GT.DXM) L13=L13+1
      IF(DST(K).GT.DXM) P13=PH
 1621 IF(DST(K).GT.DXM) GO TO 9
      PBX2=DPB(K)+2.D0*DX(K)
      IF(PBX2.GT.-16.7D0) GO TO 30
      DPBT(K)=PBSOL (K,AH,E,PH,DPB)
      IF(DPBT(K).GT.DXM.AND.L67.NE.0) GO TO 1704
      IF(DPBT(K).GT.DXM) L67=L67+1
      IF(DPBT(K).GT.DXM) P67=PH
 1704 IF(DPBT(K).GT.DXM) GO TO 8
      IF(DX(K).GT.DXCRIT.AND.L25.NE.0) GO TO 1620
      IF(DX(K).GT.DXCRIT)  L25=L25+1
      IF(DX(K).GT.DXCRIT) P25=PH
 1620 IF(DX(K).GT.DXCRIT) DX(K)=DXCRIT
      DXT(K)=XSOL (K,AH,E,DX)
      CALL UPDATE(K,PH,D,AH,N)
      IF(N.EQ.1) GO TO 11
      GO TO 9
C
C     THE COMBINATION OF ELEMENTAL LEAD AND PBS IS NOW CONSIDERED.
C
 21   IF(L14.NE.0) GO TO 1622
      L14=L14+1
```

```
      P14=PH
 1622 DPB(K)=(E+0.1260D0)/0.029567964D0
      DS(K)=-28.7864D0-DPB(K)
      CALL XANTH (K,AH,E,XINIT,DX)
      PBX2=DPB(K)+2.D0*DX(K)
      IF(PBX2.GT.-16.7D0) GO TO 33
      DST(K)=SSOL (K,E,AH,PH,DS)
      DPBT(K)=PBSOL (K,AH,E,PH,DPB)
      IF(DPBT(K).GT.DXM.AND.L15.NE.0) GO TO 1707
      IF(DPBT(K).GT.DXM) L15=L15+1
      IF(DPBT(K).GT.DXM) P15=PH
 1707 IF(DPBT(K).GT.DXM) GO TO 9
      DXT(K)=XSOL (K,AH,E,DX)
      CALL UPDATE(K,PH,D,AH,N)
      IF(N.EQ.1) GO TO 11
      GO TO 9
C
C     THIS UNIT INVOLVES THE COMBINATION OF PB(OH)2 AND PBS
C
 23   IF(L17.NE.0) GO TO 1623
      L17=L17+1
      P17=PH
 1623 DPB(K)=13.6348D0-2.D0*PH
      DS(K)=-28.7864D0-DPB(K)
      CALL XANTH (K,AH,E,XINIT,DX)
      DST(K)=SSOL (K,E,AH,PH,DS)
      DPBT(K)=PBSOL (K,AH,E,PH,DPB)
      IF(DX(K).GT.DXCRIT.AND.L26.NE.0) GO TO 1624
      IF(DX(K).GT.DXCRIT) L26=L26+1
      IF(DX(K).GT.DXCRIT) P26=PH
 1624 IF(DX(K).GT.DXCRIT) DX(K)=DXCRIT
      DXT(K)=XSOL (K,AH,E,DX)
      CALL UPDATE(K,PH,D,AH,N)
      IF(N.EQ.1) GO TO 11
      GO TO 12
 24   IF(K.EQ.1) X2=10.D0**DPB(K)
      IF(K.EQ.1) GO TO 25
      X2=10.D0**DPB(K-1)
C
C     NOW, CASES WHERE PBX2 IS STABLE ARE HANDLED. THE FIRST ONE
C     IS THE SITUATION WHEN PBX2 ALONE IS STABLE. SUBROUTINE SOLVE
C     IS CALLED UPON TO SOLVE THE APPROPRIATE MASS BALANCE EQUATION.
C     SINCE ALL THE SULFUR-BEARING SPECIES ARE DISSOLVED IN THIS
C     CIRCUMSTANCE, SUBROUTINE SULF IS USED TO CALCULATE THE CON-
C     CENTRATION OF THESE SPECIES.
C
 25   IF(L27.NE.0) GO TO 1625
      L27=L27+1
      P27=PH
 1625 LL=4
```

```
      CALL SOLVE (X2,AH,E,K,XM,PH,DPB,LL,XINIT)
      DXAN=-8.35D0-0.5D0*DPB(K)
      IF(DXAN.GT.DXCRIT.AND.L42.NE.0) GO TO 1626
      IF(DXAN.GT.DXCRIT) L42=L42+1
      IF(DXAN.GT.DXCRIT) P42=PH
 1626 IF(DXAN.GT.DXCRIT) GO TO 6
      CALL XANTH (K,AH,E,XINIT,DX)
      IF(DXAN.GT.DX(K).AND.L27.NE.0.AND.L28.NE.0) GO TO 1627
      IF(DXAN.GT.DX(K).AND.L27.NE.0) L28=L28+1
      IF(DXAN.GT.DX(K).AND.L27.NE.0) P28=PH
 1627 IF(DXAN.GT.DX(K)) GO TO 6
      DX(K)=DXAN
      CALL SULF (K,AH,E,DS,DXM,XM)
      IF(L31.NE.0) GO TO 502
      DSCRIT=-(E+0.4761D0)/0.029567964D0
      IF(DS(K).GT.DSCRIT) GO TO 29
 502  IF(L37.NE.0) GO TO 503
      PBS=DPB(K)+DS(K)
      IF(PBS.GT.-28.7864D0) GO TO 9
 503  PBHYD=13.6348D0-2.D0*PH
      IF(DPB(K).GT.PBHYD) GO TO 36
      DST(K)=SSOL (K,E,AH,PH,DS)
      DPBT(K)=PBSOL (K,AH,E,PH,DPB)
      DXT(K)=XSOL (K,AH,E,DX)
      CALL UPDATE(K,PH,D,AH,N)
      IF(N.EQ.1) GO TO 11
      GO TO 25
C
C     SOLVE IS NOW USED TO FIND A SOLUTION TO THE EQUATION FOR THE
C     CASE WHEN PBS AND PBX2 CO-EXIST.
C
 27   IF(L29.NE.0) GO TO 1628
      L29=L29+1
      P29=PH
 1628 LL=5
      CALL SOLVE (X2,AH,E,K,XM,PH,DPB,LL,XINIT)
      DS(K)=-28.7864D0-DPB(K)
      DX(K)=-8.35D0-0.5D0*DPB(K)
      IF(L33.NE.0) GO TO 887
      DSCRIT=-(E+0.4761D0)/0.029567964D0
      IF(DS(K).GT.DSCRIT) GO TO 30
 887  DPBCRT=(E+0.126D0)/0.029567964D0
      IF(DPB(K).GT.DPBCRT) GO TO 33
      DST(K)=SSOL (K,E,AH,PH,DS)
      DPBT(K)=PBSOL (K,AH,E,PH,DPB)
      IF(DST(K).GT.DXM.AND.L30.NE.0) GO TO 1630
      IF(DST(K).GT.DXM) L30=L30+1
      IF(DST(K).GT.DXM) P30=PH
 1630 IF(DST(K).GT.DXM) GO TO 24
C
```

```
C     IT IS NOW CHECKED TO SEE WHETHER THE TOTAL CONCENTRATION OF
C     DISSOLVED XANTHATE-BEARING SPECIES IS GREATER THAN THE MAX-
C     IMUM ALLOWED. IF SO, IT IS IMPOSSIBLE FOR PBX2 TO EXIST AND
C     ONLY PBS REMAINS STABLE.
C
      DXT(K)=XSOL (K,AH,E,DX)
      IF(DXT(K).GT.DXINIT.AND.L35.NE.0) GO TO 1631
      IF(DXT(K).GT.DXINIT) L35=L35+1
      IF(DXT(K).GT.DXINIT) P35=PH
 1631 IF(DXT(K).GT.DXINIT) GO TO 9
      CALL UPDATE(K,PH,D,AH,N)
      IF(N.EQ.1) GO TO 11
      GO TO 27
C
C     THE CASE WHERE ELEMENTAL SULFUR AND PBX2 ARE PRESENT SIMUL-
C     TANEOUSLY IS NOW CONSIDERED.
C
 29   IF(L31.NE.0) GO TO 1632
      L31=L31+1
      P31=PH
 1632 DS(K)=-(E+0.4761D0)/0.029567964D0
      LL=4
      IF(K.EQ.1) X2=10.D0**DPB(K)
      IF(K.EQ.1) GO TO 1700
      X2=10.D0**DPB(K-1)
 1700 CALL SOLVE (X2,AH,E,K,XM,PH,DPB,LL,XINIT)
      DX(K)=-8.35D0-0.5D0*DPB(K)
      IF(DX(K).GT.DXCRIT) L42=L42+1
      IF(DX(K).GT.DXCRIT) P42=PH
      IF(DX(K).GT.DXCRIT) GO TO 8
      DXT(K)=XSOL (K,AH,E,DX)
      IF(DXT(K).GT.DXINIT) L66=L66+1
      IF(DXT(K).GT.DXINIT) P66=PH
      IF(DXT(K).GT.DXINIT) GO TO 8
      IF(L49.NE.0) GO TO 40
      PBS=DPB(K)+DS(K)
      IF(PBS.GT.-28.7864D0) GO TO 27
 40   DPBCRT=13.6348D0-2.D0*PH
      IF(DPB(K).GT.DPBCRT) GO TO 41
      DPBCRT=-(E-2.0944D0+0.236544D0*PH)/0.08870389D0
      IF(DPB(K).GT.DPBCRT) GO TO 42
      DPBCRT=-(E-1.4495D0+0.118272D0*PH)/0.029567964D0
      IF(DPB(K).GT.DPBCRT) GO TO 43
      DST(K)=SSOL (K,E,AH,PH,DS)
      IF(DST(K).GT.DXM.AND.L32.NE.0) GO TO 1633
      IF(DST(K).GT.DXM) L32=L32+1
      IF(DST(K).GT.DXM) P32=PH
 1633 IF(DST(K).GT.DXM) GO TO 24
      DPBT(K)=PBSOL (K,AH,E,PH,DPB)
      CALL UPDATE(K,PH,D,AH,N)
```

```
      IF(N.EQ.1) GO TO 11
      GO TO 29
C
C     THE FOLLOWING CASE CONSIDERS WHEN ELEMENTAL SULFUR, PBS AND
C     PBX2 ALL ARE PRESENT AT THE SAME TIME.
C
 30   IF(L33.NE.0) GO TO 1634
      L33=L33+1
      P33=PH
 1634 DS(K)=-(E+0.4761D0)/0.029567964D0
      DPB(K)=-28.7864D0-DS(K)
      DX(K)=-8.35D0-0.5D0*DPB(K)
      DPBCRT=13.6348D0-2.D0*PH
      IF(DPB(K).GT.DPBCRT) GO TO 45
      DST(K)=SSOL (K,E,AH,PH,DS)
      IF(DST(K).GT.DXM.AND.L34.NE.0) GO TO 1635
      IF(DST(K).GT.DXM) L34=L34+1
      IF(DST(K).GT.DXM) P34=PH
 1635 IF(DST(K).GT.DXM) GO TO 27
      DPBT(K)=PBSOL (K,AH,E,PH,DPB)
      IF(DPBT(K).GT.DXM.AND.L49.NE.0) GO TO 1636
      IF(DPBT(K).GT.DXM) L49=L49+1
      IF(DPBT(K).GT.DXM) P49=PH
 1636 IF(DPBT(K).GT.DXM) GO TO 29
      DXT(K)=XSOL (K,AH,E,DX)
      CALL UPDATE(K,PH,D,AH,N)
      IF(N.EQ.1) GO TO 11
      GO TO 30
C
C     IN THE COURSE OF THESE CALCULATIONS, IT WAS DISCOVERED THAT
C     THERE IS A PBS AND PBX2 ARE PRESENT TOGETHER AT LOW PH. THEN,
C     AT SOME PH, PBX2 BECOMES UNSTABLE, LEAVING BEHIND ONLY PBS.
C     EVENTUALLY, PBX2 REAPPEARS AND SO THE COMBINATION OF THE TWO
C     IS RE-CONSIDERED. THIS IS DONE  IN THIS UNIT.
C
 28   IF(L36.NE.0) GO TO 1637
      L36=L36+1
      P36=PH
 1637 LL=5
      CALL SOLVE (X2,AH,E,K,XM,PH,DPB,LL,XINIT)
      DPBCRT=13.6348D0-2.D0*PH
      IF(DPB(K).GT.DPBCRT) GO TO 37
      DS(K)=-28.7864D0-DPB(K)
      DX(K)=-8.35D0-0.5D0*DPB(K)
      DST(K)=SSOL (K,E,AH,PH,DS)
      IF(DST(K).GT.DXM.AND.L37.NE.0) GO TO 1638
      IF(DST(K).GT.DXM) L37=L37+1
      IF(DST(K).GT.DXM) P37=PH
 1638 IF(DST(K).GT.DXM) GO TO 24
      DXT(K)=XSOL (K,AH,E,DX)
```

```
      IF(DXT(K).GT.DXINIT.AND.L38.NE.0) GO TO 1639
      IF(DXT(K).GT.DXINIT) L38=L38+1
      IF(DXT(K).GT.DXINIT) P38=PH
 1639 IF(DXT(K).GT.DXINIT) GO TO 9
      DPBT(K)=PBSOL (K,AH,E,PH,DPB)
      CALL UPDATE(K,PH,D,AH,N)
      IF(N.EQ.1) GO TO 11
      GO TO 28
C
C     THE CO-EXISTENCE OF ELEMENTAL LEAD,LEAD SULFIDE AND LEAD XAN-
C     THATE IS NOW CONSIDERED.
C
 33   IF(L39.NE.0) GO TO 1640
      L39=L39+1
      P39=PH
 1640 DPB(K)=(E+0.126D0)/0.029567964D0
      DS(K)=-28.7864D0-DPB(K)
      DX(K)=-8.35D0-0.5D0*DPB(K)
      DPBT(K)=PBSOL (K,AH,E,PH,DPB)
      IF(DPBT(K).GT.DXM.AND.L40.NE.0) GO TO 1706
      IF(DPBT(K).GT.DXM) L40=L40+1
      IF(DPBT(K).GT.DXM) P40=PH
 1706 IF(DPBT(K).GT.DXM) GO TO 27
      DST(K)=SSOL (K,E,AH,PH,DS)
      DXT(K)=XSOL (K,AH,E,DX)
      CALL UPDATE(K,PH,D,AH,N)
      IF(N.EQ.1) GO TO 11
      GO TO 1628
C
C     PB(OH)2 AND PBX2 CAN CO-EXIST.THIS UNIT COVERS THIS SITUATION
C     AND THE ONE WHEN PBX2 NO LONGER IS PRESENT. IN THE LATTER
C     CASE, ONLY PB(OH)2 IS THEN CONSIDERED. ALSO, THE POSSIBILITY
C     THAT DIXANTHOGEN EXISTS ALONG WITH PB(OH)2 IS TAKEN INTO
C     ACCOUNT.
C
 36   IF(L43.NE.0) GO TO 1641
      L43=L43+1
      P43=PH
 1641 DPB(K)=13.6348D0-2.D0*PH
      CALL XANTH (K,AH,E,XINIT,DX)
      PBX2=DPB(K)+2.D0*DX(K)
      IF(PBX2.GE.-16.7D0.AND.L44.NE.0) GO TO 1642
      IF(PBX2.GE.-16.7D0) L44=L44+1
      IF(PBX2.GE.-16.7D0) P44=PH
 1642 IF(PBX2.GE.-16.7D0) DX(K)=-8.35D0-0.5D0*DPB(K)
      IF(DX(K).GT.DXCRIT) GO TO 12
      IF(PBX2.LT.-16.7D0.AND.L44.NE.0.AND.L45.NE.0) GO TO 1643
      IF(PBX2.LT.-16.7D0.AND.L44.NE.0) L45=L45+1
      IF(PBX2.LT.-16.7D0.AND.L44.NE.0) P45=PH
 1643 IF(PBX2.LT.-16.7D0) GO TO 12
```

```
      CALL SULF (K,AH,E,DS,DXM,XM)
      DST(K)=SSOL (K,E,AH,PH,DS)
      DPBT(K)=PBSOL (K,AH,E,PH,DPB)
      DXT(K)=XSOL (K,AH,E,DX)
      CALL UPDATE(K,PH,D,AH,N)
      IF(N.EQ.1) GO TO 11
      GO TO 36
C
C     PBS, PB(OH)2 AND PBX2 ARE NOW CONSIDERED TO BE STABLE AT THE
C     SAME TIME.
C
 37   IF(L46.NE.0) GO TO 1644
      L46=L46+1
      P46=PH
 1644 DPB(K)=13.6348D0-2.D0*PH
      DS(K)=-28.7864D0-DPB(K)
      DX(K)=-8.35D0-0.5D0*DPB(K)
      DST(K)=SSOL (K,E,AH,PH,DS)
      DXT(K)=XSOL (K,AH,E,DX)
      DPBT(K)=PBSOL (K,AH,E,PH,DPB)
      IF(DST(K).GT.DXM.AND.L47.NE.0) GO TO 1645
      IF(DST(K).GT.DXM) L47=L47+1
      IF(DST(K).GT.DXM) P47=PH
 1645 IF(DST(K).GT.DXM) GO TO 36
      IF(DXT(K).GT.DXINIT.AND.L48.NE.0) GO TO 1646
      IF(DXT(K).GT.DXINIT) L48=L48+1
      IF(DXT(K).GT.DXINIT) P48=PH
 1646 IF(DXT(K).GT.DXINIT) GO TO 23
      CALL UPDATE(K,PH,D,AH,N)
      IF(N.EQ.1) GO TO 11
      GO TO 37
C
C     NOW, THE CO-EXISTENCE OF ELEMENTAL SULFUR AND LEAD HYDROXIDE
C     ARE CONSIDERED. IT IS ALSO CHECKED WHETHER PBX2 OR DIXANTHOGEN
C     IS STABLE. IF ANY OF THESE ARE, THE PROGRAM CONSIDERS THIS
C     NEXT.
C
 41   IF(L50.NE.0) GO TO 1647
      L50=L50+1
      P50=PH
 1647 DS(K)=-(E+0.4761D0)/0.029567964D0
      DPB(K)=13.6348D0-2.D0*PH
      CALL XANTH (K,AH,E,XINIT,DX)
      IF(L61.NE.0.OR.L42.NE.0) GO TO 49
      PBX2=DPB(K)+2.D0*DX(K)
      IF(PBX2.GT.-16.7D0) GO TO 45
 49   IF(DX(K).GT.DXCRIT.AND.L70.NE.0) GO TO 1771
      IF(DX(K).GT.DXCRIT) L70=L70+1
      IF(DX(K).GT.DXCRIT) P70=PH
 1771 IF(DX(K).GT.DXCRIT) DX(K)=DXCRIT
```

```
      DPBCRT=-(E-2.0944D0+0.236544D0*PH)/0.08870389D0
      IF(DPB(K).GT.DPBCRT) GO TO 42
      DPBCRT=-(E-1.4495D0+0.118272D0*PH)/0.029567964D0
      IF(DPB(K).GT.DPBCRT) GO TO 43
      DPBT(K)=PBSOL (K,AH,E,PH,DPB)
      IF(DPBT(K).GT.DXM.AND.L53.NE.0) GO TO 1648
      IF(DPBT(K).GT.DXM) L53=L53+1
      IF(DPBT(K).GT.DXM) P53=PH
 1648 IF(DPBT(K).GT.DXM) GO TO 44
      DXT(K)=XSOL (K,AH,E,DX)
      DST(K)=SSOL (K,E,AH,PH,DS)
      CALL UPDATE(K,PH,D,AH,N)
      IF(N.EQ.1) GO TO 11
      GO TO 41
C
C     THERE IS A REGION IN WHICH PB3O4,PBX2 AND S ARE ALL STABLE.
C     HOWEVER, AT SOME POINT PBX2 IS THE FIRST OF THESE TO BECOME
C     UNSTABLE. THEN,THE COMBINATION OF PB3O4 AND S MUST BE CON-
C     SIDERED AGAIN. THIS IS WHERE THIS IS DONE.
C
 42   IF(L51.NE.0) GO TO 1649
      L51=L51+1
      P51=PH
 1649 DPB(K)=-(E-2.0944D0+0.236544D0*PH)/0.08870389D0
      DS(K)=-(E+0.4761D0)/0.029567964D0
      CALL XANTH (K,AH,E,XINIT,DX)
      DPBCRT=-(E-1.4495D0+0.118272D0*PH)/0.029567964D0
      IF(DPB(K).GT.DPBCRT) GO TO 43
      IF(L63.NE.0) GO TO 50
      PBX2=DPB(K)+2.D0*DX(K)
      IF(PBX2.GT.-16.7D0) GO TO 47
 50   DPBT(K)=PBSOL (K,AH,E,PH,DPB)
      IF(DPBT(K).GT.DXM.AND.L57.NE.0) GO TO 1655
      IF(DPBT(K).GT.DXM) L57=L57+1
      IF(DPBT(K).GT.DXM) P57=PH
 1655 IF(DPBT(K).GT.DXM) GO TO 44
      DST(K)=SSOL (K,E,AH,PH,DS)
      IF(DX(K).GT.DXCRIT.AND.L68.NE.0) GO TO 1768
      IF(DX(K).GT.DXCRIT) L68=L68+1
      IF(DX(K).GT.DXCRIT) P68=PH
 1768 IF(DX(K).GT.DXCRIT) DX(K)=DXCRIT
      DXT(K)=XSOL (K,AH,E,DX)
      CALL UPDATE(K,PH,D,AH,N)
      IF(N.EQ.1) GO TO 11
      GO TO 42
C
C     AGAIN, IT IS FOUND THAT PBO2,PBX2 AND S CAN EXIST SIMULTAN-
C     EOUSLY. PBX2 IS THE FIRST TO DISAPPEAR, LEAVING BEHIND THE
C     COMBINATION PBO2 AND S.
C
```

```
 43   IF(L52.NE.0) GO TO 1656
      L52=L52+1
      P52=PH
 1656 DPB(K)=-(E-1.4495D0+0.118272D0*PH)/0.029567964D0
      DS(K)=-(E+0.4761D0)/0.029567964D0
      CALL XANTH (K,AH,E,XINIT,DX)
      IF(L64.NE.0) GO TO 51
      PBX2=DPB(K)+2.D0*DX(K)
      IF(PBX2.GT.-16.7D0) GO TO 48
 51   DPBT(K)=PBSOL (K,AH,E,PH,DPB)
      IF(DPBT(K).GT.DXM.AND.L59.NE.0) GO TO 1657
      IF(DPBT(K).GT.DXM) L59=L59+1
      IF(DPBT(K).GT.DXM) P59=PH
 1657 IF(DPBT(K).GT.DXM) GO TO 44
      DST(K)=SSOL (K,E,AH,PH,DS)
      IF(DX(K).GT.DXCRIT.AND.L69.NE.0) GO TO 1769
      IF(DX(K).GT.DXCRIT) L69=L69+1
      IF(DX(K).GT.DXCRIT) P69=PH
 1769 IF(DX(K).GT.DXCRIT) DX(K)=DXCRIT
      DXT(K)=XSOL (K,AH,E,DX)
      CALL UPDATE(K,PH,D,AH,N)
      IF(N.EQ.1) GO TO 11
      GO TO 43
C
C     THIS IS THE CASE WHERE S ALONE IS LEFT BEHIND AFTER PBX2
C     HAS BECOME UNSTABLE.
C
 44   IF(L54.NE.0) GO TO 1658
      L54=L54+1
      P54=PH
 1658 DS(K)=-(E+0.4761D0)/0.029567964D0
      CALL XANTH (K,AH,E,XINIT,DX)
      IF(DX(K).GT.DXCRIT.AND.L71.NE.0) GO TO 1772
      IF(DX(K).GT.DXCRIT) L71=L71+1
      IF(DX(K).GT.DXCRIT) P71=PH
 1772 IF(DX(K).GT.DXCRIT) DX(K)=DXCRIT
      LL=1
      X2=10.D0**DPB(K-1)
      CALL SOLVE (X2,AH,E,K,XM,PH,DPB,LL,XINIT)
      DST(K)=SSOL (K,E,AH,PH,DS)
      DPBT(K)=PBSOL (K,AH,E,PH,DPB)
      DXT(K)=XSOL (K,AH,E,DX)
      CALL UPDATE(K,PH,D,AH,N)
      IF(N.EQ.1) GO TO 11
      GO TO 44
C
C     THE CASE WHERE PB(OH)2, PBX2 AND S ARE ALL STABLE IS NOW
C     CONSIDERED.
C
 45   IF(L55.NE.0) GO TO 1659
```

```
      L55=L55+1
      P55=PH
 1659 DPB(K)=13.6348D0-2.D0*PH
      DS(K)=-(E+0.4761D0)/0.029567964D0
      DX(K)=-8.35D0-0.5D0*DPB(K)
      IF(DX(K).GT.DXCRIT) L42=L42+1
      IF(DX(K).GT.DXCRIT) P42=PH
      IF(DX(K).GT.DXCRIT) GO TO 41
      DPBT(K)=PBSOL (K,AH,E,PH,DPB)
      IF(DPBT(K).GT.DXM.AND.L60.NE.0) GO TO 1660
      IF(DPBT(K).GT.DXM) L60=L60+1
      IF(DPBT(K).GT.DXM) P60=PH
 1660 IF(DPBT(K).GT.DXM) GO TO 29
      DXT(K)=XSOL (K,AH,E,DX)
      IF(DXT(K).GT.DXINIT.AND.L61.NE.0) GO TO 1661
      IF(DXT(K).GT.DXINIT) L61=L61+1
      IF(DXT(K).GT.DXINIT) P61=PH
 1661 IF(DXT(K).GT.DXINIT) GO TO 41
      DST(K)=SSOL (K,E,AH,PH,DS)
      CALL UPDATE(K,PH,D,AH,N)
      IF(N.EQ.1) GO TO 11
      GO TO 45
C
C     NOW, THE COMBINATION OF PB304,PBX2 AND S
C
 47   IF(L56.NE.0) GO TO 1662
      L56=L56+1
      P56=PH
 1662 DPB(K)=-(E-2.0944D0+0.236544D0*PH)/0.08870389D0
      DS(K)=-(E+0.4761D0)/0.029567964D0
      DX(K)=-8.35D0-0.5D0*DPB(K)
      DPBT(K)=PBSOL (K,AH,E,PH,DPB)
      IF(DPBT(K).GT.DXM.AND.L62.NE.0) GO TO 1663
      IF(DPBT(K).GT.DXM) L62=L62+1
      IF(DPBT(K).GT.DXM) P62=PH
 1663 IF(DPBT(K).GT.DXM) GO TO 29
      DXT(K)=XSOL (K,AH,E,DX)
      IF(DXT(K).GT.DXINIT.AND.L63.NE.0) GO TO 1664
      IF(DXT(K).GT.DXINIT) L63=L63+1
      IF(DXT(K).GT.DXINIT) P63=PH
 1664 IF(DXT(K).GT.DXINIT) GO TO 42
      DST(K)=SSOL (K,E,AH,PH,DS)
      CALL UPDATE(K,PH,D,AH,N)
      IF(N.EQ.1) GO TO 11
      GO TO 47
C
C     THE COMBINATION OF PBO2,S AND PBX2 IS NEXT
C
 48   IF(L58.NE.0) GO TO 1665
      L58=L58+1
```

```
      P58=PH
 1665 DPB(K)=-(E-1.4495D0+0.118272D0*PH)/0.029567964D0
      DS(K)=-(E+0.4761D0)/0.029567964D0
      DX(K)=-8.35D0-0.5D0*DPB(K)
      DPBT(K)=PBSOL (K,AH,E,PH,DPB)
      IF(DPBT(K).GT.DXM.AND.L64.NE.0) GO TO 1666
      IF(DPBT(K).GT.DXM) L64=L64+1
      IF(DPBT(K).GT.DXM) P64=PH
 1666 IF(DPBT(K).GT.DXM) GO TO 29
      DXT(K)=XSOL (K,AH,E,DX)
      IF(DXT(K).GT.DXINIT.AND.L65.NE.0) GO TO 1667
      IF(DXT(K).GT.DXINIT) L65=L65+1
      IF(DXT(K).GT.DXINIT) P65=PH
 1667 IF(DXT(K).GT.DXINIT) GO TO 43
      DST(K)=SSOL (K,E,AH,PH,DS)
      CALL UPDATE(K,PH,D,AH,N)
      IF(N.EQ.1) GO TO 11
      GO TO 48
C
C
C     THIS IS THE END OF THE SECOND SECTION OF THE PROGRAM
C
C     SECTION 3 : OUTPUT
C
C     THE FIRST PORTION INCLUDES THE STORING THE CONCENTRATIONS
C     OF ALL SPECIES IN ARRAYS AT PH INTERVALS OF 0.1. (IT SHOULD
C     BE RECALLED THAT THE ORIGINAL CALCULATIONS WERE CARRIED
C     OUT AT INTERVALS OF 0.01.) THESE ARRAYS WILL BE SUBSEQUENTLY
C     PRINTED OUT.
C
  11  I=0
      DO 16 M=1,K,10
      I=I+1
      H(I)=D(M)
      PPB(I)=DPB(M)
      PBOH(I)=-7.0998D0+PPB(I)+H(I)
      PBOH2(I)=-17.2000D0+PPB(I)+2.D0*H(I)
      PBOH3(I)=-28.6999D0+PPB(I)+3.D0*H(I)
      PBOH4(I)=-39.3569D0+PPB(I)+4.D0*H(I)
      PB3OH4(I)=-23.3164D0+3.D0*PPB(I)+4.D0*H(I)
      PB4OH4(I)=-19.2164D0+4.D0*PPB(I)+4.D0*H(I)
      PB6OH8(I)=-42.5987D0+6.D0*PPB(I)+8.D0*H(I)
      PB4(I)=PPB(I)+E/.029567964D0-57.28159D0
      PBO3(I)=PPB(I)+E/.029567964D0-80.330184D0+6.D0*H(I)
      PBO4(I)=PPB(I)+E/.029567964D0-121.110808D0+8.D0*H(I)
      PB2OH(I)=-6.300D0+2.D0*PPB(I)+H(I)
      SS(I)=DS(M)
      HS(I)=13.8974D0-H(I)+SS(I)
      H2S(I)=20.9018D0-2.D0*H(I)+SS(I)
      PH2S(I)=20.5052D0-2.D0*H(I)+SS(I)
```

```
      S2(I)=2.D0*SS(I)+(E+0.52402D0)/0.029567964D0
      S3(I)=3.D0*SS(I)+(E+0.51938D0)/0.01478398D0
      S4(I)=4.D0*SS(I)+(E+0.51474D0)/0.00985599D0
      S5(I)=5.D0*SS(I)+(E+0.5101D0)/0.00739199D0
      PBT(I)=DPBT(M)
      ST(I)=DST(M)
      XAN(I)=DX(M)
      HXAN(I)=1.6383D0-H(I)+XAN(I)
      XAN2(I)=2.D0*XAN(I)+(E-0.08495D0)/0.029567964D0
      XT(I)=DXT(M)
      XANT=10.D0**XT(I)
C
C     PERX1 AND PERX2 ARE ARRAYS IN WHICH THE VALUES %PBX2 AND %X2
C     ARE STORED
C
      DIFF=XINIT-XANT
      IF(DIFF.LT.0.D0) PERX1(I)=0.D0
      IF(DIFF.LT.0.D0) PERX2(I)=0.D0
      IF(DIFF.GE.0.D0.AND.XAN(I).LT.DXCRIT) PERX1(I)=(XINIT-XANT)/XINIT*
     **100.D0
      IF(DIFF.GE.0.D0.AND.XAN(I).LT.DXCRIT) PERX2(I)=0.D0
      IF(DIFF.GE.0.D0.AND.XAN(I).EQ.DXCRIT) PERX1(I)=0.D0
      IF(DIFF.GE.0.D0.AND.XAN(I).EQ.DXCRIT) PERX2(I)=(XINIT-XANT)/XINIT
     **100.D0
 16   CONTINUE
C
C
C     WE ARE NOW AT THE PART OF THIS SECTION IN WHICH THE CONCENTRA-
C     TIONS ARE PRINTED OUT
C
C
      WRITE(6,100)
 100  FORMAT(T1,'1',////3X,'PH',8X,'PB++',9X,'PBOH',10X,'PBOH2',9X,'PBOH
     *3',9X,'PBOH4',8X,'PB3OH4',8X,'PB4OH4',8X,'PB6OH8',9X,'PB2OH')
      DO 102 J=1,I
 102  WRITE(6,110) H(J),PPB(J),PBOH(J),PBOH2(J),PBOH3(J),PBOH4(J),PB3OH4
     *(J),PB4OH4(J),PB6OH8(J),PB2OH(J)
 110  FORMAT(//1X,F5.2,9F14.5)
      WRITE(6,120)
 120  FORMAT(//////////3X,'PH',6X,'PB++++',10X,'PBO3',10X,'PBO4',11X,
     *'S--',11X,'HS-',11X,'H2S',9X,'PH2S',9X,'S2--',9X,'S3--')
      DO 103 J=1,I
 103  WRITE(6,130) H(J),PB4(J),PBO3(J),PBO4(J),SS(J),HS(J),H2S(J),
     *PH2S(J),S2(J),S3(J)
 130  FORMAT(//1X,F5.2,9F14.5)
      WRITE(6,140)
 140  FORMAT(//////////3X,'PH',11X,'S4--',9X,'S5--',10X,'X-',11X,'HX',11
     *X,'X2',11X,'PBT',10X,'STOT',10X,'XT')
      DO 104 J=1,I
 104  WRITE(6,150) H(J),S4(J),S5(J),XAN(J),HXAN(J),XAN2(J),PBT(J),ST(J),
```

```
     *XT(J)
 150  FORMAT(//1X,F5.2,8F14.5)
      WRITE(6,155)
 155  FORMAT(//////////3X,'PH',9X,'% PBX2',10X,'% X2')
      DO 105 J=1,I
 105  WRITE(6,165) H(J),PERX1(J),PERX2(J)
 165  FORMAT(//1X,F5.2,2F14.5)
C
C
C     IN THIS PART, THE SAME VALUES THAT HAVE JUST BEEN PRINTED OUT
C     ON PAPER ARE STORED IN A TWO-DIMENSIONAL ARRAY DISK. THIS
C     ARRAY WILL SUBSEQUENTLY WRITTEN ONTO A DISK FOR FUTURE USE.
C
C
      DO 1010 JJ=1,I
      DISK(1,JJ)=H(JJ)
      DISK(2,JJ)=PPB(JJ)
      DISK(3,JJ)=PBOH(JJ)
      DISK(4,JJ)=PBOH2(JJ)
      DISK(5,JJ)=PBOH3(JJ)
      DISK(6,JJ)=PBOH4(JJ)
      DISK(7,JJ)=PB3OH4(JJ)
      DISK(8,JJ)=PB4OH4(JJ)
      DISK(9,JJ)=PB6OH8(JJ)
      DISK(10,JJ)=PB2OH(JJ)
      DISK(11,JJ)=PB4(JJ)
      DISK(12,JJ)=PBO3(JJ)
      DISK(13,JJ)=PBO4(JJ)
      DISK(14,JJ)=SS(JJ)
      DISK(15,JJ)=HS(JJ)
      DISK(16,JJ)=H2S(JJ)
      DISK(17,JJ)=PH2S(JJ)
      DISK(18,JJ)=S2(JJ)
      DISK(19,JJ)=S3(JJ)
      DISK(20,JJ)=S4(JJ)
      DISK(21,JJ)=S5(JJ)
      DISK(22,JJ)=PBT(JJ)
      DISK(23,JJ)=ST(JJ)
      DISK(24,JJ)=XAN(JJ)
      DISK(25,JJ)=HXAN(JJ)
      DISK(26,JJ)=XAN2(JJ)
      DISK(27,JJ)=XT(JJ)
      DISK(28,JJ)=PERX1(JJ)
 1010 DISK(29,JJ)=PERX2(JJ)
      DO 1012 KK=1,29
 1012 WRITE(9,1014) (DISK(KK,JJ),JJ=1,I)
 1014 FORMAT(141D14.5)
C
C
C     THE MESSAGES GIVING THE PHASE CHANGES ARE NOW PRINTED OUT
```

```
C
C
      IF(L0.NE.0) GO TO 160
      GO TO 170
  160 WRITE(6,180) P0
  180 FORMAT(//////12X,'NO SOLID IS STABLE AT PH',F7.2)
  170 IF(L1.NE.0) GO TO 190
      GO TO 199
  190 WRITE(6,210) P1
  210 FORMAT(//////12X,'PB PRECIPITATES OUT AT PH',F7.2)
  199 IF(L2.NE.0) GO TO 220
      GO TO 230
  220 WRITE(6,240) P2
  240 FORMAT(//////12X,'S PRECIPITATES OUT AT PH',F7.2)
  230 IF(L3.NE.0) GO TO 250
      GO TO 260
  250 WRITE(6,270) P3
  270 FORMAT(//////12X,'PBS PRECIPITATES OUT AT PH',F7.2)
  260 IF(L5.NE.0) GO TO 300
      GO TO 310
  300 WRITE(6,301) P5
  301 FORMAT(//////12X,'PB(OH)2 PRECIPITATES OUT AT PH',F7.2)
  310 IF(L6.NE.0) GO TO 320
      GO TO 330
  320 WRITE(6,321) P6
  321 FORMAT(//////12X,'PB3O4 PRECIPITATES OUT AT PH',F7.2)
  330 IF(L7.NE.0) GO TO 340
      GO TO 350
  340 WRITE(6,341) P7
  341 FORMAT(//////12X,'PB2O3 PRECIPITATES OUT AT PH',F7.2)
  350 IF(L8.NE.0) GO TO 360
      GO TO 370
  360 WRITE(6,361) P8
  361 FORMAT(//////12X,'PBO2 PRECIPITATES OUT AT PH',F7.2)
  370 IF(L9.NE.0) GO TO 380
      GO TO 390
  380 WRITE(6,381) P9
  381 FORMAT(//////12X,'PBS IS NO LONGER STABLE,NO SOLIDS ARE AT PH',
     *F7.2)
  390 IF(L10.NE.0) GO TO 400
      GO TO 410
  400 WRITE(6,401) P10
  401 FORMAT(//////12X,'PB(OH)2 IS NO LONGER STABLE,NO SOLIDS ARE AT PH'
     *,F7.2)
  410 IF(L11.NE.0) GO TO 420
      GO TO 430
  420 WRITE(6,421) P11
  421 FORMAT(//////12X,'PB3O4 IS NO LONGER STABLE,NO SOLIDS ARE AT PH'
     *,F7.2)
  430 IF(L12.NE.0) GO TO 440
```

```
      GO TO 450
440   WRITE(6,441) P12
441   FORMAT(//////12X,'PBS AND S ARE BOTH STABLE AT PH',F7.2)
450   IF(L13.NE.0) GO TO 460
      GO TO 470
460   WRITE(6,461) P13
461   FORMAT(//////12X,'PBS IS STILL STABLE,BUT S IS NO LONGER AT PH',
     *F7.2)
470   IF(L14.NE.0) GO TO 480
      GO TO 490
480   WRITE(6,481) P14
481   FORMAT(//////12X,'PBS AND PB ARE BOTH STABLE AT PH',F7.2)
490   IF(L15.NE.0) GO TO 500
      GO TO 510
500   WRITE(6,501) P15
501   FORMAT(//////12X,'PBS IS STILL STABLE, BUT PB IS NO LONGER AT PH',
     *F7.2)
510   IF(L16.NE.0) GO TO 520
      GO TO 530
520   WRITE(6,521) P16
521   FORMAT(//////12X,'S IS NO LONGER STABLE AND THERE NO SOLIDS AT PH'
     *,F7.2)
530   IF(L17.NE.0) GO TO 540
      GO TO 550
540   WRITE(6,541) P17
541   FORMAT(//////12X,'PBS AND PB(OH)2 ARE BOTH STABLE AT PH',F7.2)
550   IF(L18.NE.0) GO TO 560
      GO TO 570
560   WRITE(6,561) P18
561   FORMAT(//////12X,'PB(OH)2 IS STILL STABLE,PBS IS NO LONGER AT PH',
     *F7.2)
570   IF(L19.NE.0) GO TO 580
      GO TO 590
580   WRITE(6,581) P19
581   FORMAT(//////12X,'X2 ALONE IS STABLE AT PH',F7.2)
590   IF(L20.NE.0) GO TO 600
      GO TO 610
600   WRITE(6,601) P20
601   FORMAT(//////12X,'S AND X2 ARE STABLE AT PH',F7.2)
610   IF(L21.NE.0) GO TO 620
      GO TO 630
620   WRITE(6,621) P21
621   FORMAT(//////12X,'PBS AND X2 ARE STABLE AT PH',F7.2)
630   IF(L22.NE.0) GO TO 640
      GO TO 650
640   WRITE(6,641) P22
641   FORMAT(//////12X,'PB(OH)2 AND X2 ARE STABLE AT PH',F7.2)
650   IF(L23.NE.0) GO TO 660
      GO TO 670
660   WRITE(6,661) P23
```

```
661  FORMAT(//////12X,'PB3O4 AND X2 ARE STABLE AT PH',F7.2)
670  IF(L24.NE.0) GO TO 680
     GO TO 690
680  WRITE(6,681) P24
681  FORMAT(//////12X,'PBO2 AND X2 ARE STABLE AT PH',F7.2)
690  IF(L25.NE.0) GO TO 700
     GO TO 710
700  WRITE(6,701) P25
701  FORMAT(//////12X,'S,PBS AND X2 ARE STABLE AT PH',F7.2)
710  IF(L26.NE.0) GO TO 720
     GO TO 730
720  WRITE(6,721) P26
721  FORMAT(//////12X,'PB(OH)2,PBS AND X2 ARE STABLE AT PH',F7.2)
730  IF(L27.NE.0) GO TO 740
     GO TO 750
740  WRITE(6,741) P27
741  FORMAT(//////12X,'PBX2 IS STABLE AT PH',F7.2)
750  IF(L28.NE.0) GO TO 760
     GO TO 770
760  WRITE(6,761) P28
761  FORMAT(//////12X,'PBX2 IS NO LONGER STABLE AT PH',F7.2)
770  IF(L29.NE.0) GO TO 780
     GO TO 790
780  WRITE(6,781) P29
781  FORMAT(//////12X,'PBS AND PBX2 ARE BOTH STABLE AT PH',F7.2)
790  IF(L30.NE.0) GO TO 800
     GO TO 810
800  WRITE(6,801) P30
801  FORMAT(//////12X,'PBS IS NO LONGER STABLE,BUT PBX2 IS STILL AT PH'
    *,F7.2)
810  IF(L31.NE.0) GO TO 820
     GO TO 830
820  WRITE(6,821) P31
821  FORMAT(//////12X,'PBX2 AND S ARE STABLE AT PH',F7.2)
830  IF(L32.NE.0) GO TO 840
     GO TO 850
840  WRITE(6,841) P32
841  FORMAT(//////12X,'PBX2 IS STILL STABLE,BUT S IS NO LONGER AT PH',
    *F7.2)
850  IF(L33.NE.0) GO TO 860
     GO TO 870
860  WRITE(6,861) P33
861  FORMAT(//////12X,'PBX2,PBS AND S ARE STABLE AT PH',F7.2)
870  IF(L34.NE.0) GO TO 880
     GO TO 890
880  WRITE(6,881) P34
881  FORMAT(//////12X,'PBX2 AND PBS ARE STABLE,BUT S IS NO LONGER AT
    *PH',F7.2)
890  IF(L35.NE.0) GO TO 900
     GO TO 910
```

```
900  WRITE(6,901) P35
901  FORMAT(//////12X,'PBS IS STILL STABLE,BUT PBX2 IS NO LONGER AT PH'
    *,F7.2)
910  IF(L36.NE.0) GO TO 920
     GO TO 930
920  WRITE(6,921) P36
921  FORMAT(//////12X,'PBS AND PBX2 ARE ONCE AGAIN STABLE AT PH',F7.2)
930  IF(L37.NE.0) GO TO 940
     GO TO 950
940  WRITE(6,941) P37
941  FORMAT(//////12X,'PBX2 IS STILL STABLE,BUT PBS DISAPPEARS AT PH',
    *F7.2)
950  IF(L38.NE.0) GO TO 960
     GO TO 970
960  WRITE(6,961) P38
961  FORMAT(//////12X,'PBS IS STILL STABLE,BUT PBX2 VANISHES AT PH',
    *F7.2)
970  IF(L39.NE.0) GO TO 980
     GO TO 990
980  WRITE(6,981) P39
981  FORMAT(//////12X,'PBS,PB AND PBX2 ARE ALL STABLE AT PH',F7.2)
990  IF(L40.NE.0) GO TO 1030
     GO TO 1040
1030 WRITE(6,1031) P40
1031 FORMAT(//////12X,'PBS AND PBX2 ARE STABLE,BUT PB IS NOT ANYMORE AT
    *PH',F7.2)
1040 IF(L41.NE.0) GO TO 1050
     GO TO 1060
1050 WRITE(6,1051) P41
1051 FORMAT(//////12X,'PB3O4 IS NO LONGER STABLE, BUT X2 STILL IS AT PH
    *',F7.2)
1060 IF(L42.NE.0) GO TO 1070
     GO TO 1080
1070 WRITE(6,1071) P42
1071 FORMAT(//////12X,'X2 REPLACES PBX2 AS THE STABLE SPECIES AT PH',
    *F7.2)
1080 IF(L43.NE.0) GO TO 1090
     GO TO 1100
1090 WRITE(6,1091) P43
1091 FORMAT(//////12X,'PB(OH)2 BECOMES STABLE AT PH',F7.2)
1100 IF(L44.NE.0) GO TO 1110
     GO TO 1120
1110 WRITE(6,1111) P44
1111 FORMAT(//////12X,'PB(OH)2 AND PBX2 ARE BOTH STABLE AT PH',F7.2)
1120 IF(L45.NE.0) GO TO 1130
     GO TO 1140
1130 WRITE(6,1131) P45
1131 FORMAT(//////12X,'PBX2 IS NO LONGER STABLE, BUT PB(OH)2 IS STILL
    *AT PH',F7.2)
1140 IF(L46.NE.0) GO TO 1150
```

```
     GO TO 1160
1150 WRITE(6,1151) P46
1151 FORMAT(//////12X,'PBS,PBX2 AND PB(OH)2 ARE ALL STABLE AT PH',F7.2)
1160 IF(L47.NE.0) GO TO 1170
     GO TO 1180
1170 WRITE (6,1171) P47
1171 FORMAT(//////12X,'PB(OH)2 AND PBX2 ARE STILL STABLE,WHEREAS PBS
    *IS NO LONGER AT PH',F7.2)
1180 IF(L48.NE.0) GO TO 1190
     GO TO 1200
1190 WRITE(6,1191) P48
1191 FORMAT(//////12X,'PB(OH)2 AND PBS ARE STILL PRESENT,BUT PBX2 IS
    *NOT ANYMORE AT PH',F7.2)
1200 IF(L49.NE.0) GO TO 1210
     GO TO 1220
1210 WRITE(6,1211) P49
1211 FORMAT(//////12X,'PBX2 AND S ARE STILL STABLE,BUT PBS IS NO
    *LONGER AT PH',F7.2)
1220 IF(L50.NE.0) GO TO 1230
     GO TO 1240
1230 WRITE(6,1231) P50
1231 FORMAT(//////12X,'PB(OH)2 AND S ARE BOTH STABLE AT PH',F7.2)
1240 IF(L51.NE.0) GO TO 1250
     GO TO 1260
1250 WRITE(6,1251) P51
1251 FORMAT(//////12X,'PB3O4 AND S ARE BOTH STABLE AT PH',F7.2)
1260 IF(L52.NE.0) GO TO 1270
     GO TO 1280
1270 WRITE(6,1271) P52
1271 FORMAT(//////12X,'PBO2 AND S ARE BOTH STABLE AT PH',F7.2)
1280 IF(L53.NE.0) GO TO 1290
     GO TO 1300
1290 WRITE(6,1291) P53
1291 FORMAT(//////12X,'S IS STILL STABLE,WHEREAS PB(OH)2 NO LONGER IS
    *AT PH',F7.2)
1300 IF(L54.NE.0) GO TO 1310
     GO TO 1320
1310 WRITE(6,1311) P54
1311 FORMAT(//////12X,'S IS THE ONLY STABLE SPECIES AT PH',F7.2)
1320 IF(L55.NE.0) GO TO 1330
     GO TO 1340
1330 WRITE(6,1331) P55
1331 FORMAT(//////12X,'PB(OH)2,PBX2 AND S ARE ALL STABLE AT PH',F7.2)
1340 IF(L56.NE.0) GO TO 1350
     GO TO 1360
1350 WRITE(6,1351) P56
1351 FORMAT(//////12X,'PB3O4,PBX2 AND S ARE ALL PRESENT AT PH',F7.2)
1360 IF(L57.NE.0) GO TO 1370
     GO TO 1380
1370 WRITE(6,1371) P57
```

```
1371 FORMAT(//////12X,'PB3O4 IS NO LONGER STABLE,BUT S STILL IS AT PH'
    *,F7.2)
1380 IF(L58.NE.0) GO TO 1390
     GO TO 1400
1390 WRITE(6,1391) P58
1391 FORMAT(//////12X,'PBO2,PBX2 AND S ARE ALL STABLE AT PH',F7.2)
1400 IF(L59.NE.0) GO TO 1410
     GO TO 1420
1410 WRITE(6,1411) P59
1411 FORMAT(//////12X,'S STILL IS PRESENT,BUT PBO2 NO LONGER IS AT PH',
    *F7.2)
1420 IF(L60.NE.0) GO TO 1430
     GO TO 1440
1430 WRITE(6,1431) P60
1431 FORMAT(//////12X,'PBX2 AND S ARE STILL STABLE, BUT PB(OH)2 IS NOT
    *ANYMORE AT PH',F7.2)
1440 IF(L61.NE.0) GO TO 1450
     GO TO 1460
1450 WRITE(6,1451) P61
1451 FORMAT(//////12X,'PB(OH)2 AND S ARE STILL PRESENT, BUT PBX2 DOES
    *NOT EXIST AT PH',F7.2)
1460 IF(L62.NE.0) GO TO 1470
     GO TO 1480
1470 WRITE(6,1471) P62
1471 FORMAT(//////12X,'PB3O4 DISAPPEARS,WHEREAS S AND PBX2 REMAIN AT
    *PH',F7.2)
1480 IF(L63.NE.0) GO TO 1490
     GO TO 1500
1490 WRITE(6,1491) P63
1491 FORMAT(//////12X,'S AND PB3O4 REMAIN, BUT PBX2 DOES NOT AT PH',
    *F7.2)
1500 IF(L64.NE.0) GO TO 1510
     GO TO 1520
1510 WRITE(6,1511) P64
1511 FORMAT(//////12X,'S AND PBX2 ARE STILL PRESENT, BUT PBO2 NO LONGER
    *IS AT PH',F7.2)
1520 IF(L65.NE.0) GO TO 1530
     GO TO 1540
1530 WRITE(6,1531) P65
1531 FORMAT(//////12X,'S AND PBO2 REMAIN, BUT PBX2 DOES NOT ANY LONGER
    *AT PH',F7.2)
1540 IF(L66.NE.0) GO TO 1550
     GO TO 1560
1550 WRITE(6,1551) P66
1551 FORMAT(//////12X,'PBX2 IS NO LONGER PRESENT,BUT S STILL IS AT PH',
    *F7.2)
1560 IF(L67.NE.0) GO TO 1570
     GO TO 1580
1570 WRITE(6,1571) P67
1571 FORMAT(//////12X,'PBS IS NO LONGER STABLE,BUT S STILL IS AT PH',
```

```
     *F7.2)
 1580 IF(L68.NE.0) GO TO 1590
      GO TO 1591
 1590 WRITE(6,1592) P68
 1592 FORMAT(//////12X,'S,PB3O4 AND X2 ARE ALL STABLE AT PH',F7.2)
 1591 IF(L69.NE.0) GO TO 1593
      GO TO 1594
 1593 WRITE(6,1595) P69
 1595 FORMAT(//////12X,'S,PBO2 AND X2 ARE ALL STABLE AT PH',F7.2)
 1594 IF(L70.NE.0) GO TO 1596
      GO TO 1597
 1596 WRITE(6,1598) P70
 1598 FORMAT(//////12X,'S,PB(OH)2 AND X2 ARE ALL STABLE AT PH',F7.2)
 1597 IF(L71.NE.0) GO TO 1599
      GO TO 1775
 1599 WRITE(6,1776) P71
 1776 FORMAT(//////12X,'S AND X2 ARE NOW LEFT AT PH',F7.2)
 1775 STOP
      END
C
C
C     THIS TERMINATES THE MAIN PROGRAM. WHAT FOLLOWS ARE THE SUB-
C     PROGRAMS THAT HAVE BEEN CALLED IN THE COURSE OF THE MAIN
C     PROGRAM
C
C
C     UPDATE IS THE SUBROUTINE THAT UPDATES THE PH.
C
C
      SUBROUTINE UPDATE(K,PH,D,AH,N)
      IMPLICIT REAL*8(A-H,O-Z)
      DIMENSION AH(1500),D(1500)
      PH=PH+0.01D0
      IF(PH.GT.14.D0) GO TO 10
      K=K+1
      D(K)=PH
      AH(K)=10.D0**(-PH)
      GO TO 20
 10   N=1
 20   RETURN
      END
C
C     STOTL1 IS A FUNCTION SUBPROGRAM THAT DETERMINES A FACTOR THAT
C     IS APPEARS AGAIN AND AGAIN IN THE CALCULATION OF THE DIS-
C     SOLVED SULFUR SPECIES CONCENTRATIONS
C
      FUNCTION STOTL1 (K,AH)
      IMPLICIT REAL*8(A-H,O-Z)
      DIMENSION AH(1500)
      STOTL1=1.D0+7.8959D+13*AH(K)+7.977D+20*AH(K)**2.D0+3.2002D+20*
```

```
     *AH(K)**2.D0
      RETURN
      END
C
C     PBTOTL IS A FUNCTION SUBPROGRAM THAT DETERMINES A FACTOR
C     THAT RECURS IN THE CALCULATION OF THE TOTAL CONCENTRATION
C     OF SOLUBLE LEAD SPECIES
C
      FUNCTION PBTOTL (AH,K,E,PH)
      IMPLICIT REAL*8(A-H,O-Z)
      DIMENSION AH(1500)
      A=1.D0+7.9471D-08/AH(K)+6.3096D-18/AH(K)**2.D0+1.9958D-29/AH(K)**
     *3.D0+4.3965D-40/AH(K)**4.D0
      DB=(E-1.6937D0)/0.029567964D0
      IF(DB.LT.-70.D0) B=0.D0
      IF(DB.GE.-70.D0) B=10.D0**DB
      DC=(E-2.3752D0+0.177408D0*PH)/0.029567964D0
      IF(DC.LT.-70.D0) C=0.D0
      IF(DC.GE.-70.D0) C=10.D0**DC
      DD=(E-3.5810D0+0.236544D0*PH)/0.029567964D0
      IF(DD.LT.-70.D0) D=0.D0
      IF(DD.GE.-70.D0) D=10.D0**DD
      PBTOTL=A+B+C+D
      RETURN
      END
C
C     SSOL DETERMINES THE TOTAL CONCENTRATION OF SOLUBLE SULFUR
C     SPECIES ONCE THE SULFIDE ION CONCENTRATION IS KNOWN
C
      FUNCTION SSOL (K,E,AH,PH,DS)
      IMPLICIT REAL*8(A-H,O-Z)
      DIMENSION AH(1500),DS(1500)
      Y=10.D0**DS(K)
      S=SSUM (E,Y,K,AH)
      SSOL=DLOG10(S)
      RETURN
      END
C
C     SOLVE IS A SUBROUTINE THAT USES THE SECANT METHOD TO FIND A
C     SOLUTION TO SEVERAL POLYNOMIAL MASS BALANCE EQUATIONS THAT
C     APPEAR THROUGHOUT THE PROGRAM. THE SUBROUTINE ITSELF CALLS
C     A FUNCTION SUBPROGRAM CALC WHICH EVALUATES THE POLYNOMIAL
C     AT THE DIFFERENT GUESSES FOR THE ROOT IN THE COURSE OF THE
C     ITERATION.
C
      SUBROUTINE SOLVE (X2,AH,E,K,XM,PH,DPB,LL,XINIT)
      IMPLICIT REAL*8(A-H,O-Z)
      DIMENSION AH(1500),DPB(1500),G(5)
 20   IF(LL.EQ.2) X2=4.0438D-15*DSQRT(STOTL1(K,AH)/PBTOTL(AH,K,E,PH))
      IF(K.GT.1.AND.LL.NE.2) X2=10.D0**DPB(K-1)
```

```
      X1=X2/2.D0
      F1=CALC (X1,AH,E,K,XM,PH,LL,TMAX1,DERIV1,XINIT)
      F2=CALC (X2,AH,E,K,XM,PH,LL,TMAX2,DERIV2,XINIT)
 5    IF(LL.EQ.3.OR.LL.EQ.6) GO TO 17
      GO TO 8
 17   D1=DERIV1-DERIV2
      D2=DERIV1+DERIV2
      IF(DABS(D1).GT.DABS(D2)) GO TO 6
 8    XN=F2/(F2-F1)*X1-F1/(F2-F1)*X2
      FN=CALC (XN,AH,E,K,XM,PH,LL,TMAXN,DERIVN,XINIT)
      PERDIF=FN/TMAXN
      IF(DABS(PERDIF).LT.1.D-06) GO TO 4
      X1=X2
      X2=XN
      F1=F2
      F2=FN
      IF(LL.NE.3.AND.LL.NE.6) GO TO 8
C
C     THE OCCURRENCE OF A MAXIMUM OR MINIMUM IN THE FUNCTION IN THE
C     VICINITY OF THE ROOT CAN MAKE IT IMPOSSIBLE FOR THE ITERATION
C     TO CONVERGE. WHAT OFTEN HAPPENS IS THAT THE PROCEDURE BEGINS
C     TO CYCLE OR IT MAY EVEN DIVERGE. THIS PORTION OF SOLVE
C     CHECKS FOR THE POSSIBILITY THAT THE TWO POINTS ON THE SECANT
C     OF THE FUNCTION ARE NOT ON EITHER SIDE OF A MAXIMUM OR MINI-
C     MUM. IF THIS IS THE CASE, THEN ONE OF THE POINTS IS REPLACED
C     BY A NEW ONE SO THAT BOTH POINTS ARE NOW ON THE SAME SIDE
C     OF THE EXTREMUM. MOREOVER, THE POINTS ARE CHOSEN TO BE ON
C     THE SAME SIDE AS THE ROOT.
C
      DERIV1=DERIV2
      DERIV2=DERIVN
      GO TO 5
 6    IF(K.EQ.1) X1=1.3519D-04
      IF(K.GT.1) X1=10.D0**DPB(K-1)
      X2=X1/2.D0
      F1=CALC (X1,AH,E,K,XM,PH,LL,TMAX1,DERIV1,XINIT)
      F2=CALC (X2,AH,E,K,XM,PH,LL,TMAX2,DERIV2,XINIT)
 7    XN=F2/(F2-F1)*X1-F1/(F2-F1)*X2
      FN=CALC (XN,AH,E,K,XM,PH,LL,TMAXN,DERIVN,XINIT)
      PERDIF=FN/TMAXN
      IF(DABS(PERDIF).LT.1.D-06) GO TO 4
      X2=XN
      F2=FN
      GO TO 7
 4    PB=XN
      DPB(K)=DLOG10(PB)
      IF(LL.EQ.2.OR.LL.EQ.5) GO TO 15
      GO TO 10
 15   Y=-28.7864D0-DPB(K)
      Y1=10.D0**Y
```

```
      CALL POLYS (E,Y1,G,NNN)
      CHECK1=Y-G(2)
      CHECK2=Y-G(3)
      CHECK3=Y-G(4)
      CHECK4=Y-G(5)
      IF(CHECK1.LT.6.D0.OR.CHECK2.LT.6.D0) GO TO 25
      IF(CHECK3.LT.6.D0.OR.CHECK4.LT.6.D0) GO TO 26
      GO TO 10
 25   LL=LL+1
      GO TO 20
 26   LL=LL+1
      GO TO 20
 10   RETURN
      END
C
C     CALC IS THE FUNCTION SUBPROGRAM THAT EVALUATES THE POLYNOMIALS
C     OF THE FUNCTION TO BE SOLVED. IT ALSO DETERMINES THE DERIV-
C     ATIVE OF THE FUNCTION IN THE CASE WHERE AN EXTREMUM IS FOUND
C     TO LIE BETWEEN THE TWO POINTS ON THE SECANT OF THE FUNCTION.
C     ALSO, THE MAXIMUM TERM IN THE POLYNOMIAL IS ALSO DETERMINED.
C
      FUNCTION CALC (X,AH,E,K,XM,PH,LL,TMAX,DERIV,XINIT)
      IMPLICIT REAL*8(A-H,O-Z)
      DIMENSION AH(1500),G(12),H(12),HH(12),GG(12)
      AA=PBTOTL(AH,K,E,PH)
      BB=1.0024D-06/AH(K)
      CC=1.448D-23/AH(K)**4.D0
      DD=2.4304D-19/AH(K)**4.D0
      EE=1.5115D-42/AH(K)**4.D0/AH(K)**4.D0
      FF=XM
      DIFF=0.D0
      GO TO (10,20,30,40,50,60),LL
 10   J=6
      NN=5
      H(1)=DLOG10(EE)+6.D0*DLOG10(X)
      H(2)=DLOG10(DD)+4.D0*DLOG10(X)
      H(3)=DLOG10(CC)+3.D0*DLOG10(X)
      H(4)=DLOG10(BB)+2.D0*DLOG10(X)
      H(5)=DLOG10(AA)+DLOG10(X)
      G(6)=-XM
      GO TO 650
 20   J=6
      NN=5
      H(1)=DLOG10(EE)+7.D0*DLOG10(X)
      H(2)=DLOG10(DD)+5.D0*DLOG10(X)
      H(3)=DLOG10(CC)+4.D0*DLOG10(X)
      H(4)=DLOG10(BB)+3.D0*DLOG10(X)
      H(5)=DLOG10(AA)+2.D0*DLOG10(X)
      G(6)=-1.6352D-29*STOTL1(K,AH)
      GO TO 650
```

```
30    J=10
      NN=10
      H(1)=DLOG10(EE)+11.D0*DLOG10(X)
      H(2)=DLOG10(DD)+9.D0*DLOG10(X)
      H(3)=DLOG10(CC)+8.D0*DLOG10(X)
      H(4)=DLOG10(BB)+7.D0*DLOG10(X)
      H(5)=DLOG10(AA)+6.D0*DLOG10(X)
      H(6)=-28.7864D0+DLOG10(STOTL1(K,AH))+4.D0*DLOG10(X)
      H(7)=-39.54927D0+E/0.029567964D0+3.D0*DLOG10(X)
      H(8)=-50.7509D0+E/0.01478398D0+2.D0*DLOG10(X)
      H(9)=-62.31755D0+E/0.00985599D0+DLOG10(X)
      H(10)=-74.22605D0+E/0.00739199D0
      DIFF=75.D0
      GO TO 650
40    J=8
      NN=5
      H(1)=DLOG10(EE)+7.D0*DLOG10(X)+0.30103D0
      H(2)=DLOG10(DD)+5.D0*DLOG10(X)+0.30103D0
      H(3)=DLOG10(CC)+4.D0*DLOG10(X)+0.30103D0
      H(4)=DLOG10(BB)+3.D0*DLOG10(X)+0.30103D0
      H(5)=DLOG10(AA)+2.D0*DLOG10(X)+0.30103D0
      G(6)=(XINIT-2.D0*XM)*X
      G(7)=-4.46684D-09*(1.D0+43.4783D0*AH(K))*DSQRT(X)
      G(8)=-3.99052D-17*10.D0**((E-0.08495D0)/0.029567964D0)
      GO TO 650
50    J=8
      NN=5
      H(1)=DLOG10(EE)+7.D0*DLOG10(X)
      H(2)=DLOG10(DD)+5.D0*DLOG10(X)
      H(3)=DLOG10(CC)+4.D0*DLOG10(X)
      H(4)=DLOG10(BB)+3.D0*DLOG10(X)
      H(5)=DLOG10(AA)+2.D0*DLOG10(X)
      G(6)=XINIT/2.D0*X
      G(7)=-2.23342D-09*(1.D0+43.4783D0*AH(K))*DSQRT(X)
      G(8)=-1.6352D-29*STOTL1(K,AH)-1.99526D-17*10.D0**((E-0.08495D0)/
     *0.029567964D0)
      GO TO 650
60    J=12
      NN=12
      H(1)=DLOG10(EE)+11.D0*DLOG10(X)
      H(2)=DLOG10(DD)+9.D0*DLOG10(X)
      H(3)=DLOG10(CC)+8.D0*DLOG10(X)
      H(4)=DLOG10(BB)+7.D0*DLOG10(X)
      H(5)=DLOG10(AA)+6.D0*DLOG10(X)
      H(6)=DLOG10(XINIT/2.D0)+5.D0*DLOG10(X)
      HA=1.6352D-29*STOTL1(K,AH)+1.99526D-17*10.D0**((E-0.08495D0)/
     *0.029567964D0)
      H(7)=DLOG10(HA)+4.D0*DLOG10(X)
      H(8)=-39.54927D0+E/0.029567964D0+3.D0*DLOG10(X)
      H(9)=-50.75090D0+E/0.01478398D0+2.D0*DLOG10(X)
```

```
      H(10)=-62.31755D0+E/0.00985599D0+DLOG10(X)
      H(11)=-8.65103D0+DLOG10(1.D0+43.4783D0*AH(K))+4.5D0*DLOG10(X)
      H(12)=-74.22605D0+E/0.00739199D0
      DIFF=75.D0
  650 DO 655 I=1,NN
      H(I)=H(I)+DIFF
      IF(H(I).LT.-75.D0) G(I)=0.D0
      IF(J.EQ.12) GO TO 651
      IF(H(I).GE.-75.D0.AND.I.LE.5) G(I)=10.D0**H(I)
      IF(H(I).GE.-75.D0.AND.I.GT.5) G(I)=-10.D0**H(I)
      GO TO 655
  651 IF(H(I).GE.-75.D0.AND.I.LE.6) G(I)=10.D0**H(I)
      IF(H(I).GE.-75.D0.AND.I.GT.6) G(I)=-10.D0**H(I)
  655 CONTINUE
      IF(LL.EQ.3) GO TO 661
      IF(LL.EQ.6) GO TO 662
      GO TO 660
  661 HH(1)=1.0414D0+H(1)-DLOG10(X)
      HH(2)=0.95424D0+H(2)-DLOG10(X)
      HH(3)=0.90309D0+H(3)-DLOG10(X)
      HH(4)=0.84510D0+H(4)-DLOG10(X)
      HH(5)=0.77815D0+H(5)-DLOG10(X)
      HH(6)=0.60206D0+H(6)-DLOG10(X)
      HH(7)=0.47712D0+H(7)-DLOG10(X)
      HH(8)=0.30103D0+H(8)-DLOG10(X)
      HH(9)=H(9)-DLOG10(X)
      GO TO 663
  662 HH(1)=1.0414D0+H(1)-DLOG10(X)
      HH(2)=0.95424D0+H(2)-DLOG10(X)
      HH(3)=0.90309D0+H(3)-DLOG10(X)
      HH(4)=0.84510D0+H(4)-DLOG10(X)
      HH(5)=0.77815D0+H(5)-DLOG10(X)
      HH(6)=0.69897D0+H(6)-DLOG10(X)
      HH(7)=0.60206D0+H(7)-DLOG10(X)
      HH(8)=0.47712D0+H(8)-DLOG10(X)
      HH(9)=0.30103D0+H(9)-DLOG10(X)
      HH(10)=H(10)-DLOG10(X)
      HH(11)=0.65321D0+H(11)-DLOG10(X)
  663 DERIV=0.D0
      NNY=NN-1
      JJ=J/2
      DO 670 I=1,NNY
      IF(HH(I).LT.-75.D0) GG(I)=0.D0
      IF(HH(I).GE.-75.D0.AND.I.LE.JJ) GG(I)=10.D0**HH(I)
      IF(HH(I).GE.-75.D0.AND.I.GT.JJ) GG(I)=-10.D0**HH(I)
      DERIV=DERIV+GG(I)
  670 CONTINUE
  660 CALC=0.D0
      DO 680 I=1,J
  680 CALC=CALC+G(I)
```

```
      TMAX=G(1)
      DO 700 I=1,J
      IF(DABS(G(I)).GE.TMAX) TMAX=DABS(G(I))
  700 CONTINUE
      RETURN
      END
C
C     PBSOL IS A FUNCTION SUBPROGRAM THAT CALCULATES THE TOTAL DIS-
C     SOLVED LEAD CONCENTRATION ONCE THE PB+2 CONCENTRATION IS
C     KNOWN
C
      FUNCTION PBSOL (K,AH,E,PH,DPB)
      IMPLICIT REAL*8(A-H,O-Z)
      DIMENSION AH(1500),DPB(1500)
      PB=10.D0**DPB(K)
      A=PB*PBTOTL (AH,K,E,PH)
      BB=2.D0*DPB(K)+PH-5.9990D0
      IF(BB.LT.-72.D0) B=0.D0
      IF(BB.GT.-72.D0) B=10.D0**BB
      CC=3.D0*DPB(K)+4.D0*PH-22.8392D0
      IF(CC.LT.-72.D0) C=0.D0
      IF(CC.GT.-72.D0) C=10.D0**CC
      DD=4.D0*DPB(K)+4.D0*PH-18.6143D0
      IF(DD.LT.-72.D0) D=0.D0
      IF(DD.GT.-72.D0) D=10.D0**DD
      FF=6.D0*DPB(K)+8.D0*PH-41.8206D0
      IF(FF.LT.-72.D0) F=0.D0
      IF(FF.GT.-72.D0) F=10.D0**FF
      PBSL=A+B+C+D+F
      PBSOL=DLOG10(PBSL)
      RETURN
      END
C
C     SULF IS THE SUBROUTINE THAT SOLVES THE MASS BALANCE EQUATION
C     FOR THE SULFUR-BEARING SPECIES WHEN THEY ARE ALL SOLUBLE
C
      SUBROUTINE SULF (K,AH,E,DS,DXM,XM)
      IMPLICIT REAL*8(A-H,O-Z)
      DIMENSION AH(1500),DS(1500),G(5)
      X2=XM/STOTL1(K,AH)
      CALL POLYS (E,X2,G,NNN)
      IF(NNN.EQ.1) CALL SALTER (E,K,XM,DXM,AH,DS)
      IF(NNN.EQ.1) GO TO 20
      RAT1=DXM-G(2)
      RAT2=DXM-G(3)
      RAT3=DXM-G(4)
      RAT4=DXM-G(5)
      IF(RAT1.GT.8.D0.AND.RAT2.GT.8.D0.AND.RAT3.GT.8.D0.AND.RAT4.GT.8.D0
     *) GO TO 10
      X1=X2/2.D0
```

```
      F1=SCALC (E,X1,K,AH,TMAX,XM)
      F2=SCALC (E,X2,K,AH,TMAX,XM)
 5    XN=F2/(F2-F1)*X1-F1/(F2-F1)*X2
      FN=SCALC (E,XN,K,AH,TMAX,XM)
      PERDIF=FN/TMAX
      IF(DABS(PERDIF).LT.1.D-06) GO TO 4
      X1=X2
      X2=XN
      F1=F2
      F2=FN
      GO TO 5
 4    DS(K)=DLOG10(XN)
      GO TO 20
 10   DS(K)=G(1)
 20   RETURN
      END
C
C     POLYS IS A SUBROUTINE THAT IS CALLED BY THE FUNCTION CALC
C     TO SOLVE THE POLYNOMIAL EQUATIONS.
C
      SUBROUTINE POLYS (E,X,G,NNN)
      IMPLICIT REAL*8(A-H,O-Z)
      DIMENSION G(5)
      NNN=0
      G(1)=DLOG10(X)
      G(2)=2.D0*G(1)+(E+0.52402D0)/0.029567964D0
      G(3)=3.D0*G(1)+(E+0.51938D0)/0.01478398D0
      G(4)=4.D0*G(1)+(E+0.51474D0)/0.00985599D0
      G(5)=5.D0*G(1)+(E+0.51010D0)/0.00739199D0
      DO 10 I=1,5
      IF(G(I).GE.75.D0) NNN=1
      IF(G(I).GE.75.D0) GO TO 20
 10   CONTINUE
 20   RETURN
      END
C
C     SCALC IS A FUNCTION SUBPROGRAM CALLED BY CALC FOR THE SOLU-
C     TION OF THE POLYNOMIAL EQUATIONS
C
      FUNCTION SCALC (E,X,K,AH,TMAX,XM)
      IMPLICIT REAL*8(A-H,O-Z)
      DIMENSION AH(1500),G(5),A(6)
      CALL POLYS (E,X,G,NNN)
      IF(G(5).LT.-75.D0) A(5)=0.D0
      IF(G(5).GE.-75.D0) A(5)=5.D0*10.D0**G(5)
      IF(G(4).LT.-75.D0) A(4)=0.D0
      IF(G(4).GE.-75.D0) A(4)=4.D0*10.D0**G(4)
      IF(G(3).LT.-75.D0) A(3)=0.D0
      IF(G(3).GE.-75.D0) A(3)=3.D0*10.D0**G(3)
      IF(G(2).LT.-75.D0) A(2)=0.D0
```

```
      IF(G(2).GE.-75.D0) A(2)=2.D0*10.D0**G(2)
      A(1)=10.D0**G(1)*STOTL1(K,AH)
      A(6)=-XM
      SCALC=A(1)+A(2)+A(3)+A(4)+A(5)+A(6)
      TMAX=A(1)
      DO 100 I=2,6
      IF(DABS(A(I)).GE.TMAX) TMAX=A(I)
  100 CONTINUE
      RETURN
      END
C
C     SSUM IS A FUNCTION CALLED BY THE SUBPROGRAM SSOL. SSUM EVAL-
C     UATES THE TOTAL OF SOLUBLE SULFUR SPECIES
C
      FUNCTION SSUM (E,X,K,AH)
      IMPLICIT REAL*8(A-H,O-Z)
      DIMENSION AH(1500),G(5)
      CALL POLYS (E,X,G,NNN)
      IF(G(5).LT.-75.D0) A5=0.D0
      IF(G(5).GE.-75.D0) A5=5.D0*10.D0**G(5)
      IF(G(4).LT.-75.D0) A4=0.D0
      IF(G(4).GE.-75.D0) A4=4.D0*10.D0**G(4)
      IF(G(3).LT.-75.D0) A3=0.D0
      IF(G(3).GE.-75.D0) A3=3.D0*10.D0**G(3)
      IF(G(2).LT.-75.D0) A2=0.D0
      IF(G(2).GE.-75.D0) A2=2.D0*10.D0**G(2)
      A1=10.D0**G(1)*STOTL1(K,AH)
      SSUM=A1+A2+A3+A4+A5
      RETURN
      END
C
C     THE INCLUSION OF POLYSULFIDES INTO THE CONSIDERATION COMPLI-
C     CATES THE SOLUTION OF THE MASS BALANCE EQUATION IN THE
C     SUBROUTINE SULF. SALTER IS A SUBROUTINE EXPRESSLY WRITTEN
C     TO SOLVE THE POLYNOMIAL EQUATION THAT RESULTS. IT AGAIN
C     USES THE SECANT METHOD TO SOLVE FOR THE ROOT.
C
      SUBROUTINE SALTER (E,K,XM,DXM,AH,DS)
      IMPLICIT REAL*8(A-H,O-Z)
      DIMENSION AH(1500),DS(1500)
      IF(K.GT.1) DX2=2.D0*DS(K-1)+(E+0.52402D0)/0.029567964D0
      IF(K.EQ.1) DX2=(DXM-25.39969D0-50.73058125D0*E)/2.5D0
      X2=10.D0**DX2
      X1=X2/2.D0
      F1=EQUAT (X1,K,AH,E,XM,TMAX1)
      F2=EQUAT (X2,K,AH,E,XM,TMAX2)
    5 XN=F2/(F2-F1)*X1-F1/(F2-F1)*X2
      FN=EQUAT (XN,K,AH,E,XM,TMAXN)
      PERDIF=FN/TMAXN
      IF(DABS(PERDIF).LT.1.D-06) GO TO 4
```

```
      X1=X2
      X2=XN
      F1=F2
      F2=FN
      GO TO 5
 4    DS(K)=0.5D0*DLOG10(XN)-(E+0.52402D0)/0.059135928D0
      RETURN
      END
C
C     EQUAT IS A FUNCTION SUBPROGRAM CALLED BY SUBROUTINE SALTER
C     TO EVALUATE THE POLYNOMIAL FOR VARIOUS GUESSES OF THE ROOT
C
      FUNCTION EQUAT (X,K,AH,E,XM,TMAX)
      IMPLICIT REAL*8(A-H,O-Z)
      DIMENSION AH(1500),G(6)
      DA=2.5D0*DLOG10(X)+50.73058125D0*E+24.70072002D0
      G(1)=5.D0*10.D0**DA
      DB=2.D0*DLOG10(X)+33.8203875D0*E+16.78099987D0
      G(2)=4.D0*10.D0**DB
      DC=1.5D0*DLOG10(X)+16.91019375D0*E+8.54742653D0
      G(3)=3.D0*10.D0**DC
      G(4)=2.D0*X
      G(5)=10.D0**(X/2.D0)*STOTL1(K,AH)*10.D0**(-(E+0.52402D0)/
     *0.059135928D0)
      G(6)=-XM
      EQUAT=0.D0
      TMAX=G(1)
      DO 10 I=1,6
      EQUAT=EQUAT+G(I)
      IF(DABS(G(I)).GE.TMAX) TMAX=DABS(G(I))
 10   CONTINUE
      RETURN
      END
C
C     XANTH IS A SUBROUTINE THAT SOLVES THE QUADRATIC EQUATION FOR
C     THE XANTHATE MASS BALANCE EQUATION WHEN ALL THE XANTHATE SPE-
C     CIES ARE SOLUBLE
C
      SUBROUTINE XANTH(K,AH,E,XINIT,DX)
      IMPLICIT REAL*8(A-H,O-Z)
      DIMENSION AH(1500),DX(1500)
      A=2.D0*10.D0**((E-0.08495D0)/0.029567964D0)
      B=1.D0+43.4783D0*AH(K)
      C=-XINIT
      RATIO=4.D0*A*C/B/B
      IF(DABS(RATIO).LT.1.D-06) GO TO 10
      ROOT=(-B+DSQRT(B*B-4.D0*A*C))/2.D0/A
      GO TO 20
 10   ROOT=-C/B
 20   DX(K)=DLOG10(ROOT)
```

```
      RETURN
      END
C
C     XSOL CALCULATES THE TOTAL CONCENTRATION OF SOLUBLE XANTHATE
C     SPECIES ONCE THE FREE XANTHATE ION CONCENTRATION IS KNOWN
C
      FUNCTION XSOL (K,AH,E,DX)
      IMPLICIT REAL*8(A-H,O-Z)
      DIMENSION AH(1500),DX(1500)
      X=2.D0*(10.D0**DX(K))**2.D0*10.D0**((E-0.08495D0)/0.029567964D0
     *)+10.D0**DX(K)*(1.D0+43.4783D0*AH(K))
      XSOL=DLOG10(X)
      RETURN
      END
C
C
C     THIS ENDS THE PROGRAM. WHAT FOLLOWS IS A SAMPLE DATA FILE
C     REQUIRED TO RUN THE PROGRAM.
C
C
C
  INPUT DATA  PBS-H2O-KEX SYSTEM (SULFUR IS METASTABLE) 1X10-05 M KEX
  0.00D0      0.45D0  0.4525D0     1.D-05
C
C
```

APPENDIX II.

Sample Derivation of the Relationship Between Charges Associated With a Reaction Sequence

Appendix II.

Sample Derivation of the Relationship Between Charges Associated With a Reaction Sequence

---

For the purposes of illustration, reaction sequence 1 appearing in Table 3.1 will be considered, i.e.,

A_1 $PbS + H_2O \longrightarrow PbO + S^o + 2H^+ + 2e$ [II.1]

$2PbS + 5H_2O \longrightarrow 2PbO + S_2O_3^{2-} + 10H^+ + 8e$ [II.2]

C_1 $PbO + S^o + 2H^+ + 2e \longrightarrow PbS + H_2O$ [II.3]

C_2 $PbO + 2H^+ + 2e \longrightarrow Pb^o + H_2O$ [II.4]

Letting n_{S^o} and $n_{S_2O_3^{2-}}$ represent the number of moles of S^o and $S_2O_3^{2-}$ produced by reactions [II.1] and [II.2], respectively, the total charge associated with these reactions is:

$$Q_{A1} = 2Fn_{S^o} + 8Fn_{S_2O_3^{2-}}, \quad [II.5]$$

where F is the Faraday constant.

If all the S^o that is produced at A_1 is subsequently reduced by reaction [II.3], then the charge associated with C_1 is:

$$Q_{C1} = 2Fn_{S^o}. \quad [II.6]$$

The amount of PbO reduced by reaction C_2 is the excess number of moles of PbO over S^o that is left on the galena surface at the end of oxidation. Consequently, Q_{C2} can be expressed as:

$$Q_{C2} = 2F(n_{PbO}) - (n_{SO}), \qquad [II.7]$$

where n_{PbO} is the total number of moles of PbO produced by reactions [II.1] and [II.2].

Finally, n_{PbO} is related to n_{SO} and $n_{S_2O_3^{2-}}$ by the stoichiometry of reactions [II.1] and [II.2], i.e.,

$$n_{PbO} = n_{SO} + 2n_{S_2O_3^{2-}}. \qquad [II.8]$$

Combining Eq. [II.8] and [II.7] results in the expression,

$$Q_{C2} = 4Fn_{S_2O_3^{2-}}, \qquad [II.9]$$

which can be substituted along with Eq. [II.6] into [II.5] to give:

$$Q_{A1} = Q_{C1} + 2Q_{C2}. \qquad [II.10]$$

This can be rearranged to yield the desired charge relationship for sequence 1:

$$\frac{Q_{A1} - Q_{C1}}{Q_{C2}} = 2 \qquad [II.11]$$

These expressions can also be used to derive the $n_{S_2O_3^{2-}}/n_{SO}$ ratio as given by Eq. [3.12]. Dividing [II.9] by [II.6] yields:

$$\frac{n_{S_2O_3^{2-}}}{n_{SO}} = \frac{1}{2}\frac{Q_{C2}}{Q_{C1}}. \qquad [II.12]$$

Eq. [II.12] can be given in terms of Q_{A1} and Q_{C1} only by using Eq. [II.10] to eliminate Q_{C2}. This leads to:

$$\frac{n_{S_2O_3^{2-}}}{n_{SO}} = \frac{1}{4}\,\frac{Q_{A1} - Q_{C1}}{Q_{C1}}, \qquad \text{[II.13]}$$

which, upon division of the numerator and denominator by Q_{A1}, becomes identical to Eq. [3.12], i.e.,

$$\frac{n_{S_2O_3^{2-}}}{n_{SO}} = \frac{1}{4}\,\frac{1 - Q_{C1}/Q_{A1}}{Q_{C1}/Q_{A1}}. \qquad \text{[II.14]}$$

APPENDIX III.

Expressions for the Amount of PbO Generated and Consumed During Each Cyclic Scan at pH 9.2

Appendix III.

Expressions for the Amount of PbO Generated and Consumed During Each Cyclic Scan at pH 9.2

PbO is generated by three reactions along the anodic scan of a cyclic voltammogram at pH 9.2:

A_1 $\quad PbS + H_2O \longrightarrow PbO + S^o + 2H^+ + 2e$ [III.1]

$\quad 2PbS + 5H_2O \longrightarrow 2PbO + S_2O_3^{2-} + 10H^+ + 8e$ [III.2]

A_2 $\quad Pb^o + H_2O \longrightarrow PbO + 2H^+ + 2e.$ [III.3]

From the stoichiometries of these equations, the number of moles of PbO formed $(n_{PbO})_A$ can be written as:

$$(n_{PbO})_A = n_{S^o} + 2n_{S_2O_3^{2-}} + n_{Pb^o}, \qquad [III.4]$$

where n_{S^o}, $n_{S_2O_3^{2-}}$ and n_{Pb^o} are the number of moles of S^o, $S_2O_3^{2-}$ and Pb^o, respectively, that are produced.

Using equations [II.6] and [II.9] from Appendix II, $(n_{PbO})_A$ becomes:

$$(n_{PbO})_A = \frac{Q_{C1}}{2F} + \frac{Q_{C2}}{4F} + \frac{Q_{A2}}{2F}. \qquad [III.5]$$

Since the C_2 peak is not always clearly resolved on the voltammograms, it is preferable to eliminate Q_{C2} from this equation. This can be done by substituting for Q_{C2} from Eq. [II.10] in Appendix II, and this leads to the final result:

$$(n_{PbO})_A = \frac{Q_{C1} + Q_{A1} + 2Q_{A2}}{4F} . \qquad [III.6]$$

The amount of PbO removed during each cycle, $(n_{PbO})_C$, by the reactions:

$$C_1 \quad PbO + S^o + 2H^+ + 2e \longrightarrow PbS + H_2O \qquad [III.7]$$

$$C_2 \quad PbO + 2H^+ + 2e \longrightarrow Pb^o + H_2O, \qquad [III.8]$$

is

$$(n_{PbO})_C = \frac{Q_{C1}}{2F} + \frac{Q_{C2}}{2F} . \qquad [III.9]$$

Once again, Q_{C2} can be replaced in this expression by using Eq. [II.10] to give:

$$(n_{PbO})_C = \frac{Q_{A1} + Q_{C1}}{4F} . \qquad [III.10]$$

APPENDIX IV.

Equilibrium Ratio for the Occupation of the Surface Sites by X^- and OH^-

Appendix IV.

Equilibrium Ratio for the Occupation of the Surface Sites by X^- and OH^-

---

Consider the following two chemisorption reactions that can occur on the initial monolayer of a sulfide:

$$PbS + X^- \underset{k-1}{\overset{k_1}{\rightleftharpoons}} Pb\text{—}(X)S + e \qquad [IV.1]$$

$$PbS + OH^- \underset{k-2}{\overset{k_2}{\rightleftharpoons}} Pb\text{—}(OH)S + e. \qquad [IV.2]$$

If both of these obey Temkin kinetics, then the rates of the two reactions can be written as:

$$V_X = k_1 C_X (1-\theta_{OH}-\theta_X) \exp\left(\frac{\beta_1 FE}{RT}\right) \exp[-\alpha_1 f_1(\theta_X+\theta_{OH})] -$$

$$k_{-1}\theta_X \exp\left[\frac{-(1-\beta_1)FE}{RT}\right] \exp[(1-\alpha_1) f_1(\theta_X+\theta_{OH})]. \qquad [IV.3]$$

$$V_{OH} = k_2 C_{OH} (1-\theta_{OH}-\theta_X) \exp\left(\frac{\beta_2 FE}{RT}\right) \exp[-\alpha_2 f_2(\theta_X+\theta_{OH})] -$$

$$k_{-2}\theta_{OH} \exp\left[\frac{-(1-\beta_2)FE}{RT}\right] \exp[(1-\alpha_2) f_2(\theta_X+\theta_{OH})]. \qquad [IV.4]$$

When equilibrium is reached, $V_X = 0$ and $V_{OH} = 0$ and these expressions become:

$$1 - \theta_{OH} - \theta_x = \frac{k_{-1}\theta_x}{k_1 C_x} \exp\left(\frac{-FE}{RT}\right)\exp[f_1(\theta_x+\theta_{OH})] \qquad [IV.5]$$

$$1 - \theta_{OH} - \theta_x = \frac{k_{-2}\theta_{OH}}{k_2 C_{OH}} \exp\left(\frac{-FE}{RT}\right)\exp\,[f_2(\theta_x+\theta_{OH})]. \qquad [IV.6]$$

The left-hand sides are identical and, consequently, equations [IV.5] and [IV.6] can be combined to yield:

$$\frac{\theta_x}{\theta_{OH}} = \frac{k_{-2}\, k_1}{k_2\, k_{-1}} \frac{C_x}{C_{OH}} \exp[-(f_1-f_2)(\theta_x+\theta_{OH})], \qquad [IV.7]$$

which can be seen to be equivalent to equation [6.2] by setting $k_1 = k_{-2}k_1/k_2k_{-1}$ and $k'_2 = f_1-f_2$.

The vita has been removed from the scanned document